



HAL
open science

Understanding organic aerosol formation processes in atmosphere using molecular markers : a combined measurements-model approach

Grazia Maria Lanzafame

► **To cite this version:**

Grazia Maria Lanzafame. Understanding organic aerosol formation processes in atmosphere using molecular markers : a combined measurements-model approach. Ocean, Atmosphere. Sorbonne Université, 2019. English. NNT : 2019SORUS519 . tel-03200111

HAL Id: tel-03200111

<https://theses.hal.science/tel-03200111v1>

Submitted on 16 Apr 2021

HAL is a multi-disciplinary open access archive for the deposit and dissemination of scientific research documents, whether they are published or not. The documents may come from teaching and research institutions in France or abroad, or from public or private research centers.

L'archive ouverte pluridisciplinaire **HAL**, est destinée au dépôt et à la diffusion de documents scientifiques de niveau recherche, publiés ou non, émanant des établissements d'enseignement et de recherche français ou étrangers, des laboratoires publics ou privés.

Sorbonne Université

ED 129

INERIS

**Understanding organic aerosol formation processes in
atmosphere using molecular markers: a combined
measurements-model approach**

Par Grazia Maria Lanzafame

Thèse de doctorat de Chimie de l'environnement

Dirigée par Bertrand Bessagnet

Présentée et soutenue publiquement le 12/12/2019

Devant un jury composé de :

Mme D'ANNA Barbara, Directrice de recherche, LCE	Rapporteur
Mme HODZIC Alma, Directrice de recherche, LA	Rapporteur
Mme SARTELET Karine, Directrice de recherche, CERA	Examinatrice
Mme TURQUETY Solène, Maitre de conférences, UPMC	Examinatrice
M. BALDASANO José Maria, Professeur, Université Polytechnique de Catalogne	Examinateur
M. VILLENAVE Eric, Professeur, Université de Bordeaux	Invité
Mme CAMREDON Marie, Maitre de conférences, LISA	Invitée
M. COUVIDAT Florian, Ingénieur de recherche, INERIS	Responsable de thèse
M. ALBINET Alexandre, Ingénieur de recherche, INERIS	Responsable de thèse
M. BESSAGNET Bertrand, HDR, Chargé d'Affaires Scientifiques, INERIS	Directeur de thèse

Acknowledgements

First of all I would like to thank all my supervisors, Bertrand, Olivier, Alex and Florian, for giving me the opportunity to do this PhD. Special thanks are due to Alexandre Florian. Alex, your scientific support was fundamental and the challenges you've put me up against have made me grow as a better scientist. Florian, you taught me everything I know about modeling, with a lot of patience and a smile. You believed in me till the end, also when I was driving you crazy.

I wish to acknowledge Eric Villenave and Marie Camredon for their participation during my PhD Committees, providing always a fresh and interesting point of view on my job.

I am also grateful to Barbara D'anna and Alma Hodzic for accepting reviewing this manuscript and to the examiners Karine Sartelet, José Maria Baldasano and Solène Turquety.

I would like to offer my special thanks to all the teams in which I worked during my PhD:

- The ASUR/EMIS team: Marc and Caroline for their kindness and availability, Valerie and Marie for their smile and their patience, Laurent for his support in my mother tongue :), Tanguy for his philosophic discussions, François for the nice talks, Nicolas K. and Robin for their support during Landex (I would never have survived without your help!) and Adrien for his work during the EVORA campaign. I also would like to thank and all the other team members for the nice time spent together: Florence, Nathalie M., Nathalie B., Celine, Sebastien, Olivier L., Jessica Q., Virginie, Anne-Sophie, Serge, Isaline, Jean, Benedicte, Cecile R., Vincent F., Fabrice, Hugo, Sylvie, Marion, Warda and Aline.

-The ANAE team: Jérôme and his precious help with the GC (you are the master), Hervé for his collaboration during the EVORA campaign, Claudine C. and Faustina for their understanding and support, Serguei (you will always be the ASE god for me), Yohann, Farid, Azziz, François, Cecile L., Claudine D., Ahmad, Jean-Pierre, Sylvain, Nicolas C., Valerie, Arnaud and Hugues.

-The MOCA/EDEN team: Simone, Elsa, Cynthia, Pierre, Simon, Valentin, Alicia, Florence, Fred, Blandine, Antonio, Gaël, Anthony, Jessica and Augustin. Your good mood (and your beliefs on italian food) made easier my last year at INERIS (and you also taught me new french words ahah)

My special thanks go to my family abroad, my office mates: Deep and Yunjiang, I learn a lot from both of you and please never tell anybody what we were discussing when the office door was closed :D. Lei, I know that you are still crying since I left. Camilla, one of the best person I ever met.

I wish to thank also all the other students met during this journey for the nice time spent together: Eleonora and Jasmina, the only people I trust for cooking pasta in France, Alexandre "Perlana", Marta (best road trip EVER), Adrien (BBQ king), Anitha, Ibtihel, Thi Cuc, Quentin, Pierre, Manoj, Martin, Kevin, Hugo, Vincent, Victor, Anne-Sophie, Julien, Katia, Maria, Nihal and Andrea.

I would also like to thank my friends spread all over the world who listened to my infinite complains during the PhD. Don't worry, I will soon complain about my job.

Finally, I wish to thank my parents and my sister that are proud of me also if they didn't fully understand what I was working on. Thanks for your constant support and encouragement. I owe you everything.

Contents

Chapter I.....	1
Introduction and objectives of the Thesis	1
1.1. Atmospheric aerosols	2
1.1.1. Definition	2
1.1.1. Aerosol impacts on air quality and climate.....	3
1.1.2. Air quality and air pollution policies.....	6
1.2. Aerosol chemical composition	7
1.2.1. Primary and secondary organic aerosol	7
1.2.2. SOA formation: precursors and their reactivity in atmosphere.....	8
1.2.3. Gas to particle partitioning of secondary compounds.....	11
1.2.4. Benefits of an aerosol molecular characterization	13
1.2.5. Source apportionment	15
1.2.6. Definition and use of OA markers in literature.....	16
1.3. State of art modelling secondary organic aerosol.....	18
1.3.1. Air quality model structure	18
1.3.2. SOA modelling approaches.....	19
1.3.2.1. Two-products model	19
1.3.2.2. VBS (Volatility Basis Set) approach	20
1.3.2.3. Molecular surrogate approach.....	20
1.3.2.4. Model performances	22
1.4. PhD thesis objectives.....	23
References	25
Chapter II:SOA markers measurements.....	37
Article I: One-year measurements of secondary organic aerosol (SOA) markers in the Paris region: concentrations, seasonality, gas/particle partitioning and use in SOA source apportionment.....	37
Abstract	40
1. Introduction and objectives	42
2. Experimental	44
2.1. Sampling site and sample collection.....	44
2.3. SOA markers analysis quality control/quality assurance.....	46
2.4. On-line measurements	46
3. OA source apportionment	47
3.1. SOA tracer method	47
3.2. Positive matrix factorization (PMF)	48
4. Results and discussion.....	48
4.1. SOA marker concentration levels and comparison with literature data.....	48
4.2. SOA marker temporal evolutions and seasonality.....	51
4.3. Focus on the October/November 2015 period	53
4.4. SOA markers gas/particle partitioning (GPP).....	55
4.5. SOA source apportionment.....	57

4.5.1.	SOA tracer method	57
4.5.2.	Comparison of SOA tracer method and PMF outputs	58
5.	Conclusions	60
	References	61
	Supplementary Material	77
Chapter III:	Model to measurements comparison: Anthropogenic markers	119
Article II:	Modelling organic aerosol markers in 3D air quality model. Part 1: Anthropogenic organic markers	119
	Abstract	122
1.	Introduction and objectives	123
2.	Model development	125
2.1	Overview of the marker mechanism	125
2.1.1	Marker GPP computation	126
2.2	Anthropogenic OA marker formation in the atmosphere: mechanisms and GPP parameters	128
2.2.1	Levoglucosan	129
2.2.2	Nitroguaiacols	129
2.2.3	Nitrophenols	130
2.2.4	DHOPA	131
2.2.5	Methyl-nitrocatechols	134
2.2.6	Phthalic Acid	135
3.	Comparison measurements model	136
3.1	Configuration	136
3.2	Measurements	139
4.	Results and discussion	140
4.1	Model to measurement comparison	140
4.1.1	Levoglucosan	140
4.1.2	Nitroguaiacols and nitrophenols	147
4.1.3	Methylnitrocatechols and DHOPA	148
4.1.3	Phthalic acid	151
4.1.4	Correlation between secondary markers and levoglucosan	151
4.2	GPP estimations	152
4.2.1	Levoglucosan: spatial variability and model sensitivity to thermodynamic assumptions	152
4.2.2	GPP of secondary markers at SIRTAs	155
4.2.3	Influence of partitioning and gas-phase dry deposition of secondary markers on total concentrations	158
4.2.4	Evaluation of the OA-tracer approach to evaluate the wood-burning OM: Analysis of $OM_{wb} pLEVO^{-1}$ variations	161
	Conclusions	163
	References	165
	Supplementary Material	174
Chapter IV:	Model to measurements comparison: Biogenic markers	195

Article III: Modelling organic aerosol markers in 3D air quality model. Part 2: Biogenic secondary organic markers.....	195
1. Introduction and objectives	200
2. Model overview.....	202
2.1 Development of the marker mechanism	203
2.1.1 α - and β -pinene markers	205
2.1.2 Isoprene markers	215
3. Comparison measurements model	217
3.1 Configuration: model resolution and domain	217
3.2 Measurements: SIRTA.....	218
4. Results and discussion.....	219
4.1 Model to measurement comparison	219
4.1.1 α -/ β -pinene marker temporal variations.....	221
4.1.2 Isoprene marker temporal variations	222
4.2 Influence of chemical regime on total marker concentrations.....	224
4.2.1 α -/ β -pinene markers	225
4.2.2 Isoprene markers.....	226
4.3 Pinonic acid formation process: spatial and daily variability	227
4.4 GPP estimations at SIRTA.....	230
4.4.1 Model to measurements comparison: a focus on thermodynamics.	230
4.4.2 Influence of partitioning and gas-phase dry deposition on total marker concentrations.....	232
Conclusions	235
References	237
Supplementary Material	246
References	251
Chapter V	253
Conclusions and perspectives.....	253
1. Molecular marker measurements and database.....	255
2. Molecular markers model/measurements comparison: knowledge of physicochemical processes and emissions	256
2.1 Knowledge of the emissions	257
2.2 Knowledge of the chemical processes	257
2.3 Gas/particle partitioning evaluation.....	259
3. Molecular markers for source apportionment	259
References	260
Annexes.....	261

Chapter I

*Introduction and objectives of the
Thesis*

1.1. Atmospheric aerosols

1.1.1. Definition

Aerosols are defined as suspended solid and liquid particles in a gas. In atmospheric sciences, the term aerosol is commonly used to indicate particulate matter (PM), although the original definition of the term is referred to the gaseous and the particulate phase together.

Because of the variety of sources and processes associated to atmospheric aerosol production, their concentrations in the atmosphere vary widely regionally and seasonally. Primary aerosols are directly emitted as particles in the atmosphere by both, natural (mainly vegetation, oceans, soil resuspension, volcanoes) and anthropogenic (biomass burning, traffic exhaust, industrial activities, etc.) sources. Secondary aerosols are produced in the atmosphere as a result of physical and chemical transformations of gaseous phase compounds.

Atmospheric aerosols are classified according to their aerodynamical diameters that range from a few nanometres to several micrometres. The most widely used aerosol classes are named PM₁, PM_{2.5} and PM₁₀, which correspond respectively to particles with diameter smaller than 1, 2.5 and 10 µm. Their size influences their half-life and transportation, health impacts and interactions with light.

A scheme of particle size distribution, together with the main production and removal processes associated, is presented in Figure 1.1. Fine aerosol fraction (PM_{2.5}) includes the Aitken nuclei and accumulation modes that are produced mostly from condensation of low volatility compounds and coagulation of smaller particles (ultra-fine particles). Their half-life in the atmosphere is about few days to two weeks (Kristiansen et al., 2016). These particles can either be removed from the atmosphere by dry and wet deposition or can continue to grow in size by coagulation with other particles or by condensation of low volatility compounds onto their surface (Pöschl, 2005). Most of the coarse particles (larger than 2.5 µm) are directly emitted in the atmosphere (Finlayson-Pitts and Pitts, 2009) by anthropogenic and natural sources, which includes resuspension of dust, primary biological particles (spores, pollens...) and sea spray. In the atmosphere, coarse particles are also formed by coagulation of smaller particles and low-vapor pressure compounds on their surface. Coarse aerosol half-lives range between some minutes to several days (Seinfeld and Pandis, 1998). Typical tropospheric particles concentrations are in the range of 10²-10⁵ cm⁻³ in number and 1-100 mg m⁻³ in mass (Krejci et al., 2005; Raes et al., 2000; Van Dingenen et al., 2004; Williams et al., 2002).

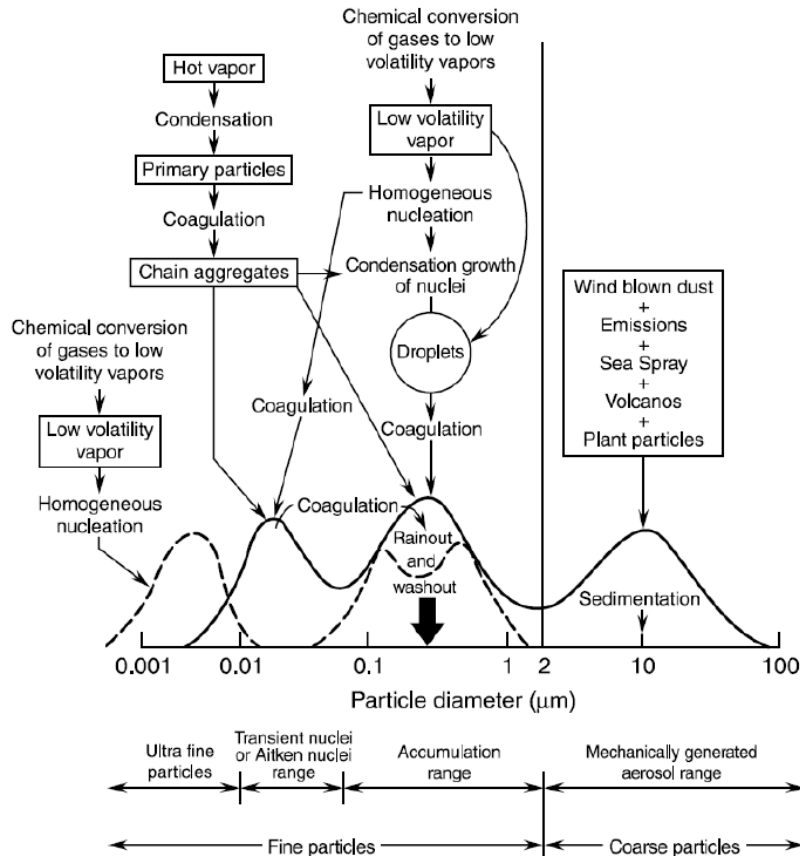


Figure 1.1. Schematic representation of principal modes, sources and aerosol formation and removal mechanisms. Adapted from:[Whitby and Sverdrup, 1980]

1.1.1. Aerosol impacts on air quality and climate.

Aerosols are getting growing attentions from the scientific community due to their proven effects on health, climate and visibility. According to the World Health Organization (WHO), 4.2 million people died because of air pollution in 2016 (WHO, 2018). Air pollution is considered as the largest environmental health hazard in Europe (EEA, 2018).

Several epidemiological studies proved the connection between particulate air pollution and an increment of respiratory diseases and adverse effect on cardiovascular system (Heal et al., 2012; Seaton et al., 1995) that can cause premature deaths (Apte et al., 2015; Burnett et al., 2018). Reduced lung function, respiratory infections and asthma have been recognized as effects of both acute and chronic exposure to air pollution. Recently, evidences of air pollution effects on diabetes, obesity, systemic inflammation and neurological diseases incidence have been also provided (RCP, 2016, and references therein; WHO, 2018).

Particle hazard depends on their size: coarse particles with a diameter between 10 and 30 μm are usually deposited in the oropharyngeal region, particles with dimensions between 2 and 16 μm can reach the terminal bronchioles and finer particles ($< 2 \mu\text{m}$) penetrate further till the alveolar sacs (Figure 1.2). Finer particles can interfere in the exchanges between air and blood, introducing toxic substances in the circulatory system. The most widely known toxic substances that can be absorbed on the aerosols are metals (Cu, Pb, Cd ...), polycyclic aromatic hydrocarbons (PAHs), polychlorobiphenyls (PCBs) and dioxins (Finlayson-Pitts and Pitts Jr, 2000; Jacobson et al., 2000). Metals and PAHs are regulated in Europe by the European Directive 2004/107/CE (European official journal, 2004).

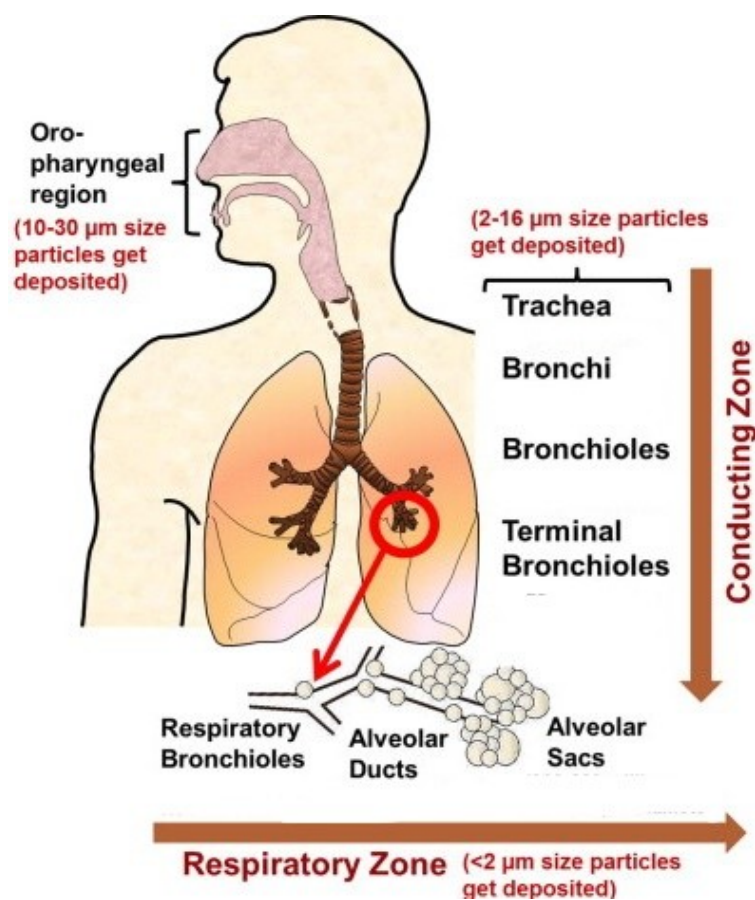


Figure 1.2. Airways of the adult lung and particle deposition in function of their sizes.

Adapted from: [Nahar et al., 2013]

Besides health impact, aerosols can scatter and absorb infrared and visible light, contributing to climate change. Three radiative forcing (RF) have been estimated for aerosol interactions with solar light: the aerosol-radiation interaction, the aerosol-cloud interaction and the impact of black carbon (BC) on snow and ice surface albedo (IPCC, 2018).

Aerosols mostly scatter solar radiation, leading to a cooling effect, and absorb solar radiation only when composed by absorbing components as black carbon (BC), causing a warming effect. The global RF estimate for the direct aerosol-light interaction is negative (-0.35 W m^{-2}), with a prevalence of the scattering effect. Besides, aerosol–cloud interactions are usually considered as indirect effects of aerosol on climate. Reflecting properties and lifetime of clouds change according to aerosol sizes and composition (Haywood and Boucher, 2000), with consequences on the RF associated to cloud albedo. RF by aerosol effect contribution is highly uncertain, and rather a total effective radiative forcing (ERF), due to aerosol-radiation and aerosol-cloud interactions, has been calculated (-0.9 W m^{-2}). Finally, the black carbon (BC) deposition reduces the snow and ice surface albedo, absorbing visible and ultraviolet light (RF $+0.04$). However, the contribution of this process is low compared to the previous ones.

Radiative forcing on climate between 1750 and 2011 is shown in Figure 1.3. Higher positive contributions to the total anthropogenic ERF are given by well mixed greenhouse gases (WMGHG), including CO_2 . Tropospheric ozone positive RF is in part compensated by the stratospheric ozone negative RF. The only forcing agents giving significant negative ERF are aerosols-radiation and aerosol-cloud interactions. These effects mitigate but not fully contrast WMGHG ERF, and total balance of anthropogenic ERFs results positive.

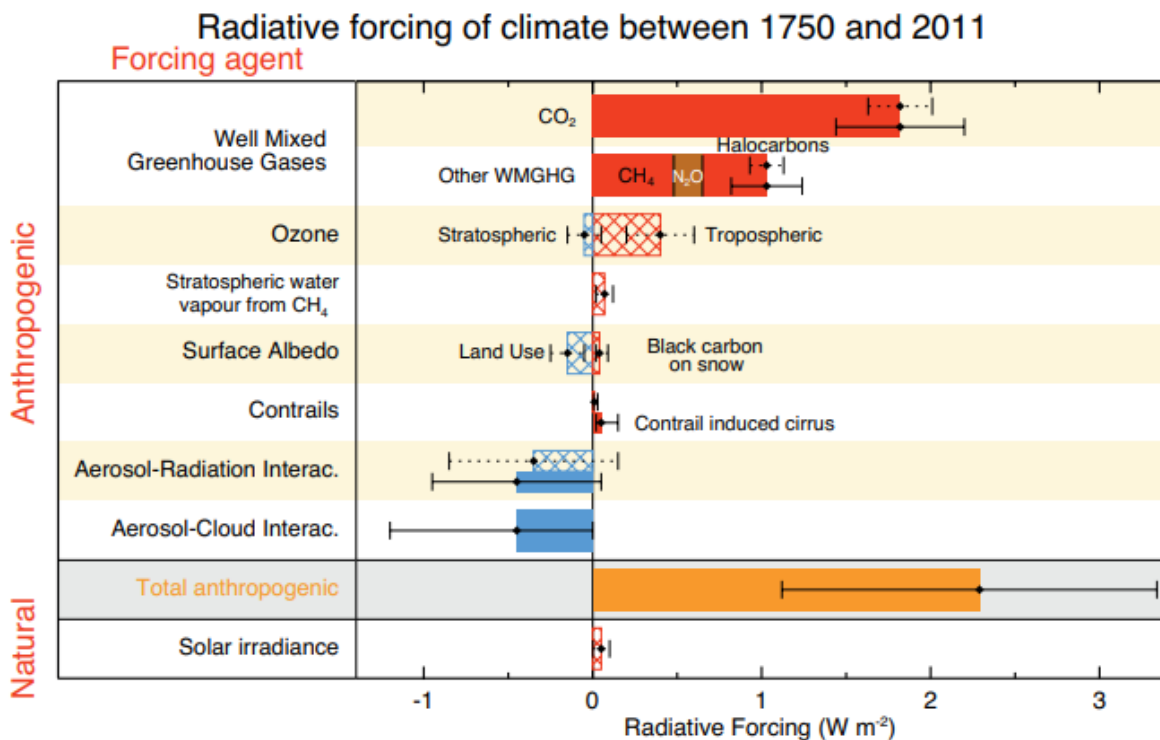


Figure 1.3. Bar chart for radiative forcing (hatched) and effective radiative forcing (solid) by concentration change between 1750 and 2011. Uncertainties (5 to 95% confidence range) are given for RF (dotted lines) and ERF (solid lines). Source: [IPCC, 2018]

1.1.2. Air quality and air pollution policies

Oxford dictionary defines air quality as “the degree to which the air in a particular place is pollution-free”. Industrialization and urbanization led to increasing emissions that modified the composition of the atmosphere. The consciousness about air quality monitoring importance has begun after the well-known acute pollution episodes of “Los Angeles smog” (1949) and “London fog” (1952). Pollution episodes usually occur when large amounts of pollutants are emitted in conditions of weak atmospheric dispersion. During severe pollution episodes respiratory disease incidence increase and excess mortality has been registered. Thus, in order to protect populations, concentrations of PM in ambient air are regulated, for example, in France and Europe by the European Directive 2008/50/EC (European official journal, 2008), which set concentration limit values for PM on annual (40 and 25 $\mu\text{g m}^{-3}$ for PM_{10} and $\text{PM}_{2.5}$ respectively) and daily (50 $\mu\text{g m}^{-3}$ for PM_{10}) timescale and with a maximum number of exceedances over the calendar year (35 days per year). However, many studies shown that there is probably no PM concentration threshold below which no health impacts would be observed (WHO, 2017).

The knowledge of PM, and especially of the organic fraction, sources is essential for policy makers to apply efficient emission regulation policies. This can be achieved from measurements as nowadays, several monitoring networks are operational and perform continuous measurements of regulated pollutants, as $\text{PM}_{2.5}$ and PM_{10} , together with a detailed aerosol chemical speciation. As an example, in France, air quality monitoring network is coordinated by the Central laboratory of air quality monitoring (LCSQA) in collaboration with the Official Air quality Monitoring Associations (AASQA) and several PM source apportionment studies have been performed in different locations (Weber et al., 2019). Air quality models are also widely used to forecast the air quality and help institutions to mitigate their effects. Daily air quality in France is forecasted with the air quality system Prev’Air (www.prevair.org). In addition, chemistry-transport models can also be used to apportion PM sources and have been applied in Europe during several studies (Brandt et al., 2013; Karamchandani et al., 2017; Skyllakou et al., 2014; Yang et al., 2019). Further details on source apportionment methodologies are given in section 1.2.5.

1.2. Aerosol chemical composition

Aerosols are constituted from both an inorganic and an organic fraction. The mineral fraction is dominated by sulfate, nitrate and ammonium and account for 40 to 60% of PM₁ dry mass, according to the kind of site considered (urban, urban background or rural) (Putaud et al., 2004; Zhang et al., 2011). OA fraction can account up to 90% (Kanakidou et al., 2005; Zhang et al., 2007, 2011) of particulate matter (PM) in ambient air (Figure 1.4). OA concentrations and compositions show large seasonal and regional variabilities and the knowledge of their sources and processes remain still poorly understood. OA is usually estimated by multiplying concentrations of OC with factors ranging from 1.5 to 2, depending on the assumed average molecular composition (Gelencsér et al., 2007; Russell, 2003). The use of a fixed factor to convert OC to OA may be insufficient to achieve high accuracy results (Brown et al., 2013). Only the identification and quantification of all OA components could make OA mass estimation possible. OA composition is extremely varied and variable and the most comprehensive OA characterization studies succeed in identifying only 10-40% of total OA (Pöschl, 2005).

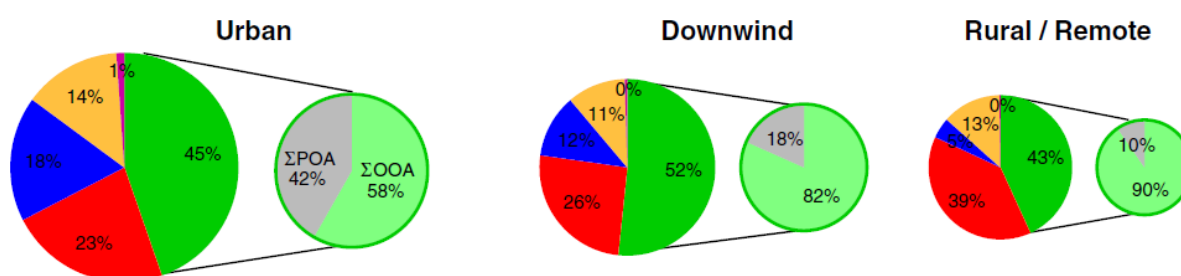


Figure 1.4 Average chemical composition of PM₁ for different types of site. Pink: chloride; Yellow: ammonium, Blu: nitrate; Red: sulfate; Green: organic matter; Light green: oxygenated organic aerosol (OOA) equivalent to SOA (secondary organic aerosol) estimation; Grey: primary organic aerosol (POA). Adapted from [Zhang et al., 2011].

1.2.1. Primary and secondary organic aerosol

Primary organic aerosols (POA) are directly emitted into the atmosphere by the combustion of biomass and fossil fuels, sea spray and resuspension of biological (plant debris, pollen, fungal spore, etc.) and anthropogenic dusts. Secondary organic aerosols (SOA) are produced in the atmosphere via gas-to-particle conversion processes of semivolatile organic compounds

(SVOCs) (Hallquist et al., 2009) and account for a significant part (20-80%) of total OA (Jimenez et al., 2009; Kroll and Seinfeld, 2008; Srivastava et al., 2018; Zhang et al., 2007, 2011). Unlike primary particles, directly emitted into the atmosphere from characterized sources, secondary aerosols, including SOA, are difficult to regulate and technological constraints restrict their monitoring. A schematic representation of the processes involved in SOA formation is reported in Figure 1.5. Gaseous phase precursors are oxidized by homogeneous and heterogeneous reactions, giving low volatility compounds. These products can nucleate into new particles or condensate onto pre-existing particles. The new-born particles can keep growing by condensation processes and coagulation with other particles. The new-born particles can keep growing by condensation processes and coagulation with other particles.

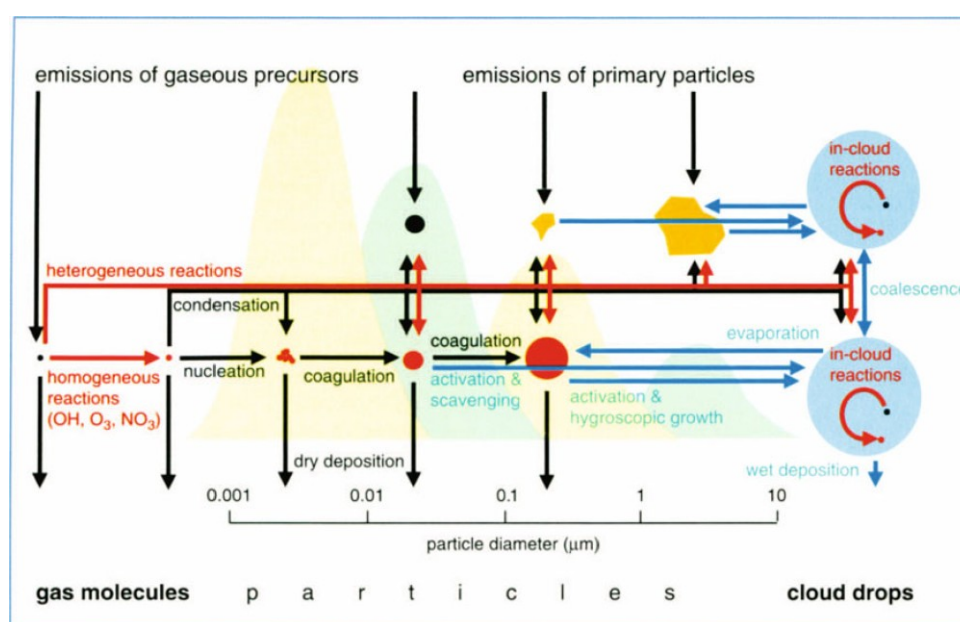


Figure 1.5 . Major microphysical and chemical processes that influence the size distribution and chemical composition of atmospheric aerosol particles. Source: [Brasseur et al., 2003]

1.2.2. SOA formation: precursors and their reactivity in atmosphere

VOCs sources are from both, natural (plant emission, forest fires...) and anthropogenic (traffic, industrial activities and domestic heating emissions) origins. The processes leading to SOA formation from VOCs are complex and still poorly understood. For this reason, numerical models generally underestimate the SOA fraction (Bessagnet et al., 2008). Once emitted into the atmosphere VOCs undergo (photo-) oxidation through photolysis and reaction with OH, NO₃ or O₃. VOCs oxidation pathways occur through several steps, leading to the formation of more functionalized, less volatile and more hydrophilic compounds. These chemical species partition onto the particle phase to form SOA until reaching thermodynamic

equilibrium. In the particle phase, SOA components can undergo further chemical (e.g. oligomerization) and physical (e.g. desorption, solubilization) processes.

Plant-emitted SOA biogenic precursors include isoprene, monoterpene and sesquiterpenes. The double C=C bonds contained by all these compounds can react with the main atmospheric oxidants (OH, NO₃ and O₃) (Calogirou et al., 1999). Monoterpenes have been identified as the major biogenic SOA precursor (Guenther et al., 1995), with a global estimated contribution between 10 and 30% to total SOA (Pye et al., 2010; Spracklen et al., 2011; Tsigaridis and Kanakidou, 2003). Isoprene SOA yields has been estimated to be low (~1%) (Carlton et al., 2009; Kroll et al., 2006). However, isoprene is the largest non-methane VOCs compound emitted (600 Tg yr⁻¹) on global scale (Guenther et al., 2006) and isoprene SOA can account for a maximum 30% to total OA (Heald et al., 2008). Sesquiterpenes have lower emissions than isoprene and monoterpenes (Acosta Navarro et al., 2014), but because of their high SOA yields they may contribute significantly to the biogenic SOA budget (Griffin et al., 1999).

Anthropogenic SOA precursors are mainly aromatic compounds (toluene, naphthalene, benzene, phenols, xylene, alkylbenzenes and PAHs) and long chain (number of carbons > 7) aliphatic alkanes (Bruns et al., 2016; Zhao et al., 2014). Their oxidation is initiated by reaction with OH, with SOA yields ranged from a few percent (Li et al., 2016; Ng et al., 2007) for aromatic compounds to 90% (Aumont et al., 2005; Lim and Ziemann, 2005, 2009) for long chain alkanes. Anthropogenic VOCs global emissions have been reported to be around 10% of total non-methane VOCs emissions (Goldstein and Galbally, 2007; Heald et al., 2010), but can become important locally in urban environments.

A schematic representation of a generic VOC oxidation pathway is reported on Figure 1.6. VOC oxidation is initiated by the reaction with an oxidant (OH, NO₃ or O₃) or by photolysis. The produced alkyl radical (R) reacts then with a molecule of oxygen, becoming an alkyl-peroxy radical (RO₂). RO₂ fate depends on the NO_x regime. At high-NO_x conditions RO₂ can be oxidized by NO or NO₂, to give in the first case, the correspondent alkoxy radical (RO) or to the correspondent nitrate (RONO₂) and in the second case, the peroxyxynitrate (ROONO₂). At low NO_x concentrations, the reactions with HO₂ and RO₂ become possible, forming stable products (hydroperoxydes, carboxylic acids, peroxyacids, alcohols and carbonyls) and RO radicals only for the RO₂+RO₂ reaction. RO undergoes isomerization or decomposition to form a stable compound. The stable compounds produced (first generation oxidation products) can be further oxidized in gas phase (producing different generation on oxidation products), following the same scheme, or can partition onto the particulate phase (organic or

aqueous phases). These compounds, less volatile than VOCs, are named semi-volatile organic compounds (SVOCs). SVOCs gas/particle partitioning (GPP) is discussed in the next section.

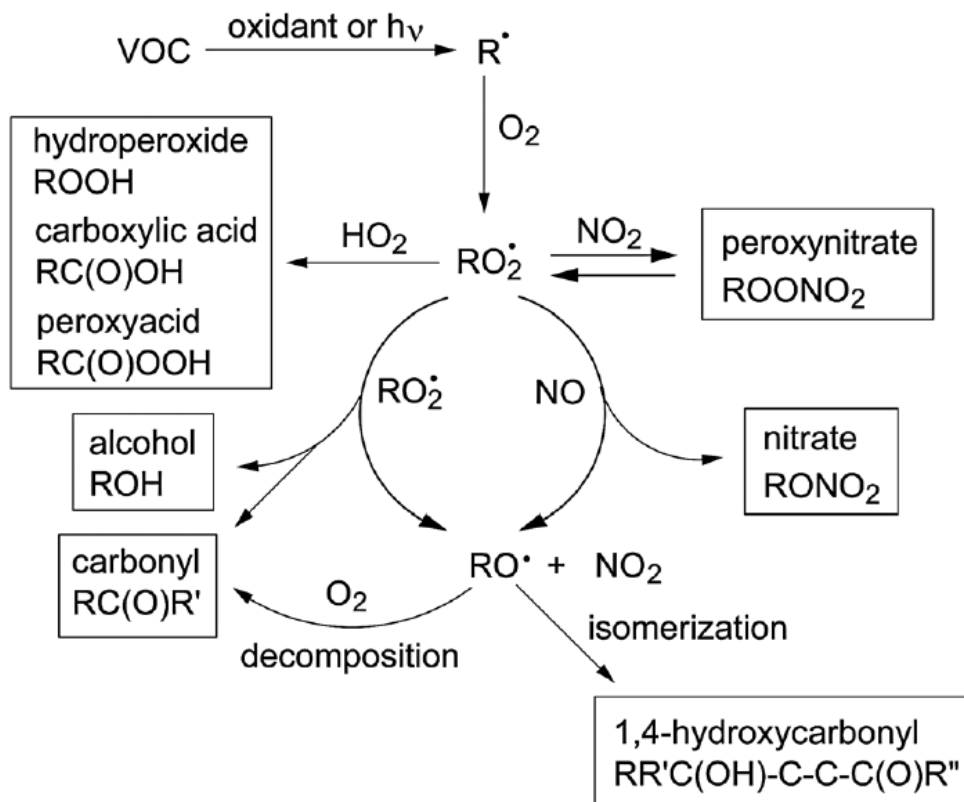


Figure 1.6 VOC atmospheric degradation reactions proceeding through formation of an alkyl or substituted alkyl radical. Source:[Ziemann and Atkinson, 2012]

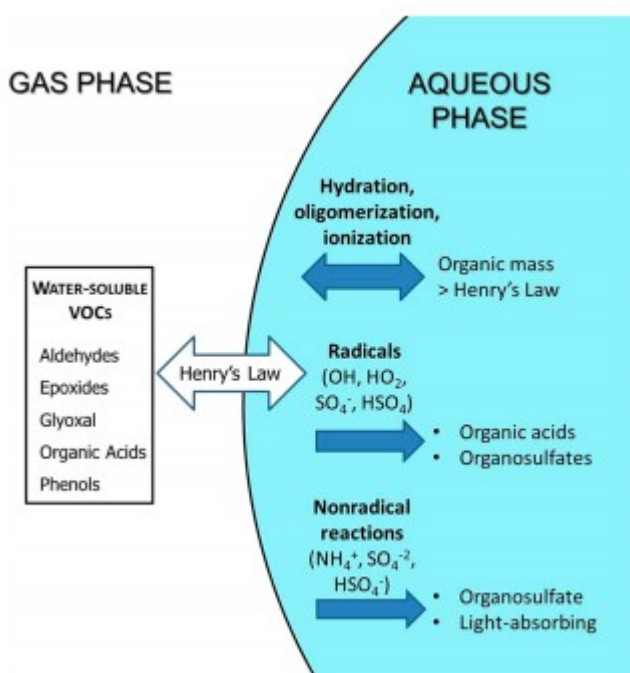


Figure 1.7. Schematic description of bulk aqueous chemical processes involved in aqueous SOA (aqSOA) formation. The same fundamental chemical mechanism applies for cloud droplets and aerosol water, however the dominant reactions differ due to differences in the chemical environment (pH, inorganic, and organic concentrations). Source: [McNeill, 2015]

The main reactions involving water-soluble organic compounds (WSOC) in the aqueous phase are (Figure 1.7):

- dark reactions, as hydration, hydrolysis, self-oligomerization and ionization,
- the radical oxidation by OH, HO₂, SO₄ and HSO₄, that generates organic acids or organosulfates. At high WSOC concentrations the organic radicals created may react together to form oligomers.
- ionic reactions operated mostly by NH₄⁺, SO₄²⁻ and HSO₄⁻. Organosulfates and light-absorbing species are produced.
- photochemical reactions: photolysis of photolabile species and activation of photosensitizers (e.g. humic and fulvic acids).

Due to the different composition of aqueous aerosol phase and cloud water, the expected predominant reactive pathways for aqueous phase SOA formation (aqSOA) are different in both media (McNeill et al., 2012; Tan et al., 2010). In the aerosol aqueous phase (0 < pH < 3 (Freedman et al., 2019), rich in organics and supersaturated in salts) acid-catalysed reactions and inorganic–organic reactions and oligomerization are favoured. In cloud water (pH > 3, less concentrated organics and salts), OH oxidation mechanism predominates.

1.2.3. Gas to particle partitioning of secondary compounds

SVOCs partition between gas-phase and the aqueous and organic phases of aerosols, generating SOA. The volatility of chemical species is directly proportional to their saturation vapor pressure, defined as the pressure at which the vapor of the compound is at the equilibrium with its solid (solid saturated vapor pressure) or liquid (liquid or subcooled saturated vapor pressure) phase. Saturated vapor pressure depends on temperature following a Clausius-Clapeyron relation: at higher temperatures saturated vapor pressure decreases, determining a particulate phase fraction decrement. According to Raoult's law the concentrations in the liquid phase and in the gas phase at equilibrium are linked by the following relation:

$$\gamma_{G,i}(P_i)P_i = \gamma_{L,i}(x_i)x_iP_i^0 \quad (\text{Eq 1.1})$$

where P_i is the partial pressure of the compound i in the gaseous phase, x_i the molar fraction of the compound i in the liquid phase, P_i^0 is the compound saturated vapor pressure of i and $\gamma_{G,i}$ and $\gamma_{L,i}$ are the activity coefficients respectively in the gaseous and the liquid phase. Activity coefficients indicate the interactions between the different species in solution. When ideality is assumed, all the interactions between the mixture components are assumed identical and therefore all the activity coefficients values are taken equal to 1. Raoult's law then become:

$$P_i = x_i P_i^0 \quad (\text{Eq 1.2})$$

This version of Raoult's law is commonly used to describe the gas to particle partitioning in air quality models. However, if atmospheric gases behavior can be assumed as ideal (as gases behavior is ideal at pressures far below the atmospheric pressure), this is not the case for the aerosol phase. The Raoult's law form to calculate gas/particle this equilibrium can be written as follows:

$$P_i = \gamma_{L,i} x_i P_i^0 \quad (\text{Eq 1.3})$$

in which only the liquid phase activity coefficients are taken in account.

A modified version of the Raoult's law to calculate the partitioning between the gaseous and the organic phases has been proposed by (Pankow, 1994):

$$K_{p,i} M_0 = \frac{A_{p,i}}{A_{g,i}} \quad (\text{Eq 1.4})$$

Where $K_{p,i}$ is the gas-particle partitioning constant ($\text{m}^3 \mu\text{g}^{-1}$), $A_{p,i}$ is the organic phase concentration in $\mu\text{g m}^{-3}$ and $A_{g,i}$ and $A_{p,i}$ are respectively the concentrations of the component i in the gas and in the particulate phase. This model assumes that the particulate phase of organic aerosol is constituted by a single and homogeneous phase, which is not the case for the real aerosols. $K_{p,i}$ is linked to the saturated vapor pressure by the following relation:

$$K_{p,i} = \frac{760 \times R \times T}{M_{ow} \gamma_i 10^6 P_i^0} \quad (\text{Eq 1.5})$$

where the temperature (T) is expressed in K, R is the perfect gas constant ($8.206 \times 10^{-5} \text{m}^3 \text{atm mol}^{-1} \text{K}^{-1}$), M_{ow} is the molar mass of the organic phase in g mol^{-1} and the saturated vapor pressure (P_i^0) is in torr.

For diluted solutions, the partitioning between the gaseous phase and the aqueous phase can be computed using Henry's law:

$$C_i = H_i \times P_i \quad (\text{Eq. 1.6})$$

where C_i , H_i and P_i are respectively the aqueous phase concentration, the Henry's law constant ($\text{mol L}^{-1} \text{atm}^{-1}$) and the molar partial pressure of i . In conditions of infinite dilution ($C_i \rightarrow 0$), Henry's law and Raoult's law can be combined:

$$H_i = \lim_{C_i \rightarrow 0} \left(\frac{C_i}{P_i} \right) = \frac{\rho_{water}}{M_{water} \times \gamma_i^\infty \times P_i^0} \quad (\text{Eq. 1.7})$$

in which ρ_{water} is the water density (g L^{-1}), M_{water} is the water molar mass (g mol^{-1}) and γ_i^∞ is the infinite dilution activity coefficient of the substance i in pure water:

$$\gamma_i^\infty = \lim_{x_i \rightarrow 0} (\gamma_i(x_i)) \quad (\text{Eq. 1.8})$$

γ_i^∞ represents the activity coefficient of i when it is surrounded only by water. Henry's law constant takes in account both the compound volatility (P_i^0) and its affinity with water (γ_i^∞). In real conditions, aerosol aqueous phase is not pure, and the compounds are not infinitely diluted. A relative activity coefficient can be calculated by the ratio of infinite dilution and liquid phase activity coefficient:

$$\zeta_i = \frac{\gamma_i}{\gamma_i^\infty} \quad (\text{Eq. 1.9})$$

To compute gaseous to aqueous phase partitioning in the aerosol aqueous phase (no infinite diluted phase) Raoult's law can be rewritten:

$$C_i = \frac{H_i \times P_i}{\zeta_i} \quad (\text{Eq. 1.10})$$

Following the model proposed by Pankow, (1994) for the partitioning with the organic phase, an analogous gas-water partitioning coefficient, $K_{aq,i}$ ($\text{m}^3 \mu\text{g}^{-1}$), can be defined:

$$K_{aq,i} LWC = \frac{A_{aq,i}}{A_{g,i}} \quad (\text{Eq. 1.11})$$

in which LWC is the liquid water content ($\mu\text{g m}^{-3}$) and $A_{aq,i}$ and $A_{g,i}$ are respectively the concentrations in aqueous and gaseous phases. Equation 1.11 can be rewritten in function of Henry's law constant:

$$K_{aq,i} = \frac{H_i \times R \times T}{\rho_{water} \zeta_i \times 1.013 \times 10^{11}} \quad (\text{Eq. 1.12})$$

1.2.4. Benefits of an aerosol molecular characterization

The characterization of the SOA composition and more generally OA has been a subject of great scientific interest in the recent years. A better knowledge of OA chemical composition is necessary to apportion OA sources and plan strategies for emission reduction. An improvement in air quality requires an understanding of the composition of ambient aerosols

and their major sources. Other reasons for this interest are related to the potential impacts of organic molecules on health (e.g. PAHs) or on climate (e.g. light-absorbing molecules and CCN activity) and on the particle formation processes (e.g. volatility and partitioning). OA major components, together with their sources, are reported in Table 1.1. The proportions reported are only indicative, since aerosol chemical composition varies considerably according to the season and the region considered.

Organic aerosol chemical characterization is usually performed on PM samples collected on filters. PM samples are extracted with solvents, selected according to the targeted compounds, or by thermal or laser desorption systems coupled with an analytical instrument. Analyses are performed using chromatographic separation and detection instruments, such as gas or liquid chromatography-mass spectrometry (GC or LC-MS). Online techniques (e.g. aerosol mass spectroscopy, AMS) are also used to deduce the OA degree of oxygenation, with no information on the identity of the individual compounds. As can be inferred from Table 1.1, some substance classes are typically from specific sources (e.g. sugars for biomass burning) and others may indicate the aerosol age (e.g. highly functionalized molecules as dicarboxylic acids). Specific molecules from these classes have been identified and used as molecular markers for source apportionment. Organic markers can be later used for source apportionment using statistical source-receptor models as described in the following section.

Table 1. 1. Prominent organic particulate matter (OPM) components. Source: [Pöschl, 2005]

Substance Classes	Proportions ^[a]	Sources
aliphatic hydrocarbons	10 ⁻²	biomass, fossil-fuel combustion
aliphatic alcohols and carbonyls	10 ⁻²	biomass, SOA/aging
levoglucosan	10 ⁻¹	biomass burning
fatty acids and other alkanolic acids	10 ⁻¹	biomass, SOA/aging
aliphatic dicarboxylic acids	10 ⁻¹	SOA/aging
aromatic (poly-)carboxylic acids	10 ⁻¹	SOA/aging, soil/dust
multifunctional aliphatic and aromatic compounds (OH, CO, COOH)	10 ⁻¹	SOA/aging, soil/dust
polycyclic aromatic hydrocarbons (PAHs)	10 ⁻³	fossil-fuel combustion, biomass burning
nitro- and oxy-PAHs	10 ⁻³	fossil-fuel combustion, biomass burning, SOA/aging
proteins and other amino compounds	10 ⁻¹	biomass
cellulose and other carbohydrates	10 ⁻²	biomass
secondary organic oligomers/polymers and humic-like substances	10 ⁻¹	SOA/aging, soil/dust

[a] Characteristic magnitudes of the mass proportion in fine OPM.

1.2.5. Source apportionment

Source apportionment can be performed using source-receptor models (PMF, CMB...), based on measurements (Srivastava et al., 2018), or by chemistry transport models (CTMs) (Burr and Zhang, 2011; Wagstrom et al., 2008; Zhang, 2005), for which general features are presented in section 1.3.1.

Source-receptor models are based on the solution of the mass balance equation. To apply these methods, the assumptions done are: (1) stable and reproducible source profile, (2) non-reactive and non-volatile receptor species, (3) receptor data representative of the geographical area studied and (4) quantification of receptor and sources has been performed with equivalent or comparable methods throughout the period considered. The chemical mass balance (CMB) only considers primary sources because the determination of profiles for secondary sources is difficult to be obtained. Thus, the OA not apportioned refers to SOA. SOA is then defined as the difference between the measured OA concentrations and the aggregated OA concentrations from all primary sources resolved by CMB. In positive matrix factorization (PMF), SOA is commonly calculated as the sum of OA loadings associated to sulfate- and nitrate-rich factors. By comparison, molecular organic markers (tracers) are source-class specific and may provide a more definitive link between factors and source classes. Molecular markers for SOA and POA can be directly included in the PMF model providing an insight into the primary–secondary split of OA sources. The effectiveness of the method depends on the molecular markers used. Besides, the SOA-tracer method developed by Kleindienst et al., (2007) allows the estimation of the SOA contributions from several biogenic and anthropogenic hydrocarbon SOA precursors to ambient OC concentrations using a series of organic molecular compounds called tracer (or marker) compounds. The SOA tracer method is based on the estimation of the SOA mass contribution using marker measured concentrations and SOA-to-marker mass fractions determined by chamber experiment. A comparison on the different existing methods to apportion SOA from filter measurements, and notably both used in this work namely PMF and SOA tracer-method, can be found in Srivastava et al., (2018). Further details on PMF and SOA tracer method are provided in Chapter II.

Two approaches are commonly used for source-oriented modelling techniques with CTMs: the brute force method (BFM) and the tagged species method (Belis et al., 2019). BFM consist in a sensitivity analysis on emission sources contributions on total PM. Emissions

from a specific set of sources can be modified, either by sectors or by geographical regions. The comparison with a baseline run, performed with unperturbed emissions, is required to quantify the contribution of that specific source. The relation between precursor emission and PM concentrations include non-linear effects, because of the contribution of SOA formation in atmosphere. The tagged species method quantifies the source contribution using extra-species, known as “reactive tracers”, that undergo chemical transformation in atmosphere generating secondary products. This method is based on a conservative mass approach, in which the sum of all the secondary product concentrations is equal to the total concentration of the sources (Yarwood et al., 2007).

1.2.6. Definition and use of OA markers in literature

A good aerosol source tracer should fulfil the following requirements: (1) to be unique to the source of origin, (2) to be produced in reasonably high yields so at sufficiently high concentrations in the atmosphere to allow for reliable quantification, (3) to be reasonably stable in the atmosphere, so that it is conserved between emission/formation and collection at a receptor location (4) to have a low vapour pressure so that it primarily partitioned to the particle phase, which minimizes possible underestimation from loss to the gas phase (Al-Naiema and Stone, 2017; Sheppard, 1963). All these conditions are rarely satisfied, so the term “marker” is more appropriate to define these species. In fact, recent studies demonstrated that most of the tracer lifetimes are in the range of couple of days (e.g. levoglucosan 0.7-2.2 days (Hennigan et al., 2010), pinonic acid ~2.1–3.3 days (Lai et al., 2015) and MBTCA ~1.2 days (Kostenidou et al., 2018)), which is shorter than the average particle half-life of 1 week (Seinfeld, 2015). Therefore, their use in source-receptor models for source apportionment may cause an underestimation of the source contributions (Robinson et al., 2007).

Commonly used POA markers include: levoglucosan for biomass burning (Simoneit et al., 1999), hopanes for vehicular exhaust (Lough et al., 2007) and odd carbon C29-C33 n-alkanes from vegetal detritus (Rogge et al., 1993).

SOA markers from both biogenic and anthropogenic sources have been identified and reported in the literature. Monoterpene (α - and β -pinene) SOA markers include multifunctional carboxylic acid, among which the most well-known and studied are pinonic acid, pinic acid, 3-methyl-1,2,3-butanetricarboxylic acid, 3-hydroxyglutaric acid and terpenylic acid (Claeys et al., 2007, 2009; Hoffmann et al., 1998; Szmigielski et al., 2007; Yu et al., 1999). MBTCA and 3-hydroglutaric have been identified as marker for aged SOA (or

second generation oxidation markers) (Claeys et al., 2007; Müller et al., 2012; Szmigielski et al., 2007). Isoprene SOA markers are methyltetrols, α -methylglyceric acid, C₅ alkene triols and their corresponding sulfate esters and nitrate esters (Claeys et al., 2004; Surratt et al., 2006). Methyltetrols are specific to low NO_x conditions, while α -methylglyceric acid is produced at high NO_x concentrations (Surratt et al., 2010). The most widely used marker for β -caryophyllene is β -caryophyllinic acid (Jaoui et al., 2007) (Figure 1.8).

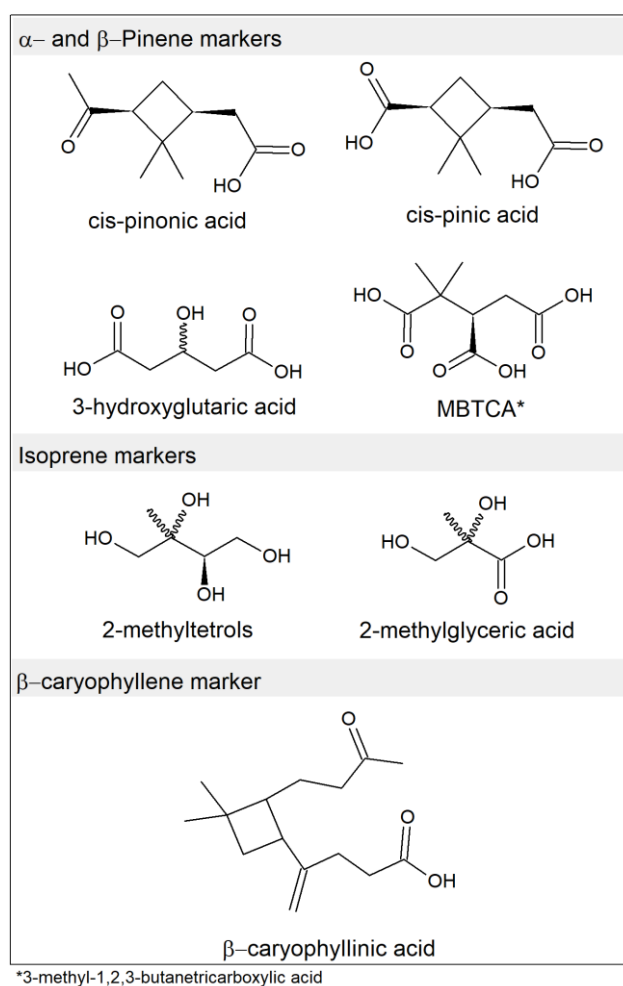


Figure 1. 8 Structures of some biogenic SOA markers divided by their precursor.

Several anthropogenic SOA markers from benzene, toluene, naphthalene and phenolic compounds oxidation have been identified (Figure 1.9). These markers are however less source specific than the biogenic ones, because their precursors can be emitted from several sources and most of them are also directly emitted. The most widely known tracer for toluene photooxidation is the 2,3-Dihydroxy-4-oxopentanoic acid (DHOPA) (Kleindienst et al., 2004), for which the formation mechanism in atmosphere has not been highlighted yet.

Phthalic acid is a tracer for naphthalene and methylnaphthalene photooxidation (Kleindienst et al., 2012) that can be also primarily emitted (Kawamura and Kaplan, 1987). Nitrated phenols and their methyl and methoxy derivatives are commonly recognized as secondary biomass burning markers (Forstner et al., 1997; Iinuma et al., 2010; Lin et al., 2015), although nitrophenols and methyl-nitrophenols have been measured also in primary emissions (Lu et al., 2019; Mkoma and Kawamura, 2013).

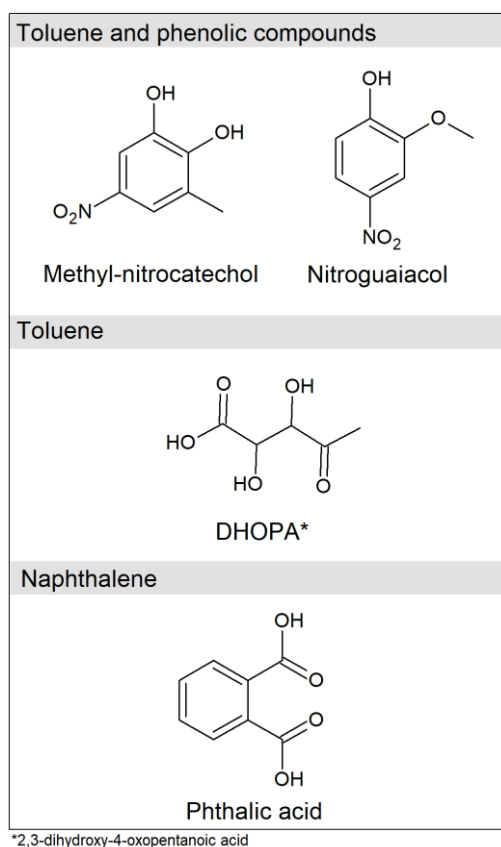


Figure 1. 9 Structures of some anthropogenic SOA markers divided by their precursor.

1.3. State of art modelling secondary organic aerosol

1.3.1. Air quality model structure

Air quality models are a powerful tool to understand atmospheric processes, forecast and monitor air quality. These models, commonly called “chemistry transport models” (CTM), use a mass conservative approach to reproduce pollutant chemical transformations and transport. The simulation domains are divided horizontally and vertically in a 3D mesh. In each box (cell) of this mesh all the variables (e.g. pollutant concentration, temperature, etc.) are homogeneous. CTMs require meteorological data, biogenic and anthropogenic emissions,

land use and topographic data, initial and boundary conditions, and embedded modules to solve chemical, thermodynamical and physical processes (Figure 1.10).

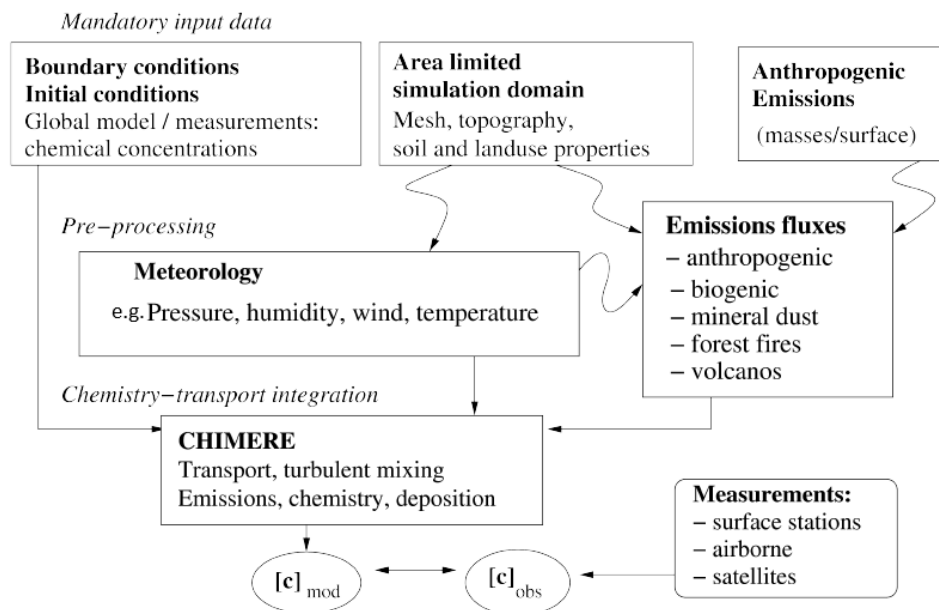


Figure 1.10 Schematic representation of a 3D chemistry transport model (CHIMERE). $[c]_{\text{mod}}$ and $[c]_{\text{obs}}$ are respectively the modelled and the observed chemical concentrations field. Adapted from: [Menut et al., 2013]

1.3.2. SOA modelling approaches

Simplified parametrizations to model secondary organic aerosol formation in the 3D CMTs have been developed, with the purpose to minimize computational costs. This kind of approach is useful for operational applications but is not sensitive to all the variations of atmospheric conditions. A brief description of the principal models used to represent SOA formation in CTMs is provided in the following paragraphs.

1.3.2.1. Two-products model

Odum et al., (1996) developed a method to parametrize secondary aerosol formation from a specific precursor using chamber experiment data. For each precursor, the fractional aerosol yield (Y) is calculated as follow:

$$Y = \frac{\Delta M_0}{\Delta ROG} \quad (\text{Eq. 1.13})$$

where ΔM_0 is the concentration of the organic aerosol mass ($\mu\text{g m}^{-3}$) produced and ΔROG is the amount of reactive organic gas reacted ($\mu\text{g m}^{-3}$).

The overall SOA yield is given by the sum of the single product yields, calculating their partitioning as proposed by Pankow, (1994):

$$Y = M_0 \sum_i \left(\frac{\alpha_i K_{om,i}}{1 + K_{om,i} M_0} \right) \quad (\text{Eq. 1.14})$$

where α_i is the stoichiometric coefficient and $K_{om,i}$ is the partitioning coefficient of each product i . Chamber experiments data are fitted to find the best combinations of α_i and $K_{om,i}$ that represent the SOA mass formed. The so-developed Secondary Organic Aerosol Module (SORGAM) has been first coupled to the EuroRADM CTM, considering aromatics, higher alkane and alkenes, pinene and limonene as SOA precursors (Schell et al., 2001).

1.3.2.2. VBS (Volatility Basis Set) approach

This approach consists in dividing semi-volatile organic compounds in classes (“bins”), according to their volatility. Compound volatility is evaluated through their saturation concentration (C_i^*), that is linked to the saturated vapor pressure (P_i^0) with the following relation:

$$C_i^* = \frac{\gamma_i \bar{M}_w}{RT} \times P_i^0 \quad (\text{Eq 1.15})$$

In the classic VBS approach, each volatility bin is treated as a unique compound regarding partitioning properties and reactivity. The compounds belonging to the same bin undergo a unique aging process, generating only bins of less volatile compounds.

This approach was developed initially to describe the partitioning of semi-volatile compounds in atmosphere (Grieshop et al., 2009; Robinson et al., 2007; Shrivastava et al., 2008). Afterwards, VBS approach has also been applied to develop parametrization of VOCs aging to form SOA (Hodzic et al., 2010; Tsimpidi et al., 2010). The oxidation is usually simulated using the same kinetic constant for all the bins, $4 \times 10^{-11} \text{ cm}^3 \text{ molecule}^{-1} \text{ s}^{-1}$, validated by comparison with measurements (Shrivastava et al., 2008). An evolution of the traditional VBS approach is the VBS-2D, in which the bins are characterized also by their oxidation degree (O:C ratio). This implementation of the traditional VBS enables to diversify the SOA composition and reactivity (Donahue et al., 2011, 2012).

1.3.2.3. Molecular surrogate approach

The main feature of this approach is the choice of molecular surrogates to represent the total SOA mass (Pun et al., 2002, 2006; Pun and Seigneur, 2007). Few molecules, identified among the major photooxidation products of a specific precursor, are chosen as molecular

surrogates based on their volatility. The advantages of this approach rely on the possibility to use molecular surrogate structures to calculate their activity coefficient, with the UNiversal Functional group Activity Coefficient; (UNIFAC, Fredenslund et al., 1975) and to simulate aerosol non-ideality.

The hydrophilic/hydrophobic organic (H²O) (Couvidat et al., 2012) mechanism has been developed with this approach, considering isoprene, monoterpenes, sesquiterpenes, toluene and xylene as precursors and it has been implemented in the 3D models Polyphemus and CHIMERE. This mechanism uses both hydrophilic (acidic or undissociated species) and hydrophobic surrogates to represent biogenic SOA and only hydrophobic surrogates to represent anthropogenic SOA (see Table 1.2).

Table 1. 2. Properties of the SOA surrogate species used in H²O. Adapted from: [Couvidat et al., 2012]

Surrogate	Type ^a	Molecular Structure	MW ^b	H ^c	p ^{0d}	ΔH_{vap} ^e	Comments
BiMT	A	methyl tetrol	136	0.805	1.45×10^{-6}	38.4	-
BiPER	A	methyl dihydroxy dihydroperoxide	168	0.111	2.61×10^{-6}	38.4	-
BiDER	A	methyl tetrol	136	2.80	4.10×10^{-7}	38.4	-
BiMGA	A	methyl glyceric acid (MGA)	120	1.13×10^{-2}	1.4×10^{-5}	43.2	pK _a = 4.0
BiNGA	B	nitrate derivative of MGA	165	-	1.4×10^{-5}	43.2	-
BiNIT3	B	methyl hydroxy trinitrate butane	272	-	1.45×10^{-6}	38.4	-
BiA0D	A	pinonaldehyde	168	4.82×10^{-5}	2.70×10^{-4}	50	-
BiA1D	A	norpinic acid	170	2.73×10^{-3}	2.17×10^{-7}	50	pK _a = 3.2
BiA2D	A	pinic acid	186	6.52×10^{-3}	1.43×10^{-7}	50	pK _{a1} = 3.4, pK _{a2} = 5.1, DRII = 0.79 ^f
BiNIT	A	Nitrooxy-limonene-1-ol	215	-	2.5×10^{-6}	109	-
BiBIP	B	C15 hydroxy nitrate aldehyde	298	-	6.0×10^{-10}	175	-
BiBmP	B	C15 oxo aldehyde	236	-	3.0×10^{-7}	175	-
AnBIP	B	methyl nitro benzoic acid	167	-	6.8×10^{-8}	50	-
AnBmP	B	methyl hydroxy benzoic acid	152	-	8.4×10^{-6}	50	-
AnCIP	C	No structure	167	-	-	-	-

^aType A: hydrophilic species, type B: hydrophobic species, type C: hydrophobic non-volatile species, which is not used to compute activity coefficients.

^bMolecular weight [g.mol⁻¹].

^cHenry's law constant [($\mu\text{g}/\mu\text{g water}$)/($\mu\text{g}/\text{m}^3$)] at 298 K.

^dSaturation vapor pressure [torr] at 298 K.

^eEnthalpy of vaporization [kJ.mol⁻¹].

^fDeliquescence relative humidity: if RII < DRII, the species is solid (Type B), if RII > DRII, the species is liquid (Type A).

The chemical scheme used to reproduce the surrogate formation is based on experimental studies and is sensitive to high and low NO_x conditions. For some biogenic compound also the oligomerization processes are taken into account.

POA are represented in this model as SVOCs. POA are splitted in three classes of volatility, POAIP, POAmP and POAhP, from the less to the most volatile. These classes have been determined by the fitting of the dilution curve of POA from diesel exhaust in Robinson et al., (2007) and represent respectively 25%, 32% and 43% of the "non-diluted" POA emissions. Each surrogate has a partitioning constant and default structures have been assigned to these surrogates to calculate their activity coefficients. Following Grieshop et al., (2009), POAIP,

POAmP and POAhP aging is simulated by reaction with OH and lead to a decrease in volatility by a factor 100. This parametrization assumes that the POA composition is constant, while it is well known that it changes according to the emission source. Although this is the main limitation of this mechanism, no exhaustive data on POA composition are available to develop an accurate parametrization for POA.

1.3.2.4. Model performances

Air quality models often underestimate SOA formation in the atmosphere. Several studies have been performed to estimate 3D CTMs performances. Tsigaridis and Kanakidou, (2003) focused on the simulation of the global SOA distribution, identifying some critical physicochemical processes in SOA modelling: the potential irreversibility of the partitioning onto the particle phase, the simulation of the aerosol mass on which SVOCs condense and the temperature dependence of the partitioning coefficients. Multiple intercomparison exercises have been performed on regional scale (Bessagnet et al., 2016; McKeen et al., 2007; Mircea et al., 2019; Pernigotti et al., 2013; Prank et al., 2016; Solazzo et al., 2012; Vautard et al., 2007). Solazzo et al., (2012) in the Air Quality Model Evaluation International Initiative (AQMEII) compared 10 air quality model outputs and none of them succeeded to represent PM₁₀ mass throughout the year. They attributed the underestimation of PM₁₀ to a misrepresentation of organic aerosol concentrations. Prank et al., (2016) identified the lack of precursor emissions from wildland fires and explicit representation of aerosol water content as the main reasons for PM₁₀ underestimation in air quality models. Concerning the EURODELTA III intercomparison exercise (Bessagnet et al., 2016; Mircea et al., 2019), similar performances related to the SOA modelling approach have been found (VBS vs SORGAM), with the difference that the VBS captured better the seasonal variations. SOA underestimation was attributed to a missing precursor emissions and SOA formation processes.

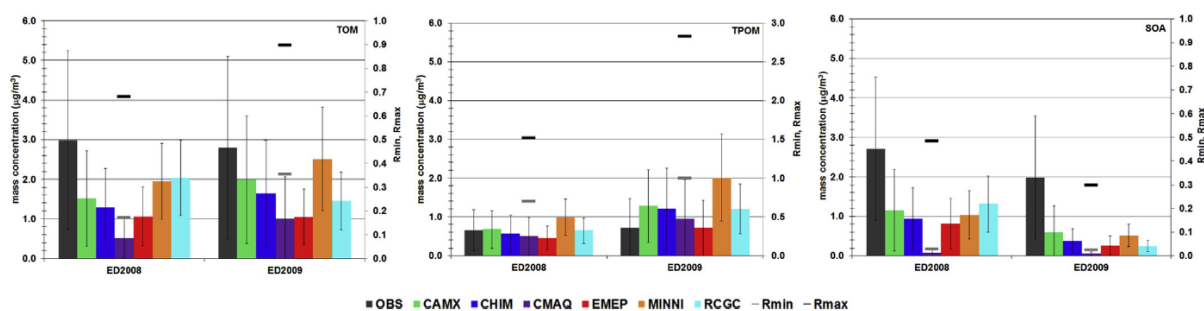


Figure 1. 11 From EURODELTA III intercomparison exercise: Comparison between observed and simulated total organic matter (TOM), total primary organic matter (TPOM)

and secondary organic aerosol (SOA) concentrations ($\mu\text{g m}^{-3}$) using 6 models (CAMX, CHIMERE, CMAQ, EMEP, MINNI and RCGC). Source: [Mircea et al., 2019]

The validation of the model outputs is normally achieved by comparison with measurements of oxidant concentration (e.g. O_3), meteorological parameters (T, wind speed etc.) and PM and carbonaceous species (EC/OC). However, compare directly the PM concentrations measured with the model output could be problematic because of the complex composition of the organic fraction.

1.4. PhD thesis objectives

A better knowledge of OA sources is required to apply efficient policies to mitigate pollution effects. As previously discussed, organic marker measurements are commonly used in source-receptor models to apportion OA sources. Source apportionment is also performed using CTMs, in which OA is often underestimated. Such underestimation increases with the photochemical aging of air masses, highlighting the incomplete identification of all SOA precursors and the poor knowledge of the processes involved in particle aging. The aim of this work was to implement a marker modelling approach in a 3D air quality model (CHIMERE). The ability of the model to reproduce marker concentrations observed in the ambient air is indicative of the model performances in representing the overall OA and SOA concentrations. Molecular markers are emitted and produced by the same sources and physicochemical processes of the organic aerosol bulk. A fair representation of the marker in a 3D CTM, could further allow to apportion OA sources using a hybrid CTM/Source-receptor model approach (Habermacher et al., 2007). The marker-implemented version of CHIMERE has been developed adding to the aerosol module detailed mechanisms for marker formation and improving emission inventories. Simulation outputs have been compared with measurements. The discrepancies observed have been investigated considering the possible model uncertainty, including primary emissions, chemical reactivity and GPP parameterization.

This PhD manuscript is divided in 4 chapters. The main results, together with the methods used, are presented in 3 scientific articles:

- In Chapter II (Article 1) the annual measurements of biogenic and anthropogenic SOA markers performed at the SIRTA facility (25 km SW of Paris city centre) during 2015 (every third day) are shown. Literature data are provided for comparison with SOA

markers concentrations measured at SIRTAs. The seasonal variations of 25 SOA marker concentrations and gas/particle partitioning are examined and discussed. SOA sources have been also apportioned using the SOA tracer method and the results obtained are compared with PMF outputs. This work constituted also the validation basis of the model developments made to simulate OA marker concentrations using CHIMERE. My contribution to the work presented in this chapter includes the development of the analysis method for the SOA markers in gaseous and particulate phase and the analysis of SOA markers in the gaseous phase.

- In Chapter III (Article 2), the primary emissions of levoglucosan, together with the formation mechanisms of 5 anthropogenic SOA markers (nitrophenols, nitroguaiacols, methyl nitrocatechols, phthalic acid and 2,3-dihydroxy-4-oxopentanoic acid) have been implemented in the 3D CTM (CHIMERE). The simulation outputs of the SOA markers are compared with the annual (2015) measurements made at SIRTAs and for levoglucosan with field observation performed during winter 2014-2015 at 10 urban locations over France. The sensitivity of gas/particle partitioning to spatial distribution and thermodynamic assumptions have been examined to highlight the key parameters in OA simulation. I personally developed the marker mechanisms and performed the 3D simulations presented in this chapter.
- In Chapter IV (Article 3), 5 biogenic SOA markers (pinonic acid, pinic acid, 3-methyl-1,2,3-butanetricarboxylic acid, 2-methyltetrols and α -methylglyceric acid) formation mechanisms from α -/ β -pinene and isoprene have been inserted in CHIMERE and compared with measurements performed at SIRTAs during 2015. Daily variations of the production rates of pinonic acid from different reaction pathways have been also investigated. A sensitivity analysis of marker concentrations to NO_x regime has been carried out. Biogenic marker gas to particle partitioning have been simulated using several thermodynamic assumptions and compared with the observed gas/particle partitioning measurements. As for Chapter III, my contribution to this chapter includes the development of the marker mechanisms and the 3D simulations execution.

The Chapter V presents the main conclusions and perspectives of this work.

References

Acosta Navarro, J. C., Smolander, S., Struthers, H., Zorita, E., Ekman, A. M. L., Kaplan, J. O., Guenther, A., Arneth, A. and Riipinen, I.: Global emissions of terpenoid VOCs from terrestrial vegetation in the last millennium, *J. Geophys. Res. Atmospheres*, 119(11), 6867–6885, doi:10.1002/2013JD021238, 2014.

Al-Naiema, I. M. and Stone, E. A.: Evaluation of anthropogenic secondary organic aerosol tracers from aromatic hydrocarbons, *Atmospheric Chem. Phys.*, 17(3), 2053–2065, doi:10.5194/acp-17-2053-2017, 2017.

Apte, J. S., Marshall, J. D., Cohen, A. J. and Brauer, M.: Addressing Global Mortality from Ambient PM_{2.5}, *Environ. Sci. Technol.*, 49(13), 8057–8066, doi:10.1021/acs.est.5b01236, 2015.

Aumont, B., Szopa, S. and Madronich, S.: Modelling the evolution of organic carbon during its gas-phase tropospheric oxidation: development of an explicit model based on a self generating approach, *Atmospheric Chem. Phys.*, 5(9), 2497–2517, 2005.

Belis, C. A., Favez, O., Mircea, M., Diapouli, E., Manousakas, M.-I., Vratolis, S., Gilardoni, S., Paglione, M., Decesari, S., Mocnik, G., Mooibroek, D., Salvador, P., Takahama, S., Vecchi, R. and Paatero, P.: European guide on air pollution source apportionment with receptor models, *Publ. Off. Eur. Union*, doi:10.2760/439106, 2019.

Bessagnet, B., Pirovano, G., Mircea, M., Cuvelier, C., Aulinger, A., Calori, G., Ciarelli, G., Manders, A., Stern, R., Tsyro, S., García Vivanco, M., Thunis, P., Pay, M.-T., Colette, A., Couvidat, F., Meleux, F., Rouïl, L., Ung, A., Aksoyoglu, S., Baldasano, J. M., Bieser, J., Briganti, G., Cappelletti, A., D'Isidoro, M., Finardi, S., Kranenburg, R., Silibello, C., Carnevale, C., Aas, W., Dupont, J.-C., Fagerli, H., Gonzalez, L., Menut, L., Prévôt, A. S. H., Roberts, P. and White, L.: Presentation of the EURODELTA III intercomparison exercise – evaluation of the chemistry transport models' performance on criteria pollutants and joint analysis with meteorology, *Atmospheric Chem. Phys.*, 16(19), 12667–12701, doi:10.5194/acp-16-12667-2016, 2016.

Brandt, J., Silver, J. D., Christensen, J. H., Andersen, M. S., Bønløkke, J. H., Sigsgaard, T., Geels, C., Gross, A., Hansen, A. B., Hansen, K. M., Hedegaard, G. B., Kaas, E. and Frohn, L. M.: Contribution from the ten major emission sectors in Europe and Denmark to the health-cost externalities of air pollution using the EVA model system – an integrated modelling approach, *Atmospheric Chem. Phys.*, 13(15), 7725–7746, doi:https://doi.org/10.5194/acp-13-7725-2013, 2013.

Brasseur, G. P., Prinn, R. G. and Pszenny, A. A. P., Eds.: *Atmospheric Chemistry in a Changing World: An Integration and Synthesis of a Decade of Tropospheric Chemistry Research*, Springer-Verlag, Berlin Heidelberg. [online] Available from: <https://www.springer.com/gp/book/9783540430506>, 2003.

Bruns, E. A., El Haddad, I., Slowik, J. G., Kilic, D., Klein, F., Baltensperger, U. and Prévôt, A. S. H.: Identification of significant precursor gases of secondary organic aerosols from residential wood combustion, *Sci. Rep.*, 6(1), doi:10.1038/srep27881, 2016.

Burnett, R., Chen, H., Szyszkowicz, M., Fann, N., Hubbell, B., Pope, C. A., Apte, J. S., Brauer, M., Cohen, A., Weichenthal, S., Coggins, J., Di, Q., Brunekreef, B., Frostad, J., Lim, S. S., Kan, H., Walker, K. D., Thurston, G. D., Hayes, R. B., Lim, C. C., Turner, M. C., Jerrett, M., Krewski, D., Gapstur, S. M., Diver, W. R., Ostro, B., Goldberg, D., Crouse, D. L., Martin, R. V., Peters, P., Pinault, L., Tjepkema, M., Donkelaar, A. van, Villeneuve, P. J., Miller, A. B., Yin, P., Zhou, M., Wang, L., Janssen, N. A. H., Marra, M., Atkinson, R. W., Tsang, H., Thach, T. Q., Cannon, J. B., Allen, R. T., Hart, J. E., Laden, F., Cesaroni, G., Forastiere, F., Weinmayr, G., Jaensch, A., Nagel, G., Concin, H. and Spadaro, J. V.: Global estimates of mortality associated with long-term exposure to outdoor fine particulate matter, *Proc. Natl. Acad. Sci.*, 115(38), 9592–9597, doi:10.1073/pnas.1803222115, 2018.

Burr, M. J. and Zhang, Y.: Source apportionment of fine particulate matter over the Eastern U.S. Part II: source apportionment simulations using CAMx/PSAT and comparisons with CMAQ source sensitivity simulations, *Atmospheric Pollut. Res.*, 2(3), 318–336, doi:10.5094/APR.2011.037, 2011.

Claeys, M., Wang, W., Ion, A. C., Kourtchev, I., Gelencsér, A. and Maenhaut, W.: Formation of secondary organic aerosols from isoprene and its gas-phase oxidation products through reaction with hydrogen peroxide, *Atmos. Environ.*, 38(25), 4093–4098, doi:10.1016/j.atmosenv.2004.06.001, 2004.

Claeys, M., Szmigielski, R., Kourtchev, I., Van der Veken, P., Vermeylen, R., Maenhaut, W., Jaoui, M., Kleindienst, T. E., Lewandowski, M., Offenberg, J. H. and Edney, E. O.: Hydroxydicarboxylic acids: markers for secondary organic aerosol from the photooxidation of α -pinene, *Environ. Sci. Technol.*, 41(5), 1628–1634, doi:10.1021/es0620181, 2007.

Claeys, M., Iinuma, Y., Szmigielski, R., Surratt, J. D., Blockhuys, F., Van Alsenoy, C., Böge, O., Sierau, B., Gómez-González, Y., Vermeylen, R., Van der Veken, P., Shahgholi, M., Chan, A. W. H., Herrmann, H., Seinfeld, J. H. and Maenhaut, W.: Terpenylic Acid and Related Compounds from the Oxidation of α -Pinene: Implications for New Particle Formation and Growth above Forests, *Environ. Sci. Technol.*, 43(18), 6976–6982, doi:10.1021/es9007596, 2009.

Couvidat, F., Debry, E., Sartelet, K. and Seigneur, C.: A hydrophilic/hydrophobic organic (H₂O) aerosol model: Development, evaluation and sensitivity analysis, *J. Geophys. Res.*, 117, D10304, doi:10.1029/2011JD017214, 2012.

Donahue, N. M., Epstein, S. A., Pandis, S. N. and Robinson, A. L.: A two-dimensional volatility basis set: 1. organic-aerosol mixing thermodynamics, *Atmospheric Chem. Phys.*, 11(7), 3303–3318, doi:https://doi.org/10.5194/acp-11-3303-2011, 2011.

Donahue, N. M., Kroll, J. H., Pandis, S. N. and Robinson, A. L.: A two-dimensional volatility basis set – Part 2: Diagnostics of organic-aerosol evolution, *Atmospheric Chem. Phys.*, 12(2), 615–634, doi:https://doi.org/10.5194/acp-12-615-2012, 2012.

EEA: Air quality in Europe - 2018 report, Eur. Environ. Agency [online] Available from: <https://www.eea.europa.eu/publications/air-quality-in-europe-2018>, 2018.

European official journal: Directive 2004/107/EC of the European Parliament and of the Council of 15 December 2004 relating to arsenic, cadmium, mercury, nickel and polycyclic aromatic hydrocarbons in ambient air., 2004.

Chapter I: Introduction of the Thesis

European official journal: Directive 2008/50/EC of the European Parliament and of the Council of 21 May 2008 on Ambient Air Quality and Cleaner Air for Europe. Official Journal of the European Union. L 152. 11/06/2008., 2008.

Finlayson-Pitts, B. J. and Pitts, J. N.: Chemistry of the upper and lower atmosphere: theory, experiments, and applications, Nachdr., Academic Press, San Diego, Calif., 2009.

Finlayson-Pitts, B. J. and Pitts Jr, J. N.: Chemistry of the upper and lower atmosphere, Academic Press., 2000.

Forstner, H. J. L., Flagan, R. C. and Seinfeld, J. H.: Secondary Organic Aerosol from the Photooxidation of Aromatic Hydrocarbons: Molecular Composition, Environ. Sci. Technol., 31(5), 1345–1358, doi:10.1021/es9605376, 1997.

Fredenslund, A., Jones, R. L. and Prausnitz, J. M.: Group-contribution estimation of activity coefficients in nonideal liquid mixtures, AIChE J., 21(6), 1086–1099, doi:10.1002/aic.690210607, 1975.

Freedman, M. A., Ott, E.-J. E. and Marak, K. E.: Role of pH in Aerosol Processes and Measurement Challenges, J. Phys. Chem. A, 123(7), 1275–1284, doi:10.1021/acs.jpca.8b10676, 2019.

Gelencsér, A., May, B., Simpson, D., Sánchez-Ochoa, A., Kasper-Giebl, A., Puxbaum, H., Caseiro, A., Pio, C. and Legrand, M.: Source apportionment of PM_{2.5} organic aerosol over Europe: Primary/secondary, natural/anthropogenic, and fossil/biogenic origin, J. Geophys. Res., 112(D23), doi:10.1029/2006JD008094, 2007.

Goldstein, A. H. and Galbally, I. E.: Known and Unexplored Organic Constituents in the Earth's Atmosphere, Environ. Sci. Technol., 41(5), 1514–1521, doi:10.1021/es072476p, 2007.

Grieshop, A. P., Logue, J. M., Donahue, N. M. and Robinson, A. L.: Laboratory investigation of photochemical oxidation of organic aerosol from wood fires 1: measurement and simulation of organic aerosol evolution, Atmospheric Chem. Phys., 9(4), 1263–1277, doi:https://doi.org/10.5194/acp-9-1263-2009, 2009.

Griffin, R. J., Cocker, D. R., Flagan, R. C. and Seinfeld, J. H.: Organic aerosol formation from the oxidation of biogenic hydrocarbons, J. Geophys. Res. Atmospheres, 104(D3), 3555–3567, doi:10.1029/1998JD100049, 1999.

Guenther, A., Hewitt, C. N., Erickson, D., Fall, R., Geron, C., Graedel, T., Harley, P., Klinger, L., Lerdau, M., Mckay, W. A., Pierce, T., Scholes, B., Steinbrecher, R., Tallamraju, R., Taylor, J. and Zimmerman, P.: A global model of natural volatile organic compound emissions, J. Geophys. Res. Atmospheres, 100(D5), 8873–8892, doi:10.1029/94JD02950, 1995.

Habermacher, F. D., Napelenok, S. L., Akhtar, F., Hu, Y. and Russell, A. G.: Area of Influence (AOI) Development: Fast Generation of Receptor-Oriented Sensitivity Fields for Use in Regional Air Quality Modeling, Environ. Sci. Technol., 41(11), 3997–4003, doi:10.1021/es0621501, 2007.

Hallquist, M., Wenger, J. C., Baltensperger, U., Rudich, Y., Simpson, D., Claeys, M., Dommen, J., Donahue, N. M., George, C., Goldstein, A. H., Hamilton, J. F., Herrmann, H., Hoffmann, T., Iinuma, Y., Jang, M., Jenkin, M. E., Jimenez, J. L., Kiendler-Scharr, A., Maenhaut, W., McFiggans, G., Mentel, T. F., Monod, A., Prevot, A. S. H., Seinfeld, J. H., Surratt, J. D., Szmigielski, R. and Wildt, J.: The formation, properties and impact of secondary organic aerosol: current and emerging issues, *Atmos Chem Phys*, 9, 5155–5236, 2009.

Haywood, J. and Boucher, O.: Estimates of the direct and indirect radiative forcing due to tropospheric aerosols: A review, *Rev. Geophys.*, 38(4), 513–543, doi:10.1029/1999RG000078, 2000.

Heal, M. R., Kumar, P. and Harrison, R. M.: Particles, air quality, policy and health, *Chem. Soc. Rev.*, 41(19), 6606, doi:10.1039/c2cs35076a, 2012.

Heald, C. L., Ridley, D. A., Kreidenweis, S. M. and Drury, E. E.: Satellite observations cap the atmospheric organic aerosol budget, *Geophys. Res. Lett.*, 37(24), doi:10.1029/2010GL045095, 2010.

Hennigan, C. J., Sullivan, A. P., Collett, J. L. and Robinson, A. L.: Levoglucosan stability in biomass burning particles exposed to hydroxyl radicals, *Geophys. Res. Lett.*, 37(9), doi:10.1029/2010GL043088, 2010.

Hodzic, A., Jimenez, J. L., Madronich, S., Canagaratna, M. R., DeCarlo, P. F., Kleinman, L. and Fast, J.: Modeling organic aerosols in a megacity: potential contribution of semi-volatile and intermediate volatility primary organic compounds to secondary organic aerosol formation, *Atmospheric Chem. Phys.*, 10(12), 5491–5514, doi:10.5194/acp-10-5491-2010, 2010.

Hoffmann, T., Bandur, R., Marggraf, U. and Linscheid, M.: Molecular composition of organic aerosols formed in the α -pinene/O₃ reaction: Implications for new particle formation processes, *J. Geophys. Res. Atmospheres*, 103(D19), 25569–25578, doi:10.1029/98JD01816, 1998.

Iinuma, Y., Böge, O., Gräfe, R. and Herrmann, H.: Methyl-nitrocatechols: atmospheric tracer compounds for biomass burning secondary organic aerosols, *Environ. Sci. Technol.*, 44(22), 8453–8459, doi:10.1021/es102938a, 2010.

IPCC: Climate Change 2013: The Physical Science Basis. Contribution of Working Group I to the Fifth Assessment Report of the Intergovernmental Panel on Climate Change. [Stocker, T.F., D. Qin, G.-K. Plattner, M. Tignor, S.K. Allen, J. Boschung, A. Nauels, Y. Xia, V. Bex and P.M. Midgley (eds.)]. Cambridge University Press, Cambridge, United Kingdom and New York, NY, USA. [online] Available from: https://www.ipcc.ch/site/assets/uploads/2018/02/WG1AR5_all_final.pdf, 2018.

Jacobson, M. C., Hansson, H.-C., Noone, K. J. and Charlson, R. J.: Organic atmospheric aerosols: Review and state of the science, *Rev. Geophys.*, 38(2), 267–294, doi:10.1029/1998RG000045, 2000.

Jaoui, M., Lewandowski, M., Kleindienst, T. E., Offenberg, J. H. and Edney, E. O.: β -caryophyllinic acid: An atmospheric tracer for β -caryophyllene secondary organic aerosol, *Geophys. Res. Lett.*, 34(5), doi:10.1029/2006GL028827, 2007.

Jimenez, J. L., Canagaratna, M. R., Donahue, N. M., Prevot, A. S. H., Zhang, Q., Kroll, J. H., DeCarlo, P. F., Allan, J. D., Coe, H., Ng, N. L., Aiken, A. C., Docherty, K. S., Ulbrich, I. M., Grieshop, A. P., Robinson, A. L., Duplissy, J., Smith, J. D., Wilson, K. R., Lanz, V. A., Hueglin, C., Sun, Y. L., Tian, J., Laaksonen, A., Raatikainen, T., Rautiainen, J., Vaattovaara, P., Ehn, M., Kulmala, M., Tomlinson, J. M., Collins, D. R., Cubison, M. J., E., Dunlea, J., Huffman, J. A., Onasch, T. B., Alfarra, M. R., Williams, P. I., Bower, K., Kondo, Y., Schneider, J., Drewnick, F., Borrmann, S., Weimer, S., Demerjian, K., Salcedo, D., Cottrell, L., Griffin, R., Takami, A., Miyoshi, T., Hatakeyama, S., Shimono, A., Sun, J. Y., Zhang, Y. M., Dzepina, K., Kimmel, J. R., Sueper, D., Jayne, J. T., Herndon, S. C., Trimborn, A. M., Williams, L. R., Wood, E. C., Middlebrook, A. M., Kolb, C. E., Baltensperger, U. and Worsnop, D. R.: Evolution of Organic Aerosols in the Atmosphere, *Science*, 326(5959), 1525–1529, doi:10.1126/science.1180353, 2009.

Kanakidou, M., Seinfeld, J. H., Pandis, S. N., Barnes, I., Dentener, F. J., Facchini, M. C., Dingenen, R. V., Ervens, B., Nenes, A. and Nielsen, C. J.: Organic aerosol and global climate modelling: a review, *Atmospheric Chem. Phys.*, 5(4), 1053–1123, 2005.

Karamchandani, P., Long, Y., Pirovano, G., Balzarini, A. and Yarwood, G.: Source-sector contributions to European ozone and fine PM in 2010 using AQMEII modeling data, *Atmospheric Chem. Phys.*, 17(9), 5643–5664, doi:https://doi.org/10.5194/acp-17-5643-2017, 2017.

Kawamura, K. and Kaplan, I. R.: Motor exhaust emissions as a primary source for dicarboxylic acids in Los Angeles ambient air, *Environ. Sci. Technol.*, 21(1), 105–110, doi:10.1021/es00155a014, 1987.

Kleindienst, T. E., Conner, T. S., McIver, C. D. and Edney, E. O.: Determination of secondary organic aerosol products from the photooxidation of toluene and their implications in ambient PM 2.5, *J. Atmospheric Chem.*, 47(1), 79–100, 2004.

Kleindienst, T. E., Jaoui, M., Lewandowski, M., Offenber, J. H., Lewis, C. W., Bhave, P. V. and Edney, E. O.: Estimates of the contributions of biogenic and anthropogenic hydrocarbons to secondary organic aerosol at a southeastern US location, *Atmos. Environ.*, 41(37), 8288–8300, doi:10.1016/j.atmosenv.2007.06.045, 2007.

Kleindienst, T. E., Jaoui, M., Lewandowski, M., Offenber, J. H. and Docherty, K. S.: The formation of SOA and chemical tracer compounds from the photooxidation of naphthalene and its methyl analogs in the presence and absence of nitrogen oxides, *Atmospheric Chem. Phys.*, 12(18), 8711–8726, doi:10.5194/acp-12-8711-2012, 2012.

Kostenidou, E., Karnezi, E., Kolodziejczyk, A., Szmigielski, R. and Pandis, S. N.: Physical and Chemical Properties of 3-Methyl-1,2,3-butanetricarboxylic Acid (MBTCA) Aerosol, *Environ. Sci. Technol.*, 52(3), 1150–1155, doi:10.1021/acs.est.7b04348, 2018.

Krejci, R., Ström, J., Reus, M. de, Williams, J., Fischer, H., Andreae, M. O. and Hansson, H.-C.: Spatial and temporal distribution of atmospheric aerosols in the lowermost troposphere over the Amazonian tropical rainforest, *Atmospheric Chem. Phys.*, 5(6), 1527–1543, doi:https://doi.org/10.5194/acp-5-1527-2005, 2005.

Kristiansen, N. I., Stohl, A., Olivie, D. J. L., Croft, B., Søvde, O. A., Klein, H., Christoudias, T., Kunkel, D., Leadbetter, S. J., Lee, Y. H., Zhang, K., Tsigaridis, K., Bergman, T.,

Evangeliou, N., Wang, H., Ma, P.-L., Easter, R. C., Rasch, P. J., Liu, X., Pitari, G., Genova, G. D., Zhao, S. Y., Balkanski, Y., Bauer, S. E., Faluvegi, G. S., Kokkola, H., Martin, R. V., Pierce, J. R., Schulz, M., Shindell, D., Tost, H. and Zhang, H.: Evaluation of observed and modelled aerosol lifetimes using radioactive tracers of opportunity and an ensemble of 19 global models, *Atmospheric Chem. Phys.*, 16(5), 3525–3561, doi:<https://doi.org/10.5194/acp-16-3525-2016>, 2016.

Kroll, J. H. and Seinfeld, J. H.: Chemistry of secondary organic aerosol: Formation and evolution of low-volatility organics in the atmosphere, *Atmos. Environ.*, 42(16), 3593–3624, doi:10.1016/j.atmosenv.2008.01.003, 2008.

Lai, C., Liu, Y., Ma, J., Ma, Q., Chu, B. and He, H.: Heterogeneous Kinetics of cis-Pinonic Acid with Hydroxyl Radical under Different Environmental Conditions, *J. Phys. Chem. A*, 119(25), 6583–6593, doi:10.1021/acs.jpca.5b01321, 2015.

Li, L., Tang, P., Nakao, S., Chen, C.-L. and Cocker III, D. R.: Role of methyl group number on SOA formation from monocyclic aromatic hydrocarbons photooxidation under low-NO_x conditions, *Atmospheric Chem. Phys.*, 16(4), 2255–2272, doi:<https://doi.org/10.5194/acp-16-2255-2016>, 2016.

Lim, Y. B. and Ziemann, P. J.: Products and Mechanism of Secondary Organic Aerosol Formation from Reactions of n-Alkanes with OH Radicals in the Presence of NO_x, *Environ. Sci. Technol.*, 39(23), 9229–9236, doi:10.1021/es051447g, 2005.

Lim, Y. B. and Ziemann, P. J.: Chemistry of Secondary Organic Aerosol Formation from OH Radical-Initiated Reactions of Linear, Branched, and Cyclic Alkanes in the Presence of NO_x, *Aerosol Sci. Technol.*, 43(6), 604–619, doi:10.1080/02786820902802567, 2009.

Lin, P., Liu, J., Shilling, J. E., Kathmann, S. M., Laskin, J. and Laskin, A.: Molecular characterization of brown carbon (BrC) chromophores in secondary organic aerosol generated from photo-oxidation of toluene, *Phys. Chem. Chem. Phys.*, 17(36), 23312–23325, doi:10.1039/C5CP02563J, 2015.

Lough, G. C., Christensen, C. G., Schauer, J. J., Tortorelli, J., Mani, E., Lawson, D. R., Clark, N. N. and Gabele, P. A.: Development of molecular marker source profiles for emissions from on-road gasoline and diesel vehicle fleets, *J. Air Waste Manag. Assoc.* 1995, 57(10), 1190–1199, doi:10.3155/1047-3289.57.10.1190, 2007.

Lu, C., Wang, X., Li, R., Gu, R., Zhang, Y., Li, W., Gao, R., Chen, B., Xue, L. and Wang, W.: Emissions of fine particulate nitrated phenols from residential coal combustion in China, *Atmos. Environ.*, 203, 10–17, doi:10.1016/j.atmosenv.2019.01.047, 2019.

McKeen, S., Chung, S. H., Wilczak, J., Grell, G., Djalalova, I., Peckham, S., Gong, W., Bouchet, V., Moffet, R., Tang, Y., Carmichael, G. R., Mathur, R. and Yu, S.: Evaluation of several PM_{2.5} forecast models using data collected during the ICARTT/NEAQS 2004 field study, *J. Geophys. Res. Atmospheres*, 112(D10), doi:10.1029/2006JD007608, 2007.

McNeill, V. F.: Aqueous Organic Chemistry in the Atmosphere: Sources and Chemical Processing of Organic Aerosols, *Environ. Sci. Technol.*, 49(3), 1237–1244, doi:10.1021/es5043707, 2015.

McNeill, V. F., Woo, J. L., Kim, D. D., Schwier, A. N., Wannell, N. J., Sumner, A. J. and Barakat, J. M.: Aqueous-phase secondary organic aerosol and organosulfate formation in atmospheric aerosols: a modeling study, *Environ. Sci. Technol.*, 46(15), 8075–8081, doi:10.1021/es3002986, 2012.

Menuet, L., Bessagnet, B., Khvorostyanov, D., Beekmann, M., Blond, N., Colette, A., Coll, I., Curci, G., Foret, G., Hodzic, A., Mailler, S., Meleux, F., Monge, J.-L., Pison, I., Siour, G., Turquety, S., Valari, M., Vautard, R. and Vivanco, M. G.: CHIMERE 2013: a model for regional atmospheric composition modelling, *Geosci. Model Dev.*, 6(4), 981–1028, doi:10.5194/gmd-6-981-2013, 2013.

Mircea, M., Bessagnet, B., D'Isidoro, M., Pirovano, G., Aksoyoglu, S., Ciarelli, G., Tsyro, S., Manders, A., Bieser, J., Stern, R., Vivanco, M. G., Cuvelier, C., Aas, W., Prévôt, A. S. H., Aulinger, A., Briganti, G., Calori, G., Cappelletti, A., Colette, A., Couvidat, F., Fagerli, H., Finardi, S., Kranenburg, R., Rouil, L., Silibello, C., Spindler, G., Poulain, L., Herrmann, H., Jimenez, J. L., Day, D. A., Tiitta, P. and Carbone, S.: EURODELTA III exercise: An evaluation of air quality models' capacity to reproduce the carbonaceous aerosol, *Atmospheric Environ. X*, 2, 100018, doi:10.1016/j.aeaoa.2019.100018, 2019.

Mkoma, S. L. and Kawamura, K.: Molecular composition of dicarboxylic acids, ketocarboxylic acids, α -dicarbonyls and fatty acids in atmospheric aerosols from Tanzania, East Africa during wet and dry seasons, *Atmospheric Chem. Phys.*, 13(4), 2235–2251, doi:https://doi.org/10.5194/acp-13-2235-2013, 2013.

Müller, L., Reinnig, M.-C., Naumann, K. H., Saathoff, H., Mentel, T. F., Donahue, N. M. and Hoffmann, T.: Formation of 3-methyl-1,2,3-butanetricarboxylic acid via gas phase oxidation of pinonic acid – a mass spectrometric study of SOA aging, *Atmospheric Chem. Phys.*, 12(3), 1483–1496, doi:10.5194/acp-12-1483-2012, 2012.

Nahar, K., Gupta, N., Gauvin, R., Absar, S., Patel, B., Gupta, V., Khademhosseini, A. and Ahsan, F.: In vitro, in vivo and ex vivo models for studying particle deposition and drug absorption of inhaled pharmaceuticals, *Eur. J. Pharm. Sci.*, 49(5), 805–818, doi:10.1016/j.ejps.2013.06.004, 2013.

Ng, N. L., Kroll, J. H., Chan, A. W. H., Chhabra, P. S., Flagan, R. C. and Seinfeld, J. H.: Secondary organic aerosol formation from m-xylene, toluene, and benzene, *Atmospheric Chem. Phys.*, 7(14), 3909–3922, 2007.

Odum, J. R., Hoffmann, T., Bowman, F., Collins, D., Flagan, R. C. and Seinfeld, J. H.: Gas/particle partitioning and secondary organic aerosol yields, *Environ. Sci. Technol.*, 30(8), 2580–2585, 1996.

Pankow, J. F.: An absorption model of gas/particle partitioning of organic compounds in the atmosphere, *Atmos. Environ.*, 28(2), 185–188, doi:10.1016/1352-2310(94)90093-0, 1994.

Pernigotti, D., Thunis, P., Cuvelier, C., Georgieva, E., Gsella, A., Meij, A., Pirovano, G., Balzarini, A., Riva, G. M., Carnevale, C., Pisoni, E., Volta, M., Bessagnet, B., Kerschbaumer, A., Viaene, P., Ridder, K. D., Nyiri, A. and Wind, P.: POMI: a model inter-comparison exercise over the Po Valley, *Air Qual. Atmosphere Health*, 4(6), 701–715, doi:10.1007/s11869-013-0211-1, 2013.

Pöschl, U.: Atmospheric Aerosols: Composition, Transformation, Climate and Health Effects, *Angew. Chem. Int. Ed.*, 44(46), 7520–7540, doi:10.1002/anie.200501122, 2005.

Prank, M., Sofiev, M., Tsyro, S., Hendriks, C., Semeena, V., Vazhappilly Francis, X., Butler, T., Denier van der Gon, H., Friedrich, R., Hendricks, J., Kong, X., Lawrence, M., Righi, M., Samaras, Z., Sausen, R., Kukkonen, J. and Sokhi, R.: Evaluation of the performance of four chemical transport models in predicting the aerosol chemical composition in Europe in 2005, *Atmospheric Chem. Phys.*, 16(10), 6041–6070, doi:https://doi.org/10.5194/acp-16-6041-2016, 2016.

Pun, B. K. and Seigneur, C.: Investigative modeling of new pathways for secondary organic aerosol formation, *Atmospheric Chem. Phys.*, 7(9), 2199–2216, doi:https://doi.org/10.5194/acp-7-2199-2007, 2007.

Pun, B. K., Griffin, R. J., Seigneur, C. and Seinfeld, J. H.: Secondary organic aerosol 2. Thermodynamic model for gas/particle partitioning of molecular constituents, *J. Geophys. Res. Atmospheres*, 107(D17), AAC 4-1-AAC 4-15, doi:10.1029/2001JD000542, 2002.

Pun, B. K., Seigneur, C. and Lohman, K.: Modeling Secondary Organic Aerosol Formation via Multiphase Partitioning with Molecular Data, *Environ. Sci. Technol.*, 40(15), 4722–4731, doi:10.1021/es0522736, 2006.

Putaud, J.-P., Raes, F., Van Dingenen, R., Brüggemann, E., Facchini, M.-C., Decesari, S., Fuzzi, S., Gehrig, R., Hüglin, C., Laj, P., Lorbeer, G., Maenhaut, W., Mihalopoulos, N., Müller, K., Querol, X., Rodriguez, S., Schneider, J., Spindler, G., Brink, H. ten, Tørseth, K. and Wiedensohler, A.: A European aerosol phenomenology—2: chemical characteristics of particulate matter at kerbside, urban, rural and background sites in Europe, *Atmos. Environ.*, 38(16), 2579–2595, doi:10.1016/j.atmosenv.2004.01.041, 2004.

Raes, F., Dingenen, R. V., Vignati, E., Wilson, J., Putaud, J.-P., Seinfeld, J. H. and Adams, P.: Formation and cycling of aerosols in the global troposphere, *Atmos. Environ.*, 34(25), 4215–4240, doi:10.1016/S1352-2310(00)00239-9, 2000.

RCP: Every breath we take: the lifelong impact of air pollution, [online] Available from: <https://www.rcplondon.ac.uk/projects/outputs/every-breath-we-take-lifelong-impact-air-pollution> (Accessed 7 October 2019), 2016.

Robinson, A. L., Donahue, N. M., Shrivastava, M. K., Weitkamp, E. A., Sage, A. M., Grieshop, A. P., Lane, T. E., Pierce, J. R. and Pandis, S. N.: Rethinking Organic Aerosols: Semivolatile Emissions and Photochemical Aging, *Science*, 315(5816), 1259–1262, doi:10.1126/science.1133061, 2007.

Rogge, W. F., Hildemann, L. M., Mazurek, M. A., Cass, G. R. and Simoneit, B. R. T.: Sources of fine organic aerosol. 4. Particulate abrasion products from leaf surfaces of urban plants, *Environ. Sci. Technol.*, 27(13), 2700–2711, doi:10.1021/es00049a008, 1993.

Russell, L. M.: Aerosol Organic-Mass-to-Organic-Carbon Ratio Measurements, *Environ. Sci. Technol.*, 37(13), 2982–2987, doi:10.1021/es026123w, 2003.

Schell, B., Ackerman, I. J., Hass, H., Binkowski, F. S. and Ebel, A.: Modeling the formation of secondary organic aerosol within a comprehensive air quality model system, *J. Geophys. Res.*, 106(D22), 28275–28293, 2001.

Seaton, A., Godden, D., MacNee, W. and Donaldson, K.: Particulate air pollution and acute health effects, *The Lancet*, 345(8943), 176–178, doi:10.1016/S0140-6736(95)90173-6, 1995.

Seinfeld, J. H.: Tropospheric chemistry and composition | Aerosols/Particles, in *Encyclopedia of Atmospheric Sciences (Second Edition)*, edited by G. R. North, J. Pyle, and F. Zhang, pp. 182–187, Academic Press, Oxford., 2015.

Seinfeld, J. H. and Pandis, S. N.: *Atmospheric Chemistry and Physics*, Wiley-Interscience, New York, USA. [online] Available from: <https://www.wiley.com/en-us/Atmospheric+Chemistry+and+Physics%3A+From+Air+Pollution+to+Climate+Change%2C+3rd+Edition-p-9781118947401>, 1998.

Sheppard, P. A.: Atmospheric tracers and the study of the general circulation of the atmosphere, *Rep. Prog. Phys.*, 26(1), 213–267, doi:10.1088/0034-4885/26/1/307, 1963.

Shrivastava, M. K., Lane, T. E., Donahue, N. M., Pandis, S. N. and Robinson, A. L.: Effects of gas particle partitioning and aging of primary emissions on urban and regional organic aerosol concentrations, *J. Geophys. Res. Atmospheres*, 113(D18), doi:10.1029/2007JD009735, 2008.

Simoneit, B. R., Schauer, J. J., Nolte, C. G., Oros, D. R., Elias, V. O., Fraser, M. P., Rogge, W. F. and Cass, G. R.: Levoglucosan, a tracer for cellulose in biomass burning and atmospheric particles, *Atmos. Environ.*, 33(2), 173–182, 1999.

Skyllakou, K., Murphy, B. N., Megaritis, A. G., Fountoukis, C. and Pandis, S. N.: Contributions of local and regional sources to fine PM in the megacity of Paris, *Atmospheric Chem. Phys.*, 14(5), 2343–2352, doi:<https://doi.org/10.5194/acp-14-2343-2014>, 2014.

Solazzo, E., Bianconi, R., Pirovano, G., Matthias, V., Vautard, R., Moran, M. D., Wyatt Appel, K., Bessagnet, B., Brandt, J., Christensen, J. H., Chemel, C., Coll, I., Ferreira, J., Forkel, R., Francis, X. V., Grell, G., Grossi, P., Hansen, A. B., Miranda, A. I., Nopmongkol, U., Prank, M., Sartelet, K. N., Schaap, M., Silver, J. D., Sokhi, R. S., Vira, J., Werhahn, J., Wolke, R., Yarwood, G., Zhang, J., Rao, S. T. and Galmarini, S.: Operational model evaluation for particulate matter in Europe and North America in the context of AQMEII, *Atmos. Environ.*, 53, 75–92, doi:10.1016/j.atmosenv.2012.02.045, 2012.

Srivastava, D., Favez, O., Perraudin, E., Villenave, E. and Albinet, A.: Comparison of Measurement-Based Methodologies to Apportion Secondary Organic Carbon (SOC) in PM_{2.5}: A Review of Recent Studies, *Atmosphere*, 9(11), 452, doi:10.3390/atmos9110452, 2018.

Surratt, J. D., Murphy, S. M., Kroll, J. H., Ng, N. L., Hildebrandt, L., Sorooshian, A., Szmigielski, R., Vermeylen, R., Maenhaut, W., Claeys, M., Flagan, R. C. and Seinfeld, J. H.: Chemical Composition of Secondary Organic Aerosol Formed from the Photooxidation of Isoprene, *J. Phys. Chem. A*, 110(31), 9665–9690, doi:10.1021/jp061734m, 2006.

Surratt, J. D., Chan, A. W. H., Eddingsas, N. C., Chan, M., Loza, C. L., Kwan, A. J., Hersey, S. P., Flagan, R. C., Wennberg, P. O. and Seinfeld, J. H.: Reactive intermediates revealed in secondary organic aerosol formation from isoprene, *Proc. Natl. Acad. Sci.*, 107(15), 6640–6645, doi:10.1073/pnas.0911114107, 2010.

Szmigielski, R., Surratt, J. D., Gómez-González, Y., Van der Veken, P., Kourtchev, I., Vermeylen, R., Blockhuys, F., Jaoui, M., Kleindienst, T. E., Lewandowski, M., Offenberg, J. H., Edney, E. O., Seinfeld, J. H., Maenhaut, W. and Claeys, M.: 3-methyl-1,2,3-butane-tricarboxylic acid: An atmospheric tracer for terpene secondary organic aerosol, *Geophys. Res. Lett.*, 34(24), doi:10.1029/2007GL031338, 2007.

Tan, Y., Carlton, A. G., Seitzinger, S. P. and Turpin, B. J.: SOA from methylglyoxal in clouds and wet aerosols: Measurement and prediction of key products, *Atmos. Environ.*, 44(39), 5218–5226, doi:10.1016/j.atmosenv.2010.08.045, 2010.

Tsigaridis, K. and Kanakidou, M.: Global modelling of secondary organic aerosol in the troposphere: a sensitivity analysis, *Atmospheric Chem. Phys.*, 3(5), 1849–1869, doi:<https://doi.org/10.5194/acp-3-1849-2003>, 2003.

Tsimpidi, A. P., Karydis, V. A., Zavala-Perez, M. A., Lei, W., Molina, L. T., Ulbrich, I. M., Jimenez, J. L. and Pandis, S. N.: Evaluation of the volatility basis-set approach for the simulation of organic aerosol formation in the Mexico City metropolitan area, *Copernicus* [online] Available from: <https://dspace.mit.edu/handle/1721.1/65641>, 2010.

Van Dingenen, R., Raes, F., Putaud, J.-P., Baltensperger, U., Charron, A., Facchini, M.-C., Decesari, S., Fuzzi, S., Gehrig, R., Hansson, H.-C., Harrison, R. M., Hüglin, C., Jones, A. M., Laj, P., Lorbeer, G., Maenhaut, W., Palmgren, F., Querol, X., Rodriguez, S., Schneider, J., Brink, H. ten, Tunved, P., Tørseth, K., Wehner, B., Weingartner, E., Wiedensohler, A. and Wählin, P.: A European aerosol phenomenology—1: physical characteristics of particulate matter at kerbside, urban, rural and background sites in Europe, *Atmos. Environ.*, 38(16), 2561–2577, doi:10.1016/j.atmosenv.2004.01.040, 2004.

Vautard, R., Builtjes, P. H. J., Thunis, P., Cuvelier, C., Bedogni, M., Bessagnet, B., Honoré, C., Moussiopoulos, N., Pirovano, G., Schaap, M., Stern, R., Tarrason, L. and Wind, P.: Evaluation and intercomparison of Ozone and PM10 simulations by several chemistry transport models over four European cities within the CityDelta project, *Atmos. Environ.*, 41(1), 173–188, doi:10.1016/j.atmosenv.2006.07.039, 2007.

Wagstrom, K. M., Pandis, S. N., Yarwood, G., Wilson, G. M. and Morris, R. E.: Development and application of a computationally efficient particulate matter apportionment algorithm in a three-dimensional chemical transport model, *Atmos. Environ.*, 42(22), 5650–5659, doi:10.1016/j.atmosenv.2008.03.012, 2008.

Weber, S., Salameh, D., Albinet, A., Alleman, L. Y., Waked, A., Besombes, J.-L., Jacob, V., Guillaud, G., Meshbah, B., Rocq, B., Hulin, A., Dominik-Sègue, M., Chrétien, E., Jaffrezo, J.-L. and Favez, O.: Comparison of PM10 Sources Profiles at 15 French Sites Using a Harmonized Constrained Positive Matrix Factorization Approach, *Atmosphere*, 10(6), 310, doi:10.3390/atmos10060310, 2019.

Whitby, K. T. and Sverdrup, G. M.: California aerosols - their physical and chemical characteristics, *Adv Env. Sci Technol U. S.*, 9 [online] Available from: <https://www.osti.gov/biblio/6572253-california-aerosols-physical-chemical-characteristics>, 1980.

WHO: Review of evidence on health aspects of air pollution – REVIHAAP project: final technical report, [online] Available from: <http://www.euro.who.int/en/health->

topics/environment-and-health/air-quality/publications/2013/review-of-evidence-on-health-aspects-of-air-pollution-revihaap-project-final-technical-report, 2017.

WHO: Burden of disease from Ambient Air Pollution for 2016, WHO. [online] Available from: https://www.who.int/airpollution/data/AAP_BoD_results_May2018_final.pdf, 2018.

Williams, J., Reus, M. de, Krejci, R., Fischer, H. and Ström, J.: Application of the variability-size relationship to atmospheric aerosol studies: estimating aerosol lifetimes and ages, *Atmospheric Chem. Phys.*, 2(2), 133–145, doi:<https://doi.org/10.5194/acp-2-133-2002>, 2002.

Yang, Y., Lou, S., Wang, H., Wang, P. and Liao, H.: Trends and source apportionment of aerosols in Europe during 1980–2018, *Atmospheric Chem. Phys. Discuss.*, 1–40, doi:<https://doi.org/10.5194/acp-2019-778>, 2019.

Yarwood, G., Morris, R. E. and Wilson, G. M.: Particulate matter source apportionment technology (PSAT) in the CAMx photochemical grid model, in *Air Pollution Modeling and Its Application XVII*, pp. 478–492, Springer., 2007.

Yu, J., Cocker, D. R., Griffin, R. J., Flagan, R. C. and Seinfeld, J. H.: Gas-Phase Ozone Oxidation of Monoterpenes: Gaseous and Particulate Products, *J. Atmospheric Chem.*, 34(2), 207–258, doi:10.1023/A:1006254930583, 1999.

Zhang, Q., Jimenez, J. L., Canagaratna, M. R., Allan, J. D., Coe, H., Ulbrich, I., Alfarra, M. R., Takami, A., Middlebrook, A. M., Sun, Y. L., Dzepina, K., Dunlea, E., Docherty, K., DeCarlo, P. F., Salcedo, D., Onasch, T., Jayne, J. T., Miyoshi, T., Shimojo, A., Hatakeyama, S., Takegawa, N., Kondo, Y., Schneider, J., Drewnick, F., Borrmann, S., Weimer, S., Demerjian, K., Williams, P., Bower, K., Bahreini, R., Cottrell, L., Griffin, R. J., Rautiainen, J., Sun, J. Y., Zhang, Y. M. and Worsnop, D. R.: Ubiquity and dominance of oxygenated species in organic aerosols in anthropogenically-influenced Northern Hemisphere midlatitudes, *Geophys. Res. Lett.*, 34(13), n/a-n/a, doi:10.1029/2007GL029979, 2007.

Zhang, Q., Jimenez, J. L., Canagaratna, M. R., Ulbrich, I. M., Ng, N. L., Worsnop, D. R. and Sun, Y.: Understanding atmospheric organic aerosols via factor analysis of aerosol mass spectrometry: a review, *Anal. Bioanal. Chem.*, 401(10), 3045–3067, doi:10.1007/s00216-011-5355-y, 2011.

Zhang, Y.: Evaluation of three probing techniques in a three-dimensional air quality model, *J. Geophys. Res.*, 110(D2), D02305, doi:10.1029/2004JD005248, 2005.

Zhao, Y., Hennigan, C. J., May, A. A., Tkacik, D. S., de Gouw, J. A., Gilman, J. B., Kuster, W. C., Borbon, A. and Robinson, A. L.: Intermediate-Volatility Organic Compounds: A Large Source of Secondary Organic Aerosol, *Environ. Sci. Technol.*, 48(23), 13743–13750, doi:10.1021/es5035188, 2014.

Ziemann, P. J. and Atkinson, R.: Kinetics, products, and mechanisms of secondary organic aerosol formation, *Chem. Soc. Rev.*, 41(19), 6582, doi:10.1039/c2cs35122f, 2012.

Chapter II

SOA markers measurements

Article I

One-year measurements of secondary organic aerosol (SOA) markers in the Paris region: concentrations, seasonality, gas/particle partitioning and use in SOA source apportionment

To be submitted in “Science of the Total Environment”

1 One-year measurements of secondary organic aerosol (SOA)
2 markers in the Paris region: concentrations, seasonality,
3 gas/particle partitioning and use in SOA source apportionment
4

5 G.M. Lanzafame^{1,2,§}, D. Srivastava^{1,§}, O. Favez^{1,*}, N. Bonnaire³, L. Alleman⁴, F.
6 Couvidat¹, B. Bessagnet^{1,2} and A. Albinet^{1,*}
7

8 ¹INERIS, Parc Technologique Alata, BP 2, 60550 Verneuil-en-Halatte, France

9 ²Sorbonne Universités, UPMC, 75252 PARIS cedex 05, France

10 ³LSCE - UMR8212, CNRS-CEA-UVSQ, Gif-sur-Yvette, France,

11 ⁴IMT Lille Douai, SAGE, 59000 Lille, France
12

13 * Correspondence to: alexandre.albinet@gmail.com; alexandre.albinet@ineris.fr

14 § These authors contributed equally to this work

15 **Abstract**

16 Twenty-five biogenic and anthropogenic SOA markers have been measured in both
17 gaseous and particulate (PM₁₀) phases, over one year in the Paris region (France). The
18 measured SOA markers concentrations agreed with the values already observed
19 worldwide. Nitroaromatic compounds (NACs) concentrations varied seasonally, with
20 higher concentrations in the winter period. This pattern was consistent with the profile of
21 biomass burning emissions, that increase during the colder season. Among biogenic
22 markers, only isoprene marker concentrations increased during summer while pinene
23 markers had no straightforward seasonal trend. An unexpected peak in most of the marker
24 concentrations has been observed in October, in which the meteorological conditions
25 favoured the accumulation of pollutants at high NO_x conditions. SOA markers gas to
26 particle partitioning (GPP) was more shifted towards the particulate phase than previously
27 reported, with a scarce temperature dependency. SOA markers were used to apportion
28 SOA sources with the SOA tracer method: the first part of the year was dominated by
29 anthropogenic Secondary Organic Carbon (SOC), summer period was mainly composed

30 by biogenic SOC and the last part of the year anthropogenic contribution was significant
31 but not predominant. SOA tracer method anthropogenic SOC agreed completely with
32 PMF estimations, while biogenic SOC estimation still require some improvements.
33 However, the overall SOA tracer method performance can be considered sufficiently
34 accurate for a first SOC estimation.

35

36 Keywords: Aerosol, SOA, Tracers, Source apportionment, PMF, Particulate matter

37

38 1. Introduction and objectives

39 Aerosols (particulate matter, PM) have significant impacts on air quality and climate (Heal et
40 al., 2012; IPCC, 2018). The organic fraction (organic aerosol (OA)) contributes to about 20 to
41 90% of the PM mass in ambient air (Kanakidou et al., 2005; Zhang et al., 2011, 2007). OA
42 originates either from anthropogenic or natural sources and includes both primary OA(POA),
43 directly emitted into the atmosphere, and secondary OA (SOA), formed in the atmosphere.
44 SOA results from the condensation and coagulation of (photo-)oxidized volatile and/or semi-
45 volatile organic compounds (VOCs and SVOCs) (Carlton et al., 2009; Hallquist et al., 2009;
46 Kroll and Seinfeld, 2008; Ziemann and Atkinson, 2012) and accounts for a major fraction of
47 OA (up to 90%) (Srivastava et al., 2018b; Zhang et al., 2011, 2007) making its
48 characterization and apportionment essential in terms of air quality or climate impacts.
49 However, the comprehension of SOA sources is still difficult to achieve and SOA is quite
50 uneasily predicted by air quality models (Bessagnet et al., 2008).

51 Different methodologies have been developed and reported to investigate OA sources
52 (Srivastava et al., 2018b). A detailed chemical characterization of OA at a molecular level can
53 provide insights into the OA sources as several organic compounds have been identified and
54 recognized as tracers (or markers) of specific sources or chemical (trans-)formation processes
55 (Srivastava et al., 2019, 2018a, 2018b, 2018c and references therein). For instance, for
56 primary sources, levoglucosan is commonly used to trace biomass burning emissions, polyols
57 for biogenic emissions (fungal spores), hopanes for vehicular emissions, etc...(Cass, 1998;
58 Samaké et al., 2019a, 2019b; Schauer et al., 1996; Simoneit et al., 1999)

59 .Similarly, key organic species have been identified as characteristic of secondary sources or
60 are typical oxidation by-products of specific precursors. They are commonly referred to as
61 SOA tracers (markers) as they can be used to apportion biogenic and anthropogenic SOA
62 sources (Kleindienst et al., 2007a). For instance, biogenic SOA markers include pinene (α -
63 and β -pinene) oxidation markers such as cis-pinonic acid, pinic acid (Christoffersen et al.,
64 1998; Jang and Kamens, 1999; Mutzel et al., 2016; Yu et al., 1999), 3-methylbutane-1,2,3-
65 tricarboxylic acid (MBTCA) (Mutzel et al., 2016; Szmigielski et al., 2007) and 3-
66 hydroxyglutaric acid (Claeys et al., 2007). Several other pinene SOA markers have been also
67 reported (Jaoui et al., 2005) and are used for source apportionment (Table 1). Isoprene SOA
68 markers include α -methylglyceric acid, 2-methylthreitol and 2-methylerythritol (Claeys et al.,
69 2004, 2004; Edney et al., 2005) while a common sesquiterpene SOA marker is β -
70 caryophyllinic acid formed from the oxidation of β -caryophyllene (Jaoui et al., 2007).
71 Anthropogenic SOA markers are generally less source (precursor) specific. For instance,
72 succinic acid has been identified as a photooxidation product of cyclic olefins but it is also
73 directly emitted by the motor vehicles(Hatakeyama et al., 1987; Kawamura and Kaplan,
74 1987). Typical toluene oxidation products are 2,3-dihydroxy-4-oxopentanoic acid (DHOPA),
75 nitrophenols and methylnitrophenols (Forstner et al., 1997; Kleindienst et al., 2004). Phthalic
76 acid has been proposed as SOA marker for the photooxidation of naphthalene and
77 methylnaphthalenes (Kleindienst et al., 2012). All these SOA precursors are both emitted by
78 biomass burning and fossil fuel combustions. Nitroguaiacols and methylnitrocatechols are
79 considered as specific products of the phenolic compounds oxidation (Iinuma et al., 2010;
80 Yee et al., 2013) and their precursors are largely emitted by biomass burning (Bruns et al.,

81 2016; Iinuma et al., 2010). In addition, phthalic acid, nitrophenols, methyl-nitrophenols and
82 methylnitrocatechols could be also directly emitted (Wang et al., 2017; Lu et al., 2019;
83 Mkoma and Kawamura, 2013).

84 As defined, a tracer should be should be unique to the source (precursor) of origin, formed in
85 reasonably high yields to induce quantifiable concentrations in the ambient air, stable in the
86 atmosphere, and so conservative between its emission/formation and its collection at a
87 receptor location, and should have a low vapour pressure, and so mainly associated with the
88 particulate phase, to minimize possible underestimation from loss to the gaseous phase.
89 However, as already specified above for source specificity, all these conditions are rarely (and
90 probably never) fulfilled and, in this case, the term marker is more appropriate. In fact, such
91 compounds may react in the atmosphere by photochemical processes involving sunlight and
92 atmospheric oxidants (O_3 , NO_x , radicals OH, NO_3 ...). For most of the SOA markers, data
93 about their stability or atmospheric lifetimes are scarce or not available. They are usually
94 based on empirical calculations (Nozière et al., 2015) and the exact values are only available
95 for few ones (e.g. cis-pinonic acid ~2.1–3.3 days(Lai et al., 2015) and MBTCA ~1.2 days
96 (Kostenidou et al., 2018)). SOA markers are then semi-volatile compounds however, their
97 gas/particle partitioning (GPP) is still poorly documented (Al-Naiema and Stone, 2017; Bao et
98 al., 2012; Isaacman-VanWertz et al., 2016; Lutz et al., 2019; Thompson et al., 2017; Xie et
99 al., 2014; Yataveli et al., 2014) while this parameter is essential in terms of further use in
100 source apportionment. Understanding SOA markers GPP is difficult, since SOA composition
101 is highly variable and the GPP process cannot be considered at the equilibrium. Simple
102 parametrizations normally based on Raoult and Henry's laws do not succeed in correctly
103 representing the SOA GPP (Lutz et al., 2019).

104 Finally, SOA markers have been widely measured, and used for source apportionment, in the
105 USA and in southeast Asia, notably in China, but are poorly documented in Europe
106 (Srivastava et al., 2018a). The SOA chemistry is expected to be quite different in Europe
107 compared to USA and/or Asia due to the differences in the predominant SOA precursor and
108 emission sources. For example, biogenic emissions in the USA and in China are largely
109 dominated by isoprene (Guenther et al., 2006; Hantson et al., 2017), while other biogenic
110 VOCs, such as monoterpenes, are significantly emitted in Europe (Simpson et al., 1995;
111 Steinbrecher et al., 2009). Similarly, coal combustion contribution to PM (and OA) is largely
112 significant in China (Huang et al., 2014) but not in western Europe and biomass burning for
113 residential heating purposes is commonly used in Europe (Crippa et al., 2014) but not
114 necessarily in the USA (Denier van der Gon et al., 2015; Viana et al., 2016). In addition, most
115 of the measurements of SOA markers in Europe were in rural or forest areas. This did not
116 give any information about the influence of anthropogenic sources and it is not relevant for
117 urban air quality purposes (Srivastava et al., 2018b).

118
119 In this work, we investigated, over a year, the concentrations of 25 SOA markers, in both,
120 particulate and gaseous phase, in the Paris region (France) in order to (1) to compare the
121 concentration levels observed with the ones reported in the literature in Europe and
122 worldwide, (2) to study their temporal variations and seasonality together with their sources
123 or the chemical processes involved, (3) to document the GPP of the SOA markers including

124 the investigation of the influence of the temperature on this parameter and (4) to apportion the
125 different SOA sources based on the use of the SOA markers into two methodologies namely,
126 SOA tracer method and positive matrix factorization (PMF). The results obtained using both
127 methods have then been compared.

128

129 **2. Experimental**

130 **2.1. Sampling site and sample collection**

131 PM₁₀ and gaseous phases were collected, every third day, from mid- November 2014 to mid-
132 December 2015 on quartz fiber filters (Tissu-quartz, Pallflex, Ø = 150 m) and polyurethane
133 foams (PUF, Tisch Environmental, L = 75 mm), respectively, at the SIRTA facility (Site
134 Instrumental de Recherche par Télédétection Atmosphérique, 2.15° E; 48.71° N; 150 m a.s.l.;
135 <http://sirta.ipsl.fr>). This site is located 25km SW from the Paris city centre (Haeffelin et al.,
136 2005) and is part of the ACTRIS European network (Aerosol, Clouds and Trace gases
137 Research InfraStructure, www.actris.eu). The location is surrounded by forests, agricultural
138 fields, residential areas and commuting roads, and is representative of the suburban
139 background air quality conditions of the Ile-de-France region (Paris), the most populated area
140 in France (Crippa et al., 2013a; Petit et al., 2014, 2017; Sciare et al., 2011; Zhang et al.,
141 2019). Samplings were achieved on 24h-basis (from 8am to 8am, UTC), using a high-volume
142 sampler (DA-80, Digitel, 30 m³ h⁻¹) and the sampling head was not heated to avoid any
143 additional sampling artifact (Albinet et al., 2007). Prior to sampling, filters were pre-baked at
144 500 °C for 12 h and PUFs were cleaned using pressurized solvent extraction (ASE 350,
145 Thermo) using hexane (1 cycle) and acetone (2 cycles): 80 °C, 100 bars, 5 min heat time, 15
146 min static time (Zielinska2008). Once collected, particulate and gaseous phase samples
147 (n=130 +15 field blanks) were wrapped in aluminium foils and stored in polyethylene bags at
148 <-18°C until the analysis. Shipping of the samples to the different laboratories for analyses
149 have been done by express post using cool boxes (<5°C). Note, as no denuder (for oxidants or
150 to trap the SVOCs in the gaseous phase) has been used for the samplings, we are aware that
151 results could be biased due to some sampling artifacts (positive, overestimation of the
152 concentrations, or negative, underestimation, due to the sorption or desorption on/from the
153 filter of semi-volatile species and/or due to the degradation/formation of chemical species by
154 heterogeneous processes involving atmospheric oxidants) (Albinet et al., 2010; Goriaux et al.,
155 2006; Mader and Pankow, 2001; Turpin et al., 2000 and references therein). However,
156 especially on annual basis, the errors induced should be relatively small by comparison to the
157 overall measurement uncertainties (Brown and Brown, 2013).

158

159 **2.2. Off-line chemical analyses**

160 Particulate phase was extensively characterized for many chemical species (n=175).
161 Elemental and organic carbon (EC/OC) were measured using a Sunset lab analyser and
162 following the EUSAAR-2 thermo-optical protocol (Cavalli et al. 2010). Major ions (Cl⁻, NO₃⁻,
163 SO₄²⁻, NH₄⁺, Na⁺, K⁺, Mg²⁺, Ca²⁺) together with methanesulfonic acid (MSA) and oxalate
164 (C₂O₄²⁻), were quantified using ion chromatography after filter extraction in ultrapure water
165 (18 MΩ) (Guinot et al., 2007). Both EC/OC and ion analyses fulfilled the recommendations
166 of the European standard procedures EN 16909 and EN 16913, respectively (CEN, 2017a,

167 2017b). Thirty seven elements and metals, notably including Ca, Ti, Mn, Fe, Ni, Sb, Cu, Zn,
168 V, and Pb, were measured using ICP-AES or ICP-MS after filter digestion using nitric acid
169 (Alleman et al., 2010; CEN, 2005; Mbengue et al., 2014). Anhydrosugars, including known
170 biomass burning markers (levoglucosan, mannosan and galactosan) and 3 polyols (arabitol,
171 sorbitol and mannitol) were quantified using LC-PAD (Verlhac et al., 2017; Yttri et al., 2015).
172 Particulate polycyclic aromatic hydrocarbons (PAHs) and their oxygenated and nitrated
173 derivatives (oxy- and nitro-PAHs) were extracted using a QuEChERS-like (Quick Easy
174 Cheap Effective Rugged and Safe) procedure with acetonitrile (ACN) as solvent. As
175 described below, a single extraction for PUF samples was performed for the analysis of both,
176 SOA markers, PAHs and PAH derivatives. For both phases, 22 PAHs, 27 oxy- and 31 nitro-
177 PAHs were quantified by UPLC/UV-Fluorescence and GC/NICI-MS, respectively (Albinet et
178 al., 2006, 2013, 2014; Srivastava et al., 2018c; Tomaz et al., 2016). PAH analyses have been
179 performed following the recommendation of European standard procedures EN 15549 and TS
180 16645 (CEN, 2014, 2008) including the control of extraction efficiency using the NIST
181 standard reference material SRM1649b (urban dust). Oxy- and nitro-PAH extraction
182 efficiencies were also checked using the same SRM. All the concentration values obtained
183 were in good agreement with the certified, reference or indicative values from the NIST
184 certificate or with the ones reported in the literature (Albinet et al., 2006, 2013, 2014).

185 Twenty-five SOA markers were quantified using the extraction and analytical procedures
186 described briefly here and in the Supplementary Material (SM) and as reported previously
187 (Albinet et al., 2019). The list of the chemicals used together with their purity, CAS number
188 and suppliers is also specified (Table S1). Particulate SOA markers extraction was achieved
189 using a QuEChERS-like extraction procedure as described previously (Albinet et al., 2019).
190 47mm filter punches were placed in centrifuge glass tubes ($\varnothing = 16$ mm, L=100mm, screw cap
191 with PTFE septum face; Duran), spiked with a known amount (800 ng) of 4 deuterated SOA
192 surrogate standards (Table S2) and 7 mL of methanol (MeOH) were added for the extraction.
193 The tubes were shaken using a multi-tube vortexer for 1.5 min (DVX-2500, VWR), then
194 centrifuged for 10min at 4500 rpm (Sigma 3-16 PK). Supernatant extracts (5 ml) were
195 collected and reduced to dryness under a gentle nitrogen stream to remove any trace of MeOH
196 or water and avoid additional consumption of derivatizing reagent. Extracts were then
197 reconstructed into 100 μ l of ACN.

198 PUF samples were extracted with acetone using pressurized liquid extraction (ASE 350,
199 Thermo; two cycles: 80 $^{\circ}$ C, 100 bars, 5 min heat time, 15 min static time) (Tomaz et al.,
200 2016). Extracts were reduced under a gentle nitrogen stream to a volume of about 200 μ L
201 (Zymark, Turbovap II) and adjusted to 2 mL with ACN. Next, a known amount of labelled
202 SOA surrogate standards (100 ng) was added to 500 μ L of the extract and then reduced to
203 dryness under a gentle nitrogen stream and finally dissolved into 50 μ l of ACN. This step was
204 necessary to eliminate any residual acetone left. Note that, the surrogates have not been added
205 before PUF extractions at that time, but extraction tests have been performed later, using
206 spiked PUFs with a standard solution of SOA markers, and showed extraction efficiencies in
207 the range of 20 to 70 %.

208 All the extracts have been subjected to derivatization (silylation) using an equal proportion
209 (ratio sample extract to derivatizing reagent of 1:1) of N-methyl-N-(trimethylsilyl)
210 trifluoroacetamide (MSTFA) with 1% trimethylchlorosilane (TMCS) for 30 minutes at 60 $^{\circ}$ C.

211 SOA marker analyses were achieved by GC/MS (Agilent 7890A GC coupled to 5975C MS,
212 EI, 70eV). Authentic SOA marker standards (liquids or solids) were used for the
213 quantification of most of the compounds (Table S1). For molecules with no authentic
214 available standards, quantification was performed using the response factor of the most
215 similar compound among the others measured: 3-(2-hydroxy-ethyl)-2,2-dimethylcyclobutane-
216 carboxylic acid (HCCA) was quantified as pinic acid (PniA); 3-isopropylpentanedioic acid
217 (IPPA), 3-acetylpentanedioic acid (APDA), 3-acetylhexanedioic acid (AHDA), 2-hydroxy-
218 4,4-dimethylglutaric acid (HDGA) were quantified as 3-hydroxyglutaric acid (HGA); 3-
219 methyl-6-nitrocatechol (3M6NC) was quantified as 3-methyl-5-nitrocatechol (3M5NC). All
220 compounds were quantified by internal calibration using appropriate deuterated surrogates
221 except methylnitrocatechols (SM, (Albinet et al., 2019)).
222

223 2.3. SOA markers analysis quality control/quality assurance

224 Fifteen field blanks for both, particulate and gaseous phases, were collected, stored and
225 analysed simultaneously with the ambient air samples. SOA marker concentrations were
226 corrected from the field blanks. Overall, field blank concentrations were for most of the
227 compounds below the limit of quantification (LOQ) or represented less than 30% of the
228 average ambient concentrations observed.

229 LOQs, defined as the lowest concentration of the compound that can be determined for a
230 signal to noise ratio $S/N = 10$, were estimated using the lowest calibration standard solution
231 (Table S2). Concentrations in the samples $< LOQ$ were replaced by $LOQ/2$.

232 SOA markers extraction efficiencies were also checked using the NIST SRM1649b (urban
233 dust). Results obtained were compared with the only concentration values available in
234 literature (Albinet et al., 2019, Table S3). Note that to date, certified concentration values in
235 any SRM do not exist for any SOA marker. Succinic acid (SuA), phthalic acid (PhA), α -
236 methylglyceric acid (MGA), 2,3-dihydroxy-4-oxopentanoic acid (DHOPA), cis-pinonic acid
237 (PnoA), 3-hydroxyglutaric acid (HGA), pinic acid (PniA), 3-methylbutane-1,2,3-tricarboxylic
238 acid (MBTCA) and β -caryophyllinic acid (CarA) concentrations obtained were relatively in
239 good agreement with the ones reported previously. The differences for 2-Methylerythritol
240 (MET), 3-Methyl-5-nitrocatechol (3M5NC) and 4-Methyl-5-nitrocatechol (4M5NC) were
241 more significant. Note that, additional and new individual concentration values are given for
242 nitrophenols and nitroguaiacols in this SRM.
243

244 2.4. On-line measurements

245 PM_{10} were monitored by TEOM-FDMS (1405F model, Thermo) following the technical
246 specifications of the standard method EN 16450 (CEN, 2017c). Black carbon (BC)
247 concentrations were measured using a multi-wavelength aethalometer (AE33, Magee
248 Scientific) and corrected from the filter-loading effect with the real-time compensation
249 algorithm using both simultaneous light attenuation measurements (Drinovec et al., 2017). BC
250 was discriminated between its two main sources, i.e. wood burning (BC_{wb}) and fossil fuel
251 (BC_{ff}) using the “aethalometer model” (Sandradewi et al., 2008). For these calculations,
252 absorption Angström exponents of 1.7 and 0.9 were used for BC_{wb} and BC_{ff} , respectively
253 (Zhang et al., 2019; Zotter et al., 2017). NO_x and O_3 were monitored using T200UP and T400

254 analysers (Teledyne API), respectively, following the standard operating procedures (SOPs)
255 from the ACTRIS network (CEN, 2012a, 2012b).

256 Meteorological parameters such as, temperature, relative humidity (RH), wind direction, wind
257 speed and planetary boundary level height (PBL) were measured at the main SIRTA facility
258 located at about 5 km east from the sampling site.

259

260 3. SOA source apportionment

261 3.1. SOA tracer method

262 Estimation of the different SOA fractions associated with individual gaseous precursors was
263 achieved applying the SOA tracer method developed by Kleindienst et al., (2007). In such
264 method, secondary organic carbon (SOC) mass fractions are determined using conversion
265 factors, obtained from smog chamber experiments, allowing to calculate SOC loadings from
266 SOA marker concentrations

267 From the smog chamber experiments, the SOA mass fraction for each precursor have been
268 calculated using Eq. (1):

$$269 f_{SOA,prec} = \frac{\sum_i tr_i}{[SOA]} \quad (1)$$

270 where $f_{SOA,I}$ is the ratio of the sum of the concentrations of all the measured SOA
271 markers $\sum_i tr_i$, to the total SOA formed from the individual class of precursor “prec”. The
272 SOA mass fractions were obtained using gravimetric measurements to convert them into SOC
273 mass fractions (f_{SOC}) using SOA/SOC mass ratios (Eq. (2)).

$$274 f_{SOC,prec} = f_{SOA,prec} \frac{[SOA]}{[SOC]} \quad (2)$$

275 Here, SOC mass fractions, from anthropogenic and biogenic origins, were estimated
276 according to a subset of markers analysed following the procedure proposed by Rutter et al.,
277 (2014) and described in the SM (Tables S6).

278 The main limitation of this methodology is the limited number of SOA markers identified
279 for specific known gaseous organic precursors (so far, only isoprene, α -pinene, β -
280 caryophyllene, naphthalene and toluene) and the few SOA/SOC data available in the literature
281 (Srivastava et al., 2018b). Biomass burning SOA is not estimated using the SOA-tracer
282 method. Neglecting this SOA source might lead to significant underestimation of the total
283 wintertime SOC concentrations in Europe due to relatively high contributions of residential
284 wood burning during the cold season (Ciarelli et al., 2017; Denier van der Gon et al., 2015;
285 Petit et al., 2014; Puxbaum et al., 2007; Srivastava et al., 2018b; Zhang et al., 2019). Here, the
286 biomass burning SOA fraction was evaluated using the measured concentrations of
287 methylnitrocatechols, previously demonstrated as secondary photooxidation products of
288 phenolic compounds (e.g., cresols, methoxy phenols) (Iinuma et al., 2010) and known to
289 account for a major fraction of SOA biomass burning (Bruns et al., 2016). Values were taken
290 from the literature (Iinuma et al., 2010) to calculate f_{SOA} using Eq. (1) with $\sum [tr]_i = 821 \text{ ng}$
291 m^{-3} ; $[SOA] = 8293 \text{ ng m}^{-3}$. The SOA mass fractions were converted into SOC mass fractions
292 using SOA to SOC mass ratios. A ratio of 2, typical for SOA (Aiken et al., 2008), was used to
293 estimate the SOC mass fraction linked to the oxidation of phenolic compounds emitted from
294 biomass burning, following Eq. (2) (Table S6). To the best of our knowledge, the only other

295 study including biomass burning SOA mass fractions in the SOA-tracer method has been
296 performed recently by Al-Naiema et al, (2019).
297

298 **3.2. Positive matrix factorization (PMF)**

299 We previously showed, that the use of key secondary organic markers into source-receptor
300 models permits the resolution of several SOA sources(Srivastava et al., 2018b, 2018c, 2019,
301 2019 and references therein). SOA marker concentrations, together with other key species
302 from the extended PM chemical characterization, were included into the data matrix of a PMF
303 analysis performed to apportion the different PM and SOA sources. Details about the PMF
304 analysis and results obtained are reported in the SM.

305

306 **4. Results and discussion**

307 **4.1. . SOA marker concentration levels and comparison with literature data**

308 Annual mean and median total SOA marker concentrations (gaseous + particulate phases),
309 together with minimum, maximum, mean concentrations during the cold (October,
310 November, December, January, February and March) and warm periods (April, May, June,
311 July, August and September), and average particulate fractions, are presented in Table 1.

312 Overall, individual SOA concentration levels observed at SIRTA were in the same range than
313 those reported worldwide (Tables S4 and S5, particulate phase only), from few pg m^{-3} , for
314 both, biogenic and anthropogenic compounds, up to $0.1\text{-}1 \mu\text{g m}^{-3}$ for nitroaromatic
315 compounds (NACs) (Table 1).

316 As expected, and mentioned before, the particulate concentrations of isoprene SOA markers
317 at SIRTA (MGA, MTR and MET) were significantly lower than the ones reported in North
318 and South America and in China due to lower isoprene emissions (Guenther et al., 2006;
319 Hantson et al., 2017). This is also true for some pinene SOA markers such as MBTCA and
320 HGA. Interestingly, the differences were significant only for these 2nd generation
321 photooxidation products(Claeys et al., 2007; Müller et al., 2012; Szmigielski et al., 2007)
322 while the concentrations of the 1st generation products such as pinic and cis-pinonic acids,
323 were comparable anywhere. Finally, except for Honk Kong (Hu et al., 2008), CarA
324 concentrations at SIRTA were comparable to worldwide reported values.

325 For the anthropogenic SOA markers, the particulate concentrations observed at SIRTA were
326 all comparable with the ones reported worldwide except for the methylnitrocatechols that
327 were largely higher than in China, probably less impacted by biomass burning emissions.

328 These results confirmed that precursor emissions, together with the chemical processes
329 involved, are significantly different in Europe than in America and Asia. A comparison of the
330 SOA marker concentrations measured at SIRTA (in particulate phase only) with the ones
331 previously reported in Europe is probably more relevant and is presented here after.

332

333

334 Table 1. Total atmospheric concentrations (gaseous + particulate phases, ng m⁻³) of biogenic
 335 and anthropogenic SOA markers measured at SIRTa (France) from mid-November 2014 to
 336 mid-December 2015. Annual average and mean values together with the average
 337 concentrations for the cold and warm period, the minimum and the maximum observed
 338 values, are reported. Average particulate fraction (F_p) is also specified (%).

Compound	Abbreviation	Annual mean (min – max)	Annual median	Cold period ^a mean	Warm period ^a mean	F _p (%)
<i>Pinene</i>						
cis-Pinonic acid	PnoA	2.8(0.1-11)	2.1	2.2	3.4	68
Pinic acid	PniA	0.8(<0.1-7.8)	0.5	0.7	1.0	94
3-(2-Hydroxy-ethyl)-2,2-dimethylcyclobutane-carboxylic acid ^b	HCCA	1.1(<0.1-16.9)	0.6	1.4	0.7	75
3-Methylbutane-1,2,3-tricarboxylic acid	MBTCA	1.0(<0.1-10.3)	0.6	1.4	0.6	99
3-Hydroxyglutaric acid	HGA	2.2(<0.1-16.4)	0.8	2.6	1.7	78
Terpenylic acid	TerA	0.3(<0.1-4.7)	0.1	0.2	0.3	51
3-Hydroxy-4,4-dimethylglutaric acid ^c	HDGA	0.3(<0.1-2.3)	0.2	0.3	0.3	44
3-Acetyl-pentanedioic acid ^c	APDA	4.2(0.1-43.4)	2.3	3.4	5.1	64
3-Acetyl-hexanedioic acid ^c	AHDA	6(<0.1-37.1)	4.0	5.0	7.2	60
3-Isopropylpentanedioic acid ^c	IPPA	10.9(<0.1-17.7)	11.1	8.9	13.3	2
<i>Isoprene</i>						
α-Methylglyceric acid	MGA	0.5(<0.1-3.3)	0.2	0.3	0.8	89
2-Methylthreitol	MTR	0.8(<0.1-6.2)	0.5	0.6	1.0	38
2-Methylerythritol	MET	3.1(<0.1-40.8)	1.0	0.7	6.0	58
<i>β-Caryophyllene</i>						
β-Caryophyllinic acid	CarA	1(<0.1-21.9)	0.4	1.5	0.4	25
<i>Anthropogenic SOA acids</i>						
Succinic acid	SuA	8.3(<0.1-53.3)	5.0	10.5	5.6	88
Phthalic acid	PhA	2.7(<0.1-25.1)	1.5	3.5	1.7	51
2,3-Dihydroxy-4-oxopentanoic acid	DHOPA	1(<0.1-9)	0.5	1.6	0.3	72
<i>Nitroaromatic compounds (NACs)</i>						
2-Nitrophenol	2NPh	52.7(<0.1-1086.3)	0.6	96.8	0.4	69
4-Nitrophenol	4NPh	6.9(<0.1-27.9)	5.3	8.6	5.0	78
2-Methyl-4-nitrophenol	2M4NPh	1.6(<0.1-12.1)	1.1	2.4	0.7	9
4-Nitroguaiacol	4NG	7.9(<0.1-98.1)	2.3	13.9	0.7	6
5-Nitroguaiacol	5NG	0.4(<0.1-6.2)	0.1	0.6	0.1	7
4-Methyl-5-nitrocatechol	4M5NC	18.9(0.1-321)	1.5	33.6	1.6	95
3-Methyl-6-nitrocatechol	3M6NC	4.4(1.7-39.6)	3.0	5.6	3.0	88
3-Methyl-5-nitrocatechol	3M5NC	15.9(0.1-263.8)	1.4	28.0	1.4	67

339 ^a Cold and warm periods were defined as follows: cold period included October, November (2014 and 2015),
 340 December (2014 and 2015), January, February and March months, and warm periods included April, May, June,
 341 July, August and September months. Average temperatures during both period of about 7.4 and 17°C,
 342 respectively.

343 ^bQuantified using pinic acid as response factor.

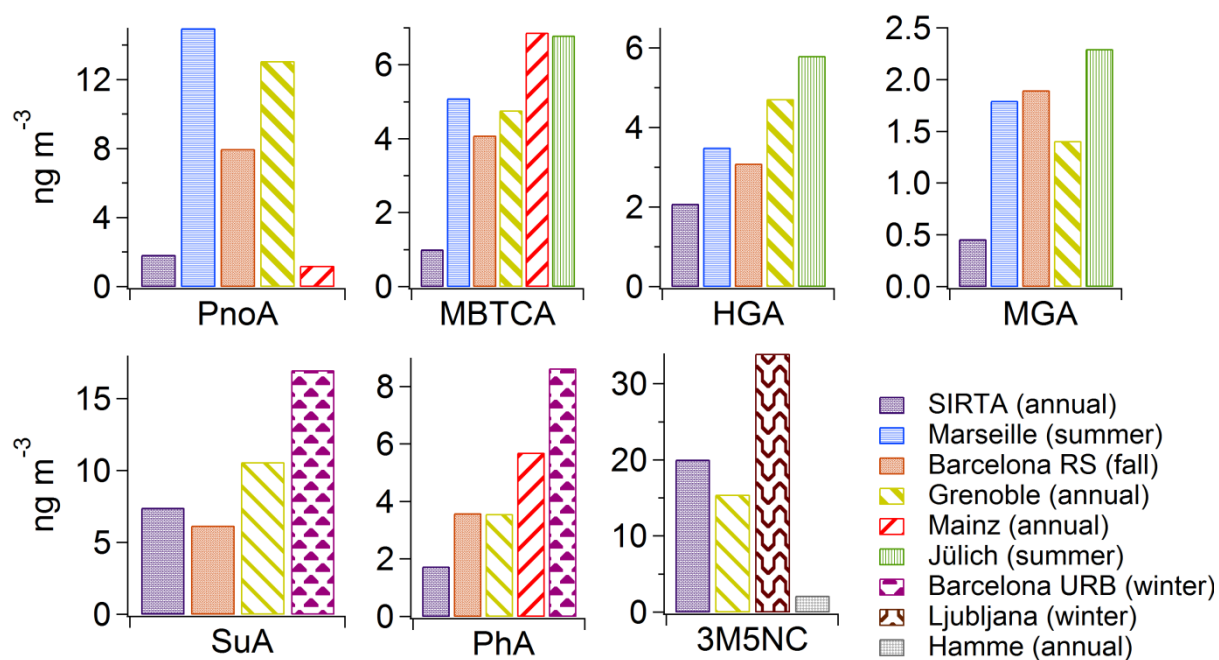
344 *Quantified by internal calibration using 3-hydroxyglutaric acid as response factor.

345

346 Fig. 1 shows a direct comparison of selected particulate SOA marker concentrations
 347 (commonly measured, from different precursors and usually used for SOA source
 348 apportionment) measured at SIRTA to the ones previously reported for several locations in
 349 Europe. European data include 4 urban sites and, as an example, one forest and 2 rural sites.
 350 Other compounds are presented in Table S5.

351 SOA marker particulate phase concentrations observed displayed the same order of magnitude
 352 at SIRTA than the ones measured at other sites. However, biogenic markers are generally in
 353 the lower concentration ranges (Table S5.1 and S5.2), due to the low biogenic influence on
 354 this site. Only β -caryophyllinic acid concentrations (0.8 ng m^{-3}) are higher than the only other
 355 value measured in Europe (0.3 ng m^{-3} in Marseille).

356 Anthropogenic marker concentrations at SIRTA are lower than in the rest of Europe, except
 357 for SuA and methylnitrocatechols, that are respectively in the lower and in the higher range of
 358 European concentrations (Fig. 1, Table S5.1 and S5.2). These comparisons are consistent with
 359 results from previous studies showing that SIRTA was highly influenced by anthropogenic
 360 emissions, and especially by biomass burning in wintertime (Bressi et al., 2014; Crippa et al.,
 361 2013b; Petit et al., 2014; Srivastava et al., 2018a; Zhang et al., 2019).



362

363 **Fig. 1.** Comparison of annual average particulate SOA marker and OC concentrations
 364 observed at SIRTA (mid-November 2014 – mid-December 2015) with literature values
 365 reported for several European locations. Urban: Marseille (France) (El Haddad et al., 2011),
 366 Barcelona (Spain) (road street, RS) (van Drooge et al., 2012) (urban, URB) (Alier et al.,
 367 2013), Grenoble (France) (Srivastava et al, 2018c) and Ljubljana (Slovenia) (Kitanovski et al.,
 368 2012). Rural: Mainz (rural urban, Germany)(Zhang et al., 2010), Hamme (Belgium) (Kahnt et

369 al., 2013). Forest: Jülich (Germany) (Kourtchev et al., 2008). Note, the sum of MNC isomers,
370 and not 3M5NC concentrations, is reported for Hamme.

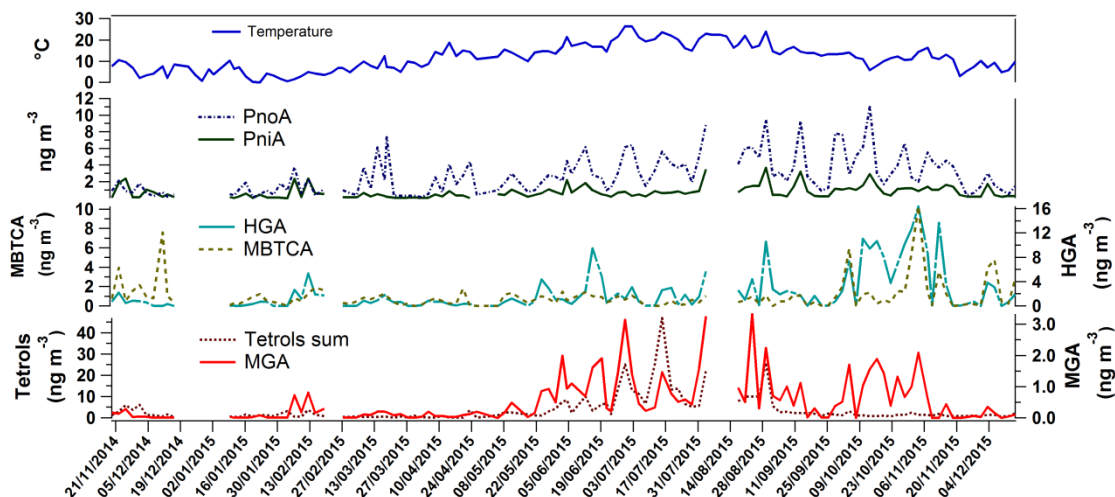
371

372 The comparison of the average total SOA marker concentrations observed during the cold and
373 warm periods gives some first clues in the seasonality of these compounds (Table 1) that is
374 further discussed into details into the following section. For biogenic species, the average sum
375 of monoterpene SOA marker concentrations in warm and cold periods were 34 and 26 ng m⁻³,
376 respectively. Although the total monoterpene marker budget varies according to the
377 temperature, with higher concentrations in the warmer periods, the individual compounds did
378 not show the same behaviour. Most of the biogenic marker concentrations were 1.5 times
379 lower in the cold period, except for HDGA, that was quite stable, and HCCA, MBTCA, and
380 HGA, for which cold period concentrations were 1.5 to 2 times higher than in warm period.
381 For isoprene SOA markers, mean total concentrations were 4.5 times higher (from 1.6 to 7.6
382 ng m⁻³) during the warm period. Into details, MGA, MTR and MET concentrations were
383 about 2.7, 1.6 and 10 times higher in this season than in the cold period. Finally, β-
384 caryophyllinic acid mean concentrations were higher in the colder period (1.5 ng m⁻³) than in
385 the warmer period (0.4 ng m⁻³) by a factor 3.7. As for HCAA, MBTCA and HGA, this was
386 mainly due to the high concentrations observed in October/November and this will be further
387 discussed in section 4.3. This may also suggest that the seasonal trend of biogenic markers did
388 not depend only from the precursor emissions.

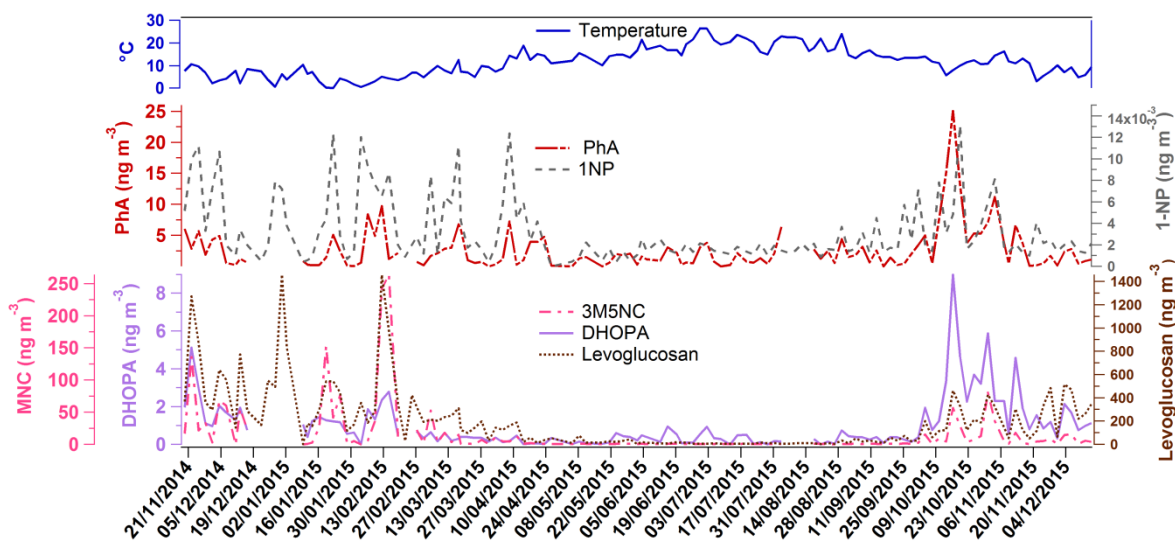
389 Anthropogenic SOA marker concentrations were overall higher in cold season than in warm
390 season. SuA, PhA and DHOPA concentrations were respectively 1.9, 2 and 5.8 times higher
391 during the cold period. Nitroaromatic compounds (NACs) dominated over the other markers
392 measured during all the year. They all showed higher concentrations in the cold period (1.7 to
393 245 times higher) depending on the compound. Major differences between the cold and the
394 warm periods were observed for 2NPh (× 245) and for 4-NG, 4M5NC and 3M5NC (× 20),
395 due to large emissions of their precursors by biomass burning from residential heating (Bruns
396 et al., 2016; Iinuma et al., 2010).

397 **4.2. SOA marker temporal evolutions and seasonality**

398 The temporal evolutions of selected biogenic (PnoA, PniA, MBTCA, HGA, MGA and
399 MET+MTR) and anthropogenic (PhA, DHOPA and 3M5NC) SOA markers (gaseous +
400 particulate phase concentrations) are shown on Figs. 2 and 3, respectively, together with the
401 temperature. All the other compounds are presented individually in the SM (Figs S2 to S8).
402 Anthropogenic SOA markers are also presented with two primary anthropogenic markers:
403 levoglucosan, a well-known biomass burning molecular tracer (Simoneit et al., 1999) and 1-
404 nitropyrene (1-NP) emitted by diesel engines (Keyte et al., 2016; Zielinska et al., 2004a). This
405 latter was used to trace vehicular emissions (Srivastava et al., 2018a, 2018c, 2019) as in
406 France in 2015 80% of the total vehicles fleet (cars+heavy trucks) was composed by diesel
407 engines (CCFA, 2016) and as supported by the correlations with BC_{ff} and NO_x (Fig S11 and
408 Fig S17, r=0.73 for both, n=130, p<0.05).



409
 410 **Fig. 2.** Temporal variations of selected total biogenic SOA markers concentrations (gaseous +
 411 particulate phases) at SIRTa (2015). Upper panel shows the temperature, central panels show
 412 the first (PnoA and PniA) and second generation (HGA and MBTCA) pinene SOA markers
 413 and the lower panel show, isoprene SOA markers (tetrols and MGA). Tetrols is the sum of 2-
 414 methylerythritol (MET) and 2-methylthreitol (MTR).



415
 416 **Fig. 3.** Temporal variations of selected total anthropogenic SOA markers concentrations
 417 (gaseous + particulate phases) at SIRTa (2015). Upper panel shows the temperature, central
 418 panel shows PhA together with 1-nitropyrene (1-NP) (diesel emission marker) and lower
 419 panel shows DHOPA and 3M5NC together with levoglucosan (marker for primary biomass
 420 burning emissions).

421
 422 Biogenic SOA marker concentrations were expected to increase during summer due to the
 423 increase of biogenic emissions and photochemical activity enhancement (Guenther, 1997;
 424 Tarvainen et al., 2005). Here, only isoprene SOA markers (e.g., MGA and MET+MTR)
 425 showed clear seasonal variations with higher concentrations observed in summer while no
 426 significant seasonal trend could be observed for all the pinene SOA makers. Several previous
 427 studies, in China and US, investigated the annual variations of biogenic SOA markers

428 concentrations in particulate phase. They showed a systematic summer increase for isoprene
429 SOA marker and a fluctuating seasonal trend for pinene markers (Ding et al., 2008, 2016;
430 Feng et al., 2013). The only study reporting PnoA, PniA and MBTCA seasonal variations in
431 Europe (Mainz, Germany, particulate phase (Zhang et al. 2010) found a general increase of
432 these compounds in summer. The different seasonal trends of these marker families are
433 related to their precursor emission annual variations. Monoterpene emissions are regulated
434 almost entirely by the temperature, while isoprene emissions depend also on the light
435 irradiance and the leaf area index (Guenther et al., 2006). Thus, in cold period, monoterpene
436 emissions are still significant, while isoprene emissions are close to zero (Oderbolz et al.,
437 2013). No significant correlations ($r > 0.7$) between biogenic SOA markers and trace gases or
438 meteorological data have been highlighted at SIRTA. Only MGA and MET correlated with
439 temperature ($r = 0.58$ and 0.63 , $n = 130$, $p < 0.05$). Considering the difference in the factors
440 driving isoprene and monoterpene emissions, the lack of a definite seasonal trend for
441 monoterpene SOA was not surprising.

442 All anthropogenic SOA markers concentrations were enhanced in colder periods, but no
443 definite seasonal trend could be highlighted for PhA and SuA. Nitrophenols and
444 nitroguaiacols concentrations were higher only in the first part of the year. Significant
445 correlations with levoglucosan have been observed for 2NPh (0.72 , $n = 130$, $p < 0.05$, Fig. S15)
446 and for methylnitrocatechols (r^2 for 4M5NC, 3M6NC and 3MNC of 0.79 , 0.74 and 0.81 ,
447 respectively, $n = 130$, $p < 0.05$, Fig. S15). The concentration increase of the biomass burning
448 related markers at low temperature was expected, since in Europe biomass burning is a large
449 source of PM due to residential heating (Denier van der Gon et al., 2015; Puxbaum et al.,
450 2007; Viana et al., 2016). No significant correlations between any anthropogenic secondary
451 markers, 1NP, trace gases and meteorological data have been observed (Fig. S15 and S17).

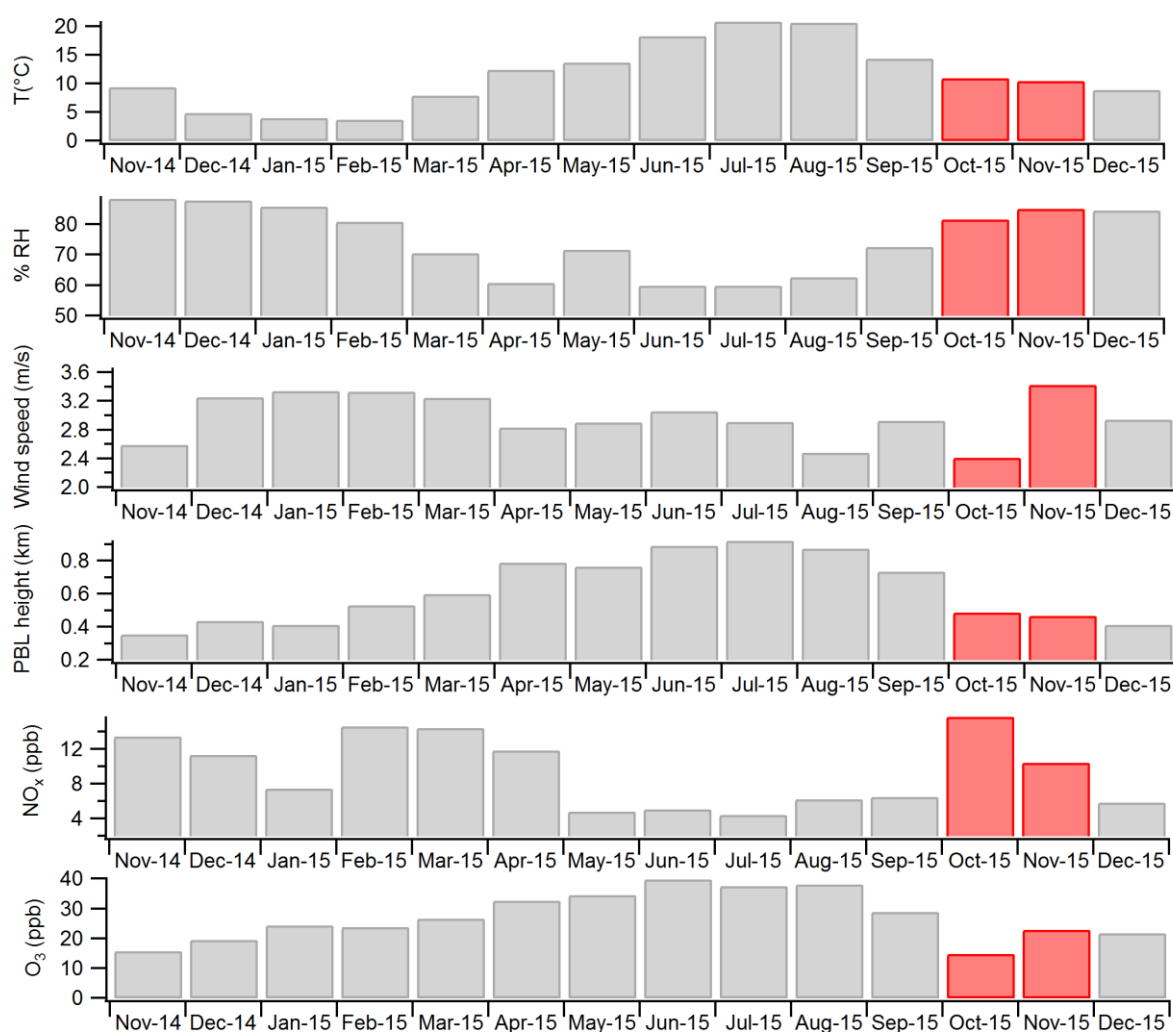
452

453 **4.3. Focus on the October/November 2015 period**

454 For most of the biogenic and anthropogenic molecular markers (primary and secondary,
455 except MTR, MET and NACs), a strong and not necessarily expected increase in the
456 concentrations was observed in fall (01/10 to 15/11) (Figs 2, 3 and Figs S2 to S8). Higher
457 concentrations of oxygenated organic aerosol (OOA, SOA proxy) have been also reported in
458 this period at SIRTA from Aerosol Chemical Speciation Monitor (ACSM) measurements
459 (Zhang et al., 2019).

460 Based on monthly data (Fig. 4), October and November 2015 showed average temperatures
461 about 11°C , for which biogenic emissions are expected to be relatively reduced. RH in
462 October rose of 10% compared to the month before, reaching a value of 80% and kept similar
463 values in November (84%). Wind speed reached the annual minimum with a mean speed of
464 2.5 m s^{-1} in October and about 3 m s^{-1} until mid-November (Fig; S13). The PBL height was
465 lower compared to the previous months (around 450 and 530m for October and November).
466 October and November 2015 were very dry compared to previous years, with significant low
467 precipitations (Météo-France, 2015). All these conditions inhibited the vertical mixing of the
468 pollutants in the atmosphere causing an accumulation of the pollutants during October and in
469 the first part of November. Then, the high wind speed in the second part of November
470 increased the dispersion of the pollutants (Fig. S13).

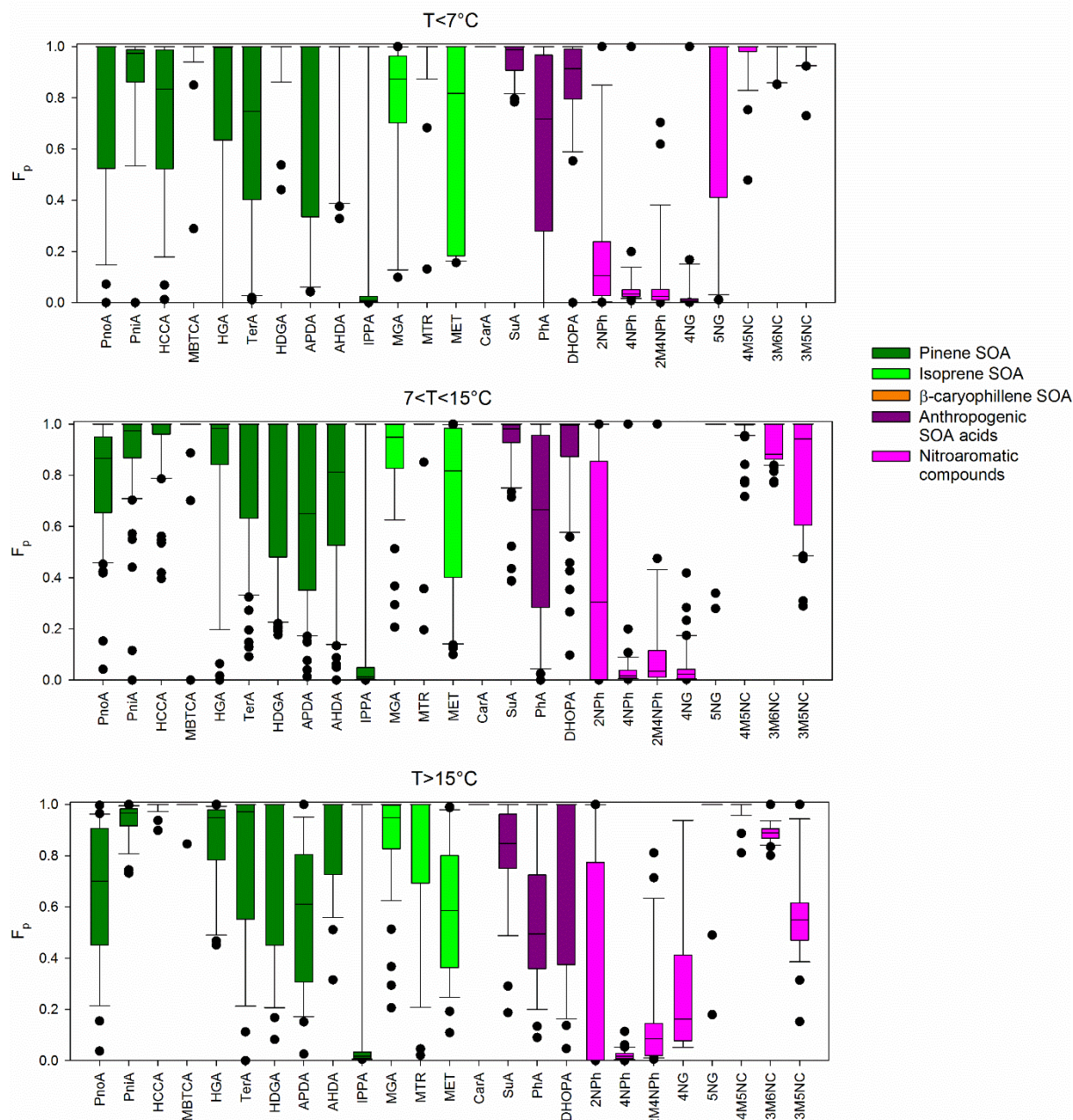
471 Several studies reported a strong effect of O₃ and NO_x concentrations on SOA composition
 472 and formation yields (Capouet et al., 2008; Dommen et al., 2006; Eddingsaas et al., 2012;
 473 Kroll et al., 2006; Lin et al., 2013; Presto et al., 2005; Sarrafzadeh et al., 2016; Xie et al.,
 474 2017; Xu et al., 2015). October mean ozone concentration was very low (16 ppb, annual mean
 475 28 ppb) and NO_x monthly mean was the highest (14.2 ppb) observed in 2015 (annual mean 9
 476 ppb). High NO_x concentrations were probably due increase in road traffic usually observed in
 477 this period, as supported by the increase in BC_{ff} and 1-NP concentrations (Fig. S11). In
 478 November, O₃ (24 ppb) and NO_x (6.3 ppb) concentrations were similar to the annual averages.
 479 Under high NO_x conditions, the formation of methyltetrols is inhibited and MGA is the main
 480 molecular marker produced (Surratt et al., 2010). High values of the ratio MGA/(MET+MTR)
 481 were observed during this period (Fig. S12) highlighting the impact of the higher NO_x
 482 concentrations on SOA formation. High NO_x conditions, when combined with significant
 483 biomass burning emissions, should also induce an increase in NACs concentrations (Harrison
 484 et al., 2005a, 2005b; Wang et al., 2019; Yuan et al., 2016) but it was not observed in our case.
 485 The low levoglucosan concentrations observed during this period suggested a moderate
 486 contribution of biomass burning (Fig. 3, S18 and S20).
 487



488

489 **Fig. 4.** Monthly average values observed for temperature ($^{\circ}\text{C}$), relative humidity (%), wind
 490 speed (m s^{-1}), planetary boundary layer height(PBL) (km), NO_x and O_3 concentrations (ppb)
 491 at SIRTa from November 2014 to December 2015. October and November 2015 are
 492 highlighted in red.

493
 494 **4.4. SOA markers gas/particle partitioning (GPP)**
 495 Particulate phase fractions (F_p) of biogenic and anthropogenic SOA markers are shown on
 496 Fig.5. F_p were split by temperature bins defined based on temperature quartiles: $T < 7^{\circ}\text{C}$ (25%
 497 of the data); $7 < T < 15^{\circ}\text{C}$ (50% of the data) and $T > 15^{\circ}\text{C}$ (25% of the data).



498 **Fig. 5.** SOA marker particulate phase fractions (F_p) divided by temperature bins. Bins
 499 were defined based on temperature quartiles (7 and 15°C were respectively the 25th and
 500

501 the 75th temperature percentiles). Data < LOQ have been excluded. The minimum data
502 considered was 15% of the total data.

503

504 All the pinene SOA markers, except IPPA, were mainly, on average, associated to the
505 particulate phase with low variations at higher and lower temperatures. Compared to the
506 literature, in which F_p values ranged from 0.1 to 0.6, PnoA was largely in particulate phase
507 but showed a shift to the gaseous phase with increasing T (F_p from 1 to 0.65 with $T < 7^\circ\text{C}$ and
508 $T > 15^\circ\text{C}$) (Al-Naiema and Stone, 2017; Lutz et al., 2019; Yatavelli et al., 2014). Similarly,
509 PniA (median $F_p \sim 0.9$), TerA (median $F_p \sim 0.8$) and HGA (median $F_p > 0.9$) partitioned more to
510 the particulate phase than previously reported (Yatavelli et al., 2014 found $F_p \sim 0.5$ for both
511 PniA and TerA, $F_p \sim 0.7$ for HGA, Kristensen et al., 2016 measured respectively mean $F_p \sim 0.38$
512 and 0.29 for PniA and TerA). Overall, our observations were in agreement with the literature,
513 showing that PniA is less volatile than PnoA (Lutz et al., 2019; Thompson et al., 2017).
514 Finally, MBTCA was mainly particulate (median $F_p \approx 1$) with no change according to the
515 temperature as shown previously (Kristensen et al., 2016; Yatavelli et al., 2014). Isoprene
516 SOA markers GPP showed also a low temperature dependency. MGA F_p ranged from 0.85 to
517 0.90 whatever the temperature bin considered. MTR partitioned in the gaseous phase only
518 above 15°C , while MET median F_p ranged from 0.6 to 0.8. Except for MTR, these results
519 were in agreement with the measurements performed by Al-Naiema and Stone, (2017) (for
520 MGA average $F_p \approx 0.85$, for MET and MTR average $F_p \approx 0.63$). Finally, β -caryophyllinic acid
521 was observed only in particulate phase ($F_p = 1$).

522 Among anthropogenic acid SOA markers, only PhA GPP was significantly affected by
523 temperature. SuA and DHOPA median F_p were above 0.8 in all bins, while PhA median F_p
524 decreased from 0.7 to 0.5 following the temperature increase. Literature data for SuA and
525 PhA are discordant on F_p estimation and temperature dependency, with F_p ranging from 0.5 to
526 0.9 for SuA (Bao et al., 2012; Limbeck et al., 2001) and from 0.2 to 0.7 for PhA (Al-Naiema
527 and Stone, 2017; Kristensen et al., 2016; Limbeck et al., 2001). In agreement with our
528 observations, Al-Naiema and Stone, (2017) showed that DHOPA was 100% associated to the
529 particulate phase.

530 No common behaviour for NACs GPP could be highlighted. Nitrophenol (2NPh, 4NPh and
531 2M4NPh) gaseous phase fractions predominated largely (median $F_p < 0.3$). Our estimation for
532 2NPh GPP agreed with the values reported by Cecinato et al., (2005) ($F_p = 0.25$), while their
533 4NPh F_p estimation ($F_p = 0.82$) was higher. Al-Naiema and Stone, (2017) reported low 4NPh
534 $F_p (= 0.3)$ in agreement with our results. Interestingly, both NG isomers, namely 4NG and
535 5NG, were in total opposition with 4NG completely in the gaseous phase, as in Al-Naiema
536 and Stone, (2017), and 5NG fully associated to the particulate phase. 3M6NC and 4M5NC
537 were mainly associated to the particulate phase whatever the T° bin considered ($1 > F_p > 0.9$), as
538 previously reported (Al-Naiema and Stone, 2017). Only 3M5NC showed a temperature
539 dependency with a shift to the gaseous phase at higher T° (F_p from 0.1 to 0.5).

540 These results highlighted that all the SOA markers studied here seemed mainly associated to
541 the particulate phase, including the compounds usually considered as semi-volatile. For
542 instance, the high functionalisation may decrease alkanolic acids volatility (Yatavelli et al.,
543 2014) and may explain the large association to the particulate as previously observed for low

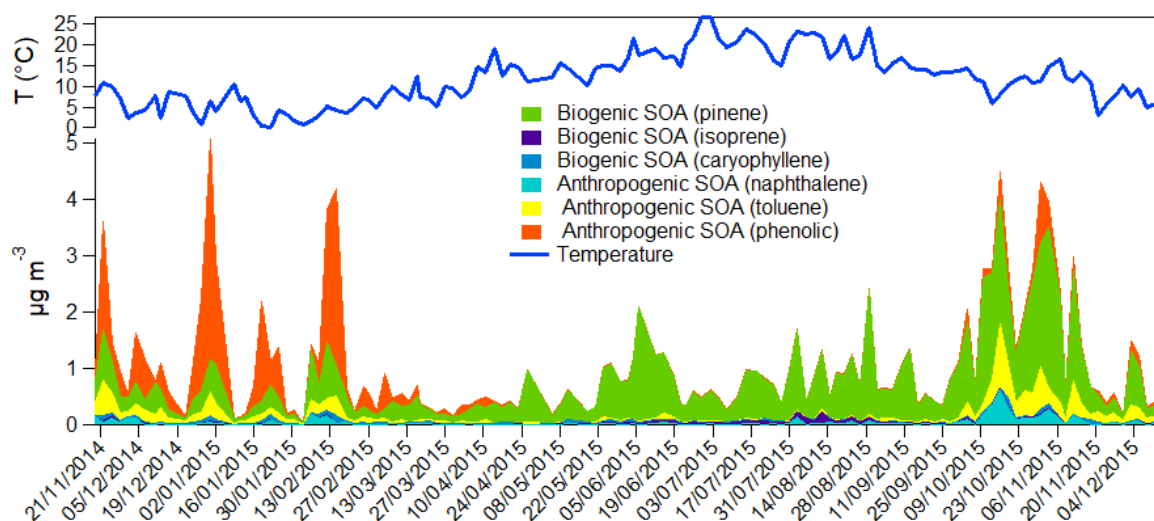
544 molecular weight dicarboxylic acids (Bilde et al., 2015; Booth et al., 2010; Falkovich et al.,
545 2004; Huisman et al., 2013; Limbeck et al., 2001; Mochida et al., 2003; Saxena and
546 Hildemann, 1996). The GPP temperature dependence observed was generally low. However,
547 GPP estimation for such compounds is still highly uncertain and the results obtained here
548 highlighted that temperature cannot fully explain their GPP in the atmosphere and other
549 parameters must be considered (aerosol chemical composition, water content...) notably for
550 modelling purposes (Kim et al., 2019; Liu et al., 2019; Pye et al., 2017; Shahpoury et al.,
551 2016).

552 4.5. SOA source apportionment

553 4.5.1. SOA tracer method

554 Fig. 6 shows the annual evolution of SOC sources estimated using the SOA tracer method.
555 The highest SOC concentrations were observed in February, October and November (2014
556 and 2015) accounting for about 9, 20 and 15% of OC. Through the year, three different
557 periods with different SOC characteristics can be highlighted: the first period, from November
558 2014 until end of March 2015 was mainly dominated by anthropogenic SOC from the
559 photooxidation of phenolic compounds and toluene, including minor contribution from the
560 SOC formed through the oxidation of naphthalene. All of these species are largely emitted by
561 biomass burning (Baudic et al., 2016; Bruns et al., 2016; Iinuma et al., 2010; Nalin et al.,
562 2016). Wood combustion used for residential heating is usually a predominant source for PM
563 and S/VOCs during the cold period in the Paris region (Bressi et al., 2014; Crippa et al.,
564 2013b; Petit et al., 2014; Srivastava et al., 2018a; Zhang et al., 2019). The stable
565 meteorological conditions (low boundary layer height and low wind speed, Fig. S10 and S11)
566 together with high S/VOC precursor concentrations from these emissions were favourable to
567 enhance anthropogenic SOA formation in this period. The second period, from April until the
568 end of September, was mainly dominated by biogenic SOC from pinene oxidation. High
569 pinene emissions are usually noticed during the warmer months (Guenther, 1997; Guenther et
570 al., 2006; Tarvainen et al., 2005), together with high solar flux (Fig. S10) and oxidant
571 concentrations (i.e. O₃ and OH) that could facilitate high biogenic SOC formation (Docherty
572 et al., 2008; Feng et al., 2013; Kleindienst et al., 2007b; Lewandowski et al., 2008; Sheesley
573 et al., 2004; Shrivastava et al., 2007; Zhang et al., 2009). In addition, increase in the biogenic
574 emissions at SIRTAs has already been found to be linked with the temperature rise (Zhang et
575 al., 2019). During the last period, from October until end of December 2015, biogenic SOC
576 (from pinene) still accounted for a significant fraction of the total SOC, however,
577 anthropogenic SOC from toluene and naphthalene oxidation contributed also significantly.
578 Other biogenic SOC, from isoprene and β -caryophyllene oxidation, and anthropogenic SOC
579 (phenolic compounds oxidation), showed low contributions to the total SOC mass. As
580 explained before (section 4.2.1.), from October to mid-November, favourable meteorological
581 conditions including increase in the relative humidity, low wind speed, low planetary
582 boundary level height, low precipitation and “warm” weather (mean temperature of 11°C)
583 induced a poor atmospheric vertical mixing with a stagnation of the pollutants over a long
584 period, and further favored SOA formation. Additionally, this period also observed high NO_x
585 levels compared to the annual average due probably to the road traffic increase leading to
586 larger primary pollutant emissions (Fig. S11). Together with favorable meteorological

587 conditions, this resulted in an enhanced SOA formation. In fact, at low temperatures,
 588 reduction in biogenic emissions is usually observed, however, prevalent anthropogenic
 589 emissions (high NO_x conditions) could induce an enhancement in the formation of biogenic
 590 SOA (at least from isoprene) as already shown previously (Claeys et al., 2004; Edney et al.,
 591 2005; Kroll et al., 2006; Surratt et al., 2006, 2010). Finally, in December 2015, the SOC
 592 composition/concentrations was found to be different from the SOC
 593 composition/concentrations observed in November-December 2014. The discrepancies could
 594 be linked to the temperature differences noticed during these periods and to the differences in
 595 terms of anthropogenic activities (low levoglucosan concentrations for instance, Fig. 3) and
 596 meteorological conditions.



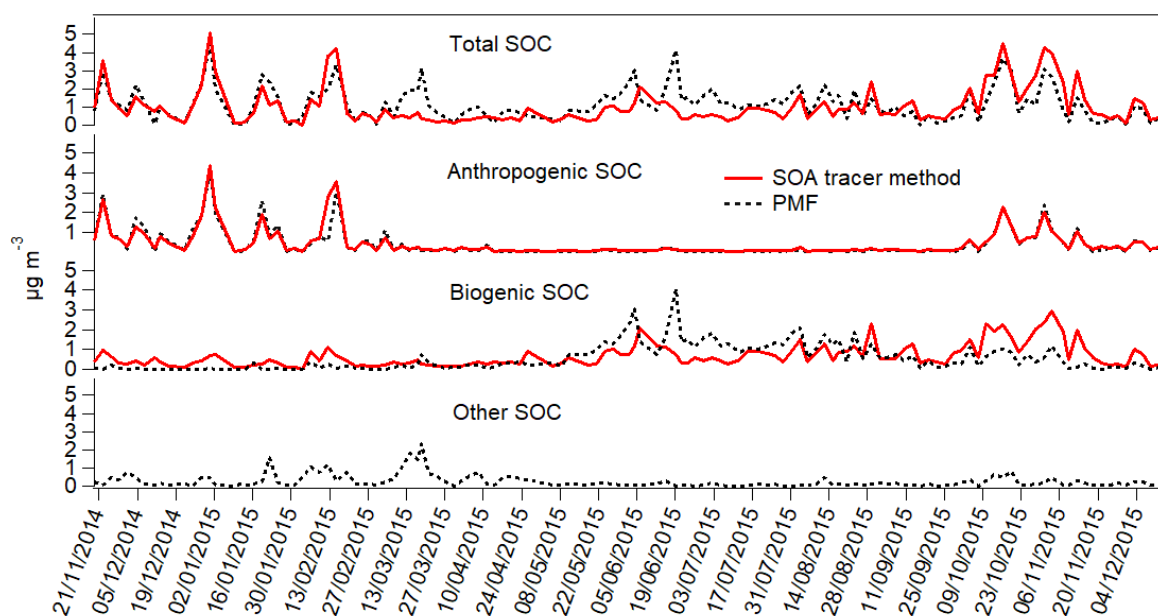
598
 599 **Fig. 6.** Temporal evolution of the identified sources to SOC mass concentrations at Sirta
 600 (2015) using the SOA tracer method.

601

602 4.5.1. Comparison of SOA tracer method and PMF outputs

603 The SOA tracer method witnesses several limitations due to the use of laboratory developed
 604 mass fractions to estimate SOC mass from the individual class of precursors, that are probably
 605 not representative of all the existing atmospheric conditions, and only determined for a
 606 limited number of SOA markers (Srivastava et al., 2018a). As suggested by Srivastava et al.,
 607 (2018a), the use of a combination of different SOC estimation methodologies to apportion the
 608 SOC concentrations is necessary to get a higher level of confidence in the results obtained.
 609 Here, we compared the SOA tracer method with the outputs from a PMF analysis. Details on
 610 PMF analysis and results are provided in the SM (Fig. S18-S20). The specific PMF SOC
 611 apportionment results are shown on Fig. S21. Fig. 7. shows the comparison of the SOC
 612 concentrations estimated using both methods.

613



614
 615 **Fig. 7.** Comparison of the SOC concentrations estimated using PMF analysis and SOA tracer
 616 method. For SOA tracer method, anthropogenic SOC includes SOA from naphthalene,
 617 toluene and phenolic compounds; biogenic SOC includes SOA from pinene, isoprene and β -
 618 caryophyllene. For PMF analysis, anthropogenic SOC includes ASOA-1 (biomass burning +
 619 traffic) and ASOA-2 (biomass burning) factors; biogenic SOC includes BSOA-A (marine)
 620 and BSOA-2 (monoterpenes + isoprene) factors. Other PMF SOC was apportioned based the
 621 on nitrate- and sulfate-rich factors.

622
 623 Overall, total SOC concentrations evaluated by both methods were in good agreement through
 624 the year. Significant differences were only observed in March and in summer (from May to
 625 August) with a systematic underestimation by the SOA tracer method. March was
 626 characterized by an intense PM pollution event ($PM_{10} > 50 \mu g m^{-3}$ for at least 3 consecutive
 627 days) over a three weeks period (Fig. S20). This type of event is typical of the late winter -
 628 early spring period in North western Europe and is characterized by large contributions of
 629 secondary organic species such as ammonium nitrate (and in a lesser extent, ammonium
 630 sulfate too), long range transportation and significant aging. Detailed discussions about the
 631 PM and OA sources of the March 2015 PM pollution event can be found elsewhere (Petit et
 632 al., 2017; Srivastava et al., 2018a, 2019). The additional SOC contribution in the PMF method
 633 (other SOC, Fig; 7) was apportioned based on the nitrate and sulfate-rich factors (Srivastava
 634 et al., 2018a) (Fig. S21). Even with advanced source apportionment method, we failed to get
 635 any better description due to the lack of specific molecular markers for such aged SOA
 636 (Srivastava et al., 2019). Similarly, as no specific markers and/or f_{SOC} have been reported in
 637 the literature for any other SOA classes, especially for organonitrates and organosulfates, the
 638 SOA tracer method underestimated the total SOC concentrations in such conditions. This is
 639 clearly one of the main limitations of this method during such highly processed PM pollution
 640 episode and it is further discussed in another paper with the comparison of several SOC
 641 apportionment methods (Srivastava et al., 2018b).

642 Into details, the anthropogenic SOC contribution for the SOA tracer method accounted for the
 643 SOC formed from the oxidation of naphthalene, toluene and phenolic compounds while 2

644 anthropogenic secondary fractions (ASOA-1 (biomass burning + traffic) and ASOA-2
645 (biomass burning) factors) were apportioned by the PMF model. A very good agreement was
646 noticed ($r^2=0.9$, slope=0.94, $n=123$, $p<0.05$) thanks to the similar species used in both
647 approaches and to the inclusion of methylnitrocatechols into the SOA tracer method
648 according to the SOA and SOC fractions calculated from Iinuma et al., (2010) data. We
649 estimated that the use of the fractions proposed by Al-Naiema et al., (2019) would have lead
650 to a lowering of phenolic SOC by a factor 10.

651 The biogenic SOC fraction resolved using the SOA tracer method was the sum of the SOC
652 formed from the oxidation of isoprene, pinene and caryophyllene while biogenic SOC from
653 the PMF model accounted two biogenic secondary fractions from marine origin
654 (dimethylsulfide oxidation, BSOA-1) and from the oxidation of isoprene/monoterpenes
655 (BSOA-2) (Figs 6, 7 and S21). Temporal profiles of biogenic SOC estimated using both
656 approaches showed significant disagreement, especially in summer and fall. The biogenic
657 SOA mass in summer included a large fraction of marine origin SOA only apportioned by the
658 PMF. Again, as no specific f_{SOC} value has been determined for the DMS oxidation, this
659 fraction could not be accounted using the SOA tracer method, explaining the significant
660 differences observed between both methods. In fall, the differences between both methods
661 with a large overestimation by the SOA tracer method were probably due to the f_{SOC} from
662 smog chamber experiments that may be different and not representative of the atmospheric
663 conditions observed in this period (NO_x concentrations, humidity, etc...).

664 5. Conclusions

665 Twenty five biogenic and anthropogenic SOA markers were measured in gaseous and
666 particulate phase during a whole year (2015) in a European suburban site (SIRTA, Paris
667 suburbs). The measured marker concentrations were in the same order of magnitude of the
668 values observed worldwide, with some differences due to different precursor emissions (e.g.
669 higher isoprene marker concentrations in America or lower biomass burning marker
670 concentrations in China than in Europe) or aerosol aging (e.g. fresher aerosol in Marseille
671 compared to SIRTA). For isoprene and biomass burning markers opposite seasonal trends
672 were identified, with respectively higher concentrations in summer and winter. No definite
673 seasonal variations have been observed for pinene and other anthropogenic markers. Stable
674 atmospheric conditions combined with high NO_x regime caused an unexpected increase in
675 concentrations for OC and some markers during October and the first part of November. Most
676 of the markers were less volatile than previously reported in literature, with low F_p variations
677 with temperature. Surprisingly, different GPP has been measured for some isomers (4NG and
678 5NG or 3M5NC, 3M6NC and 4M5NC). Finally, SOA markers were used to apportion SOA
679 sources. Biomass burning SOA was predominant in the first part of the year (until April) and
680 pinene SOA afterwards. SOA tracer approach was validated by comparison with PMF:
681 estimations for anthropogenic SOC were in good agreement, while biogenic SOC was
682 underestimated by SOA tracer method in summer and in March. The discrepancy observed is
683 probably due to missing sources or tracers specific to the processes.

684 To date, less studies on SOA marker concentrations have been performed in Europe. More
685 studies are required in order to better apportion SOA sources and identify missing sources and
686 tracers specific for European air quality conditions.

687 **References**

- 688 Aiken, A.C., DeCarlo, P.F., Kroll, J.H., Worsnop, D.R., Huffman, J.A., Docherty, K.S.,
689 Ulbrich, I.M., Mohr, C., Kimmel, J.R., Sueper, D., Sun, Y., Zhang, Q., Trimborn, A.,
690 Northway, M., Ziemann, P.J., Canagaratna, M.R., Onasch, T.B., Alfarra, M.R., Prevot,
691 A.S.H., Dommen, J., Duplissy, J., Metzger, A., Baltensperger, U., Jimenez, J.L., 2008. O/C
692 and OM/OC Ratios of Primary, Secondary, and Ambient Organic Aerosols with High-
693 Resolution Time-of-Flight Aerosol Mass Spectrometry. *Environ. Sci. Technol.* 42, 4478–
694 4485. <https://doi.org/10.1021/es703009q>
- 695 Albinet, A., Lanzafame, G.M., Srivastava, D., Bonnaire, N., Nalin, F., Wise, A., 2019.
696 Analysis and determination of secondary organic aerosol (SOA) tracers (markers) in
697 particulate matter standard reference material (SRM 1649b, urban dust). *Anal. Bioanal.*
698 *Chem.* <https://doi.org/10.1007/s00216-019-02015-6>
- 699 Albinet, A., Leoz-Garziandia, E., Budzinski, H., Villenave, E., 2006. Simultaneous analysis
700 of oxygenated and nitrated polycyclic aromatic hydrocarbons on standard reference material
701 1649a (urban dust) and on natural ambient air samples by gas chromatography–mass
702 spectrometry with negative ion chemical ionisation. *J. Chromatogr. A* 1121, 106–113.
703 <https://doi.org/10.1016/j.chroma.2006.04.043>
- 704 Albinet, A., Leoz-Garziandia, E., Budzinski, H., Villenave, E., 2007. Sampling precautions
705 for the measurement of nitrated polycyclic aromatic hydrocarbons in ambient air. *Atmos.*
706 *Environ.* 41, 4988–4994. <https://doi.org/10.1016/j.atmosenv.2007.01.061>
- 707 Albinet, A., Nalin, F., Tomaz, S., Beaumont, J., Lestremau, F., 2014. A simple QuEChERS-
708 like extraction approach for molecular chemical characterization of organic aerosols:
709 application to nitrated and oxygenated PAH derivatives (NPAH and OPAH) quantified by
710 GC-NICI MS. *Anal. Bioanal. Chem.* 406, 3131–3148. <https://doi.org/10.1007/s00216-014-7760-5>
- 712 Albinet, A., Papaiconomou, N., Estager, J., Suptil, J., Besombes, J.-L., 2010. A new ozone
713 denuder for aerosol sampling based on an ionic liquid coating. *Anal. Bioanal. Chem.* 396,
714 857–864. <https://doi.org/10.1007/s00216-009-3243-5>
- 715 Albinet, A., Tomaz, S., Lestremau, F., 2013. A really quick easy cheap effective rugged and
716 safe (QuEChERS) extraction procedure for the analysis of particle-bound PAHs in ambient
717 air and emission samples. *Sci. Total Environ.* 450–451, 31–38.
718 <https://doi.org/10.1016/j.scitotenv.2013.01.068>
- 719 Alier, M., van Drooge, B.L., Dall'Osto, M., Querol, X., Grimalt, J.O., Tauler, R., 2013.
720 Source apportionment of submicron organic aerosol at an urban background and a road site in
721 Barcelona (Spain) during SAPUSS. *Atmospheric Chem. Phys.* 13, 10353–10371.
722 <https://doi.org/10.5194/acp-13-10353-2013>
- 723 Alleman, L.Y., Lamaison, L., Perdrix, E., Robache, A., Galloo, J.-C., 2010. PM10 metal
724 concentrations and source identification using positive matrix factorization and wind
725 sectoring in a French industrial zone. *Atmospheric Res.* 96, 612–625.
726 <https://doi.org/10.1016/j.atmosres.2010.02.008>

- 727 Al-Naiema, I.M., Offenberg, J.H., Madler, C. J., Lewandoski, M., Kettler, J., Fang, T., Stone,
728 E.A., 2019. Secondary organic aerosols from aromatic hydrocarbons and their contribution to
729 fine particulate matter in Atlanta, Georgia. *Atmos. Environ.* 117227.
730 <https://doi.org/10.1016/j.atmosenv.2019.117227>.
731
- 732 Al-Naiema, I.M., Stone, E.A., 2017. Evaluation of anthropogenic secondary organic aerosol
733 tracers from aromatic hydrocarbons. *Atmospheric Chem. Phys.* 17, 2053–2065.
734 <https://doi.org/10.5194/acp-17-2053-2017>
- 735 Bao, L., Matsumoto, M., Kubota, T., Sekiguchi, K., Wang, Q., Sakamoto, K., 2012.
736 Gas/particle partitioning of low-molecular-weight dicarboxylic acids at a suburban site in
737 Saitama, Japan. *Atmos. Environ.* 47, 546–553.
738 <https://doi.org/10.1016/j.atmosenv.2009.09.014>
- 739 Baudic, A., Gros, V., Sauvage, S., Locoge, N., Sanchez, O., Sarda-Estève, R., Kalogridis, C.,
740 Petit, J.-E., Bonnaire, N., Baisnée, D., Favez, O., Albinet, A., Sciare, J., Bonsang, B., 2016.
741 Seasonal variability and source apportionment of volatile organic compounds (VOCs) in the
742 Paris megacity (France). *Atmospheric Chem. Phys.* 16, 11961–11989.
743 <https://doi.org/10.5194/acp-16-11961-2016>
- 744 Bessagnet, B., Menut, L., Curci, G., Hodzic, A., Guillaume, B., Liousse, C., Moukhtar, S.,
745 Pun, B., Seigneur, C., Schulz, M., 2008. Regional modeling of carbonaceous aerosols over
746 Europe—focus on secondary organic aerosols. *J. Atmospheric Chem.* 61, 175–202.
747 <https://doi.org/10.1007/s10874-009-9129-2>
- 748 Bilde, M., Barsanti, K., Booth, M., Cappa, C.D., Donahue, N.M., Emanuelsson, E.U.,
749 McFiggans, G., Krieger, U.K., Marcolli, C., Topping, D., Ziemann, P., Barley, M., Clegg, S.,
750 Dennis-Smith, B., Hallquist, M., Hallquist, Å.M., Khlystov, A., Kulmala, M., Mogensen,
751 D., Percival, C.J., Pope, F., Reid, J.P., Ribeiro da Silva, M.A.V., Rosenoern, T., Salo, K.,
752 Soonsin, V.P., Yli-Juuti, T., Prisle, N.L., Pagels, J., Rarey, J., Zardini, A.A., Riipinen, I.,
753 2015. Saturation Vapor Pressures and Transition Enthalpies of Low-Volatility Organic
754 Molecules of Atmospheric Relevance: From Dicarboxylic Acids to Complex Mixtures. *Chem.*
755 *Rev.* 115, 4115–4156. <https://doi.org/10.1021/cr5005502>
- 756 Booth, A.M., Barley, M.H., Topping, D.O., McFiggans, G., Garforth, A., Percival, C.J., 2010.
757 Solid state and sub-cooled liquid vapour pressures of substituted dicarboxylic acids using
758 Knudsen Effusion Mass Spectrometry (KEMS) and Differential Scanning Calorimetry.
759 *Atmospheric Chem. Phys.* 10, 4879–4892. <https://doi.org/10.5194/acp-10-4879-2010>
- 760 Bressi, M., Sciare, J., Gherzi, V., Mihalopoulos, N., Petit, J.-E., Nicolas, J.B., Moukhtar, S.,
761 Rosso, A., Féron, A., Bonnaire, N., Poulakis, E., Theodosi, C., 2014. Sources and
762 geographical origins of fine aerosols in Paris (France). *Atmospheric Chem. Phys.* 14, 8813–
763 8839. <https://doi.org/10.5194/acp-14-8813-2014>
- 764 Brown, R.J.C., Brown, A.S., 2013. Assessment of the effect of degradation by atmospheric
765 gaseous oxidants on measured annual average benzo[a]pyrene mass concentrations.
766 *Chemosphere* 90, 417–422. <https://doi.org/10.1016/j.chemosphere.2012.07.044>
- 767 Bruns, E.A., El Haddad, I., Slowik, J.G., Kilic, D., Klein, F., Baltensperger, U., Prévôt,
768 A.S.H., 2016. Identification of significant precursor gases of secondary organic aerosols from
769 residential wood combustion. *Sci. Rep.* 6. <https://doi.org/10.1038/srep27881>

- 770 Capouet, M., Müller, J.-F., Ceulemans, K., Compernelle, S., Vereecken, L., Peeters, J., 2008.
771 Modeling aerosol formation in alpha-pinene photo-oxidation experiments. *J. Geophys. Res.*
772 *Atmospheres* 113. <https://doi.org/10.1029/2007JD008995>
- 773 Carlton, A.G., Wiedinmyer, C., Kroll, J.H., 2009. A review of Secondary Organic Aerosol
774 (SOA) formation from isoprene. *Atmospheric Chem. Phys.* 9, 4987–5005.
775 <https://doi.org/10.5194/acp-9-4987-2009>
- 776 Cass, G.R., 1998. Organic molecular tracers for particulate air pollution sources. *TrAC*
777 *Trends Anal. Chem.* 17, 356–366. [https://doi.org/10.1016/S0165-9936\(98\)00040-5](https://doi.org/10.1016/S0165-9936(98)00040-5)
- 778 CCFA, 2016. The French Automotive Industry. Analysis and Statistics 2016. CCFA (Comité
779 des Constructeurs Français d'Automobiles). [WWW Document]. URL
780 [http://temis.documentation.developpement-durable.gouv.fr/document.html?id=Temis-](http://temis.documentation.developpement-durable.gouv.fr/document.html?id=Temis-0000921)
781 [0000921](http://temis.documentation.developpement-durable.gouv.fr/document.html?id=Temis-0000921) (accessed 5.5.19).
- 782 Cecinato, A., Di Palo, V., Pomata, D., Tomasi Scianò, M.C., Possanzini, M., 2005.
783 Measurement of phase-distributed nitrophenols in Rome ambient air. *Chemosphere* 59, 679–
784 683. <https://doi.org/10.1016/j.chemosphere.2004.10.045>
- 785 CEN, 2017a. European Committee for Standardization, EN-16909: 2017 - Ambient air -
786 Measurement of elemental carbon (EC) and organic carbon (OC) collected on filters. CEN,
787 Brussels (Belgium).
- 788 CEN, 2017b. European Committee for Standardization, EN-16913: 2017 - Ambient air -
789 Standard method for measurement of NO_3^- , SO_4^{2-} , Cl^- , NH_4^+ , Na^+ , K^+ , Mg^{2+} , Ca^{2+} , in $\text{PM}_{2.5}$ as
790 deposited on filters. .CEN, Brussels (Belgium)
791
- 792 CEN, 2017c. European Committee for Standardization, EN-16450: 2017 - Ambient Air –
793 automated measuring systems for the measurement of the concentration of particulate matter
794 (PM_{10} , $\text{PM}_{2.5}$). CEN, Brussels (Belgium).
- 795 CEN, 2014. European Committee for Standardization, TS-16645: 2014- Ambient Air –
796 Method for the Measurement of Benz[a]anthracene, Benzo[b]fluoranthene,
797 Benzo[j]fluoranthene, Benzo[k]fluoranthene, Dibenz[a,h]anthracene, Indeno[1,2,3- cd]pyrene
798 et Benzo[ghi]perylene. CEN, Brussels (Belgium).
- 799 CEN, 2012a. European Committee for Standardization, EN-14625: 2012 - Ambient air -
800 Standard method for the measurement of the concentration of ozone by ultraviolet
801 photometry. CEN, Brussels (Belgium).
- 802 CEN, 2012b. European Committee for Standardization, EN-14211: 2012 - Ambient air -
803 Standard method for the measurement of the concentration of nitrogen dioxide and nitrogen
804 monoxide by chemiluminescence. CEN, Brussels (Belgium).
- 805 CEN, 2008. European Committee for Standardization, EN-15549: 2008 - Air Quality -
806 Standard Method for the Measurement of the Concentration of Benzo[a]pyrene in Air. CEN,
807 Brussels (Belgium).
- 808 CEN, 2005. European Committee for Standardization, EN-14902: 2005 - Ambient air -
809 Standard method for the measurement of Pb, Cd, As and Ni in the PM_{10} fraction of
810 suspended particulate matter. CEN, Brussels (Belgium).

- 811 Christoffersen, T.S., Hjorth, J., Horie, O., Jensen, N.R., Kotzias, D., Molander, L.L., Neeb, P.,
812 Ruppert, L., Winterhalter, R., Virkkula, A., Wirtz, K., Larsen, B.R., 1998. cis-pinic acid, a
813 possible precursor for organic aerosol formation from ozonolysis of α -pinene. *Atmos.*
814 *Environ.* 32, 1657–1661. [https://doi.org/10.1016/S1352-2310\(97\)00448-2](https://doi.org/10.1016/S1352-2310(97)00448-2)
- 815 Ciarelli, G., Aksoyoglu, S., Haddad, I.E., Bruns, E.A., Crippa, M., Poulain, L., Äijälä, M.,
816 Carbone, S., Freney, E., O'Dowd, C., Baltensperger, U., Prévôt, A.S.H., 2017. Modelling
817 winter organic aerosol at the European scale with CAMx: evaluation and source
818 apportionment with a VBS parameterization based on novel wood burning smog chamber
819 experiments. *Atmospheric Chem. Phys.* 17, 7653–7669.
820 <https://doi.org/https://doi.org/10.5194/acp-17-7653-2017>
- 821 Claeys, M., Szmigielski, R., Kourtchev, I., Van der Veken, P., Vermeylen, R., Maenhaut, W.,
822 Jaoui, M., Kleindienst, T.E., Lewandowski, M., Offenberg, J.H., Edney, E.O., 2007.
823 Hydroxydicarboxylic acids: markers for secondary organic aerosol from the photooxidation of
824 α -pinene. *Environ. Sci. Technol.* 41, 1628–1634. <https://doi.org/10.1021/es0620181>
- 825 Claeys, M., Wang, W., Ion, A.C., Kourtchev, I., Gelencsér, A., Maenhaut, W., 2004.
826 Formation of secondary organic aerosols from isoprene and its gas-phase oxidation products
827 through reaction with hydrogen peroxide. *Atmos. Environ.* 38, 4093–4098.
828 <https://doi.org/10.1016/j.atmosenv.2004.06.001>
- 829 Crippa, M., Canonaco, F., Lanz, V.A., Äijälä, M., Allan, J.D., Carbone, S., Capes, G.,
830 Ceburnis, D., Dall'Osto, M., Day, D.A., DeCarlo, P.F., Ehn, M., Eriksson, A., Freney, E.,
831 Hildebrandt Ruiz, L., Hillamo, R., Jimenez, J.L., Junninen, H., Kiendler-Scharr, A.,
832 Kortelainen, A.-M., Kulmala, M., Laaksonen, A., Mensah, A.A., Mohr, C., Nemitz, E.,
833 O'Dowd, C., Ovadnevaite, J., Pandis, S.N., Petäjä, T., Poulain, L., Saarikoski, S., Sellegri, K.,
834 Swietlicki, E., Tiitta, P., Worsnop, D.R., Baltensperger, U., Prévôt, A.S.H., 2014. Organic
835 aerosol components derived from 25 AMS data sets across Europe using a consistent ME-2
836 based source apportionment approach. *Atmospheric Chem. Phys.* 14, 6159–6176.
837 <https://doi.org/https://doi.org/10.5194/acp-14-6159-2014>
- 838 Crippa, M., Canonaco, F., Slowik, J.G., Haddad, I.E., DeCarlo, P.F., Mohr, C., Heringa, M.F.,
839 Chirico, R., Marchand, N., Temime-Roussel, B., Abidi, E., Poulain, L., Wiedensohler, A.,
840 Baltensperger, U., Prévôt, A.S.H., 2013a. Primary and secondary organic aerosol origin by
841 combined gas-particle phase source apportionment. *Atmospheric Chem. Phys.* 13, 8411–
842 8426. <https://doi.org/https://doi.org/10.5194/acp-13-8411-2013>
- 843 Crippa, M., DeCarlo, P.F., Slowik, J.G., Mohr, C., Heringa, M.F., Chirico, R., Poulain, L.,
844 Freutel, F., Sciare, J., Cozic, J., Marco, C.F.D., Elsasser, M., Nicolas, J.B., Marchand, N.,
845 Abidi, E., Wiedensohler, A., Drewnick, F., Schneider, J., Borrmann, S., Nemitz, E.,
846 Zimmermann, R., Jaffrezo, J.-L., Prévôt, A.S.H., Baltensperger, U., 2013b. Wintertime
847 aerosol chemical composition and source apportionment of the organic fraction in the
848 metropolitan area of Paris. *Atmospheric Chem. Phys.* 13, 961–981.
849 <https://doi.org/https://doi.org/10.5194/acp-13-961-2013>
- 850 Denier van der Gon, H. a. C., Bergström, R., Fountoukis, C., Johansson, C., Pandis, S.N.,
851 Simpson, D., Visschedijk, A.J.H., 2015. Particulate emissions from residential wood
852 combustion in Europe – revised estimates and an evaluation. *Atmospheric Chem. Phys.* 15,
853 6503–6519. <https://doi.org/https://doi.org/10.5194/acp-15-6503-2015>

- 854 Ding, X., Zhang, Y.-Q., He, Q.-F., Yu, Q.-Q., Shen, R.-Q., Zhang, Y., Zhang, Z., Lyu, S.-J.,
855 Hu, Q.-H., Wang, Y.-S., Li, L.-F., Song, W., Wang, X.-M., 2016. Spatial and seasonal
856 variations of secondary organic aerosol from terpenoids over China. *J. Geophys. Res.*
857 *Atmospheres* 121, 14,661–14,678. <https://doi.org/10.1002/2016JD025467>
- 858 Ding, X., Zheng, M., Yu, L., Zhang, X., Weber, R.J., Yan, B., Russell, A.G., Edgerton, E.S.,
859 Wang, X., 2008. Spatial and seasonal trends in biogenic secondary organic aerosol tracers and
860 water-soluble organic carbon in the southeastern United States. *Environ. Sci. Technol.* 42,
861 5171–5176.
- 862 Docherty, K.S., Stone, E.A., Ulbrich, I.M., DeCarlo, P.F., Snyder, D.C., Schauer, J.J., Peltier,
863 R.E., Weber, R.J., Murphy, S.M., Seinfeld, J.H., Grover, B.D., Eatough, D.J., Jimenez, J.L.,
864 2008. Apportionment of Primary and Secondary Organic Aerosols in Southern California
865 during the 2005 Study of Organic Aerosols in Riverside (SOAR-1). *Environ. Sci. Technol.*
866 42, 7655–7662. <https://doi.org/10.1021/es8008166>
- 867 Dommen, J., Metzger, A., Duplissy, J., Kalberer, M., Alfarra, M.R., Gascho, A., Weingartner,
868 E., Prevot, A.S.H., Verheggen, B., Baltensperger, U., 2006. Laboratory observation of
869 oligomers in the aerosol from isoprene/NO_x photooxidation. *Geophys. Res. Lett.* 33.
870 <https://doi.org/10.1029/2006GL026523>
- 871 Drinovec, L., Gregorič, A., Zotter, P., Wolf, R., Bruns, E.A., Prévôt, A.S.H., Petit, J.-E.,
872 Favez, O., Sciare, J., Arnold, I.J., Chakrabarty, R.K., Moosmüller, H., Filep, A., Močnik, G.,
873 2017. The filter-loading effect by ambient aerosols in filter absorption photometers depends
874 on the coating of the sampled particles. *Atmospheric Meas. Tech.* 10, 1043–1059.
875 <https://doi.org/https://doi.org/10.5194/amt-10-1043-2017>
- 876 Eddingsaas, N.C., Loza, C.L., Yee, L.D., Chan, M., Schilling, K.A., Chhabra, P.S., Seinfeld,
877 J.H., Wennberg, P.O., 2012. α -pinene photooxidation under controlled chemical conditions -
878 Part 2: SOA yield and composition in low- and high-NO_x environments. *Atmospheric Chem.*
879 *Phys.* 12, 7413–7427. <https://doi.org/https://doi.org/10.5194/acp-12-7413-2012>
- 880 Edney, E.O., Kleindienst, T.E., Jaoui, M., Lewandowski, M., Offenberg, J.H., Wang, W.,
881 Claeys, M., 2005. Formation of 2-methyl tetrols and 2-methylglyceric acid in secondary
882 organic aerosol from laboratory irradiated isoprene/NO_x/SO₂/air mixtures and their detection
883 in ambient PM_{2.5} samples collected in the eastern United States. *Atmos. Environ.* 39, 5281–
884 5289. <https://doi.org/10.1016/j.atmosenv.2005.05.031>
- 885 El Haddad, I., Marchand, N., Temime-Roussel, B., Wortham, H., Piot, C., Besombes, J.-L.,
886 Baduel, C., Voisin, D., Armengaud, A., Jaffrezo, J.-L., 2011. Insights into the secondary
887 fraction of the organic aerosol in a Mediterranean urban area: Marseille. *Atmospheric Chem.*
888 *Phys.* 11, 2059–2079. <https://doi.org/10.5194/acp-11-2059-2011>
- 889 Falkovich, A.H., Graber, E.R., Schkolnik, G., Rudich, Y., Maenhaut, W., Artaxo, P., 2004.
890 Low molecular weight organic acids in aerosol particles from Rondônia, Brazil, during the
891 biomass-burning, transition and wet periods. *Atmospheric Chem. Phys. Discuss.* 4, 6867–
892 6907.
- 893 Feng, J., Li, M., Zhang, P., Gong, S., Zhong, M., Wu, M., Zheng, M., Chen, C., Wang, H.,
894 Lou, S., 2013. Investigation of the sources and seasonal variations of secondary organic

- 895 aerosols in PM_{2.5} in Shanghai with organic tracers. *Atmos. Environ.* 79, 614–622.
896 <https://doi.org/10.1016/j.atmosenv.2013.07.022>
- 897 Forstner, H.J.L., Flagan, R.C., Seinfeld, J.H., 1997. Secondary Organic Aerosol from the
898 Photooxidation of Aromatic Hydrocarbons: Molecular Composition. *Environ. Sci. Technol.*
899 31, 1345–1358. <https://doi.org/10.1021/es9605376>
- 900 <https://doi.org/https://doi.org/10.5194/acp-10-2663-2010>
- 901 Goriaux, M., Jourdain, B., Temime, B., Besombes, J.-L., Marchand, N., Albinet, A., Leoz-
902 Garziandia, E., Wortham, H., 2006. Field Comparison of Particulate PAH Measurements
903 Using a Low-Flow Denuder Device and Conventional Sampling Systems. *Environ. Sci.*
904 *Technol.* 40, 6398–6404. <https://doi.org/10.1021/es060544m>
- 905 Guenther, A., 1997. Seasonal and Spatial Variations in Natural Volatile Organic Compound
906 Emissions. *Ecol. Appl.* 7, 34–45. [https://doi.org/10.1890/1051-0761\(1997\)007\[0034:SASVIN\]2.0.CO;2](https://doi.org/10.1890/1051-0761(1997)007[0034:SASVIN]2.0.CO;2)
- 908 Guenther, A., Karl, T., Harley, P., Wiedinmyer, C., Palmer, P.I., Geron, C., 2006. Estimates
909 of global terrestrial isoprene emissions using MEGAN (Model of Emissions of Gases and
910 Aerosols from Nature). *Atmospheric Chem. Phys.* 6, 3181–3210. <https://doi.org/10.5194/acp-6-3181-2006>
- 912 Guinot, B., Cachier, H., Sciare, J., Tong, Y., Xin, W., Jianhua, Y., 2007. Beijing aerosol:
913 Atmospheric interactions and new trends. *J. Geophys. Res. Atmospheres* 112.
914 <https://doi.org/10.1029/2006JD008195>
- 915 Haeffelin, M., Barthès, L., Bock, O., Boitel, C., Bony, S., Bouniol, D., Chepfer, H., Chiriaco,
916 M., Cuesta, J., Delanoë, J., Drobinski, P., Dufresne, J.-L., Flamant, C., Grall, M., Hodzic, A.,
917 Hourdin, F., Lapouge, F., Lemaître, Y., Mathieu, A., Morille, Y., Naud, C., Noël, V.,
918 O'Hirok, W., Pelon, J., Pietras, C., Protat, A., Romand, B., Scialom, G., Vautard, R., 2005.
919 SIRTA, a ground-based atmospheric observatory for cloud and aerosol research. *Ann.*
920 *Geophys.* 23, 253–275.
- 921 Hallquist, M., Wenger, J.C., Baltensperger, U., Rudich, Y., Simpson, D., Claeys, M.,
922 Dommen, J., Donahue, N.M., George, C., Goldstein, A.H., Hamilton, J.F., Herrmann, H.,
923 Hoffmann, T., Iinuma, Y., Jang, M., Jenkin, M.E., Jimenez, J.L., Kiendler-Scharr, A.,
924 Maenhaut, W., McFiggans, G., Mentel, T.F., Monod, A., Prevot, A.S.H., Seinfeld, J.H.,
925 Surratt, J.D., Szmigielski, R., Wildt, J., 2009. The formation, properties and impact of
926 secondary organic aerosol: current and emerging issues. *Atmos Chem Phys* 9, 5155–5236.
927 <https://doi.org/10.5194/acp-9-5155-2009>
- 928 Hantson, S., Knorr, W., Schurgers, G., Pugh, T.A.M., Arneth, A., 2017. Global isoprene and
929 monoterpene emissions under changing climate, vegetation, CO₂ and land use. *Atmos.*
930 *Environ.* 155, 35–45. <https://doi.org/10.1016/j.atmosenv.2017.02.010>
- 931 Harrison, M.A.J., Barra, S., Borghesi, D., Vione, D., Arsene, C., Iulian Olariu, R., 2005a.
932 Nitrated phenols in the atmosphere: a review. *Atmos. Environ.* 39, 231–248.
933 <https://doi.org/10.1016/j.atmosenv.2004.09.044>

- 934 Harrison, M.A.J., Heal, M.R., Cape, J.N., 2005b. Evaluation of the pathways of tropospheric
935 nitrophenol formation from benzene and phenol using a multiphase model. *Atmospheric*
936 *Chem. Phys.* 5, 1679–1695. <https://doi.org/https://doi.org/10.5194/acp-5-1679-2005>
- 937 Hatakeyama, S., Ohno, M., Weng, J., Takagi, H., Akimoto, H., 1987. Mechanism for the
938 formation of gaseous and particulate products from ozone-cycloalkene reactions in air.
939 *Environ. Sci. Technol.* 21, 52–57. <https://doi.org/10.1021/es00155a005>
- 940 Heal, M.R., Kumar, P., Harrison, R.M., 2012. Particles, air quality, policy and health. *Chem.*
941 *Soc. Rev.* 41, 6606. <https://doi.org/10.1039/c2cs35076a>
- 942 Hu, D., Bian, Q., Li, T.W.Y., Lau, A.K.H., Yu, J.Z., 2008. Contributions of isoprene,
943 monoterpene, β -caryophyllene, and toluene to secondary organic aerosols in Hong Kong
944 during the summer of 2006. *J. Geophys. Res.* 113. <https://doi.org/10.1029/2008JD010437>
- 945 Huang, R.-J., Zhang, Y., Bozzetti, C., Ho, K.-F., Cao, J.-J., Han, Y., Daellenbach, K.R.,
946 Slowik, J.G., Platt, S.M., Canonaco, F., Zotter, P., Wolf, R., Pieber, S.M., Bruns, E.A.,
947 Crippa, M., Ciarelli, G., Piazzalunga, A., Schwikowski, M., Abbaszade, G., Schnelle-Kreis,
948 J., Zimmermann, R., An, Z., Szidat, S., Baltensperger, U., Haddad, I.E., Prévôt, A.S.H., 2014.
949 High secondary aerosol contribution to particulate pollution during haze events in China.
950 *Nature* 514, 218–222. <https://doi.org/10.1038/nature13774>
- 951 Huisman, A.J., Krieger, U.K., Zuend, A., Marcolli, C., Peter, T., 2013. Vapor pressures of
952 substituted polycarboxylic acids are much lower than previously reported. *Atmospheric*
953 *Chem. Phys.* 13, 6647–6662. <https://doi.org/10.5194/acp-13-6647-2013>
- 954 Iinuma, Y., Böge, O., Gräfe, R., Herrmann, H., 2010. Methyl-nitrocatechols: atmospheric
955 tracer compounds for biomass burning secondary organic aerosols. *Environ. Sci. Technol.* 44,
956 8453–8459. <https://doi.org/10.1021/es102938a>
- 957 IPCC, 2018. *Climate Change 2013: The Physical Science Basis. Contribution of Working*
958 *Group I to the Fifth Assessment Report of the Intergovernmental Panel on Climate Change.*
959 [Stocker, T.F., D. Qin, G.-K. Plattner, M. Tignor, S.K. Allen, J. Boschung, A. Nauels, Y. Xia,
960 V. Bex and P.M. Midgley (eds.)]. Cambridge University Press. Cambridge, United Kingdom
961 and New York, NY, USA.
- 962 Isaacman-VanWertz, G., Yee, L.D., Kreisberg, N.M., Wernis, R., Moss, J.A., Hering, S.V., de
963 Sá, S.S., Martin, S.T., Alexander, M.L., Palm, B.B., Hu, W., Campuzano-Jost, P., Day, D.A.,
964 Jimenez, J.L., Riva, M., Surratt, J.D., Viegas, J., Manzi, A., Edgerton, E., Baumann, K.,
965 Souza, R., Artaxo, P., Goldstein, A.H., 2016. Ambient Gas-Particle Partitioning of Tracers for
966 Biogenic Oxidation. *Environ. Sci. Technol.* 50, 9952–9962.
967 <https://doi.org/10.1021/acs.est.6b01674>
- 968 Jang, M., Kamens, R.M., 1999. Newly characterized products and composition of secondary
969 aerosols from the reaction of α -pinene with ozone. *Atmos. Environ.* 33, 459–474.
970 [https://doi.org/10.1016/S1352-2310\(98\)00222-2](https://doi.org/10.1016/S1352-2310(98)00222-2)
- 971 Jaoui, M., Kleindienst, T.E., Lewandowski, M., Offenberg, J.H., Edney, E.O., 2005.
972 Identification and Quantification of Aerosol Polar Oxygenated Compounds Bearing
973 Carboxylic or Hydroxyl Groups. 2. Organic Tracer Compounds from Monoterpenes. *Environ.*
974 *Sci. Technol.* 39, 5661–5673. <https://doi.org/10.1021/es048111b>

- 975 Jaoui, M., Lewandowski, M., Kleindienst, T.E., Offenberg, J.H., Edney, E.O., 2007. β -
976 caryophyllinic acid: An atmospheric tracer for β -caryophyllene secondary organic aerosol.
977 *Geophys. Res. Lett.* 34. <https://doi.org/10.1029/2006GL028827>
- 978 Kahnt, A., Behrouzi, S., Vermeylen, R., Safi Shalamzari, M., Vercauteren, J., Roekens, E.,
979 Claeys, M., Maenhaut, W., 2013. One-year study of nitro-organic compounds and their
980 relation to wood burning in PM10 aerosol from a rural site in Belgium. *Atmos. Environ.* 81,
981 561–568. <https://doi.org/10.1016/j.atmosenv.2013.09.041>
- 982 Kanakidou, M., Seinfeld, J.H., Pandis, S.N., Barnes, I., Dentener, F.J., Facchini, M.C.,
983 Dingenen, R.V., Ervens, B., Nenes, A., Nielsen, C.J., 2005. Organic aerosol and global
984 climate modelling: a review. *Atmospheric Chem. Phys.* 5, 1053–1123.
985 <https://doi.org/10.5194/acp-5-1053-2005>
- 986 Kawamura, K., Kaplan, I.R., 1987. Motor exhaust emissions as a primary source for
987 dicarboxylic acids in Los Angeles ambient air. *Environ. Sci. Technol.* 21, 105–110.
988 <https://doi.org/10.1021/es00155a014>
- 989 Keyte, I.J., Albinet, A., Harrison, R.M., 2016. On-road traffic emissions of polycyclic
990 aromatic hydrocarbons and their oxy- and nitro- derivative compounds measured in road
991 tunnel environments. *Sci. Total Environ.* 566–567, 1131–1142.
992 <https://doi.org/10.1016/j.scitotenv.2016.05.152>
- 993 Kim Y., Sartelet K., Couvidat F., 2019. Modeling the effect of non-ideality, dynamic mass
994 transfer and viscosity on SOA formation in a 3-D air quality model. *Atmos. Chem. Phys.*, 19,
995 1241–1261. <https://doi.org/10.5194/acp-19-1241-2019>
- 996
997 Kitanovski, Z., Grgić, I., Vermeylen, R., Claeys, M., Maenhaut, W., 2012. Liquid
998 chromatography tandem mass spectrometry method for characterization of monoaromatic
999 nitro-compounds in atmospheric particulate matter. *J. Chromatogr. A* 1268, 35–43.
1000 <https://doi.org/10.1016/j.chroma.2012.10.021>
- 1001 Kleindienst, T.E., Conner, T.S., McIver, C.D., Edney, E.O., 2004. Determination of
1002 secondary organic aerosol products from the photooxidation of toluene and their implications
1003 in ambient PM 2.5. *J. Atmospheric Chem.* 47, 79–100.
1004 <https://doi.org/10.1023/B:JOCH.0000012305.94498.28>
- 1005 Kleindienst, T.E., Jaoui, M., Lewandowski, M., Offenberg, J.H., Docherty, K.S., 2012. The
1006 formation of SOA and chemical tracer compounds from the photooxidation of naphthalene
1007 and its methyl analogs in the presence and absence of nitrogen oxides. *Atmospheric Chem.*
1008 *Phys.* 12, 8711–8726. <https://doi.org/10.5194/acp-12-8711-2012>
- 1009 Kleindienst, T.E., Jaoui, M., Lewandowski, M., Offenberg, J.H., Lewis, C.W., Bhave, P.V.,
1010 Edney, E.O., 2007a. Estimates of the contributions of biogenic and anthropogenic
1011 hydrocarbons to secondary organic aerosol at a southeastern US location. *Atmos. Environ.* 41,
1012 8288–8300. <https://doi.org/10.1016/j.atmosenv.2007.06.045>
- 1013 Kleindienst, T.E., Jaoui, M., Lewandowski, M., Offenberg, J.H., Lewis, C.W., Bhave, P.V.,
1014 Edney, E.O., 2007b. Estimates of the contributions of biogenic and anthropogenic
1015 hydrocarbons to secondary organic aerosol at a southeastern US location. *Atmos. Environ.* 41,
1016 8288–8300. <https://doi.org/10.1016/j.atmosenv.2007.06.045>

- 1017 Kostenidou, E., Karnezi, E., Kolodziejczyk, A., Szmigielski, R., Pandis, S.N., 2018. Physical
1018 and Chemical Properties of 3-Methyl-1,2,3-butanetricarboxylic Acid (MBTCA) Aerosol.
1019 *Environ. Sci. Technol.* 52, 1150–1155. <https://doi.org/10.1021/acs.est.7b04348>
- 1020 Kourtchev, I., Warnke, J., Maenhaut, W., Hoffmann, T., Claeys, M., 2008. Polar organic
1021 marker compounds in PM_{2.5} aerosol from a mixed forest site in western Germany.
1022 *Chemosphere* 73, 1308–1314. <https://doi.org/10.1016/j.chemosphere.2008.07.011>
- 1023 Kristensen, K., Bilde, M., Aalto, P.P., Petäjä, T., Glasius, M., 2016. Denuder/filter sampling
1024 of organic acids and organosulfates at urban and boreal forest sites: Gas/particle distribution
1025 and possible sampling artifacts. *Atmos. Environ., Chemical Characterization of Secondary
1026 Organic Aerosol - Dedication to Professor Claeys* 130, 36–53.
1027 <https://doi.org/10.1016/j.atmosenv.2015.10.046>
- 1028 Kroll, J.H., Ng, N.L., Murphy, S.M., Flagan, R.C., Seinfeld, J.H., 2006. Secondary Organic
1029 Aerosol Formation from Isoprene Photooxidation. *Environ. Sci. Technol.* 40, 1869–1877.
1030 <https://doi.org/10.1021/es0524301>
- 1031 Kroll, J.H., Seinfeld, J.H., 2008. Chemistry of secondary organic aerosol: Formation and
1032 evolution of low-volatility organics in the atmosphere. *Atmos. Environ.* 42, 3593–3624.
1033 <https://doi.org/10.1016/j.atmosenv.2008.01.003>
- 1034 Lai, C., Liu, Y., Ma, J., Ma, Q., Chu, B., He, H., 2015. Heterogeneous Kinetics of cis-Pinonic
1035 Acid with Hydroxyl Radical under Different Environmental Conditions. *J. Phys. Chem. A*
1036 119, 6583–6593. <https://doi.org/10.1021/acs.jpca.5b01321>
- 1037 Lewandowski, M., Jaoui, M., Offenberg, J.H., Kleindienst, T.E., Edney, E.O., Sheesley, R.J.,
1038 Schauer, J.J., 2008. Primary and secondary contributions to ambient PM in the midwestern
1039 United States. *Environ. Sci. Technol.* 42, 3303–3309. <https://doi.org/10.1021/es0720412>
- 1040 Limbeck, A., Puxbaum, H., Otter, L., Scholes, M.C., 2001. Semivolatile behavior of
1041 dicarboxylic acids and other polar organic species at a rural background site (Nylsvley, RSA).
1042 *Atmos. Environ.* 35, 1853–1862. [https://doi.org/10.1016/S1352-2310\(00\)00497-0](https://doi.org/10.1016/S1352-2310(00)00497-0)
- 1043 Lin, Y.-H., Zhang, H., Pye, H.O.T., Zhang, Z., Marth, W.J., Park, S., Arashiro, M., Cui, T.,
1044 Budisulistiorini, S.H., Sexton, K.G., Vizuete, W., Xie, Y., Luecken, D.J., Piletic, I.R., Edney,
1045 E.O., Bartolotti, L.J., Gold, A., Surratt, J.D., 2013. Epoxide as a precursor to secondary
1046 organic aerosol formation from isoprene photooxidation in the presence of nitrogen oxides.
1047 *Proc. Natl. Acad. Sci.* 110, 6718–6723. <https://doi.org/10.1073/pnas.1221150110>
- 1048 Liu, Y., Wu, Z., Huang, X., Shen, H., Bai, Y., Qiao, K., Meng, X., Hu, W., Tang, M., He, L.,
1049 2019. Aerosol Phase State and Its Link to Chemical Composition and Liquid Water Content
1050 in a Subtropical Coastal Megacity. *Environ. Sci. Technol.* 53 (9), 5027–5033.
1051 <https://doi.org/10.1021/acs.est.9b01196>
- 1052
1053 Lu, C., Wang, X., Li, R., Gu, R., Zhang, Y., Li, W., Gao, R., Chen, B., Xue, L., Wang, W.,
1054 2019. Emissions of fine particulate nitrated phenols from residential coal combustion in
1055 China. *Atmos. Environ.* 203, 10–17. <https://doi.org/10.1016/j.atmosenv.2019.01.047>
- 1056 Lutz, A., Mohr, C., Le Breton, M., Lopez-Hilfiker, F.D., Priestley, M., Thornton, J.A.,
1057 Hallquist, M., 2019. Gas to Particle Partitioning of Organic Acids in the Boreal Atmosphere.
1058 *ACS Earth Space Chem.* 3, 1279–1287. <https://doi.org/10.1021/acsearthspacechem.9b00041>

- 1059 Mader, B.T., Pankow, J.F., 2001. Gas/Solid Partitioning of Semivolatile Organic Compounds
1060 (SOCs) to Air Filters. 3. An Analysis of Gas Adsorption Artifacts in Measurements of
1061 Atmospheric SOCs and Organic Carbon (OC) When Using Teflon Membrane Filters and
1062 Quartz Fiber Filters. *Environ. Sci. Technol.* 35, 3422–3432.
1063 <https://doi.org/10.1021/es0015951>
- 1064 Mbengue, S., Alleman, L.Y., Flament, P., 2014. Size-distributed metallic elements in
1065 submicronic and ultrafine atmospheric particles from urban and industrial areas in northern
1066 France. *Atmospheric Res.* 135–136, 35–47. <https://doi.org/10.1016/j.atmosres.2013.08.010>
- 1067 Météo-France, 2015. Octobre 2015 [WWW Document]. URL <http://www.meteofrance.fr/>
1068 (accessed 6.14.19).
- 1069 Mkoma, S.L., Kawamura, K., 2013. Molecular composition of dicarboxylic acids,
1070 ketocarboxylic acids, α -dicarbonyls and fatty acids in atmospheric aerosols from Tanzania,
1071 East Africa during wet and dry seasons. *Atmospheric Chem. Phys.* 13, 2235–2251.
1072 <https://doi.org/https://doi.org/10.5194/acp-13-2235-2013>
- 1073 Mochida, M., Kawamura, K., Umemoto, N., Kobayashi, M., Matsunaga, S., Lim, H.-J.,
1074 Turpin, B.J., Bates, T.S., Simoneit, B.R.T., 2003. Spatial distributions of oxygenated organic
1075 compounds (dicarboxylic acids, fatty acids, and levoglucosan) in marine aerosols over the
1076 western Pacific and off the coast of East Asia: Continental outflow of organic aerosols during
1077 the ACE-Asia campaign. *J. Geophys. Res. Atmospheres* 108.
1078 <https://doi.org/10.1029/2002JD003249>
- 1079 Müller, L., Reinnig, M.-C., Naumann, K.H., Saathoff, H., Mentel, T.F., Donahue, N.M.,
1080 Hoffmann, T., 2012. Formation of 3-methyl-1,2,3-butanetricarboxylic acid via gas phase
1081 oxidation of pinonic acid – a mass spectrometric study of SOA aging. *Atmospheric Chem.*
1082 *Phys.* 12, 1483–1496. <https://doi.org/10.5194/acp-12-1483-2012>
- 1083 Mutzel, A., Rodigast, M., Iinuma, Y., Böge, O., Herrmann, H., 2016. Monoterpene SOA –
1084 Contribution of first-generation oxidation products to formation and chemical composition.
1085 *Atmos. Environ.* 130, 136–144. <https://doi.org/10.1016/j.atmosenv.2015.10.080>
- 1086 Nalin, F., Golly, B., Besombes, J.-L., Pelletier, C., Aujay-Plouzeau, R., Verlhac, S.,
1087 Dermigny, A., Fievet, A., Karoski, N., Dubois, P., Collet, S., Favez, O., Albinet, A., 2016.
1088 Fast oxidation processes from emission to ambient air introduction of aerosol emitted by
1089 residential log wood stoves. *Atmos. Environ.* 143, 15–26.
1090 <https://doi.org/10.1016/j.atmosenv.2016.08.002>
- 1091 Nozière, B., Kalberer, M., Claeys, M., Allan, J., D’Anna, B., Decesari, S., Finessi, E.,
1092 Glasius, M., Grgić, I., Hamilton, J.F., Hoffmann, T., Iinuma, Y., Jaoui, M., Kahnt, A., Kampf,
1093 C.J., Kourtchev, I., Maenhaut, W., Marsden, N., Saarikoski, S., Schnelle-Kreis, J., Surratt,
1094 J.D., Szidat, S., Szmigielski, R., Wisthaler, A., 2015. The Molecular Identification of Organic
1095 Compounds in the Atmosphere: State of the Art and Challenges. *Chem. Rev.* 115, 3919–3983.
1096 <https://doi.org/10.1021/cr5003485>
- 1097 Oderbolz, D.C., Aksoyoglu, S., Keller, J., Barmpadimos, I., Steinbrecher, R., Skjøth, C.A.,
1098 Plaß-Dülmer, C., Prévôt, A.S.H., 2013. A comprehensive emission inventory of biogenic
1099 volatile organic compounds in Europe: improved seasonality and land-cover. *Atmospheric*
1100 *Chem. Phys.* 13, 1689–1712. <https://doi.org/https://doi.org/10.5194/acp-13-1689-2013>

- 1101 Petit, J.-E., Amodeo, T., Meleux, F., Bessagnet, B., Menut, L., Grenier, D., Pellan, Y., Ockler,
1102 A., Rocq, B., Gros, V., Sciare, J., Favez, O., 2017. Characterising an intense PM pollution
1103 episode in March 2015 in France from multi-site approach and near real time data:
1104 Climatology, variabilities, geographical origins and model evaluation. *Atmos. Environ.* 155,
1105 68–84. <https://doi.org/10.1016/j.atmosenv.2017.02.012>
- 1106 Petit, J.-E., Favez, O., Sciare, J., Canonaco, F., Croteau, P., Močnik, G., Jayne, J., Worsnop,
1107 D., Leoz-Garziandia, E., 2014. Submicron aerosol source apportionment of wintertime
1108 pollution in Paris, France by double positive matrix factorization (PMF²) using an aerosol
1109 chemical speciation monitor (ACSM) and a multi-wavelength Aethalometer. *Atmospheric*
1110 *Chem. Phys.* 14, 13773–13787. <https://doi.org/https://doi.org/10.5194/acp-14-13773-2014>
- 1111 Presto, A.A., Huff Hartz, K.E., Donahue, N.M., 2005. Secondary Organic Aerosol Production
1112 from Terpene Ozonolysis. 2. Effect of NO_x Concentration. *Environ. Sci. Technol.* 39, 7046–
1113 7054. <https://doi.org/10.1021/es050400s>
- 1114 Puxbaum, H., Caseiro, A., Sánchez-Ochoa, A., Kasper-Giebl, A., Claeys, M., Gelencsér, A.,
1115 Legrand, M., Preunkert, S., Pio, C.A., 2007. Levoglucosan levels at background sites in
1116 Europe for assessing the impact of biomass combustion on the European aerosol background.
1117 *J. Geophys. Res. Space Phys.* 112, D23S05. <https://doi.org/10.1029/2006JD008114>
- 1118 Pye HOT, Murphy BN, Xu L, Ng NL, Carlton AG, Guo H, Weber R, Vasilakos P, Appel
1119 KW, Budisulistiorini SH, Surratt JD, Nenes A, Hu W, Jimenez JL, Isaacman-VanWertz G,
1120 Misztal PK, Goldstein AH., 2017. On the implications of aerosol liquid water and phase
1121 separation for organic aerosol mass. *Atmos Chem Phys.* 17(1):343-369.
1122 <https://doi.org/10.5194/acp-17-343-2017>.
1123
- 1124 Rutter, A.P., Snyder, D.C., Stone, E.A., Shelton, B., DeMinter, J., Schauer, J.J., 2014.
1125 Preliminary assessment of the anthropogenic and biogenic contributions to secondary organic
1126 aerosols at two industrial cities in the upper Midwest. *Atmos. Environ.* 84, 307–313.
1127 <https://doi.org/10.1016/j.atmosenv.2013.11.014>
- 1128 Samaké, A., Jaffrezo, J.-L., Favez, O., Weber, S., Jacob, V., Albinet, A., Riffault, V., Perdrix,
1129 E., Waked, A., Golly, B., Salameh, D., Chevrier, F., Oliveira, D.M., Bonnaire, N., Besombes,
1130 J.-L., Martins, J.M.F., Conil, S., Guillaud, G., Mesbah, B., Rocq, B., Robic, P.-Y., Hulin, A.,
1131 Meur, S.L., Descheemaeker, M., Chretien, E., Marchand, N., Uzu, G., 2019a. Polyols and
1132 glucose particulate species as tracers of primary biogenic organic aerosols at 28 French sites.
1133 *Atmospheric Chem. Phys.* 19, 3357–3374. <https://doi.org/https://doi.org/10.5194/acp-19-3357-2019>
1134
- 1135 Samaké, A., Jaffrezo, J.-L., Favez, O., Weber, S., Jacob, V., Canete, T., Albinet, A., Charron,
1136 A., Riffault, V., Perdrix, E., Waked, A., Golly, B., Salameh, D., Chevrier, F., Oliveira, D.M.,
1137 Besombes, J.-L., Martins, J.M.F., Bonnaire, N., Conil, S., Guillaud, G., Mesbah, B., Rocq, B.,
1138 Robic, P.-Y., Hulin, A., Le Meur, S., Descheemaeker, M., Chretien, E., Marchand, N., Uzu,
1139 G., 2019b. Arabitol, mannitol and glucose as tracers of primary biogenic organic aerosol:
1140 influence of environmental factors on ambient air concentrations and spatial distribution over
1141 France. *Atmospheric Chem. Phys. Discuss.* 1–24. <https://doi.org/10.5194/acp-2019-434>
- 1142 Sandradewi, J., Prévôt, A.S.H., Alfarra, M.R., Szidat, S., Wehrli, M.N., Ruff, M., Weimer, S.,
1143 Lanz, V.A., Weingartner, E., Perron, N., 2008. Comparison of several wood smoke markers

- 1144 and source apportionment methods for wood burning particulate mass. *Atmospheric Chem.*
1145 *Phys. Discuss.* 8, 8091–8118.
- 1146 Sarrafzadeh, M., Wildt, J., Pullinen, I., Springer, M., Kleist, E., Tillmann, R., Schmitt, S.H.,
1147 Wu, C., Mentel, T.F., Zhao, D., Hastie, D.R., Kiendler-Scharr, A., 2016. Impact of NO_x and
1148 OH on secondary organic aerosol formation from β -pinene photooxidation. *Atmospheric*
1149 *Chem. Phys.* 16, 11237–11248. <https://doi.org/https://doi.org/10.5194/acp-16-11237-2016>
- 1150 Saxena, P., Hildemann, L.M., 1996. Water-soluble organics in atmospheric particles: A
1151 critical review of the literature and application of thermodynamics to identify candidate
1152 compounds. *J. Atmospheric Chem.* 24, 57–109. <https://doi.org/10.1007/BF00053823>
- 1153 Schauer, J.J., Rogge, W.F., Hildemann, L.M., Mazurek, M.A., Cass, G.R., Simoneit, B.R.T.,
1154 1996. Source apportionment of airborne particulate matter using organic compounds as
1155 tracers. *Atmos. Environ.* 30, 3837–3855. [https://doi.org/10.1016/1352-2310\(96\)00085-4](https://doi.org/10.1016/1352-2310(96)00085-4)
- 1156 Schulte, J.K., Fox, J.R., Oron, A.P., Larson, T.V., Simpson, C.D., Paulsen, M., Beaudet, N.,
1157 Kaufman, J.D., Magzamen, S., 2015. Neighborhood-Scale Spatial Models of Diesel Exhaust
1158 Concentration Profile Using 1-Nitropyrene and Other Nitroarenes. *Environ. Sci. Technol.* 49,
1159 13422–13430. <https://doi.org/10.1021/acs.est.5b03639>
- 1160 Sciare, J., d'Argouges, O., Sarda-Estève, R., Gaimoz, C., Dolgorouky, C., Bonnaire, N.,
1161 Favez, O., Bonsang, B., Gros, V., 2011. Large contribution of water-insoluble secondary
1162 organic aerosols in the region of Paris (France) during wintertime. *J. Geophys. Res.*
1163 *Atmospheres* 116. <https://doi.org/10.1029/2011JD015756>
- 1164 Shahpoury, P., Lammel, G., Albinet, A., Sofuoglu, A., Dumanoglu, Y., Sofuoglu, S. C.,
1165 Wagner, Z. and Zdimial, V., 2016. Evaluation of a conceptual model for gas-particle
1166 partitioning of polycyclic aromatic hydrocarbons using poly-parameter linear free energy
1167 relationships, *Environ. Sci. Technol.*, 50, 22, 12312-12319.
1168 <https://doi.org/10.1021/acs.est.6b02158>.
- 1169
- 1170 Sheesley, R.J., Schauer, J.J., Bean, E., Kenski, D., 2004. Trends in Secondary Organic
1171 Aerosol at a Remote Site in Michigan's Upper Peninsula. *Environ. Sci. Technol.* 38, 6491–
1172 6500. <https://doi.org/10.1021/es049104q>
- 1173 Shrivastava, M.K., Subramanian, R., Rogge, W.F., Robinson, A.L., 2007. Sources of organic
1174 aerosol: Positive matrix factorization of molecular marker data and comparison of results
1175 from different source apportionment models. *Atmos. Environ.* 41, 9353–9369.
1176 <https://doi.org/10.1016/j.atmosenv.2007.09.016>
- 1177 Simoneit, B.R., Schauer, J.J., Nolte, C.G., Oros, D.R., Elias, V.O., Fraser, M.P., Rogge, W.F.,
1178 Cass, G.R., 1999. Levoglucosan, a tracer for cellulose in biomass burning and atmospheric
1179 particles. *Atmos. Environ.* 33, 173–182.
- 1180 Simpson, D., Guenther, A., Hewitt, C.N., Steinbrecher, R., 1995. Biogenic emissions in
1181 Europe: 1. Estimates and uncertainties. *J. Geophys. Res. Atmospheres* 100, 22875–22890.
1182 <https://doi.org/10.1029/95JD02368>
- 1183 Srivastava, D., Favez, O., Bonnaire, N., Lucarelli, F., Haeffelin, M., Perraudin, E., Gros, V.,
1184 Villenave, E., Albinet, A., 2018a. Speciation of organic fractions does matter for aerosol

- 1185 source apportionment. Part 2: Intensive short-term campaign in the Paris area (France). *Sci.*
1186 *Total Environ.* 634, 267–278. <https://doi.org/10.1016/j.scitotenv.2018.03.296>
- 1187 Srivastava, D., Favez, O., Perraudin, E., Villenave, E., Albinet, A., 2018b. Comparison of
1188 Measurement-Based Methodologies to Apportion Secondary Organic Carbon (SOC) in PM_{2.5}:
1189 A Review of Recent Studies. *Atmosphere* 9, 452. <https://doi.org/10.3390/atmos9110452>
- 1190 Srivastava, D., Favez, O., Petit, J.-E., Zhang, Y., Sofowote, U.M., Hopke, P.K., Bonnaire, N.,
1191 Perraudin, E., Gros, V., Villenave, E., Albinet, A., 2019. Speciation of organic fractions does
1192 matter for aerosol source apportionment. Part 3: Combining off-line and on-line
1193 measurements. *Sci. Total Environ.* 690, 944–955.
1194 <https://doi.org/10.1016/j.scitotenv.2019.06.378>
- 1195 Srivastava, D., Tomaz, S., Favez, O., Lanzafame, G.M., Golly, B., Besombes, J.-L., Alleman,
1196 L.Y., Jaffrezo, J.-L., Jacob, V., Perraudin, E., Villenave, E., Albinet, A., 2018c. Speciation of
1197 organic fraction does matter for source apportionment. Part 1: A one-year campaign in
1198 Grenoble (France). *Sci. Total Environ.* 624, 1598–1611.
1199 <https://doi.org/10.1016/j.scitotenv.2017.12.135>
- 1200 Steinbrecher, R., Smiatek, G., Köble, R., Seufert, G., Theloke, J., Hauff, K., Ciccioli, P.,
1201 Vautard, R., Curci, G., 2009. Intra- and inter-annual variability of VOC emissions from
1202 natural and semi-natural vegetation in Europe and neighbouring countries. *Atmos. Environ.*,
1203 Natural and Biogenic Emissions of Environmentally Relevant Atmospheric Trace
1204 Constituents in Europe 43, 1380–1391. <https://doi.org/10.1016/j.atmosenv.2008.09.072>
- 1205 Surratt, J.D., Chan, A.W.H., Eddingsaas, N.C., Chan, M., Loza, C.L., Kwan, A.J., Hersey,
1206 S.P., Flagan, R.C., Wennberg, P.O., Seinfeld, J.H., 2010. Reactive intermediates revealed in
1207 secondary organic aerosol formation from isoprene. *Proc. Natl. Acad. Sci.* 107, 6640–6645.
1208 <https://doi.org/10.1073/pnas.0911114107>
- 1209 Surratt, J.D., Murphy, S.M., Kroll, J.H., Ng, N.L., Hildebrandt, L., Sorooshian, A.,
1210 Szmigielski, R., Vermeylen, R., Maenhaut, W., Claeys, M., Flagan, R.C., Seinfeld, J.H.,
1211 2006. Chemical Composition of Secondary Organic Aerosol Formed from the Photooxidation
1212 of Isoprene. *J. Phys. Chem. A* 110, 9665–9690. <https://doi.org/10.1021/jp061734m>
- 1213 Szmigielski, R., Surratt, J.D., Gómez-González, Y., Van der Veken, P., Kourtchev, I.,
1214 Vermeylen, R., Blockhuys, F., Jaoui, M., Kleindienst, T.E., Lewandowski, M., Offenberg,
1215 J.H., Edney, E.O., Seinfeld, J.H., Maenhaut, W., Claeys, M., 2007. 3-methyl-1,2,3-
1216 butanetricarboxylic acid: An atmospheric tracer for terpene secondary organic aerosol.
1217 *Geophys. Res. Lett.* 34. <https://doi.org/10.1029/2007GL031338>
- 1218 Tarvainen, V., Hakola, H., Hellén, H., Bäck, J., Hari, P., Kulmala, M., 2005. Temperature and
1219 light dependence of the VOC emissions of Scots pine. *Atmospheric Chem. Phys.* 5, 989–998.
1220 <https://doi.org/https://doi.org/10.5194/acp-5-989-2005>
- 1221 Thompson, S.L., Yatavelli, R.L.N., Stark, H., Kimmel, J.R., Krechmer, J.E., Day, D.A., Hu,
1222 W., Isaacman-VanWertz, G., Yee, L., Goldstein, A.H., Khan, M.A.H., Holzinger, R.,
1223 Kreisberg, N., Lopez-Hilfiker, F.D., Mohr, C., Thornton, J.A., Jayne, J.T., Canagaratna, M.,
1224 Worsnop, D.R., Jimenez, J.L., 2017. Field intercomparison of the gas/particle partitioning of
1225 oxygenated organics during the Southern Oxidant and Aerosol Study (SOAS) in 2013.
1226 *Aerosol Sci. Technol.* 51, 30–56. <https://doi.org/10.1080/02786826.2016.1254719>

- 1227 Tomaz, S., Shahpoury, P., Jaffrezo, J.-L., Lammel, G., Perraudin, E., Villenave, E., Albinet,
1228 A., 2016. One-year study of polycyclic aromatic compounds at an urban site in Grenoble
1229 (France): Seasonal variations, gas/particle partitioning and cancer risk estimation. *Sci. Total*
1230 *Environ.* 565, 1071–1083. <https://doi.org/10.1016/j.scitotenv.2016.05.137>
- 1231 Turpin, B.J., Saxena, P., Andrews, E., 2000. Measuring and simulating particulate organics in
1232 the atmosphere: problems and prospects. *Atmos. Environ.* 34, 2983–3013.
1233 [https://doi.org/10.1016/S1352-2310\(99\)00501-4](https://doi.org/10.1016/S1352-2310(99)00501-4)
- 1234 van Drooge, B.L., Crusack, M., Reche, C., Mohr, C., Alastuey, A., Querol, X., Prevot, A.,
1235 Day, D.A., Jimenez, J.L., Grimalt, J.O., 2012. Molecular marker characterization of the
1236 organic composition of submicron aerosols from Mediterranean urban and rural environments
1237 under contrasting meteorological conditions. *Atmos. Environ.* 61, 482–489.
1238 <https://doi.org/10.1016/j.atmosenv.2012.07.039>
- 1239 Verlhac, S., Favez, O., Albinet, A., 2017. Interlaboratory comparison organized for the
1240 European laboratories involved in the analysis of levoglucosan and its isomers.
1241 <https://doi.org/10.13140/rg.2.2.16262.47684>
- 1242 Viana, M., Alastuey, A., Querol, X., Guerreiro, C.B.B., Vogt, M., Colette, A., Collet, S.,
1243 Albinet, A., Fraboulet, I., Lacome, J.-M., Tognet, F., de Leeuw, F., 2016. Contribution of
1244 residential-combustion to ambient air pollution and greenhouse gas emissions (No.
1245 ETC/ACM Technical Paper 2015/1). EEA, ETC/ACM.
- 1246 Wang, X., Gu, R., Wang, L., Xu, W., Zhang, Y., Chen, B., Li, W., Xue, L., Chen, J., Wang,
1247 W., 2017. Emissions of fine particulate nitrated phenols from the burning of five common
1248 types of biomass. *Environ. Pollut.* 230, 405–412. <https://doi.org/10.1016/j.envpol.2017.06.072>
- 1249 Wang, Y., Hu, M., Wang, Y., Zheng, J., Shang, D., Yang, Y., Liu, Y., Li, X., Tang, R., Zhu,
1250 W., Du, Z., Wu, Y., Guo, S., Wu, Z., Lou, S., Hallquist, M., Yu, J., 2019. The formation of
1251 nitro-aromatic compounds under high NO_x-anthropogenic VOCs dominated atmosphere in
1252 summer in Beijing, China. *Atmospheric Chem. Phys. Discuss.* 1–22.
1253 <https://doi.org/10.5194/acp-2018-1256>
- 1254 Xie, M., Chen, X., Hays, M.D., Lewandowski, M., Offenberg, J., Kleindienst, T.E., Holder,
1255 A.L., 2017. Light Absorption of Secondary Organic Aerosol: Composition and Contribution
1256 of Nitroaromatic Compounds. *Environ. Sci. Technol.* 51, 11607–11616.
1257 <https://doi.org/10.1021/acs.est.7b03263>
- 1258 Xie, M., Hannigan, M.P., Barsanti, K.C., 2014. Gas/Particle Partitioning of 2-Methyltetrols
1259 and Levoglucosan at an Urban Site in Denver. *Environ. Sci. Technol.* 48, 2835–2842.
1260 <https://doi.org/10.1021/es405356n>
- 1261 Xu, J., Griffin, R.J., Li, Y., Nakao, S., Cocker III, D.R., 2015. Simulated impact of
1262 NO_x on SOA formation from oxidation of toluene and m-xylene.
1263 *Atmos. Environ.* 101, 217–225. <https://doi.org/10.1016/j.atmosenv.2014.11.008>
- 1264 Yatavelli, R.L.N., Stark, H., Thompson, S.L., Kimmel, J.R., Cubison, M.J., Day, D.A.,
1265 Campuzano-Jost, P., Palm, B.B., Hodzic, A., Thornton, J.A., Jayne, J.T., Worsnop, D.R.,
1266 Jimenez, J.L., 2014. Semicontinuous measurements of gas–particle partitioning of organic
1267 acids in a ponderosa pine forest using a MOVI-HRToF-CIMS. *Atmospheric Chem. Phys.* 14,
1268 1527–1546. <https://doi.org/10.5194/acp-14-1527-2014>

- 1269 Yee, L.D., Kautzman, K.E., Loza, C.L., Schilling, K.A., Coggon, M.M., Chhabra, P.S., Chan,
1270 M.N., Chan, A.W.H., Hersey, S.P., Crounse, J.D., Wennberg, P.O., Flagan, R.C., Seinfeld,
1271 J.H., 2013. Secondary organic aerosol formation from biomass burning intermediates: phenol
1272 and methoxyphenols. *Atmospheric Chem. Phys.* 13, 8019–8043. [https://doi.org/10.5194/acp-](https://doi.org/10.5194/acp-13-8019-2013)
1273 13-8019-2013
- 1274 Yttri, K., Schnelle-Kreis, J., Maenhaut, W., Abbaszade, G., Alves, C., Bjerke, A., Bonnier,
1275 N., Bossi, R., Claeys, M., Dye, C., Evtugina, M., García-Gacio, D., Hillamo, R., Hoffer, A.,
1276 Hyder, M., Iinuma, Y., Jaffrezo, J., Kasper-Giebl, A., Kiss, G., López-Mahia, P., Pio, C., Piot,
1277 C., Ramirez-Santa-Cruz, C., Sciare, J., Teinilä, K., Vermeylen, R., Vicente, A., Zimmermann,
1278 R., 2015. An intercomparison study of analytical methods used for quantification of
1279 levoglucosan in ambient aerosol filter samples. *Atmospheric Meas. Tech.* 8, 125–147.
1280 <https://doi.org/10.5194/amt-8-125-2015>
- 1281 Yu, J., Cocker, D.R., Griffin, R.J., Flagan, R.C., Seinfeld, J.H., 1999. Gas-Phase Ozone
1282 Oxidation of Monoterpenes: Gaseous and Particulate Products. *J. Atmospheric Chem.* 34,
1283 207–258. <https://doi.org/10.1023/A:1006254930583>
- 1284 Yuan, B., Liggio, J., Wentzell, J., Li, S.-M., Stark, H., Roberts, J.M., Gilman, J., Lerner, B.,
1285 Warneke, C., Li, R., Leithead, A., Osthoff, H.D., Wild, R., Brown, S.S., Gouw, J.A. de, 2016.
1286 Secondary formation of nitrated phenols: insights from observations during the Uintah Basin
1287 Winter Ozone Study (UBWOS) 2014. *Atmospheric Chem. Phys.* 16, 2139–2153.
1288 <https://doi.org/https://doi.org/10.5194/acp-16-2139-2016>
- 1289 Zhang, Q., Jimenez, J.L., Canagaratna, M.R., Allan, J.D., Coe, H., Ulbrich, I., Alfarra, M.R.,
1290 Takami, A., Middlebrook, A.M., Sun, Y.L., Dzepina, K., Dunlea, E., Docherty, K., DeCarlo,
1291 P.F., Salcedo, D., Onasch, T., Jayne, J.T., Miyoshi, T., Shimojo, A., Hatakeyama, S.,
1292 Takegawa, N., Kondo, Y., Schneider, J., Drewnick, F., Borrmann, S., Weimer, S., Demerjian,
1293 K., Williams, P., Bower, K., Bahreini, R., Cottrell, L., Griffin, R.J., Rautiainen, J., Sun, J.Y.,
1294 Zhang, Y.M., Worsnop, D.R., 2007. Ubiquity and dominance of oxygenated species in
1295 organic aerosols in anthropogenically-influenced Northern Hemisphere midlatitudes.
1296 *Geophys. Res. Lett.* 34, L13801. <https://doi.org/10.1029/2007GL029979>
- 1297 Zhang, Q., Jimenez, J.L., Canagaratna, M.R., Ulbrich, I.M., Ng, N.L., Worsnop, D.R., Sun,
1298 Y., 2011. Understanding atmospheric organic aerosols via factor analysis of aerosol mass
1299 spectrometry: a review. *Anal. Bioanal. Chem.* 401, 3045–3067.
1300 <https://doi.org/10.1007/s00216-011-5355-y>
- 1301 Zhang, Y., Favez, O., Petit, J.-E., Canonaco, F., Truong, F., Bonnaire, N., Crenn, V.,
1302 Amodeo, T., Prévôt, A.S.H., Sciare, J., Gros, V., Albinet, A., 2019. Six-year source
1303 apportionment of submicron organic aerosols from near-continuous measurements at SIRTA
1304 (Paris area, France). *Atmospheric Chem. Phys. Discuss.* 1–41. [https://doi.org/10.5194/acp-](https://doi.org/10.5194/acp-2019-515)
1305 2019-515
- 1306 Zhang, Y., Sheesley, R.J., Schauer, J.J., Lewandowski, M., Jaoui, M., Offenberg, J.H.,
1307 Kleindienst, T.E., Edney, E.O., 2009. Source apportionment of primary and secondary
1308 organic aerosols using positive matrix factorization (PMF) of molecular markers. *Atmos.*
1309 *Environ.* 43, 5567–5574. <https://doi.org/10.1016/j.atmosenv.2009.02.047>
- 1310 Zhang, Y.Y., Müller, L., Winterhalter, R., Moortgat, G.K., Hoffmann, T., Pöschl, U., 2010.
1311 Seasonal cycle and temperature dependence of pinene oxidation products, dicarboxylic acids

- 1312 and nitrophenols in fine and coarse air particulate matter. *Atmospheric Chem. Phys.* 10,
1313 7859–7873. <https://doi.org/10.5194/acp-10-7859-2010>
- 1314 Zielinska, B., 2008. Analysis of Semi-Volatile Organic Compound by GC/MS, DRI Standard
1315 Operating Procedure. Desert Res. Inst. Reno NV.
- 1316 Zielinska, B., Sagebiel, J., Arnott, W.P., Rogers, C.F., Kelly, K.E., Wagner, D.A., Lighty,
1317 J.S., Sarofim, A.F., Palmer, G., 2004a. Phase and Size Distribution of Polycyclic Aromatic
1318 Hydrocarbons in Diesel and Gasoline Vehicle Emissions. *Environ. Sci. Technol.* 38, 2557–
1319 2567. <https://doi.org/10.1021/es030518d>
- 1320 Zielinska, B., Sagebiel, J., McDonald, J.D., Whitney, K., Lawson, D.R., 2004b. Emission
1321 Rates and Comparative Chemical Composition from Selected In-Use Diesel and Gasoline-
1322 Fueled Vehicles. *J. Air Waste Manag. Assoc.* 54, 1138–1150.
1323 <https://doi.org/10.1080/10473289.2004.10470973>
- 1324 Ziemann, P.J., Atkinson, R., 2012. Kinetics, products, and mechanisms of secondary organic
1325 aerosol formation. *Chem. Soc. Rev.* 41, 6582. <https://doi.org/10.1039/c2cs35122f>
- 1326 Zotter, P., Herich, H., Gysel, M., El-Haddad, I., Zhang, Y., Močnik, G., Hüglin, C.,
1327 Baltensperger, U., Szidat, S., Prévôt, A.S.H., 2017. Evaluation of the absorption Ångström
1328 exponents for traffic and wood burning in the Aethalometer-based source apportionment
1329 using radiocarbon measurements of ambient aerosol. *Atmospheric Chem. Phys.* 17, 4229–
1330 4249. <https://doi.org/https://doi.org/10.5194/acp-17-4229-2017>
- 1331
- 1332

1333
1334
1335
1336
1337
1338
1339
1340
1341
1342
1343
1344
1345
1346
1347

Supplementary Material

One-year measurements of secondary organic aerosol (SOA) markers in the Paris region: concentrations, seasonality, gas/particle partitioning and use in SOA source apportionment

G.M. Lanzafame^{1, 2, §}, D. Srivastava^{1, §}, O. Favez¹, N. Bonnaire³, V. Gros³, L. Alleman⁴, F. Couvidat¹, B. Bessagnet^{1, 2} and A. Albinet^{1, *}

¹*INERIS, Parc Technologique Alata, BP 2, 60550 Verneuil-en-Halatte, France*

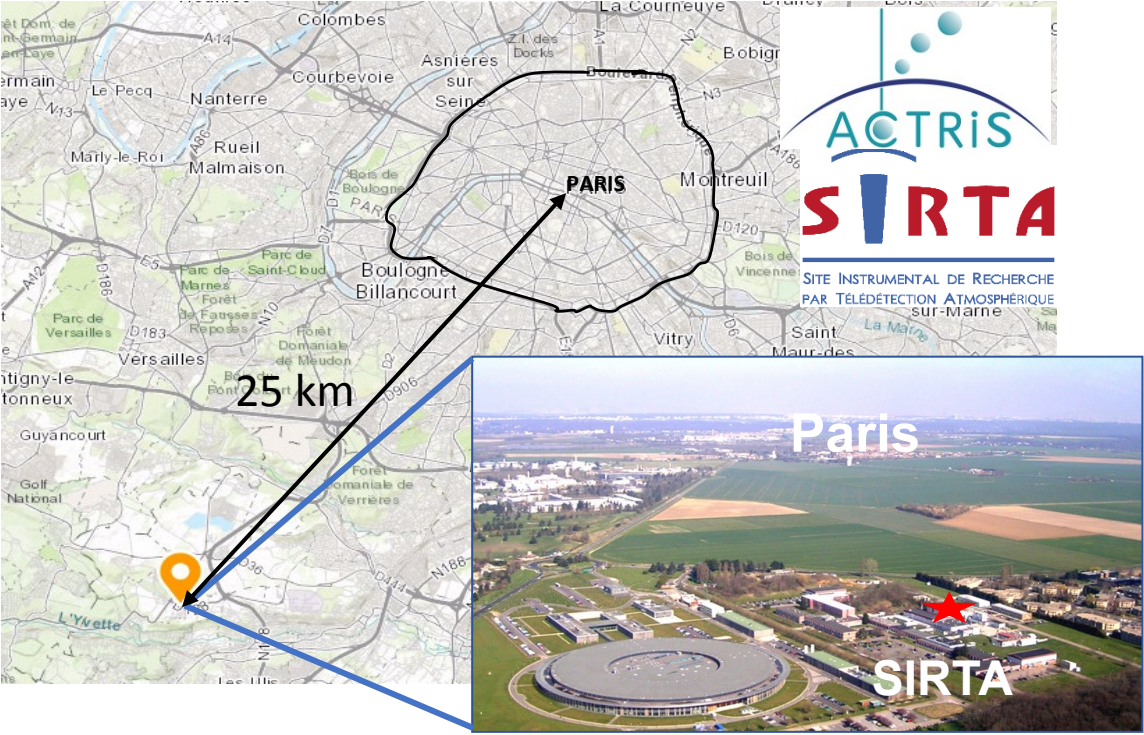
²*Sorbonne Universités, UPMC, 75252 PARIS cedex 05, France*

³*LSCE - UMR8212, CNRS-CEA-UVSQ, Gif-sur-Yvette, France,*

⁴*IMT Lille Douai, SAGE, 59000 Lille, France*

* Correspondence to: alexandre.albinet@gmail.com; alexandre.albinet@ineris.fr

§ These authors contributed equally to this work



1348
1349 **Fig. S1.** SIRTa sampling station location.

1350
1351
1352
1353
1354

1355 **1. Sample analysis**

1356 The analyses of the SOA markers were achieved using GC/MS (Agilent 7890A GC coupled
1357 to 5975C MS) in electron ionization mode (EI, 70 eV). 1 μ L of the extracts was injected in the
1358 splitless mode at 250 °C using a programmed temperature vaporizer injector system (CIS-4
1359 Gerstel, with a Restek Sky single baffle liner with wool, 3 \times 2 \times 71 mm). Compounds were
1360 separated using a capillary column with equivalent 5% phenyl-methylpolysiloxane phase 60
1361 m \times 0.25 mm \times 0.25 μ m (Agilent J&W DB5-MS with 10 m guard column) with the following
1362 temperature programs: start at 70 °C for 1 min, then ramped to 260 °C at 5 °C min⁻¹, followed
1363 by a ramp to 290 °C at 20 °C min⁻¹, further followed by a ramp to 300 °C at 5 °C min⁻¹, then
1364 ramped at 10 °C min⁻¹ to 320°C held for 10 min. The carrier gas (He) flow was set to 1.5 mL
1365 min⁻¹ throughout the analysis and transfer line heated at 310 °C. The ion source and
1366 quadrupole temperatures were 230 and 150 °C, respectively.

1367 Analyses were performed in the selected ion monitoring mode (SIM). Autotune parameters
1368 were adopted for the electron multiplier conditions with a gain factor of 10. Monitored ions
1369 and dwell times are shown in Table S2. The quantification of the SOA markers was based on
1370 8 to 10-points calibration curves (gravimetrically diluted stock standard solutions prepared in
1371 acetonitrile from 5 to 5000 pg μ l⁻¹; 0.99 > r² > 0.90 for all compounds). Most of the SOA
1372 marker compounds were quantified using authentic standards and labelled surrogate standards
1373 by internal calibration except for both methylnitrocatechols (external calibration) (Tables S1
1374 and S2).

1375
1376
1377

1378
 1379 **Table S1.** List and characteristics of the chemicals, gases and solvents used for SOA marker
 1380 analyses.

Compound	Supplier	CAS number	Purity
cis-Pinonic acid	Sigma-Aldrich	61826-55-9	98 %
Pinic acid	Santai labs	473-73-4	95 %
Terpenylic acid	Interbioscreen	116-51-8	95 %
3-Methylbutane-1,2,3-tricarboxylic acid (MBTCA)	TRC	77370-41-3	98 %
3-Hydroxyglutaric acid	Santa Cruz Biotechnology	638-18-6	95 %
α -Methylglyceric acid	Tractus/Wonderchem	21620-60-0	95 %
2-Methylerythritol	Sigma-Aldrich	58698-37-6	90 %
2-C-Methyl-D-Threitol	Sirius Chemicals	310887-92-4	99 %
β -Caryophyllinic acid	TRC	957055-11-7	97 %
Succinic acid	Sigma-Aldrich	110-15-6	99 %
Phthalic acid	Sigma-Aldrich	88-99-3	> 99.5 %
2,3-Dihydroxy-4-oxopentanoic acid (DHOPA)	TRC	37520-06-02	98 %
2-Nitrophenol	Fisher	88-75-5	99 %
4-Nitrophenol	Fisher	100-02-7	99 %
2-Methyl-4-nitrophenol	Sigma-Aldrich	99-53-6	97 %
4-Nitroguaiacol	Fisher	3251-56-7	97 %
5-Nitroguaiacol	Fisher	636-93-1	97 %
4-Methyl-5-nitrocatechol	TRC/Carbosynth	68906-21-8	96-98 %
3-Methyl-5-nitrocatechol	Santai labs	5378-76-7	97 %
Deuterated compounds			
Succinic acid-2,3,3,3- d_4	C/D/N isotopes	14493-42-6	99 %
Meso-erythritol-1,1,2,4,4- d_6	C/D/N isotopes	149-32-6(unlabelled)	99.1 %
2-Nitrophenol- d_4	Cambridge isotopes	93951-78-1	98 %
1,9-Nonanedioic- d_{14}	C/D/N isotopes	119176-67-9	99 %
Solvents, reagents			
Methanol	Sigma-Aldrich	67-56-1	> 99.9 %
Acetonitrile	VWR	75-05-8	> 99.9 %
N-Methyl-N-(trimethylsilyl) trifluoroacetamide (MSTFA) + 1% trimethylchlorosilane (TMCS)	Thermo	24589-78-4	99 %
Gases			
Helium	Air liquide	7440-59-7	99.9999 %
Nitrogen	Air liquide	7727-37-9	99.9999 %

1381
 1382
 1383
 1384
 1385
 1386
 1387
 1388

1389

1390 **Table S2.** GC/MS conditions used for SOA marker analysis and typical instrumental limits of
 1391 quantification (LOQ).

Compound	Monitored ions(m/z)	Retention time(min)	Dwell time (ms)	LOQ (pg injected)
<i>Succinic acid-2,3,3,3-d4</i>	147, 251	19.54	35	-
Succinic acid	129 , 247	19.61	35	1.1
α -Methylglyceric acid	219 , 306	19.74	35	0.7
2,3-Dihydroxy-4-oxopentanoic acid	218 , 350	24.71	50	1.6
cis-Pinonic acid	171 , 125	25.27	50	1.1
3-Hydroxyglutaric acid	185, 349	26.26	50	1.0
Terpenylic acid	158 , 229	26.60	25	1.4
3-(2-Hydroxy-ethyl)-2,2-dimethylcyclobutane-carboxylic acid ^a	158 229	26.69	25	1.4
3-Hydroxy-4,4-dimethylglutaric acid ^b	259 ,377	27.02	25	1.0
3-Acetylpentanedioic acid ^b	111 , 276	27.15	25	1.0
Pinic acid	129 , 171	28.50	50	1.4
Phthalic acid	221, 295	29.04	50	1.3
3-Acetyl hexanedioic acid ^b	204, 317	29.70	25	1.0
3-Isopropylpentanedioic acid ^b	213, 229	29.80	25	1.0
<i>2-Nitrophenol-d4</i>	155, 200	21.955	35	-
2-Nitrophenol	151, 196	21.994	35	0.2
4-Nitrophenol	196 , 211	24.878	50	0.7
2-Methyl-4-nitrophenol	210 , 225	27.158	50	0.7
4-Nitroguaiacol	211 , 226	28.66	50	2.6
5-Nitroguaiacol	211 , 226	28.997	50	4.1
<i>Meso-erythritol-1,1,2,4,4-d6</i>	208 , 220	24.50	100	-
2-Methylthreitol	203, 219	23.23	25	1.3
2-Methylerythritol	117, 219	25.74	50	4.5
<i>1,9-Nonanedioic acid-d14</i>	213, 331	31.10	35	-
3-Methylbutane-1,2,3-tricarboxylic acid	204 , 245	30.34	50	5.5
β -Caryophyllinic acid	117 , 200	36.08	50	2.9
4-Methyl-5-nitrocatechol ^c	296, 313	31.06	35	1.6
3-Methyl-6-nitrocatechol ^c	298 , 313	32.10	25	4.1
3-Methyl-5-nitrocatechol ^c	298 , 313	32.28	100	4.1

1392 ^aQuantified using response factor obtained for pinic acid.

1393 ^bQuantified using response factor obtained for 3-hydroxyglutaric acid.

1394 ^cQuantified by external calibration (Albinet et al., 2019).

1395 Quantification ions are specified in bold.

1396

1397

1398

1399

1400

1401

1402

1403 **Table S3.** SOA marker concentrations (mg kg^{-1}) (dry-mass basis) in SRM 1649b (urban dust).
 1404 obtained here and comparison with literature data.

Compounds	Mean (this study) ^a	Standard deviation (this study) ^a	Mean (Albinet et al., 2019)	Standard deviation (Albinet et al., 2019)
Succinic acid	115.1	8.6	111.0	35.0
α -Methylglyceric acid	2.8	0.2	3.3	1.3
DHOPA	1.8	0.1	1.2	0.8
cis-Pinonic acid	5.9	1.0	5.9	4.4
3-Hydroxyglutaric acid	8.4	0.7	8.5	2.5
Pinic acid	8.7	1.1	12.8	4.9
Phthalic acid	129.9	8.1	89.7	30.7
2-Nitrophenol	0.7	0.1	ND	ND
4-Nitrophenol	85.4	23.9	ND	ND
2-Methyl-4-nitrophenol	22.6	11.7	ND	ND
4-Nitroguaiacol	4.8	3.1	ND	ND
5-Nitroguaiacol	15.1	8.0	ND	ND
2-Methylerythritol ^c	198.3	14.9	28.9	33.5
MBTCA	4.0	1.5	2.1	2.1
β -Caryophyllinic acid	0.1	<0.1	0.4	0.3
4-Methyl-5-nitrocatechol	11.1	0.4	3.8	3.3
3-Methyl-5-nitrocatechol	11.2	<0.1	3.3	2.7

1405 ^an=6 full replicates (extraction and analysis, triplicate injections). Mean values and standard deviations
 1406 calculated considering all the results obtained.

1407 ND: not determined.

1408

1409 **2. Literature data**1410 **Table S4.** List of studies reporting SOA marker concentrations in ambient air for different locations worldwide.

Sampling location, Country	Abbreviation	Site typology*	Period	SOA markers measured	Reference
Europe					
Rome, Italy	Rom	Urban	February-April 2003	2NPh, 4NPh, 2M4NPh	(Cecinato et al., 2005)
Mainz, Germany	Maz	Rural urban	June 2006-May 2007	PnoA, PniA, MBTCA, PhA, 2NPh, 4NPh	(Zhang et al., 2010)
Marseille, France	Mar	Urban	July 2008	PnoA, PniA, MBTCA, HGA, MGA	(El Haddad et al., 2011)
Barcelona, Spain	BCN	Urban	February-March 2009	SuA, PhA	(van Drooge et al., 2012)
Ljubljana, Slovenia	Lju	Urban background	Winter 2010	4NPh, 2M4NPh, 4NG, 4M5NC, 3M6NC, 3MNC	(Kitanovski et al., 2012)
Barcelona, Spain	BUB	Urban background	September-October 2010	PnoA, MBTCA, HGA, MGA, MTR, MET, SuA, PhA	(Alier et al., 2013)
Barcelona, Spain	BRS	Urban, road street	September-October 2010	PnoA, MBTCA, HGA, MGA, MTR, MET, SuA, PhA	(Alier et al., 2013)
Grenoble, France	Gr	Urban background	Annual mean (2013)	PnoA, MBTCA, HGA, MGA, MET, SuA, PhA, DHOPA, 3M5NC, 4M4NC	(Srivastava et al., 2018b)
Paris, France	Par	Suburban	March 2015	PnoA, PniA, MBTCA, HGA, MGA, MTR, MET, SuA, PhA, DHOPA, 3M5NC, 4M4NC	(Srivastava et al., 2018a)
Seiffen, Germany	Sei	Rural	October 2007-March 2008	4M5NC, 3M6NC, 3M5NC	(Iinuma et al., 2010)
Montseny, Spain	MSY	Rural Background	February-March 2009	SuA, PhA	(van Drooge et al., 2012)
Hamme, Belgium	Ham	Rural background	2010-2011	NPh, MNC	(Kahnt et al., 2013)
Detling, UK	Det	Rural	Winter 2012	4NPh, 4M5NC	(Mohr et al., 2013)
Hyytiälä, Finland	HY	Forest	Summer/Fall 2004	MGA, MTR, MET	(Kourchev et al., 2005)
K-pusztá, Hungary	KP	Forest	Summer 2003	MGA, MTR, MET	(Ion et al., 2005)
Hyytiälä, Finland	HY2	Forest	July-August 2005	PniA, HGA, MTR, MET	(Kourchev et al., 2008a)

Chapter II: SOA marker measurements

Jülich, Germany	Jul	Forest	July 2003	PniA, MBTCA, HGA, MGA, MTR, MET, SuA	(Kourtchev et al., 2008b)
K-pusztá, Hungary	KP2	Forest	Summer 2003	PniA, MBTCA, HGA, SuA	(Kourtchev et al., 2009)
Silkeborg, Denmark	Sil	Forest	April-May 2008	PnoA, PniA, MBTCA, TerA	(Kristensen and Glasius, 2011)
Brasschaat, Belgium	Bra	Forest impacted by urban pollution	June-July 2007	PnoA, PniA, MBTCA, TerA	(Gómez-González et al., 2012)
North and South America					
Atlanta, USA	Atl	Urban	June 2006	MTR, MET	(Clements and Seinfeld, 2007)
Atlanta, USA	Atl2	Urban	May-August 2005	PnoA, PniA, HCCA, MBTCA, HGA, HDGA, APDA, AHDA, MGA, MTR, MET, CarA, PhA, DHOPA	(Kleindienst et al., 2010)
Birmingham, USA	Bir	Urban	June 2006	MTR, MET	(Clements and Seinfeld, 2007)
Birmingham, USA	Bir2	Urban	May-August 2005	PnoA, PniA, HCCA, MBTCA, HGA, HDGA, APDA, AHDA, MGA, MTR, MET, CarA, PhA, DHOPA	(Kleindienst et al., 2010)
Pensacola, USA	Pen	Suburban	June 2006	MTR, MET	(Clements and Seinfeld, 2007)
Pensacola, USA	Pen2	Suburban	May-August 2005	PnoA, PniA, HCCA, MBTCA, HGA, HDGA, APDA, AHDA, MGA, MTR, MET, CarA, PhA, DHOPA	(Kleindienst et al., 2010)
Toronto, Canada	Tor	Urban	2000-2001	PnoA	(Cheng et al., 2011)
Riverside, USA	Riv	Urban	August 2005	PnoA, PniA, HCCA, MBTCA, HGA, HDGA, APDA, AHDA, MGA, MTR, MET, CarA, PhA, DHOPA	(Kleindienst et al., 2010)
Cleveland, USA	Cle	Industrial	July-August 2009	PnoA, PniA, HCCA, MBTCA, HGA, HDGA, APDA, AHDA, MGA, MTR, MET, CarA, PhA, DHOPA	(Piletic et al., 2013)
Bakersfield, USA	Bak	Urban/ industrial	May-June 2010	MBTCA, HGA, HDGA, APDA, AHDA, MGA, MTR, MET, DHOPA	(Lewandowski et al., 2013)
Pasadena, USA	Pas	Urban/ industrial	May-June 2010	PniA, MBTCA, HGA, HDGA, APDA,	(Lewandowski et al., 2013)

Chapter II: SOA marker measurements

				AHDA, MGA, MTR, MET, DHOPA	
Triangle Park, USA	TP	Semi-rural	Annual mean (2003)	PnoA, PniA, HCCA, HGA, HDGA, APDA, AHDA, IPPA, MGA, MTR, MET, CarA, DHOPA	(Kleindienst et al, 2007b)
Centreville, USA	Cen	Rural	June 2004	MTR, MET	(Clements and Seinfeld, 2007)
Centreville, USA	Cen2	Rural	May-August 2005	PnoA, PniA, HCCA, MBTCA, HGA, HDGA, APDA, AHDA, MGA, MTR, MET, CarA, PhA, DHOPA	(Kleindienst et al., 2010)
Medina, USA	Med	Rural	July-August 2009	PnoA, PniA, HCCA, MBTCA, HGA, HDGA, APDA, AHDA, MGA, MTR, MET, CarA, PhA, DHOPA	(Piletic et al., 2013)
Amazonian Forest, Brasil	Ama	Forest	July 2000	HGA	(Claeys et al., 2004)
Asia					
Hong Kong, China	HK	Urban	July 2006	MBTCA, HGA, HDGA, APDA, AHDA, IPPA, MGA, MTR, MET, CarA, SuA, PhA, DHOPA	(Hu et al., 2008)
Beijing, China	Bei	Urban	Summer 2016	4NPh, 2M4NPh, 4M5NC, 3M6NC, 3M5NC	(Wang et al., 2019)
Tsuen Wan, China	TW	Urban background	Summer 2012	4NPh, 2M4NPh, 4M5NC, 3M6NC, 3MNC	(Chow et al., 2015)
Mumbai, India	Mum	Urban background	June 2006 and February 2007	PnoA, PniA, HCCA, MBTCA, HGA, MTR, MET, CarA, DHOPA	(Fu et al., 2016a)
Pearl river delta, China	PRD	Rural	Summer 2008	PnoA, PniA, HGA, MBTCA, MGA, MTR, MET, CarA, DHOPA	(Ding et al., 2012)
Tianhu, China	Tia	Rural	March 2012-February 2013	PnoA, PniA, MBTCA, HGA, HDGA, MGA, MTR, MET, PhA, DHOPA	(Yuan et al., 2018)
Tazhong, China	Taz	Desert	April 2008	PnoA, PniA, MBTCA, HGA, MGA, MTR, MET, CarA	(Fu et al., 2016b)
Hetian, China	Het	Desert	April 2008	PnoA, PniA, MBTCA, HGA, MGA, MTR, MET, CarA	(Fu et al., 2016b)
Cape Hebdo, Japan	CHe	Maritime/forested	October 2009-February 2012	PnoA, PniA, MBTCA, HGA, MGA, MTR+MET, CarA	(Zhu et al., 2016)

Chapter II: SOA marker measurements

<i>Africa</i>					
Nylsvley Nature Reserve, South Africa	NNR	Savannah	Winter 2007-2008	SuA, PhA	(Limbeck et al., 2001)

1411 *As defined by the authors.

1412

Chapter II: SOA marker measurements

1413 **Table S5.** Concentrations of SOA markers (ng m^{-3}) (particulate phase only) and of OC ($\mu\text{g m}^{-3}$) reported in previous studies and from this study.

1414 Sampling locations and periods are specified in Table S4. PM size fractions studied is also specified.

	Rom	Maz	Mar	BCN	Lju	BUB	BRS	Gr	Par	Sei	MSY	Ham	Det	HY	KP	HY2	Jul	KP2	Sil	Bra	Atl	Atl2	Bir	
PnoA		1.2	15.0			15.4	8.0	13.1	4.0										3.0	1.8*		3.2		
PniA		2.3	4.5						0.8							7.7*	4.2	12.2	1.5	0.5*		2.5		
HCCA																						4.3		
MBTCA		6.9	5.0			5.5	4.1	4.8	0.4								6.8	15.8	3.0	2.7*		23.9		
HGA			3.5			4.5	3.1	4.7	2.2						7.6	16.1*	5.8	19.7				24.2		
TerA																			0.8	2.4*				
HDGA																						2.6		
APDA																						5.4		
AHDA																						2.4		
IPPA																								
MGA			1.8			2.1	1.9	1.4	0.5					1.1	7.6*		2.3						18.1	
MTR						2.8	1.4	7.2	0.6					3.3	7.5*	4.0*	4.4			6.4*#	3.5	25.2	4.5	
MET						6.5	3.5							12.6	21.0*	8.4*	10.8				9.7	55.0	14.8	
CarA			0.3																			0.3		
SuA				17.0		7.3	6.2	10.6	14.4		11.4						8.1	15.2						
PhA		5.7		8.6		3.9	3.6	3.6	3.8		6.6											4.0		
DHOPA								4.9	1.5													1.4		
2NP	3.5	1.8										0.7*#												
4NP	17.8	3.8			1.8								<0.1											
2M4NP	7.8				0.8																			
4NG					0.4																			
5NG																								
4M5NC					29.0			15.7	41.2	2.0			8.20											
3M6NC					6.2					2.9		2.2*#												
3M5NC					34.0			15.5	30.3	0.4														
OC ($\mu\text{g m}^{-3}$)			22.0	5.5	19.4	2.1	3.5	5.6	6.8		2.5	4.0*		2.4	4.2	2.2*	4.6	4		1.7		7.5		

Chapter II: SOA marker measurements

1415

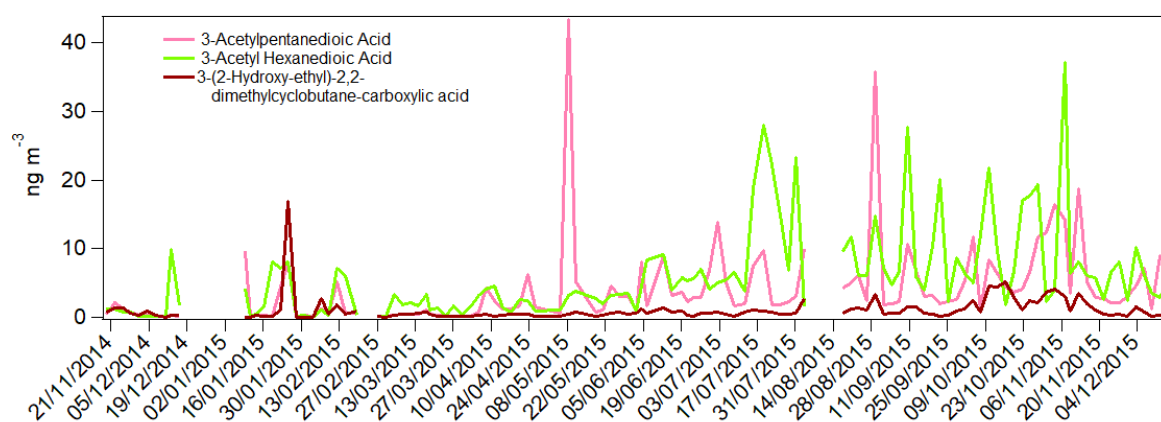
PM size fraction	PM ₅	TSP	PM _{2.5}	PM ₁	PM ₁₀	PM ₁	PM ₁	PM ₁₀	PM ₁₀	PM ₁₀	PM ₁₀	PM ₁	PM ₁	PM ₁₀	PM _{2.5}	PM _{2.5}	PM _{2.5}	PM _{2.5}	PM ₁	PM _{2.5}	PM _{2.5}	PM _{2.5}	PM _{2.5}	
	Bir2	Pen	Pen2	Tor	Riv	Cle	Bak	Pas	TP	Cen	Cen2	Med	Ama	HK	Bei	TW	Mum	PRD	Tia	Taz	Het	CHe	NNR	This work (annual average)
PnoA	1.4		1.3	3.6	4.8	0.2			0.7		2.1	0.					3.7	1.7	5.8	1	0.2	0.12		1.9
PniA	2.8		1.8		1.20	0.2		0.1	9.4		14.4	0.30					1.7	0.7	1.3	0.5	0.2	0.62		0.8
HCCA	10.0		8.1		2.	2.7			2.1		16.2	2.1					0.6							0.9
MBTCA	43.7		39.4		6.9	19.6	3.2	4.2			47.2	23.9		73.5			0.3		9.3	<0.01		0.81		1.0
HGA	46.5		44.1		19.2	21.3	5.5	10.8	28.2		46.9	22.1	12	83.8			8	2.6	11.8	0.2	0.4	0.48		2.1
TerA																								0.2
HDGA	5.0		5.6		1.5	1.8	0.4	0.6	6.0		5.9	2.3		9.7					6.9					0.2
APDA	11.0		10.4		4.9	7.8	2.0	2.1	9.2		19.1	8.2		18.5										2.0
AHDA	5.6		4.9		3.0	3.8	1.6	1.1	34.9		7.6	3.2		4.7										5.1
IPPA									1.3					8.4										0.2
MGA	22.7		9.8		14.7	18.4	6.7	2.7	11.7		24.1	22.2		1.0			0.8	7.7	2.1	3.6	0.2	0.42		0.5
MTR	49.0	1.6	28.7		2.9	30.0	2.7	1.0	19.1	4.2	66.4	45.3	40.9 [#]	8.3			0.4	25.6	8.1	0.06	0.1	1.02 [#]		0.7
MET	149	4.7	53.4		5.1	58.0	5.4	2.8	30.6	12.2	115	63.2		20.3			1.0	65.9	17.7	0.03	0.2			1.8
CarA	1.2		0.9		0.8	0.9			7.4		0.4	1.8		12.5			3.2	2.9		0.05				0.8
SuA														20.7				17.8					13.1	7.4
PhA	5.2		6.0		16.9	3.8	1.7	4.6			3.5	3.9		2.1					4.0				1.5	1.7
DHOPA	1.9		2.0		1.5	1.9	0.4	1.0	1.8		1.9	2.3		1.7			0.3		1.5					0.9
2NP																								< 0.1
4NP															2.2	0.5								0.1
2M4NP																0.3								0.1
4NG															0.8									0.1
5NG																								0.1
4M5NC															0.6	0.3								24.0
3M6NC															0.1	0.1								4.6
3M5NC															0.4	0.6								20.1
OC (µg m ⁻³)	13.5		5.9	3.8	4	2.3	5.2	3.7	4.1	6.5	6.5	1.5	2.0	5.7		6.9	9.9		6.3					3.3

Chapter II: SOA marker measurements

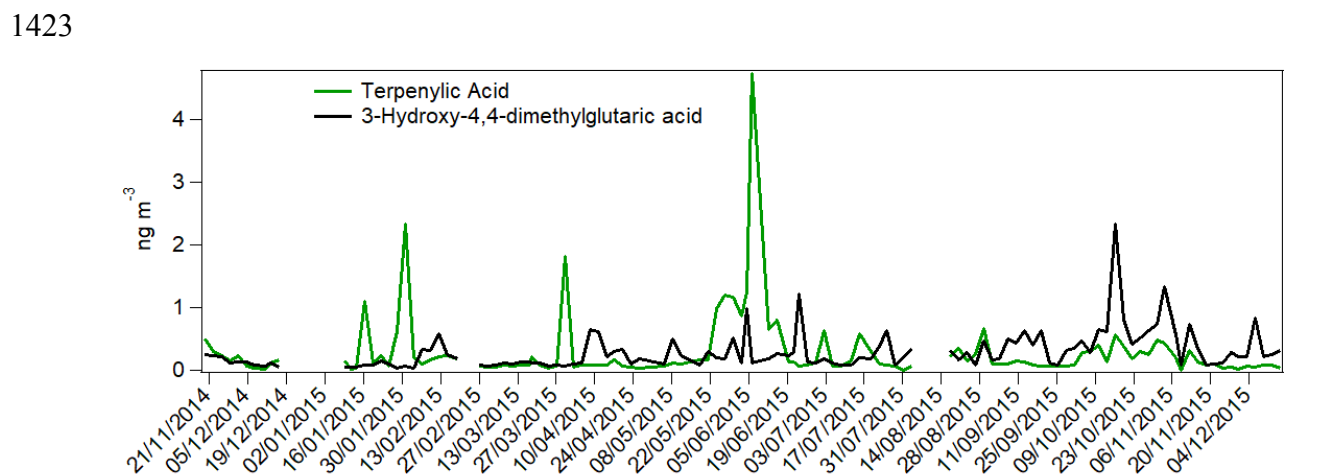
PM size fraction	PM _{2.5}	PM _{2.5}	PM _{2.5}	PM _{2.5}	PM _{2.5}	PM _{2.5}	PM _{2.5}	PM _{2.5}	PM _{2.5}	PM _{2.5}	PM _{2.5}	PM _{2.5}	PM _{2.5}	PM _{2.5}	PM _{2.5}	PM _{2.5}	PM ₁₀	PM _{2.5}	PM _{2.5}	PM _{2.5}	PM _{2.5}	TSP	-	PM ₁₀
------------------	-------------------	-------------------	-------------------	-------------------	-------------------	-------------------	-------------------	-------------------	-------------------	-------------------	-------------------	-------------------	-------------------	-------------------	-------------------	-------------------	------------------	-------------------	-------------------	-------------------	-------------------	-----	---	------------------

1416 # Sum of both isomers; *Median concentration

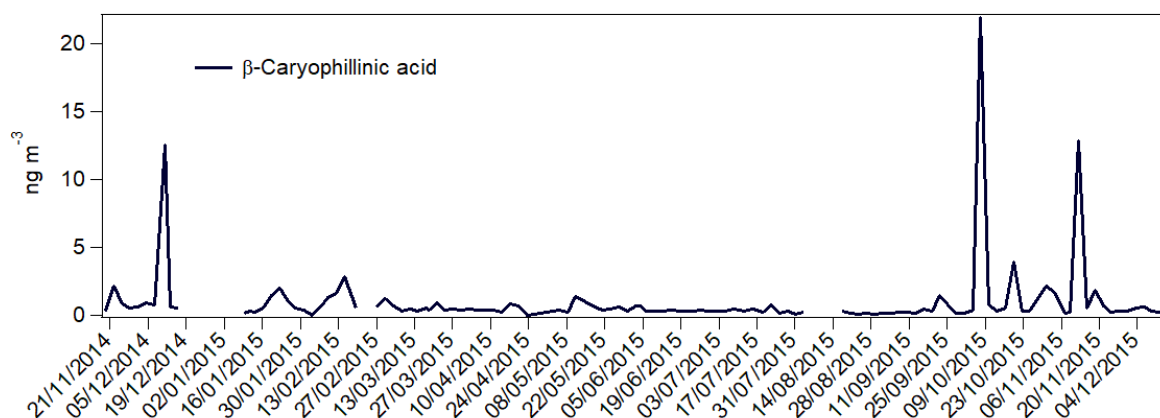
1417 **3. Temporal evolutions of total (gaseous + particulate phases) SOA marker**
 1418 **concentrations**



1419
 1420 **Fig. S2.** Temporal variations of total (gaseous+particulate phases) concentrations of 3-
 1421 acetyl pentanedioic acid, 3-acetyl hexanedioic acid and 3-(2-hydroxy-ethyl)-2,2-
 1422 dimethylcyclobutane-carboxylic acid (pinene SOA markers) at SIRT A (2015).

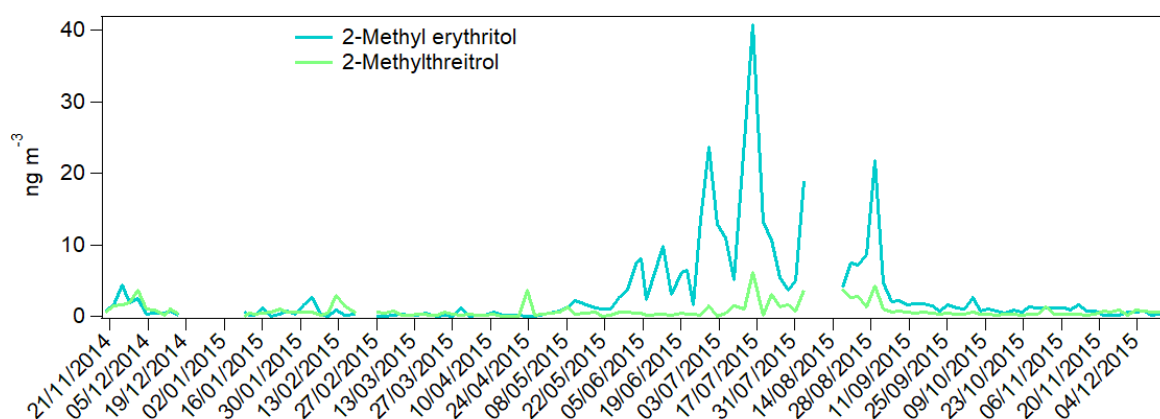


1424
 1425 **Fig. S3.** Temporal variations of total (gaseous + particulate phases) concentrations of
 1426 terpenylic acid and 3-hydroxy-4,4-dimethylglutaric acid (pinene SOA markers) at SIRT A
 1427 (2015).



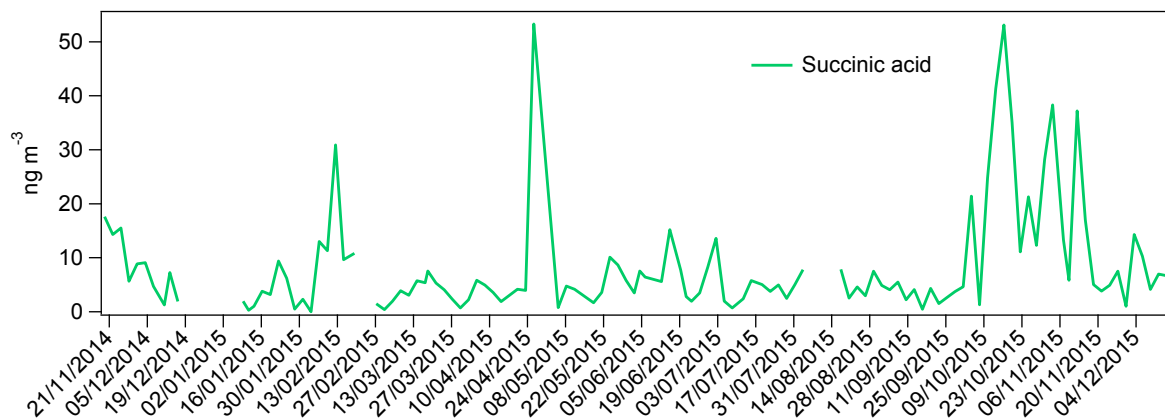
1428
1429 **Fig. S4.** Temporal variations of total (gaseous + particulate phases) concentrations of β -
1430 caryophyllinic acid (caryophyllene SOA marker) at SIRTa (2015).

1431



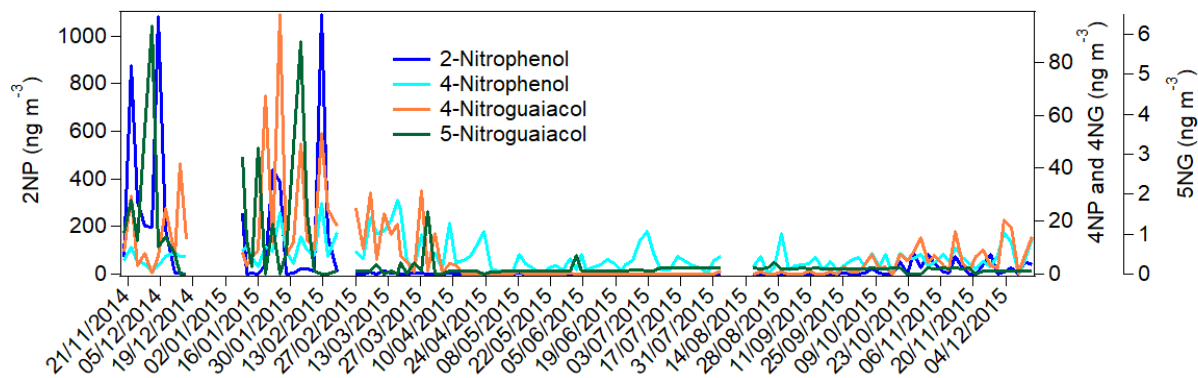
1432
1433 **Fig. S5.** Temporal variations of total (gaseous + particulate phases) concentrations of 2-
1434 methyl erythritol and 2-methylthreitol (isoprene SOA markers) at SIRTa (2015).

1435



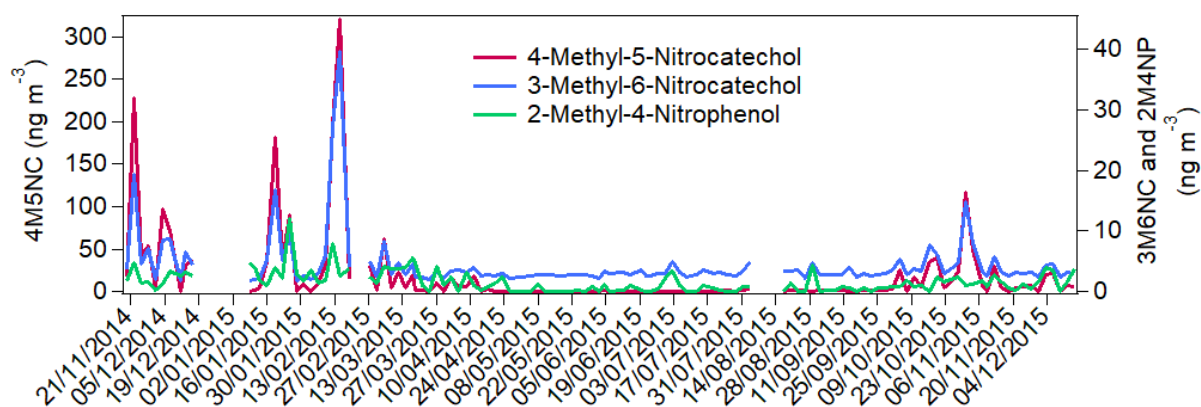
1436
 1437 **Fig.S6.** Temporal variations of total (gaseous + particulate phases) concentrations of succinic
 1438 acid (anthropogenic SOA marker) at SIRTa (2015).

1439



1440
 1441 **Fig.S7.** Temporal variations of total (gaseous + particulate phases) concentrations of
 1442 nitrophenols and nitroguaiacols (phenolic compounds oxidation SOA markers) at SIRTa
 1443 (2015).

1444

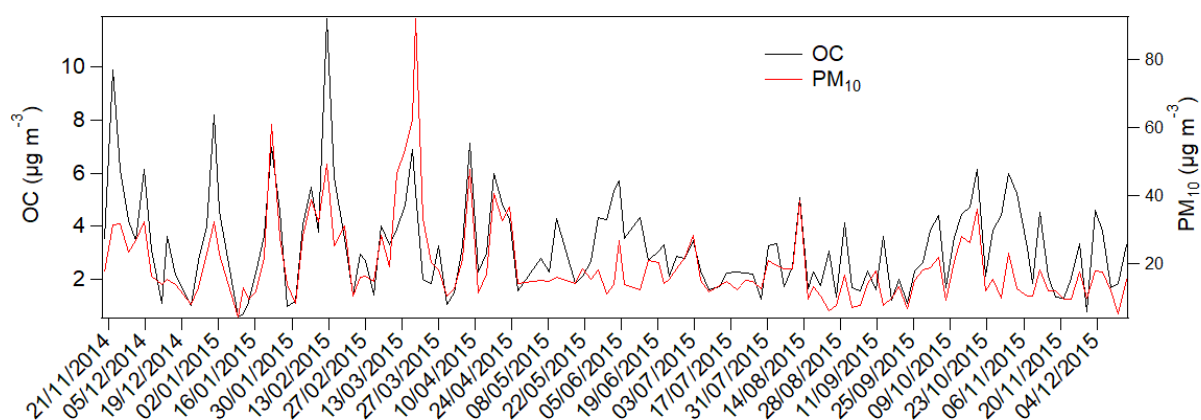


1445
 1446 **Fig. S8.** Temporal variations of total (gaseous + particulate phases) concentrations of
 1447 nitrocatechols and 2-methyl-4-nitrophenol (phenolic compounds oxidation SOA markers)
 1448 acid at SIRTa (2015).

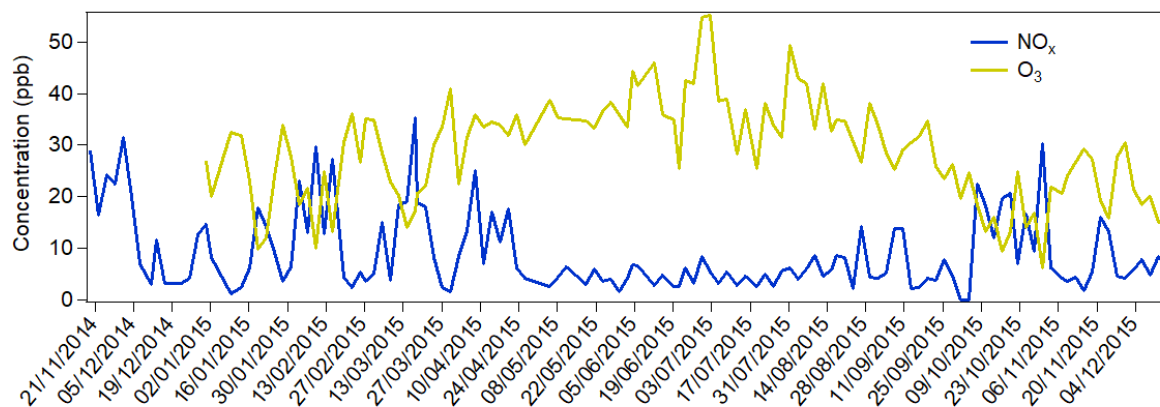
1449

1450 **4. Temporal evolutions of other species**

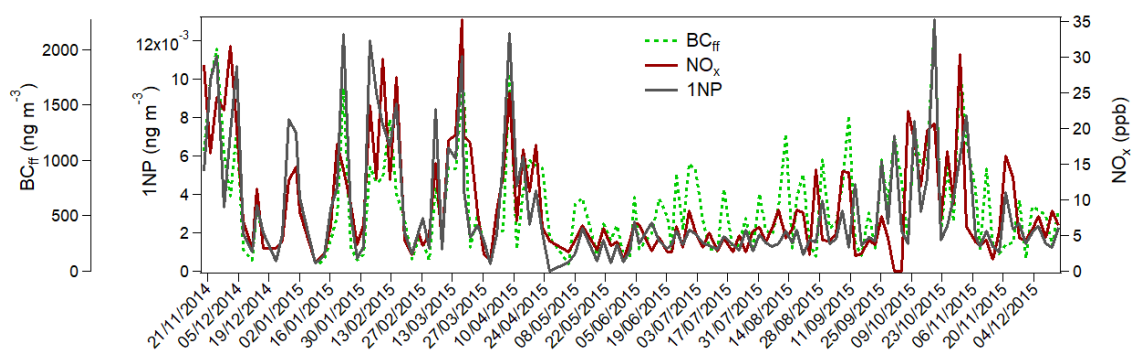
1451



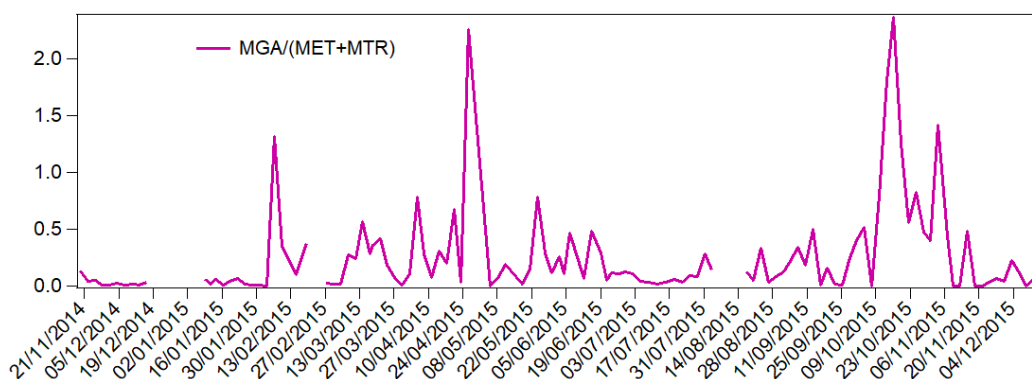
1452
 1453 **Fig.S9.** Temporal variations of organic carbon (OC) and PM₁₀ concentrations at SIRTa
 1454 (2015).



1455
1456 **Fig. S10.** Temporal evolutions of NO_x and O_3 concentrations at SIRT A (2015).



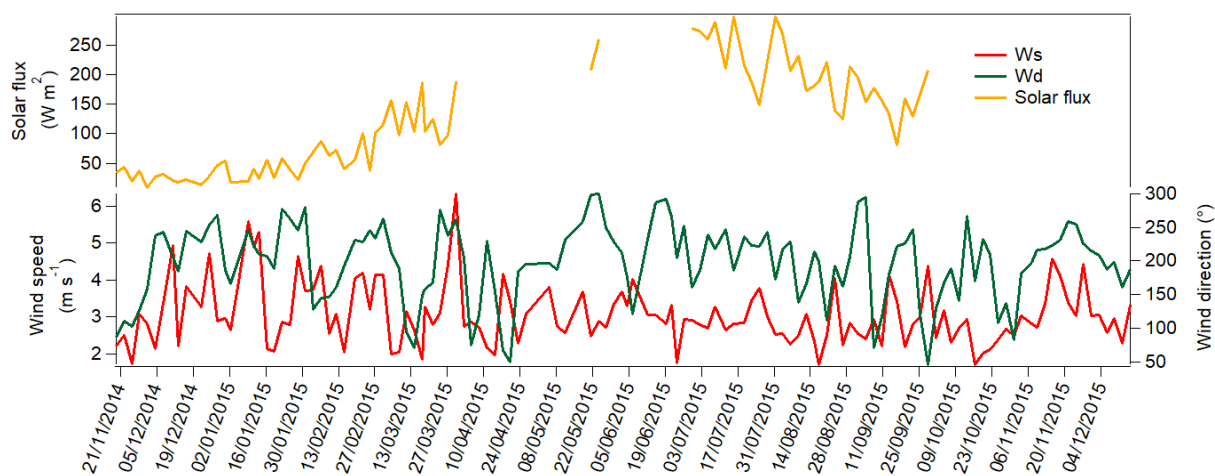
1457
1458 **Fig.S11.** Comparison of the temporal variations of 1-nitropyrene (1-NP) with BC_{ff} and NO_x
1459 observed at SIRT A (2015).



1460
1461 **Fig. S12.** Temporal variations of MGA/(MET+MTR) ratio observed at SIRT A (2015).

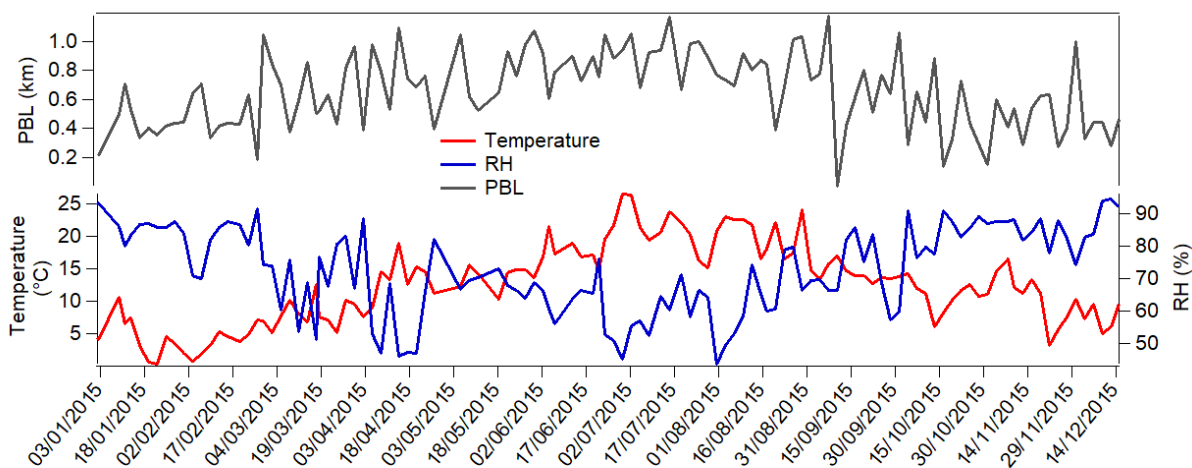
1462

1463 **5. Meteorological parameters temporal evolutions**



1464 **Fig.S13.** Temporal variations of solar flux, wind speed and direction at SIRTA (2015).
1465

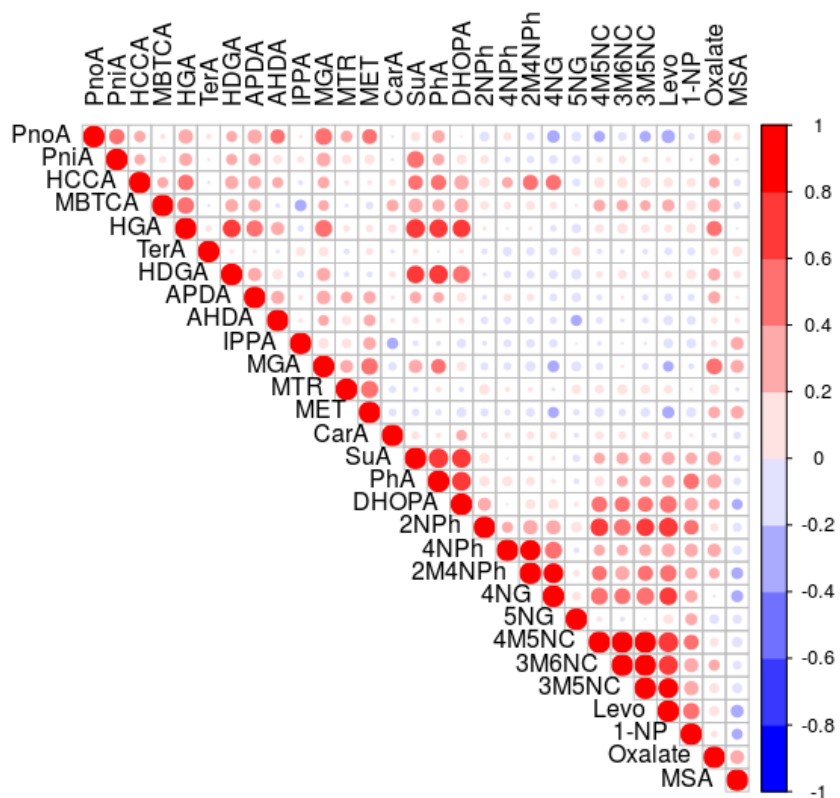
1466



1467 **Fig.S14.** Temporal variations of planetary boundary Layer (PBL), ambient air temperature and
1468 relative humidity (RH) at SIRTA (2015).
1469

1470

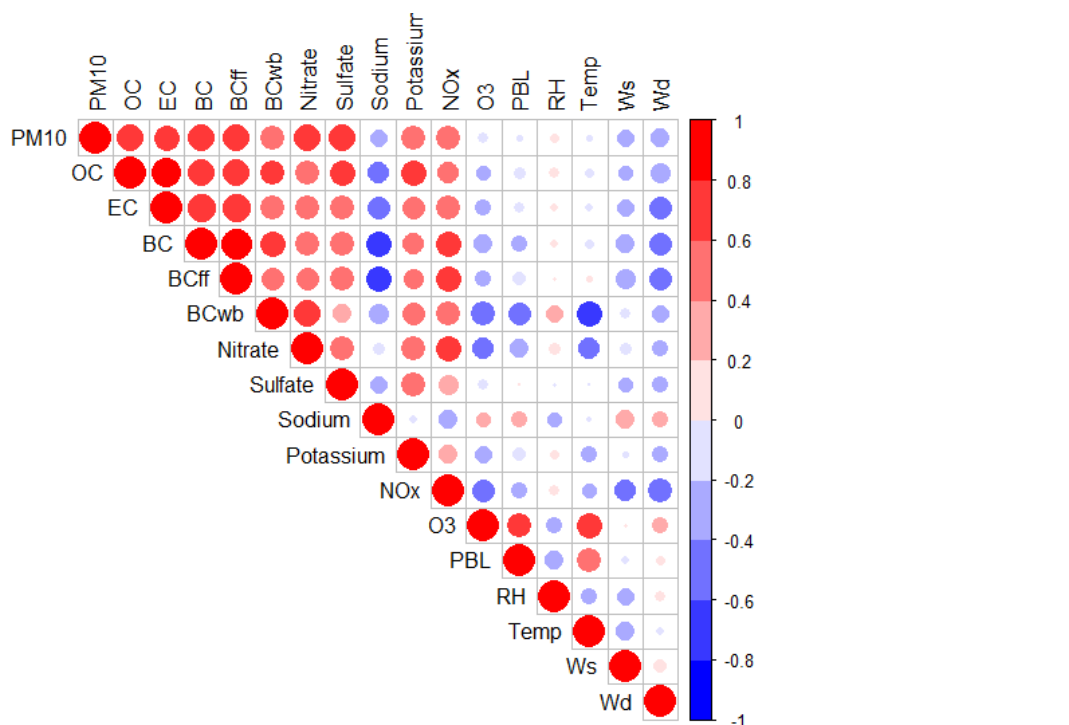
1471 **6. Correlation matrices between chemical species and external parameters**



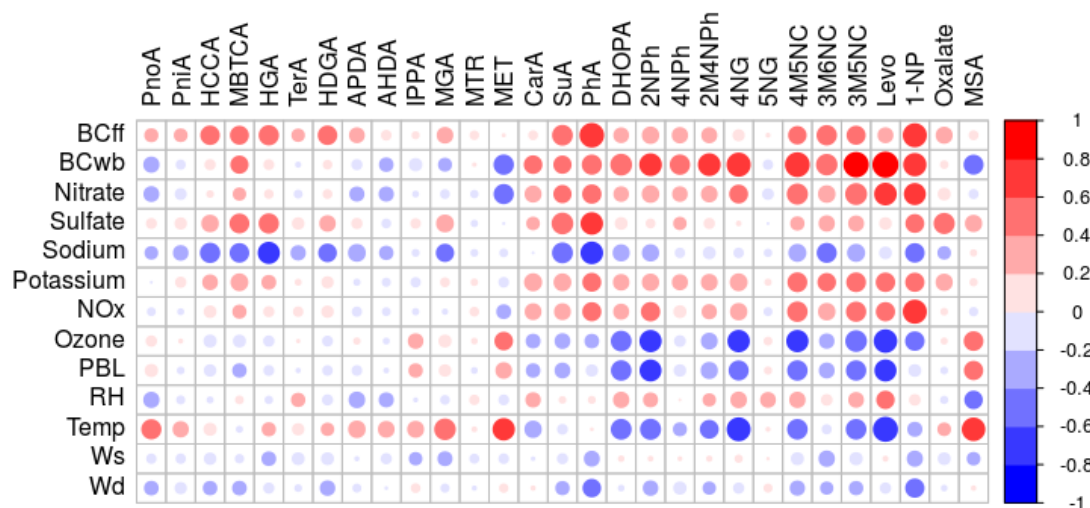
1472

1473 **Fig. S15.** Correlation matrix between molecular makers (primary and secondary) at SIRTA

1474 (2015).



1475
 1476 **Fig.S16.** Correlation matrix between PM chemical species, meteorological parameters and
 1477 trace gases (O₃ and NO_x) at SIRTA (2015).



1478
 1479 **Fig. S17.** Correlation matrix between molecular markers (primary and secondary),PM
 1480 chemical species and meteorological parameters at SIRTA (2015).

1481 **7. SOA tracer method**

1482 **Table S6.** EstimatedSOA mass fractions (f_{SOA}) and SOC mass fractions (f_{SOC}).

Chemical species	$f_{\text{SOAadjusted}}$	$f_{\text{SOCadjusted}}$
PnoA	0.0219	0.0301
PniA	0.0090	0.0124
HCCA	0.0101	0.0138
MBTCA	0.0118	0.0162
HGA	0.0243	0.0334
HDGA	0.0024	0.0033
APDA	0.0235	0.0324
AHDA	0.0600	0.0824
IPPA	0.0029	0.0039
MGA	0.0630	0.1550
MTR	0.0630	0.1550
MET	0.0630	0.1550
CarA	0.0109	0.0230
PhA	0.0206	0.0402
DHOPA	0.0040	0.0079
4M5NC	0.0489	0.0979
3M6NC	0.0093	0.0186
3M5NC	0.0409	0.0818

1483
1484
1485
1486
1487
1488
1489
1490

8. Positive matrix factorization (PMF) results.

Positive matrix factorization (PMF) is based on a weighted least squares fit, where the weights are derived from the analytical uncertainty and provides an optimal solution by minimizing the residuals (Paatero, 1997; Paatero and Tapper, 1994). The U.S. Environmental Protection Agency (US-EPA) PMF 5.0 software has been used to resolve the PM/SOA sources.

1491
1492
1493
1494
1495
1496
1497
1498
1499
1500
1501
1502
1503
1504
1505

8.1. Criteria for the selection of species

The selection of the input data for the PMF analyses is an important step, as already shown previously (Srivastava et al., 2018a, 2018b). The selection of the species was based on the following criteria: signal-to-noise ratio (S/N) (Paatero and Hopke, 2003), inclusion of compounds where at least 40% of total data points were above the detection limit, compounds considered as specific markers of a given source (e.g., 2-methylerythritol acid (2-MT) (SOA marker of isoprene oxidation), 2,3-dihydroxy-4-oxopentanoic acid (DHOPA) (SOA marker of toluene oxidation), methylnitrocatechol isomers (SOA from phenolic compounds oxidation mainly emitted by biomass burning)) (Carlton et al., 2009; Iinuma et al., 2010; Kleindienst et al., 2010)(Table S7). In addition, BC_{ff} and BC_{wb} have been used here instead of EC to improve the separation of primary emission sources such as biomass burning and traffic emissions. Note, only 20% of the species quantified has been finally used in order to keep a ratio of 1/3 between PM input species and the number of samples. Finally, a total number of 34 chemical species including inorganic species and metals, along with BC_{ff} , BC_{wb} , OC and molecular organic markers were used as input data for the PMF analysis (Table S7). PM_{10}

1506 concentrations were included as the total variable in the model to determine the source
1507 contributions.

1508
1509 The optimization of the final solution including the number of factors and the application of
1510 constraints were carried out following the same protocols as detailed by Srivastava et al.,
1511 (2018a). Briefly, wide range of factors (from 6 to 13) were explored including several
1512 constraints applied on the base run to obtain clear chemical source profiles. The details related
1513 to the constraints applied on each factor profile are given in Table S8. No significant
1514 difference ($p > 0.05$) was observed in the source chemical profiles between the base and the
1515 constrained runs (Table S9). Bootstrapping of the selected solution showed stable results with
1516 ≥ 88 out of 100 bootstrap mapped factors (Table S10). Finally, the 11-factor output provides
1517 the most reasonable solution for the selected dataset (Fig. S18 and S19). A good agreement
1518 was also noticed between the reconstructed PM_{10} contributions from all sources and the
1519 measured PM_{10} concentrations (Fig. S20). OA concentrations related to the PMF factors were
1520 further calculated applying OC-to-OA conversion factors specific to each source, i.e., 1.7 for
1521 biomass burning (Puxbaum et al., 2007), 1.2 for vehicular emissions (Drooge and Grimalt,
1522 2015) and 2.0 for secondary organics (Mohr et al., 2009). Identified aerosol sources are
1523 discussed individually below.
1524

1525 **8.2. . Primary traffic emissions**

1526 Due to the constraint applied, this factor was apportioned based on the high proportion of BC_{ff}
1527 (52%), several metals, such as Cu (53%), Sb (54%), Pb (40%) and Zn (38%) and 1-NP (59%)
1528 all considered typical species from road traffic emissions (Keyte et al., 2016; Pant and
1529 Harrison, 2012; Srivastava et al., 2016; Sternbeck et al., 2002). Note, more than half of 1-NP,
1530 good marker of diesel emissions (Keyte et al., 2016; Schulte et al., 2015; Zielinska et al.,
1531 2004a, 2004b)(Fig. S18)was attributed to this factor without applying any constraint. The use
1532 of 1-NP improved the resolution of this factor thanks to its good correlation with both, BC_{ff}
1533 and NO_x (Fig. S11).

1534 Primary traffic sources accounted for 11% of the PM_{10} mass on a yearly average (Fig. S21),
1535 with an annual mean concentration of $2.1 \mu g m^{-3}$. This value was consistent with previous
1536 studies conducted in the Paris region (14% of $PM_{2.5}$; (Bressi et al., 2014), 11% of PM_1 (Petit et
1537 al., 2014)and 5-% of PM_{10} (Srivastava et al., 2018a; Srivastava et al., 2019)
1538

1539 **8.3. Biomass burning**

1540 Biomass burning factor was characterized by the presence of levoglucosan (levo) (58%),
1541 mannosan (42%) and BC_{wb} (35%), including significant contributions of PAHs (B[a]P (24%),
1542 B[ghi]P (27%), and In[1,2,3-cd]P (32%)). The identified factor showed typical seasonal
1543 variations linked to biomass burning emissions, with maximum contributions observed in
1544 winter (38%) (Fig. S18). This source accounted for 6% of the PM_{10} mass on a yearly average
1545 ($1.2 \mu g m^{-3}$) (Fig. S20). Additionally, OC/levoglucosan ratio ($=5.2$) was in the range of the
1546 values generally reported in previously studies performed in the Paris region (Bressi et al.,
1547 2014; Sciare et al., 2011).

1548

1549 **8.4. Fungal spores**

1550 This source factor was characterized by the large proportions of polyols (arbitol (96%) and
1551 sorbitol (65%)) (Fig. S18), markers of primary biogenic emissions mainly originating from
1552 fungal spores and bacteria (Bauer et al., 2008; Caseiro et al., 2009; Rogge et al., 2007; Yttri et
1553 al., 2011). The factor contributed approximately to 8% of the PM₁₀ mass on an annual
1554 average, corresponding to a concentration of 15 µg m⁻³. As expected, high contributions
1555 during summer-autumn period were observed (Samaké et al., 2019a; Samaké et al., 2019b;
1556 Srivastava et al., 2018b).

1557

1558 **8.5. Sea salt**

1559 This factor showed major contributions of Na⁺ (75%) and Mg²⁺ (62%), highlighting the
1560 characteristic sea salt particles (Fig. S18). The Mg²⁺/Na⁺ ratio (0.09) was close to the sea
1561 water ratio (i.e., 0.11) (Curran et al., 1998; Seinfeld and Pandis, 1998) and similar to the
1562 values found in the Paris region (0.1-0.13) (Bressi et al., 2014; Srivastava et al., 2018a). In
1563 addition, this factor also showed high Cl⁻ content (84%), indicating the influence of fresh sea
1564 salt aerosols, with an annual contribution of 10% to the PM₁₀ mass (Fig.20) and a yearly
1565 average concentration of 2.0 µg m⁻³.

1566

1567 **8.6. Dust**

1568 This factor showed a relatively high content of mineral elements such as Ti (53%), Ca²⁺
1569 (49%), and Al (54%), commonly originating from soils and road dust (Andersen et al., 2007;
1570 Mossetti et al., 2005; Querol et al., 2004; Yin et al., 2005) (Fig. S16). This factor accounted
1571 for 15% of the PM₁₀ mass on an annual average corresponding to an average concentration of
1572 2.9 µg m⁻³ (Fig. S18).

1573

1574 **8.7. Sulfate-rich secondary aerosols**

1575 The factor (sulfate-rich) was characterized based on high loading of SO₄²⁻ (51%) including
1576 significant contributions from oxalate (24%) with an annual average concentration of 1.3 µg
1577 m⁻³ and accounting for approximately 7% of the PM₁₀ mass (Figs. S19 and S20). The source
1578 showed very constant temporal trend throughout the year except with very high
1579 concentrations during the spring PM pollution event (PM₁₀ > 50 µg m⁻³ for at least 3
1580 consecutive days) (Fig. S20). High contributions were related to long range transport and
1581 ageing processes highlighted previously for this same pollution event (Petit et al., 2017a;
1582 Srivastava et al., 2018a; Srivastava et al., 2019).

1583

1584 **8.8. Nitrate-rich secondary aerosols**

1585 The factor (nitrate-rich) was characterized by high contributions of NO_3^- and NH_4^+ (74% and
1586 66% of species mass being attributed to this factor, respectively), with an annual average
1587 concentration of $4.9 \mu\text{g m}^{-3}$ and accounting for approximately 25% of the PM_{10} mass (Figs.
1588 S19 and S20). The source showed a very distinctive seasonal variation with very high
1589 concentrations during the late winter-early spring period (Fig. S20). The high contributions of
1590 ammonium nitrate observed during this period was linked to secondary formation processes
1591 and long range transport of aged air masses and is typical of the late winter-early spring
1592 period in North-western Europe (Petit et al., 2017a; Srivastava et al., 2018a; Srivastava et al.,
1593 2019; Zhang et al., 2019).

1594

1595 **8.9. Biogenic SOA-1 (marine)**

1596 This factor showed very high loading (77%) of methanesulfonic acid (MSA), a known
1597 secondary oxidation product of dimethylsulfide (DMS). DMS is emitted by phytoplankton and
1598 several types of anaerobe bacteria and released from the ocean into the atmosphere (Charlson
1599 et al., 1987; Chasteen and Bentley, 2004; Crippa et al., 2013; Zorn et al., 2008). This factor
1600 accounted for 10% of the PM_{10} mass on annual average ($2.1 \mu\text{g m}^{-3}$) (Fig. S20) and followed
1601 a clear temporal variation with higher contributions during summer with a maximum
1602 contribution of 36% to the PM_{10} mass in agreement with phytoplankton blooms observed in
1603 the North Sea in summer season (Figs. S19 and S22), and was also confirmed by the results
1604 obtained from the Concentration-Weighted Trajectory (CWT) analysis (Figure S23).

1605

1606 **8.10. Biogenic SOA-2**

1607 Biogenic SOA-2 factor was resolved by using the SOA markers for oxidation of isoprene (α -
1608 methylglyceric acid (α -MGA and 2-methylerythritol (2-MT)) and pinene (3-hydroxy-4,4-
1609 dimethylglutaric acid and 3-acetylpentanedioic acid) (Carlton et al., 2009; Edney et al., 2005;
1610 Jaoui et al., 2008; Kleindienst et al., 2007). The factor showed very high loadings of these
1611 SOA markers (64-93% of the total mass of each compound), except for 3-hydroxy-4,4-
1612 dimethylglutaric acid (37%) (Fig. S19). Note, the separation of both biogenic SOA sources
1613 was not possible and resulted in a non-stable solution (poor bootstrap). Biogenic SOA factor
1614 showed a very low contribution to the PM_{10} mass of 2% on an annual average, corresponding
1615 to a concentration of $0.5 \mu\text{g m}^{-3}$ (Fig. S20). High concentrations (up to 7% of PM) observed in
1616 the summer were in good agreement with the higher biogenic activity and larger emissions of
1617 isoprene and pinene during the warm months (Kleindienst et al., 2007; Shrivastava et al.,
1618 2007; Srivastava et al., 2018b; Zhang et al., 2019, 2009).

1619 **8.11. Anthropogenic SOA-1**

1620 The factor was characterized by high loadings of succinic acid (69%), phthalic acid (73%),
1621 and DHOPA (68%) (Fig. S19). Phthalic acid and DHOPA are considered as markers of SOA
1622 formation from naphthalene and toluene photooxidation, respectively (Al-Naiema and Stone,
1623 2017; Kleindienst et al., 2004, 2007, 2012), while succinic acid is also a known oxidation
1624 product of anthropogenic precursors (Kawamura and Bikkina, 2016). Thus, this factor seemed

1625 to follow the characteristic of SOA from anthropogenic sources, including combustion
 1626 processes such as biomass burning and traffic. This source accounted for approximately 2%
 1627 of the total PM₁₀ mass, with a concentration of 0.4 µg m⁻³ (Fig. S20).

1628

1629 8.12. Anthropogenic SOA-2

1630 This factor was apportioned based on high fractions of 4-methyl-5-nitrocatechol (4-Me5Nc)
 1631 and 3-methyl-5-nitrocatechol (3-Me5Nc) (85% of each species mass being attributed to this
 1632 factor) (Fig. S19). Methyl-nitrocatechols are typical oxidation product of phenolic compounds
 1633 such as cresols, mainly originating from biomass burning emissions (Bruns et al., 2016;
 1634 Iinuma et al., 2010). In addition, this factor also showed significant contributions of
 1635 levoglucosan (23%), mannosan (23%), BC_{wb} (2%), some PAHs (B[a]P (38%), B[ghi]P
 1636 (31%), and In[1,2,3-cd]P (29%)) and DHOPA (13%). Therefore, this factor illustrated the
 1637 characteristic of biomass burning SOA.

1638 The source showed a low contribution to the PM₁₀ mass of 4% on annual average
 1639 corresponding to a concentration of 0.8 µg m⁻³ (Fig. S19 and S20). However, high
 1640 contributions (11%) were observed during winter when the biomass burning emissions were
 1641 predominant.

1642

1643 **Table S7.** List of input species in the PMF model.

PM ₁₀	Mn	Indeno[1,2,3-cd]pyrene
OC	Pb	1-Nitropyrene
BC _{ff}	Sb	Oxalate
BC _{wb}	Ti	MSA
Cl ⁻	Zn	α-Methylglyceric acid
NO ₃ ⁻	V	2-Methylerythritol
SO ₄ ²⁻	Al	3-Hydroxy-4,4- dimethylglutaric acid
Na ⁺	Levoglucosan	3-Acetylpentanedioic acid
NH ₄ ⁺	Mannosan	Succinic acid
K ⁺	Arabitol	DHOPA
Mg ²⁺	Mannitol	Phthalic acid
Ca ²⁺	Benzo[a]pyrene	4-Methyl-5-nitrocatechol
Cu	Benzo[g,h,i]perylene	3-Methyl-5-nitrocatechol

1644

1645 **Table S8.** List of the constraints applied on each factor profile in the PMF model to obtain the
 1646 final solution.

Factor	Species	Constraint type
Fungal spores	2-Methylerythritol	Pull down maximally
Fungal spores	Mannitol	Pull up maximally
Biomass burning	3-Hydroxy-4,4-dimethylglutaric acid	Pull down maximally
Primary emissions	traffic 3-Hydroxy-4,4-dimethylglutaric acid	Pull down maximally
Primary emissions	traffic BC _{ff}	Pull up maximally
Primary emissions	traffic BC _{wb}	Pull down maximally
Sulfate-rich	SO ₄ ²⁻	Pull up maximally
Nitrate-rich	NO ₃ ⁻	Set to original value
Biogenic SOA-1	2-Methylerythritol	Define limits
Biogenic SOA-2	3-Hydroxy-4,4-dimethylglutaric acid	Pull up maximally
Biogenic SOA-2	3-Acetylpentanedioic acid	Pull up maximally
Biogenic SOA-2	2-Methylerythritol	Pull up maximally
Anthropogenic SOA-1	3-Hydroxy-4,4-dimethylglutaric acid	Define limits
Anthropogenic SOA-1	Succinicacid	Pull up maximally
Anthropogenic SOA-1	DHOPA	Pull up maximally
Anthropogenic SOA-1	Phthalicacid	Pull Up Maximally

1647

1648

1649 **Table S9.** Comparison of source profiles before and after constraints. Results of observed P-value for each factor obtained using t-test.

	Biogenic SOA-1	Primary traffic emissions	Biogenic SOA-2	Sulfate-rich	Dust	Nitrate-rich	Biomass burning	Fungal spores	Sea salt	Anthropogenic SOA-1	Anthropogenic SOA-2
P-value (p<0.05)	0.36	0.75	0.20	0.22	0.17	0.26	0.18	0.09	0.47	0.17	0.10

1650

1651 **Table S10.** Results from bootstrap runs obtained for the final solution.

	Biogenic SOA-1	Primary traffic emissions	Biogenic SOA-2	Sulfate-rich	Dust	Nitrate	Biomass burning	Fungal spores	Sea salt	Anthropogenic SOA-1	Anthropogenic SOA-2
Biogenic SOA-1	97	0	0	0	0	0	0	0	0	0	0
Primary traffic emissions	0	88	0	0	9	0	0	0	0	0	0
Biogenic SOA-2	0	0	97	0	0	0	0	0	0	0	0
Sulfate-rich	0	0	0	88	0	9	0	0	0	0	0
Dust	0	0	0	0	97	0	0	0	0	0	0
Nitrate-rich	0	0	0	0	0	96	0	0	0	0	0
Biomass burning	0	1	0	0	0	0	95	0	0	0	0
Fungal spores	0	0	0	0	0	0	0	97	0	0	0
Sea salt	0	0	0	0	0	0	0	0	97	0	0
Anthropogenic	0	0	0	0	0	0	0	0	0	97	0

Chapter II: SOA marker measurements

SOA-1

Anthropogenic

SOA-2

0

0

1

0

0

0

0

0

0

0

96

1652

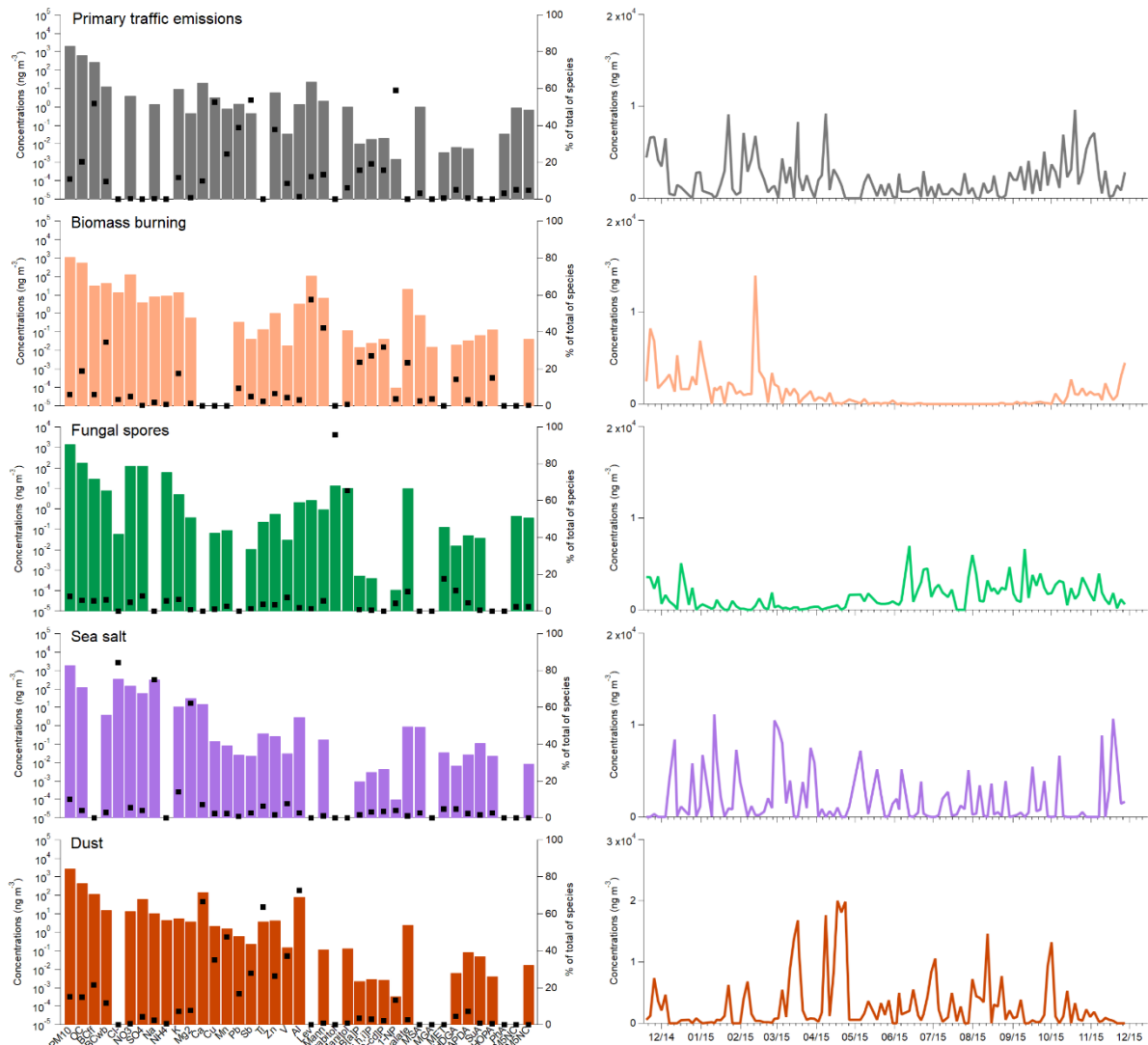


Fig. S18. Source profiles and temporal evolution of biomass burning, primary traffic emissions, fungal spores, sea salt and dust factors at SIRTA (2015).

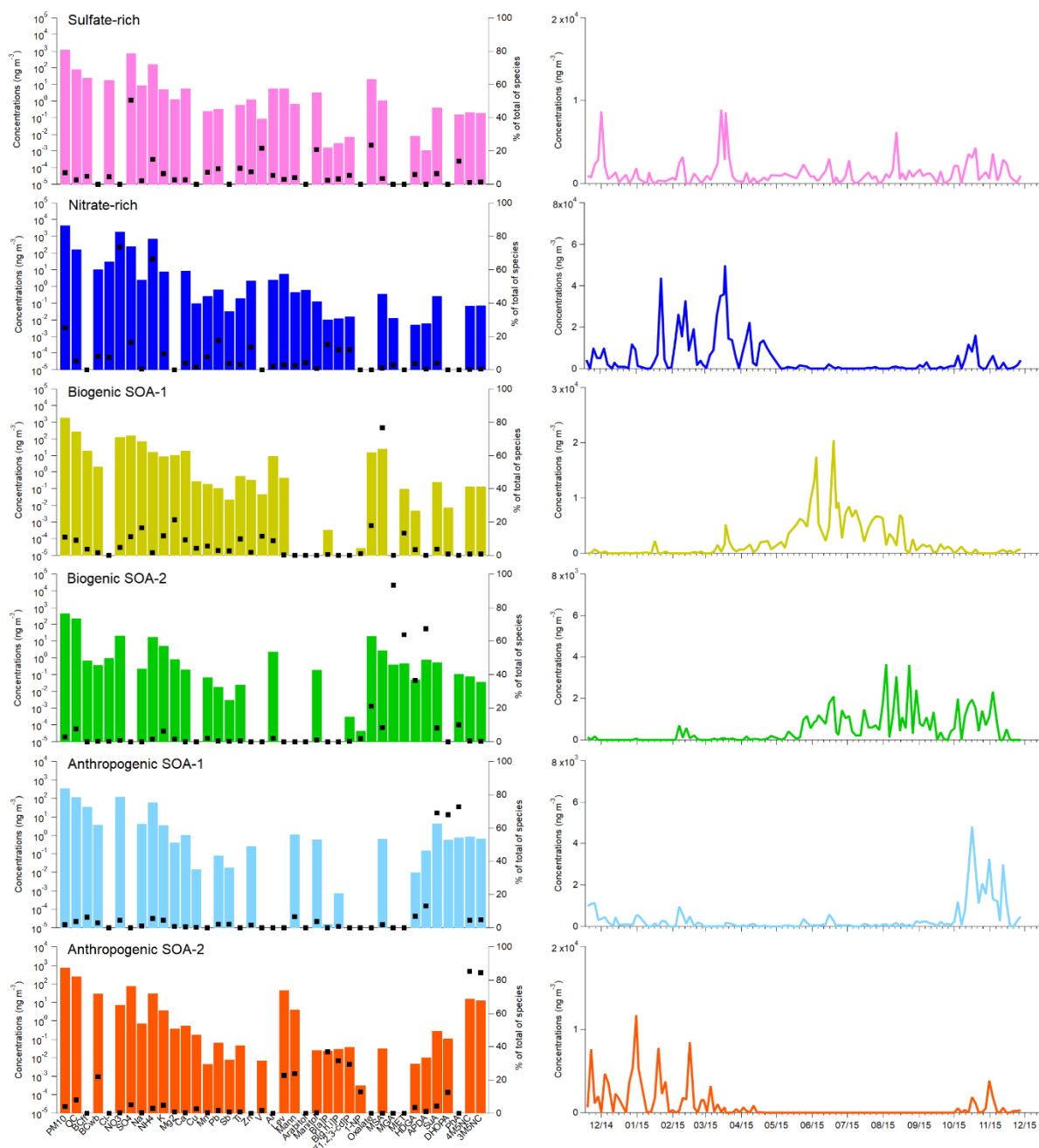


Fig. S19. Source profiles and temporal evolution of sulfate rich, nitrate rich, biogenic SOA-1, biogenic SOA-2, anthropogenic SOA-1 and anthropogenic SOA-2 factors at SIRTAs (2015).

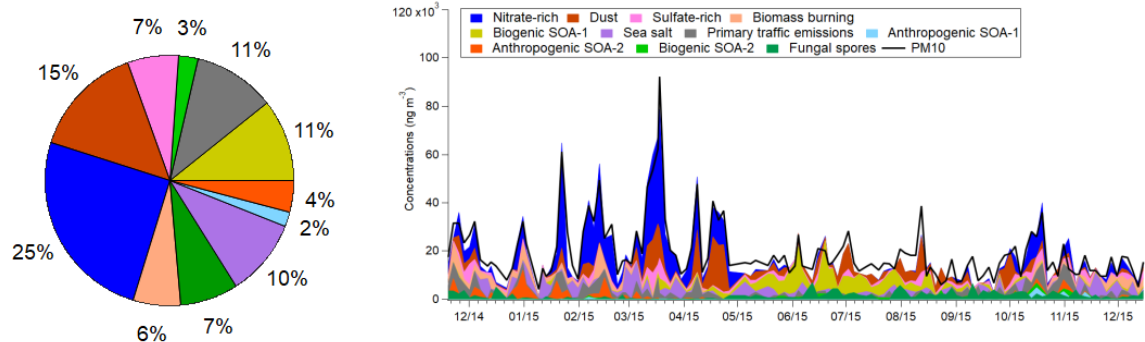


Fig. S20. Annual average contributions (left) and temporal evolution (right) of the identified sources to PM₁₀ mass concentrations at SIRT A (2015).

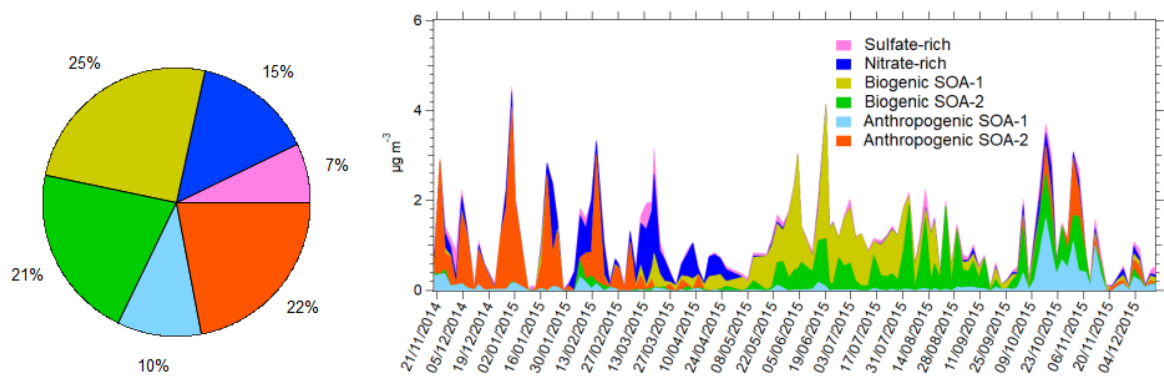


Fig. S21. Annual average contributions (left) and temporal evolution (right) of the identified sources to SOC mass concentrations at SIRT A (2015).

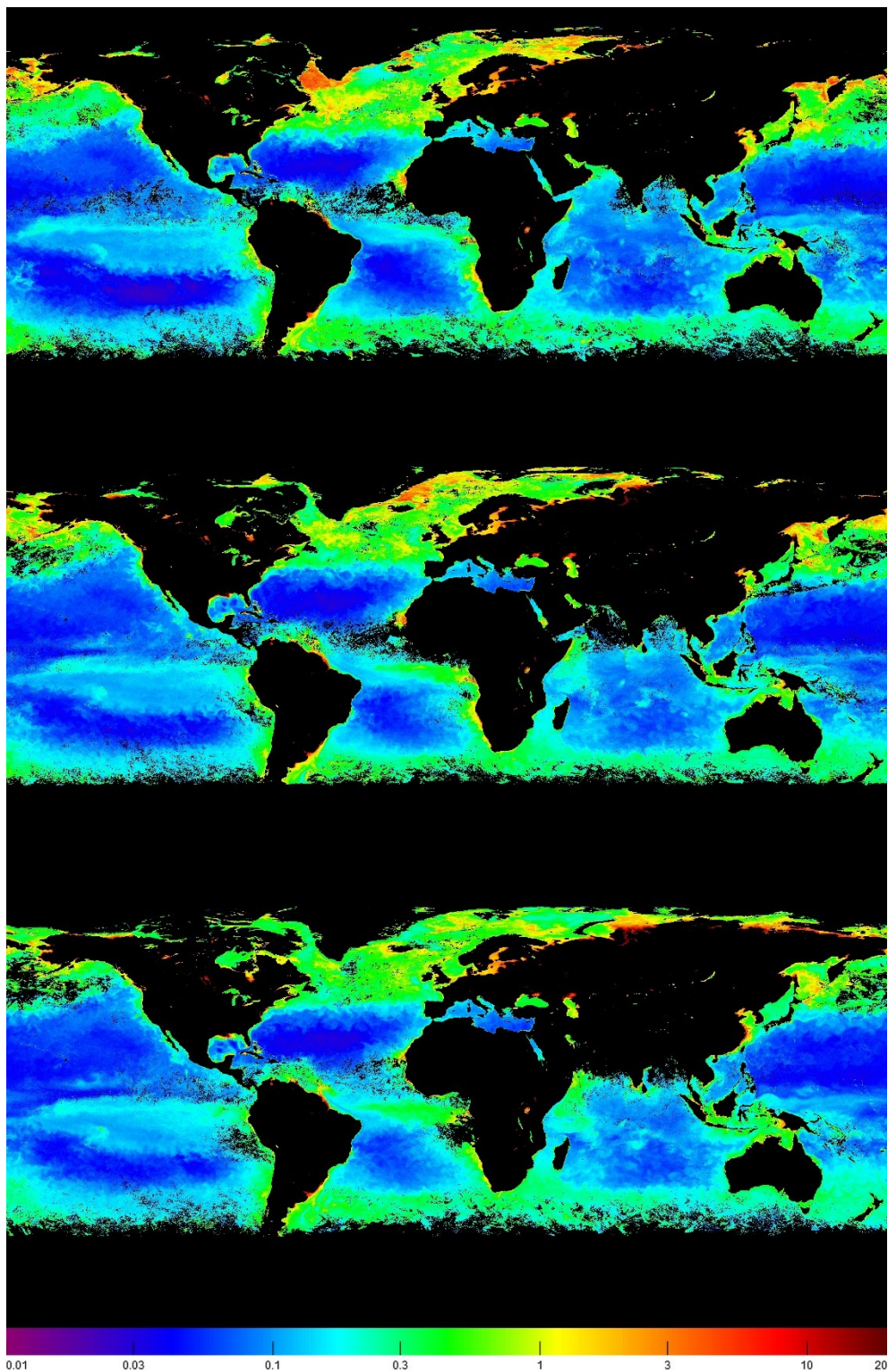


Fig. S22. Worldwide distribution of chlorophyll in mg m^{-3} for summer 2015 from satellite observations (<https://www.oceancolour.org/>). The maps show the chlorophyll distribution, from top to bottom, for June, July and August 2015, respectively.

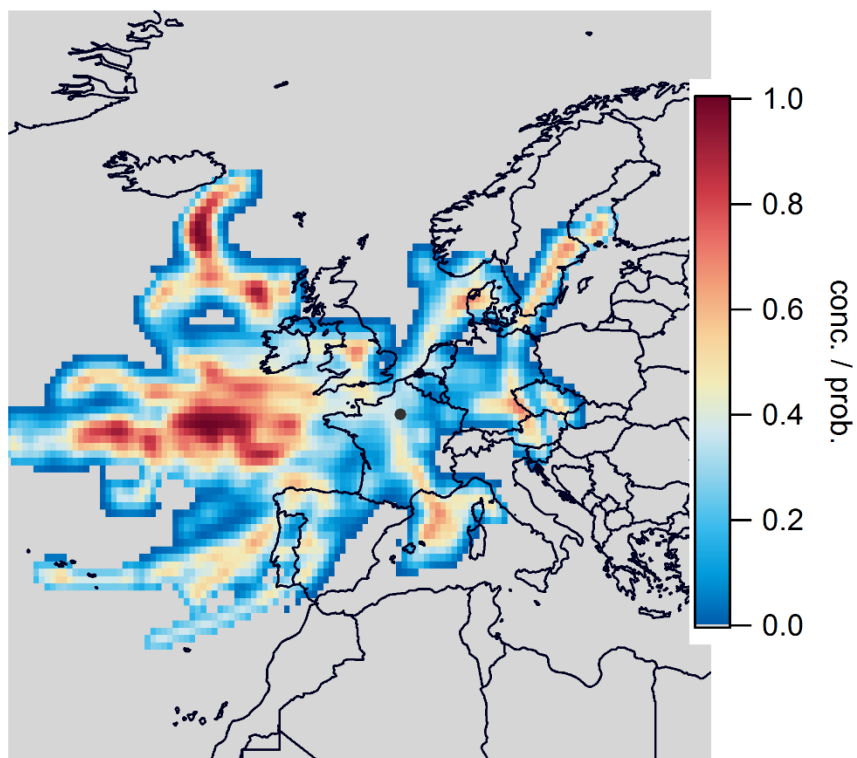


Fig. S23. Concentration-Weighted Trajectory (CWT) results for biogenic SOA-1 (marine). CWT calculations were performed using the ZeFir Igor package (Petit et al., 2017b). Details about all these calculations have been reported previously (Petit et al., 2017a).

References

- Albinet, A., Lanzafame, G.M., Srivastava, D., Bonnaire, N., Nalin, F., Wise, A., 2019. Analysis and determination of secondary organic aerosol (SOA) tracers (markers) in particulate matter standard reference material (SRM 1649b, urban dust). *Anal. Bioanal. Chem.*
- Alier, M., van Drooge, B.L., Dall'Osto, M., Querol, X., Grimalt, J.O., Tauler, R., 2013. Source apportionment of submicron organic aerosol at an urban background and a road site in Barcelona (Spain) during SAPUSS. *Atmospheric Chem. Phys.* 13, 10353–10371. <https://doi.org/10.5194/acp-13-10353-2013>
- Al-Naiema, I.M., Stone, E.A., 2017. Evaluation of anthropogenic secondary organic aerosol tracers from aromatic hydrocarbons. *Atmospheric Chem. Phys.* 17, 2053–2065. <https://doi.org/10.5194/acp-17-2053-2017>
- Andersen, Z.J., Wahlin, P., Raaschou-Nielsen, O., Scheike, T., Loft, S., 2007. Ambient particle source apportionment and daily hospital admissions among children and elderly in Copenhagen. *J. Expo. Sci. Environ. Epidemiol.* 17, 625–636. <https://doi.org/10.1038/sj.jes.7500546>
- Bauer, H., Claeys, M., Vermeylen, R., Schueller, E., Weinke, G., Berger, A., Puxbaum, H., 2008. Arabitol and mannitol as tracers for the quantification of airborne fungal spores. *Atmos. Environ.* 42, 588–593. <https://doi.org/10.1016/j.atmosenv.2007.10.013>
- Bressi, M., Sciare, J., Gherzi, V., Mihalopoulos, N., Petit, J.-E., Nicolas, J.B., Moukhtar, S., Rosso, A., Féron, A., Bonnaire, N., Poulakis, E., Theodosi, C., 2014. Sources and geographical origins of fine aerosols in Paris (France). *Atmospheric Chem. Phys.* 14, 8813–8839. <https://doi.org/10.5194/acp-14-8813-2014>
- Bruns, E.A., El Haddad, I., Slowik, J.G., Kilic, D., Klein, F., Baltensperger, U., Prévôt, A.S.H., 2016. Identification of significant precursor gases of secondary organic aerosols from residential wood combustion. *Sci. Rep.* 6. <https://doi.org/10.1038/srep27881>
- Carlton, A.G., Wiedinmyer, C., Kroll, J.H., 2009. A review of Secondary Organic Aerosol (SOA) formation from isoprene. *Atmospheric Chem. Phys.* 9, 4987–5005. <https://doi.org/10.5194/acp-9-4987-2009>
- Caseiro, A., Bauer, H., Schmidl, C., Pio, C.A., Puxbaum, H., 2009. Wood burning impact on PM₁₀ in three Austrian regions. *Atmos. Environ.* 43, 2186–2195. <https://doi.org/10.1016/j.atmosenv.2009.01.012>
- Cecinato, A., Di Palo, V., Pomata, D., Tomasi Scianò, M.C., Possanzini, M., 2005. Measurement of phase-distributed nitrophenols in Rome ambient air. *Chemosphere* 59, 679–683. <https://doi.org/10.1016/j.chemosphere.2004.10.045>
- Charlson, R.J., Lovelock, J.E., Andreae, M.O., Warren, S.G., 1987. Oceanic phytoplankton, atmospheric sulphur, cloud albedo and climate. *Nature* 326, 655–661. <https://doi.org/10.1038/326655a0>

Chasteen, T.G., Bentley, R., 2004. Volatile Organic Sulfur Compounds of Environmental Interest: Dimethyl Sulfide and Methanethiol. An Introductory Overview. *J. Chem. Educ.* 81, 1524. <https://doi.org/10.1021/ed081p1524>

Cheng, Y., Brook, J.R., Li, S.-M., Leithead, A., 2011. Seasonal variation in the biogenic secondary organic aerosol tracer cis-pinonic acid: Enhancement due to emissions from regional and local biomass burning. *Atmos. Environ.* 45, 7105–7112. <https://doi.org/10.1016/j.atmosenv.2011.09.036>

Chow, K.S., Huang, X.H.H., Yu, J.Z., 2015. Quantification of nitroaromatic compounds in atmospheric fine particulate matter in Hong Kong over 3 years: field measurement evidence for secondary formation derived from biomass burning emissions. *Environ. Chem.* 13, 665–673. <https://doi.org/10.1071/EN15174>

Claeys, M., Bim, G., Vas, G., Wang, W., Vermeylen, R., Pashynska, V., Cafmeyer, J., Guyon, P., Andreae, M.O., Artaxo, P., Maenhaut, W., 2004. Formation of secondary organic aerosols through photooxidation of isoprene. *Science* 303, 1173–1176. <https://doi.org/10.1126/science.1092805>

Clements, A.L., Seinfeld, J.H., 2007. Detection and quantification of 2-methyltetrols in ambient aerosol in the southeastern United States. *Atmos. Environ.* 41, 1825–1830. <https://doi.org/10.1016/j.atmosenv.2006.10.056>

Crippa, M., Haddad, I.E., Slowik, J.G., DeCarlo, P.F., Mohr, C., Heringa, M.F., Chirico, R., Marchand, N., Sciare, J., Baltensperger, U., Prévôt, A.S.H., 2013. Identification of marine and continental aerosol sources in Paris using high resolution aerosol mass spectrometry. *J. Geophys. Res. Atmospheres* 118, 1950–1963. <https://doi.org/10.1002/jgrd.50151>

Curran, M.A.J., Van Ommen, T.D., Morgan, V., 1998. Seasonal characteristics of the major ions in the high-accumulation Dome Summit South ice core, Law Dome, Antarctica. *Ann. Glaciol.* 27, 385–390. <https://doi.org/10.3189/1998AoG27-1-385-390>

Ding, X., Wang, X.-M., Gao, B., Fu, X.-X., He, Q.-F., Zhao, X.-Y., Yu, J.-Z., Zheng, M., 2012. Tracer-based estimation of secondary organic carbon in the Pearl River Delta, south China. *J. Geophys. Res. Atmospheres* 117, D05313. <https://doi.org/10.1029/2011JD016596>

Drooge, B.L. van, Grimalt, J.O., 2015. Particle size-resolved source apportionment of primary and secondary organic tracer compounds at urban and rural locations in Spain. *Atmospheric Chem. Phys.* 15, 7735–7752. <https://doi.org/https://doi.org/10.5194/acp-15-7735-2015>

El Haddad, I., Marchand, N., Temime-Roussel, B., Wortham, H., Piot, C., Besombes, J.-L., Baduel, C., Voisin, D., Armengaud, A., Jaffrezo, J.-L., 2011. Insights into the secondary fraction of the organic aerosol in a Mediterranean urban area: Marseille. *Atmospheric Chem. Phys.* 11, 2059–2079. <https://doi.org/10.5194/acp-11-2059-2011>

Fu, P., Aggarwal, S.G., Chen, J., Li, J., Sun, Y., Wang, Z., Chen, H., Liao, H., Ding, A., Umarji, G.S., Patil, R.S., Chen, Q., Kawamura, K., 2016a. Molecular Markers of Secondary Organic Aerosol in Mumbai, India. *Environ. Sci. Technol.* 50, 4659–4667. <https://doi.org/10.1021/acs.est.6b00372>

Fu, P., Zhuang, G., Sun, Y., Wang, Q., Chen, J., Ren, L., Yang, F., Wang, Z., Pan, X., Li, X., Kawamura, K., 2016b. Molecular markers of biomass burning, fungal spores and biogenic

SOA in the Taklimakan desert aerosols. *Atmos. Environ.* 130, 64–73. <https://doi.org/10.1016/j.atmosenv.2015.10.087>

Gómez-González, Y., Wang, W., Vermeylen, R., Chi, X., Neiryneck, J., Janssens, I.A., Maenhaut, W., Claeys, M., 2012. Chemical characterisation of atmospheric aerosols during a 2007 summer field campaign at Brasschaat, Belgium: sources and source processes of biogenic secondary organic aerosol. *Atmospheric Chem. Phys.* 12, 125–138. <https://doi.org/10.5194/acp-12-125-2012>

Iinuma, Y., Böge, O., Gräfe, R., Herrmann, H., 2010. Methyl-nitrocatechols: atmospheric tracer compounds for biomass burning secondary organic aerosols. *Environ. Sci. Technol.* 44, 8453–8459. <https://doi.org/10.1021/es102938a>

Ion, A.C., Vermeylen, R., Kourtchev, I., Cafmeyer, J., Chi, X., Gelencsér, A., Maenhaut, W., Claeys, M., 2005. Polar organic compounds in rural PM 2.5 aerosols from K-pusztá, Hungary, during a 2003 summer field campaign: Sources and diel variations. *Atmospheric Chem. Phys.* 5, 1805–1814. <https://doi.org/10.5194/acp-5-1805-2005>

Kahnt, A., Behrouzi, S., Vermeylen, R., Safi Shalamzari, M., Vercauteren, J., Roekens, E., Claeys, M., Maenhaut, W., 2013. One-year study of nitro-organic compounds and their relation to wood burning in PM10 aerosol from a rural site in Belgium. *Atmos. Environ.* 81, 561–568. <https://doi.org/10.1016/j.atmosenv.2013.09.041>

Keyte, I.J., Albinet, A., Harrison, R.M., 2016. On-road traffic emissions of polycyclic aromatic hydrocarbons and their oxy- and nitro- derivative compounds measured in road tunnel environments. *Sci. Total Environ.* 566–567, 1131–1142. <https://doi.org/10.1016/j.scitotenv.2016.05.152>

Kitanovski, Z., Grgić, I., Vermeylen, R., Claeys, M., Maenhaut, W., 2012. Liquid chromatography tandem mass spectrometry method for characterization of monoaromatic nitro-compounds in atmospheric particulate matter. *J. Chromatogr. A* 1268, 35–43. <https://doi.org/10.1016/j.chroma.2012.10.021>

Kleindienst, T.E., Conner, T.S., McIver, C.D., Edney, E.O., 2004. Determination of secondary organic aerosol products from the photooxidation of toluene and their implications in ambient PM 2.5. *J. Atmospheric Chem.* 47, 79–100.

Kleindienst, T.E., Jaoui, M., Lewandowski, M., Offenberg, J.H., Docherty, K.S., 2012. The formation of SOA and chemical tracer compounds from the photooxidation of naphthalene and its methyl analogs in the presence and absence of nitrogen oxides. *Atmospheric Chem. Phys.* 12, 8711–8726. <https://doi.org/10.5194/acp-12-8711-2012>

Kleindienst, T.E., Jaoui, M., Lewandowski, M., Offenberg, J.H., Lewis, C.W., Bhave, P.V., Edney, E.O., 2007. Estimates of the contributions of biogenic and anthropogenic hydrocarbons to secondary organic aerosol at a southeastern US location. *Atmos. Environ.* 41, 8288–8300. <https://doi.org/10.1016/j.atmosenv.2007.06.045>

Kleindienst, T.E., Lewandowski, M., Offenberg, J.H., Edney, E.O., Jaoui, M., Zheng, M., Ding, X., Edgerton, E.S., 2010. Contribution of Primary and Secondary Sources to Organic Aerosol and PM 2.5 at SEARCH Network Sites. *J. Air Waste Manag. Assoc.* 60, 1388–1399. <https://doi.org/10.3155/1047-3289.60.11.1388>

Kourtchev, I., Copolovici, L., Claeys, M., Maenhaut, W., 2009. Characterization of atmospheric aerosols at a forested site in Central Europe. *Environ. Sci. Technol.* 43, 4665–4671. <https://doi.org/10.1021/es803055w>

Kourtchev, I., Ruuskanen, T., Maenhaut, W., Kulmala, M., Claeys, M., 2005. Observation of 2-methyltetrols and related photo-oxidation products of isoprene in boreal forest aerosols from Hyytiälä, Finland. *Atmospheric Chem. Phys.* 5, 2761–2770. <https://doi.org/https://doi.org/10.5194/acp-5-2761-2005>

Kourtchev, I., Ruuskanen, T.M., Keronen, P., Sogacheva, L., Dal Maso, M., Reissell, A., Chi, X., Vermeylen, R., Kulmala, M., Maenhaut, W., Claeys, M., 2008a. Determination of isoprene and α - β -pinene oxidation products in boreal forest aerosols from Hyytiälä, Finland: diel variations and possible link with particle formation events: Isoprene and α - β -pinene oxidation products. *Plant Biol.* 10, 138–149. <https://doi.org/10.1055/s-2007-964945>

Kourtchev, I., Warnke, J., Maenhaut, W., Hoffmann, T., Claeys, M., 2008b. Polar organic marker compounds in PM_{2.5} aerosol from a mixed forest site in western Germany. *Chemosphere* 73, 1308–1314. <https://doi.org/10.1016/j.chemosphere.2008.07.011>

Kristensen, K., Glasius, M., 2011. Organosulfates and oxidation products from biogenic hydrocarbons in fine aerosols from a forest in North West Europe during spring. *Atmos. Environ.* 45, 4546–4556. <https://doi.org/10.1016/j.atmosenv.2011.05.063>

Lewandowski, M., Piletic, I.R., Kleindienst, T.E., Offenberg, J.H., Beaver, M.R., Jaoui, M., Docherty, K.S., Edney, E.O., 2013. Secondary organic aerosol characterisation at field sites across the United States during the spring–summer period. *Int. J. Environ. Anal. Chem.* 93, 1084–1103.

Limbeck, A., Puxbaum, H., Otter, L., Scholes, M.C., 2001. Semivolatile behavior of dicarboxylic acids and other polar organic species at a rural background site (Nylsvley, RSA). *Atmos. Environ.* 35, 1853–1862. [https://doi.org/10.1016/S1352-2310\(00\)00497-0](https://doi.org/10.1016/S1352-2310(00)00497-0)

Mohr, C., Huffman, J.A., Cubison, M.J., Aiken, A.C., Docherty, K.S., Kimmel, J.R., Ulbrich, I.M., Hannigan, M., Jimenez, J.L., 2009. Characterization of Primary Organic Aerosol Emissions from Meat Cooking, Trash Burning, and Motor Vehicles with High-Resolution Aerosol Mass Spectrometry and Comparison with Ambient and Chamber Observations. *Environ. Sci. Technol.* 43, 2443–2449. <https://doi.org/10.1021/es8011518>

Mohr, C., Lopez-Hilfiker, F.D., Zotter, P., Prévôt, A.S.H., Xu, L., Ng, N.L., Herndon, S.C., Williams, L.R., Franklin, J.P., Zahniser, M.S., Worsnop, D.R., Knighton, W.B., Aiken, A.C., Gorkowski, K.J., Dubey, M.K., Allan, J.D., Thornton, J.A., 2013. Contribution of nitrated phenols to wood burning brown carbon light absorption in Detling, United Kingdom during winter time. *Environ. Sci. Technol.* 47, 6316–6324. <https://doi.org/10.1021/es400683v>

Mossetti, S., Angius, S.P., Angelino, E., 2005. Assessing the impact of particulate matter sources in the Milan urban area. *Int. J. Environ. Pollut.* 24, 247. <https://doi.org/10.1504/IJEP.2005.007396>

Paatero, P., 1997. Least squares formulation of robust non-negative factor analysis. *Chemom. Intell. Lab. Syst.* 37, 23–35. [https://doi.org/10.1016/S0169-7439\(96\)00044-5](https://doi.org/10.1016/S0169-7439(96)00044-5)

Paatero, P., Hopke, P.K., 2003. Discarding or downweighting high-noise variables in factor analytic models. *Anal. Chim. Acta* 490, 277–289. [https://doi.org/10.1016/S0003-2670\(02\)01643-4](https://doi.org/10.1016/S0003-2670(02)01643-4)

Paatero, P., Tapper, U., 1994. Positive matrix factorization: A non-negative factor model with optimal utilization of error estimates of data values. *Environmetrics* 5, 111–126. <https://doi.org/10.1002/env.3170050203>

Petit, J.-E., Amodeo, T., Meleux, F., Bessagnet, B., Menut, L., Grenier, D., Pellan, Y., Ockler, A., Rocq, B., Gros, V., Sciare, J., Favez, O., 2017. Characterising an intense PM pollution episode in March 2015 in France from multi-site approach and near real time data: Climatology, variabilities, geographical origins and model evaluation. *Atmos. Environ.* 155, 68–84. <https://doi.org/10.1016/j.atmosenv.2017.02.012>

Piletic, I.R., Offenberg, J.H., Olson, D.A., Jaoui, M., Krug, J., Lewandowski, M., Turlington, J.M., Kleindienst, T.E., 2013. Constraining carbonaceous aerosol sources in a receptor model by including ¹⁴C data with redox species, organic tracers, and elemental/organic carbon measurements. *Atmos. Environ.* 80, 216–225. <https://doi.org/10.1016/j.atmosenv.2013.07.062>

Puxbaum, H., Caseiro, A., Sánchez-Ochoa, A., Kasper-Giebl, A., Claeys, M., Gelencsér, A., Legrand, M., Preunkert, S., Pio, C.A., 2007. Levoglucosan levels at background sites in Europe for assessing the impact of biomass combustion on the European aerosol background. *J. Geophys. Res. Space Phys.* 112, D23S05. <https://doi.org/10.1029/2006JD008114>

Querol, X., Alastuey, A., Viana, M.M., Rodriguez, S., Artiñano, B., Salvador, P., Garcia do Santos, S., Fernandez Patier, R., Ruiz, C.R., de la Rosa, J., Sanchez de la Campa, A., Menendez, M., Gil, J.I., 2004. Speciation and origin of PM₁₀ and PM_{2.5} in Spain. *J. Aerosol Sci.* 35, 1151–1172. <https://doi.org/10.1016/j.jaerosci.2004.04.002>

Rogge, W.F., Medeiros, P.M., Simoneit, B.R.T., 2007. Organic marker compounds in surface soils of crop fields from the San Joaquin Valley fugitive dust characterization study. *Atmos. Environ.* 41, 8183–8204. <https://doi.org/10.1016/j.atmosenv.2007.06.030>

Schulte, J.K., Fox, J.R., Oron, A.P., Larson, T.V., Simpson, C.D., Paulsen, M., Beaudet, N., Kaufman, J.D., Magzamen, S., 2015. Neighborhood-Scale Spatial Models of Diesel Exhaust Concentration Profile Using 1-Nitropyrene and Other Nitroarenes. *Environ. Sci. Technol.* 49, 13422–13430. <https://doi.org/10.1021/acs.est.5b03639>

Sciare, J., d'Argouges, O., Sarda-Estève, R., Gaimoz, C., Dolgorouky, C., Bonnaire, N., Favez, O., Bonsang, B., Gros, V., 2011. Large contribution of water-insoluble secondary organic aerosols in the region of Paris (France) during wintertime. *J. Geophys. Res. Atmospheres* 116, n/a-n/a. <https://doi.org/10.1029/2011JD015756>

Seinfeld, J.H., Pandis, S.N., 1998. *Atmospheric Chemistry and Physics*. Wiley-Interscience, New York, USA.

Shrivastava, M.K., Subramanian, R., Rogge, W.F., Robinson, A.L., 2007. Sources of organic aerosol: Positive matrix factorization of molecular marker data and comparison of results from different source apportionment models. *Atmos. Environ.* 41, 9353–9369. <https://doi.org/10.1016/j.atmosenv.2007.09.016>

Srivastava, D., Favez, O., Bonnaire, N., Lucarelli, F., Haefelin, M., Perraudin, E., Gros, V., Villenave, E., Albinet, A., 2018a. Speciation of organic fractions does matter for aerosol source apportionment. Part 2: Intensive short-term campaign in the Paris area (France). *Sci. Total Environ.* 634, 267–278. <https://doi.org/10.1016/j.scitotenv.2018.03.296>

Srivastava, D., Tomaz, S., Favez, O., Lanzafame, G.M., Golly, B., Besombes, J.-L., Alleman, L.Y., Jaffrezo, J.-L., Jacob, V., Perraudin, E., Villenave, E., Albinet, A., 2018b. Speciation of organic fraction does matter for source apportionment. Part 1: A one-year campaign in Grenoble (France). *Sci. Total Environ.* 624, 1598–1611. <https://doi.org/10.1016/j.scitotenv.2017.12.135>

van Drooge, B.L., Crusack, M., Reche, C., Mohr, C., Alastuey, A., Querol, X., Prevot, A., Day, D.A., Jimenez, J.L., Grimalt, J.O., 2012. Molecular marker characterization of the organic composition of submicron aerosols from Mediterranean urban and rural environments under contrasting meteorological conditions. *Atmos. Environ.* 61, 482–489. <https://doi.org/10.1016/j.atmosenv.2012.07.039>

Wang, Y., Hu, M., Wang, Y., Zheng, J., Shang, D., Yang, Y., Liu, Y., Li, X., Tang, R., Zhu, W., Du, Z., Wu, Y., Guo, S., Wu, Z., Lou, S., Hallquist, M., Yu, J., 2019. The formation of nitro-aromatic compounds under high NO_x-anthropogenic VOCs dominated atmosphere in summer in Beijing, China. *Atmospheric Chem. Phys. Discuss.* 1–22. <https://doi.org/10.5194/acp-2018-1256>

Yin, J., Allen, A.G., Harrison, R.M., Jennings, S.G., Wright, E., Fitzpatrick, M., Healy, T., Barry, E., Ceburnis, D., McCusker, D., 2005. Major component composition of urban PM₁₀ and PM_{2.5} in Ireland. *Atmospheric Res.* 78, 149–165. <https://doi.org/10.1016/j.atmosres.2005.03.006>

Yttri, K.E., Simpson, D., Stenström, K., Puxbaum, H., Svendby, T., 2011. Source apportionment of the carbonaceous aerosol in Norway – quantitative estimates based on ¹⁴C, thermal-optical and organic tracer analysis. *Atmospheric Chem. Phys.* 11, 9375–9394. <https://doi.org/10.5194/acp-11-9375-2011>

Yuan, Q., Lai, S., Song, J., Ding, X., Zheng, L., Wang, X., Zhao, Y., Zheng, J., Yue, D., Zhong, L., Niu, X., Zhang, Y., 2018. Seasonal cycles of secondary organic aerosol tracers in rural Guangzhou, Southern China: The importance of atmospheric oxidants. *Environ. Pollut.* 240, 884–893. <https://doi.org/10.1016/j.envpol.2018.05.009>

Zhang, Y., Sheesley, R.J., Schauer, J.J., Lewandowski, M., Jaoui, M., Offenberg, J.H., Kleindienst, T.E., Edney, E.O., 2009. Source apportionment of primary and secondary organic aerosols using positive matrix factorization (PMF) of molecular markers. *Atmos. Environ.* 43, 5567–5574. <https://doi.org/10.1016/j.atmosenv.2009.02.047>

Zhang, Y.Y., Müller, L., Winterhalter, R., Moortgat, G.K., Hoffmann, T., Pöschl, U., 2010. Seasonal cycle and temperature dependence of pinene oxidation products, dicarboxylic acids and nitrophenols in fine and coarse air particulate matter. *Atmospheric Chem. Phys.* 10, 7859–7873. <https://doi.org/10.5194/acp-10-7859-2010>

Zhu, C., Kawamura, K., Fu, P., 2016. Seasonal variations of biogenic secondary organic aerosol tracers in Cape Hedo, Okinawa. *Atmos. Environ., Chemical Characterization of*

Secondary Organic Aerosol - Dedication to Professor Claeys 130, 113–119.
<https://doi.org/10.1016/j.atmosenv.2015.08.069>

Zielinska, B., Sagebiel, J., Arnott, W.P., Rogers, C.F., Kelly, K.E., Wagner, D.A., Lighty, J.S., Sarofim, A.F., Palmer, G., 2004a. Phase and Size Distribution of Polycyclic Aromatic Hydrocarbons in Diesel and Gasoline Vehicle Emissions. *Environ. Sci. Technol.* 38, 2557–2567. <https://doi.org/10.1021/es030518d>

Zielinska, B., Sagebiel, J., McDonald, J.D., Whitney, K., Lawson, D.R., 2004b. Emission Rates and Comparative Chemical Composition from Selected In-Use Diesel and Gasoline-Fueled Vehicles. *J. Air Waste Manag. Assoc.* 54, 1138–1150. <https://doi.org/10.1080/10473289.2004.10470973>

Zorn, S.R., Drewnick, F., Schott, M., Hoffmann, T., Borrmann, S., 2008. Characterization of the South Atlantic marine boundary layer aerosol using an aerodyne aerosol mass spectrometer. *Atmospheric Chem. Phys.* 8, 4711–4728. <https://doi.org/10.5194/acp-8-4711-2008>

Chapter III

***Model to measurements comparison:
Anthropogenic markers***

Article II

Modelling organic aerosol markers in 3D air quality model. Part 1:

Anthropogenic organic markers.

To be submitted in “Atmospheric chemistry and physics”

Modelling organic aerosol markers in 3D air quality model. Part 1: Anthropogenic organic markers.

G.M. Lanzafame^{1,2}, F. Couvidat^{1,*}, O. Favez^{1,*}, A. Albinet¹ and B. Bessagnet^{1,2}

¹INERIS, Parc Technologique Alata, BP 2, 60550 Verneuil-en-Halatte, France

²Sorbonne Universités, UPMC, 75252 PARIS cedex 05, France

Correspondence to Florian Couvidat(florian.couvidat@ineris.fr)

Abstract.

Air quality models often underestimate the secondary organic aerosol (SOA) fractions in total organic aerosol (OA). The great variability of OA sources and composition make it difficult to validate model performances by in situ measurements (GPP). For these reasons, we developed and inserted in a 3D model the formation mechanisms of some anthropogenic marker: levoglucosan (primary marker), nitroaromatic compounds, DHOPA and phthalic acid (secondary markers). Simulation outputs have been compared with measurements performed in 10 urban sites in France in winter for levoglucosan and for secondary marker at SIRTA, in the Paris region, all over 2015. Gas to particle partitioning thermodynamic and spatial sensitivity have been examined.

Levoglucosan is well estimated in most of the sites, except for western cities, in which residential wood burning emissions are probably underestimated. A great uncertainty in levoglucosan concentrations is due to its recently proved semivolatility, that is reproduced by our model with a particulate phase fraction that varies between 20 and 80%. Our results suggest also a strong GPP spatial sensitivity to humidity for levoglucosan. Temporal variations and concentrations of secondary markers are well reproduced for nitrophenol and nitroguaiacols, and misrepresented and underestimated for methylnitrocatechol, DHOPA and phthalic acid. Precursors emissions and formation pathways are probably missing. GPP is well reproduced for nitroguaiacols, nitrophenols and DHOPA in non-ideal conditions and a protective effect towards degradation for the transfer to the particulate phase has been identified. Except for DHOPA (almost non-volatile), marker total concentrations are significantly affected by gas phase dry and wet deposition.

A theoretical study on the ratio between wood burning organic matter (OM_{wb}) and particulate phase levoglucosan variations in function of organic matter (OM) has also been performed. This ratio is constant only at high OM values ($<10 \mu\text{g m}^{-3}$) contrary to what is assumed in numerous studies.

1. Introduction and objectives

Air quality models are numerical tools to forecast and monitor air pollution events and assess air quality control policies. By using data such as emissions and meteorology, chemistry transport models (CTMs) simulate the main processes involved in the evolution of pollutant concentrations in the atmosphere. However, the model performances depend strongly on the model parametrizations and configurations. Outputs from different models are often discordant (Bessagnet et al., 2016). Organic aerosol (OA) is a major fraction of the fine particulate matter (PM) (Kanakidou et al., 2005; Zhang et al., 2007) originating from both, anthropogenic and biogenic sources. Whereas primary organic aerosol (POA) are directly emitted into the atmosphere, secondary organic aerosols (SOA) are produced by atmospheric (photo-)chemical reactions. Their formation occurs via photooxidation of the volatile organic compounds (VOCs) leading to semi volatile organic compounds (SVOC) products that partition between gas and particle phases. The SOA formation depends on multiple factors (reactants concentrations, meteorological parameters, various emission sources...) and their representation in air quality model remains challenging (Carlton et al., 2009; Hallquist et al., 2009; Kroll and Seinfeld, 2008; Ziemann and Atkinson, 2012).

Due to the great number of organic species, emissions sources (biomass burning, road traffic, vegetation, etc....) and phenomena involved in OA formation (aqueous-phase reactions, gas-phase reactions, oligomerization, gas-particle partitioning), it is not straightforward to analyze by comparison to in-situ observations of OA, the reasons for a lack of performances of air quality models. One way to provide information that could be used for the evaluation of CTM is to study molecular OA tracers (markers). Molecular markers from specific sources have been experimentally identified and are currently used for source apportionment (Kleindienst et al., 2007; Lough et al., 2007; Simoneit et al., 1999) and their partitioning under ambient conditions has been evaluated in several studies (Al-Naiema and Stone, 2017; Lanzafame et al., 2020; Xie et al., 2014; Yee et al., 2013). Levoglucosan, nitrophenols, nitroguaiacols, methylnitrocatechols, 2,3-dihydroxy-4-oxopentanoic acid (DHOPA), phthalic acid are examples of molecules commonly used as molecular markers. Levoglucosan has been identified as a lignin pyrolysis products and it is commonly used as a primary marker for biomass burning (Simoneit et al., 1999). Nitrated phenolic compounds (nitrophenols, nitroguaiacols and methylnitrocatechols) are usually considered as photooxidation products (secondary markers) of

biomass burning VOCs (Iinuma et al., 2010; Lauraguais et al., 2014; Olariu et al., 2002) but nitrophenols and methylnitrocatechols have also been detected in primary biomass burning emissions (Lu et al., 2019; Wang et al., 2017). DHOPA has been identified as a marker for toluene SOA (Kleindienst et al., 2007). Phthalic acid has been proposed as a marker for naphthalene and methylnaphthalene photooxidation (Kleindienst et al., 2012), but it has also been observed as a degradation product of phthalates emitted by plastic materials (Hankett et al., 2013) and as a primary marker emitted by vehicular exhaust (Kawamura and Kaplan, 1987). Although all the source apportionment tracer-based methods assume that these compounds are stable and low volatile (Nozière et al., 2015; Schauer et al., 1996; Srivastava et al., 2018), they can be degraded in atmosphere by sunlight and radical reactions and evidences of their semi volatile behavior have been provided (Bannan et al., 2017; Booth et al., 2012; Lanzafame et al., 2020; Xie et al., 2014). Based on these considerations, OA tracers should be rather called markers.

In this study, we propose to use modelling of specific OA markers and to compare the modelled concentrations to both measurements in the gas phase and in the particle phase to better evaluate the performance of air quality models. Model to measurements comparison can provide insights on the accuracy of emissions and chemical pathways representations in the model. Additionally, comparing concentrations in both the gas phase and the particle phase of specific SOA markers can be used to evaluate directly the capacity of models to reproduce GPP.

One of the challenges to include GPP in 3D air quality models is to evaluate their thermodynamic properties such as the subcooled liquid saturated vapor pressure (P_{sat}) and the vaporization enthalpy (ΔH_{vap}). However, only a few studies were performed on the marker thermodynamic properties and their partitioning in ambient air (Bannan et al., 2017; Bilde et al., 2015; Booth et al., 2011; Oja and Suuberg, 1999; Xie et al., 2014). As OA marker are generally solid at ambient conditions, P_{sat} at ambient temperature is calculated from the solid-state vapor pressure and the fusion enthalpy (Booth et al., 2012). The condensation of SVOC is also influenced by the aerosol non-ideality and aerosol viscosity. For simplification aerosol models often assume the ideality (no short-, medium- and long-range interactions between the compounds) whereas the partitioning is strongly dependent on non-ideality (Couvidat et al., 2012, Kim et al., 2019). Moreover, viscosity mixing affects the diffusion of the marker inside the particle, slowing down the exchange processes with the gaseous phase (Shrivastava et al., 2017). Kim et al. (2019) showed that considering the viscosity of the organic phase could lead to a strong increase of particle-phase concentrations of high volatility compounds.

This paper focuses on the development of chemical mechanisms of some anthropogenic markers: levoglucosan and several secondary SOA markers (nitrophenols, nitroguaiacols, methylnitrocatechols, DHOPA and phthalic acid) and presents model to measurements comparisons of concentrations and

GPP at SIRTA in the Paris region. To our knowledge, this is the first time that the anthropogenic markers mentioned are modelled in a 3D CTM. Model to measurements comparison of concentrations were also carried out for levoglucosan at several sites over France. Finally, some sensitivity analyses on GPP are presented in the final part of the paper.

2. Model development

A gaseous and aqueous phase mechanism for the formation of 14 organic markers in ambient air has been developed and inserted in the 3D chemistry-transport model CHIMERE 2017 β (Couvidat et al., 2018). The CHIMERE 2017 β aerosol module was extensively described in Couvidat et al., (2018). CHIMERE uses a sectional approach, with particles separated into 9 bins from 10nm to 10 μ m. The evaporation/condensation of semi-volatile compounds is represented with the algorithm of Pandis et al., (1993) using thermodynamic equilibria computed with the thermodynamic modules ISORROPIA for inorganics (Fountoukis and Nenes, 2007) and the secondary organic aerosol processor (SOAP, Couvidat and Sartelet, 2015) for organics. Coagulation of particles is represented as in Debry et al., (2007). H₂SO₄ nucleation parametrization is simulated as in Kulmala et al., (1998).

The model takes into account the wet and dry deposition of particles as a function of their wet diameter as presented in Couvidat et al., (2018). The dry deposition of the gas-phase concentration of SVOC can be estimated according to their Henry's law constant as in in Bessagnet et al., (2010). Similarly, the model can also consider the in-cloud and the below-cloud scavenging of SVOC.

The marker formation mechanism is added to the gas-phase mechanism MELCHIOR2 (Derognat et al., 2003) and to the Hydrophilic/Hydrophobic Organics (H²O) SOA formation mechanism (Couvidat et al., 2012) already inserted in CHIMERE. In the H²O mechanism, SOA are produced by the photooxidation of the major volatile organic compounds (VOCs: isoprene, monoterpenes, sesquiterpenes, toluene and xylene). POA is treated as SVOCs and split in 3 surrogate species with different volatility and aging products. Following Majdi et al., (2019), the H²O mechanism has been refined by adding SOA formation for the oxidation of several precursors from biomass burning: phenol, cresol, catechol, benzene, furan, guaiacol, syringol, naphthalene and methylnaphthalene.

2.1 Overview of the marker mechanism

The marker version of CHIMERE 2017 β includes 267 species and 757 reactions, against the 69 species and 215 reactions in the base version.

For secondary markers, the precursors considered are toluene, guaiacol, phenol, isoprene and α -/ β -pinene. Mechanisms for markers formation were sought in literature, taken from the Master Chemical

Mechanism (MCM, version 3.3.1) and missing information (not found in the literature and using MCM) were taken from the Generator for Explicit Chemistry and Kinetics of Organics in the Atmosphere (GECKO-A, Camredon et al., 2007) for the gaseous phase chemistry and from the Cloud Explicit Physico-chemical Scheme (CLEPS 1.0, Mouchel-Vallon et al., 2017) for the aqueous phase chemistry. These mechanisms are developed with the following procedure: the precursors are photolyzed, oxidized or hydrolyzed according to kinetics and branching ratios obtained from laboratory data, and when laboratory data are not available, the reactivity is estimated by analogy with similar better characterized systems or with structure activity relationships (SARs). The photooxidation mechanisms are usually initiated in the gaseous phase by reaction with OH, NO₃ and also O₃ for isoprene and α -/ β -pinene. Further reaction steps consider also the reactivity with HO₂, RO₂, NO and NO₂, photolysis, hydrolysis and aqueous-phase reactions. To simulate aqueous phase reactivity, the substrate and OH radicals partition between the gaseous and aqueous phases according to its Henry's law constant and solubilization enthalpy. The value chosen for OH Henry's law constant is 25 M⁻¹ atm (Lelieveld and Crutzen, 1991). Following Couvidat et al. (2013), the aqueous-phase concentration of OH has been assumed to be half of the concentration at the equilibrium, to take in account the consumption by the other species dissolved. The detailed mechanisms for anthropogenic markers are discussed below and reported in the supplementary material. The mechanisms for the biogenic markers are presented in the companion paper.

The gas to particle partitioning of markers and some reaction intermediates is computed with SOAP (Couvidat and Sartelet, 2015), briefly described in the next section. The GPP is estimated by the model by using P_{sat} and ΔH_{vap} . These parameters have been sought in literature, measured data has been preferred when available. For the markers with no published data, SARs estimations have been inserted in the model or used to deduce semi-empiric values related to experimental data for similar molecules. Henry's law constants (K_{H}) used for marker deposition have been calculated with SOAP.

2.1.1 Marker GPP computation

In SOAP, the user chooses whether the SVOC species are hydrophilic (condensed onto the aqueous phase of particles), hydrophobic (condensed onto the organic phase) or both (condensed on both phase). By using the molecular structure assigned to each species, the model computes the activity coefficients with the UNiversal Functional group Activity Coefficient; (UNIFAC, Fredenslund et al., 1975) model for short-range interactions (interactions between solvent species) and the Aerosol Inorganic–Organic Mixtures Functional groups Activity Coefficients (AIOMFAC, (Zuend et al., 2008, 2010, 2011; Zuend and Seinfeld, 2012) model for the medium-range and long-range interactions (interactions between

solvent species and ionic species) and uses them to simulate the non-ideality of aerosols. These structure activity relationship models include parameterizations to calculate activity coefficients of aerosol mixtures containing water, several organic functional groups (e.g. carboxyl, hydroxyl aldehyde, aromatic carbon ...) and inorganic ions for AIOMFAC. As some NO₂ parameters are missing, the parameters for alkanes were used instead.

P_{sat} and ΔH_{vap} are required as input data for the model. To compute the hydrophilic partitioning, the value of the Henry's law constant is used. It can be either provided by the user or be computed from the saturation vapor pressure and the activity coefficient at infinite dilution.

SOAP can use either a dynamic approach or an equilibrium approach (assuming instantaneous partitioning) to compute OA formation. For computational purposes, the equilibrium approach was used here. The effect of modeling with SOAP non-ideality and non-equilibrium was studied in a previous paper (Kim et al., 2018)

In the equilibrium approach, the partitioning between the organic phase and the gaseous phase is estimated according to a modified version of Raoult's law that evaluates the organic compounds absorption by the organic phase (Pankow, 1994):

$$\frac{A_{p,i}}{A_{g,i}} = K_{p,i} M_0 \quad (\text{Eq.1})$$

where $A_{p,i}$ is in the organic phase concentration ($\mu\text{g m}^{-3}$) of i , $A_{g,i}$ the gas-phase concentration ($\mu\text{g m}^{-3}$) of i , M_0 the organic phase concentration ($\mu\text{g m}^{-3}$) and $K_{p,i}$ the organic-phase partitioning coefficient ($\text{m}^3 \mu\text{g}^{-1}$):

$$K_{p,i} = \frac{760 \times 8.202 \times 10^{-5} \times T}{M_{ow} \gamma_{i,org} P_i^0 \times 10^6} \quad (\text{Eq.2})$$

where T is the temperature (in K), M_{ow} the organic phase mean molar mass (g mol^{-1}), $\gamma_{i,org}$ is the activity coefficient of i and P_i^0 the saturation vapor pressure (torr).

Assuming infinite dilution, the partitioning between gaseous phase and the aqueous phase can be evaluated with Henry's law. In SOAP, a modified version of this law, suitable for all dilution conditions, is used:

$$\frac{A_{aq,i}}{A_{g,i}} = K_{aq,i} AQ \quad (\text{Eq.3})$$

where $A_{aq,i}$ is the concentration of species i in the organic phase ($\mu\text{g m}^{-3}$), $A_{g,i}$ the gaseous phase concentration of i ($\mu\text{g m}^{-3}$), AQ the aqueous phase organics + inorganics concentration ($\mu\text{g m}^{-3}$) and $K_{aq,i}$ is the partitioning coefficient in the aqueous phase ($\text{m}^3 \mu\text{g}^{-1}$):

$$K_{aq,i} = \frac{K_{H,i} RT}{\rho_{water} \zeta_i \times 1.013 \times 10^{11}} \times \frac{18}{M_{aq}} \quad (\text{Eq. 4})$$

where $K_{H,i}$ is the i Henry's law constant ($M^{-1} \text{ atm}$), ρ_{water} is the aqueous phase density (kg m^{-3}), M_{aq} is the molar mass of the aqueous phase (g mol^{-1}) considering the presence of other compounds and ζ_i is the ratio of the i activity coefficient in the aqueous phase with the activity coefficient at infinite dilution in water:

$$\zeta_i = \frac{\gamma_{i,aq}}{\gamma_{i,aq}^{\infty}} \quad (\text{Eq. 5})$$

$\gamma_{i,aq}^{\infty}$ is computed with UNIFAC (Fredenslund et al., 1975). $\gamma_{i,aq}$ is computed multiplying the activity coefficients for long-, medium- and short-range interactions (Zuend et al., 2008).

$K_{aq,i}$ depends on temperature through a Clausius–Clapeyron relation as for the organic phase partitioning coefficient. A modification of partitioning coefficient to consider the acidic dissociation (by using acid dissociation constants) in the aqueous phase is added as in Pun et al. (2006). The concentrations of water and inorganics are taken from the results given by ISORROPIA.

2.2 Anthropogenic OA marker formation in the atmosphere: mechanisms and GPP parameters

The mechanisms developed for the anthropogenic markers, together with the parameters chosen to simulate their GPP at the equilibrium, are described below. For simplification, only the reactions involved in the marker formation pathways are discussed. The competitive reactions with other radicals, which do not lead to the formation of the studied markers, are also considered in the mechanism and reported in the SM. The molecules are named as in MCM or using MCM-like names. The thermodynamics properties of the markers are summarized in Table 1.

Table 1 Thermodynamic properties of the modelled anthropogenic organic markers. P_{sat} and ΔH_{vap} are used as input to calculate ΔH_{vap} and K_H with SOAP (Couvidat and Sartelet, 2015).

Modelled species	Measured markers	P_{sat} at 298K (torr)	ΔH_{vap} (KJmol^{-1})	ΔH_{solv} (KJmol^{-1})	K_H at 298 K ($M^{-1} \text{ atm}$)
DHOPA	DHOPA	1.95×10^{-6}	111.0	116.1	7.25×10^{10}
LEVO	Levogluconan	1.45×10^{-6}	52.0	61.6	2.26×10^{10}
MNCATECH	Methylnitrocatechols*	3.20×10^{-6}	41.7	68.9	1.30×10^9
NGUAIACOL	4-Nitroguaiacol	4.61×10^{-5}	30.9	51.7	5.60×10^7
NPHEN	Nitrophenols**	3.86×10^{-5}	51.2	63.8	3.90×10^7
PHTHALIC	Phthalic Acid	1.26×10^{-5}	40.0	46.7	1.20×10^8

*Sum of 3-methyl-5-nitrocatechol, 4-methyl-5-nitrocatechol and 3-methyl-6-nitrocatechol. Thermodynamic properties of a generic methylnitrocatechol.

**Sum of 2-nitrophenol and 4-nitrophenol. Thermodynamic properties of 4-nitrophenol.

2.2.1 Levoglucosan

Levoglucosan degradation in atmosphere occurs in the gaseous and in the aqueous phase. In the gaseous phase, levoglucosan reacts with the OH radical following the kinetic rate parameter proposed by Bai et al., (2013) of $2.21 \times 10^{-13} \text{ cm}^3 \text{ molecule}^{-1} \text{ s}^{-1}$. The degradation in the aqueous phase by OH radicals was also taken into account based on the the kinetic parameter measured by Yang et al., (2009) ($2.1 \times 10^9 \text{ M}^{-1} \text{ s}^{-1}$). Evidences for a semivolatile behavior of Levoglucosan are provided in Xie et al., (2014). The values chosen for levoglucosan P_{sat} and ΔH_{vap} are respectively $1.45 \times 10^{-6} \text{ torr}$ and 52 kJ mol^{-1} (measured values, 298 K) (Booth et al., 2011).

2.2.2 Nitroguaiacols

Nitroguaiacols are the photooxidation products of guaiacol, known as a primary compound emitted by biomass burning (McDonald et al., 2000). In the atmosphere, the photooxidation can be initiated by both, reaction with the hydroxy or with the nitrate radical (Fig. S1). All nitroguaiacols are represented as a single species since the SARs used to estimate the saturated vapor pressure are not able to distinguish the isomers.

For the degradation with OH, Coeur-Tourneur et al., (2010) observed in a chamber experiment a kinetic rate of $7.5 \times 10^{-11} \text{ cm}^3 \text{ molecule}^{-1} \text{ s}^{-1}$. Lauraguais et al., (2014) measured the gas-phase photooxidation yields for the guaiacol reaction with OH. With a yield of 10%, 4-nitroguaiacol was found to be the major product, followed by a mixture of 3- and 6-nitroguaiacol (yield 6%). Since no detailed mechanism was available in the literature, a yield of 16% has been used to model nitroguaiacols from OH-initiated guaiacol oxidation reaction.

The experimental value for the kinetic rate parameter of guaiacol with NO_3 is $3.2 \times 10^{-12} \text{ cm}^3 \text{ molecule}^{-1} \text{ s}^{-1}$ (Yang et al., 2016). The nitro-derivatives have been found to be the major products of this reaction (Yang et al., 2016), but no yield was provided. We assumed that the nitroguaiacols mixture has a yield of 100%. since no degradation kinetic rate of nitroguaiacols has been implemented in the gas-phase mechanism (due to lack of data in literature), the nitroguaiacol concentrations may be overestimated.

Nitroguaiacol P_{sat} and ΔH_{vap} were estimated with a semi-empiric method, taking experimental nitrocatechol P_{sat} and ΔH_{vap} ($7.50 \times 10^{-6} \text{ torr}$ and 39 kJ mol^{-1} respectively) (Booth et al., 2012) as reference. SARs P_{sat} and ΔH_{vap} have been calculated with EPIsuite (US EPA, 2015) for nitrocatechol and nitroguaiacol to estimate the effect of the -OH substitution with -OCH₃. The P_{sat} ratio and the ΔH_{vap} difference have been used as correction factors to calculate semi-empirical values, giving respectively $4.61 \times 10^{-5} \text{ torr}$ and 30.9 kJ mol^{-1} (details in Tables S8, S9 and S10).

2.2.3 Nitrophenols

The precursors of nitrophenols are toluene, benzene and phenol. In MCM there is no distinction for the nitrophenol isomer formation yields. The photooxidation process of toluene is started by reaction with OH, with a kinetic rate parameter of $1.8 \times 10^{-12} e^{(340/T)} \text{ cm}^3 \text{ molecule}^{-1} \text{ s}^{-1}$ (T being the temperature in K). This reaction generates 4 oxidation products: the benzyldioxidanyl radical (MCM name C6H5CH2O2), cresol, a dioxabicyclic-alcoholic-peroxy-hydroxy-hexene radical (TLBIPERO2) and oxobutenyl oxirane carbaldehyde (TLEPOXMUC) (see Fig 1, branching ratios are 0.07, 0.18, 0.65 and 0.10 respectively). C6H5CH2O2 is the intermediate for nitrophenol formation.

The NO₃ initiated photooxidation can also produce C6H5CH2O2, but MCM does not include this reaction. Huang et al., (2014) performed a computational study on the NO₃-initiated photooxidation of toluene. They assessed that the major isomer generated by H abstraction is the benzyl radical, with a rate constant of $6.10 \times 10^{-17} \text{ cm}^3 \text{ molecule}^{-1} \text{ s}^{-1}$. We assumed that the yield of the benzyl radical in this reaction is 100%.

The successive steps lead to the formation of the benzaldehyde as intermediate, involving reactions with HO₂, NO and photolysis. A multi-step benzaldehyde photooxidation generate the phenate radical, that reacts with NO₂ to give the nitrophenol. Phenol and benzene are also considered as nitrophenols precursors. Phenol is both a primary compound and the photooxidation intermediate from benzene. Benzene reacts with OH giving phenol, and phenate is produced by the reaction of phenol with OH and NO₃. All these reactions were coded in MCM and reported in Fig. 2. The mechanism produces a mixture of 2- and 4-nitrophenol. No evidence was provided for the formation of 3-nitrophenol (Cecinato et al., 2005). Branching ratios for nitrophenol formation are not available in the literature, however some ambient air measurements in both, gaseous and particulate phases, reported that 4-nitrophenol is the most abundant isomer (Cecinato et al., 2005). 4-nitrophenol thermodynamic parameters have therefore been chosen to simulate nitrophenols GPP. P_{sat} value is 3.86×10^{-5} torr, measured by Bannan et al., (2017). Experimental ΔH_{vap} were not available, so the arithmetic mean of SARs values (Table S1 and S3, calculated with UManSysProp (Topping et al., 2016)), $51.16 \text{ kJ mol}^{-1}$, has been used.

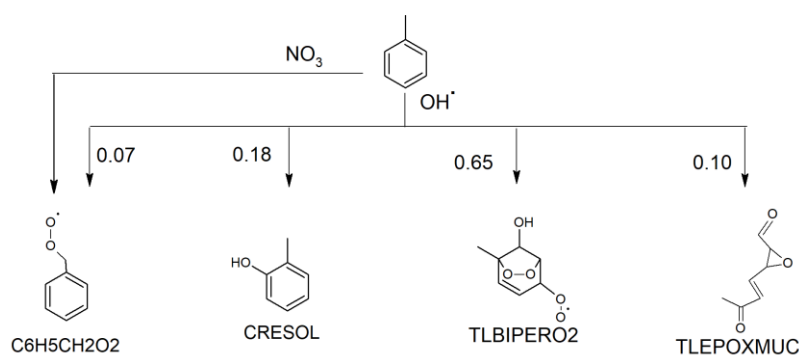
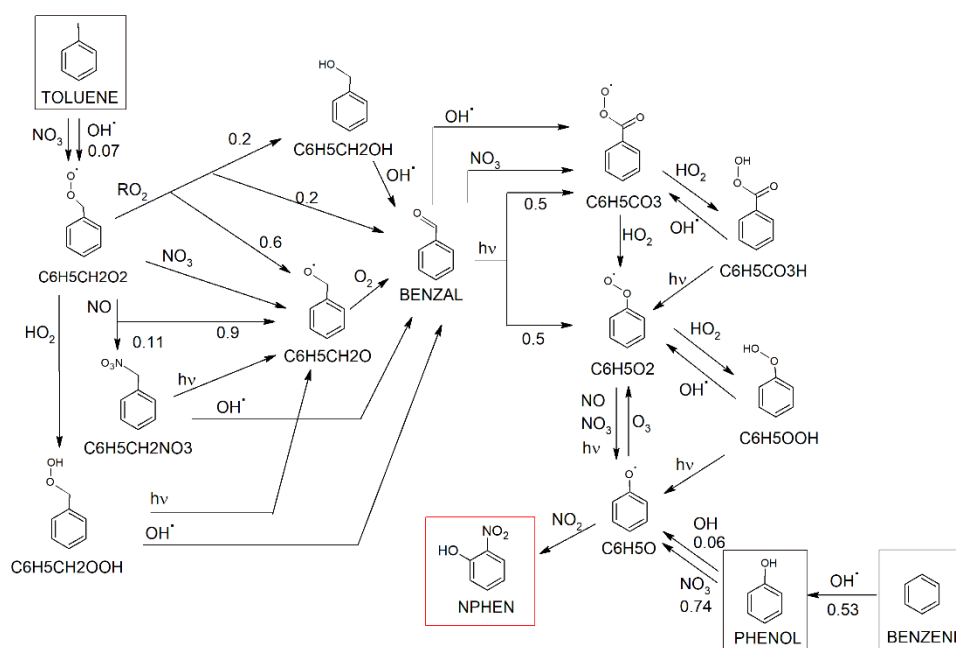


Figure 1.First step of toluene photooxidation (MCM)**Figure 2.** Nitrophenols formation pathway from cresol, benzene and phenol photooxidation. All the mechanism is included in MCM. For simplification, only the reactions directly involved in the formation pathway are shown, competitive reactions are taken in account in the model.

2.2.4 DHOPA

DHOPA has been recognized as a photooxidation product of toluene (Kleindienst et al., 2004) but to the best of our knowledge, no mechanism about the formation of DHOPA has been reported in the literature.

The 4-oxo-2-pentenal (C5DICARB) is one of the major ring-opening photooxidation products of toluene, with a yield of 4% (Bierbach et al., 1994). We supposed that this compound is the main intermediate leading to DHOPA formation. It has also been demonstrated that 2-methylfuran can be a precursor of C5DICARB, with experimental yields of 0.31, 0.60 and 0.70% (Aschmann et al., 2014; Gómez Alvarez et al., 2009 and Bierbach et al., 1995, respectively). In our model both precursors were taken into account. A yield of 31% (Aschmann et al., 2014) and a kinetic rate parameter of $6.19 \times 10^{-11} \text{ cm}^3 \text{ molecule}^{-1} \text{ s}^{-1}$ (Bierbach et al., 1992) were assumed to simulate C5DICARB formation from 2-methylfuran (Fig.3 and Table S2).

Among the OH-initiated photooxidation products of toluene listed in the previous paragraph, three of them are candidates as potential precursors of DHOPA: TLBIPERO2, TLEPOXMUC and CRESOL. TLBIPERO2 and TLEPOXMUC are photooxidized to give 3 intermediates: a dioxabicyclic-alcoolic-carbonyl-hydroxy-hexene (TLOBIPEROH), the (3E)-2,5-dioxohex-3-enal (C6125CO) and the main

intermediate C5DICARB (Fig. 4). From these intermediates two pathways have been identified to produce DHOPA (Fig. 5, Tables S3, S4 and S5). CRESOL photooxidation produce the 4-oxo-1-pentenoic acid (C5CO14OH), an intermediate of the second pathway described below.

The first pathway starts with the reaction of C5DICARB with OH, that produces the (3-hydroxy-1,4-dioxopentan-2-yl) dioxidanyl (C5DICARBO2) with a branching ratio of 0.52. The successive reaction with RO₂ radicals yields 20% of 2,3-dihydroxy-4-oxo-pentanal (C514CO23OH). In MCM, the only product of C514CO23OH reaction with OH is the 2-hydroxy-3,4-oxo-pentenal, generated from the reaction onto one of the three possible reactive sites (the two hydroxyls and the aldehyde). To form DHOPA, the H-abstraction on the aldehyde is required. The oxidation mechanism from C514CO23OH was therefore taken from GECKO-A, that estimate 43% of chances for the H-abstraction on the aldehyde to take place. The radical produced reacts with HO₂ or RO₂ to form DHOPA with a yield of 15% and 30%, respectively. Moreover, since C514CO23OH is an aldehyde, it is expected to be oxidized in the aqueous phase to the correspondent carboxylic acid (Tilgner and Herrmann, 2010), DHOPA. The reactivity in the aqueous phase has been simulated in analogy with 2,4-dihydroxy-3-oxobutanal (CLEPS 1.0). The partitioning of C514CO23OH between the gaseous and the aqueous phase has been evaluated using the SOAP Henry's constant ($3.9 \times 10^7 \text{ M}^{-1} \text{ atm}$) and solubilization enthalpy ($\Delta H_{\text{sol}} = 63.8 \text{ kJ/mol}$) (inputs $P_{\text{sat}} = 8.56 \times 10^{-4} \text{ torr}$ and a ΔH_{vap} of 83.8 kJ mol^{-1} (US EPA, 2015)). Aqueous phase branching ratios and kinetics for C514CO23OH reactions are respectively 0.29 and $1.2 \times 10^9 \text{ M}^{-1} \text{ s}^{-1}$ with OH as oxidant and 0.47 and $1 \times 10^6 \text{ M}^{-1} \text{ s}^{-1}$ with NO₃ as oxidant.

The second pathway starts with the formation of the [(2E)-4-oxopent-2-enoyl]dioxidanyl radical (C5CO14O2) from C6125CO and TLOBIPEROH by photolysis or reaction OH and from the reaction of C5DICARB reaction with NO₃. C5CO14O2 reacts with HO₂ and RO₂ (branching ratios 0.15 and 0.3) to give the 4-oxo-1-pentenoic acid (C5CO14OH). C5CO14OH can also be formed from the photooxidation of CRESOL initiated by OH and NO₃ (see Fig. 6). In MCM, the C5CO14OH reaction does not lead to the formation of DHOPA. In analogy with the MCM reactivity of the 3-esen-2,5-dione (C4DBDIKET), it has been supposed a C5CO14OH-OH reaction yields of 47% for (1-carboxy-2-hydroxy-3-oxobutyl)dioxidanyl (C5CO14OH2OO, analogous DMKOH2OO, kinetic = $1.03 \times 10^{-10} \text{ cm}^3 \text{ molecule}^{-1} \text{ s}^{-1}$). C5CO14OH2OO reacts then with RO₂ with a rate of $8.8 \times 10^{-13} \text{ cm}^3 \text{ molecule}^{-1} \text{ s}^{-1}$, producing 20% of DHOPA.

DHOPA gaseous phase degradation by reaction with OH has a kinetic of $2.42 \times 10^{-11} \text{ cm}^3 \text{ molecule}^{-1} \text{ s}^{-1}$ estimated from GECKO-A. DHOPA aqueous phase degradation is simulated by analogy with the 2,4-dihydroxy-3-oxobutanoic acid in CLEPS, with a kinetic rate of $8.1 \times 10^8 \text{ M}^{-1} \text{ s}^{-1}$.

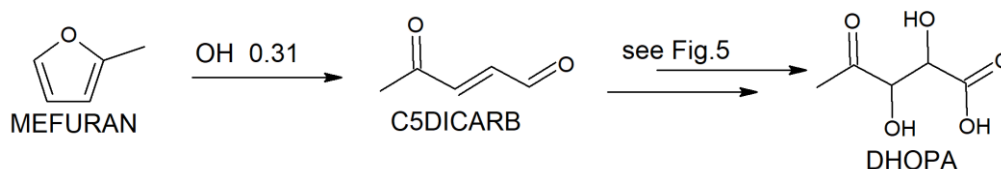


Figure 3. DHOPA formation from 2-methyl furan. Further details on the photooxidation of the 4-oxo-2-pentenal (C5DICARB) are reported on Fig.5. The 2-methylfuran reactions with O₃ and NO₃, have been considered as competitive for the reaction with OH (Table S5).

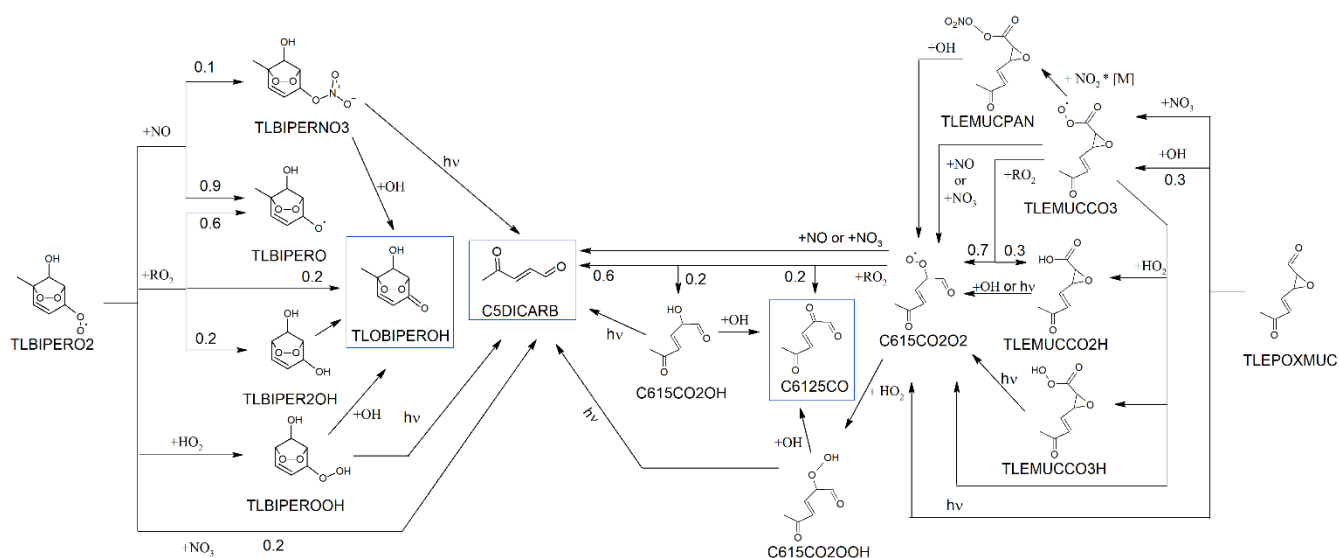


Figure 4. Photooxidation of 4-Methyl-5-hydroxy-4,6-epidioxy-2-cyclohexene-1-peroxyde (TLBIPERO₂) and of 4-Methyl-5-hydroxy-4,6-epidioxy-2-cyclohexene-1-peroxyde (TLEPOXMUC) leading to the formation of 4-Methyl-5-hydroxy-4,6-epidioxy-2-cyclohexene-1-peroxyde (TLOBIPEROH), 4-oxo-2-pentenal (C5DICARB) and (3E)-2,5-dioxohex-3-enal (C6125CO). Only the reactions involved in the DHOPA formation pathway are shown. The competitive reactions were considered in the model but omitted on this figure.

A P_{sat} of 1.95×10^{-6} torr and a ΔH_{vap} of 111 kJ mol^{-1} have been inserted in SOAP to calculate the GPP. This values are respectively the geometric mean and the arithmetic mean of the Multiphase system online property prediction (UManSysProp, Topping et al., 2016) SARs estimations. (Tables S8, S9 and S10).

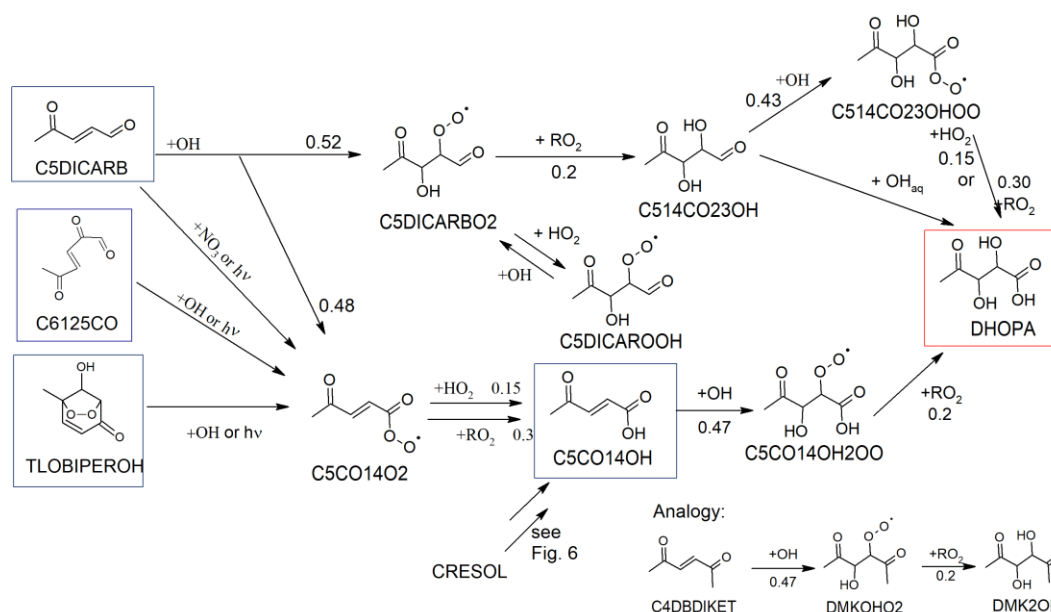


Figure 5. DHOPA formation pathways from the identified intermediates namely 4-Methyl-5-hydroxy-4,6-epidioxy-2-cyclohexene-1-peroxyde (TLOBIPEROH), 4-oxo-2-pentenal (C5DICARB) and (3E)-2,5-dioxohex-3-enal (C6125CO). The first formations pathway has been developed with GECKO and includes both, gaseous and aqueous phases. The second formation pathway was developed in analogy with the 3-esen-2,5-dione (C4DBDIKET) in gaseous phase only. Competitive reactions to the major reaction pathways were all considered in the model but are not shown here.

2.2.5 Methyl-nitrocatechols

The methyl-nitrocatechols (MNCATECH) are produced from the photooxidation of cresol. Cresol is primary emitted by biomass burning and can also be produced from toluene photooxidation (see paragraph 2.2.3 and 2.2.4). All the three possible isomers, orto-, meta- and para- cresol, have been detected in atmosphere and all the three are precursors of MNCATECH (Iinuma et al., 2010). There is no information in MCM about differences in the reactivity of o-, m- and p-cresol, so they were assumed to react in the same way. Because of this, MNCATECH is the sum of all isomers that can be produced. The mechanism for MNCATECH production is entirely reported in MCM and consists only in three steps (Fig. 6). CRESOL is oxidized by OH and form MCATECHOL (73%). MCATECHOL reacts with OH and NO₃ producing the (2-hydroxy-6-methylphenyl) oxidanyl radical (MCATEC1O) NO₂ addition to MCATEC1O generate MNCATECH.

MNCATECH P_{sat} and ΔH_{vap} were estimated as for NGUAIACOL with a semi-empiric method. Nitrocatechol experimental values (Booth et al., 2012) have been used as reference. The effect of the methyl addition on P_{sat} and ΔH_{vap} has been estimated through SARs values calculated by EPIsuite (US EPA, 2015). Semi-empiric MNCATECH P_{sat} and ΔH_{vap} are respectively 3.20×10^{-6} torr and 41.7 kJ mol^{-1} .

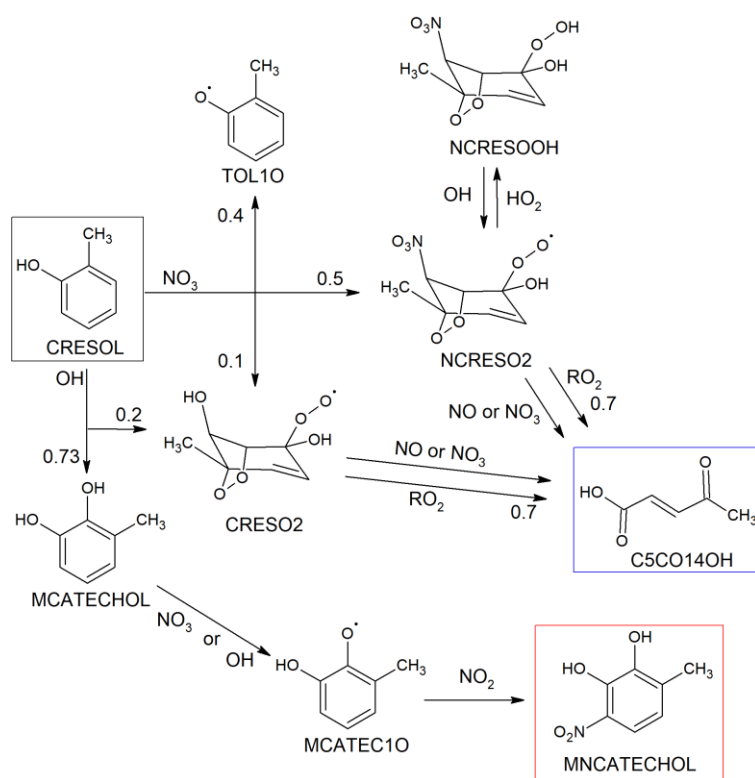


Figure 6. Cresol photooxidation to methyl-nitrocatechols and 4-oxo-1-pentenoic acid, an intermediate for DHOPA formation. The reactions not involved in the formation pathway are not displayed but considered in the model.

2.2.6 Phthalic Acid

Phthalic acid secondary formation in atmosphere is traditionally attributed to naphthalene and methylnaphthalene photooxidation (Kleindienst et al., 2012). No mechanism for naphthalene photooxidation has been provided in MCM. The formation pathway of phthalic acid from naphthalene proposed by Kautzman et al., (2010) has been taken as reference for the development of our mechanism (Fig. S2, Table S6).

Naphthalene OH-oxidation yields 45% of 2-formylcinnamaldehyde (FORMCINNAL, mean of 30–60% yield range reported in Kautzman et al., (2010)) with a rate constant of $2.4 \times 10^{-11} \text{ cm}^3 \text{ molecule}^{-1} \text{ s}^{-1}$ (Phousongphouang and Arey, 2002). Kautzman et al., (2010) proposed an alternative pathway that produces phthalaldehyde as OH-initiated naphthalene photooxidation first generation product. Sasaki et al., (1997) identified 67% of the first generation photooxidation products for the naphthalene–OH reaction. FORMCINNAL was the major product while phthalaldehyde was not observed. We supposed that the alternative pathway is negligible compared to the first one. In our mechanism phthalaldehyde (PHTHALDIAL) is a second generation photooxidation product.

FORMCINNAL-OH photooxidation can occur on the formyl double bond, yielding 35% of FCINNALOOOH, and on the aldehyde. The reaction rate and the branching ratios are calculated considering the analogous MCM reactions of pentene and pentaldehyde. The calculated overall reaction rate ($8.3 \times 10^{-11} \text{ cm}^3 \text{ molecule}^{-1} \text{ s}^{-1}$) is in good agreement with the values previously reported (7.7×10^{-11} and $2.1 \times 10^{-11} \text{ cm}^3 \text{ molecule}^{-1} \text{ s}^{-1}$ (Aschmann et al., 2013; Nishino et al., 2009)). O_3 -FORMCINNAL reactivity is simulated using the rate of $1.8 \times 10^{-18} \text{ cm}^3 \text{ molecule}^{-1} \text{ s}^{-1}$ (Aschmann et al., 2013) and a yield of 50% for FCINNALOOOH, in analogy with the alkenes in MCM. FORMCINNAL photolyzes with a rate of $0.66 \times J(\text{NO}_2)$ (Nishino et al., 2009) yielding 33% of PHTHALDIAL. The other products of this reactions are PHTHALDIAL precursors and their reactivity is parametrized in analogy with 2-pentenale in GECKO-A (Fig. S2 and Table S6). FCINNALOOOH reacts with NO (MCM generic $\text{RO}_2 + \text{NO}$, rate = $2.7 \times 10^{-12} e^{(-360/T)} \text{ cm}^3 \text{ molecule}^{-1} \text{ s}^{-1}$) giving PHTHALDIAL.

PHTHALDIAL reacts with OH ($k = 2.3 \times 10^{-11} \text{ cm}^3 \text{ molecule}^{-1} \text{ s}^{-1}$, yield 85%, Wang et al., 2006) and NO_3 ($k = 2.8 \times 10^{-12} \text{ cm}^3 \text{ molecule}^{-1} \text{ s}^{-1}$, $2 \times$ MCM generic constant for $\text{RO}_2 + \text{NO}$ reaction) giving the phthalanhydride (PHTHALAN). PHTHALDIAL photolyzes producing 35% of PHTHALAN and 53% of PHTHALIDE ($J_{(\text{aromatic carbonyl})}/J(\text{NO}_2) = 0.030$, Wang et al., 2006). PHTHALIDE reaction with OH produces 60% of PHTHALAN ($k = 8 \times 10^{-13} \text{ cm}^3 \text{ molecule}^{-1} \text{ s}^{-1}$, Wang et al., 2006).

PHTHALAN produces phthalic acid by reaction with OH in the gaseous phase and hydrolysis in the aqueous phase (SIDS, 2005). PHTHALAN half-life times in both phases (SIDS, 2005) have been used to estimate the degradation rates ($7 \times 10^{-13} \text{ cm}^3 \text{ molecule}^{-1} \text{ s}^{-1}$ and $9.9 \times 10^{-3} \text{ M}^{-1} \text{ s}^{-1}$). PHTHALAN ΔH_{sol} (61.6 kJ mol^{-1}) and K_{H} ($4.12 \times 10^5 \text{ M}^{-1} \text{ atm}$) have been calculated with SOAP, using $P_{\text{sat}} = 5.84 \times 10^{-3} \text{ torr}$ and $\Delta H_{\text{vap}} = 65 \text{ kJ mol}^{-1}$ (Crooks and Feetham, 1946).

Phthalic acid degradation in the atmosphere has been parametrized by reaction with OH ($k = 1.23 \times 10^{-12} \text{ cm}^3 \text{ molecule}^{-1} \text{ s}^{-1}$, half-life of 13 d^{-1} , $500,000 \text{ OH/cm}^3$, SIDS, 2005). Experimental P_{sat} of $1.26 \times 10^{-5} \text{ torr}$ and a ΔH_{vap} of 40 kJ mol^{-1} have been chosen (Booth et al., 2012).

3. Comparison measurements model

3.1 Configuration

The simulations have been performed at $0.06^\circ \times 0.125^\circ$ longitude/latitude resolution all over France. The number of vertical layers were 9 till 500 hPa. Meteorological data were taken from data of the Integrated Forecasting System (IFS) model from the European Centre for Medium-Range Weather Forecasts (ECMWF). Chemical boundary conditions were obtained from a lower ($0.25^\circ \times 0.4^\circ$) resolution simulation performed on the European domain.

Annual anthropogenic emissions, classified by sector, were taken from the EMEP inventory (methodology of Vestreng, 2003). Denier van der Gon et al. (2015) has shown that POA emissions are greatly underestimated due to a strong underestimation of residential wood burning emissions by a factor of 3 over Europe (between 1 and 10 depending on the countries) because emissions of condensable were often not considered. To consider this underestimation, POA emissions were corrected by applying an emission correction factor taken from the TNO inventory.

For each sector, primary organic aerosol emissions are transformed into emissions of SVOC. The SVOC emissions are split into several compounds with different volatilities. For biomass burning, SVOC are split into BOAIP (26 % of emissions, $K_p = 18.3 \text{ m}^3/\mu\text{g}$), BOAmP (31 % of emissions, $K_p = 0.04 \text{ m}^3/\mu\text{g}$) and BOAhP (43 %, $K_p = 0.00023 \text{ m}^3/\mu\text{g}$) to follow the dilution curve of POA in May et al., (2013). For other sources, emissions are split into POAIP (25 % of emissions, $K_p = 1.1 \text{ m}^3/\mu\text{g}$), POAmP (32 % of emissions, $K_p = 0.011 \text{ m}^3/\mu\text{g}$) and POAhP (43 %, $K_p = 0.00031 \text{ m}^3/\mu\text{g}$) to follow the dilution curve of POA in Robinson et al., (2007). The aging of these compounds is simulated by their reaction with OH, using a kinetic rate constant of $2 \times 10^{-11} \text{ molecules}^{-1}\text{cm}^3 \text{ s}^{-1}$. Following Grieshop et al. (2009), aging is assumed to lead to a decrease of volatility by a factor of 100 (the products BSOAIP, BSOAmP, BSOAhP, SOAIP, SOAmP and SOAhP are, respectively, less volatile by a factor of 100 than their precursors BOAIP, BOAmP, BOAhP, POAIP, POAmP and POAhP). A default “average” structure representative of atmospheric POA has been assigned to these surrogates to calculate their activity coefficients. This structure is composed by 40% of $\text{C}_{23}\text{H}_{47}\text{COOH}$, 5% of $\text{C}_8\text{H}_{17}\text{CH} = \text{CHC}_7\text{H}_{14}\text{COOH}$, 15% of 4-(2-propio)-syringone, 12% of $\text{C}_{29}\text{H}_{60}$ and 28% of 2-carboxybenzoic acid (EPRI, 1999). This approach assumes that the particle composition does not change according to the emitting source. Although we are conscious that this is not true, exhaustive molecular data for POA are still not available, so we choose this simple POA representation.

The speciation of emissions in the CHIMERE preprocessor for emission inventories is based on the data provided by Passant, (2002). Since some important precursors for biomass burning aerosols, notably the non-traditional VOCs (NTVOCs) (Chrit et al., 2018), were missing, an update of the speciation was required (Table 2). Emission speciation was taken from Nalin et al., (2016) and Schauer et al., (2001). When available, data from Nalin et al., (2016) were preferred because the wood type burnt (European beech) is typically used in France for residential heating. Levoglucosan percentage in $\text{PM}_{2.5}$ (including condensable) emitted by domestic biomass burning (3.23%–Nalin et al., (2016), unpublished data) has been estimated from this experiment. Schauer et al., (2001) estimated fireplace biomass burning emissions from 3 kind of wood typical of US: pine, oak and eucalyptus. The French Agency for the Environment and Energy Control (“Agence de l'Environnement et de la Maîtrise de l'Énergie”, ADEME) estimated that 80% of the wood used for domestic heating in France is hard wood (Pouet and

Gautier, 2013). Pine and oak emission factors have been chosen as representative of soft and hard wood, respectively. The weighted mean of oak (80%) and pine (20%) emission factors has been inserted in the model to represent biomass burning emissions in France. Also 2-methylfuran biomass burning emissions (DHOPA precursor) were included in the model and normalized according to toluene (1:1) following the experimental emission factors averages reported in McDonald et al., (2000).

For the phenolic compounds (phenol, cresol and guaiacol) only emissions from biomass burning have been updated. Although emissions from other sectors, notably livestock (Borhan et al., 2012; Cai et al., 2011; Hobbs et al., 2004), have been reported in literature, no data suitable for a robust estimation of the emissions have been provided.

The markers have been considered both hydrophilic and hydrophobic. In the reference run, dry and wet deposition removal of gas-phase concentrations was not considered.

Table 2. Marker precursor percentages in non-methane hydrocarbon VOC (NMVOC) emissions from the different sectors. Non-industrial combustion plants emissions (mainly biomass burning from domestic heating) have been especially updated in this study.

	BENZENE	CRESOL	GUAIACOL	MEFURAN	NAPHTHALENE	PHENOL	TOLUENE
SNAP							
Combustion in energy and transformation industries	1.60 ^a						1.10 ^a
Non-industrial combustion plants (domestic heating)	3.16 ^b	2.27 ^b	1.60 ^b	1.31 ^c	0.20 ^d	2.85 ^b	1.31 ^b
Combustion in manufacturing industry	12.70 ^a				0.20 ^a		2.00 ^a
Extraction and distribution of fossil fuels and geothermal energy	0.80 ^a					0.20 ^a	1.10 ^a
Solvents and other product use	0.40 ^a						0.20 ^a
Road transport							5.20 ^a
Other mobile sources and machinery	2.54 ^a						5.21 ^a
Waste treatment and disposal	3.00 ^a						4.70 ^a
Agriculture	0.30 ^a						1.10 ^a

a(Passant, 2002)

b(Schauer et al., 2001)

c(McDonald et al., 2000)

d(Nalin et al., 2016)

3.2 Measurements

The measurements compared with the model belong to different research and monitoring programs, performed in France in 2014–2015 (Fig. 7). Among the 12 sampling sites presented, 11 are urban and suburban and represent the most populated areas of France. The other is rural and less influenced by anthropic activities. This set of measurements is representative of French air quality conditions. The details about the sampling sites, online and offline measurements and analytical procedures are reported elsewhere (Lanzafame et al., 2019, Favez, 2016; Tomaz et al., 2016). The most extensively characterized campaign results used in this study come from the SIRTA facility (Site Instrumental de Recherche par Télédétection Atmosphérique, 2.15° E; 48.71° N), situated in the suburban area of Paris, 25 km SW from the city center. In this station, particulate (PM₁₀) and gaseous phase samples have been collected every third day from 19/11/2014 to 15/12/2015. 22 SOA markers have been identified in both phases, while levoglucosan has been quantified only in the particulate phase, as detailed in Lanzafame et al., (2019). The list of the SOA marker measured is reported in Table S11. Levoglucosan annual data for 2015 were available in the EBAS database (<http://ebas.nilu.no/>) for the OPE sampling site. This site is representative of rural environment and far from any anthropic influence (description available from <http://www.andra.fr>). The other sites are part of the French regional air quality monitoring network (AASQA). Particulate phase samples (PM₁₀) have been collected in the winter 2014–2015 during a campaign for the quantification of biomass burning impact on urban areas (Favez, 2016). Levoglucosan has been quantified and the Biomass Burning Organic Carbon (OC_{wb}) has been estimated using specific conversion factors from levoglucosan for each site (the estimation method is reported in Favez, (2016) and briefly described in the SM, section 2.1). The estimated OC_{wb} to levoglucosan ratio, details of sampling locations, periods and frequency for each site are reported in Table S12, for simplification in the main text each site will be named by the correspondent urban area, except for SIRTA and OPE.

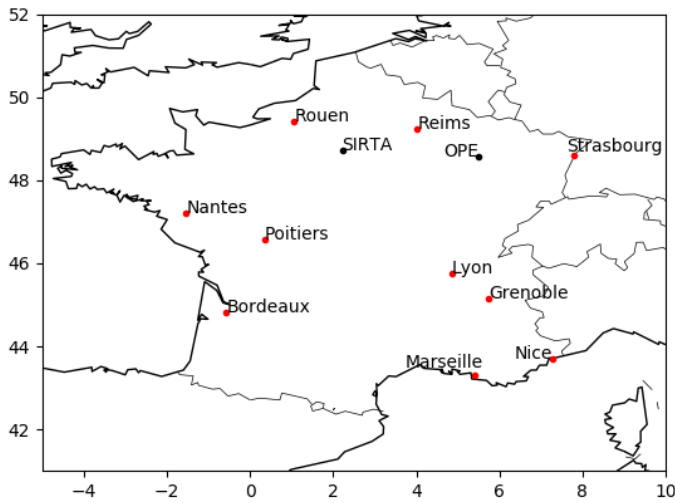


Figure 7. Map of France reporting the sampling stations mentioned in this study. Black points represent annual campaign sampling sites, red points winter time campaigns. Urban and suburban sites are named by the closer agglomeration, except for SIRTAs (25 km SO of Paris). OPE is a rural site.

1. Results and discussion

Simulations are performed over Europe and France for year 2015. In a first part, the results of the model are compared to available measurements over France in order to evaluate the performance. In a second part, sensitivity analysis on GPP are also performed.

4.1 Model to measurement comparison

4.1.1 Levoglucosan

Table 3 shows the comparison between modelled and measured particulate phase. Medians, interquartile (25th–75th) ranges, correlation coefficients, Mean Normalised Bias (MNB), modelled particulate phase fraction (F_p) and number of observations are shown for each site. The SIRTAs and the OPE stations have the highest number of samples (127 and 59 respectively) with measurements throughout all the year. For the other stations, samples have been collected only during winter with a sample number from 28 (for Strasbourg) to 58 (for Marseille and Nice).

Measured and modelled levoglucosan particulate phase median concentrations are below $1 \mu\text{g m}^{-3}$ for all the sites.

For stations in the north of France (Rouen, Reims and Strasbourg) median modelled concentrations are half of the measured ones (54, 41 and 43% less respectively). The modelled interquartile ranges underestimate the measured ones by a factor around 2. The MNBs values calculated (-0.50, -0.36 and -

0.41 respectively) agree with the discard already observed for the other parameters. Correlation is lower for Rouen (0.35) and Strasbourg (0.53) than Reims (0.63). Modelled F_p are respectively 0.65, 0.72 and 0.67 for Rouen, Reims and Strasbourg.

In the western cities Nantes, Poitiers and Bordeaux, simulations show an even stronger underestimation: median modelled concentrations are respectively 0.7, 0.10 and 0.9 $\mu\text{g m}^{-3}$ against the measured 0.28, 0.35, 0.48 $\mu\text{g m}^{-3}$, respectively. 25th and 75th percentiles are strongly underestimated by the model: for Nantes and Bordeaux the modelled 75th percentile has the same value of the measured 25th percentile (0.13 and 0.17 $\mu\text{g m}^{-3}$ respectively), for Poitiers the modelled 75th percentile (0.16 $\mu\text{g m}^{-3}$) is lower than the measured 25th percentile (0.18 $\mu\text{g m}^{-3}$). For Nantes, Poitiers and Bordeaux, MNB values are -0.71, -0.78 and -0.78 and F_p values are 0.60, 0.62, 0.54 respectively.

For stations in southeastern France (Lyon and Grenoble), results of the model are close to observations, median measured values for levoglucosan are respectively 0.29 and 0.60 $\mu\text{g m}^{-3}$ while modelled values are 0.32 and 0.49 $\mu\text{g m}^{-3}$. In these 2 sites levoglucosan is slightly overestimated, with MNB values of 0.10 and 0.12. The interquartile ranges estimation is close to observed values and the correlation is higher for Lyon (0.75) and lower for Grenoble (0.48). F_p values are 0.68 for Lyon and 0.67 for Grenoble.

In the Mediterranean cities (Nice and Marseille), levoglucosan concentrations are highly underestimated. Median modelled values (0.07 and 0.02 $\mu\text{g m}^{-3}$ respectively) are very low compared to the measured ones (0.47 and 0.24 $\mu\text{g m}^{-3}$ respectively), such as interquartile ranges (modelled values are respectively 0.02–0.17 and 0.01–0.09 $\mu\text{g m}^{-3}$ and measured values are 0.26–0.66 and 0.16–0.39 $\mu\text{g m}^{-3}$). This result is confirmed by MNBs values of -0.75 for Nice and -0.79 for Marseille. The correlation is higher for Marseille (0.67) and lower for Nice (0.38). The F_p modelled values are lower than for all the other cities (0.29 for Nice and 0.26 for Marseille).

Annual median particulate phase levoglucosan concentrations calculated for annual sites are lower than for winter sites because biomass burning emissions are lower in the warmest season. Median modelled values, 0.02 $\mu\text{g m}^{-3}$ for both sites, underestimate the measured medians of 0.06 and 0.05 $\mu\text{g m}^{-3}$ respectively for SIRTA and OPE. The modelled interquartile range for OPE (0.01–0.08 $\mu\text{g m}^{-3}$) is well estimated (measured range 0.006–0.10 $\mu\text{g m}^{-3}$), while at SIRTA the 25th and the 75th percentile (respectively 0.002 and 0.08 $\mu\text{g m}^{-3}$) are underestimated (measured interquartile range 0.01–0.21 $\mu\text{g m}^{-3}$). MNB value is negative for SIRTA, but positive for OPE (modelled concentrations are probably affected by some local maximum). Correlations are high (0.72 for SIRTA and 0.78 for OPE) and F_p values are around 0.45 for both sites. The same parameters have been also calculated for the winter period (concentrations excluded from 15/04 to 15/11), considering 58 samples for SIRTA and 23 for OPE. Winter measured median are higher than the ones calculated for the whole year, assuming the

values of 0.28 and 0.10 $\mu\text{g m}^{-3}$ respectively for SIRTA and OPE. Modelled median is underestimated for SIRTA (0.09 $\mu\text{g m}^{-3}$) and well estimated for OPE (0.11 $\mu\text{g m}^{-3}$). The interquartile range is underestimated for SIRTA (measured 0.15–0.48 $\mu\text{g m}^{-3}$, modelled 0.04–0.16 $\mu\text{g m}^{-3}$) and overestimated for OPE, with lower 25th percentile (measured and modelled respectively 0.07 and 0.05 $\mu\text{g m}^{-3}$) and higher 75th percentile (measured and modelled respectively 0.13 and 0.17 $\mu\text{g m}^{-3}$). Correlations are high (0.66 and 0.78 for SIRTA and OPE respectively) and the MNB values are lower than the annual ones (-0.39 and 0.19 respectively). Mean modelled F_p in winter is higher than in the whole year for both sites (0.66 for SIRTA and 0.68 for OPE).

Table 3. Median and interquartile range (25th–75th) of measurements and model outputs for particulate phase levoglucosan daily concentrations in 13 sites in France. Number of samples, correlation coefficients, Mean Normalized Bias (NMB) and particulate phase fraction (F_p) are also reported.

Stations	Number of samples	Measured Median (interquartile range) $\mu\text{g m}^{-3}$	Modelled Median (interquartile range) $\mu\text{g m}^{-3}$	r	MNB	Modelled F_p
<i>Winter sites</i>						
Rouen	48	0.28 (0.15–0.49)	0.13 (0.07–0.21)	0.35	-0.50	0.65
Reims	46	0.22 (0.12–0.37)	0.13 (0.07–0.19)	0.63	-0.36	0.72
Strasbourg	28	0.52 (0.33–0.91)	0.30 (0.13–0.57)	0.53	-0.43	0.67
Nantes	48	0.28 (0.13–0.57)	0.07 (0.03–0.13)	0.82	-0.71	0.60
Poitiers	47	0.35 (0.18–0.68)	0.10 (0.04–0.16)	0.65	-0.78	0.62
Bordeaux	49	0.43 (0.17–1.31)	0.09 (0.03–0.17)	0.70	-0.78	0.54
Lyon	49	0.29 (0.20–0.54)	0.32 (0.11–0.54)	0.75	0.10	0.68
Grenoble	50	0.60 (0.39–1.04)	0.49 (0.22–0.80)	0.48	0.12	0.67
Nice	58	0.47 (0.26–0.66)	0.07 (0.02–0.17)	0.38	-0.75	0.29
Marseille	58	0.24 (0.16–0.39)	0.02 (0.01–0.09)	0.67	-0.79	0.26
<i>Annual sites</i>						
SIRTA	127	0.06 (0.01–0.21)	0.02 (0.002–0.08)	0.72	-0.44	0.45
OPE*	59	0.05 (0.006–0.10)	0.02 (0.01–0.08)	0.78	0.61	0.44
<i>Annual sites - winter period</i>						
SIRTA	58	0.28 (0.15–0.48)	0.09 (0.04–0.16)	0.66	-0.39	0.66
OPE*	23	0.10 (0.07–0.13)	0.11 (0.05–0.17)	0.78	0.19	0.68

*rural site

In Fig. 8 the daily modelled mean concentrations of particulate phase levoglucosan during February 2015 is shown. The sampling sites are indicated by squares filled with the mean of levoglucosan measurements performed every 3 to 6 days (sampling frequency is reported in Table S12). February is the month in which higher concentrations of levoglucosan have been observed at SIRTA during 2015. While it seems that the spatial distribution of concentrations may be well represented in the North of

France and the southeastern cities, concentrations are strongly underestimated in Western France and in Mediterranean cities.

Different factors can influence the distribution of levoglucosan particulate phase concentrations in the model: for example, the emissions could be strongly underestimated over the western cities, especially for the city of Bordeaux, which has low modeled concentrations but high measured concentrations. For Nice and Marseille, part of the underestimation could be due to the low resolution of the model and bilinear interpolation of CHIMERE between cells onto the earth and the sea (with very low concentrations) as the stations are close to the sea (respectively ~ 1.75 and ~ 3.15 km).

Moreover, concentrations in the particle phase may be strongly affected by GPP. Whereas one can expect levoglucosan to be almost entirely in the particles (Locker, 1988), the model simulates a rather high fraction of the levoglucosan in the gas phase.

In Fig. 9 the levoglucosan simulated particulate phase fraction on the total (gas+particulate) concentration all over France is reported for February 2015. From the northern to the southern part of France particulate phase fraction gradually decrease. In the north the fraction is between 0.8 and 0.85, it decreases to 0.6–0.75 in the central and north-western part and reaches the lower values between 0.2 and 0.5 in the southern part. The spatial distribution observed in the model can be partially explained by the combined effect of temperature and humidity variations (Fig. S8 and S9). In the northern part of France, the higher humidity ($RH > 80\%$) may favor the transfer of levoglucosan in the particulate phase, while in the warmest regions ($T > 278$ K) levoglucosan will be more volatilized. The very low particle-phase concentrations observed in the southeastern cities (where the particle phase fraction of levoglucosan ranges from 20 to 60%) can be partly explained by GPP.

The influence of particle composition and thermodynamics on levoglucosan partitioning as well as the uncertainties on the GPP calculation are discussed in paragraph 4.2.1.

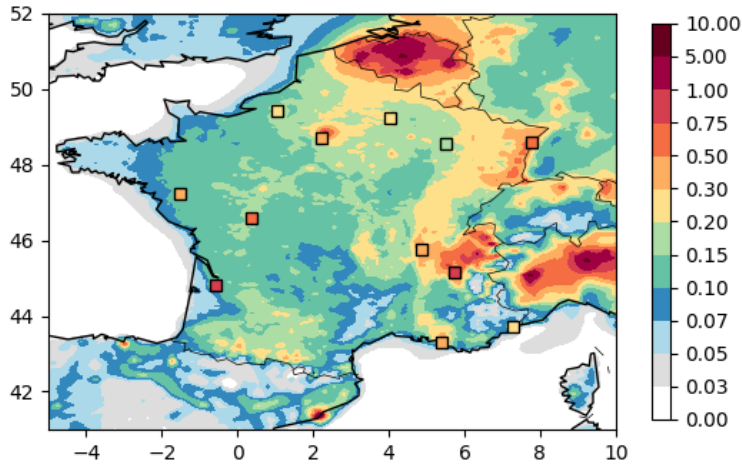


Figure 8. Mean daily particulate phase levoglucosan distribution ($\mu\text{g m}^{-3}$) simulated in France in February 2015. Sampling sites are highlighted by squares filled according to the mean concentration observed every 3 to 6 days (sampling details in Table S12).

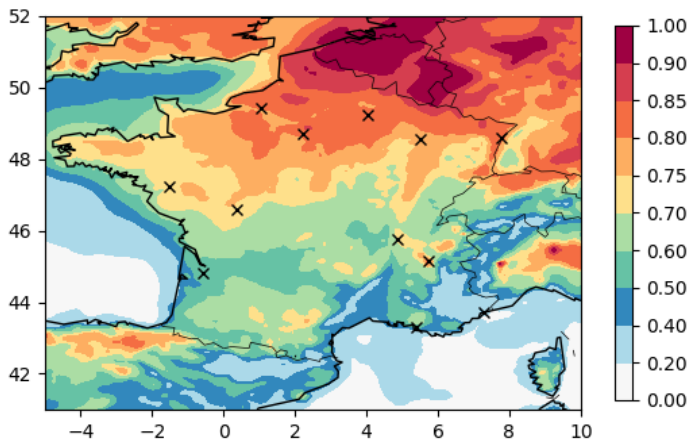


Figure 9. Modeled particulate phase fraction of levoglucosan in France in February 2015. The sampling sites are highlighted by crosses.

In Fig. 10, the temporal variations of measured and modelled particulate phase levoglucosan, together with the modelled total (gaseous+particulate phase) concentrations, (added to evaluate the importance of GPP on the modelled results) are reported for Bordeaux, Reims, Lyon and Marseille. These sites

have been selected as they are representative of the different situations (Northern, Western, South-eastern and Mediterranean cities) observed (similar results between the stations within these different regions). For the other winter sites (Rouen, Strasbourg, Nantes, Poitiers, Grenoble and Nice) the comparisons are reported in Fig. S3. Annual levoglucosan variations are reported in Fig. 12 for SIRTAs and in Fig S4 for OPE. In Bordeaux, the modelled levoglucosan concentrations are very low but reproduce the temporal trends measured (correlation of 0.7). Although almost half of the modelled levoglucosan is in the gas phase, the comparison with measurement are scarcely improved considering the total modelled concentrations. Similar considerations apply to the other 2 west side cities, Nantes and Poitiers, in which high underestimation have been observed.

In Reims (north), the model reproduces well the lower concentrations observed and the temporal trends. All the peaks are predicted, but the model cannot reach the higher measured concentrations and the extent of the peaks. Modelled gaseous phase concentrations are around 30% of the total levoglucosan and their impact on the model to measurement comparison is not significant. GPP is therefore not expected to affect simulated concentrations for these stations. Similar results are obtained for Rouen and Strasbourg.

In Lyon, southeast of France, the simulated levoglucosan concentrations reproduce both the order of magnitude and the temporal variations measured. In some days, the gaseous phase contribution to the total modelled concentrations is not negligible (up to 90%) and the total levoglucosan concentrations are higher than the measured particulate phase. A few peaks simulated by the model do not appear in the observations. Slightly better results are obtained when modelled particle-phase concentrations is compared to the measured particle-phase concentrations (MNB 0.10, correlation 0,75) than when the comparison is done with the total concentrations (MNB 0.94, correlation 0.69), especially for March and April. In Grenoble, not far from Lyon, the model estimation is similar with the one observed in Lyon from January till April. In November and December levoglucosan is underestimated and the gaseous phase contribution is required to better represent the observed concentrations.

In Marseille, situated in the south of France (Mediterranean coast), temporal evolutions are well represented (correlation of 0.67). While concentrations are underestimated when modelled particle-phase concentrations are used for the comparison, the order of magnitude is well represented by the model when the gaseous phase concentration is included. In Nice (same geographical region as Marseille), concentrations can also be reproduced when the gas-phase concentration is included. The model cannot reproduce the high concentrations observed between the 08/01 and the 18/01. These results may indicate that the underestimation of concentrations can potentially be due to an overestimation of the gas-phase fraction for these two cities.

At SIRTa, Figure, the modelled levoglucosan concentrations match well with the lower concentrations in the first part of the year, but do not reach the concentration of the major peak observed the 13/02. From May to October concentrations are low both for the measurements and for the model. At the end of the year, the peaks observed in measurements are not reproduced by the model. Although gaseous phase concentration is not negligible in some periods, its contribution is not essential to reproduce levoglucosan concentrations. Better results are obtained when modelled particle-phase concentrations is compared to the measured particle-phase concentrations (MNB -0.44, correlation 0.72) than when the comparison is done with the total concentrations (MNB 1.1, correlation 0.57)

Modelled levoglucosan at OPE has the same magnitude order and similar temporal variations of the measured levoglucosan. In the first part of the year the modelled gaseous phase has high concentrations and the sum of both phases is higher than the measured particulate phase. In the last part of the year gaseous phase contribution to the total levoglucosan is lower. Better results are obtained when modelled particle-phase concentrations is compared to the measured particle-phase concentrations (MNB 0.61, correlation 0.78) than when the comparison is done with the total concentrations (MNB 4.6, correlation 0.73).

The comparisons of measured and modelled OM concentrations temporal variation (Fig. 11 for Bordeaux, Reims, Lyon and Marseille, Fig. S5 for Rouen, Strasbourg, Nantes, Poitiers, Grenoble and Nice, Fig. 12 for SIRTa, data not provided for OPE) can help to understand the reasons of underestimation of levoglucosan concentrations. OM is generally underestimated in the cities in which levoglucosan is underestimated by a similar factor. In western (Bordeaux, Nantes and Poitiers, MNBs -0.60, -0.63 and -0.67) and northern (Reims and Rouen, MNBs -0.41 and -0.49) as the underestimation are very similar between OM and levoglucosan, the underestimation of the biomass burning emissions over these areas is a likely explanation.

For South-eastern France, as for levoglucosan, the OM is well estimated by the model, with a slight overestimation for Lyon and Grenoble (MNBs 0.18 and 0.34) and a little underestimation for Strasbourg (MNB -0.20).

For Marseille and Nice, OM underestimation is lower compared to levoglucosan underestimation (MNBs of -0.69 and -0.53). Since the total modelled levoglucosan in these cities matches well with measurements, more investigations on the GPP computation and on the biomass burning emissions are required. The mismatching between simulation and measurements could be due to an underestimation of biomass burning emissions, to a similar bias between the GPP of levoglucosan and the GPP of SVOC from biomass burning or to a cumulation of various factors (emissions, GPP, aging, meteorology, etc...).

At SIRTA the simulated OM reproduce well the measurements from January to the beginning of May, while (similarly to levoglucosan) for the rest of the year, measured OM is underestimated.

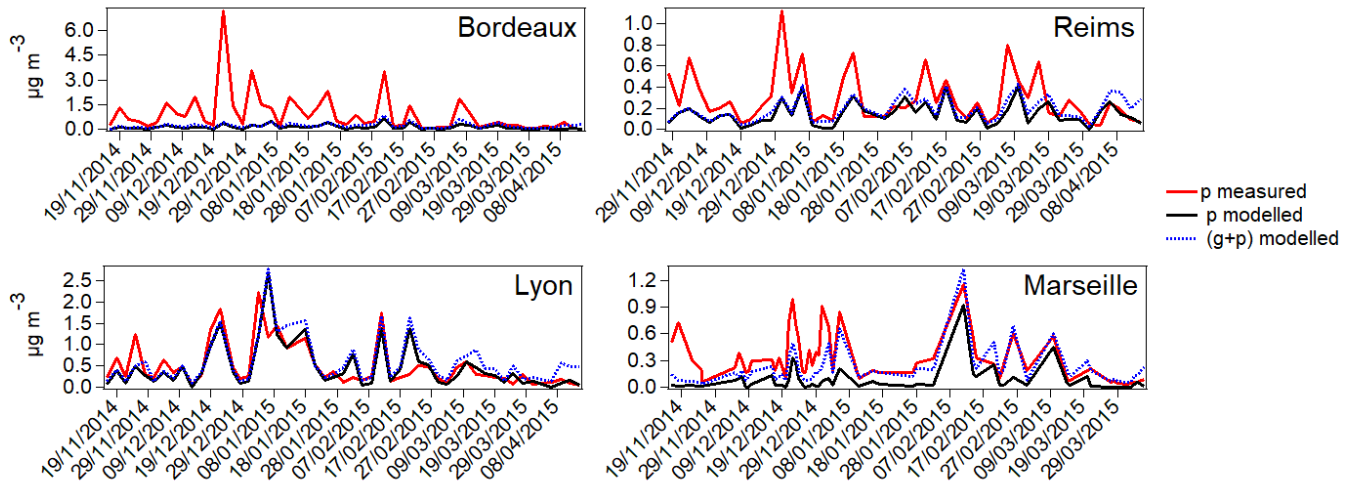


Figure 10. Model to measurements comparison of levoglucosan concentrations in 4 urban sites (Bordeaux, Reims, Lyon and Marseille) in France during the winter 2014/2015. Continuous lines are particulate phase measurements (red) and model (black). The dotted blue line represents the sum of modelled gaseous and particulate phase levoglucosan.

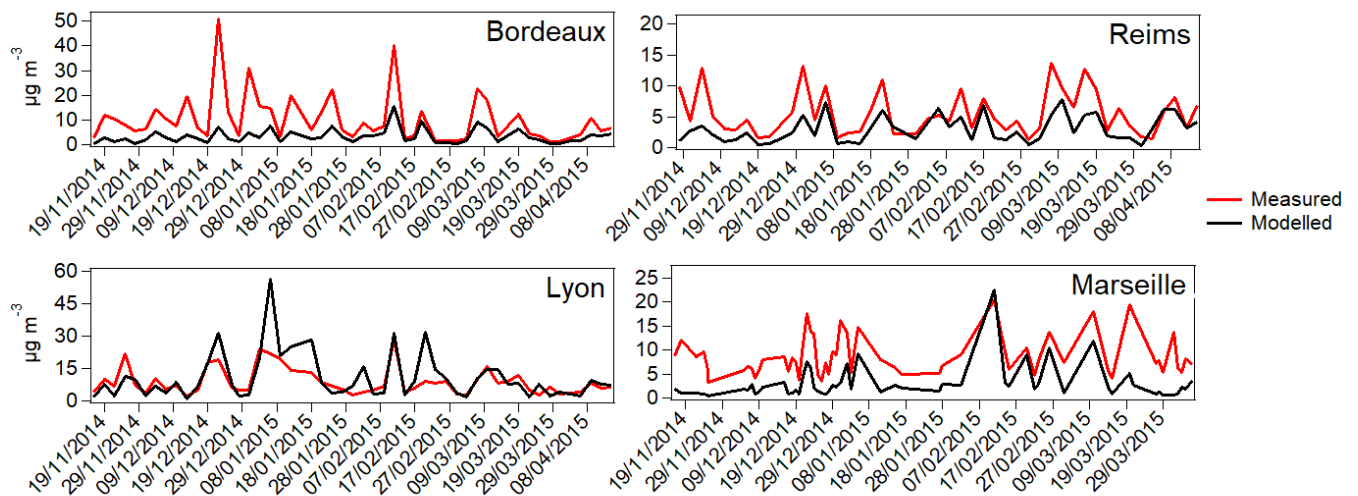


Figure 11. Model to measurements comparison of organic matter (OM) concentrations in 4 urban sites (Bordeaux, Reims, Lyon and Marseille) in France during the winter 2014/2015.

4.1.2 Nitroguaiacols and nitrophenols

As already specified in section 2.2.2, the modelled nitroguaiacols are the sum of the 3-,4- and 6-nitroguaiacol. Among these isomers, only 4-nitroguaiacol has been measured. According to (Lauraguais et al., 2014), 4-nitroguaiacol is the major nitroguaiacol isomer produced in atmosphere from the OH-initiated photooxidation (63% of the total nitroguaiacols produced by the OH-initiated photooxidation

of guaiacol). However, since no isomer specific yield from the NO₃-initiated photooxidation have been provided, it is not possible to estimate properly 4-nitroguaiacol percentage on the total nitroguaiacols. For these reasons, simulated nitroguaiacols total concentrations are compared to 4-nitroguaiacol measured concentrations, so a certain underestimation in measurements is expected.

Nitroguaiacols concentrations are simulated with the right order of magnitude. The modelled higher concentrations (mean 25.8 ng m⁻³) at the beginning of the year (January to March) matches well with the observations (mean 20.8 ng m⁻³), while in April–May the model (mean 14 ng m⁻³) overestimates the measurements (mean 1.5 ng m⁻³). In summer nitroguaiacol concentrations are very low in both model and measurements (under 6 and 1 ng m⁻³ respectively). The weak increase of concentrations observed at the end of the year has been well reproduced by the model.

Nitrophenols (2- and 4- nitrophenol sum) concentrations are well simulated for most of the year: the model succeeds to capture the high concentrations observed from January to April and the strong decrease of concentrations during summer. However, at the end of the year, the model underestimates concentrations by a factor 11 and is not able to reproduce the peaks observed. Nitrophenols precursors are toluene, benzene and phenol. The percentage of nitrophenols produced from toluene in February has been determined to be less than 1%, while primary phenol account for 40% of nitrophenols production. Therefore, benzene is the most important precursor for nitrophenols.

4.1.3 Methylnitrocatechols and DHOPA

Methylnitrocatechols (sum of 3-methyl-5-nitrocatechol, 4-methyl-5-nitrocatechol and 3-methyl-6-nitrocatechol) are underestimated by the model by a factor 60 during the cold season (January–April and September–December) and by a factor 4 in the warmest season (May–August). In winter, methylnitrocatechols measured concentrations are higher and their time evolution is well reproduced. During spring–summer, measured Methylnitrocatechols is very low, while the model simulates a strong increase of concentrations in April–May and multiple small peaks in the rest of the period. The performances of the model in reproducing methylnitrocatechols temporal variations depend on the seasonal contribution of the different emission sectors. In winter, biomass burning is expected to be the main contributor, while in summer the sum of other emission sector (such as vehicular) contributions is higher. On these bases, we can assert that biomass burning methylnitrocatechols are more underestimated than the methylnitrocatechols from other sources.

DHOPA modelled concentrations are underestimated by a factor higher than 1000. Moreover, the model failed to capture the temporal variations of DHOPA concentrations: at the beginning of the year

modelled DHOPA is higher than at the end of the year, while measured concentrations variations are opposite.

To evaluate the uncertainty due to the mechanism developed to model DHOPA concentrations from toluene photooxidation, a simpler parametrization, based on estimations from Gao et al. (2019), has been tested:



The DHOPA concentrations from toluene simulated with this reduced mechanism is higher by 40% than the DHOPA concentrations from toluene (excluding primary cresol) simulated by our model with an extended formation mechanisms (section 2.2.4). While it could be possible that the concentrations simulated by the extended mechanism are underestimated, it seems unlikely than errors on the chemical mechanism could explain a factor 1000 as the two mechanisms lead to concentrations in the same order of magnitude.

As methylnitrocatechols and DHOPA can both be formed from toluene and cresol, an evaluation of cresol and toluene contribution to simulated methylnitrocatechols and DHOPA concentrations have been performed for the month of February. Only 17% of the total modelled methylnitrocatechols turn out to be toluene generated, so we can think that primary cresol is the major precursor for methylnitrocatechols in the model. We estimated that 4% of the modelled DHOPA is produced by the dioxabicyclic-alcoholic-peroxy-hydroxy-hexene radical (TLBIPERO2) and oxobutenyl oxirane carbaldehyde (TLEPOXMUC) initiated pathways. The toluene derived DHOPA, including the secondary cresol pathway, has been estimated to account for 15% of the total simulated DHOPA. According to these results, cresol is the main precursor for both DHOPA and methylnitrocatechols.

One possible reason for the underestimation of DHOPA and methylnitrocatechols could be missing sources (especially for DHOPA that could be formed from numerous other precursors). Hobbs et al., (2004) estimated that 19% of NMVOC emission from Livestock in UK could be cresol. Based on the amount of cresol in residential wood burning emissions in Table 2 and by using emission estimates from the EMEP inventory, emissions from Livestock could therefore account for 20 times more cresol than residential wood burning. However, these emissions would not explain the high concentrations in winter and the low concentrations in summer that seem to indicate a high contribution from biomass burning.

Moreover, in our model methylcatechol (MCATECHOL in the mechanism) has been considered exclusively as intermediate, while it has been measured in primary biomass burning emissions (Gonçalves et al., 2012; Hatch et al., 2018). The eventual primary methylcatechol contribution to methylnitrocatechol concentrations has been estimated by adding to the model methylcatechol

emissions ratios (normalised to levoglucosan emissions). from Gonçalves et al., (2012). Methylnitrocatechols concentrations may increase by a factor 10, demonstrating that methylcatechol contribution to methylnitrocatechols total concentrations is not negligible.

Wang et al. (2017) measured methylnitrocatechols primary emissions from biomass burning sources. Based on this study, it only accounts for a small fraction of the PM_{2.5} emissions (between 0.0001% and 0.07%). For a concentration of biomass burning OA of 10 µg/m³, primary methylnitrocatechol concentrations would be at most around 7 ng m⁻³. In that state of knowledge, it is difficult to definitively conclude on the reasons for these underestimations. Missing precursors seem to be a likely explanation for DHOPA and methylnitrocatechols underestimation.

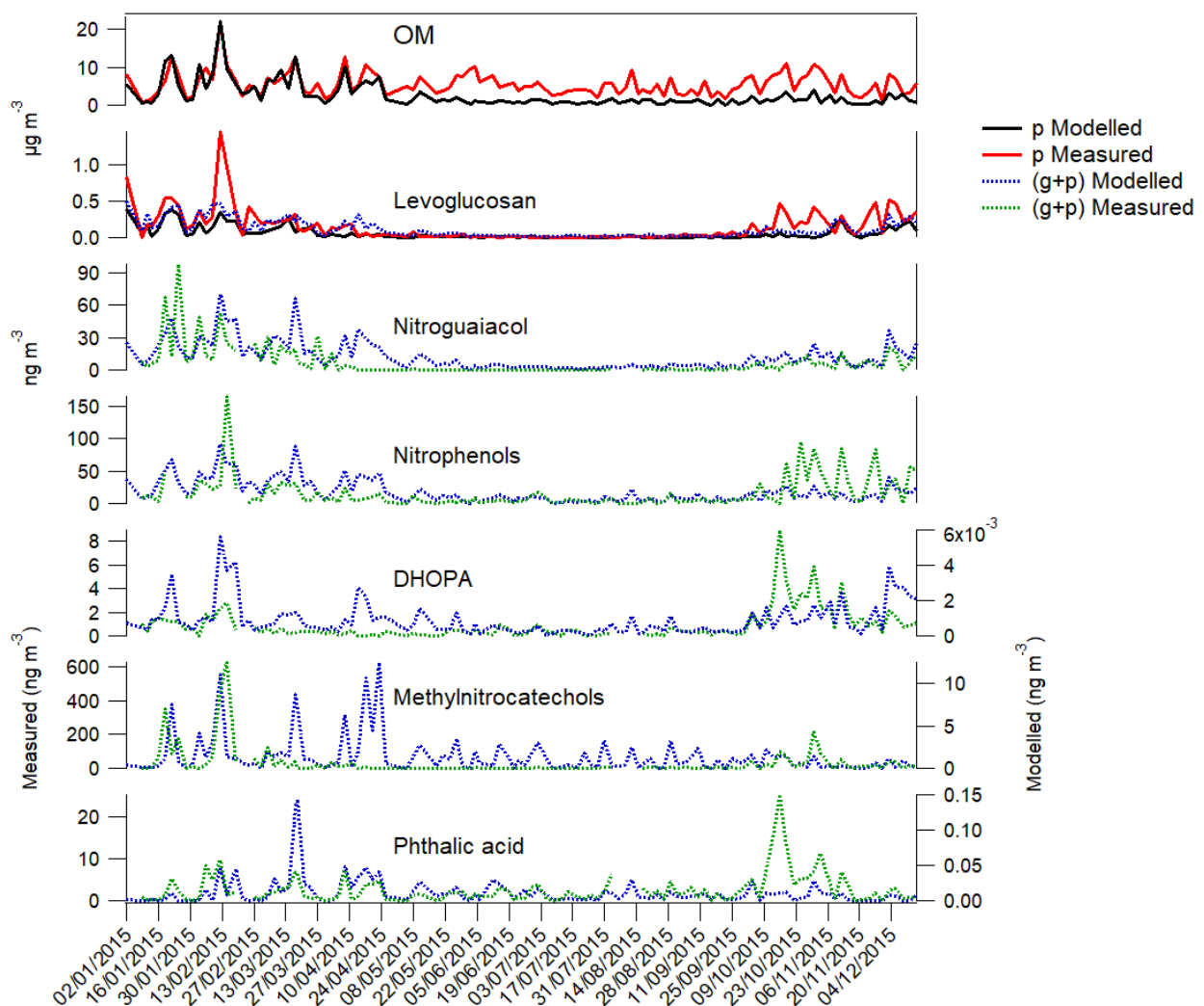


Figure 12. Annual evolution of OM, levoglucosan, nitroguaiacol, nitrophenols, DHOPA, methylnitrocatechols and phthalic acid concentrations at SIRTA, 2015.

4.1.3 Phthalic acid

Phthalic acid model to measurements comparison is presented in Fig. 12. The measured phthalic acid concentrations are below 25 ng m^{-3} , with higher concentrations observed between mid-October and the beginning of November. The modelled naphthalene-generated phthalic acid is two order of magnitude lower than the observations and the temporal variations are also misrepresented.

The potential formation of phthalic acid from naphthalene in our model has been evaluated using the experimental phthalic acid fraction in naphthalene SOA (0.02) measured by Kleindienst et al., (2012). The amount of phthalic acid estimated by the experimental fraction is 20 times lower than the phthalic acid simulated with the extended mechanism. Since also this method fails in estimating measured phthalic acid concentrations, it seems unlikely that the concentrations of phthalic acid in ambient air can be explained by the oxidation of naphthalene alone. Other phthalic acid sources should be considered to explain the discrepancies observed. Recent studies assess that phthalates concentrations are very high in urban environment (Barreca et al., 2014; He et al., 2018; Simoneit et al., 2005; Teil et al., 2006) and their degradation in atmosphere can produce phthalic acid (Hankett et al., 2013). In Paris urban area phthalate esters atmospheric levels are around 55 ngm^{-3} (Teil et al., 2006). Phthalate esters could be significant precursors of phthalic acid in atmosphere, but not enough information have been provided in the literature to quantify their contribution to total phthalic acid concentrations. Moreover, phthalic acid have been also quantified in primary vehicular emissions (Kawamura and Kaplan, 1987).

4.1.4 Correlation between secondary markers and levoglucosan

Table 4. Correlation coefficients ($p < 0.05$) of measured and modelled secondary markers with levoglucosan.

	Levoglucosan	
	measured	Modelled
DHOPA	0.55	0.52
Methylnitrocatechols	0.70	0.20
4-nitroguaiacol	0.61	0.59
Nitrophenols	0.58	0.59
Phthalic acid	0.28	0.03

Biomass burning is one of the major sources for most of the markers simulated in this study. Lanzafame et al. (in prep) reported significant correlations between some of these markers and levoglucosan for measurements. To evaluate if the relative contribution of biomass burning to marker concentrations is

well represented in the model, the correlations between levoglucosan and secondary anthropogenic markers in measurements and model are compared. The values are reported in Table 4.

DHOPA–levoglucosan measured and modeled correlations are similar and indicate a weak correlation (respectively 0.55 and 0.52). Both in measurements and model DHOPA is not attributed totally to biomass burning, because its precursors, toluene and cresol, are emitted also by other sources (Chan et al., 2009; Hobbs et al., 2004; Na et al., 2001).

Measured methylnitrocatechols and levoglucosan correlates well (0.70), demonstrating that methylnitrocatechol is a good marker for biomass burning in atmosphere. However, the correlation between these two compounds in the model (0.2) is scarce, since, as DHOPA, methylnitrocatechols precursors in the model are toluene and cresol. These results indicate that a significant contribution from biomass burning is probably missing for methylnitrocatechols.

For nitroguaiacols and nitrophenols, the correlations with levoglucosan are around 0.6 for both the model and the measurements. These non-negligible correlations are not strong enough to attribute completely these markers to biomass burning, but the similarity of the modelled and measured values is indicative of the high accuracy in representing their precursors emissions (guaiacol, toluene and phenol) in the model.

Phthalic acid correlates scarcely (0.20) in measurements with levoglucosan and even less in the model (0.03). In fact, in our model, naphthalene is emitted both from domestic and industrial biomass burning with the same percentages. The different contribution of the 2 sources throughout the year may cause the low correlation calculated in the model. Other sources for phthalic acid should be considered.

4.2 GPP estimations

4.2.1 Levoglucosan: spatial variability and model sensitivity to thermodynamic assumptions

Figure 13 shows the spatial variability of simulated daily averaged concentrations of levoglucosan fraction in the particulate phase over Europe for February 2015 (chosen to be representative of the colder season with high biomass burning emissions). Several sensitivity simulations have been performed to understand the influence of the molecular interactions on the aerosol formation and partitioning. In the “reference” run, levoglucosan is both hydrophobic and hydrophilic and all the interactions with the aerosol organic and inorganic components are considered. In the “ideal” case, levoglucosan is still considered hydrophobic and hydrophilic, but the interactions with the other aerosol organic components are not considered. Non-ideal and ideal tests have also been performed by

considering that levoglucosan is only hydrophilic (“Hyphi” and “Hyphi ideal” tests respectively) or only hydrophobic (“Hypho” and “Hypho ideal”). A map of levoglucosan total (gas+particle) concentrations during February 2015 in Europe is provided in the Supplementary material (Fig. S11). The differences simulated on the total concentrations are under $5\mu\text{g m}^{-3}$. In the “reference” run levoglucosan particulate phase fraction on the land varies from 0.2 to 1. In central Europe, the fraction is higher, with values starting from 0.75 to the maximum observed in Belgium, Luxemburg and Holland. In the northern Europe particulate phase fraction keeps high values (>0.6), with some local minimum (0.2–0.4) in the Northern part of Norway and Sweden. In Southern Europe, levoglucosan particulate phase fraction drops to lower values (0.2–0.4) over wide regions of Spain, Portugal and Greece.

In the “ideal” test, much higher aerosol fractions are simulated. The lower fraction observed on the land is between 0.75 and 0.85 (wide regions of Spain and Portugal, some spots in Norway and Sweden). In a big region covering almost all the central Europe, levoglucosan is completely in the particulate phase (particulate phase fraction 0.95–1) and more than 85% of levoglucosan is in the particulate phase in the rest of the domain.

The “hydrophilic” test gives similar results to the “reference”, with only some small local differences. Similarly, the “hydrophilic ideal” test gives similar results to the ideal test. In both, the reference and “ideal” tests, most of partitioning is due to the hydrophilic partitioning.

On the contrary, hydrophobic levoglucosan partitioning is shifted towards the gaseous phase. In the “hydrophobic non-ideal” parametrization, the levoglucosan particle-phase fraction ranges between 0 and 0.3 on the land. The higher fraction is simulated over Belgium and the North of Italy, where the simulated levoglucosan total concentrations are the highest (Fig S11). Much higher particle-phase fractions (10 to 90%) are simulated in the “hydrophilic ideal” test (but the fraction is still much lower than for the hydrophilic ideal and hydrophilic tests). The lower values (fraction 0.10–0.20) have been observed in most of the Scandinavian peninsula and in the north UK. In the rest of Europe particulate phase levoglucosan fractions are between 0.30 and 0.75, except for Spain and Portugal (0.2–0.3) and 2 local maximums in Belgium and in the north of Italy.

Levoglucosan partitioning in “reference” and “hydrophilic run” is clearly influenced by humidity (Fig S11). In the drier regions (relative humidity $<0.70\%$) less than 40% of levoglucosan is in the particulate phase.

All these results indicate that the hydrophilic partitioning is more shifted towards the particle phase than the hydrophobic partitioning and that non-ideality leads to a strong decrease of the particle phase fraction. In all the tests, the fraction of levoglucosan in the gas phase cannot be neglected. The gas phase fraction represents even most of the levoglucosan in some areas. These results can be surprising

as levoglucosan is often considered as non-volatile (Fraser and Lakshmanan, 2000; Simoneit et al., 1999) but some studies showed that the gas-phase fraction can be significant (Parshintsev et al., 2011). The highest uncertainty in this GPP parametrization is associated to the saturated vapor pressure and vaporization enthalpy choice. In this study, the values measured by Booth et al., (2011) were used. To our knowledge, no other measurements of levoglucosan P_{sat} have been performed. Xie et al., (2014) performed computation of the levoglucosan partitioning but with a much lower saturation vapor pressure (1.8×10^{-7} torr against 1.45×10^{-6} torr for the value used in this study) and higher vaporization enthalpy. This lower saturation vapor pressure was taken from Parshintsev et al., (2011) who did not explain how this value was estimated. It may therefore be possible that the value used in the present study is overestimated. Using the value from Parshintsev et al. (2011) would lead to a significant underestimation of the particle-phase levoglucosan that would almost appear as non-volatile.

In the non-ideal scenarios, the particle average composition considered (detailed in the section configuration) influences the GPP and may be a cause of uncertainty. The model cannot simulate all the factors governing aerosol composition, such as the emitting sources and the type of environment considered (Ruehl et al., 2011). High percentages of WSOC (Water Soluble Organic Compounds) providing an efficient substrate for levoglucosan condensation have been revealed in biomass burning aerosols (Gao et al., 2003). However, due to lack of information on the composition of primary aerosols, the H₂O mechanism assumes that primary aerosols are apolar.

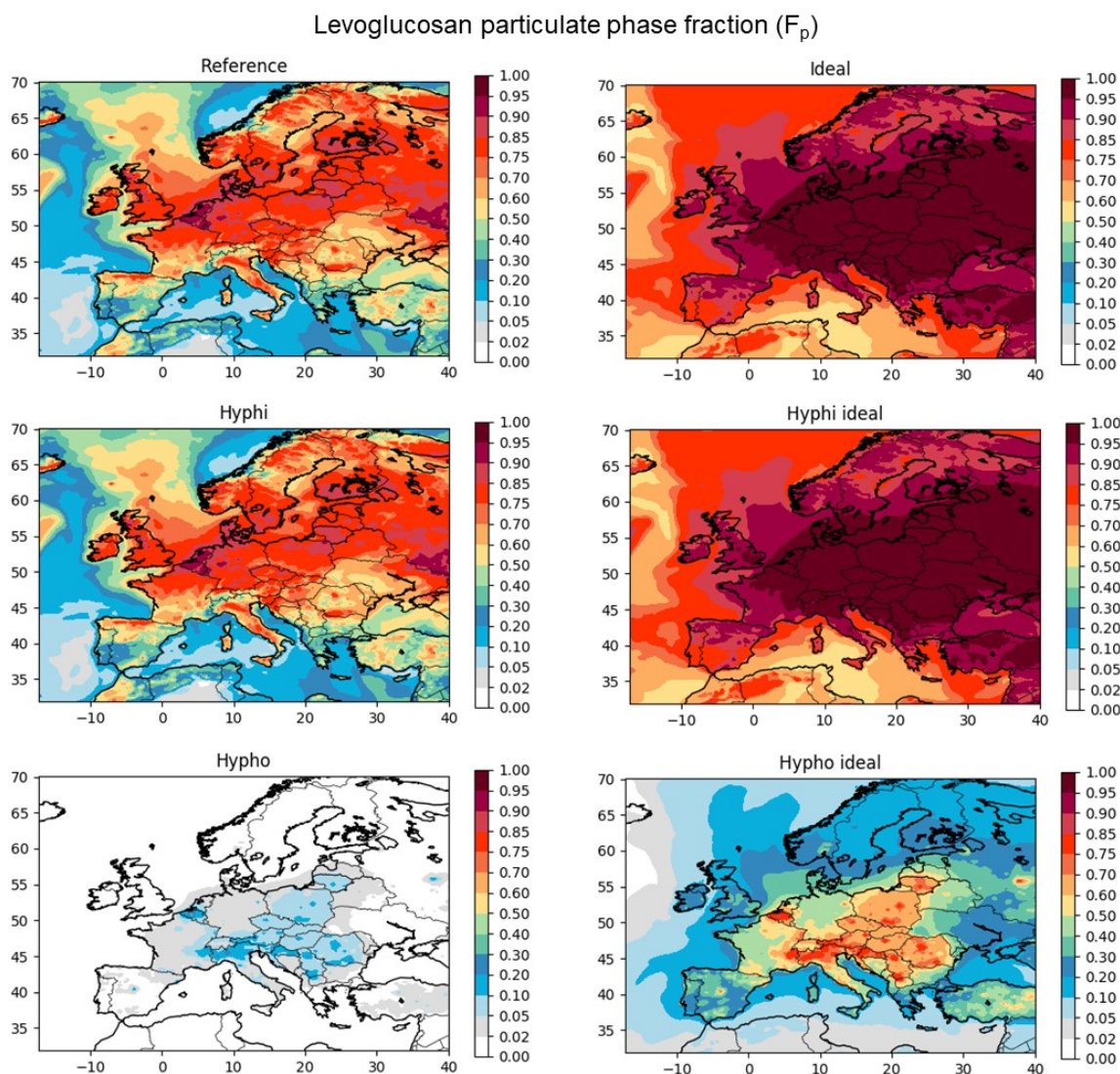


Figure 13. Maps of Levoglucosan particulate phase fraction over Europe during February 2015. The following thermodynamic conditions are shown from the top left panel to the bottom right panel: reference (non-ideal aerosol, levoglucosan is both hydrophobic and hydrophilic), ideal, hydrophilic (Hyphi), hydrophilic ideal (Hphi ideal), hydrophobic (Hypho) and hydrophobic ideal (Hypho ideal).

4.2.2 GPP of secondary markers at SIRTA.

Tests on GPP computation reference (ideal aerosol, completely hydrophobic or hydrophilic marker in non-ideal and ideal aerosol) for nitroguaiacols, nitrophenols, DHOPA, methylnitrocatechols and phthalic acid have been performed during February, mid-June to mid-July and October 2015. These months have been chosen as the more representative of all the annual weather and emission conditions. The test outputs are shown in Fig. 14, together with the results of measurements (“obs”) and of the reference simulation (ref, markers both hydrophilic and hydrophobic, non-ideal aerosol) GPP. All the markers in the only “hydrophilic” test partition similarly to the “reference” simulation. Slight

differences between the “reference” and the “hydrophilic” tests (~5% both in median and interquartile range F_p) and between the “ideal” and “hydrophilic ideal” tests (~18% for the median and interquartile range F_p) have been reported for all the markers, except DHOPA. Hence, the “hydrophilic” and “hydrophilic ideal” run outputs are very similar to the “reference” and “ideal” simulation outputs and will not be commented in the text. Hydrophobic marker F_p in non-ideal aerosol is close to zero for all the markers, with no variability indicating that all the compounds studied can be considered strongly hydrophilic.

In measurements, nitroguaiacol is mostly in the gaseous phase with a measured median F_p lower than 5%. In all the tests performed, the particulate phase fraction remains very low and the median value never exceeds 5%. The “reference” run result gives a median F_p (0.002) lower than the one observed (0.02), with narrower F_p distributions (interquartile ranges are respectively 0.16 for measurements and 0.025 for the “reference”). The partitioning on the ideal aerosol is similar to the measured one: F_p median values are similar (“ideal” median F_p 0.15), and their distribution is wider than all the other tests (interquartile range 0.047), but narrower than in the measurements. In the “ideal” simulations, hydrophobic nitroguaiacol is less volatile than in the non-ideal “hydrophobic” simulation (median F_p are respectively 0.002 and 0.0005).

Similar to nitroguaiacol, nitrophenol GPP is shifted toward the gaseous phase (all the F_p are below 0.14). Median F_p values are lower than in the “obs” (0.02) for the “reference” (0.014) and higher for the “ideal” (0.03) simulations. The F_p distribution in the observations is narrower than in the “reference” and in the “ideal” run (interquartile ranges are respectively 0.02, 0.053 and 0.11). “Hydrophobic ideal” test F_p distribution is wider than in the “hydrophobic” non-ideal test (interquartile ranges 0.026 and 0.008), median F_p value are lower (respectively 0.005 and 0.003) than in the measurements and in the “reference” run.

DHOPA F_p is shifted towards the particulate phase for the measurements, with median values close to 1. In the “reference” run, DHOPA partitioning is also shifted to the particulate phase, but the median value is lower (0.9) than in the “obs”. In the “ideal” aerosol parametrization, F_p values are close to the observed ones, with a median value slightly lower than 1. Hydrophobic DHOPA in the ideal aerosol has a median F_p around 0.2 and 25th and 75th percentiles around 0.1 and 0.6 respectively, while in non-ideal aerosol hydrophobic DHOPA is almost completely in the gaseous phase, with a median F_p of 0.005 and interquartile range of 0.035.

Methylnitrocatechols GPP is shifted towards the particle phase in the measurements (median F_p of 0.9) whereas, in all the model runs, methylnitrocatechols are mainly present in the gas phase (median F_p ranges between 0.02 and 0.2) and F_p is strongly underestimated. “Reference” run F_p are lower than 0.2, while for the “ideal” simulation, methylnitrocatechols are less volatile with median, 25th and 75th

percentile values around 0.2, 0.1 and 0.6 respectively. The median F_p for the “ideal hydrophobic” simulation (0.035) is higher than in the non-ideal “hydrophobic” simulation (0.009).

Phthalic acid median particulate phase fraction in measurements is 65%. The observed F_p are very variable, with values between 0.13 and 1. In all the simulation phthalic acid is mainly in the gas phase, with 90th F_p percentile values below 0.5. In the “reference” run, GPP has a narrow distribution around a median value lower than 5%. In the “ideal” simulation, F_p median value is around 15%, F_p distribution are wide and reach the maximum value (0.45) for particulate phase fraction. In the “hydrophobic ideal” simulation, phthalic acid is almost totally in the gaseous phase (90th F_p percentile below 0.2).

In general, we can assert that the partitioning of the markers is driven mainly by their hydrophilicity and that the model tends to underestimate the particle phase fraction. Marker partitioning in the “ideal” simulations was found to be closer to the measurements because in the “ideal” simulations the particle phase fraction is higher. These considerations should be used carefully because of the approximations used in the model: some functional group, or the combination of functional groups, could be not well represented in the SAR used to estimate the activity coefficients (e.g. the NO_2 group), the saturation vapor pressure used in this study are highly uncertain, modelled OM composition could be not representative of real OM (an apolar default structure is used for primary compounds, and the model could strongly underestimate the concentrations of hydrophilic aerosols), and OM is strongly underestimated in summer.

The sensitivity analysis (ideal aerosol, completely hydrophobic or hydrophilic marker in non-ideal and ideal aerosol) on daily mean particulate phase distribution of secondary markers all over Europe during February 2015 are reported in Fig. S14, S15, S16, S17 and S18. As already commented for levoglucosan, the hydrophilic partitioning dominates over hydrophobic partitioning. Higher F_p values (from 0.02 to 0.2 for nitroguaiacol, from 0.05 to 0.3 for nitrophenols, from 0.1 to 0.5 for methylnitrocatechols, from 0.95 to 1 for DHOPA and from 0.2 to 1 for phthalic acid) are usually observed in central Europe (North of France, Germany, Italy, Austria, Hungary, Poland, Holland, Belgium, on the Baltic coast and southern Scandinavian peninsula) for the tests including hydrophilic partitioning and non-ideal aerosol (“reference” and “hydrophilic” simulations). Lower hydrophilic (“reference” and “hydrophilic” simulations) F_p have been simulated in the drier regions (Spain and Portugal) for all the markers and for nitroguaiacol, nitrophenol and phthalic acid also in the colder regions (north of Scandinavian peninsula) (F_p from 0.01 to 0.05 for nitroguaiacol, methylnitrocatechols and phthalic acid, from 0.005 to 0.02 for nitrophenols and from 0.6 to 0.8 for DHOPA). Hydrophobic markers F_p distribution is similar to the hydrophilic, with higher values in central Europe and lower values in southern and northern Europe. Hydrophobic F_p are lower than the hydrophilic by a factor 20 for nitroguaiacol, 5 for nitrophenol, 10 for methylnitrocatechol and DHOPA and 25 for phthalic acid.

Aerosol ideality favors the partition to the particulate phase for all the markers in both hydrophilic and hydrophobic conditions, increasing F_p by a factor ranged between 0.5 to 2.

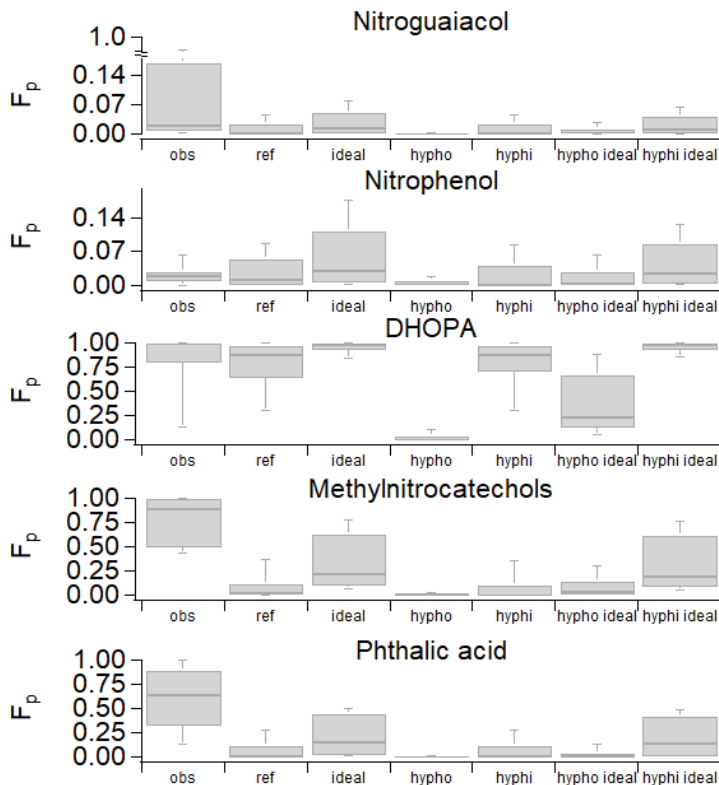


Figure 14. From the top to the bottom: nitroguaiacol, methylnitrocatechols and DHOPA gas to particle partitioning thermodynamic test. On the right side, the particulate phase fractions calculated for measurements (obs) and simulated with reference (ref), ideal aerosol (ideal), hydrophobic marker (hypho), hydrophilic marker (hyphi), hydrophobic marker and ideal aerosol (hypho ideal) and hydrophilic marker and ideal aerosol (hyphi ideal) parametrizations are shown.

4.2.3 Influence of partitioning and gas-phase dry deposition of secondary markers on total concentrations

As effect of the gas-phase oxidation and the different gas and particle deposition rates, GPP may influence total marker concentrations. Some tests on total marker concentration variations have been performed assuming a completely non-volatile and volatile behavior.

Moreover, in the “reference” simulations, dry and wet deposition of gas-phase markers were not considered (only particle deposition has been considered in the “reference” run). The influence of this phenomena is also tested (as described in part 2). The results of the different tests are compared with the “reference” run (no dry and wet deposition of gas-phase markers) in Fig. 15.

As in the “reference” simulation, nitroguaiacols are almost entirely in the gas-phase, total concentrations are very similar to those of the “volatile” case. “Non-volatile” nitroguaiacols total concentrations are lower by 30% than those of the “reference” simulation. As no gas-phase degradation of nitroguaiacols has been considered in the mechanism, the main loss process is the particle-phase deposition in the “reference” simulation. Therefore, the increase of particle-phase concentrations leads to a decrease of concentrations. As in observations, F_p 75th percentile value is around 17%, the uncertainty on F_p calculation can be expected to be of a few percent only.

Similar considerations can be applied to nitrophenol, for which F_p values are close to 0 in the reference run. Total concentrations in the “volatile” and “reference” simulations are similar, while concentrations for the “non-volatile” simulation decrease by 20%. indicating that the increase in F_p values lead to more removal due to particulate phase deposition. Indeed, nitrophenols half-life has been estimated to be around 12 days for the period tested (by using simulated radical concentrations for the period), which is longer than the average particle half-life of 1 week (Seinfeld, 2015). The degradation in the gaseous phase represent a slower loss mechanism compared to the particulate phase deposition. The uncertainty on F_p calculation is even lower than for nitroguaiacol, considered the lower F_p values.

DHOPA partitioning is shifted preferentially toward the particulate phase both in measurements and in the “reference” simulation. Compared to the “reference” simulation, DHOPA concentrations are lower by 70% in the “volatile” simulation but increase by a factor 2 in the “non-volatile” simulation. Even though DHOPA is almost non-volatile in the “reference” simulation, the differences in total concentrations between the “non-volatile” and the “reference” runs show that DHOPA concentrations depend strongly on GPP. This result can be explained by the fast degradation kinetic of DHOPA in the gaseous phase (estimated half-life of 0.84 d^{-1} for the period), that can be considered the major loss process for this marker (DHOPA can be degraded also in the aqueous phase). Therefore, the partitioning toward the particulate phase protects DHOPA from degradation. Despite DHOPA F_p values in the “reference” simulation are close to those in the measurements (0.9), the uncertainty on total concentrations associated to the GPP estimation is high (up to a factor 2) because of the high degradation rate in the gaseous phase. As methylnitrocatechols are almost entirely volatile in the “reference” simulation, their total concentrations are close to those of “volatile” run. In the “non-volatile” simulation methylnitrocatechols total concentrations increase by a factor 2. In this case, the transfer to the particulate phase protects methylnitrocatechols from their degradation mechanisms, that occur only in the gas phase (estimated half-life of 0.5 d^{-1}). As in measurements methylnitrocatechols are almost entirely inside the particle, the uncertainty on the simulated methylnitrocatechols total concentrations should be considered high (up to a factor 2).

In the “reference” simulation, phthalic acid F_p is low and total concentrations are similar to those of the “volatile” simulation. Concentrations in the “non-volatile” simulation decreased by 20%.

Therefore, the partitioning toward the particulate phase does not protect phthalic acid from degradation (half-life of 16.6 d^{-1}). In conclusion, naphthalene-generated phthalic acid concentrations may be slightly overestimated (by less than 20%) due to the discrepancy in F_p values between the model and measurements.,

These results highlight that total concentrations may be strongly influenced by GPP for some of the compounds (DHOPA, methylnitrocatechol, phthalic acid). However, the uncertainty due to GPP for these compounds is low compared to the differences between the model and measurements. The gap cannot be explained by GPP alone.

The influence of gaseous phase deposition on total marker concentrations is clearly linked to the volatility of the marker itself with a high effect for high volatile markers. For DHOPA, no significant effect of gas-phase deposition has been simulated (because the compound is almost non-volatile). A decrease of concentrations by a factor around 6 are simulated for nitroguaiacols and nitrophenol, which are volatile in both the model and measurements. While total concentrations were close to measurements in the “reference” simulation, considering the gas-phase deposition lead to a strong underestimation of concentrations. This drop of model performance when gas-phase deposition is considered can be either due to an underestimation of marker formation which compensate gas-phase deposition or due to an overestimation of the deposition rate of SVOC by CHIMERE. For methylnitrocatechol and phthalic acid, the reductions simulated (30% and 75% respectively) due to gas-phase deposition are probably strongly overestimated. In the measurements, the compounds are mostly present in the particle phase whereas simulated F_p are close to 0.

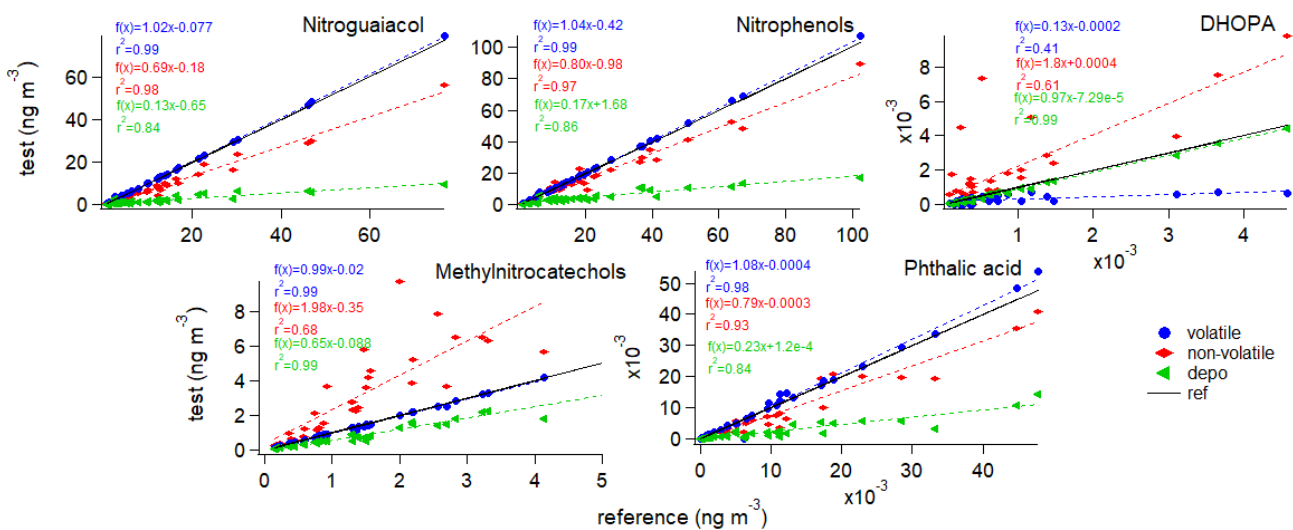


Figure 15. From the top left to the bottom right: nitroguaiacol, nitrophenol, DHOPA, methylnitrocatechols and phthalic acid thermodynamic tests. Total modelled semivolatile (reference)

marker concentrations are compared to modelled volatile, nonvolatile and affected by dry and wet deposition (depo) total marker concentrations.

4.2.4 Evaluation of the OA-tracer approach to evaluate the wood-burning OM: Analysis of OM_{wb} pLEVO-1 variations

Constant ratios between the wood burning organic matter (OM_{wb}) and particulate phase levoglucosan (pLEVO⁻¹) are often used to evaluate the contribution of wood-burning aerosol to organic aerosol (Herich et al., 2014; Puxbaum et al., 2007; Schmidl et al., 2008). Favez, (2016) calculated for the sites monitored in this study site-specific OM_{wb} pLEVO⁻¹ ratios to estimate the amount of OM_{wb} in total OM from levoglucosan measurements (details in SM). However, as shown in section 4.2.1, the partitioning of levoglucosan may depend strongly on the hydrophilic properties, on the environmental conditions and on non-ideality. Moreover, the partitioning of levoglucosan probably differs from the partitioning of wood burning SVOC. The OM_{wb} pLEVO⁻¹ should therefore depends on environmental conditions. The theoretical OM_{wb} pLEVO⁻¹ can be computed with the following algorithms:

The particulate phase levoglucosan concentration (pLEVO) can be estimated with the following equation:

$$pLEVO = (g + p)LEVO \times \frac{K_{p,levo} OM}{1 + K_{p,levo} OM} \quad (8)$$

where (g+p)LEVO is the total levoglucosan concentration and K_{p,levo} is the levoglucosan partitioning constant.

The organic matter produced from wood burning (OM_{wb}), constituted by *i* components, can be calculated as follows:

$$OM_{wb} = \sum_i \left[(A_{p,wb,i} + A_{g,wb,i}) \times \frac{K_{wb,p,i} OM}{1 + K_{wb,p,i} OM} \right] \quad (9)$$

where A_{p,wb,i} and A_{g,wb,i} are respectively the particulate and gaseous phase concentrations of the *i* component and K_{wb,p,i} is his partitioning constant. According to Eq. (8) and (9), pLEVO and OM_{wb} depend on the total OM and on temperature (Eq. (2)). The calculated OM_{wb} pLEVO⁻¹ ratio is:

$$\frac{OM_{wb}}{pLEVO} = \frac{\sum_i \left[(pA_{wb,i} + gA_{wb,i}) \times \frac{K_{wb,p,i} OM}{1 + K_{wb,p,i} OM} \right]}{(g + p)LEVO \times \frac{K_{p,levo} OM}{1 + K_{p,levo} OM}} \quad (10)$$

Based on Eq. (10), this ratio would remain constant only if K_{p,wb,i}=K_{p,levo} (all SVOCs from wood burning have the same volatility of levoglucosan).

In order to evaluate from a theoretical point of view, the validity of these assumptions, the variations of the simulated OM_{wb}pLEVO⁻¹ are studied. The simulated OM_{wb}pLEVO⁻¹ as a function of total OM at 275, 280 and 285 (±0.5) K are reported in Fig. 16 for the reference simulations as well as the ideal and

the hydrophobic ideal test (by taking all the point of the domain close to the selected temperature by ± 0.5 K). The ratio has been calculated for levoglucosan concentrations greater than $0.1 \mu\text{g m}^{-3}$. The selected temperatures have been chosen to be representative of wintertime data, in which OM_{wb} and levoglucosan emissions are expected to be higher.

All the tests indicate strong variations of the $\text{OM}_{\text{wb}}\text{pLEVO}^{-1}$ and varies strongly under $10 \mu\text{g m}^{-3}$ of OM whereas above $10 \mu\text{g m}^{-3}$, the results indicate weak of this ratio. In the hydrophobic ideal test, the ratio decreases fast at OM values below $10 \mu\text{g m}^{-3}$ (from 26 to 18) and at higher OM masses keeps a value around 18, following an inverse Odum-like curve. SVOC_{wb} concentrations grow faster than levoglucosan concentrations when OM is increasing.

In the ideal test, the $\text{OM}_{\text{wb}}\text{pLEVO}^{-1}$ ratio varies with OM according to an Odum-like curve between 8 and 16. This trend is determined by the relative variations of levoglucosan and OM_{wb} volatilities: levoglucosan is almost non-volatile (its partitioning does not depend on OM) while the condensation of SVOC_{wb} increase with OM (and follow the dilution curve of May et al., (2012)).

When non-ideality is considered, strong variability of this ratio is simulated, especially under $10 \mu\text{g m}^{-3}$ where the ratio varied in the simulations between 6 and 40. Nonetheless, this ratio tends to increase with OM and decrease with temperature. Above $10 \mu\text{g m}^{-3}$, most of the ratios are around 20.

Whatever the temperature regime, at OM values below $10 \mu\text{g m}^{-3}$, the constant ratio approach commonly used to calculate OM_{wb} cannot be validated because of the great variability. It can therefore be difficult to evaluate precisely the contribution of OM_{wb} from levoglucosan alone. However, this method could be considered as accurate for regions characterized by high OM values (e.g. Bordeaux and Lyon, Fig 10) or during OM peaks.

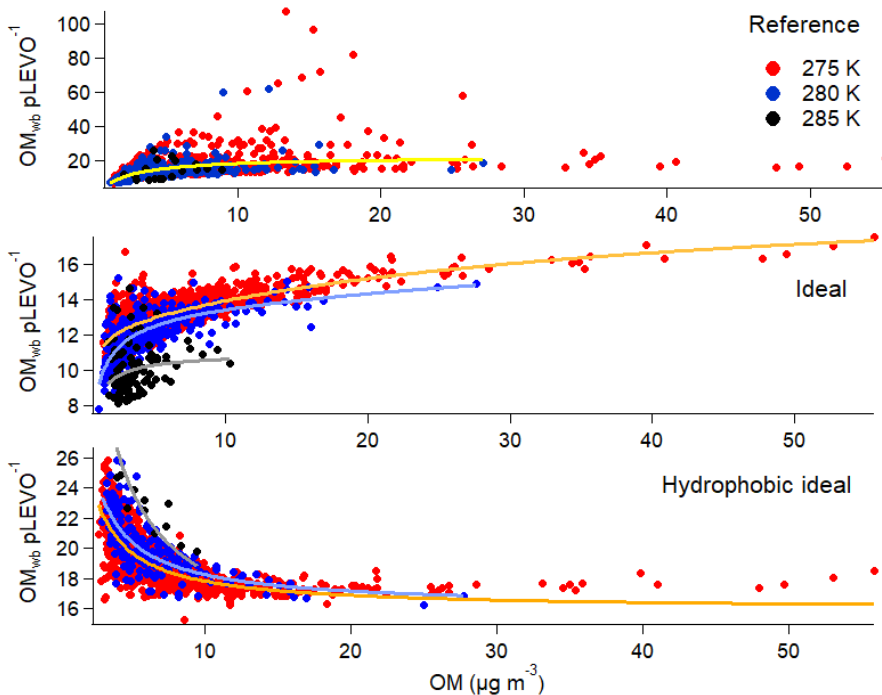


Figure 16. Odum-like curves representing $OM_{wb} pLEVO^{-1}$ as a function of total OM at 275, 280 and 285 K. From the top to the bottom: reference, ideal and hydrophobic ideal aerosol runs are shown. Hydrophobic ideal run follows an inverse Odum parametrization, which theoretical curves are reported.

Conclusions

A mechanism for the formation of molecular markers has been implemented in the 3D chemistry transport model CHIMERE. To our knowledge, this is the first time that anthropogenic OA markers have been modeled with a 3D CTM. Using marker modeling can give insights on the model performances and on several processes (such as GPP, chemistry, emissions) involving OM formation.

Levoglucosan, a primary compound, is reproduced by the model with the same performances as OM. An underestimation of the residential wood burning emissions for some cities in France is probably the cause of the mismatching between measurements and simulations outputs.

Concerning secondary markers, nitroguaiacol and nitrophenol concentrations are well simulated by the model, while methylnitrocatechol, DHOPA and phthalic acid are strongly underestimated, and their temporal variations are not consistent with the measurements. This effect may depend on an underestimation of precursor emissions (e.g. lack of emissions from some sectors), missing precursors (e.g. methylcatechol for methylnitrocatechol), non-accounted primary marker emissions (methylnitrocatechols and phthalic acid have been detected in emissions) or missing chemical pathways. Precursor emissions is probably the main source of uncertainty for these compounds. Due to the variety and the lack of data on the detailed composition of emissions, it is difficult to evaluate precisely the emissions from human activities: precursors emissions can be easily underestimated if some sector is missing.

The GPP of markers has been simulated with SOAP by considering non-ideality. For nitroguaiacol, nitrophenols and DHOPA the model reproduces well the GPP, but in general the model underestimates the measured marker F_p . A strong GPP influence on total concentrations has been found for the markers with fast degradation in the gas-phase, for which the transfer to the particle-phase protect their degradations (e.g. DHOPA). Low volatile marker total concentrations are scarcely influenced by wet and dry gas deposition, while volatile markers total concentrations are significantly affected. Although the uncertainty connected to GPP estimation is not negligible, the discrepancies between model and measurements cannot be explained by GPP alone.

For levoglucosan, the model found that the compound is semivolatile which particle-phase fraction between 20 and 100%. Recent studies proved levoglucosan semi volatility (Bertrand et al., 2018; May et al., 2012), that is reproduced in our model using the P_{sat} and ΔH_{vap} values measured by Booth et al.,

(2011). However, the greater uncertainty on the GPP estimations relies on the P_{sat} and ΔH_{vap} values chosen. In the case of levoglucosan, Booth et al., (2011) has determined a value of P_{sat} which is higher by one order of magnitude than the one used in other studies (Parshintsev et al., 2011). Using the value of Parshintsev et al. (2011) (as done by Xie et al., (2014)) would have given a much higher F_p and levoglucosan would have appear as almost non-volatile.

A theoretical study of OM $p\text{LEVO}^{-1}$ demonstrates that levoglucosan contribution to OM_{wb} is not constant at OM values typical of European aerosol ($<10 \mu\text{g m}^{-3}$) contrary to what is assumed in numerous studies. For higher OM concentrations, the ratio become constant and this approach can be validated. The model estimate that all the markers considered in this paper are very hydrophilic and that assuming that those compounds only condense on the organic phase of particles (as often assumed for SVOC by air quality models) lead to a significant underestimation of the particle phase concentrations. Moreover, their partitioning was found to strongly depend on the environmental conditions. In our simulations, humidity may play a key role in levoglucosan GPP estimation, but no measurements of both phases are available to quantify this effect.

The impact of the other approximations often done in air quality models model should also be considered: ideality, equilibrium and non-viscous aerosol. Kim et al., (2018) implemented the SOAP model in the CTM Polair3D (Sartelet et al., 2007) of air quality platform Polyphemus (Mallet et al., 2007). They tested the model using both an equilibrium and a dynamic approach, ideal and non-ideal aerosol configurations. They found that non-ideality strongly affects the condensation of hydrophilic organic compounds on the aerosol and lead to a decrease of 33% the hydrophilic SOA concentrations. The opposite findings with our study can be justified by the fact that levoglucosan and the other organic markers in this study are more polar and hydrophilic than the ones in Kim et al., (2018). To simulate correctly activity coefficients, the composition of organic aerosols must be estimated correctly, which may be very challenging in the current state of knowledge.

Kim et al., (2018) also simulated the influence of particle viscosity on hydrophobic compounds GPP using a dynamic approach. In a dynamic inviscid approach, particulate phase concentrations are close to equilibrium, while in a dynamic viscous approach hydrophobic SOA concentration increase significantly for volatile compounds.

Modeling SVOCs in atmosphere is not a simple task but may provide meaningful information to understand better OA formation and behavior in atmosphere. Further studies on aerosol dynamics, thermodynamic parameters measurements and emissions are required to improve the understanding, and consequently the modeling, of atmospheric processes.

References

- Al-Naiema, I. M. and Stone, E. A.: Evaluation of anthropogenic secondary organic aerosol tracers from aromatic hydrocarbons, *Atmospheric Chem. Phys.*, 17(3), 2053–2065, doi:10.5194/acp-17-2053-2017, 2017.
- Aschmann, S. M., Arey, J. and Atkinson, R.: Study of the Atmospheric Chemistry of 2-Formylcinnamaldehyde, *J. Phys. Chem. A*, 117(33), 7876–7886, doi:10.1021/jp404994w, 2013.
- Aschmann, S. M., Nishino, N., Arey, J. and Atkinson, R.: Products of the OH Radical-Initiated Reactions of Furan, 2- and 3-Methylfuran, and 2,3- and 2,5-Dimethylfuran in the Presence of NO, *J. Phys. Chem. A*, 118(2), 457–466, doi:10.1021/jp410345k, 2014.
- Bai, J., Sun, X., Zhang, C., Xu, Y. and Qi, C.: The OH-initiated atmospheric reaction mechanism and kinetics for levoglucosan emitted in biomass burning, *Chemosphere*, 93(9), 2004–2010, doi:10.1016/j.chemosphere.2013.07.021, 2013.
- Bannan, T. J., Booth, A. M., Jones, B. T., O’Meara, S., Barley, M. H., Riipinen, I., Percival, C. J. and Topping, D.: Measured Saturation Vapor Pressures of Phenolic and Nitro-aromatic Compounds, *Environ. Sci. Technol.*, 51(7), 3922–3928, doi:10.1021/acs.est.6b06364, 2017.
- Barreca, S., Indelicato, R., Orecchio, S. and Pace, A.: Photodegradation of selected phthalates on mural painting surfaces under UV light irradiation, *Microchem. J.*, 114, 192–196, doi:10.1016/j.microc.2014.01.004, 2014.
- Bertrand, A., Stefenelli, G., Pieber, S. M., Bruns, E. A., Temime-Roussel, B., Slowik, J. G., Wortham, H., Prévôt, A. S. H., Haddad, I. E. and Marchand, N.: Influence of the vapor wall loss on the degradation rate constants in chamber experiments of levoglucosan and other biomass burning markers, *Atmospheric Chem. Phys.*, 18(15), 10915–10930, doi:https://doi.org/10.5194/acp-18-10915-2018, 2018.
- Bessagnet, B., Seigneur, C. and Menut, L.: Impact of dry deposition of semi-volatile organic compounds on secondary organic aerosols, *Atmos. Environ.*, 44, 1781–1787, doi:10.1016/j.atmosenv.2010.01.027, 2010.
- Bessagnet, B., Pirovano, G., Mircea, M., Cuvelier, C., Aulinger, A., Calori, G., Ciarelli, G., Manders, A., Stern, R., Tsyro, S., García Vivanco, M., Thunis, P., Pay, M.-T., Colette, A., Couvidat, F., Meleux, F., Rouïl, L., Ung, A., Aksoyoglu, S., Baldasano, J. M., Bieser, J., Briganti, G., Cappelletti, A., D’Isidoro, M., Finardi, S., Kranenburg, R., Silibello, C., Carnevale, C., Aas, W., Dupont, J.-C., Fagerli, H., Gonzalez, L., Menut, L., Prévôt, A. S. H., Roberts, P. and White, L.: Presentation of the EURODELTA III intercomparison exercise – evaluation of the chemistry transport models’ performance on criteria pollutants and joint analysis with meteorology, *Atmospheric Chem. Phys.*, 16(19), 12667–12701, doi:10.5194/acp-16-12667-2016, 2016.
- Bierbach, A., Barnes, I. and Becker, K. H.: Rate Coefficients For The Gas-Phase Reactions Of Hydroxyl Radicals With Furan, 2-Methylfuran, 2-Ethylfuran And 2,5- Dimethylfuran At 300 + 2 K, *Atmos. Environ.*, 26A(5), 813–817, doi:10.1016/1352-2310(95)00096-H, 1992.
- Bilde, M., Barsanti, K., Booth, M., Cappa, C. D., Donahue, N. M., Emanuelsson, E. U., McFiggans, G., Krieger, U. K., Marcolli, C., Topping, D., Ziemann, P., Barley, M., Clegg, S., Dennis-Smith, B., Hallquist, M., Hallquist, Å. M., Khlystov, A., Kulmala, M., Mogensen, D., Percival, C. J., Pope, F., Reid, J. P., Ribeiro da Silva, M. A. V., Rosenoern, T., Salo, K., Soonsin, V. P., Yli-Juuti, T., Prisle, N.

L., Pagels, J., Rarey, J., Zardini, A. A. and Riipinen, I.: Saturation Vapor Pressures and Transition Enthalpies of Low-Volatility Organic Molecules of Atmospheric Relevance: From Dicarboxylic Acids to Complex Mixtures, *Chem. Rev.*, 115(10), 4115–4156, doi:10.1021/cr5005502, 2015.

Booth, A. M., Montague, W. J., Barley, M. H., Topping, D. O., McFiggans, G., Garforth, A. and Percival, C. J.: Solid state and sub-cooled liquid vapour pressures of cyclic aliphatic dicarboxylic acids, *Atmospheric Chem. Phys.*, 11(2), 655–665, doi:10.5194/acp-11-655-2011, 2011.

Booth, A. M., Bannan, T., McGillen, M. R., Barley, M. H., Topping, D. O., McFiggans, G. and Percival, C. J.: The role of ortho, meta, para isomerism in measured solid state and derived sub-cooled liquid vapour pressures of substituted benzoic acids, *RSC Adv.*, 2(10), 4430, doi:10.1039/c2ra01004f, 2012.

Borhan, M. S., Capareda, S., Mukhtar, S., Faulkner, W. B., McGee, R. and Jr, C. B. P.: Comparison of seasonal phenol and p-cresol emissions from ground-level area sources in a dairy operation in central Texas, *J. Air Waste Manag. Assoc.*, 62(4), 381–392, doi:10.1080/10473289.2011.646050, 2012.

Cai, L., Koziel, J. A. and Zhang, S.: Odorous chemical emissions from livestock operations in United States, *IEEE Conf. Publ.*, doi:10.1109/rsete.2011.5964331, 2011.

Camredon, M., Aumont, B., Lee-Taylor, J. and Madronich, S.: The SOA/VOC/NO_x system: an explicit model of secondary organic aerosol formation, *Atmospheric Chem. Phys.*, 7(21), 5599–5610, doi:10.5194/acp-7-5599-2007, 2007.

Carlton, A. G., Wiedinmyer, C. and Kroll, J. H.: A review of Secondary Organic Aerosol (SOA) formation from isoprene, *Atmospheric Chem. Phys.*, 9(14), 4987–5005, doi:10.5194/acp-9-4987-2009, 2009.

Cecinato, A., Di Palo, V., Pomata, D., Tomasi Scianò, M. C. and Possanzini, M.: Measurement of phase-distributed nitrophenols in Rome ambient air, *Chemosphere*, 59(5), 679–683, doi:10.1016/j.chemosphere.2004.10.045, 2005.

Chan, A. W. H., Kautzman, K. E., Chhabra, P. S., Surratt, J. D., Chan, M. N., Crouse, J. D., Kürten, A., Wennberg, P. O., Flagan, R. C. and Seinfeld, J. H.: Secondary organic aerosol formation from photooxidation of naphthalene and alkylnaphthalenes: implications for oxidation of intermediate volatility organic compounds (IVOCs), *Atmospheric Chem. Phys.*, 9(9), 3049–3060, doi:10.5194/acp-9-3049-2009, 2009.

Chrit, M., Sartelet, K., Sciare, J., Majdi, M., Nicolas, J., Petit, J.-E., and Dulac, F.: Modeling organic aerosol concentrations and properties during winter 2014 in the northwestern Mediterranean region. *Atmos. Chem. Phys.*, 18, 18079–18100, doi:10.5194/acp-18-18079-2018, 2018.

Coeur-Tourneur, C., Cassez, A. and Wenger, J. C.: Rate Coefficients for the Gas-Phase Reaction of Hydroxyl Radicals with 2-Methoxyphenol (Guaiacol) and Related Compounds, *J. Phys. Chem. A*, 114(43), 11645–11650, doi:10.1021/jp1071023, 2010.

Couvidat, F. and Sartelet, K.: The Secondary Organic Aerosol Processor (SOAP v1.0) model: a unified model with different ranges of complexity based on the molecular surrogate approach, *Geosci. Model Dev.*, 8(4), 1111–1138, doi:10.5194/gmd-8-1111-2015, 2015.

Couvidat, F., Debry, E., Sartelet, K. and Seigneur, C.: A hydrophilic/hydrophobic organic (H₂O) aerosol model: Development, evaluation and sensitivity analysis, *J. Geophys. Res.*, 117, D10304, doi:10.1029/2011JD017214, 2012.

Couvidat, F., Bessagnet, B., Garcia-Vivanco, M., Real, E., Menut, L. and Colette, A.: Development of an inorganic and organic aerosol model (CHIMERE 2017 β v1.0): seasonal and spatial evaluation over Europe, *Geosci. Model Dev.*, 11(1), 165–194, doi:10.5194/gmd-11-165-2018, 2018.

Crooks, D. A. and Feetham, F. M.: 196. The vapour pressure of phthalic anhydride, *J. Chem. Soc. Resumed*, 899–901, 1946.

Debry, E., Fahey, K., Sartelet, K., Sportisse, B. and Tombette, M.: Technical Note: A new Size REsolved Aerosol Model (SIREAM), *Atmospheric Chem. Phys.*, 7(6), 1537–1547, doi:https://doi.org/10.5194/acp-7-1537-2007, 2007.

Derognat, C., Beekmann, M., Baeumle, M., Martin, D. and Schmidt, H.: Effect of biogenic volatile organic compound emissions on tropospheric chemistry during the Atmospheric Pollution Over the Paris Area (ESQUIF) campaign in the Ile-de-France region, *J. Geophys. Res.*, 108(D17), 8560, doi:10.1029/2001JD001421, 2003.

EPRI: Organic aerosol partition module documentation, technical report, Palo Alto, California., 1999.

Favez, O.: Impact de la combustion de biomasse sur les concentrations de PM₁₀ (programme CARA - hiver 2014-2015), INERIS. [online] Available from: <https://www.lcsqa.org/fr/rapport/2015/ineris/impact-combustion-biomasse-concentrations-pm10-programme-cara-hiver-2014-2015>, 2016.

Fountoukis, C. and Nenes, A.: ISORROPIA II: a computationally efficient thermodynamic equilibrium model for K⁺–Ca²⁺–Mg²⁺–NH₄⁺–Na⁺–SO₄²⁻–NO₃–Cl–H₂O aerosols, *Atmospheric Chem. Phys.*, 7(17), 4639–4659, 2007.

Fraser, M. P. and Lakshmanan, K.: Using Levoglucosan as a Molecular Marker for the Long-Range Transport of Biomass Combustion Aerosols, *Environ. Sci. Technol.*, 34(21), 4560–4564, doi:10.1021/es991229l, 2000.

Fredenslund, A., Jones, R. L. and Prausnitz, J. M.: Group-contribution estimation of activity coefficients in nonideal liquid mixtures, *AIChE J.*, 21(6), 1086–1099, doi:10.1002/aic.690210607, 1975.

Gao, S., Hegg, D. A., Hobbs, P. V., Kirchstetter, T. W., Magi, B. I. and Sadilek, M.: Water-soluble organic components in aerosols associated with savanna fires in southern Africa: Identification, evolution, and distribution, *J. Geophys. Res. Atmospheres*, 108(D13), n/a-n/a, doi:10.1029/2002JD002324, 2003.

Gonçalves, C., Alves, C. and Pio, C.: Inventory of fine particulate organic compound emissions from residential wood combustion in Portugal, *Atmos. Environ.*, 50, 297–306, doi:10.1016/j.atmosenv.2011.12.013, 2012.

Hallquist, M., Wenger, J. C., Baltensperger, U., Rudich, Y., Simpson, D., Claeys, M., Dommen, J., Donahue, N. M., George, C., Goldstein, A. H., Hamilton, J. F., Herrmann, H., Hoffmann, T., Iinuma, Y., Jang, M., Jenkin, M. E., Jimenez, J. L., Kiendler-Scharr, A., Maenhaut, W., McFiggans, G., Mentel, T. F., Monod, A., Prevot, A. S. H., Seinfeld, J. H., Surratt, J. D., Szmigielski, R. and Wildt, J.: The

formation, properties and impact of secondary organic aerosol: current and emerging issues, *Atmos Chem Phys*, 9, 5155–5236, doi:10.5194/acp-9-5155-2009, 2009.

Hankett, J. M., Collin, W. R. and Chen, Z.: Molecular Structural Changes of Plasticized PVC after UV Light Exposure, *J. Phys. Chem. B*, 117(50), 16336–16344, doi:10.1021/jp409254y, 2013.

Hatch, L. E., Rivas-Ubach, A., Jen, C. N., Lipton, M., Goldstein, A. H. and Barsanti, K. C.: Measurements of I/SVOCs in biomass-burning smoke using solid-phase extraction disks and two-dimensional gas chromatography, *Atmospheric Chem. Phys.*, 18(24), 17801–17817, doi:https://doi.org/10.5194/acp-18-17801-2018, 2018.

He, X., Huang, X. H. H., Chow, K. S., Wang, Q., Zhang, T., Wu, D. and Yu, J. Z.: Abundance and Sources of Phthalic Acids, Benzene-Tricarboxylic Acids, and Phenolic Acids in PM_{2.5} at Urban and Suburban Sites in Southern China, *ACS Earth Space Chem.*, 2(2), 147–158, doi:10.1021/acsearthspacechem.7b00131, 2018.

Herich, H., Gianini, M. F. D., Piot, C., Močnik, G., Jaffrezo, J.-L., Besombes, J.-L., Prévôt, A. S. H. and Hueglin, C.: Overview of the impact of wood burning emissions on carbonaceous aerosols and PM in large parts of the Alpine region, *Atmos. Environ.*, 89, 64–75, doi:10.1016/j.atmosenv.2014.02.008, 2014.

Hobbs, P. J., Webb, J., Mottram, T. T., Grant, B. and Misselbrook, T. M.: Emissions of volatile organic compounds originating from UK livestock agriculture, *J. Sci. Food Agric.*, 84(11), 1414–1420, doi:10.1002/jsfa.1810, 2004.

Huang, M., Liao, Y., Wang, Z., Hao, L. and Zhang, W.: A theoretical investigation of NO₃-initiated oxidation of toluene, *Comput. Theor. Chem.*, 1037, 63–69, doi:10.1016/j.comptc.2014.03.032, 2014.

Iinuma, Y., Böge, O., Gräfe, R. and Herrmann, H.: Methyl-nitrocatechols: atmospheric tracer compounds for biomass burning secondary organic aerosols, *Environ. Sci. Technol.*, 44(22), 8453–8459, doi:10.1021/es102938a, 2010.

Kanakidou, M., Seinfeld, J. H., Pandis, S. N., Barnes, I., Dentener, F. J., Facchini, M. C., Dingenen, R. V., Ervens, B., Nenes, A. and Nielsen, C. J.: Organic aerosol and global climate modelling: a review, *Atmospheric Chem. Phys.*, 5(4), 1053–1123, doi:10.5194/acp-5-1053-2005, 2005.

Kautzman, K. E., Surratt, J. D., Chan, M. N., Chan, A. W. H., Hersey, S. P., Chhabra, P. S., Dalleska, N. F., Wennberg, P. O., Flagan, R. C. and Seinfeld, J. H.: Chemical Composition of Gas- and Aerosol-Phase Products from the Photooxidation of Naphthalene, *J. Phys. Chem. A*, 114(2), 913–934, doi:10.1021/jp908530s, 2010.

Kawamura, K. and Kaplan, I. R.: Motor exhaust emissions as a primary source for dicarboxylic acids in Los Angeles ambient air, *Environ. Sci. Technol.*, 21(1), 105–110, doi:10.1021/es00155a014, 1987.

Kim, Y., Sartelet, K. and Couvidat, F.: Modeling the effect of non-ideality, dynamic mass transfer and viscosity on SOA formation in a 3-D air quality model, *Atmospheric Chem. Phys. Discuss.*, 1–29, doi:10.5194/acp-2018-177, 2018.

Kleindienst, T. E., Conner, T. S., McIver, C. D. and Edney, E. O.: Determination of secondary organic aerosol products from the photooxidation of toluene and their implications in ambient PM_{2.5}, *J. Atmospheric Chem.*, 47(1), 79–100, doi:10.1023/B:JOCH.0000012305.94498.28, 2004.

Kleindienst, T. E., Jaoui, M., Lewandowski, M., Offenberg, J. H., Lewis, C. W., Bhave, P. V. and Edney, E. O.: Estimates of the contributions of biogenic and anthropogenic hydrocarbons to secondary organic aerosol at a southeastern US location, *Atmos. Environ.*, 41(37), 8288–8300, doi:10.1016/j.atmosenv.2007.06.045, 2007.

Kleindienst, T. E., Jaoui, M., Lewandowski, M., Offenberg, J. H. and Docherty, K. S.: The formation of SOA and chemical tracer compounds from the photooxidation of naphthalene and its methyl analogs in the presence and absence of nitrogen oxides, *Atmospheric Chem. Phys.*, 12(18), 8711–8726, doi:10.5194/acp-12-8711-2012, 2012.

Kroll, J. H. and Seinfeld, J. H.: Chemistry of secondary organic aerosol: Formation and evolution of low-volatility organics in the atmosphere, *Atmos. Environ.*, 42(16), 3593–3624, doi:10.1016/j.atmosenv.2008.01.003, 2008.

Kulmala, M., Laaksonen, A. and Pirjola, L.: Parameterizations for sulfuric acid/water nucleation rates, *J. Geophys. Res. Atmospheres*, 103(D7), 8301–8307, doi:10.1029/97JD03718, 1998.

Lanzafame, G. M., Srivastava, D., Favez, O., Bonnaire, N., Gros, V., Alleman, L. Y., Couvidat, F., Bessagnet, B. and Albinet, A.: One-year measurements of secondary organic aerosol (SOA) markers in the Paris region: concentrations, seasonality, gas/particle partitioning and use in OA source apportionment, *Sci. Total Environ.*, 2020.

Lauraguais, A., Coeur-Tourneur, C., Cassez, A., Deboudt, K., Fourmentin, M. and Choël, M.: Atmospheric reactivity of hydroxyl radicals with guaiacol (2-methoxyphenol), a biomass burning emitted compound: Secondary organic aerosol formation and gas-phase oxidation products, *Atmos. Environ.*, 86, 155–163, doi:10.1016/j.atmosenv.2013.11.074, 2014.

Lelieveld, J. and Crutzen, P. J.: The role of clouds in tropospheric photochemistry, *J. Atmospheric Chem.*, 12(3), 229–267, doi:10.1007/BF00048075, 1991.

Locker, H. B.: The use of levoglucosan to assess the environmental impact of residential wood-burning on air quality, Dartmouth College, Hanover, NH. [online] Available from: <https://www.osti.gov/biblio/7069111> (Accessed 5 August 2019), 1988.

Lough, G. C., Christensen, C. G., Schauer, J. J., Tortorelli, J., Mani, E., Lawson, D. R., Clark, N. N. and Gabele, P. A.: Development of molecular marker source profiles for emissions from on-road gasoline and diesel vehicle fleets, *J. Air Waste Manag. Assoc.* 1995, 57(10), 1190–1199, doi:10.3155/1047-3289.57.10.1190, 2007.

Lu, C., Wang, X., Li, R., Gu, R., Zhang, Y., Li, W., Gao, R., Chen, B., Xue, L. and Wang, W.: Emissions of fine particulate nitrated phenols from residential coal combustion in China, *Atmos. Environ.*, 203, 10–17, doi:10.1016/j.atmosenv.2019.01.047, 2019.

Majdi, M., Sartelet, K., Lanzafame, G. M., Couvidat, F., Kim, Y., Chrit, M. and Turquety, S.: Precursors and formation of secondary organic aerosols from wildfires in the Euro-Mediterranean region, *Atmospheric Chem. Phys.*, 19(8), 5543–5569, doi:https://doi.org/10.5194/acp-19-5543-2019, 2019.

Mallet, V., Quélo, D., Sportisse, B., Ahmed de Biasi, M., Debry, É., Korsakissok, I., Wu, L., Roustan, Y., Sartelet, K., Tombette, M. and Foudhil, H.: Technical Note: The air quality modeling system Polyphemus, *Atmospheric Chem. Phys.*, 7(20), 5479–5487, doi:https://doi.org/10.5194/acp-7-5479-2007, 2007.

May, A. A., Saleh, R., Hennigan, C. J., Donahue, N. M. and Robinson, A. L.: Volatility of Organic Molecular Markers Used for Source Apportionment Analysis: Measurements and Implications for Atmospheric Lifetime, *Environ. Sci. Technol.*, 46(22), 12435–12444, doi:10.1021/es302276t, 2012.

May, A. A., Levin, E. J. T., Hennigan, C. J., Riipinen, I., Lee, T., Collett, J. L., Jimenez, J. L., Kreidenweis, S. M. and Robinson, A. L.: Gas-particle partitioning of primary organic aerosol emissions: 3. Biomass burning, *J. Geophys. Res. Atmospheres*, 118(19), 11,327–11,338, doi:10.1002/jgrd.50828, 2013.

McDonald, J. D., Zielinska, B., Fujita, E. M., Sagebiel, J. C., Chow, J. C. and Watson, J. G.: Fine Particle and Gaseous Emission Rates from Residential Wood Combustion, *Environ. Sci. Technol.*, 34(11), 2080–2091, doi:10.1021/es9909632, 2000.

Mouchel-Vallon, C., Deguillaume, L., Monod, A., Perroux, H., Rose, C., Ghigo, G., Long, Y., Leriche, M., Aumont, B., Patryl, L., Armand, P. and Chaumerliac, N.: CLEPS 1.0: A new protocol for cloud aqueous phase oxidation of VOC mechanisms, *Geosci. Model Dev.*, 10(3), 1339–1362, doi:10.5194/gmd-10-1339-2017, 2017.

Na, K., Kim, Y. P., Moon, K.-C., Moon, I. and Fung, K.: Concentrations of volatile organic compounds in an industrial area of Korea, *Atmos. Environ.*, 35(15), 2747–2756, doi:10.1016/S1352-2310(00)00313-7, 2001.

Nalin, F., Golly, B., Besombes, J.-L., Pelletier, C., Aujay-Plouzeau, R., Verlhac, S., Dermigny, A., Fievet, A., Karoski, N., Dubois, P., Collet, S., Favez, O. and Albinet, A.: Fast oxidation processes from emission to ambient air introduction of aerosol emitted by residential log wood stoves, *Atmos. Environ.*, 143, 15–26, doi:10.1016/j.atmosenv.2016.08.002, 2016.

Nishino, N., Arey, J. and Atkinson, R.: Formation and Reactions of 2-Formylcinnamaldehyde in the OH Radical-Initiated Reaction of Naphthalene, *Environ. Sci. Technol.*, 43(5), 1349–1353, doi:10.1021/es802477s, 2009.

Nozière, B., Kalberer, M., Claeys, M., Allan, J., D'Anna, B., Decesari, S., Finessi, E., Glasius, M., Grgić, I., Hamilton, J. F., Hoffmann, T., Iinuma, Y., Jaoui, M., Kahnt, A., Kampf, C. J., Kourchev, I., Maenhaut, W., Marsden, N., Saarikoski, S., Schnelle-Kreis, J., Surratt, J. D., Szidat, S., Szmigielski, R. and Wisthaler, A.: The Molecular Identification of Organic Compounds in the Atmosphere: State of the Art and Challenges, *Chem. Rev.*, 115(10), 3919–3983, doi:10.1021/cr5003485, 2015.

Oja, V. and Suuberg, E. M.: Vapor Pressures and Enthalpies of Sublimation of D -Glucose, D -Xylose, Cellobiose, and Levoglucosan, *J. Chem. Eng. Data*, 44(1), 26–29, doi:10.1021/je980119b, 1999.

Olariu, R. I., Klotz, B., Barnes, I., Becker, K. H. and Mocanu, R.: FT-IR study of the ring-retaining products from the reaction of OH radicals with phenol, o-, m-, and p-cresol, *Atmos. Environ.*, 36(22), 3685–3697, 2002.

Pandis, S. N., Wexler, A. S. and Seinfeld, J. H.: Secondary organic aerosol formation and transport - II. Predicting the ambient secondary organic aerosol size distribution, *Atmospheric Environ. Part Gen. Top.*, 27(15), 2403–2416, doi:10.1016/0960-1686(93)90408-Q, 1993.

Pankow, J. F.: An absorption model of gas/particle partitioning of organic compounds in the atmosphere, *Atmos. Environ.*, 28(2), 185–188, doi:10.1016/1352-2310(94)90093-0, 1994.

Parshintsev, J., Ruiz-Jimenez, J., Petäjä, T., Hartonen, K., Kulmala, M. and Riekkola, M.-L.: Comparison of quartz and Teflon filters for simultaneous collection of size-separated ultrafine aerosol particles and gas-phase zero samples, *Anal. Bioanal. Chem.*, 400(10), 3527–3535, doi:10.1007/s00216-011-5041-0, 2011.

Passant, N. R.: Speciation of UK emissions of non-methane volatile organic compounds, Oxon., 2002.

Phouongphouang, P. T. and Arey, J.: Rate Constants for the Gas-Phase Reactions of a Series of Alkyl-naphthalenes with the OH Radical, *Environ. Sci. Technol.*, 36(9), 1947–1952, doi:10.1021/es011434c, 2002.

Pouet, J.-C. and Gautier, A.: Etude sur le chauffage domestique au bois: marches et approvisionnement, ADEME., 2013.

Puxbaum, H., Caseiro, A., Sánchez-Ochoa, A., Kasper-Giebl, A., Claeys, M., Gelencsér, A., Legrand, M., Preunkert, S. and Pio, C. A.: Levoglucosan levels at background sites in Europe for assessing the impact of biomass combustion on the European aerosol background, *J. Geophys. Res. Space Phys.*, 112(23), D23S05, doi:10.1029/2006JD008114, 2007.

Robinson, A. L., Donahue, N. M., Shrivastava, M. K., Weitkamp, E. A., Sage, A. M., Grieshop, A. P., Lane, T. E., Pierce, J. R. and Pandis, S. N.: Rethinking Organic Aerosols: Semivolatile Emissions and Photochemical Aging, *Science*, 315(5816), 1259–1262, doi:10.1126/science.1133061, 2007.

Ruehl, C. R., Ham, W. A. and Kleeman, M. J.: Temperature-induced volatility of molecular markers in ambient airborne particulate matter, *Atmospheric Chem. Phys.*, 11(1), 67–76, doi:https://doi.org/10.5194/acp-11-67-2011, 2011.

Sartelet, K., Debry, E., Fahey, K., Tombette, M., Roustan, Y. and Sportisse, B.: Simulation of aerosols and gas-phase species over Europe with the POLYPHEMUS system: Part I - Model-to-data comparison for 2001, [online] Available from: <https://hal.inria.fr/inria-00633774>, 2007.

Sasaki, J., Aschmann, S. M., Kwok, E. S., Atkinson, R. and Arey, J.: Products of the gas-phase OH and NO₃ radical-initiated reactions of naphthalene, *Environ. Sci. Technol.*, 31(11), 3173–3179, 1997.

Schauer, J. J., Rogge, W. F., Hildemann, L. M., Mazurek, M. A., Cass, G. R. and Simoneit, B. R. T.: Source apportionment of airborne particulate matter using organic compounds as tracers, *Atmos. Environ.*, 30(22), 3837–3855, doi:10.1016/1352-2310(96)00085-4, 1996.

Schauer, J. J., Kleeman, M. J., Cass, G. R. and Simoneit, B. R. T.: Measurement of Emissions from Air Pollution Sources. 3. C₁–C₂₉ Organic Compounds from Fireplace Combustion of Wood, *Environ. Sci. Technol.*, 35(9), 1716–1728, doi:10.1021/es001331e, 2001.

Schmidl, C., Bauer, H., Dattler, A., Hitzemberger, R., Weissenboeck, G., Marr, I. L. and Puxbaum, H.: Chemical characterisation of particle emissions from burning leaves, *Atmos. Environ.*, 42(40), 9070–9079, doi:10.1016/j.atmosenv.2008.09.010, 2008.

Seinfeld, J. H.: Tropospheric chemistry and composition | Aerosols/Particles, in *Encyclopedia of Atmospheric Sciences (Second Edition)*, edited by G. R. North, J. Pyle, and F. Zhang, pp. 182–187, Academic Press, Oxford., 2015.

Shrivastava, M., Cappa, C. D., Fan, J., Goldstein, A. H., Guenther, A. B., Jimenez, J. L., Kuang, C., Laskin, A., Martin, S. T., Ng, N. L., Petaja, T., Pierce, J. R., Rasch, P. J., Roldin, P., Seinfeld, J. H., Shilling, J., Smith, J. N., Thornton, J. A., Volkamer, R., Wang, J., Worsnop, D. R., Zaveri, R. A.,

Zelenyuk, A. and Zhang, Q.: Recent advances in understanding secondary organic aerosol: Implications for global climate forcing: *Advances in Secondary Organic Aerosol*, *Rev. Geophys.*, 55(2), 509–559, doi:10.1002/2016RG000540, 2017.

SIDS: Initial Assessment Report on phthalic anhydride, OECD, Paris, France., 2005.

Simoneit, B. R., Schauer, J. J., Nolte, C. G., Oros, D. R., Elias, V. O., Fraser, M. P., Rogge, W. F. and Cass, G. R.: Levoglucosan, a tracer for cellulose in biomass burning and atmospheric particles, *Atmos. Environ.*, 33(2), 173–182, 1999.

Simoneit, B. R. T., Medeiros, P. M. and Didyk, B. M.: Combustion Products of Plastics as Indicators for Refuse Burning in the Atmosphere, *Environ. Sci. Technol.*, 39(18), 6961–6970, doi:10.1021/es050767x, 2005.

Srivastava, D., Favez, O., Perraudin, E., Villenave, E. and Albinet, A.: Comparison of Measurement-Based Methodologies to Apportion Secondary Organic Carbon (SOC) in PM_{2.5}: A Review of Recent Studies, *Atmosphere*, 9(11), 452, doi:10.3390/atmos9110452, 2018.

Teil, M. J., Blanchard, M. and Chevreuil, M.: Atmospheric fate of phthalate esters in an urban area (Paris-France), *Sci. Total Environ.*, 354(2), 212–223, doi:10.1016/j.scitotenv.2004.12.083, 2006.

Tilgner, A. and Herrmann, H.: Radical-driven carbonyl-to-acid conversion and acid degradation in tropospheric aqueous systems studied by CAPRAM, *Atmos. Environ.*, 44(40), 5415–5422, doi:10.1016/j.atmosenv.2010.07.050, 2010.

Tomaz, S., Shahpoury, P., Jaffrezo, J.-L., Lammel, G., Perraudin, E., Villenave, E. and Albinet, A.: One-year study of polycyclic aromatic compounds at an urban site in Grenoble (France): Seasonal variations, gas/particle partitioning and cancer risk estimation, *Sci. Total Environ.*, 565, 1071–1083, doi:10.1016/j.scitotenv.2016.05.137, 2016.

Topping, D., Barley, M., Bane, M. K., Higham, N., Aumont, B., Dingle, N. and McFiggans, G.: UManSysProp v1.0: an online and open-source facility for molecular property prediction and atmospheric aerosol calculations, *Geosci. Model Dev.*, 9(2), 899–914, doi:10.5194/gmd-9-899-2016, 2016.

US EPA, O.: EPI Suite™-Estimation Program Interface, US EPA [online] Available from: <https://www.epa.gov/tsca-screening-tools/epi-suitetm-estimation-program-interface>, 2015.

Vestreng, V.: Review and Revision. Emission data reported to CLRTAP Tech. Rep., EMEP MSW-W, Norwegian Meteorological Institute, Oslo, Norway. [online] Available from: https://www.emep.int/publ/reports/2003/mscw_note_1_2003.pdf, 2003.

Wang, L., Arey, J. and Atkinson, R.: Kinetics and Products of Photolysis and Reaction with OH Radicals of a Series of Aromatic Carbonyl Compounds, *Environ. Health*, 40, 5465–5471, 2006.

Wang, X., Gu, R., Wang, L., Xu, W., Zhang, Y., Chen, B., Li, W., Xue, L., Chen, J. and Wang, W.: Emissions of fine particulate nitrated phenols from the burning of five common types of biomass, *Environ. Pollut.*, 230, 405–412, doi:10.1016/j.envpol.2017.06.072, 2017.

Xie, M., Hannigan, M. P. and Barsanti, K. C.: Gas/Particle Partitioning of 2-Methyltetrols and Levoglucosan at an Urban Site in Denver, *Environ. Sci. Technol.*, 48(5), 2835–2842, doi:10.1021/es405356n, 2014.

Yang, B., Zhang, H., Wang, Y., Zhang, P., Shu, J., Sun, W. and Ma, P.: Experimental and theoretical studies on gas-phase reactions of NO₃ radicals with three methoxyphenols: Guaiacol, creosol, and syringol, *Atmos. Environ.*, 125, 243–251, doi:10.1016/j.atmosenv.2015.11.028, 2016.

Yang, L., Minh Nguyen, D. and Yu, L.: Photooxidation of levoglucosan in atmospheric aqueous aerosols., *Geochim. Cosmochim. Acta Suppl.*, 73, A1477, doi:10.1016/j.gca.2009.05.018, 2009.

Yee, L. D., Kautzman, K. E., Loza, C. L., Schilling, K. A., Coggon, M. M., Chhabra, P. S., Chan, M. N., Chan, A. W. H., Hersey, S. P., Crounse, J. D., Wennberg, P. O., Flagan, R. C. and Seinfeld, J. H.: Secondary organic aerosol formation from biomass burning intermediates: phenol and methoxyphenols, *Atmospheric Chem. Phys.*, 13(16), 8019–8043, doi:10.5194/acp-13-8019-2013, 2013.

Zhang, Q., Jimenez, J. L., Canagaratna, M. R., Allan, J. D., Coe, H., Ulbrich, I., Alfarra, M. R., Takami, A., Middlebrook, A. M., Sun, Y. L., Dzepina, K., Dunlea, E., Docherty, K., DeCarlo, P. F., Salcedo, D., Onasch, T., Jayne, J. T., Miyoshi, T., Shimojo, A., Hatakeyama, S., Takegawa, N., Kondo, Y., Schneider, J., Drewnick, F., Borrmann, S., Weimer, S., Demerjian, K., Williams, P., Bower, K., Bahreini, R., Cottrell, L., Griffin, R. J., Rautiainen, J., Sun, J. Y., Zhang, Y. M. and Worsnop, D. R.: Ubiquity and dominance of oxygenated species in organic aerosols in anthropogenically-influenced Northern Hemisphere midlatitudes, *Geophys. Res. Lett.*, 34(13), L13801, doi:10.1029/2007GL029979, 2007.

Ziemann, P. J. and Atkinson, R.: Kinetics, products, and mechanisms of secondary organic aerosol formation, *Chem. Soc. Rev.*, 41(19), 6582, doi:10.1039/c2cs35122f, 2012.

Zuend, A. and Seinfeld, J. H.: Modeling the gas-particle partitioning of secondary organic aerosol: the importance of liquid-liquid phase separation, *Atmospheric Chem. Phys.*, 12(9), 3857–3882, doi:10.5194/acp-12-3857-2012, 2012.

Zuend, A., Marcolli, C., Luo, B. P. and Peter, T.: A thermodynamic model of mixed organic-inorganic aerosols to predict activity coefficients, *Atmospheric Chem. Phys.*, 8(16), 4559–4593, doi:https://doi.org/10.5194/acp-8-4559-2008, 2008.

Zuend, A., Marcolli, C., Peter, T. and Seinfeld, J. H.: Computation of liquid-liquid equilibria and phase stabilities: implications for RH-dependent gas/particle partitioning of organic-inorganic aerosols, *Atmospheric Chem. Phys.*, 10(16), 7795–7820, doi:https://doi.org/10.5194/acp-10-7795-2010, 2010.

Zuend, A., Marcolli, C., Booth, A. M., Lienhard, D. M., Soonsin, V., Krieger, U. K., Topping, D. O., McFiggans, G., Peter, T. and Seinfeld, J. H.: New and extended parameterization of the thermodynamic model AIOMFAC: calculation of activity coefficients for organic-inorganic mixtures containing carboxyl, hydroxyl, carbonyl, ether, ester, alkenyl, alkyl, and aromatic functional groups, *Atmos Chem Phys*, 11(17), 9155–9206, doi:10.5194/acp-11-9155-2011, 2011.

Supplementary Material

Modelling organic aerosol markers in 3D air quality model. Part 1:

Anthropogenic organic markers.

G.M. Lanzafame^{1,2}, F. Couvidat¹, O. Favez¹, A. Albinet¹ and B. Bessagnet^{1,2}

¹INERIS, Parc Technologique Alata, BP 2, 60550 Verneuil-en-Halatte, France

²Sorbonne Universités, UPMC, 75252 PARIS cedex 05, France

Correspondence to Florian Couvidat (florian.couvidat@ineris.fr)

1. Mechanisms

1.1 Nitroguaiacol

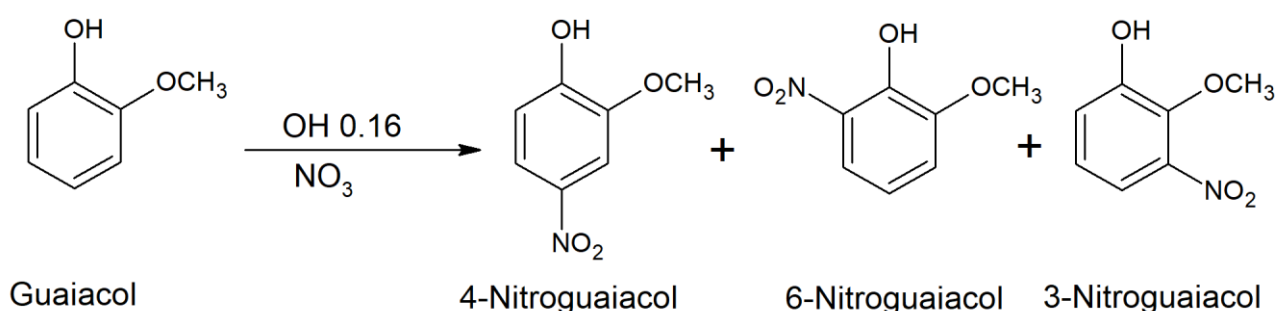


Figure S1. Guaiacol photooxidation

Table S1. Mechanisms of nitroguaiacols formation. All the kinetic constants are in $\text{cm}^3 \text{ molecule}^{-1} \text{ s}^{-1}$.

GUAIACOL+NO ₃ ->NO ₃ +NGUAIACOL	$k=3.2 \times 10^{-12}$	(Yang et al., 2016)
GUAIACOL+OH->OH+0.16*(MM _{GUAI} /MM _{NGUAI})*NGUAIACOL	$k=7.5 \times 10^{-11}$	K from (Coeur-Tourneur et al., 2010) Yields from (Lauraguais et al., 2014)

1.2 DHOPA

Table S2. DHOPA formation from 2-methyl furan. All the kinetic constants are in $\text{cm}^3 \text{ molecule}^{-1} \text{ s}^{-1}$.

MEFURAN+OH->OH+0.31*C5DICARB	$k=6.19 \times 10^{-11}$	K is from (Bierbach et al., 1992); Yield is from (Aschmann et al., 2014)
MEFURAN+NO ₃ ->NO ₃	$k=2.57 \times 10^{-11}$	(Kind et al., 1996)
MEFURAN+O ₃ ->O ₃	$k=2.05 \times 10^{-17}$	(Alvarado et al., 1996)

Table S3. First pathway for DHOPA formation: gaseous phase. Mechanism from GECKO-A (Aumont et al., 2005; Camredon et al., 2007). All the kinetic constants are in $\text{cm}^3 \text{molecule}^{-1} \text{s}^{-1}$.

$\text{C514CO23OH} + \text{OH} \rightarrow \text{OH} + 0.28 * \text{C5134CO2OH} + 0.28 * \text{CH3COCHOHCOCHO} + 0.43 * \text{C514CO23OHOO}$	$k = 6.26 \times 10^{-11}$, k from MCM, branching ratio from GECKO-A
$\text{C514CO23OH} + \text{NO3} \rightarrow \text{NO3} + \text{CH3COCHOHCOCHO}$	$k = 4.54 \times 10^{-12}$
$\text{C514CO23OH} \rightarrow \text{CO2H3CHO}$	$J(Z) = \text{photorate}(\text{RCHO})$ from MCM
$\text{C514CO23OH} \rightarrow \text{CO2H3CHO}$	$J(Z) = \text{photorate}(\text{CH3COE})$ from MCM
$\text{C514CO23OHOO} + \text{HO2} \rightarrow \text{HO2} + 0.45 * \text{C514CO23OHOOH} + 0.40 * \text{CH3COCHOHCHO} + 0.15 * \text{DHOPA}$	$k(T) = 3.2 \times 10^{-13} \exp(925/T)$
$\text{C514CO23OHOO} + \text{NO} \rightarrow \text{NO} + \text{CH3COCHOHCHO}$	$k(T) = 8.1 \times 10^{-12} \exp(270/T)$
$\text{C514CO23OHOO} + \text{NO3} \rightarrow \text{NO3} + \text{CH3COCHOHCHO}$	$k = 5 \times 10^{-12}$
$\text{C514CO23OHOO} + \text{oRO2} \rightarrow \text{oRO2} + 0.70 * \text{CH3COCHOHCHO} + 0.30 * \text{DHOPA}$	$k = 1 \times 10^{-11}$
$\text{C514CO23OHOO} + \text{obio} \rightarrow \text{obio} + 0.70 * \text{CH3COCHOHCHO} + 0.30 * \text{DHOPA}$	$k = 1 \times 10^{-11}$
$\text{C514CO23OHOO} + \text{CH3O2} \rightarrow \text{CH3O2} + 0.70 * \text{CH3COCHOHCHO} + 0.30 * \text{DHOPA}$	$k = 1 \times 10^{-11}$
$\text{C514CO23OHOO} + \text{CH3COO} \rightarrow \text{CH3COO} + 0.70 * \text{CH3COCHOHCHO} + 0.30 * \text{DHOPA}$	$k = 1 \times 10^{-11}$
$\text{DHOPA} + \text{OH} \rightarrow \text{OH} + \text{X}$	$k = 2.42 \times 10^{-11}$

Table S4. First pathway for DHOPA formation: aqueous phase. Mechanism from (Mouchel-Vallon et al., 2017) aqueous phase reactions – Analogy with 2,4-dihydroxy-3-oxobutanal for C514CO23OH and 2,4-dihydroxy-3-oxobutanoic acid for DHOPA. All the kinetic constants are in $\text{M}^{-1} \text{s}^{-1}$.

$\text{C514CO23OH} + \text{OH} \rightarrow \text{OH} + 0.29 * \text{DHOPA}$	$k = 1.2 \times 10^9$
$\text{C514CO23OH} + \text{NO3} \rightarrow \text{NO3} + 0.47 * \text{DHOPA}$	$k = 1.0 \times 10^6$
$\text{DHOPA} + \text{OH} \rightarrow \text{OH} + \text{X}$	$k = 8.1 \times 10^8$

K_H and ΔH_{vap} for C514CO23OH are $3.9 \times 10^7 \text{M}^{-1} \text{atm}$ and 63.8kJ mol^{-1} (SOAP, Couvidat and Sartelet, 2015)

K_H and ΔH_{vap} for DHOPA are $7.24 \times 10^{10} \text{M}^{-1} \text{atm}$ and 116kJ mol^{-1} (SOAP, Couvidat and Sartelet, 2015)

Table S5. Second pathway for DHOPA formation. Analogy with C4DBDIKET MCM v3.2 (Jenkin et al., 1997; Saunders et al., 2003) via website: <http://mcm.leeds.ac.uk/MCM>. All the kinetic constants are in $\text{cm}^3 \text{molecule}^{-1} \text{s}^{-1}$.

$\text{C5CO14OH} + \text{OH} \rightarrow \text{OH} + 0.47 * \text{C5CO14OH2OO} + 0.53 * \text{C5CO14CO2}$	$k = 1.03 \times 10^{-10}$
$\text{C5CO14OH} + \text{O3} \rightarrow \text{O3} + \text{X}$	$k = 5 \times 10^{-18}$
$\text{C5CO14OH} \rightarrow \text{X}$	$J(Z) = \text{photorate}(\text{CH3COE})$
$\text{C5CO14OH2OO} + \text{HO2} \rightarrow \text{HO2} + \text{X}$	$k(T) = 2.91 \times 10^{-13} \exp(1300/T)$
$\text{C5CO14OH2OO} + \text{NO} \rightarrow \text{NO} + \text{X}$	$k(T) = 2.7 \times 10^{-12} \exp(360/T)$
$\text{C5CO14OH2OO} + \text{NO3} \rightarrow \text{NO3} + \text{X}$	$k = 2.3 \times 10^{-12}$
$\text{C5CO14OH2OO} + \text{oRO2} \rightarrow \text{oRO2} + 0.2 * \text{DHOPA}$	$k = 8.8 \times 10^{-13}$
$\text{C5CO14OH2OO} + \text{obio} \rightarrow \text{obio} + 0.2 * \text{DHOPA}$	$k = 8.8 \times 10^{-13}$
$\text{C5CO14OH2OO} + \text{CH3O2} \rightarrow \text{CH3O2} + 0.2 * \text{DHOPA}$	$k = 8.8 \times 10^{-13}$
$\text{C5CO14OH2OO} + \text{CH3COO} \rightarrow \text{CH3COO} + 0.2 * \text{DHOPA}$	$k = 8.8 \times 10^{-13}$

1.3 Phthalic acid

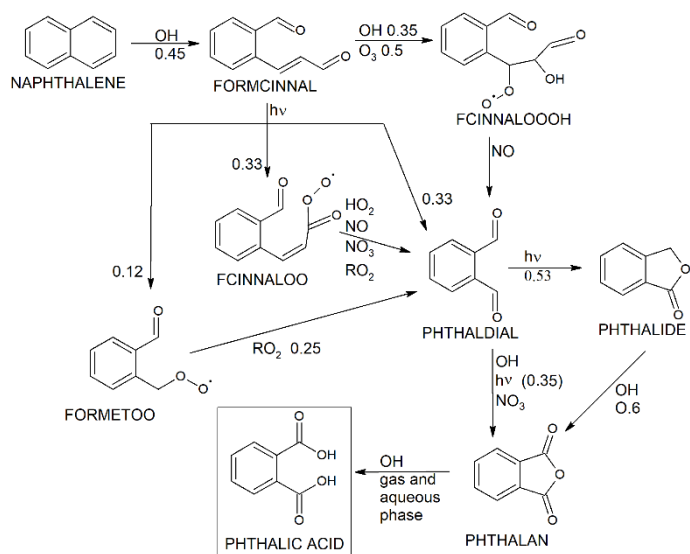


Figure S2. Phthalic acid formation pathway

Table S6. Phthalic Acid formation from naphthalene. When not specified, kinetic constants are in $\text{cm}^3 \text{ molecule}^{-1} \text{ s}^{-1}$.

NAPHTHALENE+OH->OH+0.45*FORMCINNAL	$k=2.4 \times 10^{-11}$	(Phousongphouang and Arey, 2002) 0.45 is the average yield (30-60%)(Kautzman et al., 2010)
NAPHTHALENE+NO3->NO3+NONAPHTH	$k=3.4 \times 10^{-28}$	Phousongphouang and Arey, 2003
FORMCINNAL+OH->OH+0.35*FCINNALOOOH	$K_{298K \text{ total}}=8.83 \times 10^{-11}$ Literature: (Nishino et al., 2009)= 7.7×10^{-11} (Aschmann et al., 2013)= 2.1×10^{-11}	35% reacts on the double bond: $K_{298K}(\text{pentene})=3.13 \times 10^{-11}$ $K_{298K}(\text{pentaldehyde})=2.85 \times 10^{-11}$ $K_{298K}(\text{pentaldehyde}) \times 2=5.70 \times 10^{-11}$
FORMCINNAL+O3->O3+0.5*FCINNALOOOH	$k=1.8 \times 10^{-18}$	(Aschmann et al., 2013) Reactivity in analogy with BUTENAL and all the alkenes*
FORMCINNAL+NO3->NO3+FCINNALNO3	$k=4.3 \times 10^{-14}$	(Aschmann et al., 2013)
FORMCINNAL-> 0.33*PHTHALDIAL+0.12*FORMETOO+0.33FCINNAL OO	$J(Z)=\text{photorate}(\text{FORMC I})$	(Nishino et al., 2009), products yield in analogy with 2-pentenale from GECKO-A
FCINNALOOOH+NO->NO+PHTHALDIAL	$k(T)=2.7 \times 10^{-12} \exp(360/T)$	generic constant RO2+NO (KRO2NO)*
FCINNALOOOH+HO2->HO2+X	$k(T)=2.91 \times 10^{-13} \exp(1300/T)$	generic constant RO2+HO2 (KRO2HO2)*
FCINNALOOOH+NO3->NO3+X	$k=2.3 \times 10^{-12}$	generic constant RO2+NO3 (KRO2NO3)*
FCINNALOOOH+oRO2->oRO2+X	$k=2.5 \times 10^{-13}$	Analogy with 2-hydroxy-2-phenylethyl peroxide(STYRENO2)*
FCINNALOOOH+obio->obio+X	$k=2.5 \times 10^{-13}$	
FCINNALOOOH+CH3O2->CH3O2+X	$k=2.5 \times 10^{-13}$	
FCINNALOOOH+CH3COO->CH3COO+X	$k=2.5 \times 10^{-13}$	
FCINNALOO+HO2->HO2+0.4*PHTHALDIAL	$k(T)=6.4 \times 10^{-13} \exp(925/T)$	GECKO-A, in analogy with 2-pentenale (Camredon et al., 2007)
FCINNALOO+NO->NO+PHTHALDIAL	$k(T)=8.1 \times 10^{-12} \exp(270/T)$	
FCINNALOO+NO2->NO2+X	$k=(1/T)=3.3 \times 10^{-8}/T$	
FCINNALOO+NO3->NO3+PHTHALDIAL	$k=5 \times 10^{-12}$	
FCINNALOO+ oRO2->oRO2+0.7*PHTHALDIAL	$k=1 \times 10^{-11}$	
FCINNALOO+obio->obio+0.7*PHTHALDIAL	$k=1 \times 10^{-11}$	
FCINNALOO+CH3O2->CH3O2+0.7*PHTHALDIAL	$k=1 \times 10^{-11}$	
FCINNALOO+CH3COO->CH3COO+0.7*PHTHALDIAL	$k=1 \times 10^{-11}$	

FORMETOO+NO->NO+X	$k=2.66 \times 10^{-12}$	
FORMETOO+HO2->HO2+X	$k=1.79 \times 10^{-13}$	
FORMETOO+NO3->NO3+X	$k=2.30 \times 10^{-12}$	
FORMETOO+RO2->RO2+0.25*PHTHALDIAL	$k=5 \times 10^{-12}$	
PHTHALDIAL+OH->OH+0.85*PHTHALAN	$k=2.3 \times 10^{-11}$	(Wang et al., 2006)
PHTHALDIAL+NO3->NO3+PHTHALAN	$k(T)=2.8 \times 10^{-12} \exp(-1860/T)$	2x generic constant RO2+NO3 (KNO3AL)*
PHTHALDIAL+O3->O3+X	$k=2.0 \times 10^{-18}$	Analogy with malonic aldehyde (MALDIAL)*
PHTHALDIAL->0.35*PHTHALAN+0.53*PHTHALIDE	J(Z)=photorate(PHTHAL)	(Wang et al., 2006)
PHTHALIDE+OH->OH+0.6*PHTHALAN	$k=8 \times 10^{-13}$	(Wang et al., 2006)
PHTHALAN+OH->OH+PHTHALICACID	$K=7.50 \times 10^{-13}$	Half time life= $21.4d^{-1}$, [OH]= $5 \times 10^{-5} \text{ mol/cm}^3$ SRC-AOPWIN (SIDS, 2005)
PHTHALAN->PHTHALICACID	$k_{\text{hydrolysis}}=9.9 \times 10^{-3} s^{-1}$ $K_H=41 \times 10^4$ $\Delta H=61.6$	$K_{\text{react}}=\ln 2/70s$ Half-life time from (SIDS, 2005) at $0 < \text{pH} < 6$ ΔH_{sol} calculated with SOAP using P_{sat} and ΔH_{vap} from (Crooks and Feetham, 1946)
PHTHALICACID+OH->OH+X	$k=1.23 \times 10^{-12}$	Half time life= $13d^{-1}$, [OH]= $5 \times 10^{-5} \text{ mol/cm}^3$ SRC-AOPWIN (SIDS, 2005)

*The chemical mechanistic information was taken from the Master Chemical Mechanism, MCM v3.2 (Bloss et al., 2005; Jenkin et al., 1997, 2003; Saunders et al., 2003), via website: <http://mcm.leeds.ac.uk/MCM>.

Table S8. SARs used to estimate the Psat at 298K. All the estimations are performed through the online platform UManSysProp (Topping et al., 2016)

Vapor pressure	Boiling point	Abbreviations
(Nannoolal et al., 2008)	(Nannoolal et al., 2004)	N-N
(Nannoolal et al., 2008)	(Joback and Reid, 2007)	N-J
(Nannoolal et al., 2008)	(Stein and Brown, 1994)	N-S
(Myrdal and Yalkowsky, 1997)	(Nannoolal et al., 2004)	M-N
(Myrdal and Yalkowsky, 1997)	(Joback and Reid, 2007)	M-J
(Myrdal and Yalkowsky, 1997)	(Stein and Brown, 1994)	M-S
(Compernelle et al., 2011)	Independent from T_b	Comp.
EPIsuite (US EPA, 2015)	EPIsuite (US EPA, 2015)	EPIsuite

Table S9. Marker subcooled saturated vapor pressure at 298 K. Literature and chosen values.

Vapor pressure at 298K (torr)				
Marker	Literature	Min	Max	Chosen Value
DHOPA ^{a, g}		1.67×10^{-7}	6.09×10^{-5}	1.95×10^{-6}
LEVO ^b	1.45×10^{-6} (Booth et al., 2011) 1.80×10^{-7} (Parshintsev et al., 2011) 1.77×10^{-7} (Pankow and Asher, 2008)*	1.15×10^{-6}	2.34×10^{-4}	1.45×10^{-6}
3-Methyl-5-Nitrocatechol ^c	Semi-empiric, reference: nitrocatechol ⁱ			3.20×10^{-6}
Nitrocatechol ^c	7.50×10^{-6} (Booth et al., 2012)	1.08×10^{-2}	1.98×10^{-1}	7.50×10^{-6}
4-Nitroguaiacol ^d	Semi-empiric, reference: nitrocatechol ⁱ	1.04×10^{-1}	6.76×10^{-1}	4.61×10^{-5}
4-Nitrophenol ^e	3.86×10^{-5} (Bannan et al., 2017)	9.88×10^{-1}	7.14	3.86×10^{-5}
Phthalic acid ^f	1.26×10^{-5} (Booth et al., 2012)	1.69×10^{-7}	1.22×10^{-5}	1.26×10^{-5}

*not specified if the value is measured or calculate, not specified if it is a subcooled or a solid saturated vapor pressure

Table S10. Marker vaporization enthalpies. ΔH_{vap} is estimated though the Clausius Clapeyron equation when possible.

ΔH_{vap} (KJ mol ⁻¹)				
Marker	Literature	Min	Max	Chosen Value
DHOPA ^{a, h}		92.1	122.5	111
LEVO ^b	52 (Booth et al., 2011) 84 (Xie et al., 2014)	86.5	116.8	52
3-Methyl-5-Nitrocatechol ^c	Semi-empiric, reference: nitrocatechol ⁱ	66.1	78.0	41.7
Nitrocatechol ^c	39(Booth et al., 2012)	62.5	73.3	39
4-Nitroguaiacol ^d	Semi-empiric, reference: nitrocatechol ⁱ	55.4	64.2	30.9
4-Nitrophenol ^{e, h}		46.2	56.8	51.16
Phthalic acid ^f	40 (Booth et al., 2012)	95.7	123.5	40

a. Small polyacids: N-J and M-S are not considered

b. N-J and M-N are not considered

c. N-J and Comp. are not considered

d. M-J and Comp. are not considered

e. M-S and Comp. are not considered

f. N-J and M-S are not considered

g. Geometric average of the SAR methods estimations

h. Average of the SAR methods estimations

i. Ratio method: EPIsuite ($P_{\text{sat marker}}/P_{\text{sat reference}}$) * measured($P_{\text{sat reference}}$)

l. Difference method: EPIsuite ($\Delta H_{\text{marker}} - \Delta H_{\text{reference}}$) + measured($\Delta H_{\text{reference}}$)

2. Experimental

Table S11. Secondary markers quantified in SIRT A (2015) samples.

Secondary markers measured
Succinic acid
α -Methylglyceric acid
2,3-Dihydroxy-4-oxopentanoic acid (DHOPA)
cis-Pinonic acid
3-Hydroxyglutaric acid

Terpenylic acid
3-(2-Hydroxy-ethyl)-2,2-dimethylcyclobutane-carboxylic acid
3-Hydroxy-4,4-dimethylglutaric acid ^b
3-Acetylpentanedioic acid
Pinic acid
Phthalic acid
3-Acetyl hexanedioic acid
3-Isopropylpentanedioic acid
2-Nitrophenol
4-Nitrophenol
2-Methyl-4-nitrophenol
4-Nitroguaiacol
5-Nitroguaiacol
2-Methylthreitol
2-Methylerythritol
3-Methylbutane-1,2,3-tricarboxylic acid (MBTCA)S
β -Caryophyllinic acid
4-Methyl-5-nitrocatechol
3-Methyl-6-nitrocatechol
3-Methyl-5-nitrocatechol

2.1 OC_{wb} levoglucosan⁻¹ estimation (Favez, 2016)

Experimental studies estimate biomass burning aerosols measuring levoglucosan. OC_{wb} is determined using the following equation:

$$OC_{wb} = f \times \text{levoglucosan} \quad (\text{Eq.S1})$$

where $f = (OC_{wb} \text{ levoglucosan}^{-1})$ is a source-specific factor. Literature experimental values for f are ranged between 3 and 15

(Herich et al., 2014; Puxbaum et al., 2007; Schmidl et al., 2008). These differences could be explained by the different burning conditions (leading to different particle composition). A mean factor of 7 has been proposed by Puxbaum et al., (2007) for different European sites and used in this study. However, to avoid any overestimation, a site-specific upper limit for f has been fixed considering the 3 lowest OC_{tot} levoglucosan⁻¹ ratio mean. OM_{wb} has been estimated using a factor 1.8 (Favez et al., 2010).

3. Model vs Measurements

Table S12: Sampling site locations, periods, frequency and estimated OC_{wb} levoglucosan⁻¹

Site name	Urban area	Geographical coordinates	Sampling Period	Sampling frequency (1 day every n days)	OC_{wb} levoglucosan ⁻¹
Jean d'Aulan	Reims	4.02° E 49.22° N	28/11/2014 - 15/04/2015	3	6.8
SIRTA	Paris suburbs	2.15° E 48.72° N	19/11/2014 - 15/12/2015	3	ND
STG Nord	Strasbourg	7.78° E 48.61° N	25/12/2014 - 16/03/2015	3	4
Cim Bouteillerie	Nantes	-1.54° E 47.22° N	16/11/2014 - 15/04/2015	3	5.2
Augouard	Poitiers	0.35° E 46.58° N	16/11/2014 - 15/04/2015	3	5.1

Talence	Bordeaux	-0.59° E 44.80° N	16/11/2014 - 15/04/2015	3	4.6
Lyon Centre	Lyon	4.85° E 45.76° N	16/11/2014 - 15/04/2015	3	6.1
Les Frenes	Grenoble	5.73° E 45.16° N	14/11/2014 - 16/04/2015	3	5.9
Arson	Nice	7.27° E 43.71° N	16/11/2014 - 15/04/2015	3	7.1
5 avenues	Marseille	5.40° E 43.30° N	16/11/2014 - 15/04/2015	3	7.1
OPE	rural	5.50° E 48.56° N	01/01/2015 - 26/12/2015	6	ND

3.1 Levoglucosan

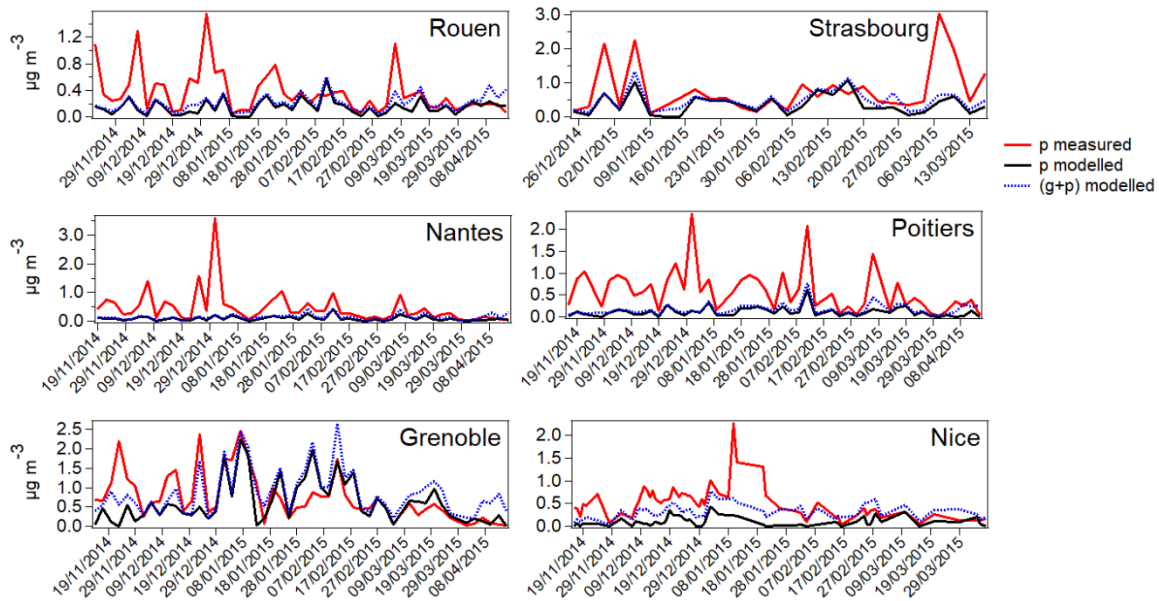


Figure S3. Model to measurements comparison in 6 urban sites all over France in winter 2014–2015.

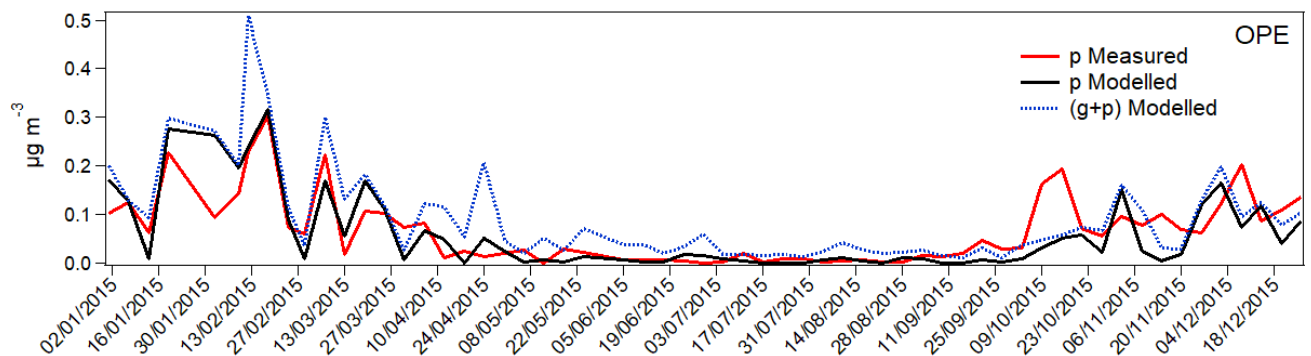


Figure S4. Model to measurements comparison at OPE sampling site in 2015.

3.2 Organic matter

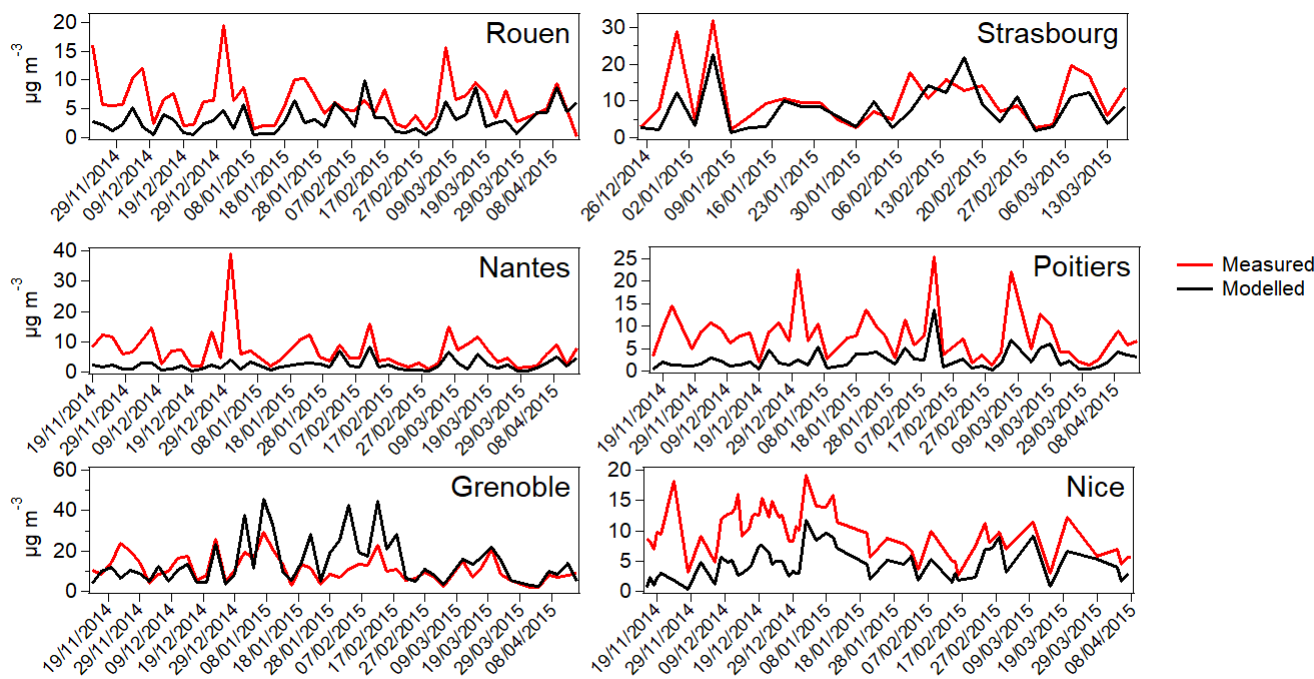


Figure S5. Comparison of measured and modelled organic matter in 7 sites in France during winter 2014–2015.

3.3 Primary vs secondary marker

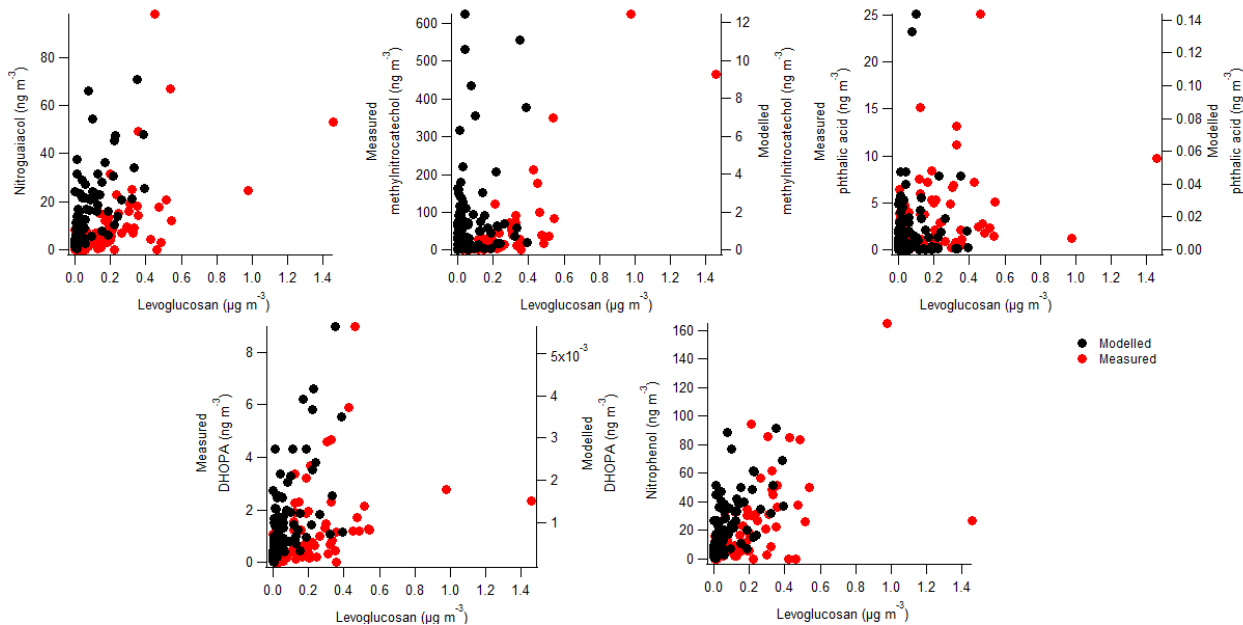


Figure S7. Correlation of measured and modelled levoglucosan and secondary markers. From top left to right bottom panel: nitroguaiacol, methylnitrocatechols, phthalic acid, DHOPA, nitrophenol.

4. Meteorological data

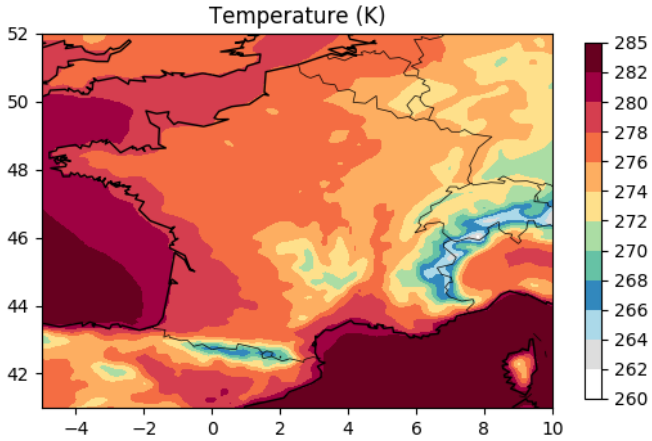


Figure S8. Mean daily temperature in France in February 2015.

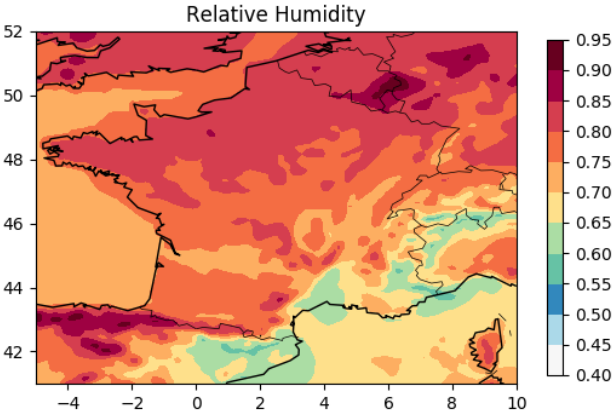


Figure S9. Mean daily relative humidity in France during February 2015.

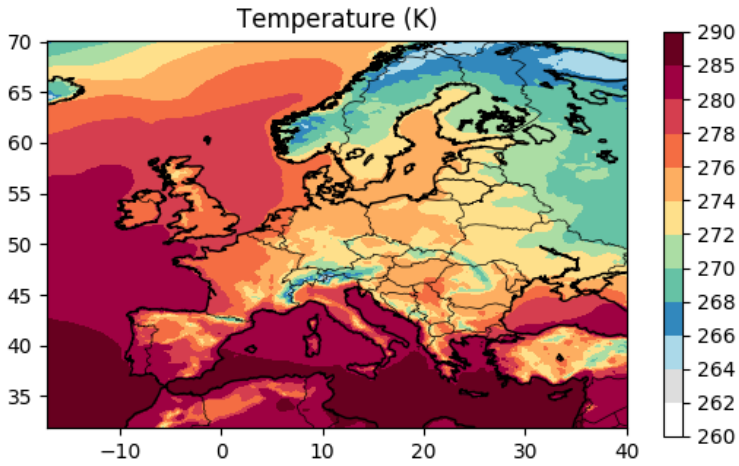


Figure S10. Mean daily temperature in Europe in February 2015.

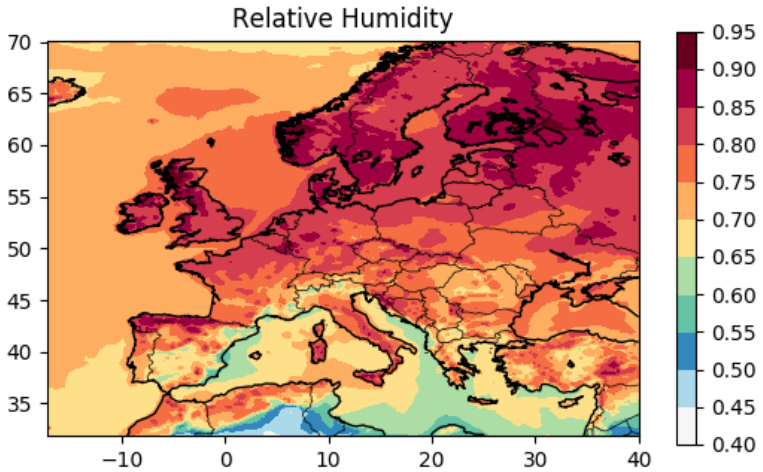


Figure S11. Mean daily relative humidity in Europe during February 2015

5. GPP estimation and sensitivity

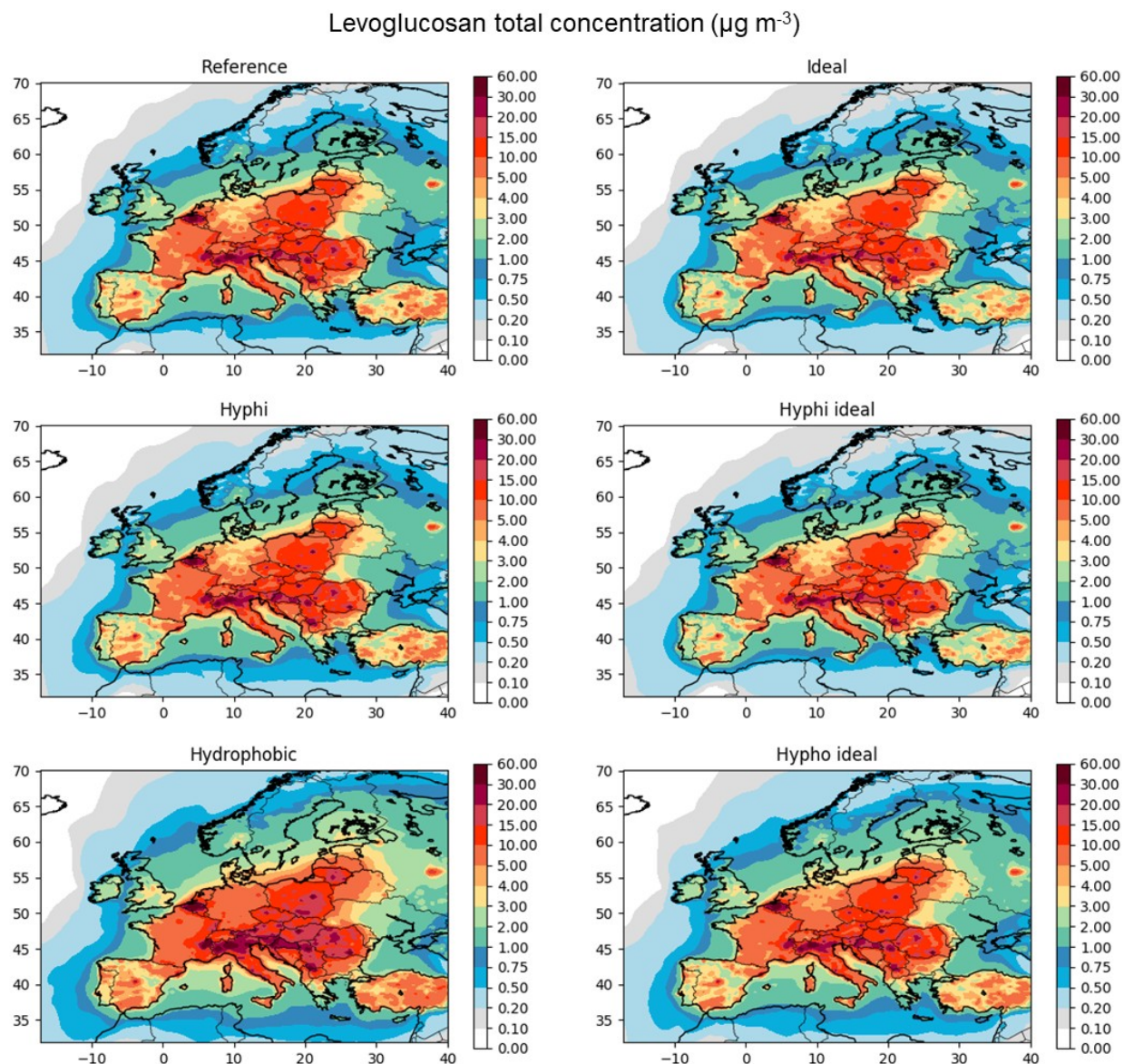


Figure S12. Spatial distribution of levoglucosan daily total concentrations during February 2015 in Europe.

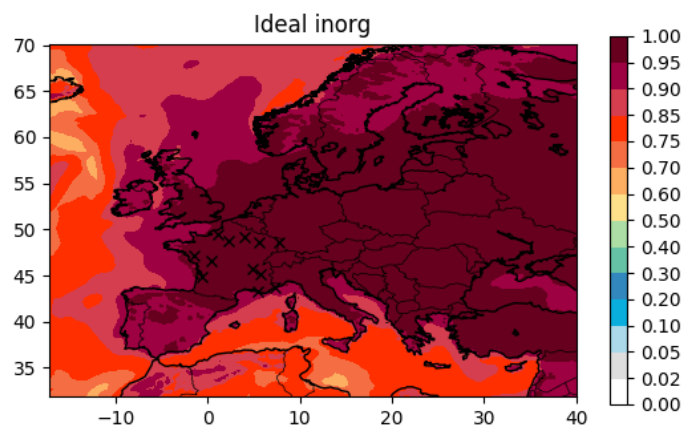


Figure. S13. Spatial distribution of levoglucosan daily particulate phase fraction in an “ideal inorganic” configuration during February 2015 in Europe. In the ideal inorganic configuration both the interactions between organics and inorganics are not taken in account.

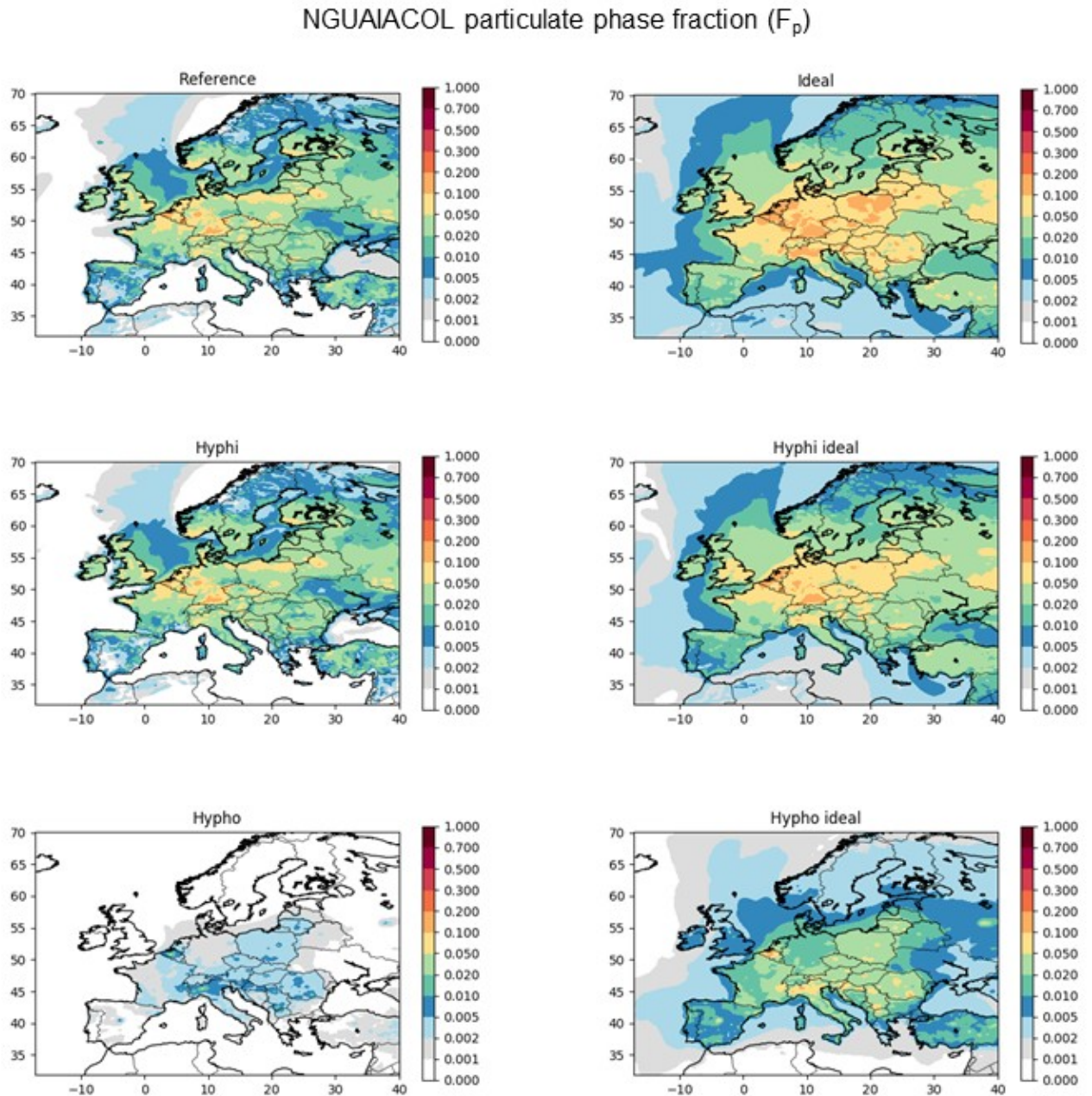


Figure S14. Nitroguaiacol particulate phase fraction variability in Europe during February 2015. The following thermodynamic conditions are shown from the top left panel: “reference” (non-ideal aerosol, nitroguaiacol is both hydrophobic and hydrophilic), “ideal”, “hydrophilic”, “hydrophilic ideal”, “hydrophobic” and “hydrophobic ideal”.

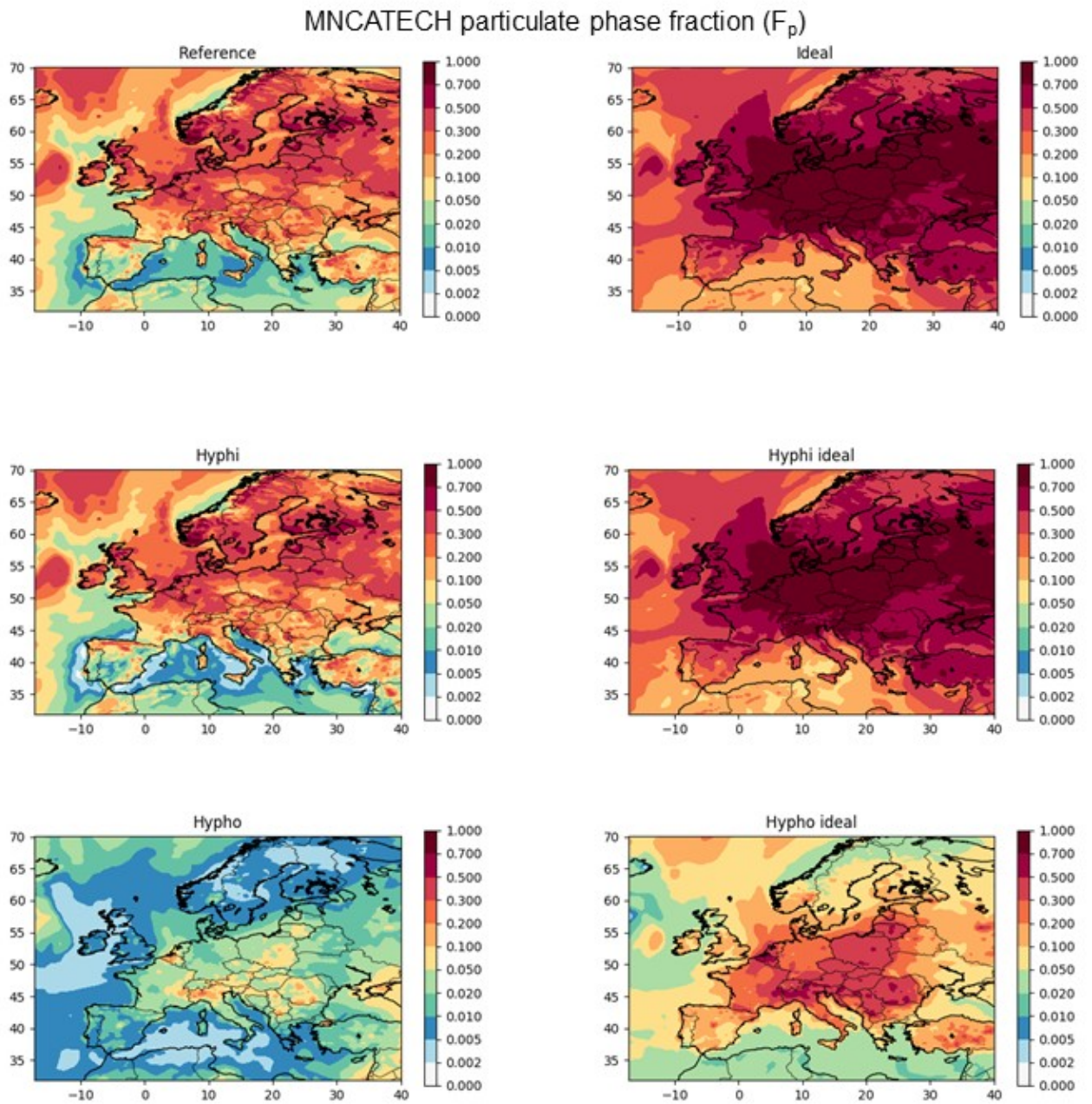


Figure S15. Methylmethylcatechols particulate phase fraction variability in Europe during February 2015. The following thermodynamic conditions are shown from the top left panel: "reference" (non-ideal aerosol, methylnitrocatechols is both hydrophobic and hydrophilic), "ideal", "hydrophilic", "hydrophilic ideal", "hydrophobic" and "hydrophobic ideal".

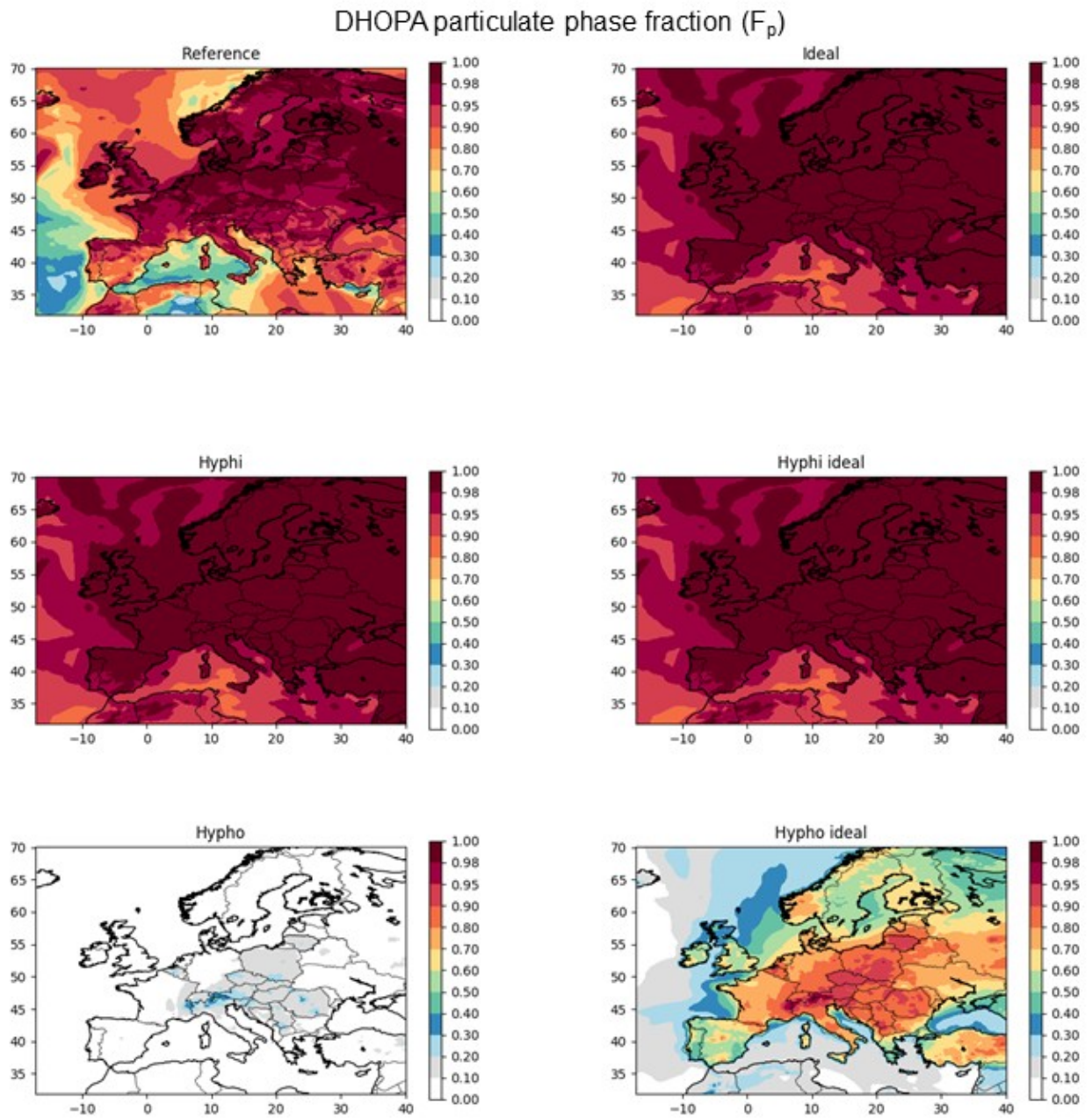


Figure S10. DHOPA particulate phase fraction variability in Europe during February 2015. The following thermodynamic conditions are shown from the top left panel: “reference” (non-ideal aerosol, DHOPA is both hydrophobic and hydrophilic), “ideal”, “hydrophilic”, “hydrophilic ideal”, “hydrophobic” and “hydrophobic ideal”.

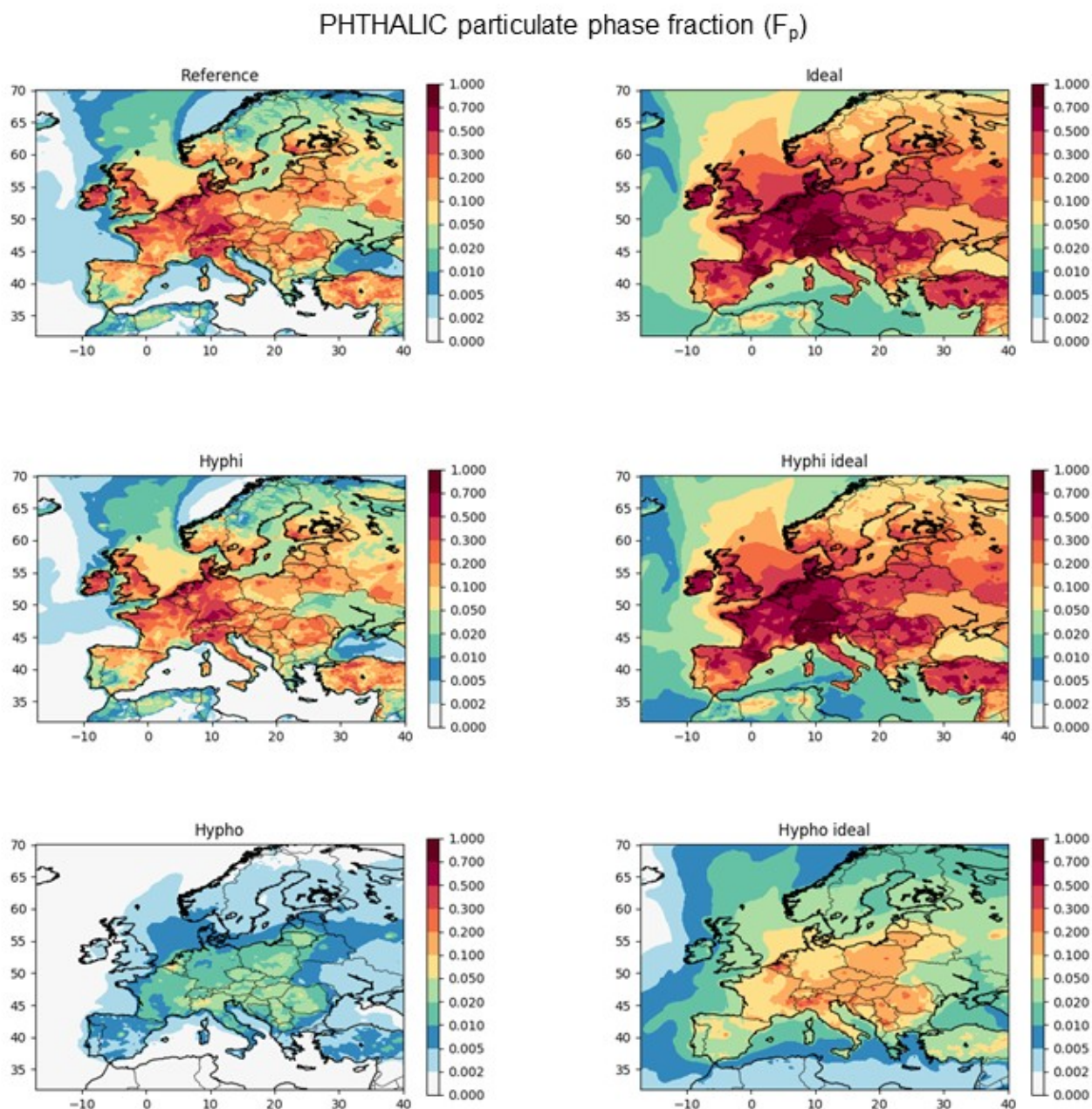


Figure S17. Phthalic acid particulate phase fraction variability in Europe during February 2015. The following thermodynamic conditions are shown from the top left panel: “reference” (non-ideal aerosol, phthalic acid is both hydrophobic and hydrophilic), “ideal”, “hydrophilic”, “hydrophilic ideal”, “hydrophobic” and “hydrophobic ideal”.

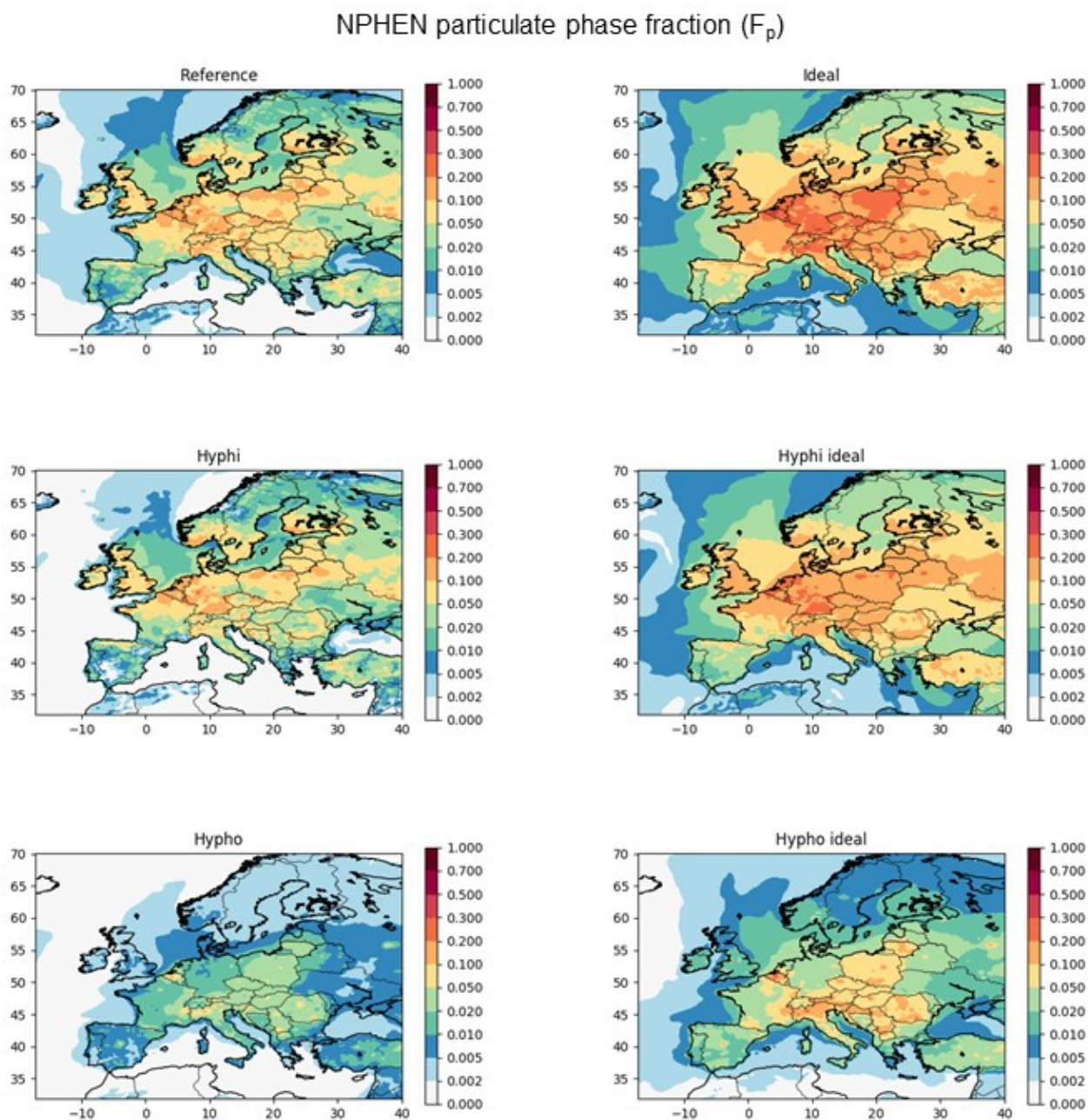


Figure S18. Nitrophenol acid particulate phase fraction variability in Europe during February 2015. The following thermodynamic conditions are shown from the top left panel: “reference” (non-ideal aerosol, nitrophenol is both hydrophobic and hydrophilic), “ideal”, “hydrophilic”, “hydrophilic ideal”, “hydrophobic” and “hydrophobic ideal”.

References

- Alvarado, A., Atkinson, R. and Arey, J.: Kinetics of the gas-phase reactions of NO₃ radicals and O₃ with 3-methylfuran and the OH radical yield from the O₃ reaction, *Int. J. Chem. Kinet.*, 28(12), 905–909, 1996.
- Aschmann, S. M., Arey, J. and Atkinson, R.: Study of the Atmospheric Chemistry of 2-Formylcinnamaldehyde, *J. Phys. Chem. A*, 117(33), 7876–7886, doi:10.1021/jp404994w, 2013.
- Aschmann, S. M., Nishino, N., Arey, J. and Atkinson, R.: Products of the OH Radical-Initiated Reactions of Furan, 2- and 3-Methylfuran, and 2,3- and 2,5-Dimethylfuran in the Presence of NO, *J. Phys. Chem. A*, 118(2), 457–466, doi:10.1021/jp410345k, 2014.
- Aumont, B., Szopa, S. and Madronich, S.: Modelling the evolution of organic carbon during its gas-phase tropospheric oxidation: development of an explicit model based on a self generating approach, *Atmospheric Chem. Phys.*, 5(9), 2497–2517, 2005.
- Bannan, T. J., Booth, A. M., Jones, B. T., O’Meara, S., Barley, M. H., Riipinen, I., Percival, C. J. and Topping, D.: Measured Saturation Vapor Pressures of Phenolic and Nitro-aromatic Compounds, *Environ. Sci. Technol.*, 51(7), 3922–3928, doi:10.1021/acs.est.6b06364, 2017.
- Bierbach, A., Barnes, I. and Becker, K. H.: Rate Coefficients For The Gas-Phase Reactions Of Hydroxyl Radicals With Furan, 2-Methylfuran, 2-Ethylfuran And 2,5- Dimethylfuran At 300 + 2 K, *Atmos. Environ.*, 26A(5), 813–817, 1992.
- Bloss, C., Wagner, V., Jenkin, M. E., Volkamer, R., Bloss, W. J., Lee, J. D., Heard, De., Wirtz, K., Martin-Reviejo, M. and Rea, G.: Development of a detailed chemical mechanism (MCMv3. 1) for the atmospheric oxidation of aromatic hydrocarbons, *Atmospheric Chem. Phys.*, 5(3), 641–664, 2005.
- Booth, A. M., Montague, W. J., Barley, M. H., Topping, D. O., McFiggans, G., Garforth, A. and Percival, C. J.: Solid state and sub-cooled liquid vapour pressures of cyclic aliphatic dicarboxylic acids, *Atmospheric Chem. Phys.*, 11(2), 655–665, doi:10.5194/acp-11-655-2011, 2011.
- Booth, A. M., Bannan, T., McGillen, M. R., Barley, M. H., Topping, D. O., McFiggans, G. and Percival, C. J.: The role of ortho, meta, para isomerism in measured solid state and derived sub-cooled liquid vapour pressures of substituted benzoic acids, *RSC Adv.*, 2(10), 4430, doi:10.1039/c2ra01004f, 2012.
- Camredon, M., Aumont, B., Lee-Taylor, J. and Madronich, S.: The SOA/VOC/NO_x system: an explicit model of secondary organic aerosol formation, *Atmospheric Chem. Phys.*, 7(21), 5599–5610, 2007.
- Coeur-Tourneur, C., Cassez, A. and Wenger, J. C.: Rate Coefficients for the Gas-Phase Reaction of Hydroxyl Radicals with 2-Methoxyphenol (Guaiacol) and Related Compounds, *J. Phys. Chem. A*, 114(43), 11645–11650, doi:10.1021/jp1071023, 2010.
- Compernelle, S., Ceulemans, K. and Müller, J.-F.: EVAPORATION: a new vapour pressure estimation method for organic molecules including non-additivity and intramolecular interactions, *Atmospheric Chem. Phys.*, 11(18), 9431–9450, doi:10.5194/acp-11-9431-2011, 2011.
- Couvidat, F. and Sartelet, K.: The Secondary Organic Aerosol Processor (SOAP v1.0) model: a unified model with different ranges of complexity based on the molecular surrogate approach, *Geosci. Model Dev.*, 8(4), 1111–1138, doi:10.5194/gmd-8-1111-2015, 2015.
- Crooks, D. A. and Feetham, F. M.: 196. The vapour pressure of phthalic anhydride, *J. Chem. Soc. Resumed*, 899–901, 1946.
- Favez, O.: Impact de la combustion de biomasse sur les concentrations de PM₁₀ (programme CARA - hiver 2014-2015), INERIS. [online] Available from: <https://www.lcsqa.org/fr/rapport/2015/ineris/impact-combustion-biomasse-concentrations-pm10-programme-cara-hiver-2014-2015>, 2016.
- Favez, O., El Haddad, I., Piot, C., Boréave, A., Abidi, E., Marchand, N., Jaffrezo, J.-L., Besombes, J.-L., Personnaz, M.-B., Sciare, J., Wortham, H., George, C. and D’Anna, B.: Inter-comparison of source

Chapter III: Model to measurements comparison: anthropogenic markers

apportionment models for the estimation of wood burning aerosols during wintertime in an Alpine city (Grenoble, France), *Atmospheric Chem. Phys.*, 10(12), 5295–5314, doi:10.5194/acp-10-5295-2010, 2010.

Herich, H., Gianini, M. F. D., Piot, C., Močnik, G., Jaffrezo, J.-L., Besombes, J.-L., Prévôt, A. S. H. and Hueglin, C.: Overview of the impact of wood burning emissions on carbonaceous aerosols and PM in large parts of the Alpine region, *Atmos. Environ.*, 89, 64–75, doi:10.1016/j.atmosenv.2014.02.008, 2014.

Jenkin, M. E., Saunders, S. M. and Pilling, M. J.: The tropospheric degradation of volatile organic compounds: a protocol for mechanism development, *Atmos. Environ.*, 31(1), 81–104, 1997.

Jenkin, M. E., Saunders, S. M., Wagner, V. and Pilling, M. J.: Protocol for the development of the Master Chemical Mechanism, MCM v3 (Part B): tropospheric degradation of aromatic volatile organic compounds, *Atmospheric Chem. Phys.*, 3(1), 181–193, doi:https://doi.org/10.5194/acp-3-181-2003, 2003.

Joback, K. G. and Reid, R. C.: Estimation of pure-component properties from group-contributions, *Chem. Eng. Commun.*, 57, 233–243, doi:10.1080/00986448708960487, 2007.

Kautzman, K. E., Surratt, J. D., Chan, M. N., Chan, A. W. H., Hersey, S. P., Chhabra, P. S., Dalleska, N. F., Wennberg, P. O., Flagan, R. C. and Seinfeld, J. H.: Chemical Composition of Gas- and Aerosol-Phase Products from the Photooxidation of Naphthalene, *J. Phys. Chem. A*, 114(2), 913–934, doi:10.1021/jp908530s, 2010.

Kind, I., Berndt, T., Böge, O. and Rolle, W.: Gas-phase rate constants for the reaction of NO₃ radicals with furan and methyl-substituted furans, *Chem. Phys. Lett.*, 256(6), 679–683, 1996.

Lauraguais, A., Coeur-Tourneur, C., Cassez, A., Deboudt, K., Fourmentin, M. and Choël, M.: Atmospheric reactivity of hydroxyl radicals with guaiacol (2-methoxyphenol), a biomass burning emitted compound: Secondary organic aerosol formation and gas-phase oxidation products, *Atmos. Environ.*, 86, 155–163, doi:10.1016/j.atmosenv.2013.11.074, 2014.

Mouchel-Vallon, C., Deguillaume, L., Monod, A., Perroux, H., Rose, C., Ghigo, G., Long, Y., Leriche, M., Aumont, B., Patryl, L., Armand, P. and Chaumerliac, N.: CLEPS 1.0: A new protocol for cloud aqueous phase oxidation of VOC mechanisms, *Geosci. Model Dev.*, 10(3), 1339–1362, doi:10.5194/gmd-10-1339-2017, 2017.

Myrdal, P. B. and Yalkowsky, S. H.: Estimating pure component vapor pressures of complex organic molecules, *Ind. Eng. Chem. Res.*, 36(6), 2494–2499, 1997.

Nannoolal, Y., Rarey, J., Ramjugernath, D. and Cordes, W.: Estimation of pure component properties Part 1. Estimation of the normal boiling point of non-electrolyte organic compounds via group contributions and group interactions, *Fluid Phase Equilibria*, 226, 45–63, doi:10.1016/j.fluid.2004.09.001, 2004.

Nannoolal, Y., Rarey, J. and Ramjugernath, D.: Estimation of pure component properties Part 3. Estimation of the vapor pressure of non-electrolyte organic compounds via group contributions and group interactions, *Fluid Phase Equilibria*, 269(1–2), 117–133, doi:10.1016/j.fluid.2008.04.020, 2008.

Nishino, N., Arey, J. and Atkinson, R.: Formation and Reactions of 2-Formylcinnamaldehyde in the OH Radical-Initiated Reaction of Naphthalene, *Environ. Sci. Technol.*, 43(5), 1349–1353, doi:10.1021/es802477s, 2009.

Pankow, J. F. and Asher, W. E.: SIMPOL. 1: a simple group contribution method for predicting vapor pressures and enthalpies of vaporization of multifunctional organic compounds, *Atmospheric Chem. Phys.*, 8(10), 2773–2796, 2008.

Parshintsev, J., Ruiz-Jimenez, J., Petäjä, T., Hartonen, K., Kulmala, M. and Riekkola, M.-L.: Comparison of quartz and Teflon filters for simultaneous collection of size-separated ultrafine aerosol particles and gas-phase zero samples, *Anal. Bioanal. Chem.*, 400(10), 3527–3535, doi:10.1007/s00216-011-5041-0, 2011.

Phouongphouang, P. T. and Arey, J.: Rate Constants for the Gas-Phase Reactions of a Series of Alkyl-naphthalenes with the OH Radical, *Environ. Sci. Technol.*, 36(9), 1947–1952, doi:10.1021/es011434c, 2002.

Chapter III: Model to measurements comparison: anthropogenic markers

Phousongphouang, P. T. and Arey, J.: Rate constants for the gas-phase reactions of a series of alkyl-naphthalenes with the nitrate radical, *Environ. Sci. Technol.*, 37(2), 308–313, 2003.

Puxbaum, H., Caseiro, A., Sánchez-Ochoa, A., Kasper-Giebl, A., Claeys, M., Gelencsér, A., Legrand, M., Preunkert, S. and Pio, C. A.: Levoglucosan levels at background sites in Europe for assessing the impact of biomass combustion on the European aerosol background, *J. Geophys. Res. Space Phys.*, 112(23), D23S05, doi:10.1029/2006JD008114, 2007.

Saunders, S. M., Jenkin, M. E., Derwent, R. G. and Pilling, M. J.: Protocol for the development of the Master Chemical Mechanism, MCM v3 (Part A): tropospheric degradation of non-aromatic volatile organic compounds, *Atmospheric Chem. Phys.*, 3(1), 161–180, 2003.

Schmidl, C., Bauer, H., Dattler, A., Hitzemberger, R., Weissenboeck, G., Marr, I. L. and Puxbaum, H.: Chemical characterisation of particle emissions from burning leaves, *Atmos. Environ.*, 42(40), 9070–9079, doi:10.1016/j.atmosenv.2008.09.010, 2008.

SIDS: Initial Assessment Report on phthalic anhydride, OECD, Paris, France., 2005.

Stein, S. E. and Brown, R. L.: Estimation of normal boiling points from group contributions, *J. Chem. Inf. Comput. Sci.*, 34(3), 581–587, 1994.

US EPA, O.: EPI Suite™-Estimation Program Interface, US EPA [online] Available from: <https://www.epa.gov/tsca-screening-tools/epi-suite-estimation-program-interface>, 2015.

Wang, L., Arey, J. and Atkinson, R.: Kinetics and Products of Photolysis and Reaction with OH Radicals of a Series of Aromatic Carbonyl Compounds, *Environ. Health*, 40, 5465–5471, 2006.

Xie, M., Hannigan, M. P. and Barsanti, K. C.: Gas/Particle Partitioning of 2-Methyltetrols and Levoglucosan at an Urban Site in Denver, *Environ. Sci. Technol.*, 48(5), 2835–2842, doi:10.1021/es405356n, 2014.

Yang, B., Zhang, H., Wang, Y., Zhang, P., Shu, J., Sun, W. and Ma, P.: Experimental and theoretical studies on gas-phase reactions of NO₃ radicals with three methoxyphenols: Guaiacol, creosol, and syringol, *Atmos. Environ.*, 125, 243–251, doi:10.1016/j.atmosenv.2015.11.028, 2016.

Chapter IV

*Model to measurements comparison:
Biogenic markers*

Article III

Modelling organic aerosol markers in 3D air quality model.

Part 2: Biogenic organic markers.

To be submitted in “Atmospheric chemistry and physics

Modelling organic aerosol markers in 3D air quality model.

Part 2: Biogenic secondary organic markers.

G.M. Lanzafame^{1,2}, F. Couvidat^{1,*}, O. Favez^{1,*}, A. Albinet¹, B. Bessagnet^{1,2,3,*}

¹INERIS, Parc Technologique Alata, BP 2, 60550 Verneuil-en-Halatte, France

²Sorbonne Universités, UPMC, 75252 PARIS cedex 05, France

³Now at: Hangzhou Futuris Environmental Technology Co. Ltd, Zhejiang, China

*Correspondence to: florian.couvidat@ineris.fr

Abstract

Biogenic secondary organic aerosols (SOA) have been identified as a large fraction of organic aerosol (OA) in Europe in summer. The major biogenic SOA precursors are monoterpenes and isoprene. Several chamber experiments have been performed to quantify the aerosols yields from each precursor at different conditions and have been used to develop SOA formation mechanism. These results are used in 1D and 3D air quality models to estimate SOA formation. However, SOA formation in air quality models is difficult to investigate due to the myriad of compounds and phenomena involved.

In this paper and its companion paper, we propose marker modelling as a way to investigate SOA formation. For the first time, a comprehensive and detailed mechanism for isoprene and α - and β -pinene SOA marker formation has been inserted in a 3D air quality model. Model outputs have been compared with measurements performed in a site located in the Paris region, France.

First generation oxidation α - and β -pinene markers (pinonic acid and pinic acid) formation in the gas-phase has been modelled according to the Master Chemical Mechanism (MCM) v3. For the second generation oxidation product MBTCA, the gas-phase formation has been modelled with the mechanism proposed by Müller et al., (2012). Isoprene SOA markers have been modelled using an updated version of Couvidat et al., (2013) parametrizations.

The concentrations of almost all the markers are underestimated and simulated with wrong temporal variations. Pinonic acid, pinic acid and MBTCA median measured values are underestimated respectively by a factor 3, 50 and 4.5. Methyltetrols are simulated with the right magnitude order, while α -methylglyceric acid is underestimated by a factor 100.

NO_x regime affect pinic acid and methyltetrols formation, that depend strongly on HO_2 and RO_2 radicals concentrations. Strong daily variations for pinonic acid formation processes have been observed. MBTCA and α -methylglyceric acid formation mechanisms are sensitive to aqueous phase reactivity representation.

GPP has been well simulated for MBTCA and methyltetrols, for which the hydrophilic non-ideal partitioning is predominant. For the other markers particulate phase fraction is underestimated. The gap between model and measurements can be explained by the synergy of chemical pathway representation, GPP estimation and OM simulation.

1. Introduction and objectives

Secondary organic aerosols (SOA) constitute an important fraction (20-80%) of total organic aerosol (OA) (Jimenez et al., 2009; Kroll and Seinfeld, 2008; Srivastava et al., 2018a; Zhang et al., 2007, 2011a). Their formation occurs in the atmosphere, through nucleation and condensation of volatile organic compounds (VOCs) (photo-) oxidation products. VOCs are emitted in the atmosphere by biogenic and anthropogenic sources and their reactivity has been widely characterized. In Europe, SOA has been reported as the major contributor to OA in summer (Bozzetti et al., 2016, 2017b, 2017a; Canonaco et al., 2015; Daellenbach et al., 2016; Lanz et al., 2010; Reyes-Villegas et al., 2016; Schlag et al., 2016) and biogenic sources contribution has been assumed to be large (Bonvalot et al., 2016; Vlachou et al., 2018; Zotter et al., 2014).

Several chamber experiments have been conducted to study SOA yields from biogenic volatile organic compounds (BVOCs) under different conditions (e.g. temperature, humidity, NO_x regime). Isoprene and monoterpenes have been recognized as the most important biogenic aerosol precursors (Guenther et al., 1995; Heald et al., 2008). SOA mass yield and composition dependence on the BVOC oxidation initiation process has been established (Draper et al., 2015; Surratt et al., 2010; Zhao et al., 2015) and the so-determined mass yields are often used to design biogenic SOA (BSOA) formation mechanism in the atmosphere (Friedman and Farmer, 2018). However, this approach do not consider the great variability associated to BSOA production at different atmospheric conditions and increases uncertainties in predicting the total SOA budget in 3D CTMs.

Isoprene SOA have been modelled in the 3D CTM CMAQ considering high and low NO_x regimes (Pye et al., 2013). The formation of some known isoprene SOA oxidation products

(markers) has been simulated in the aerosol aqueous phase, using detailed chemical mechanisms. The modelled aerosol mass is composed by α -methylglyceric acid (formed under high NO_x conditions), methyltetrols (formed under low NO_x conditions) (Surratt et al., 2010) but also organosulfates and organonitrates. The performances of the model have been evaluated by comparison with marker measurements performed on several sampling sites across US and with the results of a classic 2-product Odum parametrization for isoprene SOA. They found that the detailed mechanism outputs correlated better than the 2-products model with measurements. Similarly, Couvidat et al., (2013) studied the formation of IEPOX SOA and the importance of the Henry's law constant of IEPOX. The authors determined that a Henry's law constant for IEPOX around $2 \times 10^7 \text{ M atm}^{-1}$ would be necessary to explain concentrations of IEPOX SOA observed over Europe during different campaigns. This value was close to the one measured by Nguyen et al., (2014) onto sea salts ($3 \times 10^7 \text{ M atm}^{-1}$). Jo et al., (2019) recently developed a 3-surrogate parametrization for isoprene SOA formation that can reproduce well spatial and temporal variation of IEPOX SOA with lower computational costs. However, this parametrization cannot reproduce the diurnal variations due to the chemical and meteorological variations.

Several studies focus on modeling of monoterpene SOA in chamber experiments. Jenkin, (2004) succeeded in reproducing the certain features (e.g. the high contribution of multifunctional acids) of α -pinene ozonolysis SOA, using a detailed SOA formation mechanism from the Master Chemical Mechanism (MCM) v3, optimized with chamber experiments yields. Capouet et al., (2008) developed the Biogenic hydrocarbon Oxidation and related Aerosol formation Model (BOREAM) that include a quasi-explicit gas phase mechanism for the first oxidation generation products of α - and β -pinene and a simplified representation of the further photooxidation processes. Roldin et al., (2019) inserted the MCM+PRAM mechanism for α -pinene OH- and O_3 -initiated oxidation in the 3D CTM ADCHEM, using a Lagrangian approach. They succeeded to simulate new particle formation (NPF) episodes and high oxidized molecules (HOM) SOA in a forested site in Finland during spring with high accuracy. However, no SOA formation from isoprene or α -pinene+ NO_3 oxidation has been modelled and no specific molecule formation was targeted in their simulations.

Xavier et al., (2019) simulated a near explicit mechanism combining MCM and the peroxy radical autoxidation mechanism (PRM, Roldin et al., 2019) to model SOA mass yields from isoprene, α - and β -pinene, limonene and β -caryophyllene in an oxidative flow reactor (OFR).

The parameters individued as critical for SOA yields were the NO_x regime (for α -pinene ozonolysis) and the temperature.

In all these studies the gas to particle partitioning was either not considered, e.g. non-volatile markers as in Pye et al., (2013), or treated using a “classical” approach, with ideal aerosol and no partitioning in the hydrophilic phase (Pankow, 1994).

The hydrophobic and hydrophilic gas-to-particle partitioning has been considered by Chrit et al., (2017), which model isoprene, monoterpene and sesquiterpene SOA formation in the 3D CTM Polyphemus. They used known markers, such as methyl glyceric acids or 3-methyl-1,2,3-butanetricarboxylic acid (MBTCA), as surrogates for the biogenic SOA. However, this kind approach exclude the validation of the gas-to-particle partitioning by direct comparison with the marker measurements.

In this study, biogenic SOA marker formation in ambient air is investigated by using a multistep reaction scheme inserted in a 3D chemistry transport model. Detailed formation mechanism for pinonic acid, pinic acid, MBTCA, 2-methyltetrols and α -methylglyceric acid have been developed and the simulation output has been compared to measurements performed at SIRTAs sampling station, in Paris region. Gas to particle partitioning (GPP) is simulated with the Secondary Organic Aerosol Processor (SOAP) thermodynamic model able to compute the non-ideal partitioning between the gas, organic and aqueous phases of semivolatile organic compounds. The simulated GPP has been evaluated, with a focus on thermodynamical sensitivity. Sensitivity analysis to radical concentrations has also been carried out. In the companion paper, the anthropogenic SOA marker formation is presented.

2. Model overview

A Gaseous and aqueous phase chemical mechanism for the formation of 11 organic marker have been developed and inserted in the 3D chemistry-transport model CHIMERE 2017 β (Couvidat et al., 2018). In this paper 5 biogenic markers formation mechanisms and simulation outputs are presented, as a part of the marker implemented version of CHIMERE. The biogenic precursors considered are α -/ β -pinene and isoprene. Anthropogenic markers mechanisms and simulations are already described in the companion paper. A description of CHIMERE 2017 β aerosol module is available in the companion paper and in Couvidat et al., (2018). Thermodynamic equilibria have been simulated by ISORROPIA (Fountoukis and Nenes, 2007) for inorganics and by the Secondary Organic Aerosol Processor SOAP (Couvidat and Sartelet, 2015) for organics. SOAP estimates the partitioning of organic markers by using

their saturation vapor pressure and takes into account the condensation on both the organic and aqueous phases by estimating activity coefficients with the Aerosol Inorganic–Organic Mixtures Functional groups Activity Coefficients (AIOMFAC) parameterizations.

2.1 Development of the marker mechanism

The gaseous and aqueous phase chemical mechanism of CHIMERE have been modified to insert the marker formation mechanisms. The atmospheric chemistry in CHIMERE is represented with the MELCHIOR2 (Derognat et al., 2003) mechanism and SVOC formation by the Hydrophilic/Hydrophobic Organics (H²O) (Couvidat et al., 2012) mechanisms. H²O was implemented as in Majdi et al., (2019) by adding several aerosol precursors from biomass burning. Therefore, the marker version of CHIMERE has isoprene, monoterpenes, sesquiterpenes, toluene, xylene, phenol, cresol, catechol, benzene, furan, guaiacol, syringol, naphthalene and methylnaphthalenes as SOA precursors.

Table 1. Subcooled saturated vapor pressure (P_{sat}), evaporation and solubilization enthalpies (ΔH_{vap} and ΔH_{sol}) and Henry's law constant (K_{H}) for the modelled biogenic markers. ΔH_{sol} and K_{H} have been calculated with SOAP (Couvidat and Sartelet, 2015).

Marker	$P_{\text{sat}298\text{K}}$ (torr)	ΔH_{vap} (KJmol ⁻¹)	ΔH_{sol} (KJmol ⁻¹)	K_{H} (M ⁻¹ atm)
Pinonic Acid	5.86×10^{-6}	86	81.7	2.3×10^7
Pinic Acid	1.01×10^{-7}	80	84.2	1.1×10^{10}
MBTCA	2.85×10^{-10}	135	145.2	1.37×10^{14}
Methylthreitol*	1.94×10^{-6}	106.4	107.6	3.3×10^{10}
α -methylglyceric acid	1.4×10^{-5}	91.7	98.5	6.31×10^9

*sum of 2-methylerythritol and 2-methylthreitol

The marker formation is initiated by the oxidation of toluene, guaiacol, phenol, isoprene and α -/ β -pinene. Mechanistic data were taken from literature, the Master Chemical Mechanism (MCM, version 3.3.1) (Bloss et al., 2005; Jenkin et al., 1997, 2003; Saunders et al., 2003), from the Generator for Explicit Chemistry and Kinetics of Organics in the Atmosphere (GECKO-A) (Camredon et al., 2007) and from the Cloud Explicit Physico-chemical Scheme (CLEPS 1.0) (Mouchel-Vallon et al., 2017) for the aqueous phase chemistry. In all these

mechanisms, experimental kinetic data are preferred when available, otherwise mechanistic data are estimated through structure activity relationships (SARs) or determined by analogy to similar better characterized reactions.

The OH oxidation in the aqueous phase is modelled assuming for both OH and the substrate an instantaneous equilibrium with the gaseous phase, computed using the Henry's law constant (K_H) and the solubilization enthalpy (ΔH_{sol}) (calculated with SOAP for the substrate). OH Henry's constant has been assumed to be $25.0 \text{ M}^{-1} \text{ atm}$ (Lelieveld and Crutzen, 1991) and its consumption by reactive aqueous species has been taken in account dividing by a factor 2 the concentrations at the equilibrium (Couvidat et al., 2013).

SOAP has been used to evaluate the marker gas to particle partitioning (GPP), providing as input the subcooled saturated vapor pressure (P_{sat}) and the evaporation enthalpy (ΔH_{vap}) (Table 1). SOAP is a powerful tool in which the user can choose for each molecule to compute the hydrophilic (condensation onto the aqueous phase) and/or the hydrophobic (condensation onto the organic phase) partitioning considering a non-ideal aerosol, at the equilibrium or in a dynamic configuration. The hydrophilic partitioning is estimated according to a modified version of Henry's law, dependent on the infinite dilution activity coefficient ($\gamma_{i,aq}^\infty$) calculated with the UNiversal Functional group Activity Coefficient (UNIFAC) (Fredenslund et al., 1975) and on activity coefficient in the aqueous phase ($\gamma_{i,aq}$) computed with the AIOMFAC parameterizations (Zuend et al., 2008, 2010, 2011; Zuend and Seinfeld, 2012). The hydrophobic partitioning is estimated with a non-ideal Raoult's law (Pankow, 1994). Experimental P_{sat} and ΔH_{vap} have been preferred for markers GPP evaluation when available, semi-empiric values and SARs estimation have been used as alternative. When experimental data are not available, P_{sat} and ΔH_{vap} were estimated from the measured P_{sat} and ΔH_{vap} for a similar molecule by applying correction factors, based on SARs ratios (for P_{sat}) or differences (for ΔH_{vap}) between the two molecules.

Further details are described in the companion paper. In the mechanism descriptions, only the reactions directly involved in the formation pathways of biogenic markers are shown, however the competitive reactions (reactions that lead to a loss of intermediate species) are also taken into account in the model. The full mechanism for pinonic and pinic acid is available online (MCM website: <http://mcm.leeds.ac.uk/MCM/>) and in supplementary materials for MBTCA (Table S1) and isoprene markers (Table S2).

2.1.1 α - and β -pinene markers

In this section pinonic acid, pinic acid and 3-methylbutane-1,2,3-tricarboxylic acid (MBTCA) formation pathways are presented. Pinonic and pinic acid are commonly recognized as first generation photooxidation products (Jaoui and Kamens, 2001), while MBTCA is a second generation product (Müller et al., 2012). The gaseous phase mechanism for the first generation product formation have been provided by MCM. For MBTCA, a formation mechanism from pinonic acid based on Müller et al., (2012) have been used. The names assigned to the intermediates in MCM have been kept, in order to assure the reproducibility of the model and the possible interaction between different pathways. The kinetic constants provided by MCM have not been reported in the text.

2.1.1.1 Pinonic Acid

The only precursor of pinonic acid in MCM is α -pinene (APINENE). α -pinene photooxidation is initiated by reaction with OH, NO₃ and O₃ and leads to pinonic acid formation through several reactions. Pinonaldehyde (PINAL) has been identified as the major intermediate for this process in the 3 pathways.

The OH initiated process (Fig.1) generate two pinonic acid precursors: the 3-hydroxy- and the 2-hydroxy- isomers of (2,6,6-trimethylbicyclo[3.1.1]heptan-2-yl)dioxidanyl (APINAO2 and APINBO2) with the branching ratios respectively of 0.57 and 0.35. APINAO2 and APINBO2 oxidation pathways proceed similarly, involving the reactions with:

- NO₃, producing 100% of PINAL from both isomers.
- NO, producing 77% of PINAL and 23% of the 3- and the 2- hydroxyperoxy-2,6,6-trimethylbicyclo[3.1.1]heptan-2-yl nitrates (APINANO3 and APINBNO3) respectively. APINANO3 and APINBNO3 react with OH giving respectively PINAL and the 2-hydroxy-2,6,6-trimethylbicyclo[3.1.1]heptan-3-one (APINBCO).
- HO₂, leading to the formation of the hydroperoxydes conjugates (stoichiometric coefficient of 0.9, the 3- and the 2-hydroxyperoxy-2,6,6-trimethylbicyclo[3.1.1]heptan-2-ol, APINAOOH and APINBOOH respectively). APINAOOH and APINBOOH undergo photolysis generating 100% of PINAL.
- RO₂, producing respectively for APINAO2 and APINBO2 70% and 60% of PINAL, 30% and 20% of 3,6,6-trimethylbicyclo[3.1.1]heptane-2,3-diol (APINBOH), and 20% of APINBCO only from APINBO2. APINBOH react with OH producing APINBCO.

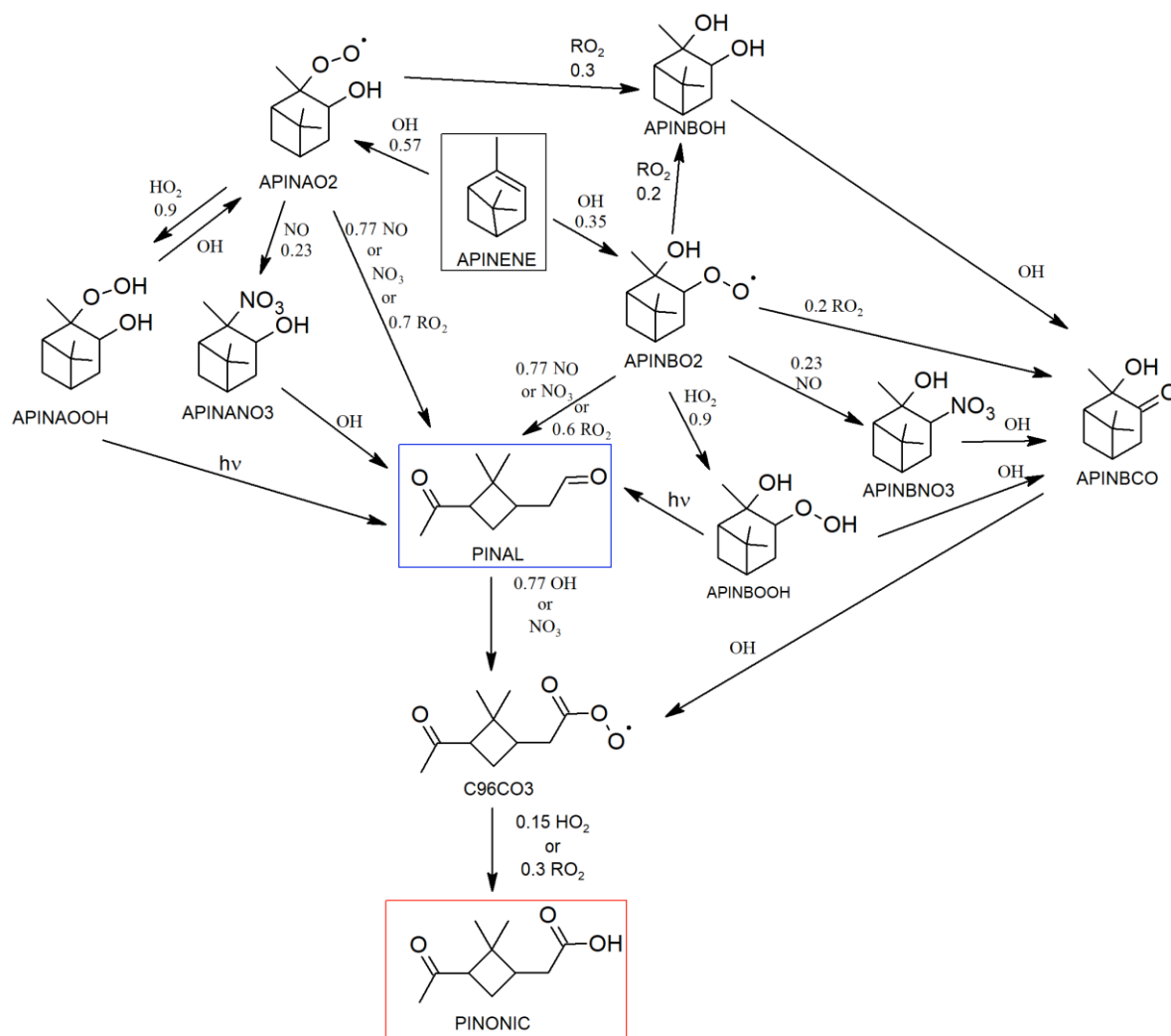


Figure 1. OH-initiated α -pinene oxidation process in atmosphere according to MCM v3.3.1.

The competitive reactions are not reported in figure, but considered in the model.

The NO_3 initiated α -pinene photooxidation (Fig.2) gives 35% of [2,6,6-trimethyl-3-(nitrooxy)bicyclo[3.1.1]heptan-2-yl]dioxidanyl (NAPINAO2) and 65% of [2,6,6-trimethyl-2-(nitrooxy)bicyclo[3.1.1]heptan-3-yl]dioxidanyl (NAPINBO2). The oxidation pathway proceed similarly to the one already described for OH-initiated mechanism. The two intermediates react with:

- NO_3 and NO , producing 100% of PINAL from both isomers.
- HO_2 , leading to the formation of the hydroperoxydes conjugates (branching ratio=0.9, the 2- and the 3-hydroperoxy-2,6,6-trimethylbicyclo[3.1.1]heptan-3-yl nitrate, NAPINAOOH and NAPINBOOH respectively). NAPINAOOH and NAPINBOOH undergo photolysis generating 100% of PINAL. NAPINBOOH reacts with OH, giving 78% of the 2,6,6-trimethyl-3-oxobicyclo[3.1.1]heptan-2-yl nitrate (NC101CO) at

298K (the competitive reaction with OH is temperature dependent, while the current reaction is not). NC101CO undergoes photolysis producing C96CO3.

- RO₂, generating respectively for NAPINAO2 and NAPINBO2 90% and 80% of PINAL, and respectively 10% of 2- and 3-hydroxy-2,6,6-trimethylbicyclo[3.1.1]heptan-3-yl nitrate (APINBNO3 and APINANO3), and 10% of NC101CO only from NAPINBO2. APINBNO3 and APINANO3 reactions have been already commented in the OH initiated pathway.

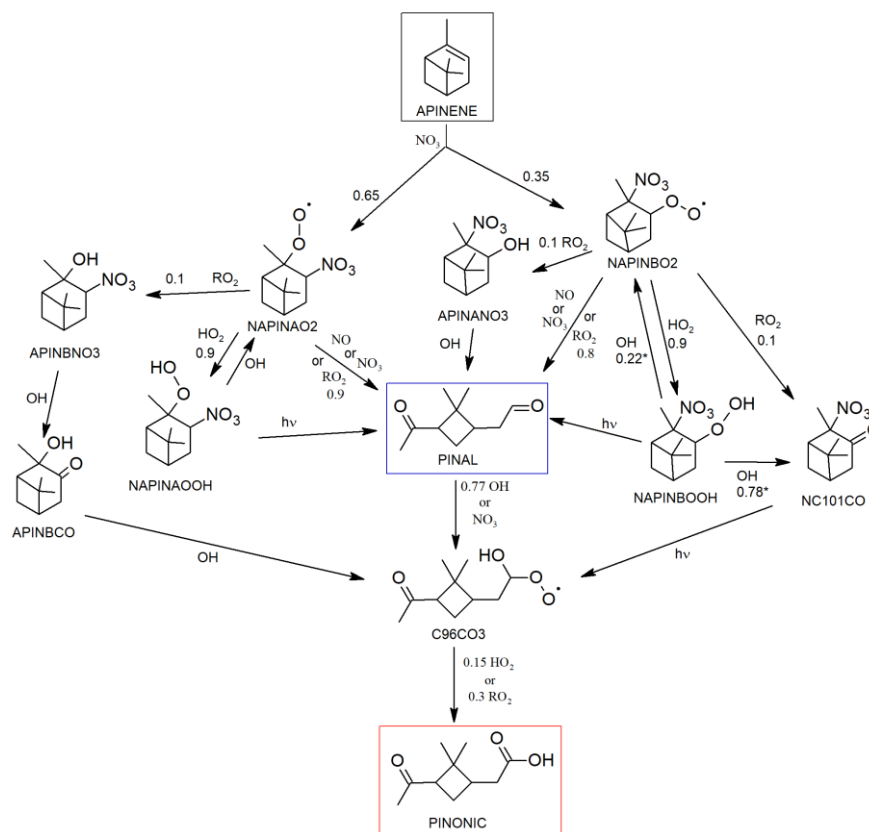


Figure 2. NO₃-initiated α -pinene oxidation process in atmosphere according to MCM v3.3.1.

The competitive reactions are not reported in figure, but considered in the model.

The O₃ initiated α -pinene photooxidation pathway generates 20% of 2-[2-(3-acetyl-2,2-dimethylcyclobutyl)ethylidene]dioxidan-2-ium-1-ide (APINBOO) and 27% of {2-[2,2-dimethyl-3-(2-oxoethyl)cyclobutyl]-2-oxoethyl}dioxidanyl (C109O2). APINBOO reacts with CO, NO, NO₂ or SO₂ giving 100% of PINAL, and with H₂O giving 88% of PINAL and 12% of pinonic acid (PINONIC). The photooxidation of C109O2 lead to the formation of pinic acid (PINIC) and is commented in the next paragraph.

The final oxidation steps are the same for all the pathways: PINAL reacts with OH and NO₃ producing 77% and 100% of [(3-acetylcyclobutyl)acetyl]dioxidanyl (C96CO3). APINBCO

photooxidation by OH give 100% of C96CO3. C96CO3 further reacts with HO₂ and RO₂ producing pinonic acid (PINONIC, branching ratios 0.15 and 0.3).

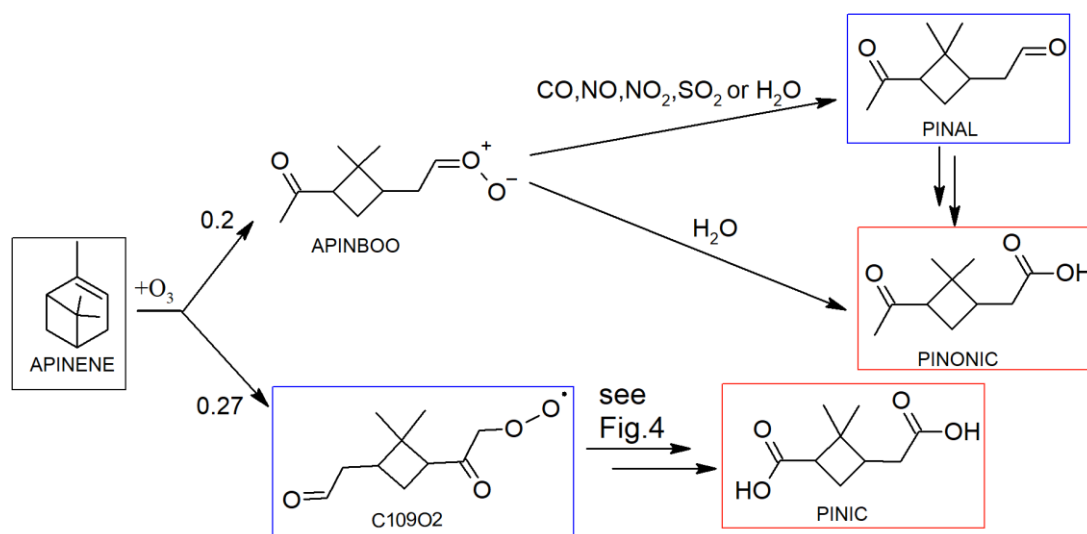


Figure 3. O₃-initiated α-pinene oxidation mechanism. Just the reactions directly involved in the pathway are displayed, the other possible reactions are considered in the model. The double arrow stands for multiple chemical steps (see Fig.4).

According to Tilgner and Herrmann, (2010) aldehydes can be oxidized to carboxylic acids in aqueous phase, therefore PINAL oxidation to PINONIC in the aqueous phase has been considered. The partitioning with the aqueous phase has been evaluated using Henry's law constant ($K_H=809 \text{ M atm}^{-1}$) and solubilization enthalpy ($\Delta H_{\text{sol}}=61.2 \text{ kJ mol}^{-1}$) calculated with SOAP, based on the P_{sat} from Hallquist et al., (1997) ($P_{\text{sat}}=3.83 \times 10^{-2} \text{ torr}$). PINAL oxidation by OH and NO₃ has been modelled in analogy with 2,3 dioxobutenale (CLEPS 1.0):



PINONIC degradation in gas and aqueous phase produce MBTCA (Müller et al., 2012) and is discussed in section 2.2.3. Experimental pinonic acid P_{sat} ($5.86 \times 10^{-6} \text{ torr}$) and ΔH_{vap} (86 kJ mol^{-1}) from Booth et al., (2011) have been inserted in SOAP as input for GPP calculation.

2.1.1.2 Pinic Acid

According to MCM, pinic acid is produced from α-pinene ozonolysis and from the OH-, NO₃- and O₃-initiated oxidation of β-pinene. The major intermediate for pinic acid formation, the nopinone, is produced only by β-pinene oxidation.

C109O2 is the precursor of pinic acid produced by α -pinene reaction with O_3 (yield 27%) (Fig. 3 and 4). C109O2 reacts with NO and NO_3 producing for both reactions 80% of 2,2-dimethyl-3-(oxoacetyl)cyclobutane-1-carbaldehyde (C89CO3). C109O2 oxidation by RO_2 gives 5% of 3-(1-hydroxy-2-oxoethyl)-2,2-dimethylcyclobutane-1-carbaldehyde (C109OH), 5% of 2,2-dimethyl-3-(oxoacetyl)cyclobutane-1-carbaldehyde (C109CO) and 90% of C89CO3. C109OH and C109OOH undergo similar oxidation pathways: their reaction with OH generates C109OH and their photolysis produces C89CO3. C109CO OH-oxidation and photolysis produce C89CO3.

C89CO3 reacts with NO_3 , RO_2 and HO_2 giving respectively 100, 70 and 44% of 3-(carboxymethyl)-2,2-dimethylcyclobutane-1-carboxylic acid (C811CO3). The C89CO3 reaction with HO_2 produce also respectively 15% and 41% of 2,2-dimethyl-3-(2-oxoethyl)cyclobutane-1-carboperoxoic acid (C89CO3H) and 2,2-dimethyl-3-(2-oxoethyl)cyclobutane-1-carboxylic acid (C89CO2H). C89CO3 is also at equilibrium with his peroxyacetylnitrate (C89PAN). C811CO3 is produced by C89CO3H and C89CO2H photolysis, and also by OH-oxidation of C89CO2H. C811CO3 is at the equilibrium with his correspondent PAN (C811PAN), and is the direct precursor of pinic acid (PINIC), by reaction with RO_2 and HO_2 (stoichiometric coefficients are respectively 0.3 and 0.15). HO_2 oxidation has also the 3-(2-hydroperoxy-2-oxoethyl)-2,2-dimethylcyclobutane-1-carboxylic acid (C811CO3H) as product, that restore C811CO3 by photolysis and OH oxidation.

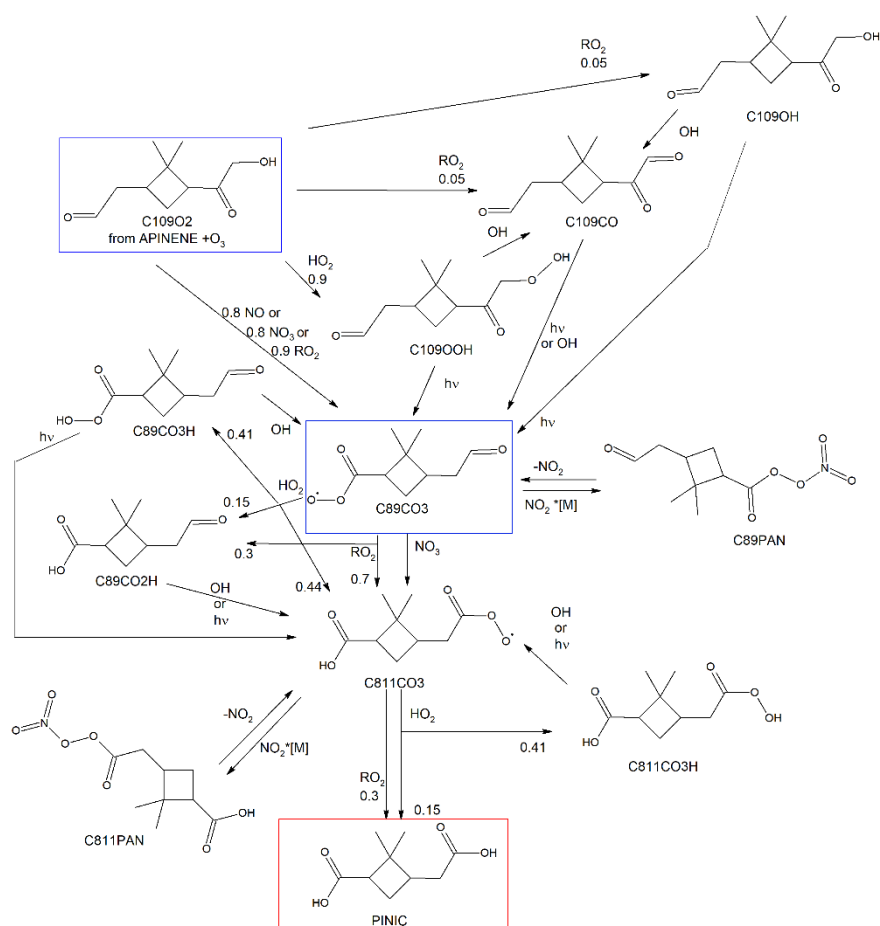


Figure 4. Pinic acid formation pathway from {2-[2,2-dimethyl-3-(2-oxoethyl)cyclobutyl]-2-oxoethyl}dioxidanyl (C109O2), an α -pinene ozonolysis product.

β -pinene (BPINENE)+OH (Fig. 5) produces 85% of [2-(hydroxymethyl)-6,6-dimethylbicyclo[3.1.1]heptan-2-yl]dioxidanyl (BPINAO2) and 8% of [2-(hydroxymethyl)-6,6-dimethylbicyclo[3.1.1]heptan-2-yl]dioxidanyl (BPINBO2). BPINAO2 and BPINBO2 generate nopinone reacting with NO (yield 76% for both), NO₃(yield 100% for both) and RO₂ (yields 70 and 60% respectively). BPINAO2 and BPINBO2 reaction with RO₂ give respectively 30 and 20% of 2-(hydroxymethyl)-6,6-dimethylbicyclo[3.1.1]heptan-2-ol (BPINAOH). BPINBO2+RO₂ produce also 20% of 2-hydroxy-6,6-dimethylbicyclo[3.1.1]heptane-2-carbaldehyde (C918CHO). BPINAOH oxidation by OH give 100% of C918CHO. BPINANO2 and BPINBO2 react with NO, producing the correspondent nitrate, respectively [2-(hydroxymethyl)-6,6-dimethylbicyclo[3.1.1]heptan-2-yl]azonic acid (BPINANO3) and [(2-hydroxy-6,6-dimethylbicyclo[3.1.1]heptan-2-yl)methyl]azonic acid (BPINBNO3). BPINANO3 and BPINBNO3 OH-oxidation products are respectively nopinone and C918CHO. The HO₂-oxidation of BPINANO2 and BPINBO2 produce 90% of (2-hydroperoxy-6,6-dimethylbicyclo[3.1.1]heptan-2-yl)methanol

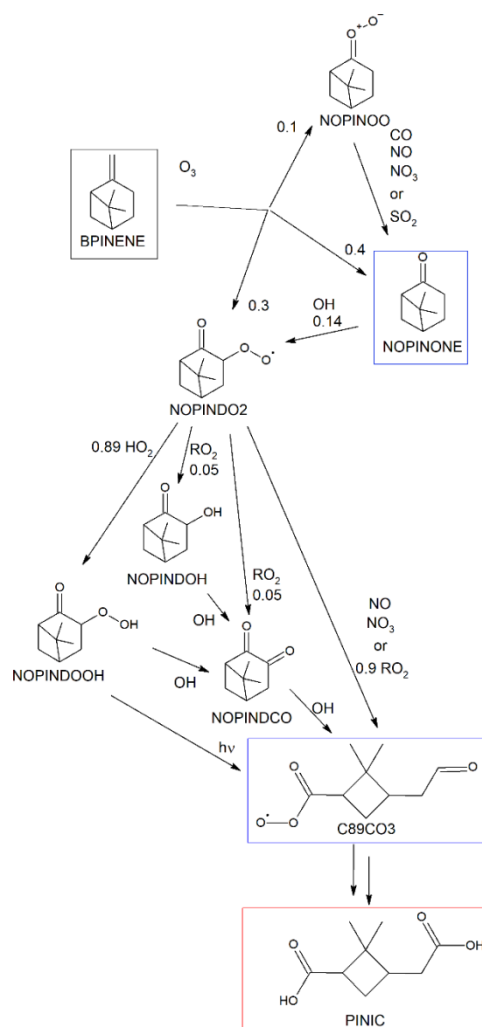


Figure 7. O_3 -initiated β -pinene photooxidation to nopinone and the successive oxidation steps to 2,2-dimethyl-3-(oxoacetyl)cyclobutane-1-carbaldehyde (C89CO3). The reactions of the mechanism not directly involved in the formation pathway are not shown.

The O_3 β -pinene photooxidation (Fig. 7) yields 10% of (2E)-2-(6,6-dimethylbicyclo[3.1.1]heptan-2-ylidene)dioxidan-2-ium-1-ide (NOPINOO), 40% of nopinone and 30% of (6,6-dimethyl-2-oxobicyclo[3.1.1]heptan-3-yl)dioxidanyl (NOPINDO2). NOPINOO is a precursor of nopinone (by reaction with CO, NO, NO_2 or SO_2). The reaction of nopinone with OH yields 14% of NOPINDO2. NOPINDO2 is a direct and indirect precursor of C89CO3. By reaction with NO, NO_3 and RO_2 (branching ratio 0.9), NOPINDO2 produces C89CO3. The other products of NOPINDO2+ RO_2 reaction are the 3-hydroxy-6,6-dimethylbicyclo[3.1.1]heptan-2-one and the 6,6-dimethylbicyclo[3.1.1]heptane-2,3-dione (respectively NOPINDOH and NOPINDCO, branching ratio is 0.05 for both). NOPINDO2 reacts with HO_2 leading to the formation of the 3-hydroperoxy-6,6-dimethylbicyclo[3.1.1]heptan-2-one (NOPINDOOH). C89CO3 is produced by NOPINDOH

and NOPINDOOH+OH and also from NOPINDOOH photolysis. The successive oxidation steps leading to pinic acid formation have been already commented at the beginning of this section and are illustrated in Fig.4. Pinic acid loss mechanism occurs via reaction with OH, as described in MCM.

Since no experimental value for PINIC subcooled vapor pressure and vaporization enthalpy has been found in literature, a semi-empiric estimation from experimental Booth et al., (2011) pinonic acid values has been performed to simulate the GPP. The P_{sat} and ΔH_{vap} estimated with this method are respectively 1.01×10^{-7} torr and 80 kJ mol^{-1} .

2.1.1.3 MBTCA

MBTCA is a so called “second generation” photooxidation product of α - and β -pinene. Müller et al., (2012) proposed a formation mechanism of MBTCA from pinonic acid (first generation photooxidation product) composed by 3 pathways. These pathways are started with H-abstraction by OH from pinonic acid C-4 (3.5%), C-5 (18%) and C-7 (0.8%) carbon atoms, named respectively pathways A, B and C. The overall MBTCA yields of the pathway A, B and C have been estimated by Müller et al., (2012) to be respectively 1.6, 0.0004 and 0.011. In our mechanism, only the pathways with higher yields, A and C, have been considered which are favoured by high NO_x conditions (Table S1).

In pathway A, the C-4 alkyl radical (R31) oxidation by NO leads to the opening of the aliphatic cycle with formation of a carboxyl (47%, R33). The successive step consists in a 1,5-shift (99%) and another NO-oxidation, with the production of the 2-(carboxymethyl)-4-hydroxy-3,3-dimethyl-5-oxohexanoyl (R35). R35 is oxidized by NO and after a 1,5 shift the 5,6-dicarboxy-3-hydroxy-4,4-dimethyl-2-oxohexan-3-yl radical is produced (R37). The last step to form MBTCA (yield 98%) involves NO and the loss of an acetyl.

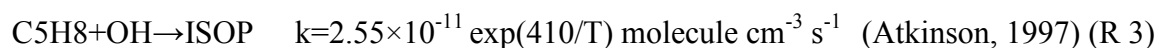
After the first reaction step with NO (which has {2-[3-(carboxymethyl)-2,2-dimethylcyclobutyl]-2-oxoethyl}oxidanyl radical (R11) as product), the pathway C is splitted in 2 sub-path, leading both to the formation of MBTCA. 98% of R11 is degraded, losing formaldehyde, into 3-(carboxymethyl)-2,2-dimethylcyclobutane-1-carbonyl radical (R12-path referred hereafter as C1) while the residual 2% undergoes 1,5 shift giving the 2-(carboxymethyl)-4-(hydroxyacetyl)-3,3-dimethylcyclobutyl radical (R1'2-path referred hereafter as C2). The path C1 progresses through 5 NO reaction steps, together with one decarboxylation and two 1,5 shifts, to produce MBTCA. In the C2 pathway, 4 reactions with NO take place, with two 1,5 shifts and a final loss of the hydroxyacetyl radical to form MBTCA.

According to experimental results from Aljawhary et al., (2016), MBTCA is also produced in the aqueous phase by pinonic acid reaction with OH, with a kinetic constant of $3.3 \times 10^9 \text{ M}^{-1} \text{ s}^{-1}$ and a maximum yield of 1%. The K_H ($2.28 \times 10^7 \text{ M}^{-1} \text{ atm}$) and ΔH_{sol} (81.68 kJ/mol) of pinonic acid have been calculated with SOAP, using the P_{sat} and ΔH_{vap} values reported in section 2.2.1 and in Table 1.

According to Aljawhary et al., (2016) MBTCA loss process in the aqueous phase occur by reaction with OH ($k=3.1 \times 10^8 \text{ M}^{-1} \text{ s}^{-1}$). The parameters to compute the transfer from the gaseous to the aqueous phase have been computed with SOAP ($K_H=1.37 \times 10^{14} \text{ M}^{-1} \text{ s}^{-1}$, $\Delta H_{\text{sol}}=145.21 \text{ kJ mol}^{-1}$) from the P_{sat} ($2.58 \times 10^{-10} \text{ torr}$) and ΔH_{vap} (135 kJ mol^{-1}) of MBTCA measured by Kostenidou et al., (2018).

2.1.2 Isoprene markers

Isoprene (C₅H₈) photooxidation is strongly dependent on the NO_x regime. The mechanisms have been developed following Couvidat et al., (2013) and using MELCHIOR2 (Derognat et al., 2003) as the base gaseous phase mechanism. The reaction with OH starts the oxidation process:



ISOP is the mixture of peroxy radicals produced from isoprene by H-abstraction and O₂ addition. The successive reactions of this species depend on the NO_x regime.

2.1.2.1 Methyltetrols

Methyltetrols have been identified as low NO_x isoprene markers. The major SOA formation pathway at low NO_x conditions occurs in the aqueous phase via methyl-epoxy-butanediols (IEPOX) hydrolysis (Surratt et al., 2010), and to a minor extent in the gaseous phase by reaction with RO₂ (Couvidat et al., 2013). In our model, the secondary compounds produced by IEPOX hydrolysis (methyltetrols and C₅-alkene triols) were already simulated as a single species, named BiMT. The parametrization used in this study for BiMT formation has been modified as explained below. Methyltetrol concentrations are then determined as 54% of BiMT (Rattanavaraha et al., 2016).

According to Couvidat et al. (2013), gaseous phase BiMT formation mechanism occurs via the following reaction:

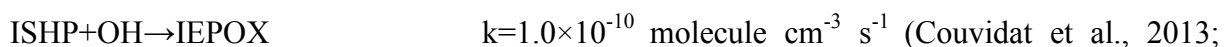


In which methacrolein (MACR), an α -methylglyceric acid precursor, is also produced.

A two step mechanism lead to IEPOX formation in the gas phase:



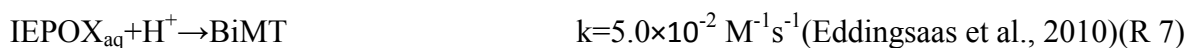
(Goliff et al., 2013) (R 5)



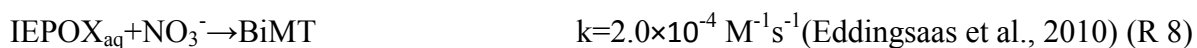
Goliff et al., 2013) (R 6)

Differently from Couvidat et al., (2013) we supposed an IEPOX yield of 100% for this last reaction, because of the high yields reported previously (Surratt et al., 2010). The oxidation mechanism of IEPOX in the aqueous phase is treated as in Couvidat et al., (2013). IEPOX K_H has been taken equal to $2 \times 10^7 \text{ M atm}^{-1}$, as the best estimated value in Couvidat et al., (2013), which is close to the Henry's law constant onto sea salts measured by Nguyen et al. (2014).

BiMT formation in cloud droplets and aerosol aqueous phase is catalyzed by acids:



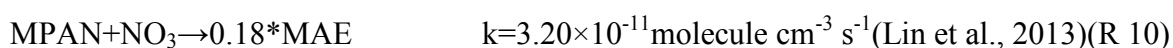
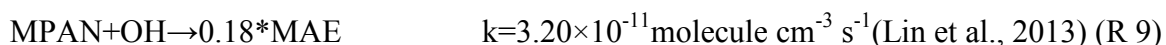
IEPOX_{aq} reacts also with nitrates and sulfates in aqueous solution, producing respectively organonitrates and sulfate esters (Darer et al., 2011; Eddingsaas et al., 2010). Although sulfate esters have been reported to be stable during the SOA average lifetime, organonitrates hydrolyse fast to methyltetrols (Darer et al., 2011). BiMT is therefore considered the product of the IEPOX reaction with nitrate:



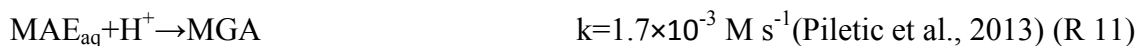
The competitive reaction with sulfates is reported in the supplementary material (Table S2). BiMT degradation process has not been considered due to lack of data. A semi-empiric P_{sat} and ΔH_{vap} have been calculated for methyl tetrols based on threitol values measured by Barone et al., (1990) (threitol $P_{\text{sat}} = 1.83 \times 10^{-7} \text{ torr}$ and $\Delta H_{\text{vap}} = 114 \text{ kJ mol}^{-1}$). The calculated methyl tetrols P_{sat} and ΔH_{vap} are respectively $1.94 \times 10^{-6} \text{ torr}$ and $106.4 \text{ kJ mol}^{-1}$.

2.1.2.2 α -methylglyceric acid

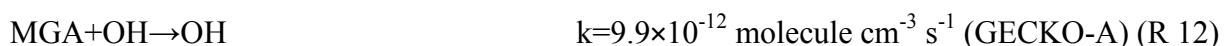
α -methylglyceric acid (MGA) is a marker for isoprene photooxidation under high- NO_x conditions (Surratt et al., 2010). MGA formation takes places via hydrolysis of the methacrylic acid epoxide (MAE) in the aqueous phase (Lin et al., 2013). MAE is a photooxidation product of peroxy methacryloynitrate (MPAN), generated in our model according to the MELCHIOR2 mechanism (Derognat et al., 2003). MAE has been added as product of MPAN OH- and NO_3 -initiated oxidation:



MAE partitioning between the gaseous and aqueous phases is assumed instantaneous and is computed with an Henry's law constant of $1.2 \times 10^5 \text{ M atm}^{-1}$. This value was estimated by Pye et al., (2013) by using Henry Win. As for IEPOX, MAE is hydrolysed in cloud droplets and aerosol water depending on pH:



The gaseous phase degradation of MAE by reaction with OH ($k = 1 \times 10^{-12} \text{ molecule cm}^{-3} \text{ s}^{-1}$ (Lin et al., 2013)) has been considered as competitive for the reaction R11. The degradation kinetic of MGA in the gaseous phase has been evaluated with GECKO-A:



Due to lack of data on thermodynamic properties of MAE, SIMPOL (Pankow and Asher, 2008) SARs estimations are used to estimate the values of P_{sat} and ΔH_{vap} (respectively of $1.4 \times 10^{-5} \text{ torr}$ and 91.7 kJ mol^{-1}).

3. Comparison measurements model

3.1 Configuration: model resolution and domain

The reference run for model to measurements comparison has been performed all over France (resolution $0.06^\circ \times 0.125^\circ$ longitude x latitude). Several runs on European domain (resolution $0.25^\circ \times 0.4^\circ$) have been performed to obtain boundary conditions and to perform sensitivity tests (for which European domain base run will be taken as reference). Nine vertical layers have been simulated till 500 hPa. Meteorological data from the operational analysis of the Integrated Forecasting System (IFS) were taken from the European Centre for Medium-Range Weather Forecasts (ECMWF). The sector-specific EMEP inventory (methodology described in Vestreng, 2003) has been used for annual anthropogenic emissions. Biogenic emissions have been computed with the Model of Emissions and Gases and Aerosol from Nature (MEGAN) 2.1 algorithm (Guenther et al., 2012). MEGAN simulates BVOCs emissions considering several parameters concerning the sources (such as the plant functional type (PFT) and the leaf area index (LAI)) and the meteorological data (for example T and the photosynthetically active radiation (PAR)). An example of MEGAN output for isoprene, α - and β -pinene is reported in Fig. 8.

Biogenic aerosols formation from isoprene, monoterpenes and sesquiterpenes is parametrized with the hydrophilic/hydrophobic organic (H^2O) aerosol model (Couvidat et al., 2012). In this mechanism the precursors are oxidized by OH, NO_3 and O_3 (under low NO_x and high

NO_x conditions) to give more oxidized and less volatile compounds, that are surrogates of biogenic secondary aerosols. Surrogate and marker GPP has been calculated with SOAP. A non-ideal configuration (taking into account interactions between organics and with inorganics) assuming thermodynamic equilibrium, in which both the hydrophilic and the hydrophobic partitioning has been evaluated, was chosen. Wet and dry deposition of particles in the reference run has been computed as in Couvidat et al., (2018) , using the method described by to Bessagnet et al., (2010) for dry deposition of organic vapors. The influence of dry and wet (in-cloud and the below-cloud scavenging) deposition of the gas-phase concentration has been tested separately.

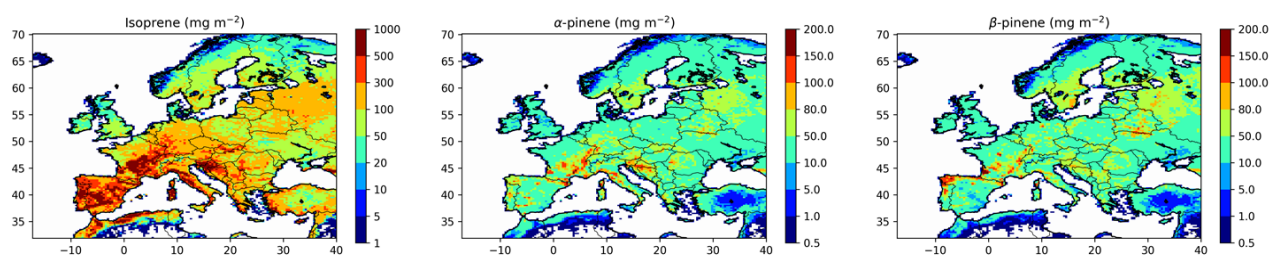


Figure 8. Biogenic emissions of isoprene, α - and β -pinene (mg m^{-2}) all over Europe computed with MEGAN 2.1 between 15/06/2015 and 15/07/2015.

3.2 Measurements: SIRTA

SOA marker simulations have been compared to a one-year (2015) campaign measurements performed 25 Km SW of Paris city center, at SIRTA facility (Site Instrumental de Recherche par Télédétection Atmosphérique, 2.15° E; 48.71° N). This site is surrounded by agricultural fields, highways and residential areas and can be considered representative of Paris region (Ile-de-France) which is the most populated area in France (Crippa et al., 2013; Petit et al., 2014, 2017; Sciare et al., 2011; Srivastava et al., 2018b). Both particle- (PM_{10}) and gas-phase samples have been collected every third day from the 19/11/2014 to the 15/12/2015, for 24h. 25 SOA markers have been quantified by GC/EI-MS after derivatization, using authentic standards. These samples were extensively characterized and all the measurements details are reported in Lanzafame et al., (2020). In this paper only the biogenic markers measurements will be shown with the aim of comparing to the model output.

4. Results and discussion

4.1 Model to measurement comparison

Table 2 shows measured and modelled annual median concentrations, 25th and 75th quartiles, and mean particulate phase fractions (F_p), together with correlation coefficients (r) and mean fractional bias (MFB) for the 5 biogenic SOA markers. Measured median total (gas + particle) concentration values are higher for all the markers by factors that seem independent of the precursors. The correlations between observations and simulations are low and exceed 0.3 only for α -methylglyceric acid.

Pinonic acid measured median concentration (2.12 ng m^{-3}) is 3 times higher than the modelled one (0.71 ng m^{-3}). Over the whole period, measured concentrations are higher and more dispersed than in the simulations, with measured and modelled interquartile ranges between $0.94\text{--}3.89$ and $0.43\text{--}2.25 \text{ ng m}^{-3}$, respectively. The correlation coefficient between simulated pinonic acid and measurements is low (0.28). MFB value is negative (-0.51), indicating that the model underestimates measurements. The model underestimate also the particulate phase fraction, with a simulated mean F_p of 0.12 against the observed value of 0.68.

Pinic acid modelled median concentration (0.011 ng m^{-3}) is 50 times lower than median measured concentration (0.51 ng m^{-3}). 25th and 75th percentiles are underestimated respectively by a factor 450 and 25 (interquartile ranges are $0.0005\text{--}0.043 \text{ ng m}^{-3}$ in simulations and $0.22\text{--}1.05 \text{ ng m}^{-3}$ in measurements). In agreement with the other underestimation indications, MFB has a high negative value (-1.68). Correlation coefficient is positive but low (0.22). GPP is misrepresented: in simulations pinic acid is quite volatile, being only at 37% in the particulate phase, while in measurements is almost completely in the particulate phase (94%).

MBTCA concentrations and variability are underestimated by the model. The median concentration in the simulation is 0.14 ng m^{-3} and the interquartile range is equal to 0.192 ng m^{-3} , median measured concentration and interquartile range are 4.5 times higher (median 0.64 ng m^{-3} , interquartile range 0.88 ng m^{-3}). The correlation coefficient is low (0.2) and MFB value is close to -1. Partitioning is well represented in the model, in which MBTCA is completely in particulate phase, as in measurements, which is coherent with the low saturation vapor pressure (2.58×10^{-10} torr) used in this study.

For methyltetrols measured (1.47 ng m^{-3}) and modelled (0.76 ng m^{-3}) median concentrations differ by a factor 2. The simulated 25th interquartile (0.14 ng m^{-3}) is underestimated compared

to measurements (0.79 ng m^{-3}) by a factor higher than 5, while the gap between 75th quartiles is only of 22% (modelled and measured values are respectively 3.05 and 3.72 ng m^{-3}). Correlation is positive but low (0.28) and not significant, MFB has been calculated to be -0.59 . The simulated particulate phase fraction is 0.56 , 15% lower than the measured one of 0.64 .

The marker with the strongest underestimation in this study is α -methylglyceric acid. The modelled median and quartiles (median 0.20 ng m^{-3} , 25th and 75th quartiles are respectively 0.03 and 0.71 ng m^{-3}) differ from measured values (median 0.0018 ng m^{-3} , 25th and 75th quartiles are respectively 0.0003 and 0.0052 ng m^{-3}) by a factor higher than 100 and MFB is equal to -1.77 . However, α -methylglyceric acid simulation has the highest, though not significant, correlation with measurements observed in this paper (0.32). In measurements α -methylglyceric acid is less volatile, with a mean particulate phase fraction of 0.89 while the simulated value is lower (0.54).

The significant underestimation can be due to a precursor emission underestimation, a wrong representation of the marker formation pathways and a wrong estimation of radical concentrations. An analysis of markers temporal variability at different atmospheric conditions is required in order to understand to which extent every process can influence marker formation. Moreover, the gas to particle partitioning is strongly underestimated for pinonic acid, pinic acid, α -methylglyceric acid that may be due to an overestimation of the saturation vapor pressure.

Table 2. Model to measurement comparison for 5 SOA markers at SIRTA, from 19/11/2014 to 15/12/2015. Measured and modelled median concentration, 25th and 75th percentiles and mean particulate phase fraction (F_p) are shown, together with the correlation (r , $p < 0.01$) and the mean fractional bias (NFB) between the 2 time series.

	Measured		Modelled		R	MFB
	Median (25 th –75 th quartiles) concentration (ng m^{-3})	Mean F_p	Median (25 th –75 th quartiles) concentration (ng m^{-3})	Mean F_p		
Pinonic acid	2.12 (0.94–3.89)	0.68	0.71 (0.43–2.25)	0.12	0.28	-0.51
Pinic acid	0.51 (0.22–1.05)	0.94	0.011 (0.0005–0.043)	0.37	0.22	-1.68
MBTCA	0.65 (0.31–1.19)	0.99	0.14 (0.088–0.28)	0.99	0.20	-0.99

Methyltetrols	1.47 (0.79–3.72)	0.64	0.76 (0.14–3.05)	0.56	0.28	-0.59
α -methylglyceric acid	0.20 (0.03–0.71)	0.89	0.0018 (0.0003–0.0052)	0.54	0.32	-1.77

4.1.1 α -/ β -pinene marker temporal variations

Model to measurements annual comparison (gas+particle phase) for pinic acid, pinonic acid and MBTCA are shown in Fig.9. Each marker is underestimated by a different factor and the temporal variations are not well represented. However, the model to measurements comparison for pinene marker is not straightforward, since no clear annual evolution has been observed in measurements (Lanzafame et al., 2020).

The concentrations simulated for pinic acid are below 0.1 ng m^{-3} for most of the year, except for some peak observed between May and August. On the opposite, measured concentrations are normally above 0.1 ng m^{-3} , except for most of winter and the beginning of spring, and several peaks have been observed throughout the year. The maximal concentration have been simulated in summer (02/07), with a value around 5 ng m^{-3} , while the maximum measured value (7.75 ng m^{-3}) has been observed in April (26/04). The overall underestimation is lower in summer (from May to August, MFB -1.2) than in winter (MFB -1.9). The model is not able to reproduce the moderate concentrations (between 0.002 and 3.5 ng m^{-3}) measured from September to the end of the year.

Although the highest simulated pinonic acid concentration (22.5 ng m^{-3} , 29/08) is higher than the measured one (11 ng m^{-3} , 13/10), the model output is lower than measurements for most of 2015. The low pinonic acid measured concentrations at the beginning of the year (January–April) are slightly underestimated (MFB -0.2) by the model. In the rest of the year, the peak concentrations are higher than measurements, while the lower concentrations are underestimated. The average MFB calculated from May to December is around -0.7. Only for this marker, model and measurements variations partially match from May to August.

MBTCA measured average summer (May–August) concentration (1.2 ng m^{-3}) is lower than the winter average (0.7 ng m^{-3}), while simulated concentrations have an average of 0.2 ng m^{-3} both during the warmer and the colder period. MFB value is close to -1 throughout the year. The maximal measured concentration is 10 times higher than the simulated maximum (respectively 10.3 ng m^{-3} on 03/11 and 1 ng m^{-3} on 10/10). Peak concentrations are scarcely reproduced and the increase of concentrations at the end of the year is not reproduced by the model.

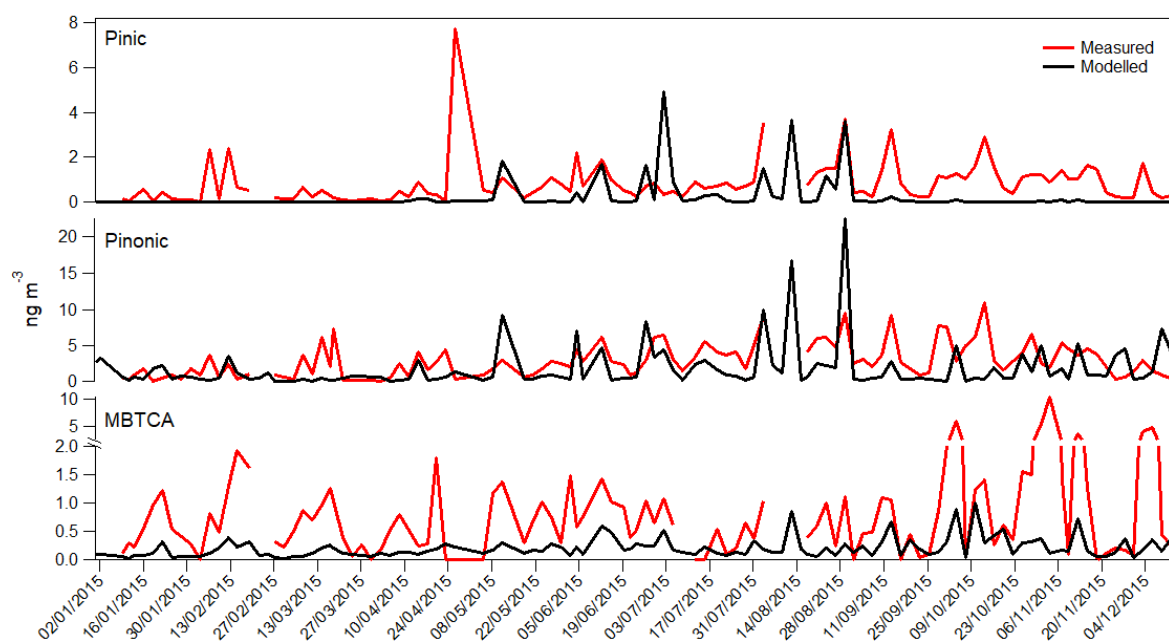


Figure 9. α - and β -pinene markers model to measurements comparison during 2015 at SIRTa, France. Measurements have been compared to model output on French domain.

4.1.2 Isoprene marker temporal variations

Modelled and measured isoprene marker concentrations (gas+particle phase) are shown in Fig. 10. Higher concentrations have been observed for both methyltetrols and α -methylglyceric acid in the warmer periods (Lanzafame et al., 2020).

Methyltetrols are represented in the model with the right magnitude order. The model simulates well the overall annual trend, with an increase of concentrations in summer. However, mean concentrations for the colder period is underestimated by a factor 2 (measured and modelled mean are respectively 1.4 and 0.7 ng m^{-3}) and the summertime simulated mean (14.5 ng m^{-3}) is 1.5 times higher than in measurements (9.9 ng m^{-3}). The mean simulated concentrations calculated for the warmer period are biased from the maximum (175 ng m^{-3}) simulated on 02/07. This anomalous concentration is due to the high isoprene emissions generated in the south of France and in Germany (Fig. S1), in which temperature in those days (from 29/06 to 03/07) is higher than in the rest of the year. According to Guenther et al. (2006), biogenic emissions depend on hydrological stress and no biogenic emissions are possible when the soil moisture is below the wilting point). However, in the MEGAN version inserted in CHIMERE, the soil moisture effect on biogenic emissions is not considered. The volumetric soil water content (θ) over this period is around 0.157 $\text{m}^3 \text{m}^{-3}$

³ at SIRTA whereas the wilting point (θ_m) is equal to $0.166 \text{ m}^3 \text{ m}^{-3}$ (Fig. S2). In these conditions ($\theta_m < \theta < \theta_m + 0.06$) biogenic emissions are reduced by a factor ranged between 0 and 1 (Guenther et al., 2006). For this reason, CHIMERE likely overestimates strongly the emissions over this period, explaining why the 02/07 peak has not been observed in measurements and the maximum has been rather measured on 15/07 (47 ng m^{-3}). MFB mean value is quite low in summer (-0.2, from May to August) and higher in winter (-0.76) where the concentrations are very low (under 6 ng m^{-3}).

α -methylglyceric acid is underestimated in the model by a factor 10^2 . Simulated concentrations are higher in summer than in winter, with a similar seasonal trend with measurements. The maximal simulated concentration is 40 pg m^{-3} (on 12/06), while the maximal measured concentration is 3.3 ng m^{-3} (on 23/08). The reason for this high underestimation may be linked to the parameters used to simulate α -methylglyceric acid formation in the aqueous phase from MAE. To quantify the influence of the parameters used for aqueous phase MAE oxidation on total α -methylglyceric acid concentrations, MAE Henry's law constant has been taken higher by a factor 10 ($K_H = 1.2 \times 10^6 \text{ kJ mol}^{-1}$) and its kinetic constant has been increased to the same value used for IEPOX oxidation, as in Pye et al., (2013). This test was performed from the 15/06 and the 15/07. We noticed an increase by a factor 190 of α -methylglyceric acid simulated concentrations at SIRTA, and an increment of the European maximum by a factor 10^2 (Fig. S3). This new parametrization brings α -methylglyceric acid concentrations to the same order of magnitude of the measured ones, leading to an overestimation by a factor 2 at SIRTA. These results fit better the measurements than the ones in the reference run, nevertheless they are still not sufficiently accurate. The choice of both Henry's law and aqueous phase kinetic constants must be considered critical for a good representation of α -methylglyceric acid formation in the aerosol phase and more experimental values should be provided to reach a more accurate result.

The model succeeds in representing the seasonal variations observed for biogenic markers, with no definite annual trend for pinene markers and higher isoprene marker concentrations in summer. The underestimation of simulated markers can depend from different factors, such as the radical concentration estimation and the OM mass and composition in the model. The next section is dedicated to a sensitivity analysis of marker formation towards radicals concentrations change.

Model to measurements comparison for OM at SIRTA during 2015 is reported in Fig. S4. OM is well represented in the first part of the year (January to April) and underestimated by a

factor ~ 5 for the rest of the year (May to December). This gap may play a decisive role on GPP estimation, especially for biogenic markers, which concentrations are expected to be higher in summer (e.g. α -methylglyceric acid). According to Pankow, (1994), the ratio between particulate and gaseous phase concentrations is directly proportional to OM, which means that OM underestimation lead to an underestimation of the particulate phase fraction and potentially of the total marker concentrations. The influence of GPP on total marker concentrations is discussed in section 4.3.

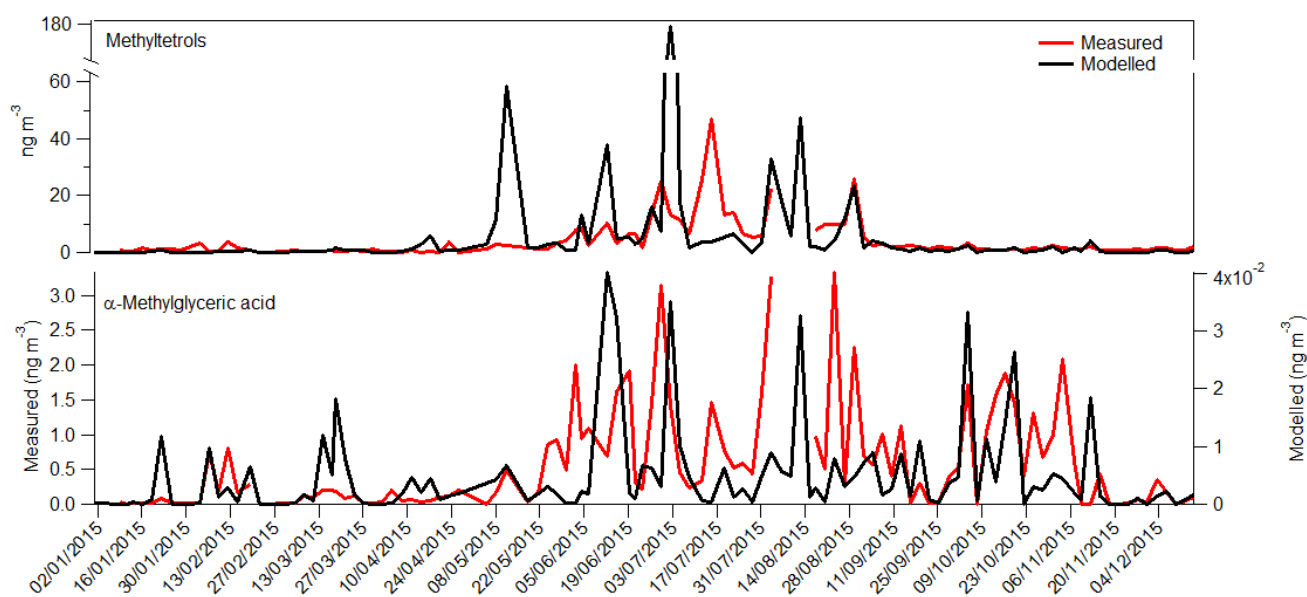


Figure 10. Isoprene markers model to measurements comparison during 2015 at SIRTA, France. The model output shown is from simulations performed on French domain.

4.2 Influence of chemical regime on total marker concentrations

As already reported in the model development section, very detailed mechanisms have been inserted in CHIMERE to simulate marker formation with many reaction steps depending on radical concentrations. Some compounds may be very sensitive to the chemical regime (low- NO_x or high- NO_x conditions). Moreover, different gas-phase mechanism may simulate very different radical concentrations (Kim et al., 2009, 2011; Sarwar et al., 2013). It is therefore important to test the robustness of this novel approach. For this purpose, the sensitivity to radical concentration has been tested to determine if the results may change significantly with different radical concentrations. Sensitivity to radical concentrations on marker formation has been tested dividing and multiplying the kinetic constants of the reactions involved in the marker formation with NO , HO_2 and RO_2 by a factor 2 in 8 different simulations. This is

equivalent to multiply and divide the concentrations of the radicals involved by a factor 2. The tests have been performed in the European domain over 3 months, February, mid-June to mid-July and October, chosen to be the most representative in terms of weather conditions and emissions. The sensitivity tests results, compared to the reference run, at SIRTA are presented.

4.2.1 α -/ β -pinene markers

Pinic acid sensitivity tests to radical concentrations are shown in Fig S5. Pinic acid formation seems strictly dependent on NO_x regime and RO_2 concentration. In “double NO” simulation, pinic acid concentrations decrease by 40%, while they do not vary in “half NO” simulation. In parallel, pinic acid concentrations respectively increase by ~30% and decrease by ~20% in the “double HO_2 ” and “half HO_2 ” runs. These results indicates that pinic acid in the model is favoured by low- NO_x conditions, as already observed by Eddingsaas et al., (2010). This result is coherent with the mechanism of pinic acid formation shown in Fig. 4, where low- NO_x conditions are needed for the formation of carboxylic acid functional groups.

In the “half RO_2 ” test pinic acid formation decrease of 33% and increase of 57% in the “double RO_2 ” test. We can conclude that, according to the reaction scheme used, pinic acid formation is enhanced at low NO_x regimes, being RO_2 and HO_2 the principal oxidants involved. However, high incertitudes have to be attributed to HO_2 concentrations, that in may be underestimated by the model by 50% (Ma et al., 2019).

In Fig. 11 the outputs of pinonic acid sensitivity analysis to radical concentrations is reported. Pinonic acid concentrations are scarcely affected by the NO_x regime and the variations observed in the “double NO”, “half NO”, “double HO_2 ” and “half HO_2 ” simulations are always below 10%. Low variations have been observed also in the “half RO_2 ” and “double RO_2 ” simulations, in which pinonic acid concentrations decrease and increase respectively of 14% and of 19%. However, the concentration variation effect seems not completely omogeneous for this radical and test concentrations are not perfectly linear compared to reference.

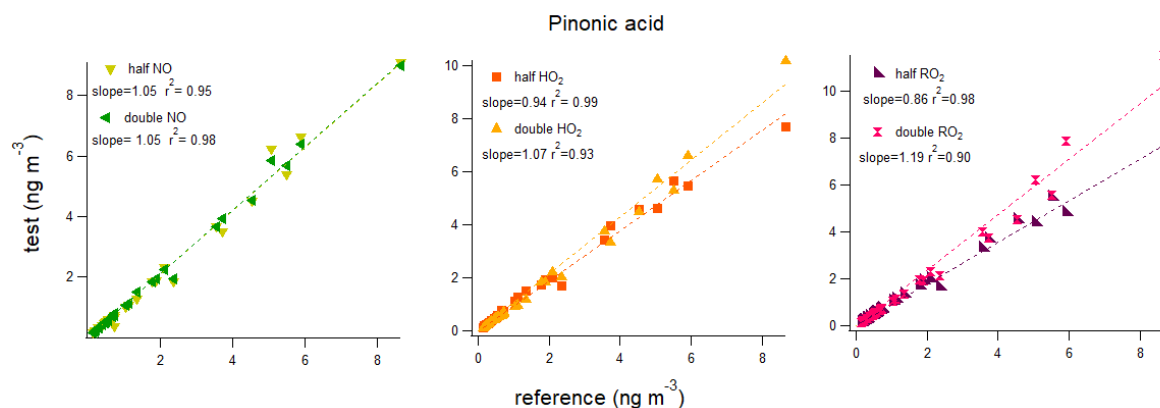


Figure 11. Pinonic acid formation sensitivity to radical concentrations. Reference and test runs have been performed on European domain. The results shown are the mean daily concentrations at SIRTA, during February, mid-June to mid-July and October.

MBTCA concentrations at SIRTA are scarcely sensitive to NO, HO₂ and RO₂ variations (Fig. S6). Whereas the formation of MBTCA should be favoured by high NO_x conditions, the competition between NO and HO₂ in the oxidation process scarcely affect MBTCA concentrations in the model. This is due to the fact that MBTCA is formed almost entirely (around 80%) by the aqueous-phase oxidation of the pinonic acid in the model (for which no dependence on NO_x concentrations was taken into account).

4.2.2 Isoprene markers

Isoprene markers sensitivity tests to radical concentrations have been reported in Fig. S7 for methyltetrols and in Fig S8 for α -methylglyceric acid. As already underlined in the method development section, the relative concentrations of these markers are expected to be strictly dependent on the NO_x regime.

In the “half NO” simulation methyltetrols concentrations slightly increased (4% of variation) while in the “double NO” run methyltetrols concentrations decrease of 36%. On the other hand, methyltetrols concentrations respectively increase (by 38%) and decrease (by 34%) in the “double HO₂” and in the “half HO₂” runs. These results are consistent with the fact that methyltetrols are low NO_x regime markers (Surratt et al., 2010). α -methylglyceric acid variations with the NO_x regime are opposite compared to methyltetrols variations but remain low (below 10%). For both marker no sensitivity to NO₃ and RO₂ concentrations has been observed.

4.3 Pinonic acid formation process: spatial and daily variability

Pinonic acid is produced by α -pinene atmospheric degradation, initiated by 3 competitive reaction with OH, NO₃ and O₃ as oxidant (see section 2.2.1). According to the local radical concentrations, the degradation may be dominated by the reaction with one of oxidant. However, it should not be assumed that the final amount of pinonic acid produced by each pathway depend only from the α -pinene oxidation initiation reaction. The fractional oxidation initiation rates (fraction of α -pinene reacting with the considered oxidant) of α -pinene with OH, NO₃ and O₃ over Europe are shown in Fig. 12, together with pinonic acid fractional amount (amount of pinonic acid produced by the reaction with one of the oxidants divided by total pinonic acid concentrations) from the 3 pathways. From the comparison between the fractional oxidation initiation rates and pinonic acid fractional amount we can deduce that:

- Although NO₃ fractional reaction rate predominate over OH and O₃ reaction rates in central Europe, the pinonic acid fractions produced by this pathway is the lowest.
- A large part of pinonic acid (20% to 50%) is formed by the OH initiated pathway.
- O₃ initiated pathways dominates pinonic acid formation in the Scandinavian peninsula (where O₃ is the main oxidant of α -pinene), Ireland (but with very low simulated concentrations of pinonic acid) and in several areas with strong biogenic emissions (like Southern France, Portugal or the Balkans)and UK. A high fraction was expected for the Scandinavian peninsula in which the O₃ initiation rate is high.

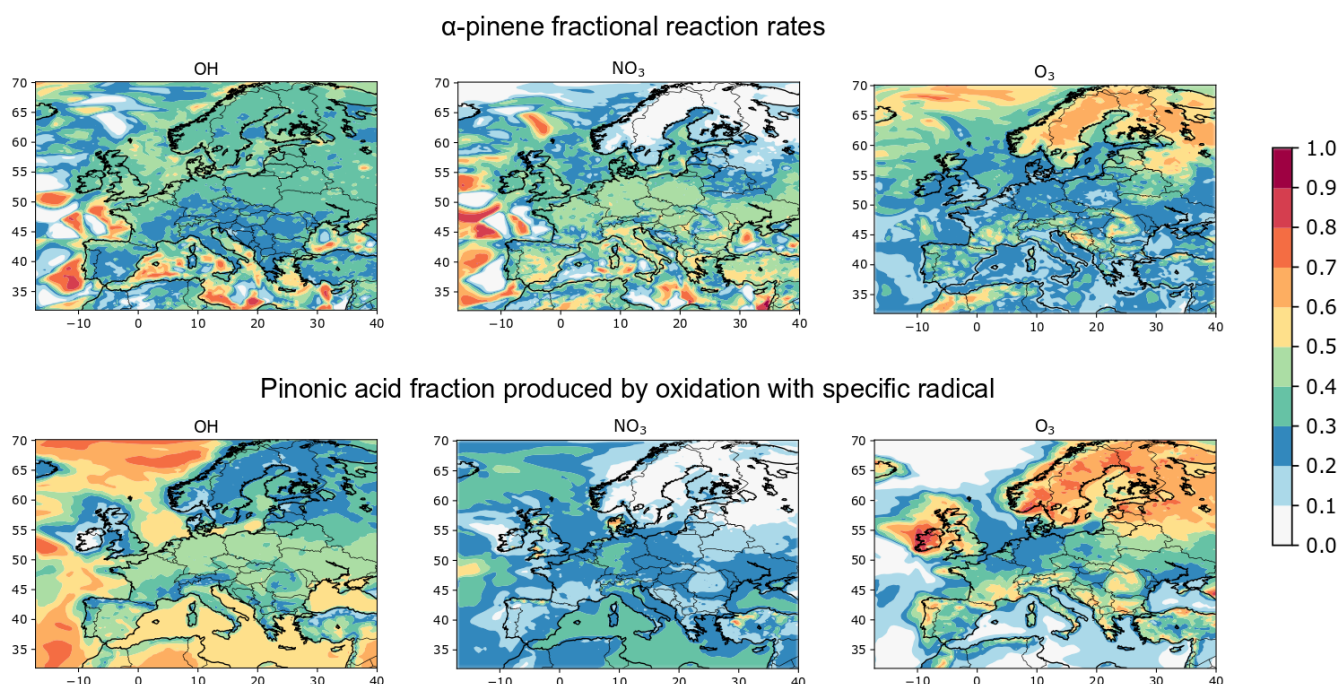


Figure 12. Spatial distribution of α -pinene fractional reaction rate (on the top) for the reactions with OH, NO₃ and O₃ (respectively left, middle and right panels) over Europe. On

the bottom the spatial distribution of pinonic acid fractions produced respectively from left to right by OH-, NO₃- and O₃-initiated oxidation pathways.

To understand why pinonic acid formation by the NO₃ initiated pathway is a minor contributor of pinonic acid formation, the processes influencing pinonic acid formation have been further investigated. In Fig. 13, the daily variations of α -pinene, pinonaldehyde and pinonic acid concentrations, together with production and degradation rates of the principal species involved in pinonic acid formation, are presented. The results shown are averaged all over Europe and integrated on all the altitude level of the model, for the period included between the 15/06 and the 15/07/2015.

Pinonic acid vertically integrated concentrations are slightly above 3 $\mu\text{g m}^{-2}$ in the nighttime and decrease below 1 $\mu\text{g m}^{-3}$ during the daytime. α -pinene and pinonaldehyde vary daily as pinonic acid: higher concentrations (~ 70 and $\sim 90 \mu\text{g m}^{-2}$ respectively) have been simulated before 4:00 UTC and after 21:00 UTC and lower concentrations (minimum ~ 25 and $\sim 10 \mu\text{g m}^{-2}$ respectively) in the rest of the day. The nighttime α -pinene degradation, that occurs mainly by reaction with NO₃ (rate $\sim 7 \text{ ng m}^{-2} \text{ s}^{-1}$), is the predominant process of pinonaldehyde formation, as previously reported (Calogirou et al., 1999). In the daytime, α -pinene+NO₃ reaction rate is very low ($0.5 \text{ ng m}^{-2} \text{ s}^{-1}$) and α -pinene reaction with OH is the main degradation process (maximal rate $\sim 5 \text{ ng m}^{-2} \text{ s}^{-1}$). The α -pinene+O₃ reaction rate has a lower diurnal vary less between night and day, with a minimum around 7:00 UTC ($2 \text{ ng m}^{-2} \text{ s}^{-1}$) and maximum around 21:00 UTC ($4 \text{ ng m}^{-2} \text{ s}^{-1}$). In the gas-phase, pinonaldehyde is quickly degraded by OH in the first hours of the day (peak rate of $\sim 4 \text{ ng m}^{-2} \text{ s}^{-1}$ at 5 UTC), while the oxidation rate with NO₃ as oxidant is always neglectable.

However, pinonic acid formation from pinonaldehyde in the gaseous phase requires several oxidation steps and these processes are not indicative of the total pinonic acid formation yield. The processes directly involved in pinonic acid formation are shown in Fig. 13c. APINBOO, C96CO3 and pinonaldehyde (via aqueous phase reactions) are pinonic acid direct precursors (see section 2.2.1). APINBOO reaction rate with H₂O is almost constant during all the day, keeping a value around $0.1 \text{ ng m}^{-2} \text{ s}^{-1}$. C96CO3 reactions with HO₂ and RO₂ are faster during daytime (from 7:00 to 18:00 UTC), with a peak rate of $0.2 \text{ ng m}^{-2} \text{ s}^{-1}$ at 12 UTC. This is the major pinonic acid production process. The pinonaldehyde reaction with OH in the aqueous phase is the second process for pinonic acid yield, with a peak rate of $0.15 \text{ ng m}^{-2} \text{ s}^{-1}$ at 3:00 UTC. This rate is low during most of the day and correspond to the maximal pinonic acid degradation rate ($0.2 \text{ ng m}^{-2} \text{ s}^{-1}$), occurring by aqueous phase reaction with OH at the same

time of the day. The other processes (pinonaldehyde+NO₃ in the aqueous phase and pinonic acid degradation by OH in the gas-phase) rates are negligible compared to the rates already commented.

The courbe gathering all these processes has a minimum at 4:00 UTC (rate next to 0) and a maximum around 12:00 UTC. Pinonic acid is produced mostly during the daytime, between 9:00 and 18:00 UTC, in which the major process is the C96CO3 oxidation. However, pinonic acid formation from APINBOO (radical formed from α -pinene+O₃) dominates pinonic acid after 18:00 UTC for a large part of the night. In the first hours of the morning, aqueous phase reactions become dominant and the total balance between production and degradation in the aqueous phase is negative, part of the pinonic acid produced in the gaseous phase is degraded together with the pinonic acid produced in the aqueous phase. Due to the aqueous phase degradation, pinonic acid concentrations decrease sharply between 3:00 to 9:00 UTC, and start to increase after, when the gaseous phase processes are predominant.

Therefore, the high O₃-pinonic acid fractional yield shown in Fig. 12 are explained by the low sensitivity to the daily variations of pinonic acid production rate from APINBOO compared to the other processes. The NO₃ initiated pathway only produces low concentrations of pinonic acid because during nighttime pinonaldehyde oxidation is very low while the accumulated pinonaldehyde during the night is fastly oxidized by aqueous-phase reactions. However, the pinonic acid formed by the aqueous phase reacts rapidly and is destroyed. During the day, most of the pinonic acid is formed by the OH initiated pathway.

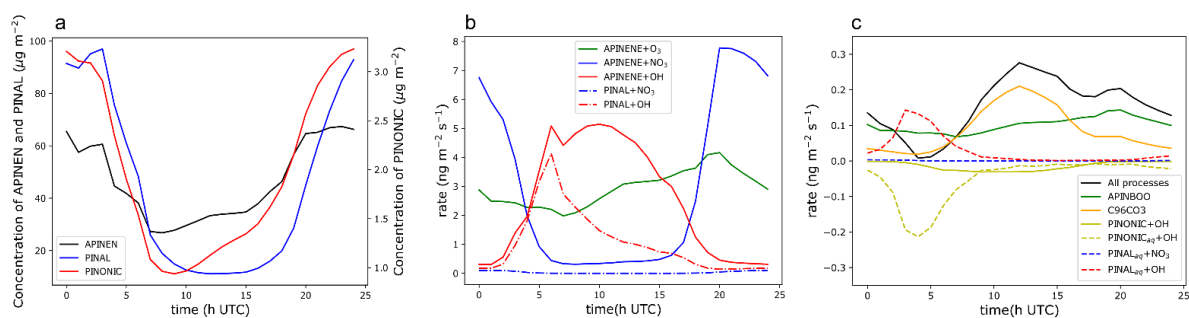


Figure 13. Mean daily variations of (a) α -pinene, pinonaldehyde and pinonic acid concentrations ($\mu\text{g m}^{-2}$); (b) α -pinene+O₃, α -pinene+NO₃, α -pinene+OH, pinonaldehyde+NO₃ and pinonaldehyde+OH rates ($\text{ng m}^{-2} \text{s}^{-1}$); (c) APINBOO, C96CO3, pinonic acid+OH or NO₃(both in gaseous and aqueous phase) degradation rates ($\text{ng m}^{-2} \text{s}^{-1}$). All the results shown are the mean of European domain, integrated over all the atmospheric levels (till 500 hPa), simulated from 15/06 to 15/07/2019.

4.4 GPP estimations at SIRTA

4.4.1 Model to measurements comparison: a focus on thermodynamics.

The sensitivity analysis on marker GPP at SIRTA is presented in Fig. 14. The tests have been performed to understand the contribution of hydrophobic and hydrophilic partitioning to the reference GPP in ideal and non-ideal aerosol. Pinonic acid, pinic acid, MBTCA, methyltetrols and α -methylglyceric acid GPP has been examined considering both hydrophobic and hydrophilic partitioning on ideal aerosol (“ideal” simulation), only hydrophobic or only hydrophilic partitioning on non-ideal aerosol (abbreviated in the figures as “hypho” and “hyphi”) and on ideal aerosol (abbr. “hypho ideal” and “hyphi ideal”). The test simulations have been performed during February, mid-June to mid-July and October. Together with the tests outputs, measurements and “reference” run (sum of hydrophobic and hydrophilic partitioning on the non-ideal aerosol) particulate phase fractions (F_p) at SIRTA (calculated for the tested periods) are presented.

Measure pinonic acid F_p median value is around 0.82 and half of the values are ranged between 0.47 (25th) and 0.97 (75th percentiles). On the opposite, the simulated pinonic acid partitioning is shifted towards the gaseous phase in all the simulations. In the “reference” simulation, 90% of the calculated F_p are below 0.44, with a median value of 0.05. Pinonic acid partitioning is mainly hydrophobic and assuming ideality lead to a slight increase of F_p values that cannot explain the high F_p values observed in measurements. Incertitudes in the calculation of activity coefficients and the significant underestimation (by a factor 5 in summer) of the organic aerosol concentrations probably contribute to the F_p underestimation, but cannot fully explain the discrepancies between observed and simulated F_p .

In the observations, pinic acid partition scarcely between the 2 phases, being almost completely in the particulate phase (median, 25th and 75th percentiles are respectively 0.98, 0.95 and 0.99). On the contrary, in simulations, pinic acid is always semivolatile. In the “reference” run the median F_p value is 0.66. The change in volatility is quite wide, being the 25th and the 75th percentiles respectively 0.33 and 0.88 (interquartile range 0.55). Pinic acid is mainly hydrophobic except when ideality is assumed (similar median F_p are obtained in the “hydrophilic” and “hydrophobic” simulations). Higher F_p are obtained when assuming ideality (median F_p of 0.9).

MBTCA is almost completely in the particulate phase in the measurements and the simulations (minimum 10th percentile F_p 0.96). In measurements, 100% of MBTCA is in the particulate phase, with no variability. the median F_p are above 0.99 for all the simulations.

The model was able to reproduce the partitioning of methyltetrols. Methyl tetrols are semivolatile both in measurements and in the “reference” run, with median F_p values respectively of 0.65 and 0.63. F_p distribution is also similar: for measurements and reference 25th percentiles are respectively 0.29 and 0.20, 75th percentiles are 0.99 and 0.95. Interquartile range is slightly higher for “reference” (0.75) compared to the “obs” (0.70). Taking only into account the hydrophobic partitioning, methyltetrols are totally in the gaseous phase, with a F_p 75th percentile of 0.02 (median of 0.003). Assuming an ideal partitioning would lead to an overestimation of F_p values (median F_p of 0.98 for the ideal simulation).

In measurements α -methylglyceric acid has low volatility, having 75% of their F_p higher than 0.71 (25th percentile). Median measured F_p is 0.91 and the interquartile range is quite narrow (0.26). In the “reference” run, α -methylglyceric acid has a median F_p of 0.60 and 50% of F_p values are between 0.24 and 0.92 (respectively 25th and 75th quartiles). A great variability is associated with this simulation (interquartile range 0.68). As for methyltetrols, only taking into account the hydrophobic partitioning, would lead to almost all the α -methylglyceric acid in the gaseous phase, with a F_p 75th percentile of 0.02 (median of 0.003). Assuming an ideal partitioning lead to F_p similar with the measurements (median F_p 0.91) except for the lower 25th quartile value (0.50).

GPP is underestimated for most of the markers, excluded MBTCA and methyltetrols. Great incoherence in GPP computation is related to the choice of the marker thermodynamic parameters (e.g. P_{sat} , K_H). The value chosen for α -methylglyceric acid was very uncertain as it was calculated with the SIMPOL (Pankow and Asher, 2008) SARs estimations whereas P_{sat} (of the marker or a similar molecule) from measurements was used for the other compounds. P_{sat} value available in the literature could also be very uncertain. Moreover for pinic and pinonic acids, which are mainly hydrophobic, the underestimation of OM may lead to a significant underestimation of the simulated particulate phase fraction.

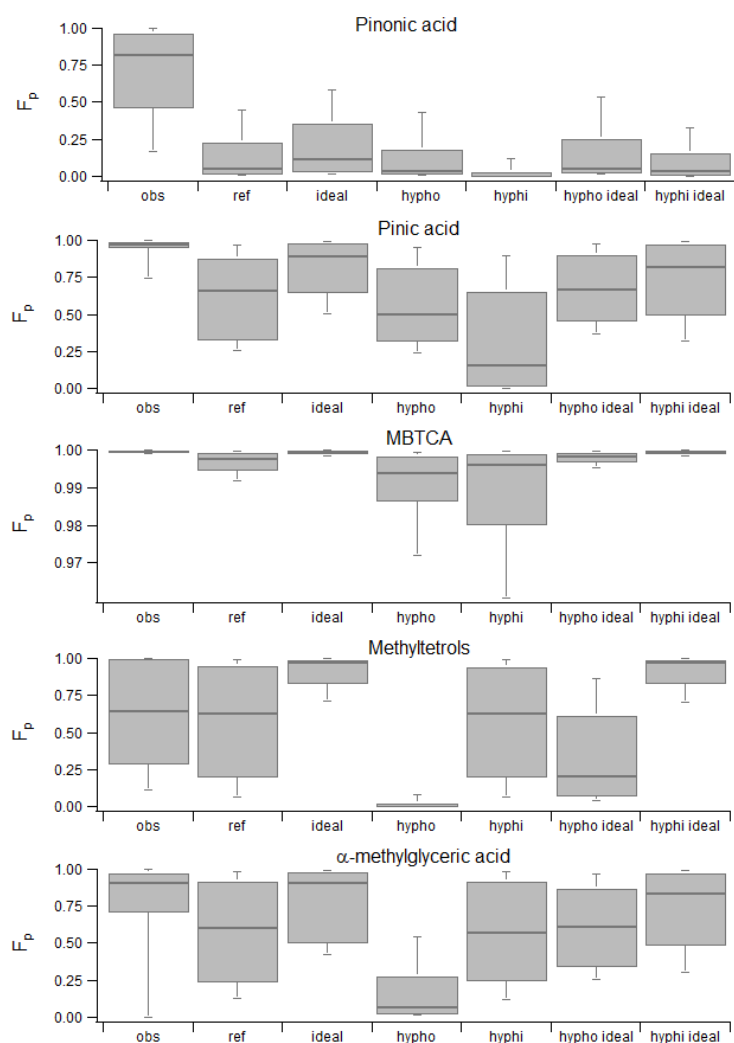


Figure 14. Particulate phase fraction (F_p) thermodynamic sensitivity for (from the top to the bottom): pinonic acid, pinic acid, MBTCA, methyltetrols and α -methylglyceric acid at SIRTA. The boxes represent from left to right: measurements (obs), reference (ref), ideal aerosol (ideal), hydrophobic (hypho) and hydrophilic (hyphi) partitioning in non-ideal aerosol, hydrophobic (hypho ideal) and hydrophilic (hyphi ideal) partitioning in ideal aerosol. The tests have been performed during 3 months: February, mid June–mid July and October. The measurements data shown for the comparison have been taken from the same period.

4.4.2 Influence of partitioning and gas-phase dry deposition on total marker concentrations

Several multiphase processes are involved in the formation and degradation mechanisms of the simulated markers. As a consequence, the GPP may affect the simulated concentrations, condensation in the particle phase can for example protect the molecule from its gas-phase degradation. To quantify the GPP influence on marker concentrations some tests have been performed assuming: (1) completely volatile markers, (2) completely non-volatile markers. A

third test was also performed to evaluate the potential effect of the dry and wet deposition of gas-phase markers. The outputs at SIRTA of “volatile”, “non-volatile” and “deposition” simulations have been compared with the “reference” run, in which markers are semivolatile (according to their P_{sat}) and only particulate phase deposition has been considered (Fig. 15). The sensitivity tests have been performed during February, mid-June to mid-July and October. The tests are not performed for MBTCA for which the non-volatility was reproduced and because in the “non-volatile” simulation MBTCA formation would be prevented. The effect of the tests on concentrations at SIRTA are shown.

Pinonic and pinic acid are less volatile in measurements (median F_p respectively 0.82 and 0.98) than in the “reference” run (median F_p respectively 0.05 and 0.66). The gap observed in comparison with the “reference” for pinonic acid and pinic acid for the “volatile” (respectively -12% and -45%) and the “non-volatile” (increase by a factor 4.5 and 2.15) simulations suggests a protective effect from degradation of the condensation onto the particle phase. For both markers the principal loss mechanism is the gas-phase oxidation by OH, for which average half lives in the tested periods (considering the simulated OH concentrations) have been evaluated to be respectively $\sim 3 \text{ d}^{-1}$ and 2.8 d^{-1} for pinonic and pinic acid. These marker half-lives are considerably shorter than the average particle half-life of 1 week for particles (Seinfeld, 2015). This result suggests that simulated total concentrations could be significantly higher and could explain the gap between measurements and observations.

As the CHIMERE species BiMT (representing methyltetrols and other IEPOX derived SOA) was already present in the model, methyltetrols are the only markers for which gas-phase deposition has been already considered in the “reference”. “Volatile” methyltetrols concentrations decrease by 63% while “non-volatile” methyltetrols concentrations increase by 61%. Since no degradation mechanism has been inserted for methyltetrols in the model, the only degradation process for methyltetrols is deposition. Therefore, the variations observed between the “volatile” and “non-volatile” simulations depends on the relative deposition rate of gaseous and particulate phase. GPP effect on total concentrations of methyltetrols at SIRTA can be quite high. However, as shown in section 4.3.1, GPP was reproduced with the right order of magnitude in the model.

α -methylglyceric acid variations with volatility are coherent with the ones observed for pinonic acid and pinic acid. A concentration decrease in the “volatile” (by 25%) parametrization is due to an enhancement of gas-phase removal process. In the “non-volatile” simulation, α -methyl glyceric acid concentrations increase by a factor 2.41, because of the partitioning protecting effect. The uncertainty due to GPP estimation for this marker (gap

between median measured and simulated F_p 0.31) should be considered lower than the one associated to pinonic acid, which measured and “reference” F_p have a gap of 0.77, and similar to the one associated to pinic acid (median F_p gap between measurement and “reference” of 0.32).

A strong effect of gas-phase deposition was simulation with a decrease of concentrations close to a factor 2 for pinonic acid, pinic acid and α -methylglyceric acid indicating that gas-phase deposition may be a very efficient removal process. However, the extent of this removal process is probably overestimated due to the fact that F_p values are strongly underestimated for these 3 compounds.

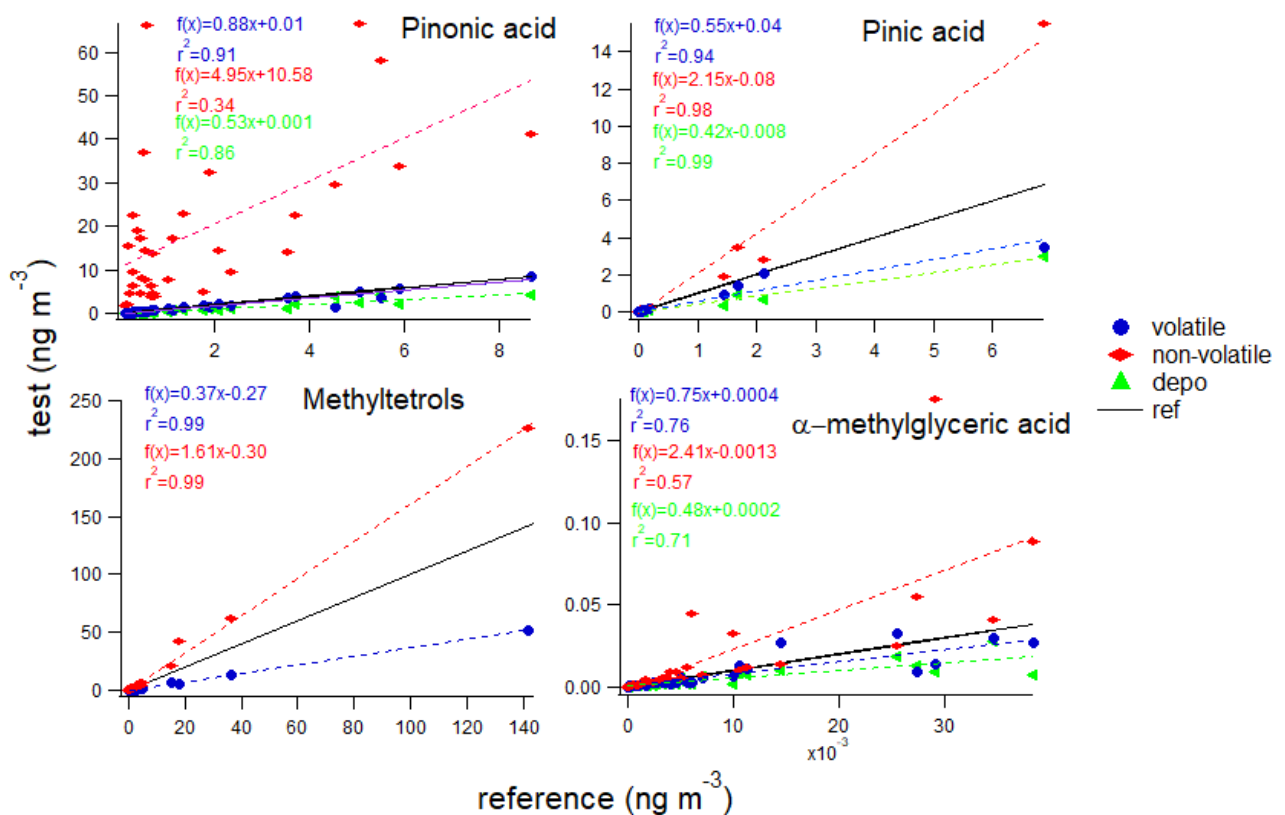


Figure 15. Simulated total (gas+particle) marker concentrations at SIRTA as a function of the concentrations for the reference simulation where markers are not considered semivolatile (“completely volatile or non-volatile) and when gaseous phase deposition is considered. From the top left to the bottom right: pinonic acid, pinic acid, α -methylglyceric acid and methyltetrols tests are presented. The tests have been performed during February, mid-June to mid-July and October.

Conclusions

A comprehensive and detailed chemical mechanism for molecular marker formation from isoprene and α -/ β -pinene has been developed and inserted in the 3D chemistry transport model CHIMERE. Useful information about the sensitivity of aerosol formation to the radical concentrations and GPP have been obtained.

Except for some peak in summer, pinene markers (pinonic acid, pinic acid and MBTCA) are underestimated, especially in the last part of the year (from September to December). Concerning isoprene markers, methyltetrols are simulated with the right magnitude order, but with a wrong temporality (probably due to the fact that the effect of soil moisture on isoprene emissions is not taken into account into CHIMERE), while α -methylglyceric acid are strongly underestimated (factor 100).

The sensitivity analysis performed allowed to understand the critical parameters for each marker simulation. Pinonic acid formation sensitivity to α -pinene oxidation initiation reaction and concentrations has been widely investigated. Although the α -pinene + NO₃ rate predominates in large regions of the domain, most of the pinonic acid in the model is formed by α -pinene + OH and α -pinene + O₃ reactions. The use of detailed mechanisms is required to model daily variations of aerosol formation processes, instead of constant aerosol yields from a defined precursor+radical reaction.

Pinic acid and methyltetrols concentrations are affected by NO_x regime and HO₂ concentrations. Only pinic acid formation is also affected by RO₂ concentrations. The sensitivity of these markers to NO_x regime was expected (Eddingsaas et al., 2012; Surratt et al., 2010). However, it is difficult to quantify accurately the influence of radical concentrations on marker formation, because of the high uncertainty connected with the radical concentration estimation and because no measurements of HO₂ and RO₂ are available for comparison. Additionally, methyltetrol formation are overestimated during heat episodes, in which isoprene emissions are computed not taking in account the effect of soil moisture variation.

MBTCA and α -methylglyceric acid formation are sensitive to aqueous phase processes, for which parametrization are still highly uncertain (K_H and k choice). When simulated with the parameters used by Pye et al., (2013) (using the same kinetic parameters as IEPOX instead of the parameters measured by Piletic et al., (2013) for MAE and using a higher Henry's law constant for MAE), α -methylglyceric acid concentrations increase by a factor 200, becoming of the same magnitude order of the measurements. It may seem surprising that methylglyceric

acid was found not to be sensitive to NO concentrations. However, Couvidat et al. (2011) showed that methyl-glyceric acid formation is strongly dependent on the NO₂/NO ratio. Moreover, it should be also strongly dependent on the particle pH. The high underestimation observed for MBTCA concentrations may be due also to the lack of a low NO_x conditions formation mechanism.

Our results seem to indicate that the good estimation of GPP is critical for SOA modeling. For some markers (pinonic acid, pinic acid, α -methylglyceric acid) F_p is significantly underestimated in the model in all conditions. Pinonic acid and pinic acid partitioning is mostly hydrophobic, and thus strictly dependent on OM mass and OM composition. The underestimation of F_p can (at least partly) be attributed to OM mass underestimation. α -methylglyceric acid partitioning is mostly hydrophilic and a great uncertainty in its partitioning should be attributed to the P_{sat} estimation by SARs. MBTCA and methyltetrols are mostly hydrophilic and their partitioning is well estimated. Our results showed that estimating the non-ideal hydrophilic partitioning is essential to reproduce the partitioning of methyltetrols and that assuming an ideal hydrophobic partitioning would lead to a strong underestimation of F_p .

Part of the gap observed between model and measurements for pinonic acid, pinic acid and α -methylglyceric acid may depend on an overestimation of removal processes entity in the gas phase. Various effect could modify marker volatility (such as aerosol viscosity), which makes markers less volatile than simulated and prevent them from the loss processes occurring in the gaseous phase. Similarly, considering these markers more volatile than observed may lead to an overestimation of their gas-phase deposition, which seems to decrease the total concentrations by a factor 2. GPP can be considered a critical parameter for the simulated pinonic acid concentrations, that underestimate measurements by a factor 3.

References

- Aljawhary, D., Zhao, R., Lee, A. K. Y., Wang, C. and Abbatt, J. P. D.: Kinetics, Mechanism, and Secondary Organic Aerosol Yield of Aqueous Phase Photo-oxidation of α -Pinene Oxidation Products, *J. Phys. Chem. A*, 120(9), 1395–1407, doi:10.1021/acs.jpca.5b06237, 2016.
- Atkinson, R.: Gas-Phase Tropospheric Chemistry of Volatile Organic Compounds: 1. Alkanes and Alkenes, *J. Phys. Chem. Ref. Data*, 26(2), 215–290, doi:10.1063/1.556012, 1997.
- Barone, G., Della Gatta, G., Ferro, D. and Piacente, V.: Enthalpies and entropies of sublimation, vaporization and fusion of nine polyhydric alcohols, *J. Chem. Soc. Faraday Trans.*, 86(1), 75–79, 1990.
- Bessagnet, B., Seigneur, C. and Menut, L.: Impact of dry deposition of semi-volatile organic compounds on secondary organic aerosols, *Atmos. Environ.*, 44, 1781–1787, doi:10.1016/j.atmosenv.2010.01.027, 2010.
- Bloss, C., Wagner, V., Jenkin, M. E., Volkamer, R., Bloss, W. J., Lee, J. D., Heard, D., Wirtz, K., Martin-Reviejo, M. and Rea, G.: Development of a detailed chemical mechanism (MCMv3.1) for the atmospheric oxidation of aromatic hydrocarbons, *Atmospheric Chem. Phys.*, 5(3), 641–664, 2005.
- Bonvalot, L., Tuna, T., Fagault, Y., Jaffrezo, J.-L., Jacob, V., Chevrier, F. and Bard, E.: Estimating contributions from biomass burning, fossil fuel combustion, and biogenic carbon to carbonaceous aerosols in the Valley of Chamonix: a dual approach based on radiocarbon and levoglucosan, *Atmospheric Chem. Phys.*, 16(21), 13753–13772, doi:https://doi.org/10.5194/acp-16-13753-2016, 2016.
- Booth, A. M., Montague, W. J., Barley, M. H., Topping, D. O., McFiggans, G., Garforth, A. and Percival, C. J.: Solid state and sub-cooled liquid vapour pressures of cyclic aliphatic dicarboxylic acids, *Atmospheric Chem. Phys.*, 11(2), 655–665, doi:10.5194/acp-11-655-2011, 2011.
- Bozzetti, C., Daellenbach, K. R., Hueglin, C., Fermo, P., Sciare, J., Kasper-Giebl, A., Mazar, Y., Abbaszade, G., El Kazzi, M., Gonzalez, R., Shuster-Meiseles, T., Flasch, M., Wolf, R., Křepelová, A., Canonaco, F., Schnelle-Kreis, J., Slowik, J. G., Zimmermann, R., Rudich, Y., Baltensperger, U., El Haddad, I. and Prévôt, A. S. H.: Size-Resolved Identification, Characterization, and Quantification of Primary Biological Organic Aerosol at a European Rural Site, *Environ. Sci. Technol.*, 50(7), 3425–3434, doi:10.1021/acs.est.5b05960, 2016.
- Bozzetti, C., Sosedova, Y., Xiao, M., Daellenbach, K. R., Ulevicius, V., Dudoitis, V., Mordas, G., Byčenkienė, S., Plauškaitė, K., Vlachou, A., Golly, B., Chazeau, B., Besombes, J.-L., Baltensperger, U., Jaffrezo, J.-L., Slowik, J. G., Haddad, I. E. and Prévôt, A. S. H.: Argon offline-AMS source apportionment of organic aerosol over yearly cycles for an urban, rural, and marine site in northern Europe, *Atmospheric Chem. Phys.*, 17(1), 117–141, doi:https://doi.org/10.5194/acp-17-117-2017, 2017a.
- Bozzetti, C., El Haddad, I., Salameh, D., Daellenbach, K. R., Fermo, P., Gonzalez, R., Minguillón, M. C., Inuma, Y., Poulain, L., Elser, M., Müller, E., Slowik, J. G., Jaffrezo, J.-L., Baltensperger, U., Marchand, N. and Prévôt, A. S. H.: Organic aerosol source

apportionment by offline-AMS over a full year in Marseille, *Atmospheric Chem. Phys.*, 17(13), 8247–8268, doi:10.5194/acp-17-8247-2017, 2017b.

Calogirou, A., Larsen, B. R. and Kotzias, D.: Gas-phase terpene oxidation products: a review, *Atmos. Environ.*, 33(9), 1423–1439, doi:10.1016/S1352-2310(98)00277-5, 1999.

Camredon, M., Aumont, B., Lee-Taylor, J. and Madronich, S.: The SOA/VOC/NO_x system: an explicit model of secondary organic aerosol formation, *Atmospheric Chem. Phys.*, 7(21), 5599–5610, 2007.

Canonaco, F., Slowik, J. G., Baltensperger, U. and Prévôt, A. S. H.: Seasonal differences in oxygenated organic aerosol composition: implications for emissions sources and factor analysis, *Atmospheric Chem. Phys.*, 15(12), 6993–7002, doi:https://doi.org/10.5194/acp-15-6993-2015, 2015.

Capouet, M., Müller, J.-F., Ceulemans, K., Compernelle, S., Vereecken, L. and Peeters, J.: Modeling aerosol formation in alpha-pinene photo-oxidation experiments, *J. Geophys. Res. Atmospheres*, 113(D2), doi:10.1029/2007JD008995, 2008.

Chrit M., Sartelet K., Sciare J., Pey J., Marchand N., Couvidat F., Sellegri K. and Beekmann M.: Modelling organic aerosol concentrations and properties during ChArMEx summer campaigns of 2012 and 2013 in the western Mediterranean region *Atmos. Chem. Phys.*, 17, 12509-12531, doi:10.5194/acp-17-12509-2017, 2017.

Couvidat, F. and Sartelet, K.: The Secondary Organic Aerosol Processor (SOAP v1.0) model: a unified model with different ranges of complexity based on the molecular surrogate approach, *Geosci. Model Dev.*, 8(4), 1111–1138, doi:10.5194/gmd-8-1111-2015, 2015.

Couvidat, F., Debry, E., Sartelet, K. and Seigneur, C.: A hydrophilic/hydrophobic organic (H₂O) aerosol model: Development, evaluation and sensitivity analysis, *J. Geophys. Res.*, 117, D10304, doi:10.1029/2011JD017214, 2012.

Couvidat, F., Sartelet, K. and Seigneur, C.: Investigating the Impact of Aqueous-Phase Chemistry and Wet Deposition on Organic Aerosol Formation Using a Molecular Surrogate Modeling Approach, *Environ. Sci. Technol.*, 47(2), 914–922, doi:10.1021/es3034318, 2013.

Couvidat, F., Bessagnet, B., Garcia-Vivanco, M., Real, E., Menut, L. and Colette, A.: Development of an inorganic and organic aerosol model (CHIMERE 2017β v1.0): seasonal and spatial evaluation over Europe, *Geosci. Model Dev.*, 11(1), 165–194, doi:10.5194/gmd-11-165-2018, 2018.

Crippa, M., Canonaco, F., Slowik, J. G., Haddad, I. E., DeCarlo, P. F., Mohr, C., Heringa, M. F., Chirico, R., Marchand, N., Temime-Roussel, B., Abidi, E., Poulain, L., Wiedensohler, A., Baltensperger, U. and Prévôt, A. S. H.: Primary and secondary organic aerosol origin by combined gas-particle phase source apportionment, *Atmospheric Chem. Phys.*, 13(16), 8411–8426, doi:https://doi.org/10.5194/acp-13-8411-2013, 2013.

Daellenbach, K. R., Bozzetti, C., Křepelová, A., Canonaco, F., Wolf, R., Zotter, P., Fermo, P., Crippa, M., Slowik, J. G., Sosedova, Y., Zhang, Y., Huang, R.-J., Poulain, L., Szidat, S., Baltensperger, U., El Haddad, I. and Prévôt, A. S. H.: Characterization and source apportionment of organic aerosol using offline aerosol mass spectrometry, *Atmospheric Meas. Tech.*, 9(1), 23–39, doi:https://doi.org/10.5194/amt-9-23-2016, 2016.

Darer, A. I., Cole-Filipiak, N. C., O'Connor, A. E. and Elrod, M. J.: Formation and Stability of Atmospherically Relevant Isoprene-Derived Organosulfates and Organonitrates, *Environ. Sci. Technol.*, 45(5), 1895–1902, doi:10.1021/es103797z, 2011.

Derognat, C., Beekmann, M., Baeumle, M., Martin, D. and Schmidt, H.: Effect of biogenic volatile organic compound emissions on tropospheric chemistry during the Atmospheric Pollution Over the Paris Area (ESQUIF) campaign in the Ile-de-France region, *J. Geophys. Res.*, 108(D17), 8560, doi:10.1029/2001JD001421, 2003.

Draper, D. C., Farmer, D. K., Desyaterik, Y. and Fry, J. L.: A qualitative comparison of secondary organic aerosol yields and composition from ozonolysis of monoterpenes at varying concentrations of NO₂, *Atmospheric Chem. Phys.*, 15(21), 12267–12281, doi:https://doi.org/10.5194/acp-15-12267-2015, 2015.

Eddingsaas, N. C., VanderVelde, D. G. and Wennberg, P. O.: Kinetics and Products of the Acid-Catalyzed Ring-Opening of Atmospherically Relevant Butyl Epoxy Alcohols, *J. Phys. Chem. A*, 114(31), 8106–8113, doi:10.1021/jp103907c, 2010.

Eddingsaas, N. C., Loza, C. L., Yee, L. D., Chan, M., Schilling, K. A., Chhabra, P. S., Seinfeld, J. H. and Wennberg, P. O.: α -pinene photooxidation under controlled chemical conditions - Part 2: SOA yield and composition in low- and high-NO_x environments, *Atmospheric Chem. Phys.*, 12(16), 7413–7427, doi:https://doi.org/10.5194/acp-12-7413-2012, 2012.

Fountoukis, C. and Nenes, A.: ISORROPIA II: a computationally efficient thermodynamic equilibrium model for K⁺–Ca²⁺–Mg²⁺–NH₄⁺–Na⁺–SO₄²⁻–NO₃–Cl–H₂O aerosols, *Atmospheric Chem. Phys.*, 7(17), 4639–4659, 2007.

Fredenslund, A., Jones, R. L. and Prausnitz, J. M.: Group-contribution estimation of activity coefficients in nonideal liquid mixtures, *AIChE J.*, 21(6), 1086–1099, doi:10.1002/aic.690210607, 1975.

Friedman, B. and Farmer, D. K.: SOA and gas phase organic acid yields from the sequential photooxidation of seven monoterpenes, *Atmos. Environ.*, 187, 335–345, doi:10.1016/j.atmosenv.2018.06.003, 2018.

Goliff, W. S., Stockwell, W. R. and Lawson, C. V.: The regional atmospheric chemistry mechanism, version 2, *Atmos. Environ.*, 68, 174–185, doi:10.1016/j.atmosenv.2012.11.038, 2013.

Guenther, A., Hewitt, C. N., Erickson, D., Fall, R., Geron, C., Graedel, T., Harley, P., Klinger, L., Lerdau, M., McKay, W. A., Pierce, T., Scholes, B., Steinbrecher, R., Tallamraju, R., Taylor, J. and Zimmerman, P.: A global model of natural volatile organic compound emissions, *J. Geophys. Res. Atmospheres*, 100(D5), 8873–8892, doi:10.1029/94JD02950, 1995.

Guenther, A., Karl, T., Harley, P., Wiedinmyer, C., Palmer, P. I. and Geron, C.: Estimates of global terrestrial isoprene emissions using MEGAN (Model of Emissions of Gases and Aerosols from Nature), *Atmospheric Chem. Phys.*, 6(11), 3181–3210, doi:10.5194/acp-6-3181-2006, 2006.

Guenther, A. B., Jiang, X., Heald, C. L., Sakulyanontvittaya, T., Duhl, T., Emmons, L. K. and Wang, X.: The Model of Emissions of Gases and Aerosols from Nature version 2.1 (MEGAN2.1): an extended and updated framework for modeling biogenic emissions, *Geosci. Model Dev.*, 5(6), 1471–1492, doi:10.5194/gmd-5-1471-2012, 2012.

Hallquist, M., Wängberg, I. and Ljungström, E.: Atmospheric fate of carbonyl oxidation products originating from α -pinene and Δ^3 -carene: determination of rate of reaction with OH and NO₃ radicals, UV absorption cross sections, and vapor pressures, *Environ. Sci. Technol.*, 31(11), 3166–3172, 1997.

Heald, C. L., Henze, D. K., Horowitz, L. W., Feddema, J., Lamarque, J.-F., Guenther, A., Hess, P. G., Vitt, F., Seinfeld, J. H., Goldstein, A. H. and Fung, I.: Predicted change in global secondary organic aerosol concentrations in response to future climate, emissions, and land use change, *J. Geophys. Res. Atmospheres*, 113(D5), doi:10.1029/2007JD009092, 2008.

Jaoui, M. and Kamens, R. M.: Mass balance of gaseous and particulate products analysis from α -pinene/NO_x/air in the presence of natural sunlight, *J. Geophys. Res. Atmospheres*, 106(D12), 12541–12558, 2001.

Jenkin, M. E.: Modelling the formation and composition of secondary organic aerosol from α - and β -pinene ozonolysis using MCM v3, *Atmospheric Chem. Phys.*, 4(7), 1741–1757, doi:https://doi.org/10.5194/acp-4-1741-2004, 2004.

Jenkin, M. E., Saunders, S. M. and Pilling, M. J.: The tropospheric degradation of volatile organic compounds: a protocol for mechanism development, *Atmos. Environ.*, 31(1), 81–104, 1997.

Jenkin, M. E., Saunders, S. M., Wagner, V. and Pilling, M. J.: Protocol for the development of the Master Chemical Mechanism, MCM v3 (Part B): tropospheric degradation of aromatic volatile organic compounds, *Atmospheric Chem. Phys.*, 3(1), 181–193, doi:https://doi.org/10.5194/acp-3-181-2003, 2003.

Jimenez, J. L., Canagaratna, M. R., Donahue, N. M., Prevot, A. S. H., Zhang, Q., Kroll, J. H., DeCarlo, P. F., Allan, J. D., Coe, H., Ng, N. L., Aiken, A. C., Docherty, K. S., Ulbrich, I. M., Grieshop, A. P., Robinson, A. L., Duplissy, J., Smith, J. D., Wilson, K. R., Lanz, V. A., Hueglin, C., Sun, Y. L., Tian, J., Laaksonen, A., Raatikainen, T., Rautiainen, J., Vaattovaara, P., Ehn, M., Kulmala, M., Tomlinson, J. M., Collins, D. R., Cubison, M. J., E., Dunlea, J., Huffman, J. A., Onasch, T. B., Alfarra, M. R., Williams, P. I., Bower, K., Kondo, Y., Schneider, J., Drewnick, F., Borrmann, S., Weimer, S., Demerjian, K., Salcedo, D., Cottrell, L., Griffin, R., Takami, A., Miyoshi, T., Hatakeyama, S., Shimojo, A., Sun, J. Y., Zhang, Y. M., Dzepina, K., Kimmel, J. R., Sueper, D., Jayne, J. T., Herndon, S. C., Trimborn, A. M., Williams, L. R., Wood, E. C., Middlebrook, A. M., Kolb, C. E., Baltensperger, U. and Worsnop, D. R.: Evolution of Organic Aerosols in the Atmosphere, *Science*, 326(5959), 1525–1529, doi:10.1126/science.1180353, 2009.

Jo, D. S., Hodzic, A., Emmons, L. K., Marais, E. A., Peng, Z., Nault, B. A., Hu, W., Campuzano-Jost, P. and Jimenez, J. L.: A simplified parameterization of isoprene-epoxydiol-derived secondary organic aerosol (IEPOX-SOA) for global chemistry and climate models: a case study with GEOS-Chem v11-02-rc, *Geosci. Model Dev.*, 12(7), 2983–3000, doi:https://doi.org/10.5194/gmd-12-2983-2019, 2019.

Kim, Y., Sartelet, K. and Seigneur, C.: Comparison of two gas-phase chemical kinetic mechanisms of ozone formation over Europe, *J. Atmospheric Chem.*, 62(2), 89–119, doi:10.1007/s10874-009-9142-5, 2009.

Kim, Y., Couvidat, F., Sartelet, K. and Seigneur, C.: Comparison of Different Gas-Phase Mechanisms and Aerosol Modules for Simulating Particulate Matter Formation, *J. Air Waste Manag. Assoc.*, 61(11), 1218–1226, doi:10.1080/10473289.2011.603999, 2011.

Kostenidou, E., Karnezi, E., Kolodziejczyk, A., Szmigielski, R. and Pandis, S. N.: Physical and Chemical Properties of 3-Methyl-1,2,3-butanetricarboxylic Acid (MBTCA) Aerosol, *Environ. Sci. Technol.*, 52(3), 1150–1155, doi:10.1021/acs.est.7b04348, 2018.

Kroll, J. H. and Seinfeld, J. H.: Chemistry of secondary organic aerosol: Formation and evolution of low-volatility organics in the atmosphere, *Atmos. Environ.*, 42(16), 3593–3624, doi:10.1016/j.atmosenv.2008.01.003, 2008.

Lanz, V. A., Prévôt, A. S. H., Alfarra, M. R., Weimer, S., Mohr, C., DeCarlo, P. F., Gianini, M. F. D., Hueglin, C., Schneider, J., Favez, O., D'Anna, B., George, C. and Baltensperger, U.: Characterization of aerosol chemical composition with aerosol mass spectrometry in Central Europe: an overview, *Atmospheric Chem. Phys.*, 10(21), 10453–10471, doi:https://doi.org/10.5194/acp-10-10453-2010, 2010.

Lanzafame, G. M., Srivastava, D., Favez, O., Bonnaire, N., Gros, V., Alleman, L. Y., Couvidat, F., Bessagnet, B. and Albinet, A.: One-year measurements of secondary organic aerosol (SOA) markers in the Paris region: concentrations, seasonality, gas/particle partitioning and use in OA source apportionment, *Sci. Total Environ.*, 2020.

Lelieveld, J. and Crutzen, P. J.: The role of clouds in tropospheric photochemistry, *J. Atmospheric Chem.*, 12(3), 229–267, doi:10.1007/BF00048075, 1991.

Lin, Y.-H., Zhang, H., Pye, H. O. T., Zhang, Z., Marth, W. J., Park, S., Arashiro, M., Cui, T., Budisulistiorini, S. H., Sexton, K. G., Vizuete, W., Xie, Y., Luecken, D. J., Piletic, I. R., Edney, E. O., Bartolotti, L. J., Gold, A. and Surratt, J. D.: Epoxide as a precursor to secondary organic aerosol formation from isoprene photooxidation in the presence of nitrogen oxides, *Proc. Natl. Acad. Sci.*, 110(17), 6718–6723, doi:10.1073/pnas.1221150110, 2013.

Ma, X., Tan, Z., Lu, K., Yang, X., Liu, Y., Li, S., Li, X., Chen, S., Novelli, A., Cho, C., Zeng, L., Wahner, A. and Zhang, Y.: Winter photochemistry in Beijing: Observation and model simulation of OH and HO₂ radicals at an urban site, *Sci. Total Environ.*, 685, 85–95, doi:10.1016/j.scitotenv.2019.05.329, 2019.

Majdi, M., Sartelet, K., Lanzafame, G. M., Couvidat, F., Kim, Y., Chrit, M. and Turquety, S.: Precursors and formation of secondary organic aerosols from wildfires in the Euro-Mediterranean region, *Atmospheric Chem. Phys.*, 19(8), 5543–5569, doi:https://doi.org/10.5194/acp-19-5543-2019, 2019.

Mouchel-Vallon, C., Deguillaume, L., Monod, A., Perroux, H., Rose, C., Ghigo, G., Long, Y., Leriche, M., Aumont, B., Patryl, L., Armand, P. and Chaumerliac, N.: CLEPS 1.0: A new protocol for cloud aqueous phase oxidation of VOC mechanisms, *Geosci. Model Dev.*, 10(3), 1339–1362, doi:10.5194/gmd-10-1339-2017, 2017.

Müller, L., Reinnig, M.-C., Naumann, K. H., Saathoff, H., Mentel, T. F., Donahue, N. M. and Hoffmann, T.: Formation of 3-methyl-1,2,3-butanetricarboxylic acid via gas phase oxidation of pinonic acid – a mass spectrometric study of SOA aging, *Atmospheric Chem. Phys.*, 12(3), 1483–1496, doi:10.5194/acp-12-1483-2012, 2012.

Nguyen, T. B., Coggon, M. M., Bates, K. H., Zhang, X., Schwantes, R. H., Schilling, K. A., Loza, C. L., Flagan, R. C., Wennberg, P. O. and Seinfeld, J. H.: Organic aerosol formation from the reactive uptake of isoprene epoxydiols (IEPOX) onto non-acidified inorganic seeds, *Atmospheric Chem. Phys.*, 14(7), 3497–3510, doi:10.5194/acp-14-3497-2014, 2014.

Pankow, J. F.: An absorption model of gas/particle partitioning of organic compounds in the atmosphere, *Atmos. Environ.*, 28(2), 185–188, doi:10.1016/1352-2310(94)90093-0, 1994.

Pankow, J. F. and Asher, W. E.: SIMPOL. 1: a simple group contribution method for predicting vapor pressures and enthalpies of vaporization of multifunctional organic compounds, *Atmospheric Chem. Phys.*, 8(10), 2773–2796, 2008.

Petit, J.-E., Favez, O., Sciare, J., Canonaco, F., Croteau, P., Močnik, G., Jayne, J., Worsnop, D. and Leoz-Garziandia, E.: Submicron aerosol source apportionment of wintertime pollution in Paris, France by double positive matrix factorization (PMF²) using an aerosol chemical speciation monitor (ACSM) and a multi-wavelength Aethalometer, *Atmospheric Chem. Phys.*, 14(24), 13773–13787, doi:https://doi.org/10.5194/acp-14-13773-2014, 2014.

Petit, J.-E., Amodeo, T., Meleux, F., Bessagnet, B., Menut, L., Grenier, D., Pellan, Y., Ockler, A., Rocq, B., Gros, V., Sciare, J. and Favez, O.: Characterising an intense PM pollution episode in March 2015 in France from multi-site approach and near real time data: Climatology, variabilities, geographical origins and model evaluation, *Atmos. Environ.*, 155, 68–84, doi:10.1016/j.atmosenv.2017.02.012, 2017.

Piletic, I. R., Edney, E. O. and Bartolotti, L. J.: A computational study of acid catalyzed aerosol reactions of atmospherically relevant epoxides, *Phys. Chem. Chem. Phys.*, 15(41), 18065, doi:10.1039/c3cp52851k, 2013.

Pye, H. O. T., Pinder, R. W., Piletic, I. R., Xie, Y., Capps, S. L., Lin, Y.-H., Surratt, J. D., Zhang, Z., Gold, A., Luecken, D. J., Hutzell, W. T., Jaoui, M., Offenberg, J. H., Kleindienst, T. E., Lewandowski, M. and Edney, E. O.: Epoxide Pathways Improve Model Predictions of Isoprene Markers and Reveal Key Role of Acidity in Aerosol Formation, *Environ. Sci. Technol.*, 47(19), 11056–11064, doi:10.1021/es402106h, 2013.

Rattanavaraha, W., Chu, K., Budisulistiorini, S. H., Riva, M., Lin, Y.-H., Edgerton, E. S., Baumann, K., Shaw, S. L., Guo, H., King, L., Weber, R. J., Neff, M. E., Stone, E. A., Offenberg, J. H., Zhang, Z., Gold, A. and Surratt, J. D.: Assessing the impact of anthropogenic pollution on isoprene-derived secondary organic aerosol formation in PM_{2.5} collected from the Birmingham, Alabama, ground site during the 2013 Southern Oxidant and Aerosol Study, *Atmospheric Chem. Phys.*, 16(8), 4897–4914, doi:10.5194/acp-16-4897-2016, 2016.

Reyes-Villegas, E., Green, D. C., Priestman, M., Canonaco, F., Coe, H., Prévôt, A. S. H. and Allan, J. D.: Organic aerosol source apportionment in London 2013 with ME-2: exploring the solution space with annual and seasonal analysis, *Atmospheric Chem. Phys.*, 16(24), 15545–15559, doi:https://doi.org/10.5194/acp-16-15545-2016, 2016.

Roldin, P., Ehn, M., Kurtén, T., Olenius, T., Rissanen, M. P., Sarnela, N., Elm, J., Rantala, P., Hao, L., Hyttinen, N., Heikkinen, L., Worsnop, D. R., Pichelstorfer, L., Xavier, C., Clusius, P., Öström, E., Petäjä, T., Kulmala, M., Vehkamäki, H., Virtanen, A., Riipinen, I. and Boy, M.: The role of highly oxygenated organic molecules in the Boreal aerosol-cloud-climate system, *Nat. Commun.*, 10(1), 1–15, doi:10.1038/s41467-019-12338-8, 2019.

Sarwar, G., Godowitch, J., Henderson, B. H., Fahey, K., Pouliot, G., Hutzell, W. T., Mathur, R., Kang, D., Goliff, W. S. and Stockwell, W. R.: A comparison of atmospheric composition using the Carbon Bond and Regional Atmospheric Chemistry Mechanisms, *Atmospheric Chem. Phys.*, 13(19), 9695–9712, doi:https://doi.org/10.5194/acp-13-9695-2013, 2013.

Saunders, S. M., Jenkin, M. E., Derwent, R. G. and Pilling, M. J.: Protocol for the development of the Master Chemical Mechanism, MCM v3 (Part A): tropospheric degradation of non-aromatic volatile organic compounds, *Atmospheric Chem. Phys.*, 3(1), 161–180, doi: 10.5194/acp-3-161-2003, 2003.

Schlag, P., Kiendler-Scharr, A., Blom, M. J., Canonaco, F., Henzing, J. S., Moerman, M., Prévôt, A. S. H. and Holzinger, R.: Aerosol source apportionment from 1-year measurements at the CESAR tower in Cabauw, the Netherlands, *Atmospheric Chem. Phys.*, 16(14), 8831–8847, doi:https://doi.org/10.5194/acp-16-8831-2016, 2016.

Sciare, J., d'Argouges, O., Sarda-Estève, R., Gaimoz, C., Dolgorouky, C., Bonnaire, N., Favez, O., Bonsang, B. and Gros, V.: Large contribution of water-insoluble secondary organic aerosols in the region of Paris (France) during wintertime, *J. Geophys. Res. Atmospheres*, 116(D22), n/a-n/a, doi:10.1029/2011JD015756, 2011.

Seinfeld, J. H.: Tropospheric chemistry and composition | Aerosols/Particles, in *Encyclopedia of Atmospheric Sciences (Second Edition)*, edited by G. R. North, J. Pyle, and F. Zhang, pp. 182–187, Academic Press, Oxford., 2015.

Srivastava, D., Favez, O., Perraudin, E., Villenave, E. and Albinet, A.: Comparison of Measurement-Based Methodologies to Apportion Secondary Organic Carbon (SOC) in PM_{2.5}: A Review of Recent Studies, *Atmosphere*, 9(11), 452, doi:10.3390/atmos9110452, 2018a.

Srivastava, D., Favez, O., Bonnaire, N., Lucarelli, F., Haefelin, M., Perraudin, E., Gros, V., Villenave, E. and Albinet, A.: Speciation of organic fractions does matter for aerosol source apportionment. Part 2: Intensive short-term campaign in the Paris area (France), *Sci. Total Environ.*, 634, 267–278, doi:10.1016/j.scitotenv.2018.03.296, 2018b.

Surratt, J. D., Chan, A. W. H., Eddingsaas, N. C., Chan, M., Loza, C. L., Kwan, A. J., Hersey, S. P., Flagan, R. C., Wennberg, P. O. and Seinfeld, J. H.: Reactive intermediates revealed in secondary organic aerosol formation from isoprene, *Proc. Natl. Acad. Sci.*, 107(15), 6640–6645, doi:10.1073/pnas.0911114107, 2010.

Tilgner, A. and Herrmann, H.: Radical-driven carbonyl-to-acid conversion and acid degradation in tropospheric aqueous systems studied by CAPRAM, *Atmos. Environ.*, 44(40), 5415–5422, doi:10.1016/j.atmosenv.2010.07.050, 2010.

Vlachou, A., Daellenbach, K. R., Bozzetti, C., Chazeau, B., Salazar, G. A., Szidat, S., Jaffrezo, J.-L., Hueglin, C., Baltensperger, U., Haddad, I. E. and Prévôt, A. S. H.: Advanced source apportionment of carbonaceous aerosols by coupling offline AMS and radiocarbon

size-segregated measurements over a nearly 2-year period, *Atmospheric Chem. Phys.*, 18(9), 6187–6206, doi:<https://doi.org/10.5194/acp-18-6187-2018>, 2018.

Xavier, C., Rusanen, A., Zhou, P., Dean, C., Pichelstorfer, L., Roldin, P. and Boy, M.: Aerosol Mass yields of selected Biogenic Volatile Organic Compounds - a theoretical study with near explicit gas-phase chemistry, *Atmospheric Chem. Phys. Discuss.*, 1–26, doi:<https://doi.org/10.5194/acp-2019-424>, 2019.

Zhang, Q., Jimenez, J. L., Canagaratna, M. R., Allan, J. D., Coe, H., Ulbrich, I., Alfarra, M. R., Takami, A., Middlebrook, A. M., Sun, Y. L., Dzepina, K., Dunlea, E., Docherty, K., DeCarlo, P. F., Salcedo, D., Onasch, T., Jayne, J. T., Miyoshi, T., Shimono, A., Hatakeyama, S., Takegawa, N., Kondo, Y., Schneider, J., Drewnick, F., Borrmann, S., Weimer, S., Demerjian, K., Williams, P., Bower, K., Bahreini, R., Cottrell, L., Griffin, R. J., Rautiainen, J., Sun, J. Y., Zhang, Y. M. and Worsnop, D. R.: Ubiquity and dominance of oxygenated species in organic aerosols in anthropogenically-influenced Northern Hemisphere midlatitudes, *Geophys. Res. Lett.*, 34(13), L13801, doi:[10.1029/2007GL029979](https://doi.org/10.1029/2007GL029979), 2007.

Zhang, Q., Jimenez, J. L., Canagaratna, M. R., Ulbrich, I. M., Ng, N. L., Worsnop, D. R. and Sun, Y.: Understanding atmospheric organic aerosols via factor analysis of aerosol mass spectrometry: a review, *Anal. Bioanal. Chem.*, 401(10), 3045–3067, doi:[10.1007/s00216-011-5355-y](https://doi.org/10.1007/s00216-011-5355-y), 2011.

Zhao, D. F., Kaminski, M., Schlag, P., Fuchs, H., Acir, I.-H., Bohn, B., Häsel, R., Kiendler-Scharr, A., Rohrer, F., Tillmann, R., Wang, M. J., Wegener, R., Wildt, J., Wahner, A. and Mentel, T. F.: Secondary organic aerosol formation from hydroxyl radical oxidation and ozonolysis of monoterpenes, *Atmospheric Chem. Phys.*, 15(2), 991–1012, doi:<https://doi.org/10.5194/acp-15-991-2015>, 2015.

Zotter, P., Ciobanu, V. G., Zhang, Y. L., El-Haddad, I., Macchia, M., Daellenbach, K. R., Salazar, G. A., Huang, R.-J., Wacker, L., Hueglin, C., Piazzalunga, A., Fermo, P., Schwikowski, M., Baltensperger, U., Szidat, S. and Prévôt, A. S. H.: Radiocarbon analysis of elemental and organic carbon in Switzerland during winter-smog episodes from 2008 to 2012 – Part 1: Source apportionment and spatial variability, *Atmospheric Chem. Phys.*, 14(24), 13551–13570, doi:<https://doi.org/10.5194/acp-14-13551-2014>, 2014.

Zuend, A. and Seinfeld, J. H.: Modeling the gas-particle partitioning of secondary organic aerosol: the importance of liquid-liquid phase separation, *Atmospheric Chem. Phys.*, 12(9), 3857–3882, doi:[10.5194/acp-12-3857-2012](https://doi.org/10.5194/acp-12-3857-2012), 2012.

Zuend, A., Marcolli, C., Luo, B. P. and Peter, T.: A thermodynamic model of mixed organic-inorganic aerosols to predict activity coefficients, *Atmospheric Chem. Phys.*, 8(16), 4559–4593, doi:<https://doi.org/10.5194/acp-8-4559-2008>, 2008.

Zuend, A., Marcolli, C., Peter, T. and Seinfeld, J. H.: Computation of liquid-liquid equilibria and phase stabilities: implications for RH-dependent gas/particle partitioning of organic-inorganic aerosols, *Atmospheric Chem. Phys.*, 10(16), 7795–7820, doi:<https://doi.org/10.5194/acp-10-7795-2010>, 2010.

Zuend, A., Marcolli, C., Booth, A. M., Lienhard, D. M., Soonsin, V., Krieger, U. K., Topping, D. O., McFiggans, G., Peter, T. and Seinfeld, J. H.: New and extended parameterization of the thermodynamic model AIOMFAC: calculation of activity coefficients for organic-inorganic

Chapter IV: Model to measurements comparison: biogenic markers

mixtures containing carboxyl, hydroxyl, carbonyl, ether, ester, alkenyl, alkyl, and aromatic functional groups, *Atmos Chem Phys*, 11(17), 9155–9206, doi:10.5194/acp-11-9155-2011, 2011.

Supplementary Material

Modelling organic aerosol markers in 3D air quality model.

Part 2: Biogenic organic markers.

G.M. Lanzafame^{1,2}, F. Couvidat^{1,*}, O. Favez¹, A. Albinet¹, B. Bessagnet^{1,2}¹INERIS, Parc Technologique Alata, BP 2, 60550 Verneuil-en-Halatte, France²Sorbonne Universités, UPMC, 75252 PARIS cedex 05, France*Correspondence to: florian.couvidat@ineris.fr

1. Marker formation mechanisms

1.1 MBTCA

Table S1. MBTCA formation mechanism in gaseous (Müller et al., 2012) and aqueous phase. Gas phase constants are in molecule cm⁻³ s⁻¹, aqueous phase constants are in M⁻¹s⁻¹

PINONIC ACID OXIDATION		
PINONIC+OH- >OH+0.075*C96O2+0.18*R21+0.035*R31 +0.008*R10b+0.063*MBTCA2	k=6.65×10 ⁻¹²	MCM
PINONIC+OH->OH+0.01*MBTCA	k=3.3×10 ⁹ K _H =2.28×10 ⁷ M ⁻¹ atm ΔH _{sol} =81.68 kJ/mol	(Aljawhary et al., 2016) K ΔH _{sol}
PATH A		
R31+NO->NO+0.47*R33	k(T)=2.7×10 ⁻¹² exp(360/T)	KRO2NO
R31+HO2->HO2+R32OH	k(T)=2.91×10 ⁻¹³ exp(1300/T)	KRO2HO2
R33+NO->NO+R35	k(T)=2.7×10 ⁻¹² exp(360/T)	KRO2NO
R33+HO2->HO2+R34HO2	k(T)=2.91×10 ⁻¹³ exp(1300/T)	KRO2HO2
R35+NO->NO+R37	k(T)=2.7×10 ⁻¹² exp(360/T)	KRO2NO
R35+HO2->HO2+R36HO2	k(T)=2.91×10 ⁻¹³ exp(1300/T)	KRO2HO2
R37+NO->NO+0.98*MBTCA	k(T)=2.7×10 ⁻¹² exp(360/T)	KRO2NO
R37+HO2->HO2+R38HO2	k(T)=2.91×10 ⁻¹³ exp(1300/T)	KRO2HO2
PATH C		
R10b+oRO2->oRO2+P10b	k=1×10 ⁻¹¹	In analogy with C96CO3
R10b+obio->obio+P10b	k=1×10 ⁻¹¹	

R10b+CH3O2->CH3O2+P10b	$k=1\times 10^{-11}$	
R10b+CH3COO->CH3COO+P10b	$k=1\times 10^{-11}$	
R10b+NO->NO+0.98*R12+0.02*R1b2	$k(T)=2.7\times 10^{-12}\exp(360/T)$	KRO2NO
R10b+HO2->HO2+R11bHO2	$k(T)=2.91\times 10^{-13}\exp(1300/T)$	KRO2HO2
PATH C1		
R12+NO->NO+0.45*R14	$k(T)=2.7\times 10^{-12}\exp(360/T)$	KRO2NO
R12+HO2->HO2+R14HO2	$k(T)=2.91\times 10^{-13}\exp(1300/T)$	KRO2HO2
R14+NO->NO+0.01*R16	$k(T)=2.7\times 10^{-12}\exp(360/T)$	KRO2NO
R14+HO2->HO2+R15HO2	$k(T)=2.91\times 10^{-13}\exp(1300/T)$	KRO2HO2
R16+NO->NO+0.99*R18	$k(T)=2.7\times 10^{-12}\exp(360/T)$	KRO2NO
R16+HO2->HO2+R17HO2	$k(T)=2.91\times 10^{-13}\exp(1300/T)$	KRO2HO2
R18+NO->NO+0.32*R110	$k(T)=2.7\times 10^{-12}\exp(360/T)$	KRO2NO
R18+HO2->HO2+R19HO2	$k(T)=2.91\times 10^{-13}\exp(1300/T)$	KRO2HO2
R110+NO->NO+0.1*MBTCA	$k(T)=2.7\times 10^{-12}\exp(360/T)$	KRO2NO
R110+HO2->HO2+R111HO2	$k(T)=2.91\times 10^{-13}\exp(1300/T)$	KRO2HO2
PATH C2		
R1b2+NO->NO+0.47*R1b4	$k(T)=2.7\times 10^{-12}\exp(360/T)$	KRO2NO
R1b2+HO2->HO2+R1b3HO2	$k(T)=2.91\times 10^{-13}\exp(1300/T)$	KRO2HO2
R1b4+NO->NO+0.99*R1b6	$k(T)=2.7\times 10^{-12}\exp(360/T)$	KRO2NO
R1b4+HO2->HO2+R1b5HO2	$k(T)=2.91\times 10^{-13}\exp(1300/T)$	KRO2HO2
R1b6+NO->NO+0.99*R1b8	$k(T)=2.7\times 10^{-12}\exp(360/T)$	KRO2NO
R1b6+HO2->HO2+R1b7HO2	$k(T)=2.91\times 10^{-13}\exp(1300/T)$	KRO2HO2
R1b8+NO->NO+0.97*MBTCA	$k(T)=2.7\times 10^{-12}\exp(360/T)$	KRO2NO
R1b8+HO2->HO2+R1b9HO2	$k(T)=2.91\times 10^{-13}\exp(1300/T)$	KRO2HO2
LOSS REACTIONS		
MBTCA->X	$k=1\times 10^{-18}$	
MBTCA2->X	$k=1\times 10^{-18}$	
MBTCA+OH->OH	$k=3.1\times 10^8\text{ M}^{-1}\text{ s}^{-1}$ $K_H=1.37\times 10^{14}\text{ M}^{-1}\text{ s}^{-1}$ $\Delta H_{\text{sol}}=145.21\text{ kJ mol}^{-1}$	(Aljawhary et al., 2016)
MBTCA2+OH->OH	$k=3.1\times 10^8\text{ M}^{-1}\text{ s}^{-1}$ $K_H=1.37\times 10^{14}\text{ M}^{-1}\text{ s}^{-1}$ $\Delta H_{\text{sol}}=145.21\text{ kJ mol}^{-1}$	(Aljawhary et al., 2016)

1.2 Isoprene SOA markers

Table S2. Isoprene SOA marker formation mechanism. Gas phase constants are in molecule $\text{cm}^{-3}\text{ s}^{-1}$, aqueous phase constants are in $\text{M}^{-1}\text{ s}^{-1}$

C5H8+OH->0.32*MAC+0.42*MVK+0.74*HCHO+ISOP	$k(T)=2.55 \times 10^{-11} \exp(410/T)$	MELCHIOR 2 (Derognat et al., 2003)+(Couvidat et al., 2013)
C5H8+NO3->C5H8+NO3+ISON	$k(T)=3.03 \times 10^{-12} \exp(-448/T)$	
ISOP+HO2->ISHP+HO2	$k(T)=2.05 \times 10^{-13} \exp(1300/T)$	
ISHP+OH->IEPOX+0.282*BiPER+0.030*BiDER+OH	$k=1.0 \times 10^{-10}$	
ISOP+CH3COO->0.026*BiMT+0.219*MACR+CH3COO	$k(T)=8.40 \times 10^{-14} \exp(221/T)$	
ISOP+CH3O2->0.026*BiMT+0.219*MACR+CH3O2	$k(T)=3.40 \times 10^{-14} \exp(221/T)$	
ISOP+NO->0.418*MACR+0.046*ISON+NO	$k(T)=2.43 \times 10^{-12} \exp(360/T)$	
ISOP+NO3->0.438*MACR+NO3	$k=1.20 \times 10^{-12}$	
MACR+OH->MACP+OH	$k(T)=1.86 \times 10^{-11} \exp(176/T)$	
MACR+NO3->0.5*MACP+NO3	$k=3.4 \times 10^{-12}$	
MACR+O3->O3	$k(T)=1.36 \times 10^{-15} \exp(2112/T)$	
MACP+NO->NO	$k(T)=2.54 \times 10^{-12} \exp(360B/T)$	
MACP+HO2->MAHP+HO2	$k(T)=1.82 \times 10^{-13} \exp(1300/T)$	
MACP+CH3O2->CH3O2	$k(T)=3.40 \times 10^{-14} \exp(221/T)$	
MACP+NO2->MPAN+NO2	$k(T)=2.80 \times 10^{-12} \exp(181/T)$	
MPAN->MACR	$k(T)=1.60 \times 10^{-16} \exp(13486/T)$	
MAHP+OH->MACP+OH	$k=3.0 \times 10^{-11}$	(Couvidat et al., 2013)+(Lin et al., 2013)
MPAN+OH->0.067*BiMGA+0.047*BiNGA+0.18*MAE+OH	$k=3.20 \times 10^{-11}$	
MPAN+NO3->0.067*BiMGA+0.047*BiNGA+0.18*MAE+NO3	$k=3.20 \times 10^{-11}$	
ISON+OH->OH	$k=1.30 \times 10^{-11}$	
ISON+NO3->0.074*BiNIT3+NO3	$k=6.61 \times 10^{-13}$	
IEPOX+OH->OH	$k=2.0 \times 10^{-11}$	
IEPOX _{aq} +H ⁺ ->BiMT	$k=5.0 \times 10^{-2}$ and $k_H=2.0 \times 10^7$	
IEPOX _{aq} +H ₂ SO ₄ ->BiSULF	$k=2.0 \times 10^{-4}$ and $k_H=2.0 \times 10^7$	
IEPOX _{aq} +HNO ₃ ->BiMT	$k=2.0 \times 10^{-4}$ and $k_H=2.0 \times 10^7$	
MAE+OH->OH	$k=1.0 \times 10^{-12}$	
MAE _{aq} +H ⁺ ->MGA	$k=1.7 \times 10^{-3}$ and $k_H=1.2 \times 10^5$	(Piletic et al., 2013a)
MGA+OH->OH	$k=9.9 \times 10^{-12}$	(GECKO-A)

2. Temporal variations

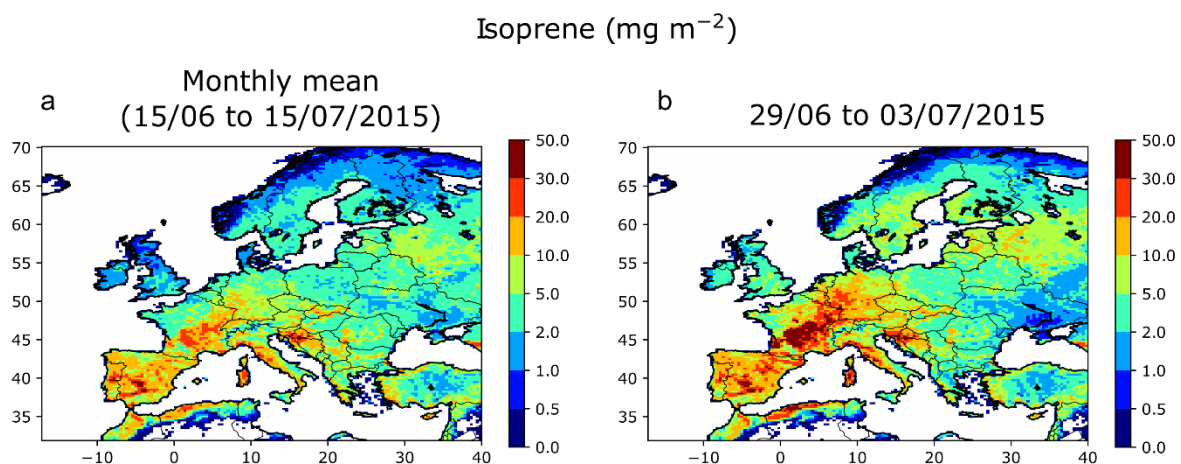


Figure S1. Isoprene mean emissions (mg m^{-2}) computed with MEGAN 2.0, during mid June to mid July (a) and between 29/06 and 03/07/2015.

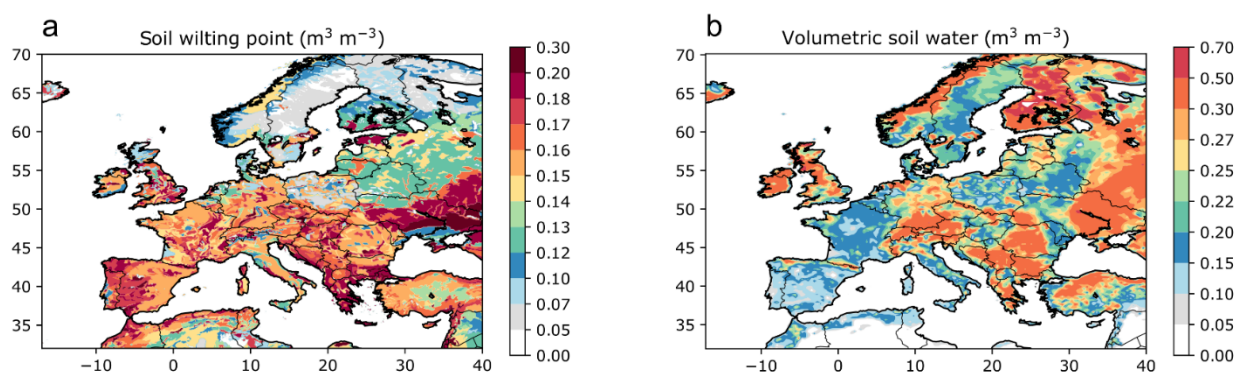


Figure S2. (a) Soil wilting point ($\text{m}^3 \text{m}^{-3}$) over Europe (Global Soil Data Task Group, 2000; ORNL DAAC, 2017) and (b) Volumetric soil water ($\text{m}^3 \text{m}^{-3}$) simulated with MEGAN 2.1 between 29/06 and 03/07/2019.

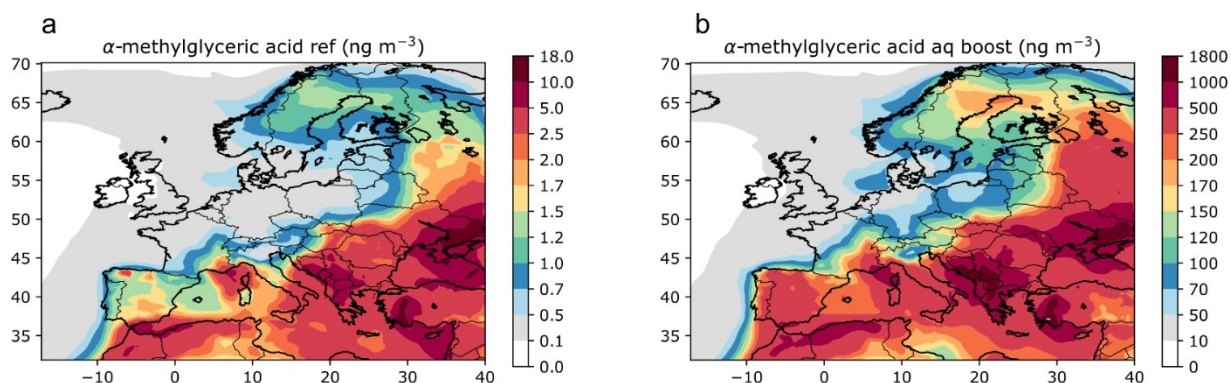


Figure S3. α -methylglyceric acid daily mean concentrations over Europe from 15/06 to 15/07/2019, in the reference run ($K_H=1.2 \times 10^5 \text{ kJ mol}^{-1}$ and $k=1.7 \times 10^{-3} \text{ M s}^{-1}$) (a) and using a Henry's law constant increased by a factor ten ($K_H=1.2 \times 10^6 \text{ kJ mol}^{-1}$) and the same IEPOX oxidation kinetic constant in the aqueous phase ($5.0 \times 10^{-2} \text{ M}^{-1} \text{ s}^{-1}$) (b).

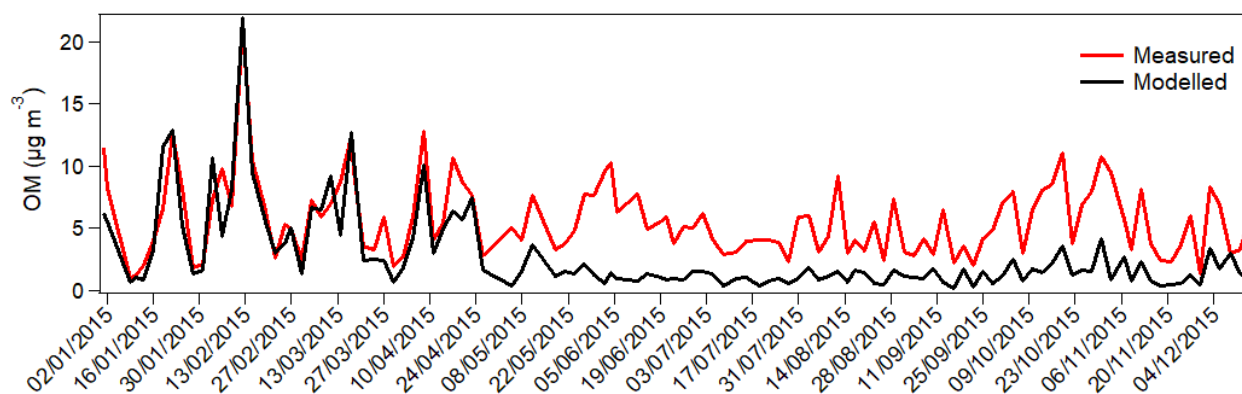


Figure S4. Annual trend of measured and simulated organic matter (OM) at SIRTA during 2015.

3. Sensitivity analysis

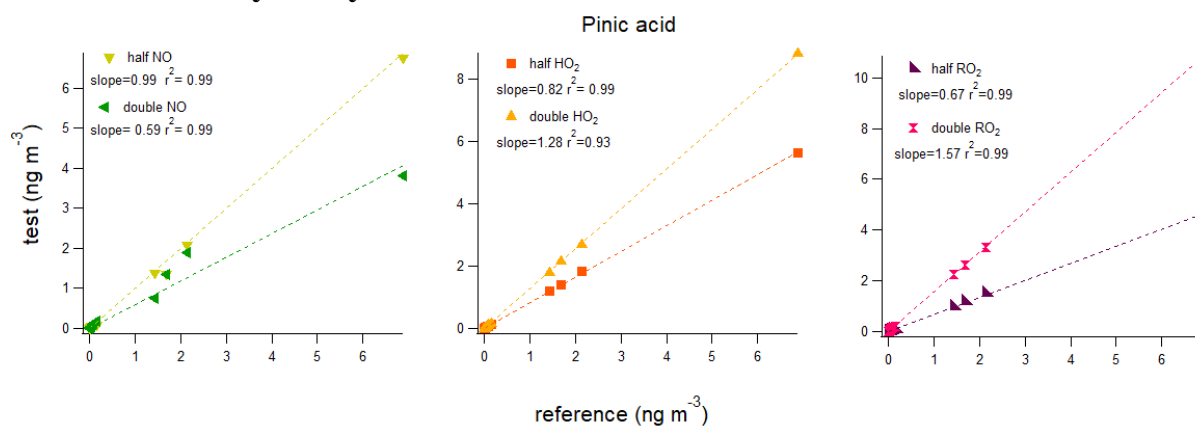


Figure S5. Sensitivity analysis to radical concentrations on pinic acid formation. Test and reference runs have been performed on European domain. The results shown are the mean daily concentrations at SIRTA, during February, mid-June to mid-July and October.

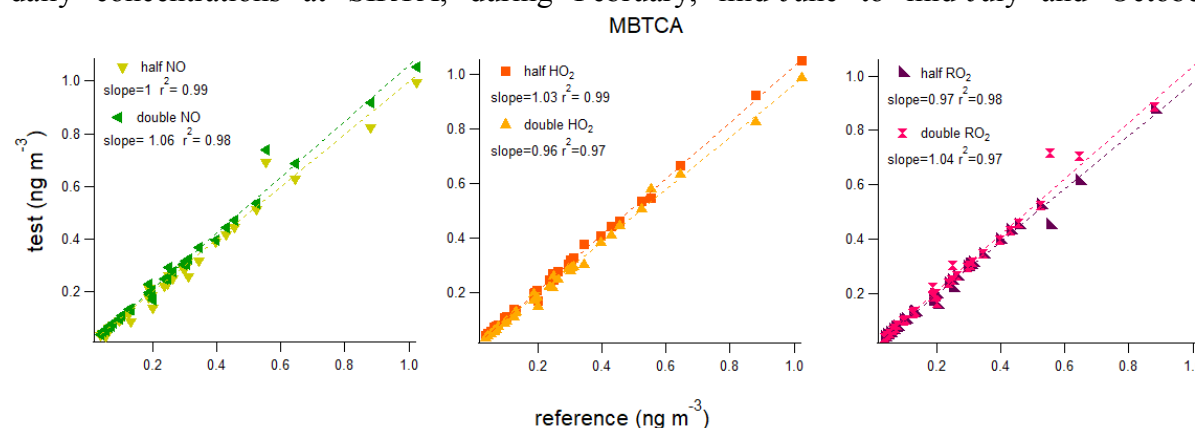


Figure S6. MBTCA formation sensitivity to radical concentrations. Simulations have been performed on European domain. The results shown are the mean daily concentrations at SIRTA, during February, mid-June to mid-July and October.

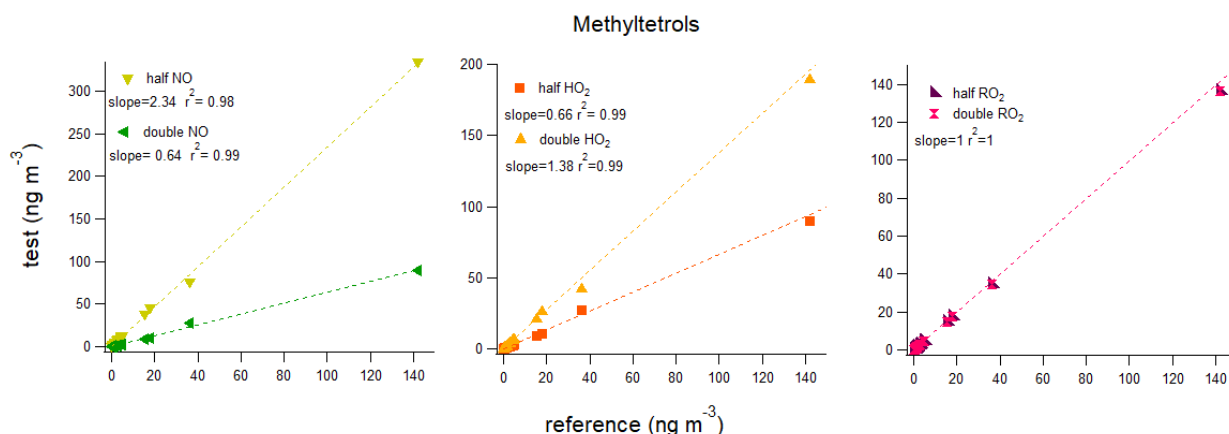


Figure S7. Methyltetrols sensitivity to radical concentrations. All the runs have been performed on European domain. The results shown are the mean daily concentrations at SIRTa, during February, mid-June to mid-July and October.

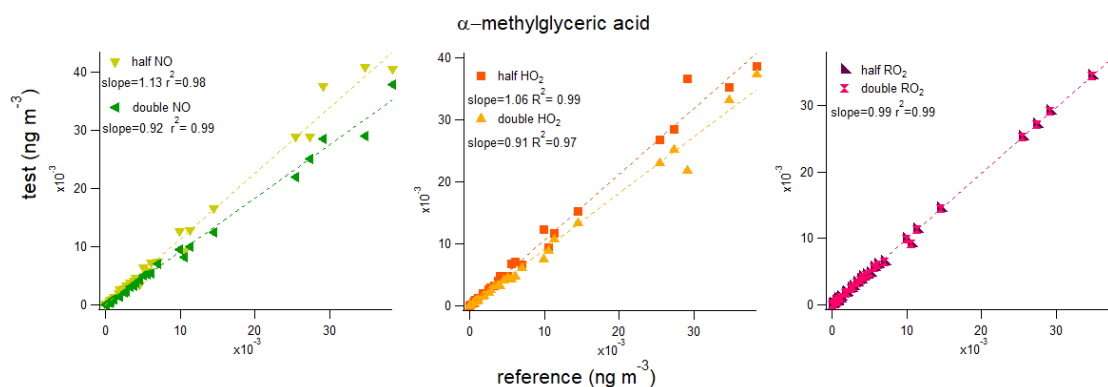


Figure S8. Sensitivity of α -methylglyceric acid formation to radical concentrations. All the outputs are from simulations on European domain. The results shown are the mean daily concentrations at SIRTa, during February, mid-June to mid-July and October.

References

Aljawhary, D., Zhao, R., Lee, A. K. Y., Wang, C. and Abbatt, J. P. D.: Kinetics, Mechanism, and Secondary Organic Aerosol Yield of Aqueous Phase Photo-oxidation of α -Pinene Oxidation Products, *J. Phys. Chem. A*, 120(9), 1395–1407, doi:10.1021/acs.jpca.5b06237, 2016.

Couvidat, F., Debry, E., Sartelet, K. and Seigneur, C.: A hydrophilic/hydrophobic organic (H₂O) aerosol model: Development, evaluation and sensitivity analysis, *J. Geophys. Res.*, 117, D10304, doi:10.1029/2011JD017214, 2012.

Couvidat, F., Sartelet, K. and Seigneur, C.: Investigating the Impact of Aqueous-Phase Chemistry and Wet Deposition on Organic Aerosol Formation Using a Molecular Surrogate Modeling Approach, *Environ. Sci. Technol.*, 47(2), 914–922, doi:10.1021/es3034318, 2013.

Derognat, C., Beekmann, M., Baeumle, M., Martin, D. and Schmidt, H.: Effect of biogenic volatile organic compound emissions on tropospheric chemistry during the Atmospheric Pollution Over the Paris Area (ESQUIF) campaign in the Ile-de-France region, *J. Geophys. Res.*, 108(D17), 8560, doi:10.1029/2001JD001421, 2003.

Global Soil Data Task Group: Global Gridded Surfaces of Selected Soil Characteristics (IGBP-DIS), ORNL DAAC Oak Ridge Tenn. USA, doi:10.3334/ornl daac/569, 2000.

Lin, Y.-H., Zhang, H., Pye, H. O. T., Zhang, Z., Marth, W. J., Park, S., Arashiro, M., Cui, T., Budisulistiorini, S. H., Sexton, K. G., Vizuete, W., Xie, Y., Luecken, D. J., Piletic, I. R., Edney, E. O., Bartolotti, L. J., Gold, A. and Surratt, J. D.: Epoxide as a precursor to secondary organic aerosol formation from isoprene photooxidation in the presence of nitrogen oxides, *Proc. Natl. Acad. Sci.*, 110(17), 6718–6723, doi:10.1073/pnas.1221150110, 2013.

Müller, L., Reinnig, M.-C., Naumann, K. H., Saathoff, H., Mentel, T. F., Donahue, N. M. and Hoffmann, T.: Formation of 3-methyl-1,2,3-butanetricarboxylic acid via gas phase oxidation of pinonic acid – a mass spectrometric study of SOA aging, *Atmospheric Chem. Phys.*, 12(3), 1483–1496, doi:10.5194/acp-12-1483-2012, 2012.

ORNL DAAC: Spatial Data Access Tool (SDAT), ORNL DAAC Oak Ridge Tenn. USA, Accessed September 01, 2019, doi:10.3334/ornl daac/1388, 2017.

Piletic, I. R., Edney, E. O. and Bartolotti, L. J.: A computational study of acid catalyzed aerosol reactions of atmospherically relevant epoxides, *Phys. Chem. Chem. Phys.*, 15(41), 18065, doi:10.1039/c3cp52851k, 2013.

Pye, H. O. T., Pinder, R. W., Piletic, I. R., Xie, Y., Capps, S. L., Lin, Y.-H., Surratt, J. D., Zhang, Z., Gold, A., Luecken, D. J., Hutzell, W. T., Jaoui, M., Offenberg, J. H., Kleindienst, T. E., Lewandowski, M. and Edney, E. O.: Epoxide Pathways Improve Model Predictions of Isoprene Markers and Reveal Key Role of Acidity in Aerosol Formation, *Environ. Sci. Technol.*, 47(19), 11056–11064, doi:10.1021/es402106h, 2013.

Chapter V

Conclusions and perspectives

The main goal of this PhD was to improve OA modelling by implementing specific organic molecular marker emissions and formation processes into a 3D air quality model namely, CHIMERE. This work was based on a combination and comparison of results from field measurements and model outputs. A good description of the organic marker formation mechanisms in the model may improve the knowledge of OA sources, giving valuable information on: (1) the estimation of the source/precursor emissions; (2) the knowledge of the chemical processes leading to SOA formation in the atmosphere, (3) the gas/particle partitioning of OA components.

1. Molecular marker measurements and database

SOA marker concentrations seasonality have been examined at the SIRTAs sampling site (25 km SW of Paris city centre). Observed concentrations were comparable to the ones reported in the literature for sites in Europe and for studies worldwide with similar characteristics (sampling seasons and site typologies). Overall, nitroaromatic compounds (NACs) concentrations showed higher concentrations in the winter period in agreement with the main precursor emission source of these compounds namely wood combustion used for residential heating purposes. Among biogenic SOA markers, only isoprene marker concentrations increased in summer period while pinene markers did not show any typical seasonal trend.

Further works should include the development of a wide database for OA molecular marker measurements in Europe from different site typologies (urban, suburban, rural, forest...). This may provide valuable information on the spatial variations of SOA sources and would be essential in terms of development and validation of the model developed in this work at a larger scale than France. Besides independent field campaigns such as Landex (The Landes Experiment) in “summer” 2017 in which I have been involved during my PhD, the development of such database could take advantage of the European research networks such as the Aerosols, Clouds, and Trace gases Research InfraStructure (ACTRIS) or the Co-operative programme for monitoring and evaluation of long range transmission of air pollutants in Europe (EMEP). Long term data for levoglucosan are already available and the modelling outputs obtained here may promote long term measurements of some key SOA molecular markers such as MBTCA, as already suggested in ACTRIS. Ideally, gas-phase measurements should be performed, including for markers that are traditionally considered non-volatile, as levoglucosan. In such case, prior specific sampling development and validation must be performed.

2. Molecular markers model/measurements comparison: knowledge of physicochemical processes and emissions

A mechanism for the formation of five anthropogenic (single species or several isomers including nitrophenols, nitroguaiacols, methylnitrocatecols, DHOPA and phthalic acid) and five biogenic (pinonic acid, pinic acid, MBTCA, methyltetrols and α -methylglyceric acid) SOA marker has been developed and inserted into the 3D CTM CHIMERE, together with primary levoglucosan emissions. Marker concentrations have been simulated and compared with measurements at SIRTA (1-year data, in 2015) and at 10 urban sites in France for levoglucosan for the winter 2014-2015 period.

Levoglucosan concentrations were simulated with the right order of magnitude. In the western part of France, levoglucosan underestimation was linked to the general underestimation of OA from wood burning in the model. Based on levoglucosan saturation vapor pressure reported in the literature, levoglucosan was found to be semi-volatile with a major dependence on humidity. The use of fixed ratios (conversion factors) to estimate OA from wood burning from levoglucosan concentrations has been investigated from a theoretical point of view. Results obtained highlighted the accuracy of this approach under high biomass burning influences (high OM concentrations due to this source) and during OM concentration peaks (PM pollution events in winter related to biomass burning from residential heating). In future studies, levoglucosan non-volatility should be re-considered and the quantification in gas phase during field campaigns should be addressed together with its partitioning under different humidity conditions.

Besides, SOA molecular marker such as nitrophenols and nitroguaiacols from both, measurements and model, agreed well in terms of concentrations and temporal variations. For methyltetrols, concentrations were simulated with the right magnitude order, but other markers were largely underestimated (till 1000 times lower) probably due to different factors not well described in the model, such as their emission/ precursor sources, formation pathways and/or thermodynamic properties, depending on the marker considered. Finally, GPP was well reproduced for nitroguaiacols, nitrophenols, DHOPA, MBTCA and methyltetrols.

2.1 Knowledge of the emissions

For anthropogenic SOA marker simulations, emission representation appeared as the most critical parameter. Missing or underestimated precursor emissions may contribute substantially to the discrepancies between measured and simulated SOA marker concentrations. For instance, methylnitrocatechol and DHOPA concentrations (underestimated respectively by a factor 60 and 1000) could increase significantly if cresol livestock emission in France were considered, as this sector could emit 20 times more cresol than wood burning. Methylcatechols primary emission from biomass burning, not currently considered, could also contribute significantly (factor 10) to methylnitrocatechols budget. Moreover, methylnitrocatechol and phthalic acid could be also directly emitted. Thus, anthropogenic VOC emissions inventories should be updated considering the emissions from sectors (e.g. livestock in France) and precursors (as methylcatechol) traditionally neglected. Primary emissions of the SOA markers should be also evaluated. Additionally, intermediate volatility organic compounds (IVOCs), now recognized as a large source of SOA from vehicular emissions, biomass burning and industrial sector (Hatch et al., 2018; Wu et al., 2019; Zhao et al., 2014, 2015, 2016), should be also added to the emission inventories. In this way, the research project EVORA (Determination of Semi-Volatile Organic compounds emissions by volatility classes. Impact on air quality modelling; ADEME CORTEA 2017-2020), in which I have been involved during my PhD, has been initiated by Ineris. The main objective of this project is to evaluate the IVOC emissions from light-duty vehicles (gasoline and diesel cars from Euro 3 to Euro 5 emission standards). Thanks to a quantification by volatility classes that I developed on purpose (Lu et al., 2018; Zhao et al., 2016), the emissions will be ready to use in a chemical-transport model such as CHIMERE. Such analytical strategy will be also applied to other emission sources such as biomass burning from public small to medium boiler size ranges (< 1-10 MW) within the research project ACIBIOQA (Improving knowledge of the impact of biomass boilers on Air Quality, ADEME CORTEA 2019-2022) and must be extended in the future to the industrial sector and residential sector (wood combustion for residential heating) to get a representative emission inventory of IVOCs in France.

2.2 Knowledge of the chemical processes

Concerning anthropogenic SOA markers, the results obtained for DHOPA and phthalic acid, underestimated by 3 and 2 order of magnitude respectively, showed that their formation

mechanisms are highly uncertain and experimental mechanistic studies are needed to support the parametrization developed here.

In this context, chamber experiments could be performed in different conditions of temperature, humidity and NO_x concentrations to elucidate the formation pathways of these species. Both, gaseous and particulate phases, must be characterized. Advanced instrumentation such as (TD)-ToF-CiMS (thermal-desorption-time-of-flight-chemical ionization mass spectrometry), CHARON-PTR-ToF-MS (chemical analysis of aerosol online-proton transfer reaction-time-of-flight-mass spectrometry) and EESI-ToF-MS (extractive electrospray ionization-time-of-flight-mass spectrometry) would be the most appropriate to monitor online and study the gas/particulate intermediate species formed. Additionally, the use of the MOVI (Multi-Orifice Volatilization Impactor) or FIGAERO inlet (Filter Inlet for Gases and AEROSols) would allow to estimate the saturated vapor pressure of the aerosol components identified and this would be of great value to improve and decrease the model uncertainties.

For biogenic SOA markers, simulation results showed that MBTCA and MGA formation seemed highly dependent on the aqueous phase formation processes. More specifically, 80% of MBTCA was produced by the aqueous phase oxidation of pinonic acid and MGA formation seemed better represented when methacrylic acid epoxide (MAE) Henry's law constant was increased by a factor 10 and oxidised with the IEPOX kinetic constant. Pinic acid and methyltetrols formation was sensitive to the NO_x regime. When NO concentrations were doubled, a decrease around 40% in marker formation was observed. In addition, strong daily variations have been observed in the formation rates of the main processes involved in pinonic acid formation from α -pinene. Despite of the higher rate of the $\text{NO}_3 + \alpha$ -pinene reaction compared to the ones with OH and O_3 , the oxidation pathways initiated by the latter ones gave higher pinonic acid yields.

Thus, the development of extended aqueous phase mechanisms (liquid phase such as cloud droplets but also in the aqueous aerosol phases) for VOC oxidation (number of carbon > 4) would be required, in order to take in account these processes currently neglected. For this purpose, experimental studies on the degradation of non-soluble SOA intermediates (e.g. pinonaldehyde) in aqueous phases (aerosols or clouds) should be performed. In addition, the investigation of all the phases together, gaseous, particulate and aqueous phases during measurement field campaigns should be investigated simultaneously and ideally, at high time resolution (< 1 hour).

Finally, the effective competition between NO_x and HO_2 or RO_2 oxidants is difficult to evaluate due to high uncertainties in HO_2 and RO_2 estimations in the model. A direct comparison of HO_2 and RO_2 model outputs with measurements performed simultaneously with OA marker measurements would be helpful to lower the model uncertainties of the biogenic OA (but also probably anthropogenic) marker simulations.

2.3 Gas/particle partitioning evaluation

Finally, all the results obtained showed that the major implication of the GPP on OA markers is linked to the protective effect to gaseous phase degradation and deposition due to the mass transfer to the particulate phase. If considered completely volatile, concentrations of low volatility compounds as DHOPA decrease till a factor 10 because of the degradation process occurring in gaseous phase. Concentrations of volatile compounds, as nitrophenols and nitroguaiacols, could decrease by a factor 6 when gas phase deposition is considered. In order to fill the gap between model and measurements, additional measurements of OA marker thermodynamic parameters, such as saturated vapor pressure, should be performed, since literature data are often discordant and for some molecular markers (e.g. α -methylglyceric acid and DHOPA) no experimental value is available. Secondly, a dynamic approach may be used to simulate particles composition, that changes according to the region and seasons, including their viscosity. This kind of partitioning could be represented using a Lagrangian approach. Additional studies on dry and wet deposition of gaseous phase compounds should be also performed, since markers concentrations in the gas phase are very sensitive to these processes, that may be overestimated.

3. Molecular markers for source apportionment

Organic molecular markers are useful species to apportion OA sources. The use of SOA markers in both, SOA tracer method and PMF allowed to apportion SOA at SIRTAs over the year 2015. Overall, total SOC concentrations evaluated by both methods were in good agreement through the year. Significant differences were only observed in March and in summer (from May to August) with a systematic underestimation by the SOA tracer method. These results highlighted that one of the main limitations of the SOA tracer method occurred under highly processed period, such as in March due to missing markers for SOA classes such as organonitrates and organosulfates while it was apportioned in the PMF based on the nitrate

and sulfate-rich factors. Similarly, in the PMF, part the biogenic SOA was apportioned using markers specific of marine biogenic SOA (dimethylsulfide oxidation) while no specific f_{SOC} value has been determined for the DMS oxidation and this fraction could not be accounted using the SOA tracer method.

A successful simulation of OA (SOA or POA) markers may represent a useful diagnostic tool in the apportionment of OA sources using CTM and in the understanding of the variability of atmospheric processes by comparison with long term measurements. Further, we could expect to use such model outputs in a dual approach combining first OA marker concentrations simulated and then, their use in a source-receptor model or based on an improved SOA tracer method to apportion SOA over larger scales than only based on measurements.

References

Hatch, L. E., Rivas-Ubach, A., Jen, C. N., Lipton, M., Goldstein, A. H. and Barsanti, K. C.: Measurements of I/SVOCs in biomass-burning smoke using solid-phase extraction disks and two-dimensional gas chromatography, *Atmospheric Chem. Phys.*, 18(24), 17801–17817, doi:<https://doi.org/10.5194/acp-18-17801-2018>, 2018.

Lu, Q., Zhao, Y. and Robinson, A. L.: Comprehensive organic emission profiles for gasoline, diesel, and gas-turbine engines including intermediate and semi-volatile organic compound emissions, *Atmospheric Chem. Phys. Discuss.*, 1–28, doi:[10.5194/acp-2018-752](https://doi.org/10.5194/acp-2018-752), 2018.

Wu, L., Wang, X., Lu, S., Shao, M. and Ling, Z.: Emission inventory of semi-volatile and intermediate-volatility organic compounds and their effects on secondary organic aerosol over the Pearl River Delta region, *Atmospheric Chem. Phys.*, 19(12), 8141–8161, doi:<https://doi.org/10.5194/acp-19-8141-2019>, 2019.

Zhao, Y., Hennigan, C. J., May, A. A., Tkacik, D. S., de Gouw, J. A., Gilman, J. B., Kuster, W. C., Borbon, A. and Robinson, A. L.: Intermediate-Volatility Organic Compounds: A Large Source of Secondary Organic Aerosol, *Environ. Sci. Technol.*, 48(23), 13743–13750, doi:[10.1021/es5035188](https://doi.org/10.1021/es5035188), 2014.

Zhao, Y., Nguyen, N. T., Presto, A. A., Hennigan, C. J., May, A. A. and Robinson, A. L.: Intermediate Volatility Organic Compound Emissions from On-Road Diesel Vehicles: Chemical Composition, Emission Factors, and Estimated Secondary Organic Aerosol Production, *Environ. Sci. Technol.*, 49(19), 11516–11526, doi:[10.1021/acs.est.5b02841](https://doi.org/10.1021/acs.est.5b02841), 2015.

Zhao, Y., Nguyen, N. T., Presto, A. A., Hennigan, C. J., May, A. A. and Robinson, A. L.: Intermediate Volatility Organic Compound Emissions from On-Road Gasoline Vehicles and Small Off-Road Gasoline Engines, *Environ. Sci. Technol.*, 50(8), 4554–4563, doi:[10.1021/acs.est.5b06247](https://doi.org/10.1021/acs.est.5b06247), 2016.

Annexes

Annex A



Speciation of organic fraction does matter for source apportionment. Part 1: A one-year campaign in Grenoble (France)



Deepchandra Srivastava^{a,b,c}, Sophie Tomaz^{a,b,c}, Olivier Favez^{a,*}, Grazia Maria Lanzafame^a, Benjamin Golly^{d,f}, Jean-Luc Besombes^d, Laurent Y. Alleman^e, Jean-Luc Jaffrezo^f, Véronique Jacob^f, Emilie Perraudin^{b,c}, Eric Villenave^{b,c}, Alexandre Albinet^{a,*}

^a INERIS, Parc Technologique Alata, BP 2, 60550 Verneuil-en-Halatte, France

^b CNRS, EPOC, UMR 5805 CNRS, 33405 Talence, France

^c Université de Bordeaux, EPOC, UMR 5805 CNRS, 33405 Talence, France

^d Univ. Savoie Mont Blanc, LCME, 73000 Chambéry, France

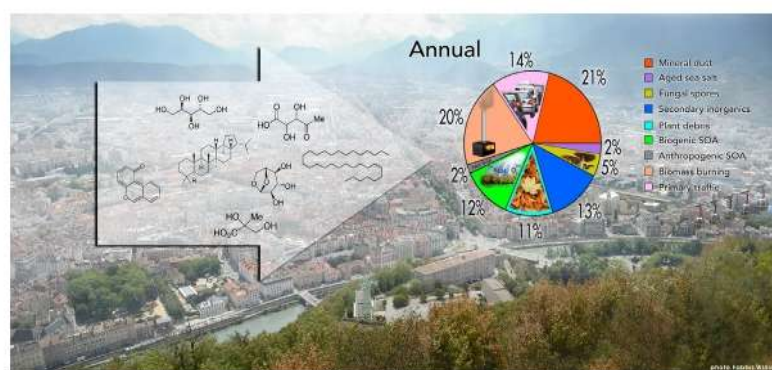
^e IMT Lille Douai, SAGE, 59000 Lille, France

^f Univ. Grenoble Alpes, CNRS, IRD, IGE, F-38000 Grenoble, France

HIGHLIGHTS

- Source apportionment using key primary and secondary organic molecular markers
- Uncommon resolved sources: plant debris, fungal spores, biogenic & anthropogenic SOA
- High contribution of anthropogenic SOA (PAH SOA) noticed in winter PM pollution event
- Investigation of HuLiS origins: both, primary and secondary contributions highlighted

GRAPHICAL ABSTRACT



ARTICLE INFO

Article history:

Received 3 October 2017

Received in revised form 11 December 2017

Accepted 12 December 2017

Available online 21 December 2017

Editor: D. Barcelo

Keywords:

Aerosol
Source apportionment
Primary biogenic organics
SOA
Molecular markers
HuLiS

ABSTRACT

PM₁₀ source apportionment was performed by positive matrix factorization (PMF) using specific primary and secondary organic molecular markers on samples collected over a one year period (2013) at an urban station in Grenoble (France). The results provided a 9-factor optimum solution, including sources rarely apportioned in the literature, such as two types of primary biogenic organic aerosols (fungal spores and plant debris), as well as specific biogenic and anthropogenic secondary organic aerosols (SOA). These sources were identified thanks to the use of key organic markers, namely, polyols, odd number higher alkanes, and several SOA markers related to the oxidation of isoprene, α -pinene, toluene and polycyclic aromatic hydrocarbons (PAHs). Primary and secondary biogenic contributions together accounted for at least 68% of the total organic carbon (OC) in the summer, while anthropogenic primary and secondary sources represented at least 71% of OC during winter-time. A very significant contribution of anthropogenic SOA was estimated in the winter during an intense PM pollution event (PM₁₀ > 50 $\mu\text{g m}^{-3}$ for several days; 18% of PM₁₀ and 42% of OC). Specific meteorological conditions with a stagnation of pollutants over 10 days and possibly Fenton-like chemistry and self-amplification cycle of SOA formation could explain such high anthropogenic SOA concentrations during this period. Finally, PMF outputs were also used to investigate the origins of humic-like substances (HuLiS), which represented 16% of OC on an annual average basis. The results indicated that HuLiS were mainly associated with biomass burning

* Corresponding authors.

E-mail addresses: olivier.favez@ineris.fr (O. Favez), alexandre.albinet@ineris.fr, alexandre.albinet@gmail.com (A. Albinet).

(22%), secondary inorganic (22%), mineral dust (15%) and biogenic SOA (14%) factors. This study is probably the first to state that HuLiS are significantly associated with mineral dust.

© 2017 Elsevier B.V. All rights reserved.

1. Introduction

Airborne particles (particulate matter, PM) are a major concern of current research in atmospheric science due to their impact on both climate (Boucher et al., 2013) and air quality (Heal et al., 2012). Elucidating their emission sources and transformation processes constitutes a crucial step for the elaboration of efficient and cost-effective abatement strategies.

Organic matter (OM) is a major PM component. Organic aerosols (OA) are categorized into either primary organic aerosol (POA), directly emitted from anthropogenic and natural sources, or secondary organic aerosol (SOA), formed in the atmosphere notably via gas-particle conversion processes such as nucleation, condensation and heterogeneous multiphase chemical reactions involving (semi-) volatile compounds (VOCs or SVOCs) (Carlton et al., 2009; Ziemann and Atkinson, 2012). Due to the multiplicity of sources and of transformation mechanisms, the apportionment of the relative contribution of each of the different primary and secondary OA fractions is still fairly uncertain.

Specific organic compounds can provide insight into OA sources (Schauer et al., 1996). They are commonly referred to as molecular markers (tracers), such as levoglucosan for biomass burning (Simoneit et al., 1999a) or α -methylglyceric acid for SOA from isoprene oxidation (Carlton et al., 2009). Source-receptor models, such as positive matrix factorization (PMF), have been widely implemented using traditional aerosol chemical speciation, such as elemental carbon (EC), organic carbon (OC), major ions, and metals. The inclusion of a comprehensive set of organic molecular markers potentially offers a closer link between factors and sources, but it has been rarely applied in PMF studies because it requires large datasets and intensive lab-work (Jaekels et al., 2007; Laing et al., 2015; Schembari et al., 2014; Shrivastava et al., 2007; Srimuruganandam and Shiva Nagendra, 2012; Waked et al., 2014; Wang et al., 2012; Zhang et al., 2009).

Source apportionment studies based on the use of source-receptor models assume that organic molecular markers are chemically stable in the atmosphere (defined as tracer compounds) (Schauer et al., 1996). However, these compounds can react in the atmosphere by photochemical processes involving sunlight and atmospheric oxidants such as O_3 , NO_x , radicals OH, NO_3 ... For instance, levoglucosan is usually assumed to be very stable (Simoneit et al., 1999b) but recent studies have shown its significant atmospheric chemical degradation (Hennigan et al., 2010; Kessler et al., 2010; Mochida et al., 2010; Zhao et al., 2014). For most of these compounds, experimental data about their stability or atmospheric lifetimes are very scarce or not available. They are usually based on empirical calculations like for SOA markers (Nozière et al., 2015). If some markers have tendency to undergo a rapid decay in the atmosphere, so short lifetime, their use may cause a bias in the source apportionment results.

The main objective of this work is to apportion specific primary and secondary OA fractions using various and distinctive molecular markers in a PMF model. The present paper is based on results obtained from a year-long campaign conducted in an Alpine city, while a following paper will be dedicated to the use of a similar approach in the Paris region during a 3-week intensive sampling campaign, with a higher time resolution for filter samplings (every 4 h) through an intense PM pollution event (Srivastava et al., in preparation). A focus has been put here on usually unresolved PM sources, such as primary biogenic sources and secondary sources such as biogenic SOA formed from pinene or isoprene oxidation, and anthropogenic SOA formed from the oxidation of polycyclic aromatic hydrocarbons (PAHs), toluene and phenol. In addition, this work provides insight into the sources of total OC and of

humic-like substances (HuLiS), a significant fraction of OM which plays an important role in the atmosphere (Graber and Rudich, 2006) and has not been extensively explored.

2. Methodology

2.1. Sampling site

The sampling site was located at the urban background sampling station of “Les Frênes” (45°09'41" N, 5°44'07" E) in Grenoble (France). The city, surrounded by three mountain ranges, is considered the most densely populated area (160,000 inhabitants) of the French Alps (Fig. S1). In addition to the urbanized area, forests, including both deciduous and coniferous species, and agriculture areas (pastures) dominate the land cover around Grenoble (Fig. S2). This region experiences frequent severe PM pollution events ($PM_{10} > 50 \mu g m^{-3}$ for at least 3 consecutive days) in the winter due to the formation of thermal inversion layers that may promote pollutant accumulation. Previous studies have shown that residential heating, mainly biomass burning, accounts for a major fraction of $PM_{2.5}$ in the winter (Favez et al., 2010). In addition, traffic and industrial activities contribute significantly to the observed PM concentration levels in Grenoble (Polo-Rehn et al., 2014).

2.2. Sample collection

PM_{10} samples (Tissu-quartz, Pallflex, $\varnothing = 150$ mm) were collected every third day for one year from 01/01/2013 to 01/01/2014 using two parallel high volume samplers (DA-80, Digitec; sampling duration of 24 h at $30 m^3 h^{-1}$). Details on the preparation and conservation of these filter samples have already been presented elsewhere (Tomaz et al., 2017; Tomaz et al., 2016) and are reported in the Supplementary material. A total of 123 samples and 9 field blanks were collected and analysed for an extended chemical characterization following the protocols described in Section 2.3.

Atmospheric concentrations of PM_{10} and $PM_{2.5}$ (1405FTEOM-FDMS, Thermo), NO_x (TEI 42I, Thermo) and O_3 (TEI 49I, Thermo) were monitored by the local air quality network in Grenoble (Atmo Rhône-Alpes-Auvergne) at a 15-min resolution. Together with the ROMMA network (Meteorological network of the Alpine massif), they also measured and provided meteorological parameters (temperature, wind direction, wind speed and relative humidity) (Figs. 1 and S3). Temperature and pressure data from several locations at different altitudes were used to evaluate the duration of thermal inversion layers in the valley. Details of the calculation of thermal inversion layers have been described previously (Tomaz et al., 2017).

2.3. Analytical procedures

Overall, approximately 194 species were quantified in each sample. EC/OC was measured using a Sunset lab analyzer using the EUSAAR-2 thermal protocol (Cavalli et al., 2010). HuLiS were analysed following the protocol described by Baduel et al. (2010). Anions (Cl^- , NO_3^- , SO_4^{2-}), cations (NH_4^+ , Ca^{2+} , Na^+ , Mg^{2+} , K^+), methanesulfonic acid (MSA) and oxalate ($C_2O_4^{2-}$) were analysed by ionic chromatography (Jaffrezou et al., 2005). Thirty-four metals and trace elements were quantified by ICP-MS (Alleman et al., 2010). Cellulose combustion markers (biomass burning) (levoglucosan, mannosan and galactosan), 3 polyols (arabitol, sorbitol and mannitol) and glucose were quantified using HPLC-PAD (Piot et al., 2012). Twenty-one PAHs, 27 oxy-PAHs, and 32 nitro-PAHs were quantified using UPLC/UV-Fluorescence and GC/NICI-

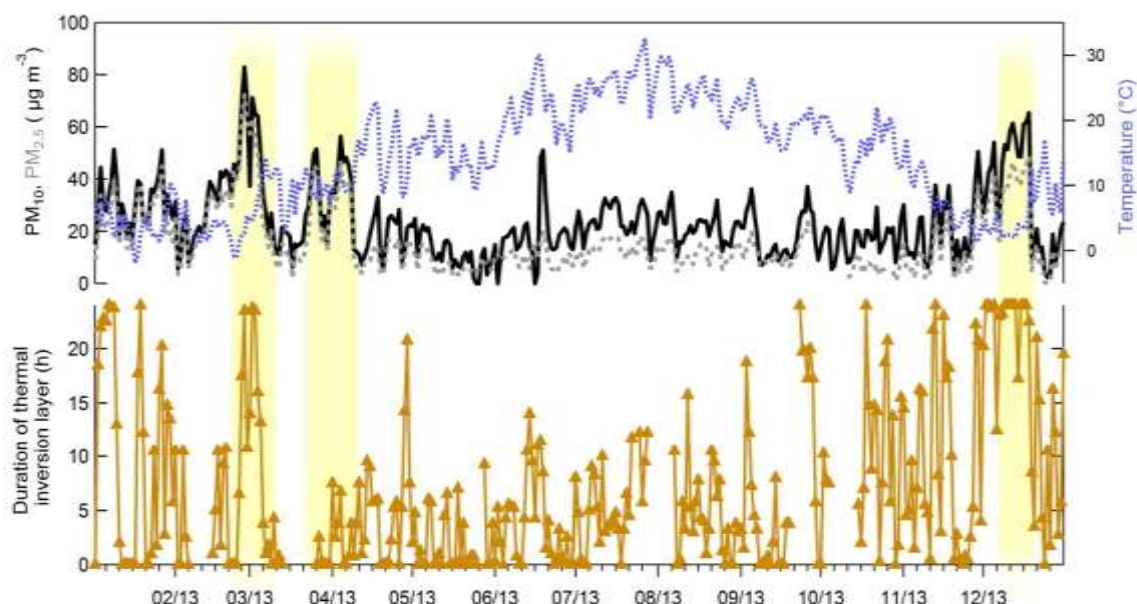


Fig. 1. Temporal variation of PM_{10} and $PM_{2.5}$ concentrations along with the temperature and duration of thermal inversion layers at Grenoble, Les Frénes (2013).

MS (Albinet et al., 2006; Albinet et al., 2014; Albinet et al., 2013; Tomaz et al., 2016). Twenty-seven higher alkanes (C13–C39), 10 hopanes, pristane, phytane, 5 sulfur containing PAHs, 5 lignin combustion markers (vanillin, coniferaldehyde ...) (Golly et al., 2015) and 11 compounds usually recognized as SOA markers (α -methylglyceric acid, pinic acid, methyl-nitrocatechols...) (Nozière et al., 2015) were analysed by GC/EI-MS. Note that the quantification of all SOA markers was performed using authentic standards. Details of the analytical procedures and sample preparation for the analysis of the SOA markers are provided in the Supplementary material (Tables S1 and S2).

2.4. Source apportionment methodology

2.4.1. Receptor modelling

The goal of receptor models is to solve the chemical mass balance equation between the measured species concentrations and source profiles as a linear combination of factors p , species profile f of each source, and the amount of mass g contributed to each individual sample (Eq. (1)):

$$X_{ij} = \sum_{k=1}^p g_{ik} f_{kj} + e_{ij} \quad (1)$$

where X_{ij} represents the measured data for species j in sample i , and e_{ij} represents the residual of each sample/species not fitted by the model.

PMF is a multivariate factor analysis tool that decomposes a matrix of the observed chemistry of the samples into two matrices (factor contributions (G) and factor profiles (F)) that need to be ascribed to a specific source. The best model solution is obtained by minimizing the function Q (Eq. (2)):

$$Q = \sum_i \sum_j \left(\frac{e_{ij}}{\sigma_{ij}} \right)^2 \quad (2)$$

where σ_{ij} represents the measurement uncertainty of each data point.

In this work, we used the U.S. Environmental Protection Agency (USEPA) PMF 5.0 software to perform the source apportionment.

2.4.2. Uncertainty calculations

The estimation of uncertainties for the filter-based measurements was calculated using Eq. (3) (Polissar et al., 1998):

$$\sigma_{ij} = \begin{cases} \frac{5}{6} LD_j & \text{if } X_{ij} < LD_j \\ \sqrt{(LD_j)^2 + (CV_j X_{ij})^2 + (a X_{ij})^2} & \text{if } X_{ij} \geq LD_j \end{cases} \quad (3)$$

where LD_j is the detection limit for compound j (defined as the lowest concentrations of the compound that can be measured with a signal to noise ratio of 3), CV_j is the coefficient of variation for compound j (calculated as the standard deviation of repeated analyses divided by the mean value of the repeated analyses), and a is a factor (0.03) applied to account for additional sources of uncertainty (Gianini et al., 2012). Missing concentration values were replaced by the geometric mean of the concentrations of compound j , and their accompanying uncertainties were set at 4 times this value.

2.4.3. Criteria for the selection of species

Inclusion or exclusion of a chemical species in the PMF matrix is usually based on the signal to noise ratio (S/N) (Paatero and Hopke, 2003). S/N ratios for all the quantified species in this study are given in Table S3. Species with an S/N ratio below 0.2 were automatically excluded. Additional criteria for the final selection of the input species in the PMF have been applied; compounds that are analytically difficult to quantify, i.e., with a large number of data points below the detection limit (>60% of total data points), those mainly associated with the gas phase (e.g., pinonic acid, low molecular weight PAHs, oxy and nitro-PAHs) (Albinet et al., 2007; Albinet et al., 2008; Isaacman-VanWertz et al., 2016; Tomaz et al., 2016), and those that are not specific markers of a given source or those with no observed temporal trends (single events or spikes, e.g., pinic acid) were excluded.

In addition, to limit the input data matrix according to the total number of samples ($n = 123$), some species were also not included if they belonged to a single source and were well correlated with another marker of this source (e.g., cellulose combustion: levoglucosan, mannosan, galactosan ($r = 0.97$ – 0.99 , $n = 123$, $p < 0.05$); fungal spores: arabitol, sorbitol, glucose, mannitol ($r = 0.85$ – 0.92 , $n = 123$, $p < 0.05$)). In this case, only one or two representative species were kept for the input matrix. Some other specific organic compounds, such as oxalate, MSA and methyl-nitrocatechols, were also discarded due to poor

predictions by the preliminary model runs. Finally, a total of 47 species were used in the model (Table S4). Details about the species in the final input and the exclusion of the former ones are reported in the Supplementary material and Table S4. PM_{10} concentrations were included as the total variable in the model to directly determine the source contributions to the daily mass concentrations. The total variable was defined as weak (low weight) in the model to not have influence on the solution obtained.

2.4.4. Applied constraints

Several constraints were applied to the base run to obtain clearer chemical source profiles in the final solution. To limit the change in the Q-value, only “soft pulling” constraints were applied. Change in the Q-robust was finally approximately 7%. Details related to the constraints applied to each factor profile are given in Table S5.

2.4.5. Optimization of the final solution

The selection of the final solution was made based on three criteria, including the bootstrap results to evaluate its stability, the comparison between observed and predicted concentrations, and the evaluation of the sensitivity to the applied constraints. A mapping of over 80% of the factors for the bootstrap was taken as the threshold to indicate that the chosen solution may be appropriate. Species showing poor correlations ($r < 0.5$) between observed and modelled concentrations were evaluated carefully to determine whether they should be down-weighted or excluded. A few species were finally kept despite their low correlation coefficients due to their significant role in the interpretation of selected factors (Table S6). Student's *t*-test was used to evaluate the effectiveness of applied constraints on the base model run and to verify whether the differences were statistically insignificant for all source profiles (two-tailed paired *t*-test significance test at $p < 0.05$ probability).

3. Results and discussions

3.1. Overview of the PM_{10} concentrations and pollution events

The daily PM_{10} mass concentrations ranged from 2 to $83 \mu\text{g m}^{-3}$, with an annual average of approximately $24 \mu\text{g m}^{-3}$ (Fig. 1). Two severe PM pollution events, which also affected the rest of France (Favez, 2013), were observed in early spring (02/25–04/08/2013) and winter (12/09–12/19/2013). A large contribution of OM and the presence of thermal inversion layers were observed during the first part of the spring PM pollution events, while the second part was influenced by long range transport and characterized by a large contribution of inorganic species, such as ammonium nitrate and sulfate. The winter pollution episode was associated with the occurrence of thermal inversion layers over a period of 10 consecutive days (Tomaz et al., 2017), where OM was the major contributor to the total PM_{10} loadings (Fig. 1). During this winter pollution event, air quality was expected to be mainly influenced by local combustion sources, such as residential

heating, notably wood combustion, and traffic, as shown by the high concentrations of primary species such as levoglucosan, NO, and PAHs (Tomaz et al., 2017; Tomaz et al., 2016).

3.2. PM_{10} source apportionment

A nine-factor output provides the most reasonable solution for this PM_{10} source apportionment in the Grenoble valley (Fig. 2). It includes traditional aerosol sources, such as primary traffic, biomass burning, mineral dust, secondary inorganics and aged sea salt, and uncommonly resolved ones, such as primary biogenic organic aerosols (fungal spores and plant debris), as well as specific biogenic and anthropogenic SOA, all identified by the chosen molecular organic markers analysed in the PM_{10} fraction. The selection of factors was based on the variability explained by the Q/Q_{exp} ratio, the chemical interpretation of the obtained factors and the total reconstructed mass. Forcing PMF to explain the variability with a less number of factors (<8) resulted in high Q value (Fig. S4), thus only solutions with eight factors and more were checked. The solutions with eight sources were less explanatory, and some factors were merged (Figs. S5 and S6). Conversely, an increase in the number of sources led to the split of meaningful source profiles into two unrealistic ones (Figs. S7 and S8). In the final solution, the comparison of the reconstructed PM_{10} contributions from all sources with measured PM_{10} concentrations showed very good mass closure ($r = 0.93$, $n = 123$, $p < 0.05$) (Fig. 2 and Table S6). Note that results from the chemical characterization of the last 2 days of the year were not validated and were excluded from the PMF matrix. In addition, most of the species showed good agreement with the measured concentrations. Few of them were poorly reconstructed by the PMF (e.g., Sb, hopanes, DHOPA (2,3-Dihydroxy-4-oxopentanoic acid) and phthalic acid ($r < 0.34$)). Low correlation coefficients were due to some single events that occurred during the year and were not well reproduced by the model. Bootstrapping on the final solution showed stable results with ≥ 84 out of 100 bootstrap mapped factors (Table S7). Finally, no significant difference ($p > 0.05$) was observed in the source chemical profiles between the base and the constrained runs (Table S8, Figs. S9 and S10).

Overall, mineral dust (21%) and biomass burning (20%) sources were the main contributors to the total PM_{10} mass on an annual scale. Primary traffic emissions, secondary inorganic aerosols, plant debris and biogenic SOA also presented significant contributions (11 to 14%). Aged sea salt, fungal spores and anthropogenic SOA contributed to approximately 2 to 5% of total PM_{10} (Fig. 2). Identified aerosol sources, chemical profiles and temporal evolutions are shown in Figs. 3 and 4 and discussed individually below.

3.2.1. Secondary inorganics

The secondary inorganics source factor (nitrate-rich) was characterized by high contributions of NO_3^- and NH_4^+ (69% and 63% of these species being attributed to this factor, respectively), with an annual average concentration of $2.9 \mu\text{g m}^{-3}$ and accounted for approximately 13% of PM_{10} mass on an annual scale (Figs. 2 and 3). Cl^- and SO_4^{2-} also

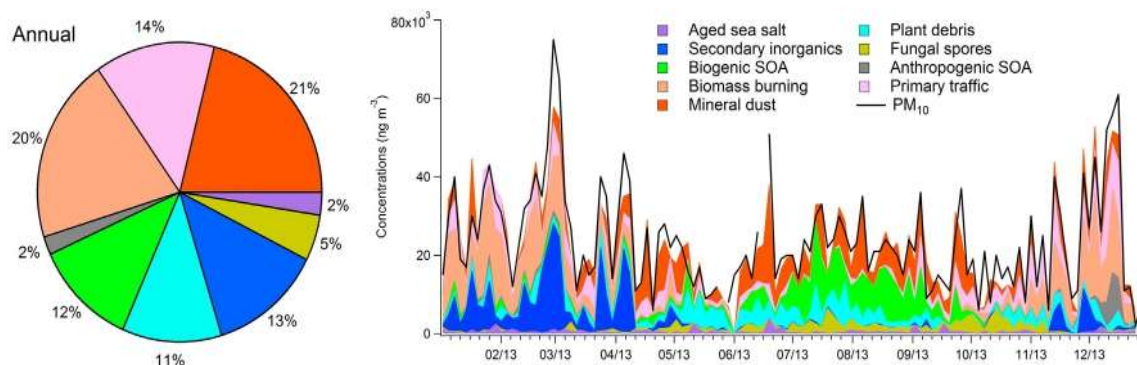


Fig. 2. Annual average contributions (left) and temporal evolution (right) of the identified sources to PM_{10} mass concentrations in Grenoble, Les Frères (2013).

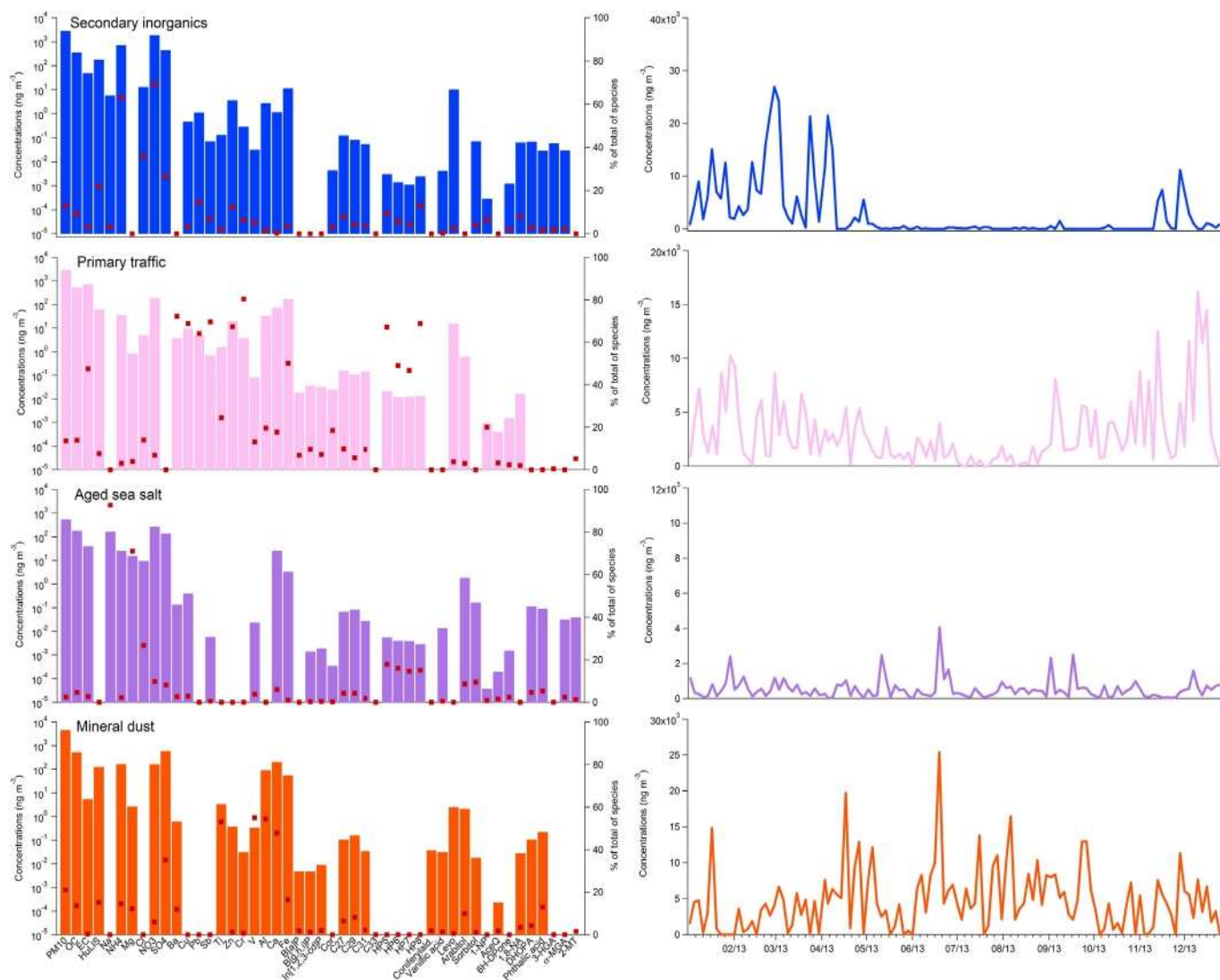


Fig. 3. Source profiles and temporal evolution of secondary inorganic, primary traffic, aged sea salt and mineral dust factors identified at Grenoble, Les Frères (2013).

contributed to this source factor by approximately 30–35%. The source showed large seasonal variations with very high concentrations and PM contributions during both severe PM pollution events in the early spring and, to a lesser extent, in the winter (Fig. 3). In the early spring, the high PM₁₀ concentration levels, concomitant to the high contributions of ammonium nitrate, were related to secondary formation processes, long range transport of aged air masses and direct emissions from biomass burning (Tomaz et al., 2017). On average, the sources of secondary inorganics accounted for approximately 47% of the PM₁₀ mass during this spring pollution event. Conversely, during the December PM pollution event, this factor accounted for only approximately 1% of the total PM₁₀ mass.

3.2.2. Primary traffic (exhaust and non-exhaust)

The PMF model always grouped the four hopanes (HP5 to HP8, 46% to 69% of the total mass of each compound) together with a significant amount of EC (48% of its total mass) into one factor (Fig. 3). These species are typical of traffic exhaust emissions and this factor was significantly correlated with NO_x ($r = 0.6$, $n = 123$, $p < 0.05$). As expected and following the applied constraints, this factor showed high contributions of several metals, such as Ba (72%), Cu (69%), Sb (70%), Pb (64%) and Fe (50%), known as additional good indicators of road traffic emissions (Pant and Harrison, 2012; Srivastava et al., 2016; Stembeck et al., 2002). In particular, Ba and Sb are known as specific markers of

vehicular brake abrasion (Johansson et al., 2009), showing that this factor accounted for both exhaust and non-exhaust traffic emissions. Regarding OC/EC (0.9) and PM₁₀/EC (4.3) ratios in the factor profile, their values obtained here are in good agreement with the literature data reported for primary traffic emissions (El Haddad et al., 2009; Fine et al., 2002). Interestingly, only 20% of 1-nitropyrene (1-NP), expected to be a marker of diesel emissions (Keyte et al., 2016), was associated with this factor. Despite several efforts, PMF was unable to increase the 1-NP contribution into this factor and it remained distributed in the biomass burning factor due its strong correlation with levoglucosan. The mixing of sources on 24 h filter samples, together with the specific geomorphology of Grenoble as well the atmospheric dynamic could explain such observed correlations.

Primary traffic sources accounted for 14% of the PM₁₀ mass on a yearly average (Fig. 2), corresponding to an annual mean concentration of 3.0 $\mu\text{g m}^{-3}$. These values are in the range of those commonly observed at other urban background locations in Europe (5–25%) (Belis et al., 2013; Waked et al., 2014) and with a previous study conducted at an heavy traffic site in Grenoble (traffic exhaust = 17%, traffic non-exhaust = 13%, contribution to PM₁₀) (Polo-Rehn et al., 2014). This source showed seasonal variations with higher concentrations in a cold period, notably due to the typical atmospheric dynamic in the valley of Grenoble. However, its contribution to PM₁₀ was rather constant through the year, except in July–August (summer vacations) when it

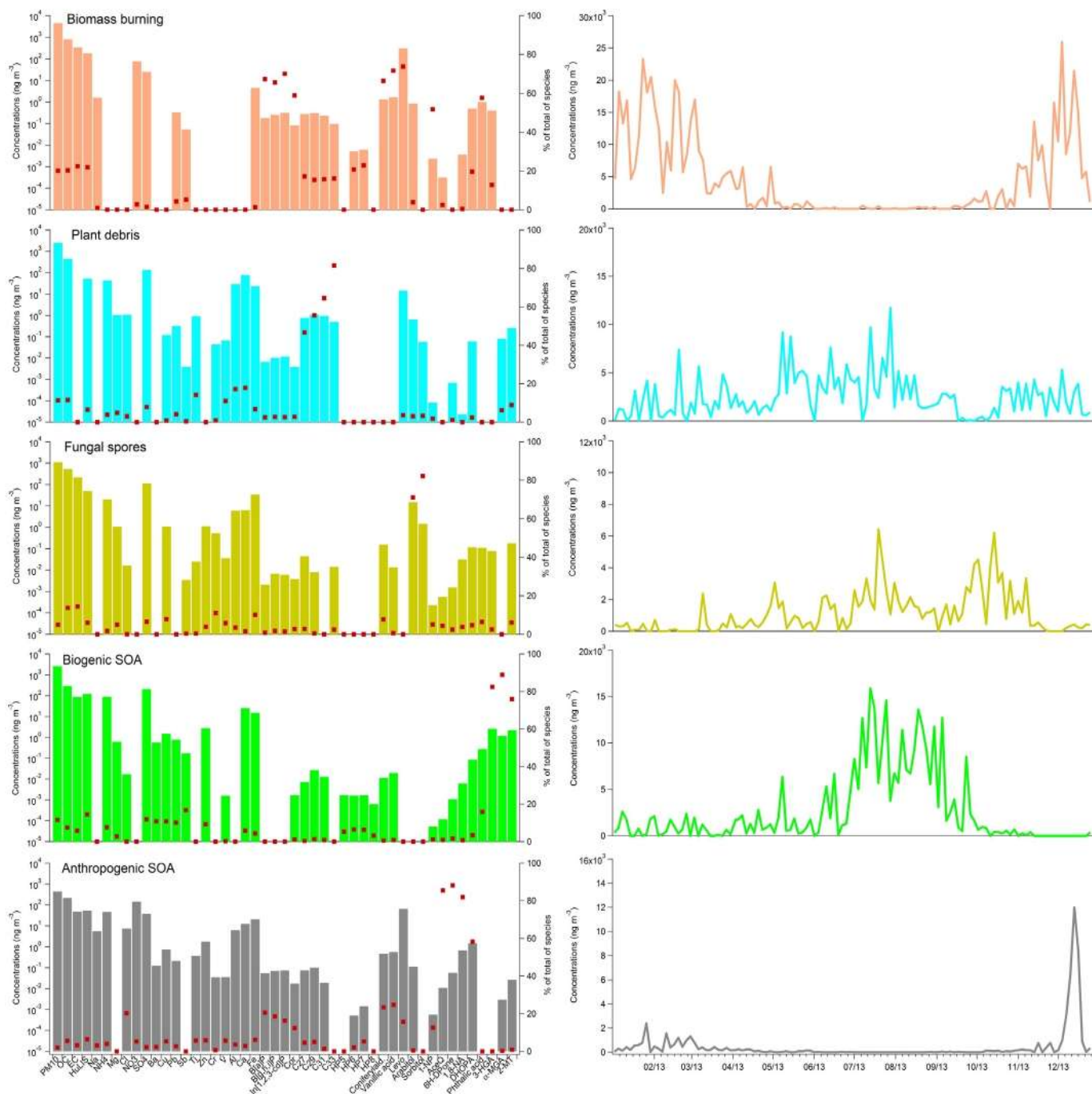


Fig. 4. Source profiles and temporal evolution of plant debris, fungal spores, biogenic SOA and anthropogenic SOA identified at Grenoble, Les Frènes (2013).

was slightly lower (Fig. 3). The highest concentrations of this source were observed during the December PM pollution event, but no drastic change of its relative contribution to PM₁₀ was noticed even during this episode.

3.2.3. Aged sea salt

Given the constraints applied, this factor showed major contributions of Na⁺ (92% in this factor) and Mg²⁺ (71% in this factor), highlighting that this source was chiefly from sea salt particles (Fig. 3). The Mg²⁺/Na⁺ ratio (0.10) was comparable to the expected ratio found for sea water (i.e., 0.11) (Curran et al., 1998; Seinfeld and Pandis, 2012) and similar to the values found at the same site in a previous study (Polo-Rehn et al., 2014). The low Cl⁻ content (27%) resulted in ageing processes, including well-known heterogeneous reactions between airborne sea-salt particles and acidic pollutants (e.g., nitric and sulfuric acid) leading to the volatilization of HCl (Seinfeld and Pandis, 2012). This source was rather constant throughout the year, with a

very low annual contribution (2%) to the PM₁₀ mass (Fig. 2) and a yearly average concentration of 0.5 μg m⁻³, which was in agreement with the sampling site location relatively far from the Atlantic and Mediterranean coasts (~200–500 km).

3.2.4. Mineral dust

This factor showed a relatively high content of mineral elements such as Ti (53% in this factor), Ca (49% in this factor), and Al (54% in this factor), commonly originating from soils and road dust (Andersen et al., 2007; Mossetti et al., 2005; Querol et al., 2004a; Yin et al., 2005) (Fig. 3). This was one of the major PM sources, corresponding to an average of 4.7 μg m⁻³ and accounting for 21% of the PM₁₀ mass on an annual average (Fig. 2). It showed a typical seasonal evolution with high concentrations and contributions in the summer (dry season). Significant amounts of OM (including HuLiS) and sulfate were also observed in the chemical profile of this source, in agreement with the presence of these species in soils, within resuspended particles, and/or as

condensation products onto crustal material (Falkovich et al., 2004; Kögel-Knabner, 2000).

3.2.5. Biomass burning

The source of the biomass burning factor was characterized by very high loadings of levoglucosan (levo), coniferaldehyde (conyferald.), and vanillic acid. This factor also showed significant contributions of PAHs (B[a]P, B[ghi]P, In[1,2,3-cd]P and Cor). It followed typical seasonal variations, with a largely higher contribution in winter (Fig. 4). This source accounted for 20% of the PM₁₀ mass on a yearly average ($4.5 \mu\text{g m}^{-3}$) (Fig. 2), with maximum contributions in winter of approximately 39%. These results were in very good agreement with previous observations reported in Europe (Herich et al., 2014; Viana et al., 2015) and at the same site in the winter by Favez et al. (2010). Approximately 22–25% of OC and HuLiS were associated with this factor on an annual average. Both species showed strong correlations with levoglucosan, especially during the cold period ($r = 0.85$ and 0.71 , $n = 91$, $p < 0.05$, i.e., late autumn and winter months). These results highlighted that biomass burning is a significant source of HuLiS, as already shown in previous field studies (Baduel et al., 2010; El Haddad et al., 2011; Lin et al., 2010). Finally, OC/levoglucosan and OC/EC ratios ($= 4.2$ and 3.8 , respectively) were in good agreement with those generally reported for aerosols from biomass burning (El Haddad et al., 2009; Favez et al., 2010; Fine et al., 2002; Gianini et al., 2013).

The biomass burning factor also included significant contributions from phthalic acid (58%) and, to a lesser extent, from DHOPA (20%). Both compounds are known as markers of SOA formation from the photooxidation of naphthalene and toluene, respectively (Al-Naiema and Stone, 2017; Kleindienst et al., 2004; Kleindienst et al., 2012; Kleindienst et al., 2007). In addition to vehicle exhaust, both these latter species are largely emitted by biomass burning (Baudic et al., 2016; Nalin et al., 2016; Shen et al., 2012), and previous chamber experiments have shown that SOA formation from biomass burning mainly involved the photooxidation of phenolic compounds, naphthalene, and benzene, which could together contribute up to 80% of the total observed SOA (Bruns et al., 2016). It is then expected that the factor obtained here includes both fresh and processed aerosols from biomass burning.

3.2.6. Primary biogenics 1: plant debris

This factor was characterized by a typical chemical fingerprint from plant waxes with significant amounts (47–82%) of odd number higher alkanes (C27 to C31) (Rogge et al., 1993) (Fig. 4). This source accounted for 11% of the PM₁₀ mass on an annual average ($2.5 \mu\text{g m}^{-3}$) (Fig. 2) and exhibited a clear seasonal pattern, with relatively higher concentrations in the warm period (May–August), in agreement with plant metabolic activity. However, concentrations were also significant for the rest of the year. PM source apportionment from plant emissions is usually not achieved in the literature. To the best of our knowledge, this is the first report of the identification of a plant debris source factor using higher alkanes in a PMF model (at least in Europe). A similar source has been identified in similar studies using other source apportionment models (van Drooge and Grimalt, 2015). However, as shown by the presence of elements such as Ti, V, Al, and Ca, the influence of other sources, such as resuspension from road dust and soil particles, cannot be ruled out.

3.2.7. Primary biogenics 2: fungal spores

This source factor was characterized by the large proportions of polyols (arabitol and sorbitol, 75–85% of the total mass of each compound in this factor) (Fig. 2). These compounds have been identified in the literature as markers of primary biogenic emissions originating from primary biological aerosol particles, notably fungal spores and microbes (Bauer et al., 2008; Caseiro et al., 2009; Rogge et al., 2007; Yttri et al., 2011), and previously used to apportion primary biogenic aerosols via a PMF analysis in France (Lens) (Waked et al., 2014). This factor contributed approximately 5% of the PM₁₀ mass on an annual average, with

a concentration of $1.1 \mu\text{g m}^{-3}$, which was significantly lower than the contribution estimated by Waked et al. (2014) (9% on a yearly average). This lower contribution might be explained by the fact that the present study allowed for better separation between two types of primary biogenic aerosols, as well as between primary and secondary organic aerosols.

Temporal evolution showed a clear seasonality, with maximum concentrations observed in the summer and fall seasons (from June to early November), in agreement with the higher biological activity due to higher temperatures and humidity inducing an increase in the emissions of fungal spores, fern spores and pollen grains (Graham et al., 2003; Verma et al., 2017). Maximum concentrations of arabitol and sorbitol have already been observed during the warm period in several previous studies (Bauer et al., 2008; Verma et al., 2017; Waked et al., 2014; Yttri et al., 2011).

3.2.8. Biogenic SOA

The sources of the biogenic SOA factor was resolved by the use of oxidation products of isoprene (α -methylglyceric acid (α -MGA and 2-methylerythritol (2-MT)) and of α -pinene (hydroxyglutaric acid (3-HGA)) (Carlton et al., 2009; Jaoui et al., 2008). The source factor showed very high contributions of these three SOA markers (78–90% of the total mass of each compound). The apportionment of biogenic SOA is not commonly achieved in PMF or other models based studies (Heo et al., 2013; Hu et al., 2010; Shrivastava et al., 2007; van Drooge and Grimalt, 2015; Zhang et al., 2009). Here, the evaluation of both biogenic SOA precursors to the total biogenic SOA contribution was not possible due to the strong correlation observed between isoprene and α -pinene SOA markers (e.g., (α -MGA and 2-MT vs 3-HGA, $r = 0.84$ and 0.86 , respectively; $n = 123$, $p < 0.05$)). The source of biogenic SOA showed a significant contribution to the PM₁₀ mass of 12% on an annual average, corresponding to a concentration of $2.6 \mu\text{g m}^{-3}$ (Fig. 2). A clear seasonal variation with larger contributions and concentrations in the summer was observed (up to 20% of PM and $16 \mu\text{g m}^{-3}$), in agreement with the higher biogenic SOC contributions already noticed during the warmer months in related studies (Kleindienst et al., 2007; Shrivastava et al., 2007; Zhang et al., 2009) (Fig. 4).

3.2.9. Anthropogenic SOA

The last factor was characterized by high loadings of acenaphthenequinone (86%), 6H-dibenzo[b,d]pyran-6-one (88%), 1,8-naphthalic anhydride (83%) and DHOPA (58%). As mentioned previously, DHOPA is considered a marker of SOA formation from toluene photooxidation (Al-Naiema and Stone, 2017; Kleindienst et al., 2004; Kleindienst et al., 2007), while the three other compounds are typically by-products of PAH oxidation (phenanthrene, acenaphthene and acenaphthylene) resulting in SOA formation (Lee and Lane, 2010; Lee et al., 2012; Perraudin et al., 2007; Tomaz et al., 2017; Zhou and Wenger, 2013a; Zhou and Wenger, 2013b). Thus, this factor seemed characteristic of SOA from anthropogenic sources, including combustion processes such as biomass burning and traffic. Note that the primary emission of PAH oxidation products, notably by biomass burning, cannot be ignored. However, poor correlations with levoglucosan have been observed ($r < 0.39$, $n = 123$, $p < 0.05$) and confirmed that these compounds were mainly originated from secondary processes in the Grenoble valley.

Anthropogenic SOA accounted for approximately 2% of the total PM₁₀ mass, with a concentration of $0.5 \mu\text{g m}^{-3}$ on an annual average (Fig. 2).

The source showed higher concentrations during the winter season and especially in December during the severe PM pollution event, with a contribution to PM₁₀ of up to 18% (Fig. 4).

To the best of our knowledge, this study is probably the first report of the use of PAH derivatives (here oxy-PAHs) for the apportionment of an anthropogenic SOA (PAH SOA) source. Additional tests have been performed to investigate the validity of this factor. To do this, we excluded

the December data points from the complete dataset and ran the PMF model again (Table S9). The new PMF results showed that the nine factors solution was also found to be optimum and quite stable (with bootstrap >98%) (Table S10). The chemical and temporal profiles for all the factors were totally similar to those obtained with the entire dataset, even including this factor (Figs. S11 and S12, Table S11). These results confirmed the robustness of PMF outputs, which are not perturbed by the severe winter pollution event.

The large concentration peak of the source of anthropogenic SOA observed during the December PM pollution event was also noticed for all primary pollutants, including EC, levoglucosan, hopanes, several alkanes, PAHs, 1-nitropyrene and NO, underlining the large impact of primary combustion sources during this period (Tomaz et al., 2017; Tomaz et al., 2016). In addition, several secondary compounds from anthropogenic precursors, such as DHOPA, methyl-nitrocatechols (markers for biomass burning SOA) (Iinuma et al., 2010), succinic and phthalic acids (Kawamura and Ikushima, 1993; Kleindienst et al., 2012) and nitro- and oxy-PAHs, exhibited very high concentrations during this period (Fig. 5).

Such an event and anthropogenic SOA concentrations could be explained by a combination of several factors. First, the meteorological conditions and the geomorphology around Grenoble promoted the formation and the occurrence of thermal inversion layers for >10 consecutive days (Fig. 1) (Tomaz et al., 2017). Together with the low wind speed (<2 m s⁻¹) (Fig. S3), this led to the stagnation of polluted air masses over a long period, allowing favourable conditions for chemical reactions and intense secondary formation processes. Second and interestingly, most of the metallic species and notably the transition metals (Fe, Cu, Cr, V...) showed a concentration peak during the December PM pollution event (Fig. 6). Such an increase of concentrations is still not fully understood, but these redox-active metals, and especially Fe and Cu, are known to be involved in the catalysis of Fenton-like reactions in which they may react with hydrogen peroxide (H₂O₂) to generate OH radicals (Walling, 1975). In addition, recent studies have stated the role of a Fenton reagent (Fe, Cu/H₂O₂) in both SOA formation and PAH oxidation (Singh and Gupta, 2016; Singh and Gupta, 2017; Singh et al., 2017). Thus, transition metals could have played a significant role in the enhancement of the chemical processes and the anthropogenic SOA formation during this period. Last, Tong et al. (2016) have recently shown that SOA decomposition may also lead to the formation of OH radicals. The OH production rate by SOA decomposition depends on Fe²⁺, SOA precursors and concentrations. Such a process seems quantitatively comparable to the Fenton reaction in most conditions and may

be the main source of OH radicals at low concentrations of H₂O₂ and Fe²⁺. Then, the OH radicals generated would promote SOA chemical ageing, especially in the presence of iron, increasing auto-oxidation in the condensed phase and further resulting in a self-amplification cycle of SOA formation (Tong et al., 2016). All these conditions were present during the December PM pollution event to promote these processes and enhance SOA formation.

3.3. Sources of coarse and fine aerosol fractions

Overall, the coarse aerosol fraction (PM₁₀-PM_{2.5}) accounted for one-third of the PM₁₀ mass. Such a proportion is in agreement with those previously reported in many different urban environments (Masri et al., 2015; Querol et al., 2004b). Fig. 7 shows the tentative reconstruction of both aerosol fractions using apportioned PM sources. Interestingly, the sum of the three source factors, namely plant debris, aged sea salt, and mineral dust, showed a significant correlation with the PM mass concentration of the coarse particle mode ($r = 0.71$; $n = 123$, $p < 0.05$). Note that to date, no consensus has emerged to precisely decide whether the source of fungal spores belongs to the fine or the coarse aerosol fraction (Liang et al., 2013; Waked et al., 2014; Wang et al., 2011). The sum of the 5 or 6 other source factors identified (PM_{2.5} vs. Σ_5 factors, $r = 0.91$; $n = 123$, $p < 0.05$) (PM_{2.5} vs. Σ_6 factors, $r = 0.92$; $n = 123$, $p < 0.05$) was in very good agreement with the fine aerosol mass fraction. These results highlighted that fine particles were associated mostly with primary carbonaceous emissions together with secondary processes, while coarse particles consisted mostly of mineral dust and organic matter.

3.4. Organic aerosol source apportionment

3.4.1. Organic carbon (OC)

OC source contributions apportioned from the present PMF analysis are presented in Fig. 8. On an annual average, the major contributors to OC were biomass burning (25%), primary traffic (12%), mineral dust (13%), fungal spores (12%), secondary inorganics (11%) and plant debris (10%), followed by both SOA fractions (14% in total) and aged sea salt (3%).

These results highlighted the large contributions of primary OA sources, namely, biomass burning, traffic and biogenic source (59% in total on an annual average). The significant impact of biomass burning within OC was in good agreement with previous findings at Grenoble (Favez et al., 2010). As expected, elevated contributions of this source

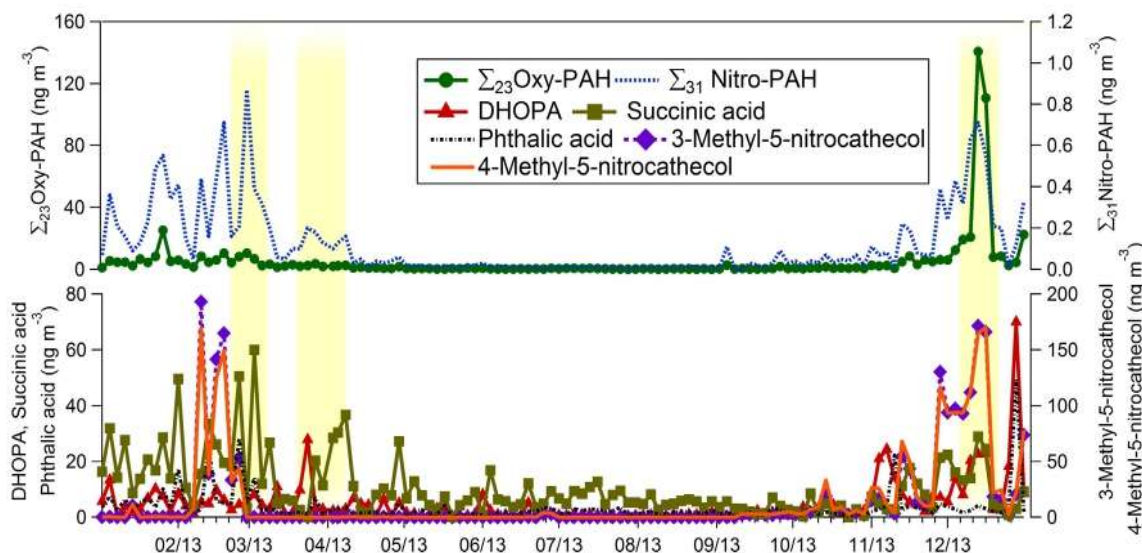


Fig. 5. Temporal variation of the concentrations of Σ_{23} Oxy-PAHs, Σ_{31} Nitro-PAHs, DHOPA, methyl-nitrocatechols, succinic and phthalic acids observed at Grenoble, Les Frères (2013).

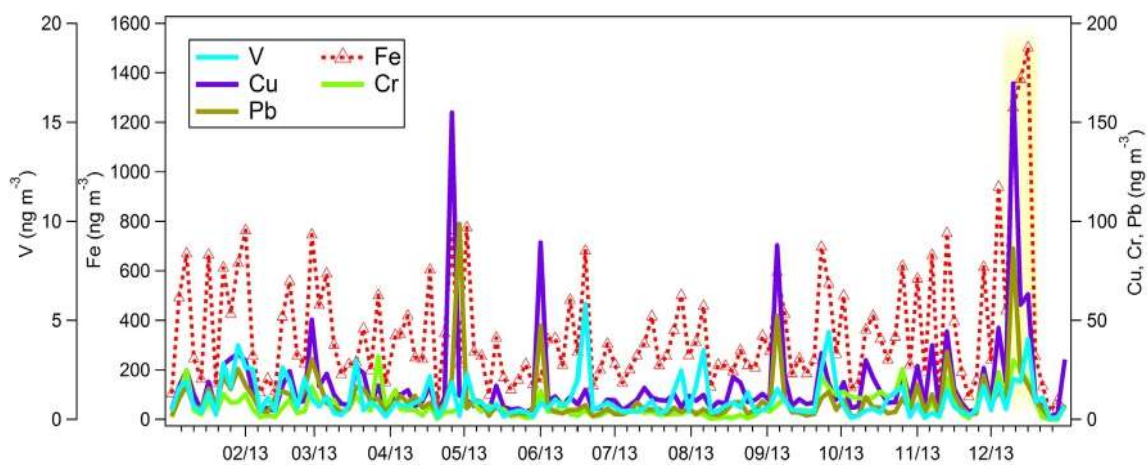


Fig. 6. Temporal variation of selected metal concentrations (Fe, Cu, Cr, Pb, and V) observed at Grenoble, Les Frênes (2013).

to OC were obtained during the long residential heating periods in this region (20%, 20% and 43% for the spring, fall and winter seasons, respectively). In addition, the traffic contribution was in the same range as that previously reported (Favez et al., 2010). The primary biogenic fraction, consisting of fungal spores and plant debris, accounted for a considerable fraction of OC (22%), with a typical seasonal variation along with maximum concentrations and contributions up to 40% in the summer, which was related to the increase in biological activity.

Other sources, secondary inorganics, mineral dust and aged sea salt accounted together for 27% of the total OC load on a yearly basis. The primary or secondary origins of OC for these sources are discussed hereafter. The source of secondary inorganics showed a conspicuous seasonal time trend. High contributions during the spring and winter seasons were likely associated with the PM pollution events. This source factor showed a good correlation with oxalate only in the winter ($r = 0.84$, $n = 31$, $p < 0.05$) and fall ($r = 0.70$, $n = 30$, $p < 0.05$), indicating the influence of secondary origins for this OA source. The source of mineral dust showed a higher contribution in the summer (22%), similar to the time trend, followed by secondary processes. The presence of HuLiS, phthalic acid, and sulfate in this source factor suggested that a part of OC was likely to be secondary. The condensation of secondary organic species on mineral dust could occur during long range transport. In addition, mineral dust may facilitate very active redox chemistry on its surface under certain conditions (i.e., in the presence of metal oxides

such as TiO_2 , ZnO, iron oxides and their exposure to sunlight) and lead to the formation of a number of different oxidized products (Aymoz et al., 2004; George et al., 2015). Similarly, the OC fraction in the aged sea-salt factor may be produced via a primary or bubble-mediated production mechanism at the ocean surface (Ceburnis et al., 2008), but their ageing could be explained by exposure to secondary organic aerosols precursors during the transport of air masses (Song and Carmichael, 1999).

SOA fractions from clearly identified biogenic and anthropogenic precursor origins together accounted for 14% of OC on an annual basis and ranged from 7% to 27% depending on the season. This rather low contribution could be explained by the presence of SOA in other source factors, as discussed above. The maximum contribution was observed in the summer and is of biogenic origin. Conversely, anthropogenic SOA accounted for 15% of OC in the winter and up to 42% during the December PM pollution event.

Clear-cut anthropogenic sources (i.e., primary traffic, biomass burning and anthropogenic SOA) and biogenic sources (primary and secondary) accounted for 43% and 30% of total OC on an annual average, respectively. The remaining 27% (distributed between mineral dust, secondary inorganics and aged sea salt factors) could not be unambiguously ascribed to either anthropogenic or biogenic origins. The maximum anthropogenic OC contribution was obtained during the winter season (>71%), notably due to the impact of residential heating and

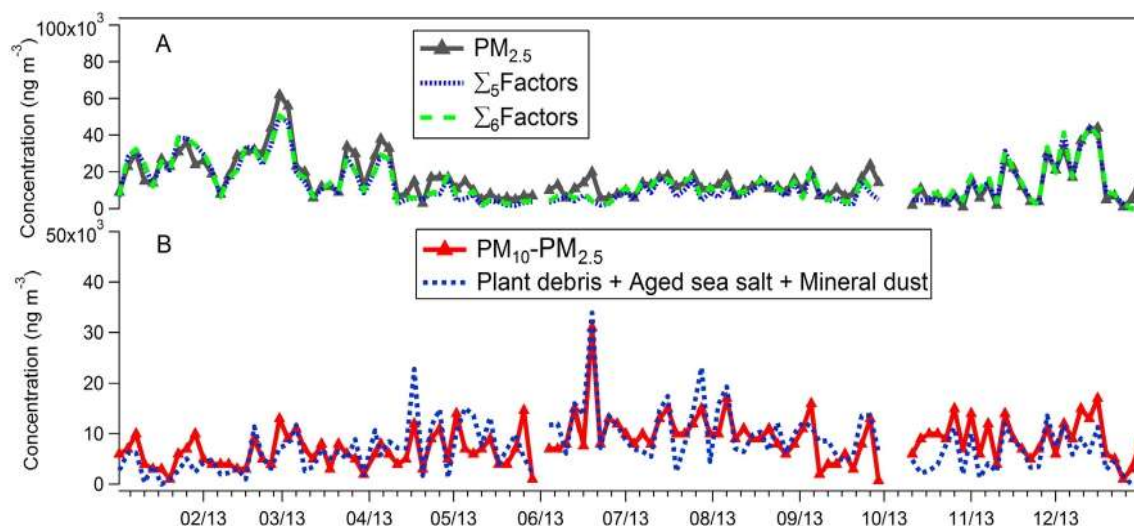


Fig. 7. Tentative reconstruction of fine ($\text{PM}_{2.5}$) (A) and coarse ($\text{PM}_{10}-\text{PM}_{2.5}$) (B) aerosol fractions observed at Grenoble, Les Frênes (2013) using identified PM sources by PMF model. $\Sigma_5\text{Factors}$ = Primary traffic + Secondary inorganic + Biomass burning + Anthropogenic SOA + Biogenic SOA; $\Sigma_6\text{Factors}$ = Primary traffic + Secondary inorganic + Biomass burning + Anthropogenic SOA + Biogenic SOA + Fungal spores.

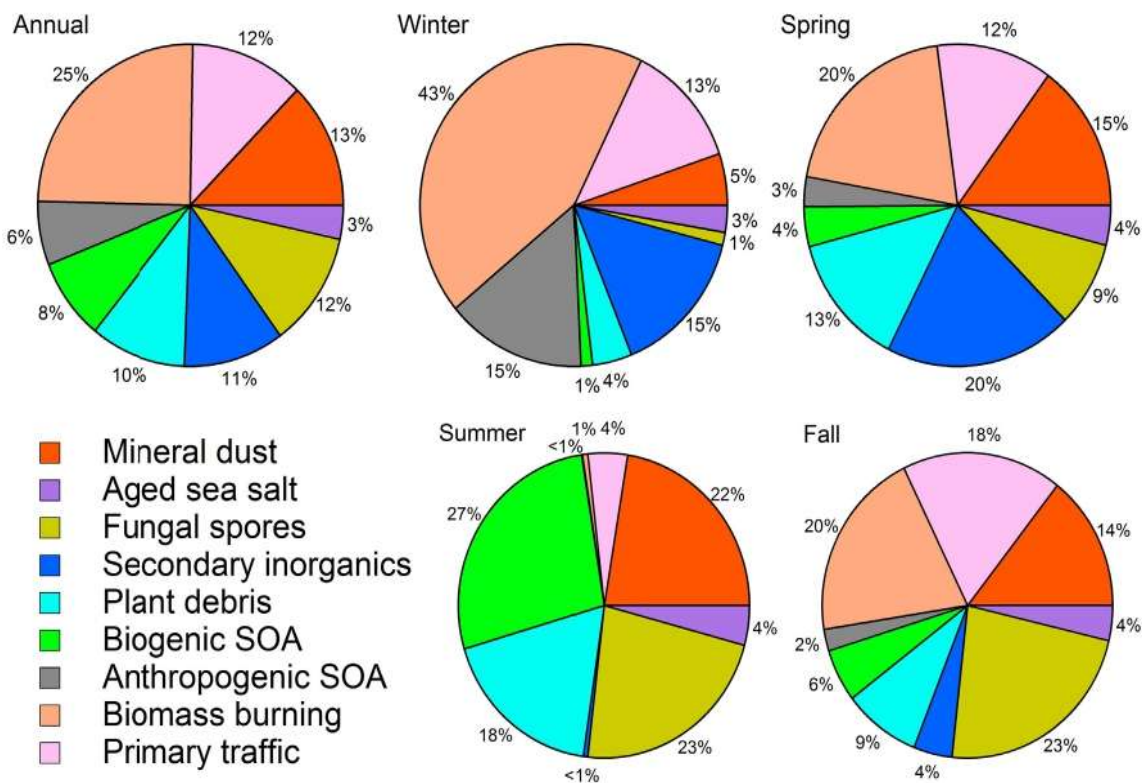


Fig. 8. Annual and seasonal contributions of the identified sources to OC concentrations at Grenoble, Les Frênes (2013).

the accumulation of pollutants in the valley of Grenoble, whereas the biogenic OC contribution was greatest in the summer (>68%).

3.4.2. Humic like substances (HuLiS)

HuLiS play an important role in the atmosphere by affecting the growth of particles (Gysel et al., 2004), cloud condensation and ice nuclei formation (Facchini et al., 1999; Wang and Knopf, 2011) due to their

hygroscopic and surface-active properties. They account for a significant fraction of OM (approximately 10 to 30%) (Feczko et al., 2007). They are probably poorly photoactive (Albinet et al., 2010) but may directly react with oxidants (Baduel et al., 2011). They have been found to catalytically enhance the generation of reactive oxygen species (ROS) under simulated physiological conditions and may contribute to PM health impacts (Lin and Yu, 2011). The current knowledge and understanding

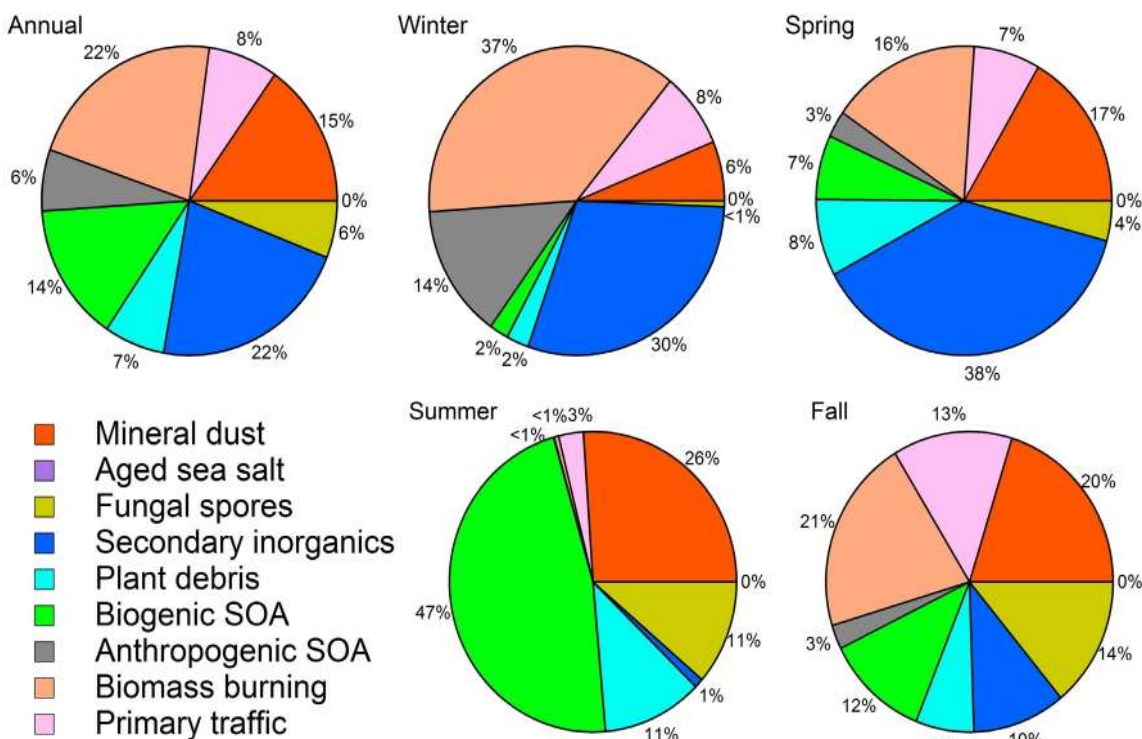


Fig. 9. Annual and seasonal contributions of the identified sources to HuLiS concentrations at Grenoble, Les Frênes (2013).

of the sources and formation mechanisms of HuLiS are still rather poor due to the lack of source apportionment studies of this OA component (Baduel et al., 2010).

On an annual average, HuLiS accounted for approximately 8% of OM in Grenoble (from 2 to 20%) and among the nine sources resolved by PMF, only aged sea salt did not contribute to HuLiS mass (Fig. 9). Overall, 22%, 22%, 15%, and 14% of HuLiS mass were respectively associated with biomass burning, secondary inorganics, mineral dust and biogenic SOA on an annual average. PMF outputs also indicated that a non-negligible amount of HuLiS mass was attributed to plant debris, primary biogenic and primary traffic. Each of these latter sources contributed to approximately 6–8% on annual average of total HuLiS, with higher contributions in the summer for plant debris (11%) and in the summer and fall for fungal spores (11–14%). While traffic emission origins have already been assigned to HuLiS (Kuang et al., 2015), no previous study explicitly reported the contribution of primary biogenics (fungal spores + plant debris) OA to these compounds.

The contribution of biomass burning to HuLiS showed a strong seasonal trend (Fig. 9). It is well known that biomass combustion processes release large quantities of aromatic species into the atmosphere (Graham et al., 2002) and represent the most likely contributor to HuLiS mass in urban areas during the cold season (Baduel et al., 2010). This was confirmed by the strong correlation observed between HuLiS and levoglucosan ($r = 0.81$) and the major contribution of this source to HuLiS in the winter (37%).

Secondary inorganics showed high contributions to HuLiS in the spring and winter (30–38%) and negligible input in the summer. Significant correlations were observed between HuLiS and secondary inorganic species in the spring (HuLiS vs. NH_4^+ , SO_4^{2-} , NO_3^- , $r = 0.82$ – 0.84 , $n = 30$, $p < 0.05$) and winter (HuLiS vs. NH_4^+ , SO_4^{2-} , NO_3^- , $r = 0.68$ – 0.76 , $n = 31$, $p < 0.05$). Both chamber and field studies reported up to now have shown that heterogeneous reactions of organic compounds with sulfate aerosols lead to the formation of organosulfates (Riva et al., 2015; Surratt et al., 2008), which are a major class of compounds of the HuLiS fraction (Lin et al., 2012). Sulfate aerosols, VOCs and SVOCs (including PAHs) were abundant in the Grenoble valley during the PM pollution events and could cause enhanced HuLiS formation. In addition to organosulfates, nitrated organic compounds (organonitrates) have been reported to be constituents of HuLiS (Lin et al., 2012). Organonitrates may contribute substantially to OM, especially in Europe (Kiedler-Scharr et al., 2009), and notably could have been formed during the spring PM pollution events, as has been shown for nitro-PAHs (Tomaz et al., 2017).

The large contribution of the biogenic SOA factor to HuLiS observed in the summer (47%) can also be explained by secondary formation processes. Indeed, aqueous-phase oxidation and heterogeneous reactions involving oxidation products of biogenic VOCs (i.e., isoprene, α -pinene, limonene, etc.) are known to produce HuLiS (Surratt et al., 2008). In addition, anthropogenic SOA showed a low contribution to HuLiS on an annual average (6%) but was remarkably higher in winter (14%), especially during the December PM pollution event, as described previously. Organosulfate formation from the gas phase oxidation of PAHs (Riva et al., 2015) and the formation of HuLiS from secondary processes in liquid phase from aromatic acid precursors during biomass burning events (Altieri et al., 2008; Baduel et al., 2010; El Haddad et al., 2011) may explain such observations.

Finally, mineral dust also contributed significantly to HuLiS, especially in the warm period (17%–26%), with the highest contribution in the summer, which could be explained by both primary and secondary origins. HuLiS are known to be partly emitted as a primary source from soils (Graber and Rudich, 2006). High correlations were noticed between HuLiS and oxalate and O_3 ($r = 0.60$ – 0.70 , $n = 31$, $p < 0.05$) in the summer (Fig. S13). As discussed before, mineral dust could also play a major role in secondary redox processes under favourable atmospheric conditions (George et al., 2015), and the link between HuLiS and mineral dust could be partly related to such processes.

4. Conclusion

Source apportionment performed using specific primary and secondary molecular markers indicated nine major PM_{10} sources in Grenoble (France), including sources rarely apportioned, such as primary biogenics (fungal spores + plant debris) as well as explicit SOA factors. Major contributors to PM_{10} mass on an annual average were biomass burning and mineral dust (~20% of PM_{10} for each of them), followed by primary traffic (14%). A high contribution of anthropogenic SOA was also observed during an intense wintertime PM pollution event. This could be explained by the accumulation of pollutants due to specific meteorological conditions and the enhancement of SOA formation via probable Fenton-like reactions and self-amplification cycles.

PMF outputs also allowed the clear identification of the overwhelming biogenic origins of organic aerosols during the summer season (>68% of total OC), contrasting with the predominance of anthropogenic OC during wintertime. Moreover, a peculiar emphasis was put on the sources of HuLiS, a class of compounds that constitutes a significant fraction of organic matter and is commonly considered a proxy of low volatile oxygenated organic aerosols. The results obtained here enlightened the diversity of the primary and secondary origins of these compounds, being mainly associated with biomass burning (22%), secondary inorganics (22%), mineral dust (15%), and biogenic SOA (14%) on an annual scale in Grenoble.

The findings presented in this paper demonstrate that the speciation of the organic aerosol fraction and the input of specific molecular markers into source-receptor model are powerful tools to evaluate the contributions of discriminated OA sources and to get a better understanding of PM origins. Future works could try to incorporate even more markers (e.g., organosulfates and organonitrates) to further discriminate the nature (e.g., biogenic vs. anthropogenic) of organic aerosols that are associated with secondary inorganics, as well as mineral dusts. The use of higher time-resolution datasets (e.g., filter sampling every 6 h or less) could also allow the better apportionment of the influence of various secondary formation mechanisms that present different diurnal cycles.

Acknowledgements

The authors wish to thank the French Ministry of the Environment (MTE) and the French Ministry of Research for their financial support. This work was done as part of the LCSQA activities (French reference laboratory for air quality monitoring). The authors thank Atmo Rhône-Alpes-Auvergne for filter samplings, air quality and meteorological data, Nadine Guillaumet and Noémie Nuttens for PAH analyses, Coralie Connes and Vincent Lucaire for the EC/OC, IC, sugars, organic acids and HuLiS measurements, Nathalie Bocquet and Robin Aujay-Plouzeau for sample preparation and Patrick Bodu for the graphical abstract design. The Labex OSUG@2020 (ANR-10-LABX-56) is gratefully acknowledged for the analytical equipment at IGE.

Appendix A. Supplementary data

Supplementary data to this article can be found online at <https://doi.org/10.1016/j.scitotenv.2017.12.135>.

References

- Albinet, A., Leoz-Garziandia, E., Budzinski, H., Villenave, E., 2006. Simultaneous analysis of oxygenated and nitrated polycyclic aromatic hydrocarbons on standard reference material 1649a (urban dust) and on natural ambient air samples by gas chromatography-mass spectrometry with negative ion chemical ionisation. *J. Chromatogr. A* 1121, 106–113.
- Albinet, A., Leoz-Garziandia, E., Budzinski, H., Villenave, E., 2007. Polycyclic aromatic hydrocarbons (PAHs), nitrated PAHs and oxygenated PAHs in ambient air of the Marseilles area (south of France): concentrations and sources. *Sci. Total Environ.* 384, 280–292.

- Albinet, A., Leoz-Garziandia, E., Budzinski, H., Villenave, E., Jaffrezo, J.-L., 2008. Nitrate and oxygenated derivatives of polycyclic aromatic hydrocarbons in the ambient air of two French alpine valleys: part 1: concentrations, sources and gas/particle partitioning. *Atmos. Environ.* 42, 43–54.
- Albinet, A., Minero, C., Vione, D., 2010. Photochemical generation of reactive species upon irradiation of rainwater: negligible photoactivity of dissolved organic matter. *Sci. Total Environ.* 408, 3367–3373.
- Albinet, A., Tomaz, S., Lestremay, F., 2013. A really quick easy cheap effective rugged and safe (QuEChERS) extraction procedure for the analysis of particle-bound PAHs in ambient air and emission samples. *Sci. Total Environ.* 450–451, 31–38.
- Albinet, A., Nalin, F., Tomaz, S., Beaumont, J., Lestremay, F., 2014. A simple QuEChERS-like extraction approach for molecular chemical characterization of organic aerosols: application to nitrated and oxygenated PAH derivatives (NPAH and OPAH) quantified by GC-NICMS. *Anal. Bioanal. Chem.* 406, 3131–3148.
- Alleman, L.Y., Lamaison, L., Perdrix, E., Robache, A., Galloo, J.-C., 2010. PM10 metal concentrations and source identification using positive matrix factorization and wind sectoring in a French industrial zone. *Atmos. Res.* 96, 612–625.
- Al-Naiema, I.M., Stone, E.A., 2017. Evaluation of anthropogenic secondary organic aerosol tracers from aromatic hydrocarbons. *Atmos. Chem. Phys.* 17, 2053–2065.
- Altieri, K., Seitzinger, S., Carlton, A., Turpin, B., Klein, G., Marshall, A., 2008. Oligomers formed through in-cloud methylglyoxal reactions: chemical composition, properties, and mechanisms investigated by ultra-high resolution FT-ICR mass spectrometry. *Atmos. Environ.* 42, 1476–1490.
- Andersen, Z.J., Wahlin, P., Raaschou-Nielsen, O., Scheike, T., Loft, S., 2007. Ambient particle source apportionment and daily hospital admissions among children and elderly in Copenhagen. *J. Expo. Sci. Environ. Epidemiol.* 17, 625.
- Aymoz, G., Jaffrezo, J.-L., Jacob, V., Colomb, A., George, C., 2004. Evolution of organic and inorganic components of aerosol during a Saharan dust episode observed in the French Alps. *Atmos. Chem. Phys.* 4, 2499–2512.
- Baduel, C., Voisin, D., Jaffrezo, J.L., 2010. Seasonal variations of concentrations and optical properties of water soluble HULIS collected in urban environments. *Atmos. Chem. Phys.* 10, 4085–4095.
- Baduel, C., Monge, M.E., Voisin, D., Jaffrezo, J.-L., George, C., Haddad, I.E., Marchand, N., D'anna, B., 2011. Oxidation of atmospheric humic like substances by ozone: a kinetic and structural analysis approach. *Environ. Sci. Technol.* 45, 5238–5244.
- Baudic, A., Gros, V., Sauvage, S., Locoge, N., Sanchez, O., Sarda-Estève, R., Kalogridis, C., Petit, J.-E., Bonnaire, N., Baisnée, D., 2016. Seasonal variability and source apportionment of volatile organic compounds (VOCs) in the Paris megacity (France). *Atmos. Chem. Phys.* 16, 11961–11989.
- Bauer, H., Claeys, M., Vermeylen, R., Schueller, E., Weinke, G., Berger, A., Puxbaum, H., 2008. Arabitol and mannitol as tracers for the quantification of airborne fungal spores. *Atmos. Environ.* 42, 588–593.
- Belis, C.A., Karagulian, F., Larsen, B.R., Hopke, P.K., 2013. Critical review and meta-analysis of ambient particulate matter source apportionment using receptor models in Europe. *Atmos. Environ.* 69, 94–108.
- Boucher, O., Randall, D., Artaxo, P., Bretherton, C., Feingold, G., Forster, P., Kerminen, V.-M., Kondo, Y., Liao, H., Lohmann, U., 2013. Clouds and Aerosols. *Climate Change 2013: The Physical Science Basis. Contribution of Working Group I to the Fifth Assessment Report of the Intergovernmental Panel on Climate Change.* Cambridge University Press, pp. 571–657.
- Bruns, E.A., El Haddad, I., Slowik, J.G., Kilic, D., Klein, F., Baltensperger, U., Prévôt, A.S.H., 2016. Identification of significant precursor gases of secondary organic aerosols from residential wood combustion. *Sci. Rep.* 6, 27881.
- Carlton, A.G., Wiedinmyer, C., Kroll, J.H., 2009. A review of secondary organic aerosol (SOA) formation from isoprene. *Atmos. Chem. Phys.* 9, 4987–5005.
- Caseiro, A., Bauer, H., Schmidl, C., Pio, C.A., Puxbaum, H., 2009. Wood burning impact on PM10 in three Austrian regions. *Atmos. Environ.* 43, 2186–2195.
- Cavalli, F., Viana, M., Yttri, K., Genberg, J., Putaud, J.-P., 2010. Toward a standardised thermal-optical protocol for measuring atmospheric organic and elemental carbon: the EUSAAR protocol. *Atmos. Meas. Tech.* 3, 79–89.
- Ceburnis, D., O'Dowd, C.D., Jennings, G.S., Facchini, M.C., Emblico, L., Decesari, S., Fuzzi, S., Sakaly, J., 2008. Marine aerosol chemistry gradients: elucidating primary and secondary processes and fluxes. *Geophys. Res. Lett.* 35.
- Curran, M.A., Van Ommen, T.D., Morgan, V., 1998. Seasonal characteristics of the major ions in the high-accumulation Dome Summit South ice core, Law Dome, Antarctica. *Ann. Glaciol.* 27, 385–390.
- van Drooge, B.L., Grimalt, J.O., 2015. Particle size-resolved source apportionment of primary and secondary organic tracer compounds at urban and rural locations in Spain. *Atmos. Chem. Phys.* 15, 7735–7752.
- El Haddad, I., Marchand, N., Dron, J., Temime-Roussel, B., Quivet, E., Wortham, H., Jaffrezo, J.L., Baduel, C., Voisin, D., Besombes, J.L., Gille, G., 2009. Comprehensive primary particulate organic characterization of vehicular exhaust emissions in France. *Atmos. Environ.* 43, 6190–6198.
- El Haddad, I., Marchand, N., Temime-Roussel, B., Wortham, H., Piot, C., Besombes, J.L., Baduel, C., Voisin, D., Armengaud, A., Jaffrezo, J.L., 2011. Insights into the secondary fraction of the organic aerosol in a Mediterranean urban area: Marseille. *Atmos. Chem. Phys.* 11, 2059–2079.
- Facchini, M.C., Fuzzi, S., Zappoli, S., Andracchio, A., Gelencsér, A., Kiss, G., Krivácsy, Z., Mészáros, E., Hansson, H.C., Albers, T., 1999. Partitioning of the organic aerosol component between fog droplets and interstitial air. *J. Geophys. Res.-Atmos.* 104, 26821–26832.
- Falkovich, A.H., Schkolnik, G., Ganor, E., Rudich, Y., 2004. Adsorption of organic compounds pertinent to urban environments onto mineral dust particles. *J. Geophys. Res.-Atmos.* 109.
- Favez, O., 2013. Synthèse des travaux 2013 du programme CARA. LCSQA (French language). DR-13-136071-14096A. <https://www.lcsqa.org/rapport/2013/ineris/synthese-travaux-2013-programme-cara>.
- Favez, O., El Haddad, I., Piot, C., Boréave, A., Abidi, E., Marchand, N., Jaffrezo, J.L., Besombes, J.L., Personnaz, M.B., Sciare, J., Wortham, H., George, C., D'Anna, B., 2010. Inter-comparison of source apportionment models for the estimation of wood burning aerosols during wintertime in an alpine city (Grenoble, France). *Atmos. Chem. Phys.* 10, 5295–5314.
- Feczko, T., Puxbaum, H., Kasper-Giebl, A., Handler, M., Limbeck, A., Gelencsér, A., Pio, C., Preunkert, S., Legrand, M., 2007. Determination of water and alkaline extractable atmospheric humic-like substances with the TU Vienna HULIS analyzer in samples from six background sites in Europe. *J. Geophys. Res.-Atmos.* 112, D23510.
- Fine, P.M., Cass, G.R., Simoneit, B.T., 2002. Chemical characterization of fine particle emissions from the fireplace combustion of woods grown in the southern United States. *Environ. Sci. Technol.* 36, 1442–1451.
- George, C., Ammann, M., D'Anna, B., Donaldson, D.J., Nizkorodov, S.A., 2015. Heterogeneous photochemistry in the atmosphere. *Chem. Rev.* 115, 4218–4258.
- Gianini, M.F.D., Fischer, A., Gehrig, R., Ulrich, A., Wichser, A., Piot, C., Besombes, J.L., Hueglin, C., 2012. Comparative source apportionment of PM10 in Switzerland for 2008/2009 and 1998/1999 by positive matrix factorisation. *Atmos. Environ.* 54, 149–158.
- Gianini, M., Piot, C., Herich, H., Besombes, J.-L., Jaffrezo, J.-L., Hueglin, C., 2013. Source apportionment of PM10, organic carbon and elemental carbon at Swiss sites: an inter-comparison of different approaches. *Sci. Total Environ.* 454, 99–108.
- Golly, B., Brulfert, G., Berlioux, G., Jaffrezo, J.L., Besombes, J.L., 2015. Large chemical characterisation of PM10 emitted from graphite material production: application in source apportionment. *Sci. Total Environ.* 538, 634–643.
- Graber, E.R., Rudich, Y., 2006. Atmospheric HULIS: how humic-like are they? A comprehensive and critical review. *Atmos. Chem. Phys.* 6, 729–753.
- Graham, B., Mayol-Bracero, O.L., Guyon, P., Roberts, G.C., Decesari, S., Facchini, M.C., Artaxo, P., Maenhaut, W., Koll, P., Andreae, M.O., 2002. Water-soluble organic compounds in biomass burning aerosols over Amazonia - 1. Characterization by NMR and GC-MS. *J. Geophys. Res.-Atmos.* 107.
- Graham, B., Guyon, P., Maenhaut, W., Taylor, P.E., Ebert, M., Matthias-Maser, S., Mayol-Bracero, O.L., Godoi, R.H., Artaxo, P., Meixner, F.X., 2003. Composition and diurnal variability of the natural Amazonian aerosol. *J. Geophys. Res.-Atmos.* 108.
- Gysel, M., Weingartner, E., Nyeki, S., Paulsen, D., Baltensperger, U., Galambos, I., et al., 2004. Hygroscopic properties of water-soluble matter and humic-like organics in atmospheric fine aerosol. *Atmos. Chem. Phys.* 4, 35–50.
- Heal, M.R., Kumar, P., Harrison, R.M., 2012. Particles, air quality, policy and health. *Chem. Soc. Rev.* 41, 6606–6630.
- Hennigan, C.J., Sullivan, A.P., Collett, J.L., Robinson, A.L., 2010. Levoglucosan stability in biomass burning particles exposed to hydroxyl radicals. *Geophys. Res. Lett.* 37, L09806.
- Heo, J., Dulger, M., Olson, M.R., McGinnis, J.E., Shelton, B.R., Matsunaga, A., Sioutas, C., Schauer, J.J., 2013. Source apportionments of PM2.5 organic carbon using molecular marker positive matrix factorization and comparison of results from different receptor models. *Atmos. Environ.* 73, 51–61.
- Herich, H., Gianini, M., Piot, C., Močnik, G., Jaffrezo, J.-L., Besombes, J.-L., Prévôt, A., Hueglin, C., 2014. Overview of the impact of wood burning emissions on carbonaceous aerosols and PM in large parts of the Alpine region. *Atmos. Environ.* 89, 64–75.
- Hu, D., Bian, Q., Lau, A.K.H., Yu, J.Z., 2010. Source apportioning of primary and secondary organic carbon in summer PM2.5 in Hong Kong using positive matrix factorization of secondary and primary organic tracer data. *J. Geophys. Res.-Atmos.* 115.
- Iinuma, Y., Boge, O., Grafe, R., Herrmann, H., 2010. Methyl-nitrocatechols: atmospheric tracer compounds for biomass burning secondary organic aerosols. *Environ. Sci. Technol.* 44, 8453–8459.
- Isaacman-VanWertz, G., Yee, L.D., Kreisberg, N.M., Wernis, R., Moss, J.A., Hering, S.V., De Sá, S.S., Martin, S.T., Alexander, M.L., Palm, B.B., 2016. Ambient gas-particle partitioning of tracers for biogenic oxidation. *Environ. Sci. Technol.* 50, 9952–9962.
- Jaekels, J.M., Bae, M.-S., Schauer, J.J., 2007. Positive matrix factorization (PMF) analysis of molecular marker measurements to quantify the sources of organic aerosols. *Environ. Sci. Technol.* 41, 5763–5769.
- Jaffrezo, J.L., Aymoz, G., Delaval, C., Cozic, J., 2005. Seasonal variations of the water soluble organic carbon mass fraction of aerosol in two valleys of the French Alps. *Atmos. Chem. Phys.* 5, 2809–2821.
- Jaoui, M., Edney, E.O., Kleindienst, T.E., Lewandowski, M., Offenber, J.H., Surratt, J.D., Seinfeld, J.H., 2008. Formation of secondary organic aerosol from irradiated α -pinene/toluene/NOx mixtures and the effect of isoprene and sulfur dioxide. *J. Geophys. Res.-Atmos.* 113, D09303.
- Johansson, C., Norman, M., Burman, L., 2009. Road traffic emission factors for heavy metals. *Atmos. Environ.* 43, 4681–4688.
- Kawamura, K., Ikushima, K., 1993. Seasonal changes in the distribution of dicarboxylic acids in the urban atmosphere. *Environ. Sci. Technol.* 27, 2227–2235.
- Kessler, S.H., Smith, J.D., Che, D.L., Worsnop, D.R., Wilson, K.R., Kroll, J.H., 2010. Chemical sinks of organic aerosol: kinetics and products of the heterogeneous oxidation of erythritol and levoglucosan. *Environ. Sci. Technol.* 44, 7005–7010.
- Keyte, I.J., Albinet, A., Harrison, R.M., 2016. On-road traffic emissions of polycyclic aromatic hydrocarbons and their oxy- and nitro- derivative compounds measured in road tunnel environments. *Sci. Total Environ.* 566–567, 1131–1142.
- Kiendler-Scharr, A., Zhang, Q., Hohaus, T., Kleist, E., Mensah, A., Mentel, T.F., Spindler, C., Uerlings, R., Tillmann, R., Wildt, J., 2009. Aerosol mass spectrometric features of biogenic SOA: observations from a plant chamber and in rural atmospheric environments. *Environ. Sci. Technol.* 43, 8166–8172.
- Kleindienst, T., Conner, T., McIver, C., Edney, E., 2004. Determination of secondary organic aerosol products from the photooxidation of toluene and their implications in ambient PM2.5. *J. Atmos. Chem.* 47, 79–100.
- Kleindienst, T.E., Jaoui, M., Lewandowski, M., Offenber, J.H., Lewis, C.W., Bhavsar, P.V., Edney, E.O., 2007. Estimates of the contributions of biogenic and anthropogenic

- hydrocarbons to secondary organic aerosol at a southeastern US location. *Atmos. Environ.* 41, 8288–8300.
- Kleindienst, T.E., Jaoui, M., Lewandowski, M., Offenberg, J.H., Docherty, K.S., 2012. The formation of SOA and chemical tracer compounds from the photooxidation of naphthalene and its methyl analogs in the presence and absence of nitrogen oxides. *Atmos. Chem. Phys.* 12, 8711–8726.
- Kögel-Knabner, I., 2000. Analytical approaches for characterizing soil organic matter. *Org. Geochem.* 31, 609–625.
- Kuang, B., Lin, P., Huang, X.H., Yu, J., 2015. Sources of humic-like substances in the Pearl River Delta, China: positive matrix factorization analysis of PM_{2.5} major components and source markers. *Atmos. Chem. Phys.* 15, 1995–2008.
- Laing, J.R., Hopke, P.K., Hopke, E.F., Husain, L., Dutkiewicz, V.A., Paatero, J., Viisanen, Y., 2015. Positive matrix factorization of 47 years of particle measurements in Finnish Arctic. *Aerosol Air Qual. Res.* 15, 188–207.
- Lee, J., Lane, D.A., 2010. Formation of oxidized products from the reaction of gaseous phenanthrene with the OH radical in a reaction chamber. *Atmos. Environ.* 44, 2469–2477.
- Lee, J.Y., Lane, D.A., Heo, J.B., Yi, S.-M., Kim, Y.P., 2012. Quantification and seasonal pattern of atmospheric reaction products of gas phase PAHs in PM_{2.5}. *Atmos. Environ.* 55, 17–25.
- Liang, L., Engling, G., He, K., Du, Z., Cheng, Y., Duan, F., 2013. Evaluation of fungal spore characteristics in Beijing, China, based on molecular tracer measurements. *Environ. Res. Lett.* 8, 014005.
- Lin, P., Yu, J.Z., 2011. Generation of reactive oxygen species mediated by humic-like substances in atmospheric aerosols. *Environ. Sci. Technol.* 45, 10362–10368.
- Lin, P., Huang, X.-F., He, L.-Y., Zhen Yu, J., 2010. Abundance and size distribution of HULIS in ambient aerosols at a rural site in South China. *J. Aerosol Sci.* 41, 74–87.
- Lin, P., Yu, J.Z., Engling, G., Kalberer, M., 2012. Organosulfates in humic-like substance fraction isolated from aerosols at seven locations in East Asia: a study by ultra-high-resolution mass spectrometry. *Environ. Sci. Technol.* 46, 13118–13127.
- Masri, S., Kang, C.M., Koutrakis, P., 2015. Composition and sources of fine and coarse particles collected during 2002–2010 in Boston, MA. *J. Air Waste Manage. Assoc.* 65, 287–297.
- Mochida, M., Kawamura, K., Fu, P., Takemura, T., 2010. Seasonal variation of levoglucosan in aerosols over the western North Pacific and its assessment as a biomass-burning tracer. *Atmos. Environ.* 44, 3511–3518.
- Mossetti, S., Angius, S.P., Angelino, E., 2005. Assessing the impact of particulate matter sources in the Milan urban area. *Int. J. Environ. Pollut.* 24, 247–259.
- Nalin, F., Golly, B., Besombes, J.-L., Pelletier, C., Aujay-Plouzeau, R., Verlhac, S., Dermigny, A., Fievet, A., Karoski, N., Dubois, P., 2016. Fast oxidation processes from emission to ambient air introduction of aerosol emitted by residential log wood stoves. *Atmos. Environ.* 143, 15–26.
- Nozière, B., Kalberer, M., Claeys, M., Allan, J., D'Anna, B., Decesari, S., Finessi, E., Glasius, M., Grgić, I., Hamilton, J.F., Hoffmann, T., Iinuma, Y., Jaoui, M., Kahnt, A., Kampf, C.J., Kourtschev, I., Maenhaut, W., Marsden, N., Saarikoski, S., Schnelle-Kreis, J., Surratt, J.D., Szidat, S., Szmigielski, R., Wisthaler, A., 2015. The molecular identification of organic compounds in the atmosphere: state of the art and challenges. *Chem. Rev.* 115, 3919–3983.
- Paatero, P., Hopke, P.K., 2003. Discarding or downweighting high-noise variables in factor analytic models. *Anal. Chim. Acta* 490, 277–289.
- Pant, P., Harrison, R.M., 2012. Critical review of receptor modelling for particulate matter: a case study of India. *Atmos. Environ.* 49, 1–12.
- Perraudin, E., Budzinski, H., Villenave, E., 2007. Identification and quantification of ozonation products of anthracene and phenanthrene adsorbed on silica particles. *Atmos. Environ.* 41, 6005–6017.
- Piot, C., Jaffrezo, J.-L., Cozic, J., Pissot, N., El Haddad, I., Marchand, N., Besombes, J.-L., 2012. Quantification of levoglucosan and its isomers by high performance liquid chromatography-electrospray ionization tandem mass spectrometry and its application to atmospheric and soil samples. *Atmos. Meas. Tech.* 5, 141–148.
- Polissar, A.V., Hopke, P.K., Paatero, P., Malm, W.C., Sisler, J.F., 1998. Atmospheric aerosol over Alaska: 2. Elemental composition and sources. *J. Geophys. Res.-Atmos.* 103, 19045–19057.
- Polo-Rehn, L., Waked, A., Charron, A., Piot, C., Besombes, J.-L., Marchand, N., Guillaud, G., Favez, O., Jaffrezo, J.-L., 2014. Estimation de la contribution des émissions véhiculaires à l'échappement et hors échappement aux teneurs atmosphériques en PM₁₀ par Positive Matrix Factorization (PMF). *Pollut. Atmos.* 221.
- Querol, X., Alastuey, A., Viana, M., Rodriguez, S., Artiñano, B., Salvador, P., Do Santos, S.G., Patier, R.F., Ruiz, C., De la Rosa, J., 2004a. Speciation and origin of PM₁₀ and PM_{2.5} in Spain. *J. Aerosol Sci.* 35, 1151–1172.
- Querol, X., Alastuey, A., Viana, M.M., Rodriguez, S., Artiñano, B., Salvador, P., Garcia do Santos, S., Fernandez Patier, R., Ruiz, C.R., de la Rosa, J., Sanchez de la Campa, A., Menendez, M., Gil, J.L., 2004b. Speciation and origin of PM₁₀ and PM_{2.5} in Spain. *J. Aerosol Sci.* 35, 1151–1172.
- Riva, M., Tomaz, S., Cui, T., Lin, Y.H., Perraudin, E., Gold, A., Stone, E.A., Villenave, E., Surratt, J.D., 2015. Evidence for an unrecognized secondary anthropogenic source of organosulfates and sulfonates: gas-phase oxidation of polycyclic aromatic hydrocarbons in the presence of sulfate aerosol. *Environ. Sci. Technol.* 49, 6654–6664.
- Rogge, W.F., Hildemann, L.M., Mazurek, M.A., Cass, G.R., Simoneit, B.R.T., 1993. Sources of fine organic aerosol. 4. Particulate abrasion products from leaf surfaces of urban plants. *Environ. Sci. Technol.* 27, 2700–2711.
- Rogge, W.F., Medeiros, P.M., Simoneit, B.R., 2007. Organic marker compounds in surface soils of crop fields from the San Joaquin Valley fugitive dust characterization study. *Atmos. Environ.* 41, 8183–8204.
- Schauer, J.J., Rogge, W.F., Hildemann, L.M., Mazurek, M.A., Cass, G.R., Simoneit, B.R., 1996. Source apportionment of airborne particulate matter using organic compounds as tracers. *Atmos. Environ.* 30, 3837–3855.
- Schembari, C., Bove, M.C., Cuccia, E., Cavalli, F., Hjorth, J., Massabò, D., Nava, S., Udusti, R., Prati, P., 2014. Source apportionment of PM₁₀ in the western Mediterranean based on observations from a cruise ship. *Atmos. Environ.* 98, 510–518.
- Seinfeld, J.H., Pandis, S.N., 2012. *Atmospheric Chemistry and Physics: From Air Pollution to Climate Change*. John Wiley & Sons.
- Shen, G., Tao, S., Wei, S., Zhang, Y., Wang, R., Wang, B., Li, W., Shen, H., Huang, Y., Chen, Y., 2012. Emissions of parent, nitro, and oxygenated polycyclic aromatic hydrocarbons from residential wood combustion in rural China. *Environ. Sci. Technol.* 46, 8123–8130.
- Shrivastava, M.K., Subramanian, R., Rogge, W.F., Robinson, A.L., 2007. Sources of organic aerosol: positive matrix factorization of molecular marker data and comparison of results from different source apportionment models. *Atmos. Environ.* 41, 9353–9369.
- Simoneit, B.R., Schauer, J.J., Nolte, C., Oros, D.R., Elias, V.O., Fraser, M., Rogge, W., Cass, G.R., 1999a. Levoglucosan, a tracer for cellulose in biomass burning and atmospheric particles. *Atmos. Environ.* 33, 173–182.
- Simoneit, B.R.T., Schauer, J.J., Nolte, C.G., Oros, D.R., Elias, V.O., Fraser, M.P., Rogge, W.F., Cass, G.R., 1999b. Levoglucosan, a tracer for cellulose in biomass burning and atmospheric particles. *Atmos. Environ.* 33, 173–182.
- Singh, D.K., Gupta, T., 2016. Role of transition metals with water soluble organic carbon in the formation of secondary organic aerosol and metallo-organics in PM₁ sampled during post monsoon and pre-winter time. *J. Aerosol Sci.* 94, 56–69.
- Singh, D.K., Gupta, T., 2017. Role of ammonium ion and transition metals in the formation of secondary organic aerosol and metallo-organic complex within fog processed ambient deliquescent submicron particles collected in central part of Indo-Gangetic Plain. *Chemosphere* 181, 725–737.
- Singh, D.K., Kawamura, K., Yanase, A., Barrie, L.A., 2017. Distributions of polycyclic aromatic hydrocarbons, aromatic ketones, carboxylic acids, and trace metals in Arctic aerosols: long-range atmospheric transport, photochemical degradation/production at polar sunrise. *Environ. Sci. Technol.* 51, 8992–9004.
- Song, C.H., Carmichael, G.R., 1999. The aging process of naturally emitted aerosol (sea-salt and mineral aerosol) during long range transport. *Atmos. Environ.* 33, 2203–2218.
- Srimuruganandam, B., Shiva Nagendra, S.M., 2012. Application of positive matrix factorization in characterization of PM₁₀ and PM_{2.5} emission sources at urban roadside. *Chemosphere* 88, 120–130.
- Srivastava, D., Goel, A., Agrawal, M., 2016. Particle bound metals at major intersections in an urban location and source identification through use of metal markers. *Proc. Natl. Acad. Sci., India. Sect. A* 86, 209–220.
- Srivastava, D., Favez, O., Bonnaire, N., Lucarelli, F., Perraudin, E., Gros, V., Villenave, E., Albinet, A. (in preparation). Speciation of organic fractions does matter for aerosol source apportionment. Part 2: intensive campaign in the Paris area (France). *Sci. Total Environ.*
- Sternbeck, J., Sjödin, Å., Andréasson, K., 2002. Metal emissions from road traffic and the influence of resuspension—results from two tunnel studies. *Atmos. Environ.* 36, 4735–4744.
- Surratt, J.D., Gómez-González, Y., Chan, A.W.H., Vermeylen, R., Shahgholi, M., Kleindienst, T.E., Edney, E.O., Offenberg, J.H., Lewandowski, M., Jaoui, M., Maenhaut, W., Claeys, M., Flagan, R.C., Seinfeld, J.H., 2008. Organosulfate formation in biogenic secondary organic aerosol. *J. Phys. Chem. A* 112, 8345–8378.
- Tomaz, S., Shahpoury, P., Jaffrezo, J.-L., Lammel, G., Perraudin, E., Villenave, E., Albinet, A., 2016. One-year study of polycyclic aromatic compounds at an urban site in Grenoble (France): seasonal variations, gas/particle partitioning and cancer risk estimation. *Sci. Total Environ.* 565, 1071–1083.
- Tomaz, S., Jaffrezo, J.-L., Favez, O., Perraudin, E., Villenave, E., Albinet, A., 2017. Sources and atmospheric chemistry of oxy- and nitro-PAHs in the ambient air of Grenoble (France). *Atmos. Environ.* 161, 144–154.
- Tong, H., Arangio, A.M., Lakey, P.S.J., Berkemeier, T., Liu, F., Kampf, C.J., Brune, W.H., Pöschl, U., Shiraiwa, M., 2016. Hydroxyl radicals from secondary organic aerosol decomposition in water. *Atmos. Chem. Phys.* 16, 1761–1771.
- Verma, S.K., Kawamura, K., Chen, J., Fu, P., 2017. Thirteen-years of observations on primary sugars and sugar alcohols over remote Chidijima Island in the western North Pacific. *Atmos. Chem. Phys.* 2017, 1–50.
- Viana, M., Alastuey, A., Querol, X., Guerreiro, C., Vogt, M., Colette, A., Collet, S., Albinet, A., Fraboulet, I., Lacombe, J.-M., 2015. Contribution of Residential Combustion to Ambient Air Pollution and Greenhouse Gas Emissions. ETC/ACM Technical Paper. 1.
- Waked, A., Favez, O., Alleman, L.Y., Piot, C., Petit, J.E., Delaunay, T., Verlinden, E., Golly, B., Besombes, J.L., Jaffrezo, J.L., Leoz-Garziandia, E., 2014. Source apportionment of PM₁₀ in a north-western Europe regional urban background site (Lens, France) using positive matrix factorization and including primary biogenic emissions. *Atmos. Chem. Phys.* 14, 3325–3346.
- Walling, C., 1975. Fenton's reagent revisited. *Acc. Chem. Res.* 8, 125–131.
- Wang, B., Knopf, D.A., 2011. Heterogeneous ice nucleation on particles composed of humic-like substances impacted by O₃. *J. Geophys. Res.-Atmos.* 116.
- Wang, G., Chen, C., Li, J., Zhou, B., Xie, M., Hu, S., Kawamura, K., Chen, Y., 2011. Molecular composition and size distribution of sugars, sugar-alcohols and carboxylic acids in airborne particles during a severe urban haze event caused by wheat straw burning. *Atmos. Environ.* 45, 2473–2479.
- Wang, Y., Hopke, P.K., Xia, X., Rattigan, O.V., Chalupa, D.C., Utell, M.J., 2012. Source apportionment of airborne particulate matter using inorganic and organic species as tracers. *Atmos. Environ.* 55, 525–532.
- Yin, J., Allen, A., Harrison, R., Jennings, S., Wright, E., Fitzpatrick, M., Healy, T., Barry, E., Ceburnis, D., McCusker, D., 2005. Major component composition of urban PM₁₀ and PM_{2.5} in Ireland. *Atmos. Res.* 78, 149–165.
- Yttri, K.E., Simpson, D., Stenström, K., Puxbaum, H., Svendby, T., 2011. Source apportionment of the carbonaceous aerosol in Norway—quantitative estimates based on 14 C, thermal-optical and organic tracer analysis. *Atmos. Chem. Phys.* 11, 9375–9394.

- Zhang, Y., Sheesley, R.J., Schauer, J.J., Lewandowski, M., Jaoui, M., Offenberg, J.H., Kleindienst, T.E., Edney, E.O., 2009. Source apportionment of primary and secondary organic aerosols using positive matrix factorization (PMF) of molecular markers. *Atmos. Environ.* 43, 5567–5574.
- Zhao, R., Mungall, E.L., Lee, A.K.Y., Aljawhary, D., Abbatt, J.P.D., 2014. Aqueous-phase photooxidation of levoglucosan – a mechanistic study using aerosol time-of-flight chemical ionization mass spectrometry (aerosol ToF-CIMS). *Atmos. Chem. Phys.* 14, 9695–9706.
- Zhou, S., Wenger, J.C., 2013a. Kinetics and products of the gas-phase reactions of acenaphthene with hydroxyl radicals, nitrate radicals and ozone. *Atmos. Environ.* 72, 97–104.
- Zhou, S., Wenger, J.C., 2013b. Kinetics and products of the gas-phase reactions of acenaphthylene with hydroxyl radicals, nitrate radicals and ozone. *Atmos. Environ.* 75, 103–112.
- Ziemann, P.J., Atkinson, R., 2012. Kinetics, products, and mechanisms of secondary organic aerosol formation. *Chem. Soc. Rev.* 41, 6582–6605.

Annex B



Precursors and formation of secondary organic aerosols from wildfires in the Euro-Mediterranean region

Marwa Majdi^{1,2}, Karine Sartelet¹, Grazia Maria Lanzafame³, Florian Couvidat³, Youngseob Kim¹, Mounir Chrit¹, and Solene Turquety²

¹CEREA – joint laboratory École des Ponts ParisTech-EDF R&D, Université Paris-Est, 77455 Champs-sur-Marne, France

²Laboratoire de Météorologie Dynamique (LMD) – IPSL, Sorbonne Université, CNRS UMR 8539, École Polytechnique, Paris, France

³INERIS – Institut national de l'environnement industriel et des risques, Verneuil-en-Halatte, France

Correspondence: Marwa Majdi (marwa.majdi@enpc.fr)

Received: 5 October 2018 – Discussion started: 22 October 2018

Revised: 15 February 2019 – Accepted: 1 April 2019 – Published: 29 April 2019

Abstract. This work aims at quantifying the relative contribution of secondary organic aerosol (SOA) precursors emitted by wildfires to organic aerosol (OA) formation during summer of 2007 over the Euro-Mediterranean region, where intense wildfires occurred. A new SOA formation mechanism, H^2O_{aro} , including recently identified aromatic volatile organic compounds (VOCs) emitted from wildfires, is developed based on smog chamber experiment measurements under low- and high- NO_x regimes. The aromatic VOCs included in the mechanism are toluene, xylene, benzene, phenol, cresol, catechol, furan, naphthalene, methyl-naphthalene, syringol, guaiacol, and structurally assigned and unassigned compounds with at least six carbon atoms per molecule ($\text{USC}>6$). This mechanism H^2O_{aro} is an extension of the H^2O (hydrophilic–hydrophobic organic) aerosol mechanism: the oxidation of the precursor forms surrogate species with specific thermodynamic properties (volatility, oxidation degree and affinity to water). The SOA concentrations over the Euro-Mediterranean region in summer of 2007 are simulated using the chemistry transport model (CTM) Polair3D of the air-quality platform Polyphemus, where the mechanism H^2O_{aro} was implemented. To estimate the relative contribution of the aromatic VOCs, intermediate volatility, semi-volatile and low-volatility organic compounds (I/S/L-VOCs), to wildfires OA concentrations, different estimations of the gaseous I/S/L-VOC emissions (from primary organic aerosol – POA – using a factor of 1.5 or from non-methanic organic gas – NMOG – using a factor of 0.36) and their ageing

(one-step oxidation vs. multi-generational oxidation) are also tested in the CTM.

Most of the particle OA concentrations are formed from I/S/L-VOCs. On average during the summer of 2007 and over the Euro-Mediterranean domain, they are about 10 times higher than the OA concentrations formed from VOCs. However, locally, the OA concentrations formed from VOCs can represent up to 30 % of the OA concentrations from biomass burning. Amongst the VOCs, the main contributors to SOA formation are phenol, benzene and catechol (CAT; 47 %); $\text{USC}>6$ compounds (23 %); and toluene and xylene (12 %). Sensitivity studies of the influence of the VOCs and the I/S/L-VOC emissions and chemical ageing mechanisms on $\text{PM}_{2.5}$ concentrations show that surface $\text{PM}_{2.5}$ concentrations are more sensitive to the parameterization used for gaseous I/S/L-VOC emissions than for ageing.

Estimating the gaseous I/S/L-VOC emissions from POA or from NMOG has a high impact on local surface $\text{PM}_{2.5}$ concentrations (reaching –30 % in the Balkans, –8 % to –16 % in the fire plume and +8 % to +16 % in Greece). Considering the VOC as SOA precursors results in a moderate increase in $\text{PM}_{2.5}$ concentrations mainly in the Balkans (up to 24 %) and in the fire plume (+10 %).

1 Introduction

Atmospheric particulate matter (PM) has a strong impact on human health (Pope et al., 2002; Naeher et al., 2006; Johnston et al., 2012), climate (Pilinis et al., 1995; Bond et al., 2013) and visibility (Eldering and Cass, 1996; Hand et al., 2007). Chemistry transport models (CTMs) play an important role in simulating the formation of these particles and their concentrations. PM is composed of different compounds, namely organic and inorganic compounds, dust, and black carbon (Jimenez et al., 2009).

Organic aerosols (OA) are classified either as primary organic aerosols (POA) or as secondary organic aerosols (SOA). POA are directly emitted into the atmosphere, whereas SOA are formed by gas–particle conversion of oxidation products of precursors. OA can be classified based on their saturation concentrations (C^*): volatile organic compounds (VOCs; with $C^* > 10^6 \mu\text{g m}^{-3}$), intermediate volatility organic compounds (I-VOCs; with $10^4 < C^* < 10^6 \mu\text{g m}^{-3}$), semi-volatile organic compounds (S-VOCs; with $0.1 < C^* < 10^4 \mu\text{g m}^{-3}$) and low-volatility organic compounds (L-VOCs; with $C^* < 0.1 \mu\text{g m}^{-3}$; Lipsky and Robinson, 2006; Grieshop et al., 2009). Both SOA and POA may be composed of components of different volatilities such as S-VOCs and L-VOCs, which may partition between the gas and particle phases (Robinson et al., 2007). Depending on the ambient concentrations, some components only exist in the gas phase (e.g., I-VOCs). In the following, OA_{tot} denotes the sum of gaseous and particle-phase organic aerosol concentrations with volatility lower than VOCs.

POA_{tot} originates mostly from anthropogenic (e.g., traffic and industry) sources and from biomass burning, which is considered to be one of the major sources of PM (Bian et al., 2017), with contributions from both anthropogenic (e.g., residential heating) as well as natural sources such as wildfires.

Wildfires are one of the largest sources of primary carbonaceous aerosols globally. They are also an important source of trace gases including organic vapors, which themselves can serve as precursors of SOA (Akagi et al., 2011; Stockwell et al., 2015). SOA from wildfires may contribute significantly to organic aerosol loading in the atmosphere (Konovalov et al., 2015). However, the concentration of SOA is highly uncertain because of the complexities of physical and chemical evolution of wildfire plumes (Bian et al., 2017). Although several modeling studies have examined SOA formation from VOCs released from biomass burning (Marson et al., 2006; Alvarado and Prinn, 2009; Alvarado et al., 2015), the compounds that act as precursors of SOA are still not well understood. Considering only traditional SOA precursors (mainly toluene, xylene, benzene and naphthalene; Appel et al., 2017) in SOA models leads to a substantial underestimation of SOA concentrations (Dawson et al., 2016; Bian et al., 2017). This can probably partly be explained by the limited knowledge about SOA precursors. Recently, aromatic VOCs (namely toluene, xylene, benzene,

phenol, cresol, catechol, furan, guaiacol, syringol, naphthalene and methyl-naphthalene) were identified as the major SOA precursors emitted by biomass burning (Akagi et al., 2011; Stockwell et al., 2015; Bruns et al., 2016). To develop mechanisms of SOA formation from these aromatic compounds, many laboratory studies have investigated the gas-phase oxidation of VOCs (mainly initiated by reactions with a hydroxyl radical – OH; Calvert et al., 2002; Atkinson and Arey, 2003; Chhabra et al., 2011; Nakao et al., 2011; Yee et al., 2013), and SOA yields have been measured under various conditions (Odum et al., 1996; Ng et al., 2007): a low- NO_x regime where the concentrations of NO_x are low and the production of ozone and oxidants is mainly governed by the NO_x levels and a high- NO_x regime where the production of ozone and oxidants is controlled by the VOC levels (Sillman et al., 1990; Kleinman, 1994). Odum et al. (1996) model SOA formation by a gas–particle partitioning absorption scheme (Pankow, 1994) using data from smog chamber experiments. In CTMs, the SOA formation may be represented using different approaches mostly based on data from smog chamber experiments: the two-lumped-product approach, which uses an empirical representation of SOA formation (Odum et al., 1996; Schell et al., 2001), the molecular or surrogate approach (Pun et al., 2006; Bessagnet et al., 2008; Carlton et al., 2010; Couvidat et al., 2012; Chrit et al., 2017), which represents the formation of SOA using surrogate molecules with associated physico-chemical properties, and the volatility basis set (VBS) approach (Donahue et al., 2006) in which surrogates are associated to classes of different volatilities. The ageing (oxidation by OH) of each surrogate may lead to the formation of surrogates of lower volatility classes through the competition of two processes: fragmentation and functionalization. Fragmentation corresponds to the cleavage of C–C bonds, and it leads to oxidation products of a lower carbon number and higher volatility than the precursor. Functionalization corresponds to the addition of oxygen-containing functional groups, and it leads to oxidation products of a higher oxygen number.

SOA formation mechanisms may rely not only on smog chamber experiments but also on explicit chemical mechanisms when experimental data are not available. Examples of such mechanisms are the master chemical mechanisms (MCMs; Saunders et al., 1997) or the generator for explicit chemistry and kinetics of organics in the atmosphere (GECKO-A; Aumont et al., 2005).

Recent studies take into account not only the oxidation of selected VOCs but also gaseous intermediate volatility, semi-volatile and low-volatility organic compounds (I/S/L-VOCs) emitted by biomass burning to model SOA formation (Koo et al., 2014; Konovalov et al., 2015; Ciarelli et al., 2017). Majdi et al. (2019) show that near fire regions and during the summer of 2007, 52 % to 87 % of the $\text{PM}_{2.5}$ concentrations are organic aerosol that is mainly composed of primary and secondary I/S/L-VOCs (62 % to 84 %). They highlight that neglecting primary gaseous I/S/L-VOC emissions from

wildfires tends to lessen the surface $PM_{2.5}$ concentrations (-30%). Since ignoring primary gaseous I/S/L-VOC emissions biases model predictions of SOA production, several studies based on smog chamber data aim at estimating them (Yokelson et al., 2013; Jathar et al., 2014, 2017). The primary gaseous I/S/L-VOCs emitted by biomass burning are usually calculated using the emissions of POA (Couvidat et al., 2012; Koo et al., 2014) because a part of these I/S/L-VOCs may correspond to POA due to the gas-to-particle partitioning. However, these gaseous I/S/L-VOC emissions may also correspond to an unspciated fraction of non-methane organic gas (NMOG; Jathar et al., 2014, 2017). Jathar et al. (2014) estimate that about 20% of the total NMOG emitted from biomass burning is assumed to be I/S/L-VOCs in the gas phase, while Yokelson et al. (2013) estimate that as much as 35% to 64% of NMOG is I/S/L-VOCs in the gas phase.

Although primary gaseous I/S/L-VOCs are not considered to be or classified as unspciated NMOG in emission inventories, their contribution to the SOA budget may be substantial, despite being a small fraction of the overall organic gas emissions (Koo et al., 2014; Kononov et al., 2015; Ciarelli et al., 2017). The gaseous I/S/L-VOCs are usually classified according to their volatilities (Couvidat et al., 2012; May et al., 2013) by taking into account the variation in their average oxidation state (Koo et al., 2014). Different parameterizations have been used to simulate the ageing of gaseous I/S/L-VOCs emitted by the biomass burning: a simple one-step oxidation scheme (Couvidat et al., 2012) or a multi-generational oxidation scheme taking simultaneously functionalization and fragmentation into account at each step (Koo et al., 2014; Ciarelli et al., 2017).

The objective of this work is to quantify the contribution of recently identified SOA precursors from wildfires (guaiacol, syringol, benzene, phenol, catechol, cresol, furan, naphthalene, methylnaphthalene and USC>6 compounds). To that end, a new SOA formation mechanism is developed for those precursors, based on smog chamber experiments under low- and high- NO_x conditions. This new mechanism is used in conjunction with the H^2O mechanism previously developed for biogenic and anthropogenic VOC precursors (xylene, toluene, isoprene, monoterpenes, sesquiterpenes, etc.).

This study aims also to quantify the relative contribution of VOCs and I/S/L-VOCs to OA formation. The OA concentrations are simulated using the chemistry transport model (CTM) Polair3D of the Polyphemus modeling air-quality platform.

This study focuses on two severe fire events that occurred during the summer of 2007 over the Euro-Mediterranean area. Majdi et al. (2019) show a large contribution of wildfires (reaching $\sim 90\%$), mainly in Greece (24–30 August 2007) and in the Balkans (20–31 July 2007, 24–30 August 2007).

This paper is structured as follows. Section 2 details the SOA formation mechanisms from VOCs and I/S/L-VOCs. Then, Sect. 3 describes the model and the simulation setup

during summer of 2007. The main OA_{tot} precursors (VOCs and 4 gaseous I/S/L-VOCs) emitted from wildfires, their emission factors and their emissions are detailed in Sect. 4. Section 5 presents the sensitivity simulations performed to understand the relative impact of VOCs and I/S/L-VOCs on OA formation.

2 SOA formation from VOCs and I/S/L-VOCs

2.1 SOA formation from VOC oxidation

This section presents a new SOA formation mechanism H^2O_{aro} developed to represent the SOA formation from the main aromatic VOCs that are estimated to be SOA precursors. The new mechanism (H^2O_{aro}) is an extension of the hydrophilic–hydrophobic organic (H^2O) SOA mechanism, which details the formation of organic aerosols from the oxidation of precursors (Couvidat et al., 2012). Laboratory chamber studies provide the fundamental data that are used to parameterize the atmospheric SOA formation under low- or high- NO_x conditions. The formed organic aerosols are represented by surrogate compounds, with varying water affinity (hydrophobic and hydrophilic). In the original H^2O mechanism, the precursors are I/S/L-VOCs, aromatics (xylene and toluene), isoprene, monoterpenes and sesquiterpene. In the extension H^2O_{aro} developed here, other VOCs are considered to be SOA precursors (phenol, cresol, catechol, benzene, furan, guaiacol, syringol, naphthalene and methylnaphthalene).

Laboratory chamber studies provide the fundamental data that are used to parameterize the atmospheric SOA formation under low- or high- NO_x conditions. All the experiments used in this paper were conducted under dry conditions, with a relative humidity (RH) lower than 10% and a temperature ranging between 292 and 300 K.

For each VOC, precursor of SOA and chamber experiment, the SOA mass yield (Y) is defined as the fraction of the reactive organic gas (ROG) that is converted to SOA. The relationship between the yield and the measured organic aerosol mass concentration (i.e., formed SOA) M_0 (Odum et al., 1996) is

$$Y = \sum_{i=1}^n \frac{\alpha_i K_{p,i} \cdot M_0}{(1 + K_{p,i} \cdot M_0)}, \quad (1)$$

where α_i is the molar stoichiometric coefficient of the product (surrogate) i , and $K_{p,i}$ is its gas–particle partitioning equilibrium constant.

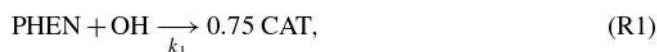
The chamber experimental results are analyzed according to the absorption gas–particle partitioning model developed by Pankow (1994) and Odum et al. (1996). For each VOC, the experimental results (Y , M_0) are fitted (with the least-mean-square method) either with a one-product model or two-product model by plotting the Odum curve. The stoichiometric coefficients of SOA products, their saturation va-

por pressures and their partitioning gas–particle constants are determined from the experimental results and the Odum curve. Then candidates for SOA surrogates formed by the VOC oxidation are estimated from the literature. For each candidate, the saturation vapor pressure and the partitioning constant are estimated from an empirical method called “the group contribution method” proposed by SIMPOL.1 (Pankow and Asher, 2008). These parameters are used to choose the SOA surrogates amongst the candidates: the SOA surrogates are chosen so that their saturation pressure and partitioning constant are the closest to the ones determined experimentally from the Odum plot.

2.1.1 Oxidation of phenol and catechol

Under low- NO_x conditions, the chamber experiments of Yee et al. (2013), Chhabra et al. (2011) and Nakao et al. (2011) are used to model the SOA formation from phenol oxidation.

In their studies, and in agreement with the explicit chemical mechanism MCM version 3.3.1 (MCM.v3.3.1), CAT is the dominant product of the first oxidation step of phenol. Therefore, catechol is assumed to be the main intermediary leading to SOA formation from OH oxidation of phenol following Reaction (R1):



where the kinetic constant $k_1 = 4.7 \times 10^{-13} \exp(1220/T) \text{ molecule}^{-1} \text{ cm}^3 \text{ s}^{-1}$ and the stoichiometric coefficient of catechol are given by MCM.v3.3.1. SOA from phenol are produced essentially from the oxidation of catechol, which is mostly present in the gas phase ($K_p = 2.57 \text{ m}^3 \text{ g}^{-1}$). The yields of the SOA surrogates formed from the catechol oxidation by OH are estimated, assuming that Reaction (R1) holds and using the Odum approach with the results (yields and M_0) of the experiments conducted by Yee et al. (2013) and Chhabra et al. (2011) for phenol oxidation. The Odum approach (Odum et al., 1996) is used here with only one surrogate (one-product model) to estimate SOA formation parameters, as similar partitioning constants and stoichiometric coefficients are obtained with two surrogates. Figure 1 shows the plots of the SOA yields against the SOA concentrations M_0 . The blue stars are yields from smog chamber experiments, and the red circles are yields estimated by the one-product model.

The one-product model with a stoichiometric coefficient α_1 of 0.28 and a vapor pressure of 4.59×10^{-8} torr correctly reproduces the experimental data. To quantify the spread between the model and experimental data, the root-mean-square error (RMSE) is used as a statistical estimator and calculated as

$$\text{RMSE} = \left(\sqrt{\frac{1}{N} \sum_{i=1}^n (\text{Yield}_{\text{exp}} - \text{Yield}_{\text{model}})^2} \right) \cdot 100, \quad (2)$$

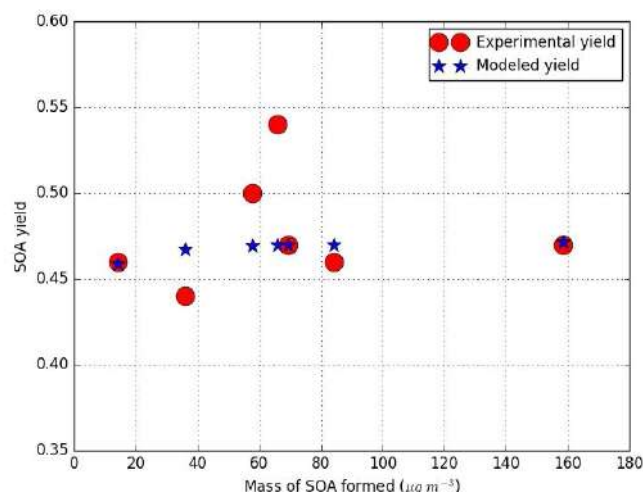


Figure 1. SOA yield from smog chamber experiments under low- NO_x conditions (Yee et al., 2013; Chhabra et al., 2011; Nakao et al., 2011), and yield curve for phenol–OH reaction using one-product model.

where $\text{Yield}_{\text{model}}$ refers to the modeled SOA yield, $\text{Yield}_{\text{exp}}$ is the experimental SOA yield and N is the number of experiments. A small amount of spread between the model and experimental data (RMSE of 3.1 %) is quantified. Note that this stoichiometric coefficient (0.28) is similar to the one obtained using the experimental result of Nakao et al. (2011) for the OH oxidation of catechol (0.26). Yee et al. (2013) identified SOA products from phenol oxidation under low- NO_x conditions. For each product proposed by Yee et al. (2013), vapor saturation pressures are calculated with SIMPOL.1 using the group contribution method. The surrogate is chosen so that its estimated saturation vapor pressure corresponds to the experimental one estimated from the Odum curve. The product ACIDMAL ($\text{C}_6\text{H}_6\text{O}_5$, maleylacetic acid) is chosen, as its theoretical vapor pressure (5.76×10^{-8} torr) is the closest to the experimental one (4.59×10^{-8} torr). The van Krevelen diagram in Chhabra et al. (2011) presents the properties of SOA from phenol oxidation in terms of O/C and H/C ratios. According to the van Krevelen diagram, the O/C and H/C ratios of SOA from phenol vary from 0.8 to 1 and between 1 and 1.5 respectively. This confirms that ACIDMAL is an acceptable SOA surrogate for the OH oxidation of phenol (O/C = 0.83 and H/C = 1). Because of the lack of experimental data of phenol oxidation under high NO_x , ACIDMAL is also used as a high- NO_x surrogate.

Finally, the oxidation of catechol is modeled following Reaction (R2):



where the kinetic constant $k_2 = 9.9 \times 10^{-10} \text{ molecule}^{-1} \text{ cm}^3 \text{ s}^{-1}$ is taken from MCM.v3.3.1.

2.1.2 Oxidation of cresol

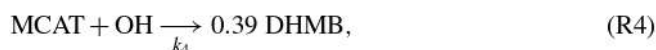
As detailed in the chemical mechanism MCM.v3.3.1, the OH oxidation of cresol (CRESp) leads to the formation of methylcatechol (MCAT), which is the dominant product of the first oxidation step of cresol, presented in Reaction (R3):



where the kinetic constant $k_3 = 4.65 \times 10^{-10} \text{ molecule}^{-1} \text{ cm}^3 \text{ s}^{-1}$, and the stoichiometric coefficient are from MCM.v3.3.1.

The oxidation of methylcatechol by OH leads to the formation of SOA, following a chemical mechanism detailed in Schwantes et al. (2017). Because of the lack of the experimental data under high- NO_x conditions, we consider cresol chemical mechanisms under low- and high- NO_x conditions to be similar. Aerosol yields from the experiments of Nakao et al. (2011) under low- NO_x conditions are used for the Odum approach. The one-product model is sufficiently accurate to reproduce correctly the data from the smog chamber. Figure 2 plots the SOA yields against the SOA concentrations. A stoichiometric coefficient and a saturation vapor pressure 0.39 and 3.52×10^{-6} torr respectively are found to fit the experimental data accurately, with small differences between the model and experimental data (RMSE of $\sim 3\%$). The oxidation mechanism of MCAT developed by Schwantes et al. (2017) presents the potential candidates of SOA surrogates. For each candidate, the theoretical vapor saturation pressure is calculated using SIMPOL.1 DHMB ($\text{C}_7\text{H}_6\text{O}_4$, dihydroxymethylbenzoquinone) has the closest vapor saturation pressure (4.2×10^{-6} torr) to the experimental vapor pressure calculated from the Odum plot (3.52×10^{-6} torr), and it is also close to the experimental pressure given in Schwantes et al. (2017) (6.3×10^{-6} torr).

Finally, the oxidation of methylcatechol is modeled following Reaction (R4):



where the kinetic constant $k_4 = 2 \times 10^{-10} \text{ molecule}^{-1} \text{ cm}^3 \text{ s}^{-1}$ is from MCM.v3.3.1, and the stoichiometric coefficient of DHMB is deduced from the Odum plot.

Several studies focus also on the oxidation of cresol by NO_3 (Olariu et al., 2013; Grosjean, 1990). This oxidation may not contribute significantly to SOA formation because the NO_3 oxidation products of cresol are highly volatiles.

2.1.3 Oxidation of benzene

According to MCM.v3.3.1, benzene (BENZ) reacts with OH to form phenol, as presented in Reaction (R5).

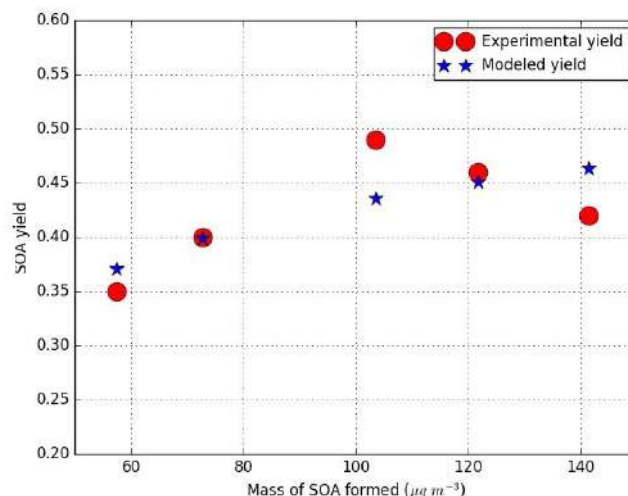
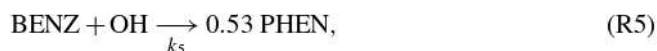
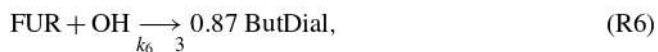


Figure 2. SOA yield data from smog chamber under low- NO_x conditions (Nakao et al., 2011), and yield curve for cresol–OH reaction using one-product model.

where $k_5 = 2.3 \times 10^{-12} \exp(-190/T) \text{ molecule}^{-1} \text{ cm}^3 \text{ s}^{-1}$ is from MCM.v3.3.1. For the case of benzene, only the formation through the phenolic route is taken into account for simplification purposes. However, due to the high SOA yield of phenol and the high amount of phenol formed through benzene oxidation, the phenolic route should be one of the main pathways for SOA formation. By using the phenol SOA mechanism developed previously in Sect. 2.1.1, the SOA yield through the phenolic of 0.28 is evaluated. This yield is within the range of SOA yields from benzene oxidation (between 0.22 and 0.33) reported by Nakao et al. (2011) for low- NO_x conditions. It confirms that phenol is probably the main intermediate for the formation of SOA.

2.1.4 Oxidation of furan

According to MCM.v3.3.1, furan (FUR) reacts with OH to form an unsaturated 1,4-dicarbonyl product (butendial – ButDial), following Reaction (R6):



where $k_6 = 4.19 \times 10^{-11} \text{ molecule}^{-1} \text{ cm}^3 \text{ s}^{-1}$ is from MCM.v3.3.1.

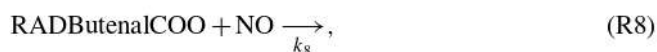
According to MCM.v3.3.1, ButDial reacts with OH to form highly volatile products (not detailed here because they may not form SOA) and a radical (RADButenalCOO), as presented in Reaction (R7):



where $k_7 = 5.2 \times 10^{-11} \text{ molecule}^{-1} \text{ cm}^3 \text{ s}^{-1}$ is from MCM.v3.3.1.

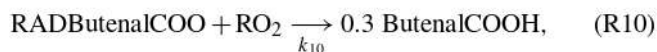
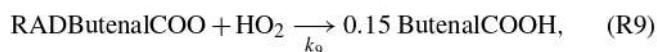
Under high- NO_x conditions, according to MCM.v3.3.1, the oxidation of RADButenalCOO forms highly volatile

products (glyoxal and maleic anhydride), which are not considered here for SOA formation (Reaction R8):



where $k_8 = 7.5 \times 10^{-12} \exp(980/T) \text{ molecule}^{-1} \text{ cm}^3 \text{ s}^{-1}$ is from MCM.v3.3.1.

Under low- NO_x conditions, the oxidation of RADButenalCOO forms malealdehydic acid (ButenalCOOH) as shown in Reactions (R9) and (R10):

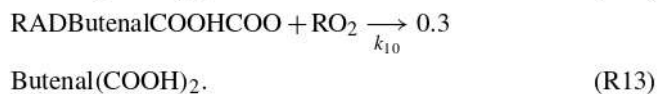
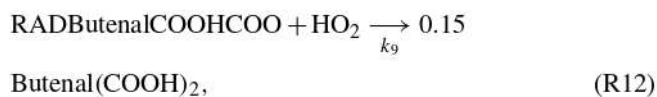


where $k_9 = 5.2 \times 10^{-13} \exp(980/T) \text{ molecule}^{-1} \text{ cm}^3 \text{ s}^{-1}$, and $k_{10} = 1.10 \times 10^{-11} \text{ molecule}^{-1} \text{ cm}^3 \text{ s}^{-1}$ are from MCM.v3.3.1.

ButenalCOOH is mostly in the gas phase ($K_p = 1.53 \times 10^{-5} \text{ m}^3 \text{ g}^{-1}$) and not in the particle phase. However, according to GECKO-A, it may be oxidized by OH to form a radical (RADButenalCOOHCOO) following Reaction (R11):



where $k_{11} = 2.12 \times 10^{-11} \text{ molecule}^{-1} \text{ cm}^3 \text{ s}^{-1}$ is from GECKO-A. The radical RADButenalCOOHCOO can react similarly to RADButenalCOO under low- NO_x conditions to form the diacid (Buten(COOH)₂) as presented in Reactions (R12) and (R13):



Note that the oxidation mechanism of furan presented in this section probably overestimates the SOA concentrations from the OH-oxidation route because several reactions such as ozonolysis and photolysis of both ButenalCOOH and Buten(COOH)₂ are not considered. These reactions may lead to the loss of the main intermediary responsible of SOA formation (ButenalCOOH and Buten(COOH)₂).

Furthermore, other routes may be more efficient at forming SOA from furan. Jiang et al. (2018) showed that NO_x levels and relative humidity (RH) may significantly influence SOA formation from furan, with higher SOA concentrations at high- NO_x levels and high humidity.

2.1.5 Oxidation of syringol and guaiacol

According to Lauraguais et al. (2014), the SOA formation mechanisms from methoxyphenols, namely syringol and

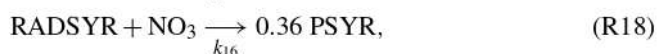
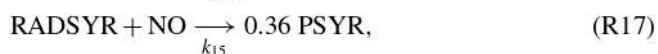
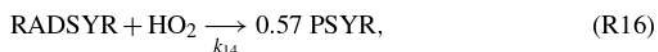
guaiacol, are split into two steps. The first step consists of Reactions (R14) and (R15) with the radical OH:



where $k_{12} = 9.63 \times 10^{-11} \text{ molecule}^{-1} \text{ cm}^3 \text{ s}^{-1}$ and $k_{13} = 7.53 \times 10^{-11} \text{ molecule}^{-1} \text{ cm}^3 \text{ s}^{-1}$ are given by Lauraguais et al. (2012) and Coeur-Tourneur et al. (2010a) respectively.

The parameterization is developed for syringol and guaiacol by considering low- NO_x and high- NO_x conditions based on SOA yields reported by Chhabra et al. (2011), Yee et al. (2013), Lauraguais et al. (2012) and Yee et al. (2013). Generally this compound represents low- NO_x oxidation products. In this first parameterization it is also used as a high- NO_x surrogate. Figure 3 shows the modeled Odum plots for syringol SOA formation under both low- NO_x and high- NO_x conditions. A one-product parameterization is sufficient for properly representing the experimental data for the two regimes. The same surrogate compound can be used for both regimes, as similar partitioning constants are estimated. Among the compounds recognized as syringol oxidation products, $\text{C}_8\text{H}_{10}\text{O}_5$ (PSYR) is the only product with a vapor saturation pressure, calculated with SIMPOL.1 (7.53×10^{-6} torr), close to the experimental one estimated from the Odum plot (7.72×10^{-6} torr). Stoichiometric coefficients of 0.57 and 0.36 are also estimated from the Odum curve under low- and high- NO_x conditions respectively.

The second reaction step for SOA formation is then represented with the following Reactions (R16), (R17) and (R18):



where $k_{14} = 2.91 \times 10^{-13} \exp(1300/T) \text{ molecule}^{-1} \text{ cm}^3 \text{ s}^{-1}$, $k_{15} = 2.70 \times 10^{-13} \exp(360/T) \text{ molecule}^{-1} \text{ cm}^3 \text{ s}^{-1}$ and $k_{16} = 2.30 \times 10^{-12} \text{ molecule}^{-1} \text{ cm}^3 \text{ s}^{-1}$ are from MCM.v3.3.1.

Similarly, for guaiacol, the two NO_x regimes are distinguished. One surrogate compound is used for the high- NO_x and the low- NO_x parameterizations. Odum plots are presented in Fig. 4.

The surrogate compound chosen to represent SOA formation in both conditions is $\text{C}_7\text{H}_{10}\text{O}_5$ (GHDPerox), a hydroperoxide proposed as an oxidation product for guaiacol in Yee et al. (2013). It was chosen because the calculated saturation vapor pressure with SIMPOL.1 (1.05×10^{-6} torr) is close to the one estimated by the Odum method (6.01×10^{-7} torr). Stoichiometric coefficients of 0.37 and 0.32 are also estimated from the Odum curve under low- NO_x and high- NO_x conditions respectively. Moreover, according to the van

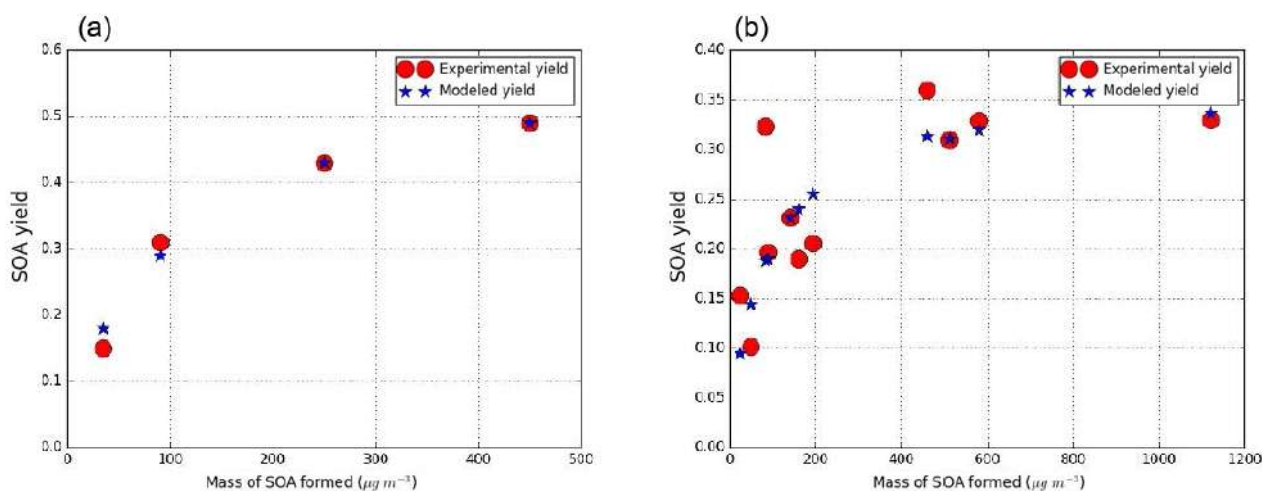


Figure 3. SOA experimental and modeled yield data from smog chamber for syringol under low- NO_x conditions (a) (experimental data from Chhabra et al., 2011; Yee et al., 2013) and under high- NO_x conditions (b) (experimental data from Yee et al., 2013; Lauraguais et al., 2012).

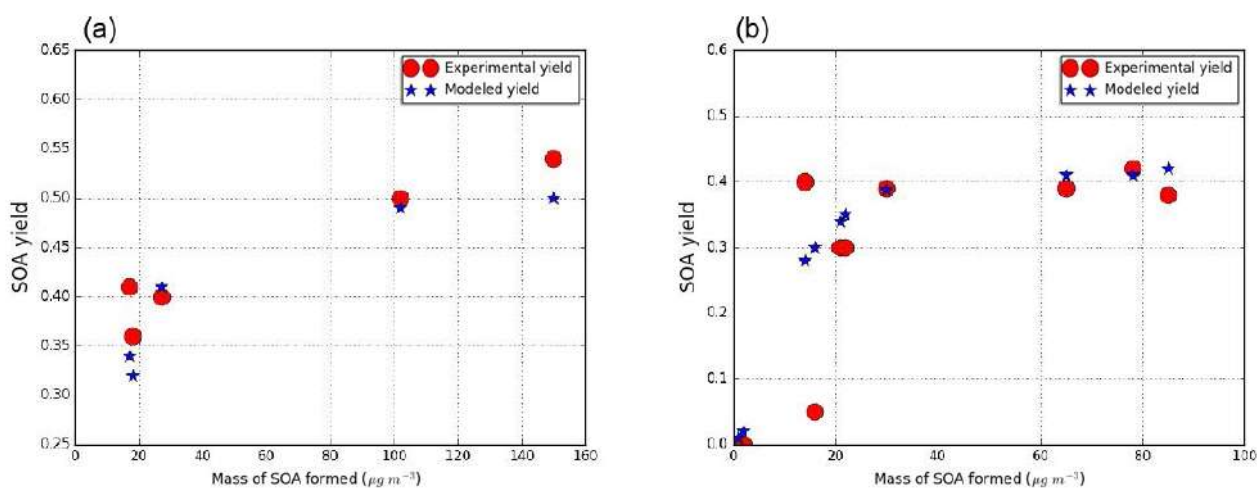


Figure 4. SOA experimental and modeled yield data from smog chamber for guaiacol under low- NO_x conditions (a) (experimental data from Chhabra et al., 2011; Yee et al., 2013) and under high- NO_x conditions (b) (experimental data from Yee et al., 2013; Lauraguais et al., 2012).

Krevelen plot proposed by Chhabra et al. (2011), the most appropriate guaiacol SOA surrogate has an O/C and H/C ratio respectively in the ranges 0.7–1 and 1.2–1.5. With its O/C and H/C ratios of 0.71 and 1.43 ratios, GHDPerox is in the right position of the van Krevelen plot.

The second part of the OH-oxidation mechanism for guaiacol follows Reactions (R19), (R20) and (R21):



2.1.6 Oxidation of naphthalene and methylnaphthalene

As detailed in Couvidat et al. (2013), data from the chamber experiments of Chan et al. (2009) are used to fit two products from the oxidation of naphthalene and methylnaphthalene under low- NO_x and high- NO_x conditions. The SOA surrogates are chosen amongst the compounds detected by Kautzman et al. (2010). Under low- NO_x conditions (reactions with HO_2 , the methylperoxy radical MEO_2 and the peroxyacetyl radical C_2O_3), BBPAHIN ($\text{C}_6\text{H}_6\text{O}_6$, dihydroxyterephthalic acid) is the surrogate chosen to represent SOA formation from the oxidation of naphthalene and methylnaphthalene. Under high- NO_x conditions, BBPAHhN ($\text{C}_8\text{H}_6\text{O}_4$, phthalic acid) is the surrogate chosen because its theoretical saturation vapor pressure (2.04×10^{-7} torr), estimated with SIMPOL.1

(Pankow and Asher, 2008), is the closest to the experimental one (10^{-6} torr) estimated from the Odum curve plotted by Couvidat et al. (2013). The oxidation reactions leading to SOA formation from naphthalene and methyl-naphthalene are presented in Table B3 of Appendix B.

2.1.7 Oxidation of USC >6 compounds

It is not easy to design a chemical mechanism for the structurally assigned and unassigned compounds with at least six carbon atoms per molecule (USC>6 compounds). Because Bruns et al. (2016) estimated that SOA yields for USC>6 compounds are high, they are represented in the model by a high-yield compound. Phenol and naphthalene are good candidates. Because the oxidation products of naphthalene and phenol are very different (e.g., volatility), a sensitivity simulation is performed by choosing the oxidation mechanism of naphthalene rather than phenol to evaluate the impact of changing the oxidation mechanism.

Table B3 in Appendix B summarizes the oxidation reactions added to the chemical mechanism CB05 for each VOC. All properties of the added compounds are presented in Table B1 of Appendix B. The chemical structure of the SOA compounds is given in Table B2.

2.2 SOA formation from I/S/L-VOCs

Different parameterizations may be used to describe the formation of SOA from the gaseous I/S/L-VOCs emitted from wildfires, with or without an ageing scheme: a one-step oxidation scheme (no ageing) and multi-generational oxidation scheme.

In the one-step oxidation scheme, used, for example, in Couvidat et al. (2012), Zhu et al. (2016) and Sartelet et al. (2018), the primary organic aerosols emitted by biomass burning (BBPOA_{IP} for compounds of low volatility, BBPOA_{MP} for compounds of medium volatility and BBPOA_{HP} for compounds of high volatility of saturation concentration C^* : $\log(C^*)$ is -0.04 , 1.93 and 3.5 respectively) undergo one oxidation step in the gas phase, leading to the formation of secondary surrogates (BBSOA_{IP}, BBSOA_{MP} and BBSOA_{HP}).

Compared to the primary products, the volatility of the secondary products is reduced by a factor of 100, and their molecular weight is increased by 40 % (Couvidat et al., 2012; Grieshop et al., 2009). Tables in Appendix C list the three OH-oxidation reactions and the properties of the primary and secondary surrogates.

For the multi-generational scheme, the VBS approach based on the hybrid VBS (Donahue et al., 2006, 2011; Koo et al., 2014; Ciarelli et al., 2017) is used. In this scheme (Koo et al., 2014; Ciarelli et al., 2017), the basis set uses five volatility surrogates with different saturation concentrations ranging from 0.1 to $1000 \mu\text{g m}^{-3}$. BBPOA₀, BBPOA₁, BBPOA₂, BBPOA₃ and BBPOA₄ refer to the

primary surrogates, and BBSOA₀, BBSOA₁, BBSOA₂ and BBSOA₃ refer to the secondary ones (see Table D2 of Appendix D for their properties). In the gas phase, the primary and secondary surrogates react with OH at a rate of $4 \times 10^{-11} \text{ molecule}^{-1} \text{ cm}^3 \text{ s}^{-1}$ (Robinson et al., 2007). During each oxidation step, the oxidation of the surrogate increases the surrogate oxygen number and decreases its volatility and carbon number due to functionalization and fragmentation, which are considered simultaneously during each oxidation reaction. The reactions and the properties of the surrogates of the multi-generational scheme are shown in Appendix D.

3 3-D simulation over the Mediterranean region

The impact of wildfires on PM concentrations and optical depths in the Euro-Mediterranean during the summer of 2007 was studied by Majdi et al. (2019).

Here, the CTM Polair3D or Polyphemus (Mallet et al., 2007; Sartelet et al., 2012) is used with a similar setup to Majdi et al. (2019) and summarized here. A modified version of the Carbon Bond 05 model (CB05; Yarwood et al., 2005; Kim et al., 2011) is used for gas-phase chemistry with the Size Resolved Aerosol Model (SIREAM; Debry et al., 2007) for aerosol dynamics (coagulation and condensation or evaporation). The meteorological fields are provided by the European Centre for Medium-Range Weather Forecasts (ECMWF; ERA-Interim). Boundary conditions of the nesting domain are obtained from the global chemistry transport model MOZART-GEOS5 6-hourly simulation outputs (Emmons et al., 2010). Anthropogenic emissions are generated from EMEP inventory for 2007 (European Monitoring and Evaluation Programme; <http://www.emep.int>, last access: 19 April 2019). Biogenic emissions are estimated with the Model of Emissions of Gases and Aerosols from Nature (MEGAN-LHIV, Guenther et al., 2006). Sea-salt emissions are parameterized following Monahan (1986). The soil and surface database of Menut et al. (2013) is used to calculate the dust emissions considering the spatial extension of potentially emitted area in Europe described in Briant et al. (2017). The daily fire emissions are calculated using the APIFLAME fire emission model v1.0 (Turquety et al., 2014), as described in Majdi et al. (2019).

Two domains are considered in this study (Fig. 5): one nesting domain covering Europe and North Africa and one nested over the Mediterranean. The horizontal resolutions used are $0.5^\circ \times 0.5^\circ$ and $0.25^\circ \times 0.25^\circ$ for the nesting and nested domains respectively. The vertical dimension is discretized with 14 levels in Polyphemus (from the ground to 12 km). Since the largest fires in the Euro-Mediterranean domain occur mainly in the Balkans and eastern Europe (between 20 July and 31 July 2007), in Greece (between 24 August and 30 August), and in southern Italy (between 9 July and 31 July 2007; Majdi et al., 2019), we choose to focus on the subregion indicated in the green box in Fig. 5.

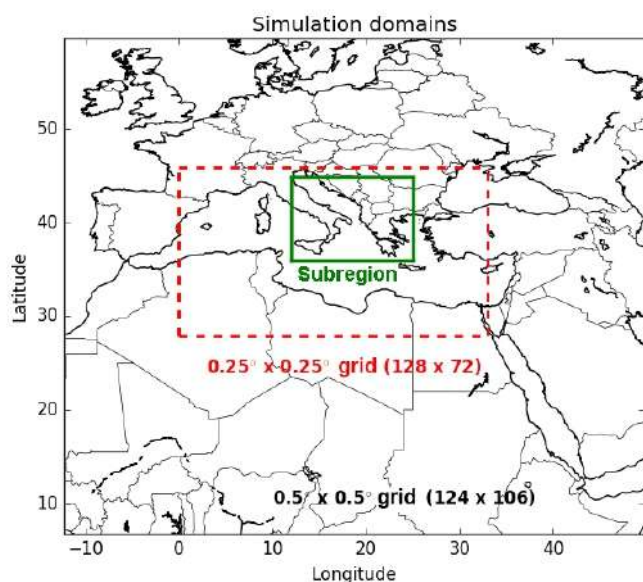


Figure 5. Simulation domains, including one large domain (with a $0.5^\circ \times 0.5^\circ$ horizontal resolution) and a smaller domain (at a $0.25^\circ \times 0.25^\circ$ horizontal resolution) delimited by the dotted red box. The subregion (Balkans, Greece, Eastern Europe and Italy) indicated in green box, is used in this study.

The CB05 gas-phase chemical mechanism is used in conjunction with the chemical mechanism H^2O to model the formation of SOA from five classes of precursors, namely I/S/L-VOCs of anthropogenic emissions, aromatic VOCs, isoprene, monoterpene and sesquiterpenes (Kim et al., 2011; Couvidat et al., 2012). In this work, the SOA mechanism H^2O_{aro} developed in Sect. 2.1 for aromatic VOCs, precursors of SOA, is added. Gas–particle partitioning is modeled using a thermodynamic equilibrium model for multiphase multicomponent inorganic aerosols (ISORROPIA; Nenes et al., 1999) for inorganics and using a secondary organic aerosol processor (SOAP) for organics (Couvidat and Sartelet, 2015), assuming thermodynamic equilibrium between gases and particles.

As in Majdi et al. (2019), POA from fire and anthropogenic emissions are assumed to be the condensed phase of I/S/L-VOCs. The gaseous emissions of I/S/L-VOCs from wildfires and their ageing are described in Sect. 2.2.

Dry deposition of gaseous I/S/L-VOCs from wildfires is parameterized based on Wesely (1989), modeling deposition as a series of resistors consisting of an atmospheric, laminar sublayer and bulk surface resistance. The surface resistance is a function of the effective Henry's law constant (H_{eff} ; $M \text{ atm}^{-1}$). For I/S/L-VOCs, this constant varies with the volatility, as detailed in Hodzic et al. (2016). The reactivity factor f_0 , which corresponds to the ability of a dissolved gas to oxidize biological substances in solution, may range from 0 for non-reactive species to 1 for highly reactive species. In this work, the f_0 value is set to 0.1 (Karl

et al., 2010; Knote et al., 2015). All the parameters used to compute the dry-deposition velocities of the I/S/L-VOCs are summarized in Table E1 of Appendix E.

The reference simulation uses the same setup as Majdi et al. (2019). The evaluation of Majdi et al. (2019) of the simulation includes both ground-based and satellite remote-sensing (MODIS) observations. Ground-based observations of $PM_{2.5}$ at eight AIRBASE stations and of aerosol optical depth at six AERONET stations are used. The evaluation shows good performances of the model, especially when wildfires are taken into account in the simulation. Enhancements in PM concentrations due to wildfires are simulated at ± 1 d of uncertainty in the timing compared to satellite observations (MODIS), with a strong contribution from organic compounds (61 %; Majdi et al., 2019).

4 Sensitivity simulations

To assess the relative influence of emissions of VOCs and I/S/L-VOCs from wildfires on OA concentrations, six sensitivity simulations are performed. The setup of the different simulations is summarized in Table 1.

The reference simulation OnestepISLVOC uses the default setup, i.e., the setup used in the previous study (Majdi et al., 2019): for VOC emissions, only toluene and xylene are considered (as detailed in Sect. 5.1), while gaseous I/S/L-VOC emissions are estimated from POA emissions, and their ageing is modeled using a one-step oxidation scheme. The simulation MultstepISLVOC is conducted to highlight the impact of the ageing scheme of the gaseous I/S/L-VOCs from wildfires on SOA formation. To do so, the multi-generational scheme (Ciarelli et al., 2017) is used for the gaseous I/S/L-VOCs from wildfires.

To assess the impact of VOCs on SOA formation, the simulation Multstep-withVOC uses the same setup as the simulation MultstepISLVOC, but all the VOCs, which are SOA precursors, are added to the model, as detailed in Sect. 5. Because the relative impact of I/S/L-VOCs on OA formation depends on how gaseous I/S/L-VOC emissions are computed, the simulation Multstep-UnNMOG-withVOC is the same as the simulation Multstep-withVOC, but the gaseous I/S/L-VOC emissions are assumed to be unidentified NMOG, and they are estimated from NMOG emissions (as described in Sect. 5.2).

The sensitivity of two parameters involved in the modeling of the ageing of these VOCs is also assessed: the enthalpy of vaporization (ΔH_{vap}) of the SOA formed from the oxidation of the VOCs and the SOA formation mechanism from USC>6 compounds.

Several studies consider ΔH_{vap} of the formed SOA to be constant (Sheehan and Bowman, 2001; Donahue et al., 2005; Stanier et al., 2007). For SOA from α -pinene, Donahue et al. (2005) estimated ΔH_{vap} to be about 30 kJ mol^{-1} . This is lower than the ΔH_{vap} values calculated for individual com-

ponents using SIMPOL.1. The calculated ΔH_{vap} values are in the range of 54–132 kJ mol⁻¹. Stanier et al. (2007) also estimated ΔH_{vap} to be in the range of 10–50 kJ mol⁻¹. In the simulation Multstep-withVOC-Enthalpy-SIMPOL.1, the enthalpy of vaporization is calculated for the SOA surrogates formed from VOCs using SIMPOL.1 rather than being constant as in the simulation Multstep-withVOC. In the simulation Multstep-withVOC-USC>6naph, the SOA formation mechanism from USC>6 compounds is taken to be the formation mechanism of naphthalene, rather than being the same as the formation mechanism of phenol in the simulation Multstep-withVOC.

5 Emissions of SOA precursors from wildfires

To better understand the contribution of OA_{tot} precursors emitted by wildfires and their relative importance for OA_{tot} and OA formation, the estimation of OA_{tot} precursors emissions is first detailed. Two categories of SOA precursors are distinguished depending on their volatilities: VOCs and gaseous I/S/L-VOCs.

5.1 VOC emissions

Bruns et al. (2016) identified the most significant gaseous VOC precursors of SOA from residential wood combustion and presented their contribution to SOA concentrations. Although wood fire stove smoke emissions may not be representative of wildfires, they provide some indication of the SOA precursors involved during wildfires. In this work, VOC precursors emitted from wildfires are chosen based on the list of Bruns et al. (2016), their emission factors for wildfires and SOA yields. Toluene, xylene, phenol, benzene, catechol, cresol, furan, naphthalene, methylnaphthalene, and the structurally assigned and unassigned compounds with at least six carbon atoms per molecule (USC>6 compounds) are retained. Table A1 in Appendix A shows the VOCs, the corresponding SOA yields and emission factors from fires of various vegetation types. Note that although Biogenic VOC (BVOC) emissions may increase during wildfires, as suggested by Ciccioli et al. (2014), the potential increase in BVOC emissions from wildfires is not considered here due to a lack of data.

Daily fire emissions of toluene, xylene, phenol, benzene and furan are estimated by the APIFLAME fire emission model (Turquety et al., 2014). The emissions of factors in Akagi et al. (2011) are used to calculate the emissions of each species from the carbon emissions. The emission factors of toluene, xylene, benzene, furan and phenol are available in the Akagi et al. (2011) inventory and provided in terms of grams of species per kilogram of dry biomass burned for different standard vegetation types (temperate forest, crop residues, pasture maintenance, savanna and chaparral). Using

an aggregation matrix, emissions of these inventory VOCs are converted to model species.

However, cresol, catechol, syringol, guaiacol, naphthalene and methylnaphthalene emission factors are missing from the Akagi et al. (2011) inventory. For cresol, catechol, guaiacol and syringol, these emission factors are calculated from the molar emission ratio to phenol, and for naphthalene and methylnaphthalene, they are calculated from the molar emission ratio to benzene (Stockwell et al., 2015) following Eq. (3):

$$EF_i = ER_{\text{mass},i} \cdot EF_x = \left(ER_{\text{mol},i} \cdot \frac{M_{w,i}}{M_{w,x}} \right) \cdot EF_x, \quad (3)$$

where i represents a VOC (cresol, catechol, guaiacol, syringol, naphthalene and methylnaphthalene), $ER_{\text{mass},i}$ is the mass emission ratio of the VOC i to phenol or benzene, EF_x is the mass emission factor of phenol or benzene (determined using APIFLAME), $ER_{\text{mol},i}$ is the molar emission ratio of the VOC i (cresol, catechol, guaiacol, syringol, naphthalene and methylnaphthalene), $M_{w,i}$ is the molar weight of the VOC i , and $M_{w,x}$ is the molar weight of phenol (= 90 g mol⁻¹) or benzene (= 78 g mol⁻¹).

For two types of vegetation j (chaparral and crop residue), the emission ratios $ER_{\text{mol},i,j}$ are obtained from Stockwell et al. (2015). Then in each model grid cell, the emission ratio of the VOC i (cresol, catechol, guaiacol, syringol, naphthalene or methylnaphthalene) to phenol or benzene is obtained by weighting the emission ratios over the burned vegetation types:

$$ER_{\text{mol},i} = \sum_{j=1}^n F_{\text{veg},j} \cdot ER_{\text{mol},i,j}, \quad (4)$$

where $F_{\text{veg},j}$ is the burning fraction for each vegetation type, and $ER_{\text{mol},i,j}$ is the emission ratio of the VOC i to phenol or benzene for each vegetation type.

Considering only these two types of vegetation (crop residue and chaparral) for which emission ratios are available may lead to an underestimation of the emission factors and therefore the emissions of cresol, catechol, guaiacol, syringol, naphthalene and methylnaphthalene emissions. Indeed, Fig. 6 shows the percentages of the different vegetation types in the burned area detected over the subregion. Chaparral and crop residue make only 29.5 % of burned area detections. Savanna and temperate forest are considered to be the dominant vegetation types detected in the burned areas, and their contributions to burned area detections reach 32.7 % and 37.2 % respectively. Therefore, neglecting the emission factors for temperate forest and savanna would lead to a significant underestimation of the SOA precursor emissions. Because the EF of VOCs emitted by wildfires of crop residue, chaparral, temperate forest and savanna in the inventory of Akagi et al. (2011) are often of the same order of magnitude (Table A1 of Appendix A), it is assumed here that temperate forest and savanna have the same EF as chaparral for

Table 1. Summary of the sensitivity simulations performed by Polyphemus (n/a: not applicable).

Simulations	Wildfires				
	Gaseous I/S/L-VOC emissions	Gaseous I/S/L-VOC ageing	Added VOCs precursors	ΔH_{vap} (kJ mol ⁻¹)	USC>6 mechanism
OnestepISLVOC	From POA	One step	No	n/a	n/a
MultstepISLVOC	From POA	Multi-generational	No	n/a	n/a
Multstep-withVOC	From POA	Multi-generational	Yes	50	Phenol mechanism
Multstep-UnNMOG-withVOC	From NMOG	Multi-generational	Yes	50	Phenol mechanism
Multstep-withVOC-Enthalpy-SIMPOL.1	From POA	Multi-generational	Yes	SIMPOL.1	Phenol mechanism
Multstep-withVOC-USC>6naph	From POA	Multi-generational	Yes	50	Naphthalene mechanism

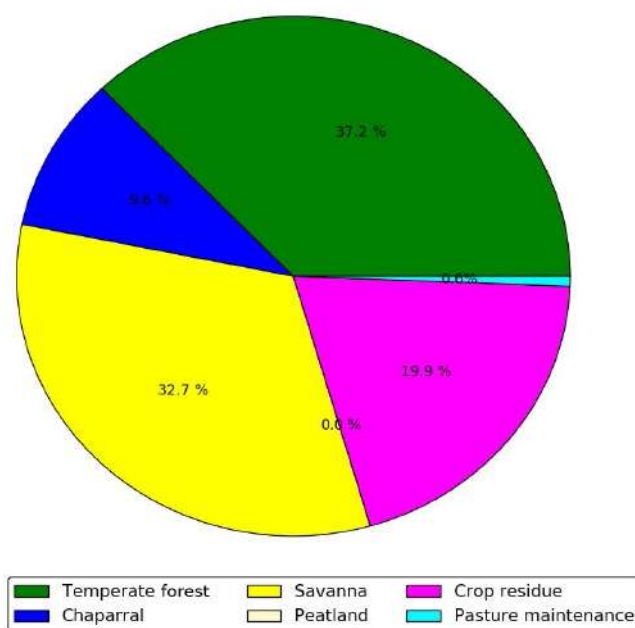
cresol, catechol, guaiacol, syringol, naphthalene and methyl-naphthalene. This assumption is justified by considering uncertainties linked to emissions: Turquetty et al. (2014) estimated that the uncertainties in the emitted carbon related to fire emissions can reach 100%. They found that the database used for the type of vegetation burned plays a significant role in the emitted carbon (~75% associated uncertainty). Moreover, the inventory used in this work (APIFLAME Turquetty et al., 2014) is mainly based on the emission factors of Akagi et al. (2011) using data from different field and laboratory experiments. Uncertainties related to these emission factors are high. For example, Alves et al. (2011) measured carbon monoxide (CO) emissions for forest fires in Portugal that were 2.6 times higher than the values of Akagi et al. (2011) for extra-tropical forests.

According to Bruns et al. (2016), the structurally assigned and unassigned compounds with at least six carbon atoms per molecule (USC>6 compounds) are expected to contribute to SOA formation based on their structures, but their SOA yields are unknown. In this work, USC>6 compound emissions are deduced by multiplying phenol emissions by a factor of 1.7, deduced from the ratio of the SOA contribution of USC>6 compounds to the SOA contribution of phenol (Bruns et al., 2016).

5.2 I/S/L-VOC emissions

The gaseous I/S/L-VOC emissions from wildfires are estimated either from the POA emissions released from wildfires, by multiplying them by a constant ratio of I/S/L-VOC/POA=1.5 (Kim et al., 2016), or from the unspiciated NMOG released from wildfires (Jathar et al., 2014). The fraction of unspiciated NMOG is estimated as the difference between the total NMOG emissions from the Akagi et al. (2011) inventory and the VOC emissions, which represent the sum of the total identified NMOG in the Akagi et al. (2011) inventory plus the VOCs previously added to the Akagi et al. (2011) inventory (cresol, catechol, guaiacol, syringol, naphthalene, methyl-naphtha-

Vegetation types in the burned area detected in subregion (%)

**Figure 6.** Percentage of the different vegetation types in the burned area detected over the subregion during the summer of 2007.

lene and USC>6 compounds). In this work, as in Jathar et al. (2017), these unspiciated NMOG are assumed to be gaseous I/S/L-VOCs. They represent 36% of the total NMOG emissions, consistent with the work of Yokelson et al. (2013), which estimates that between 35% to 64% of NMOG are the gaseous I/S/L-VOCs. Similarly to anthropogenic emissions (detailed in Sect. 3), the gaseous I/S/L-VOC emissions from wildfires are distributed into three volatility bins depending on their saturation concentration ($\log(C^*)$): low volatility – BBPOAIP, $\log(C^*) = -0.04$; medium volatility – BBPOAmP, $\log(C^*) = 1.93$; and high

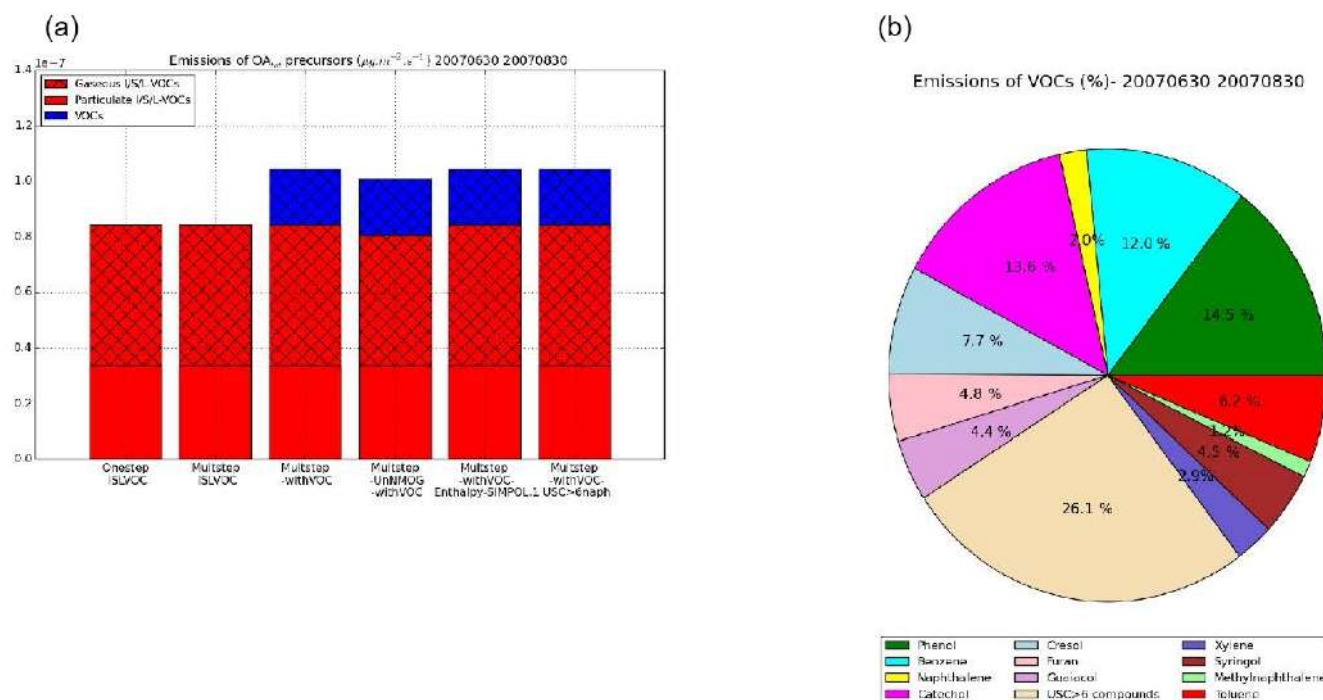


Figure 7. Emissions of the OA_{tot} precursors from wildfires for the different sensitivity simulations (a) and percentage of emissions for each VOC (b) over the subregion during the summer of 2007.

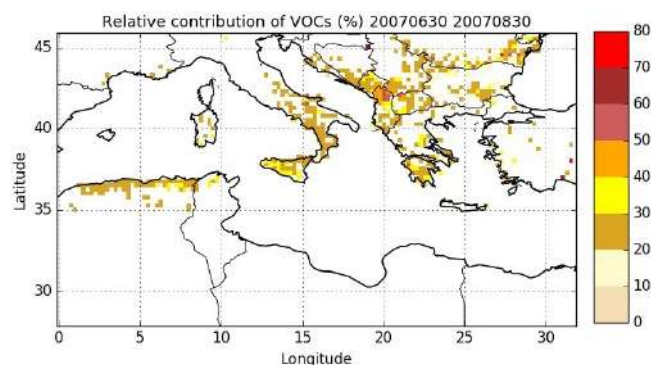


Figure 8. Relative contribution of VOCs to gaseous precursors (VOCs plus gaseous I/S/L-VOCs; %) emitted by wildfires over the Mediterranean area during the summer of 2007.

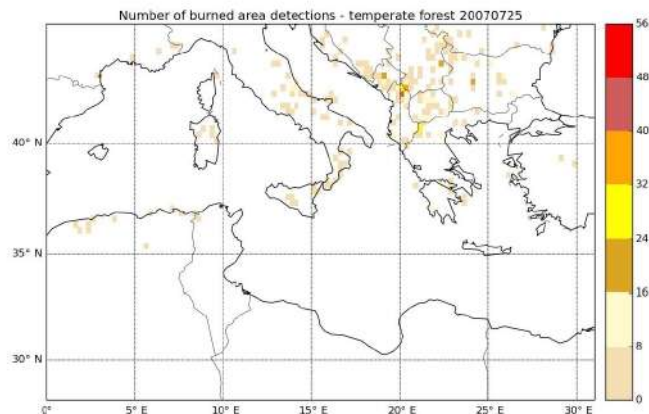


Figure 9. Number of burned area detections for temperate forest on 25 July 2007.

volatility – BBPOAhP, $\log(C^*) = 3.5$). The volatility distribution at emission is 25%, 32% and 43% for BBPOAIP, BBPOAmP and BBPOAhP respectively (Couvidat et al., 2012; May et al., 2013; Ciarelli et al., 2017).

5.3 Emissions over the Mediterranean domain

Fig. 7a presents the emissions of total (gas plus particle) OA_{tot} precursors (VOCs and I/S/L-VOCs) for the different sensitivity simulations, spatially and temporally averaged over the subregion (Fig. 5) and during the summer of 2007. The emissions of VOCs and I/S/L-VOCs are sim-

ilar in all the sensitivity simulations except for the simulation Multistep-UnNMOC-withVOC, which estimates the gaseous I/S/L-VOC emissions from NMOG. The emissions of gaseous I/S/L-VOCs estimated from NMOG emissions are slightly lower than those estimated from POA emissions. The emissions of gaseous I/S/L-VOCs (estimated from POA or from NMOG) are higher by a factor of about 2.5 than the emissions of VOCs.

The spatial distribution of the relative contribution of VOCs to gaseous precursors emissions (I/S/L-VOCs from NMOG plus VOCs) is assessed in Fig. 8. Emissions of wild-

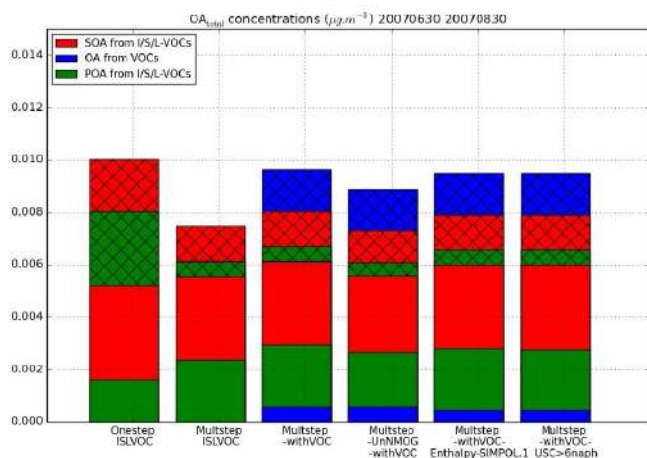


Figure 10. Mean surface OA_{tot} concentrations from different OA_{tot} precursors over the subregion for each sensitivity simulation. The cross-hatched part corresponds to OA concentrations in the gaseous phase, while the plain parts correspond to OA concentrations in the particle phase.

fires occur mostly over the Balkans, Greece, southern Italy, Eastern Europe and northern Algeria, with a relative contribution of VOCs mostly between 20 % and 40 %. Locally, over the Balkans, the contribution of VOCs can be higher (between 40 % and 60 %). Figure 9 shows the number of burned area detections for temperate forest. The high contribution of VOCs in the Balkans is probably explained by the high number of burned areas detected for temperate forest, which is considered one of the dominant vegetation types in the burned areas.

Fig. 7b shows the distribution of VOCs between the different compounds emitted over the subregion during the summer of 2007. USC>6 compounds dominate (26.1 %), followed by phenol (14.5 %), catechol (13.6 %), benzene (12 %), toluene (7 %), furan (5 %) and cresol (4 %). The other VOCs (SOA precursors) contribute to 3 % or less of the VOC emissions.

6 Results and discussion

The influence of VOCs and I/S/L-VOCs on OA and OA_{tot} concentrations is discussed in this section as well as the sensitivity to some parameters for OA and OA_{tot} formation from VOCs and gaseous I/S/L-VOCs.

6.1 Influence on OA concentrations

Figure 10 presents the OA_{tot} concentrations from different precursors emitted by biomass burning (VOCs and I/S/L-VOCs). The contributions of the different OA_{tot} precursors from different simulations are compared. In the simulation Multistep-withVOC, the precursors are VOCs and I/S/L-VOCs with gaseous emissions estimated from POA and with

ageing by the multi-step oxidation scheme. In the simulations OnestepISLVOC and MultistepISLVOC, the precursors are I/S/L-VOCs with gaseous emissions estimated from POA emissions and with ageing by the one-step and the multi-step oxidation schemes respectively. In the simulation Multistep-UnNMOG-withVOC, the precursors are VOCs and I/S/L-VOCs with gaseous emissions estimated from NMOG emissions and with ageing by the multi-step oxidation scheme.

The emissions of VOCs are lower than those of gaseous I/S/L-VOCs estimated from NMOG (or POA) emissions by almost a factor of about 2.5. This preponderance of I/S/L-VOCs is observed not only for emissions but also for concentrations. The primary and secondary OA concentrations from gaseous I/S/L-VOCs (estimated from NMOG emissions and from POA emissions) are about 10 times higher than the OA concentrations from VOCs. Most of the OA and OA_{tot} concentrations are formed from I/S/L-VOCs (about 90 % and 75 % respectively). The OA concentrations are slightly higher (by about 10 %) when the gaseous I/S/L-VOCs are estimated from POA rather than from NMOG emissions. This difference corresponds to the difference observed in emissions (gaseous I/S/L-VOC emissions estimated from POA are slightly higher than those estimated from NMOG).

Across our cases, 28 % to 42 % of the OA concentrations from I/S/L-VOC emissions are primary. The amount of POA from I/S/L-VOC emissions in simulation OnestepISLVOC (28 %) is lower than the one in the simulation MultistepISLVOC (42 %) because of the differences in the volatility properties of the species in the two ageing schemes.

The OA concentrations simulated with the one-step and the multi-generational schemes are nearly similar (about 5 % difference). However, the primary and secondary OA_{vapor} concentrations (the gas phase of OA_{tot} concentrations) are lower with the multi-generational scheme because of fragmentation.

A large part of OA_{tot} concentrations from VOCs ($\sim 70\%$) is in the gas phase. This suggests that the influence of the VOC emissions on particle OA concentrations could be larger if the surrogates from these VOC oxidations partition more easily to the particle phase. This could be the case if further ageing mechanisms are considered for these VOCs or if the particles are very viscous (Kim et al., 2019).

Using the SOA formation mechanism of naphthalene rather than the SOA formation mechanism of phenol affects the OA_{tot} concentrations from VOCs slightly ($\sim 3\%$). Similar results are found when calculating the enthalpy of vaporization of the formed SOA with SIMPOL.1 instead of using a constant ($\Delta H = 50 \text{ kJ mol}^{-1}$). This shows that the SOA formation from VOCs is poorly sensitive to these parameters involved in the modeling of the VOCs ageing.

Figure 11 presents the contribution of VOCs to biomass-burning OA concentrations, as simulated by the simulation Multistep-withVOC. In agreement with the preponderance of the contribution of I/S/L-VOCs discussed above, the VOC contribution is between 10 % and 25 % in most of the

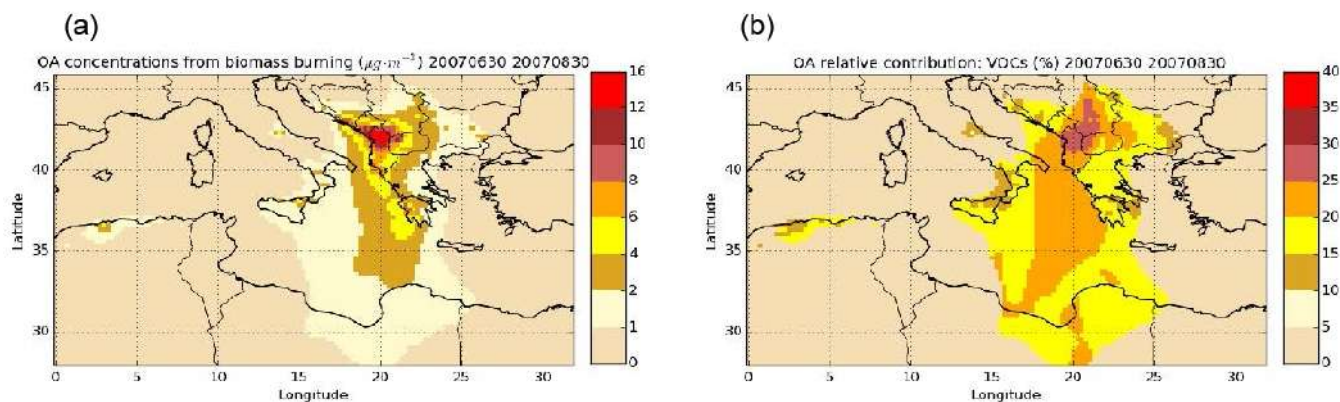


Figure 11. Daily mean surface OA concentrations from wildfires (a) and the relative contribution of VOCs (%) to OA from wildfires (b) during the summer of 2007 (simulation Multstep-withVOC).

Contribution to OA from VOC oxidation (%) - 20070630 20070830

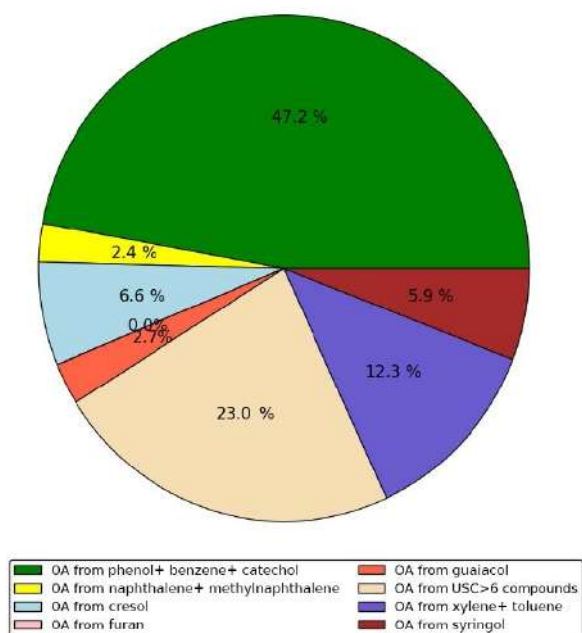


Figure 12. Distribution of the OA concentrations formed from the different VOCs emitted by wildfires over the subregion during the summer of 2007 (simulation Multstep-withVOC).

Mediterranean where biomass-burning OA concentrations are above $1 \mu\text{g m}^{-3}$. A larger contribution of VOCs (reaching 30 %) is observed in the Balkans, where the biomass-burning OA concentrations are the highest, with a large fraction of temperate forests burning.

Figure 12 shows the distribution of the OA concentrations formed from the different VOCs emitted by wildfires in the simulation Multstep-withVOC over the subregion during the summer of 2007. The largest contribution comes from phe-

nol, benzene and catechol. It represents about 47 % of the OA concentrations from VOCs and 40 % of the VOC emissions. The second-largest contribution comes from USC>6 compounds. It represents about 23 % of the OA concentrations from VOCs and 26 % of the VOC emissions. Toluene and xylene, which were taken into account in the previous version of the model, have a high yield compared to other VOCs. They make about 12 % of the OA concentrations from VOCs, whereas their emissions represent about 9 % of the VOC emissions. Furan, which makes about 5 % of VOC emissions, does not contribute to OA concentrations (contribution lower than 1 %). Cresol contributes equally to VOC emissions and SOA concentrations (about 7 %). Syringol, which contributes to only 4 % of VOC emissions, contributes to about 6 % of the OA concentrations. The other VOCs (naphthalene, methylnaphthalene and guaiacol) have a low contribution (equal to or lower than 3 %).

6.2 Sensitivity of $\text{PM}_{2.5}$ concentrations

To assess the sensitivity of $\text{PM}_{2.5}$ concentrations to VOCs and gaseous I/S/L-VOCs and parameters related to their emissions or ageing, differences of $\text{PM}_{2.5}$ concentrations among the sensitivity simulations are compared. The sensitivity to the gaseous I/S/L-VOC ageing scheme is assessed by computing relative differences between the simulations OnestepISLVOC and MultstepISLVOC. The sensitivity to the gaseous I/S/L-VOC emissions is assessed by computing the relative difference between the simulations Multstep-withVOC and Multstep-UnNMOG-withVOC. The sensitivity to the VOC emissions is assessed by computing the relative difference between the simulations Multstep-withVOC and MultstepISLVOC.

Figure 13 shows the average $\text{PM}_{2.5}$ concentrations as well as relative differences of $\text{PM}_{2.5}$ concentrations among the sensitivity simulations. The $\text{PM}_{2.5}$ concentrations are especially high, with average concentrations above $20 \mu\text{g m}^{-3}$ where wildfires occur, especially in the Balkans and Greece.

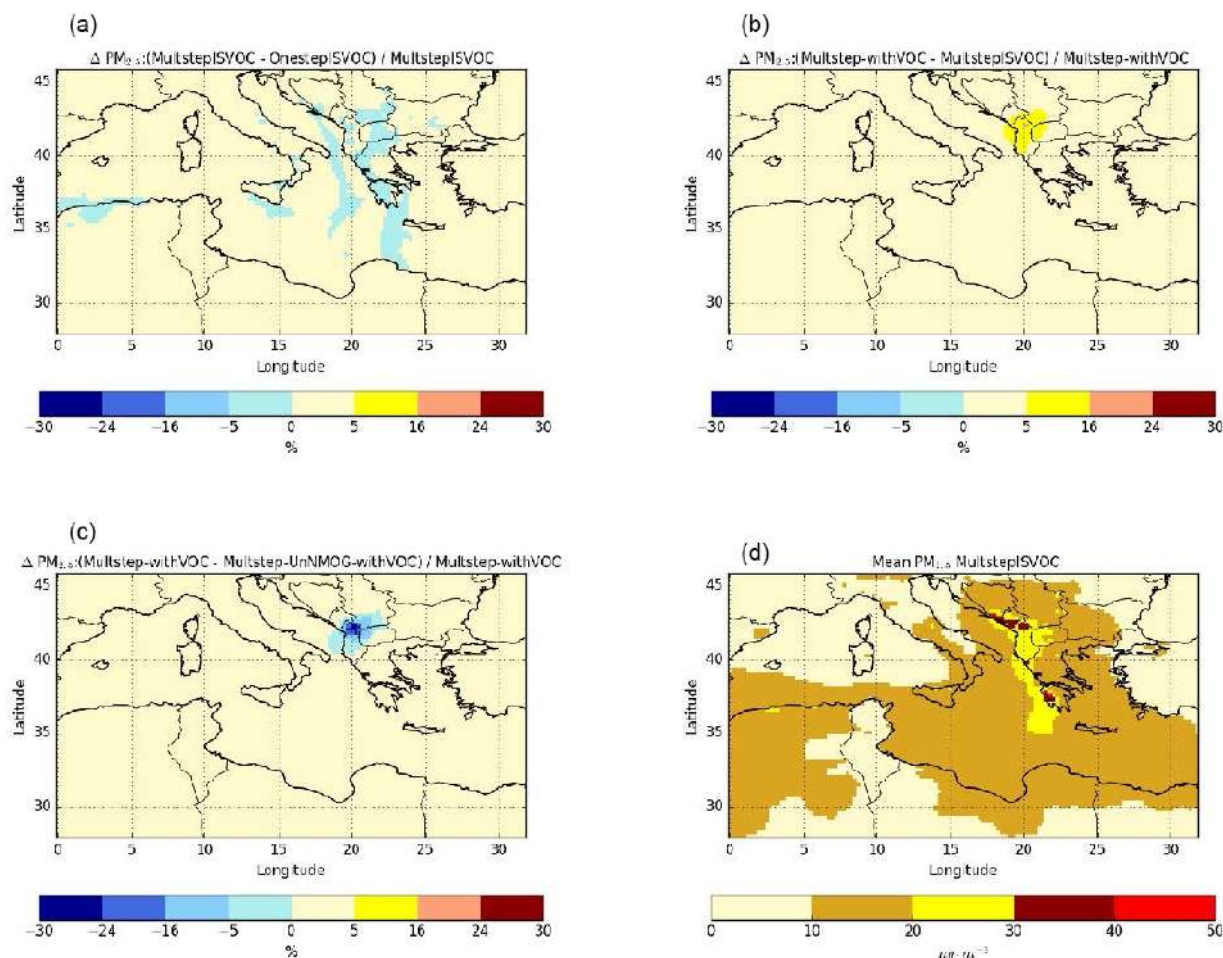


Figure 13. Sensitivity of surface $\text{PM}_{2.5}$ concentrations to the gaseous I/S/L-VOC ageing scheme (a), the SOA from the selected VOC (b), the SOA from gaseous I/S/L-VOC emissions estimated from NMOG (c) and daily mean $\text{PM}_{2.5}$ concentrations from the Multistep-withVOC simulation (d) during the summer of 2007 (from 30 June to 30 August 2007).

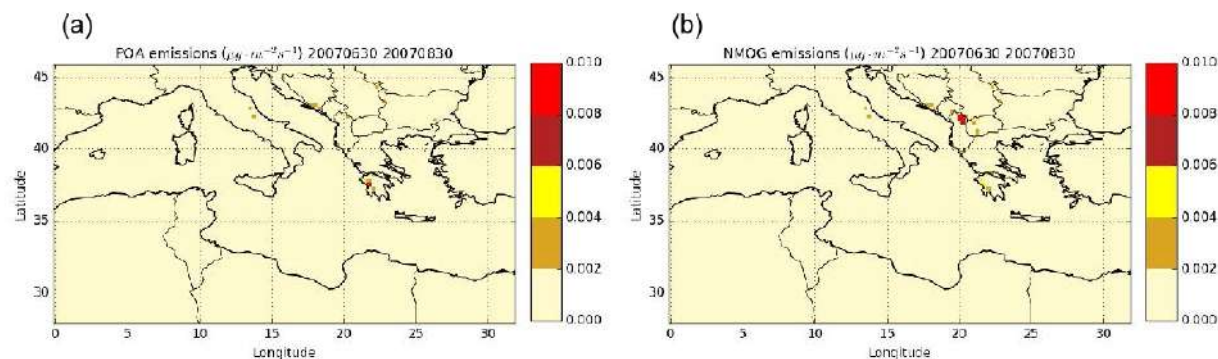


Figure 14. Daily mean POA (a) and NMOG (b) emissions from wildfires during the summer of 2007.

Majdi et al. (2019) studied the simulation OnestepIS-LVOC and found that comparing to $\text{PM}_{2.5}$ observations, the model tends to underestimate $\text{PM}_{2.5}$ concentrations (MFB = -32%). Moreover, they highlighted that surface $\text{PM}_{2.5}$ concentrations are sensitive to gaseous I/S/L-VOC emissions,

and their impact on surface $\text{PM}_{2.5}$ concentrations over the fire regions can reach 10%–20% in the fire plume and 30% locally.

Concerning the influence of the gaseous I/S/L-VOC ageing scheme, the relative differences between the simulations

OnestepISLVOC and MultstepISLVOC are low (below 5 %). The differences can be positive or negative because the one-step oxidation scheme and the multi-step oxidation schemes lead to SOA of different volatilities. The sign of the differences depends on the SOA volatilities and on the partitioning between the gas and the particle phases of I/S/L-VOCs, which itself depends on PM_{2.5} concentrations. The comparison of the relative difference of PM_{2.5} concentrations between the simulations OnestepISLVOC and MultstepISLVOC (Fig. 13a) and the daily mean PM_{2.5} concentrations (Fig. 13d) shows that the differences tend to be positive (higher concentrations with multi-generational ageing than with one-step ageing) in the regions of strong fires where PM_{2.5} concentrations are high and negative in the fire plume where PM_{2.5} concentrations are lower.

The emissions of the added VOCs (namely benzene, phenol, cresol, catechol, furan, guaiacol, syringol, naphthalene, methylnaphthalene, and the structurally assigned and unassigned compounds with at least six carbon atoms per molecule (USC>6) lead to a moderate increase in PM_{2.5} concentrations (up to 25 % in the Balkans; Fig. 13b). PM_{2.5} concentrations are more sensitive to the parameterization used to estimate the gaseous I/S/L-VOC emissions.

Estimating the gaseous I/S/L-VOC emissions from POA rather than from NMOG results in higher local PM_{2.5} concentrations (+8 % to +16 % in Greece) and lower PM_{2.5} concentrations mainly in the Balkans (−30 %) and in the fire plume that is visually determined (−8 % to −16 %). The larger fraction of PM_{2.5} concentrations is shown in the Balkans, where the gaseous I/S/L-VOC emissions from NMOG are higher than those emitted from POA. This is explained by differences in NMOG and POA emissions. Figure 14 shows daily mean emissions of POA and NMOG from wildfires during the summer of 2007. The main differences between POA and NMOG emissions are located in the Balkans, where the largest fraction of burned temperate forest is observed. In Akagi et al. (2011), the emission factor of POA is unavailable for temperate forest. This may be explained by the lower POA emissions in the Balkans.

7 Conclusions

This study quantified the relative contribution of OA_{tot} precursors (VOCs and I/S/L-VOCs) emitted by wildfires to OA formation and particle concentrations during the summer of 2007 over the Euro-Mediterranean region. A new chemical mechanism H²O_{aro} was developed to represent the SOA formation from selected VOCs, namely toluene, xylene, benzene, phenol, cresol, catechol, furan, guaiacol, syringol, naphthalene, methylnaphthalene, and the structurally assigned and unassigned compounds with at least six carbon atoms per molecule (USC>6), based on smog chamber experiments under low- and high-NO_x conditions. This mechanism was implemented in the chemistry transport model

Polair3D of the air-quality platform Polyphemus. Over the Euro-Mediterranean area, the OA concentrations emitted by wildfires originate mostly from I/S/L-VOCs. The OA concentrations from gaseous I/S/L-VOCs are about 10 times higher than the OA concentrations from VOCs. However, the contribution of the oxidation of VOCs to the OA concentrations is locally significant (it reaches 30 % in the area close to where wildfires are emitted and 20 % in the fire plume). Air-quality models often represent SOA formation from only a few VOCs, such as toluene and xylene. This study points out the need to consider the contribution of a variety of VOCs, namely, phenol, benzene, catechol, cresol, xylene, toluene and syringol, when modeling SOA formation from wildfires. The contribution of these VOCs may even be underestimated here for two reasons. First, the yields from smoke chamber experiments were not corrected for wall losses, and they may therefore be underestimated, leading to an underestimation of the SOA formation from VOCs in the model. Second, a large part of OA concentrations from VOCs is in the gas phase (~70 %). This suggests that the influence of the VOC emissions on OA concentrations could be larger if the surrogates from these VOC oxidations partition more easily to the particle phase. This could be the case if further ageing mechanisms are considered for these VOCs or if the particles are very viscous (Kim et al., 2019). Emissions of gaseous I/S/L-VOCs are a large source of uncertainties. However, similar estimates were obtained here by using, as a proxy, POA emissions (with a factor of 1.5) or NMOG emissions (with a factor of 0.36). Sensitivity simulations were performed to quantify the uncertainties in OA and PM_{2.5} concentrations linked to I/S/L-VOC emissions and chemical evolution (ageing). They are found to be lower than the uncertainties associated with SOA formation from VOC emissions. This stresses the need to consider a variety of VOCs in SOA formation model and to better characterize their emission factors.

Data availability. Data can be requested from the corresponding author (marwa.majdi@enpc.fr).

Appendix A

Table A1. The VOCs that are SOA precursors and their emission factors (EFs) and SOA yields. EFs from Akagi et al. (2011) are in regular font, ERs from Stockwell et al. (2015) are in italic font, and EFs in bold font are deduced from the assumption considering that temperate forest and savanna have the same EF as chaparral.

VOCs	EF* (g kg ⁻¹)					Y _{SOA}	NO _x regime
	Savanna	Crop residue	Pasture maintenance	Temperate forest	Chaparral		
Phenol	0.52	0.52	1.68	0.33	0.45	0.44 ^a	Low or high NO _x
Cresol	0.26 ¹	<i>0.35</i> ¹	–	0.26 ¹	<i>0.26</i> ¹	0.36 ^b	Low NO _x
Benzene	0.20	0.15	0.70	–	–	0.33 ^c	Low or high NO _x
Catechol	0.90 ¹	<i>0.48</i> ¹	–	0.90 ¹	<i>0.90</i> ¹	0.39 ^b	Low NO _x
Furan	0.17	0.11	2.63	0.2	0.18	0.05 ^c	High NO _x
Syringol	0.27 ¹	<i>0.23</i> ¹	–	0.27 ¹	<i>0.27</i> ¹	0.26 ^{a,f}	Medium-high NO _x
Guaiacol	0.27 ¹	<i>0.81</i> ¹	–	0.27 ¹	<i>0.27</i> ¹	0.45 ^{a,f}	Medium NO _x
Naphthalene	0.16 ²	<i>0.31</i> ²	–	0.16 ²	<i>0.16</i> ²	0.52 ^{e,f}	Medium NO _x
Methylnaphthalene	0.06 ²	<i>0.22</i> ²	–	0.06 ²	<i>0.06</i> ²	0.52 ^{e,f}	Medium-low NO _x
Toluene	0.08	0.19	0.34	–	–	0.24 ^{c,g}	Low or high NO _x
Xylene	0.01	–	–	0.11	–	0.20 ^{c,f}	Low or high NO _x

^a Yee et al. (2013), ^b Nakao et al. (2011), ^c Ng et al. (2007), ^d Gómez et al. (2008), ^e Chan et al. (2009), ^f Chhabra et al. (2011), ^g Hildebrandt et al. (2009).

¹ Emission ratio (ER) of the VOC to phenol from Stockwell et al. (2015). ² Emission ratio of the VOC to benzene from Stockwell et al. (2015).

Appendix B

Table B1. Properties of the compounds added to the model.

Species	Species names	Formula molecular	Mw ^a	ΔH_{vap}^b	P_{sat}^c	K_{p}^d	H^e
PHEN	Phenol	C ₆ H ₆ O	94	60.88	99.99×10^2	1.98×10^{-6}	–
CAT	Catechol	C ₆ H ₆ O ₂	110	76.91	6.5×10^{-4}	2.57×10^{-4}	–
ACIDMAL	Maleylacetic acid	C ₆ H ₆ O ₅	158	81.66	4.59×10^{-8}	2.56	8.68×10^{11}
BENZ	Benzene	C ₆ H ₆	78	43.25	15.23	1.30×10^{-8}	–
CRESp	Cresol	C ₇ H ₈ O	108	64.53	3.98×10^{-6}	3.75×10^{-12}	–
MCAT	Methylcatechol	C ₇ H ₈ O ₂	124	81.36	2.46×10^{-4}	6.08×10^{-4}	–
DHMB	Dihydroxymethylbenzoquinone	C ₇ H ₆ O ₄	154	81.73	3.52×10^{-6}	3.4×10^{-2}	3.62×10^9
FUR	Furan	C ₄ H ₄ O	68	27.45	5.925×10^2	2.5×10^{-7}	–
ButDial	Butendial	C ₄ H ₄ O ₂	84	54.03	1.89	1.17×10^{-7}	–
RADButenalCOO	Radical	C ₄ H ₃ O ₃	99	–	–	–	–
ButenalCOOH	Malealdehydic acid	C ₄ H ₄ O ₃	100	66.92	0.0122	1.53×10^{-5}	–
RADButenCOOHCOO	Radical	C ₄ H ₃ O ₄	115	–	–	–	–
Buten2COOH	Maleic acid	C ₄ H ₄ O ₄	116	79.83	7.803×10^{-5}	0.00238	1.03×10^9
SYR	Syringol	C ₈ H ₁₀ O ₃	154	77.41	5.49×10^{-4}	0.0002195	–
GUAI	Guaiacol	C ₇ H ₈ O ₂	124	68.89	7.41×10^{-3}	2.02×10^{-3}	–
RADSYR	Radical	C ₈ H ₉ O ₃ *	171	–	–	–	–
RADGUAI	Radical	C ₇ H ₇ O ₂ *	141	–	–	–	–
PSYR	Syringol SOA	C ₈ H ₁₀ O ₅	186	96.25	7.53×10^{-6}	1.294×10^{-2}	$1.45 \times 10^{+9}$
GHDPerox	Guaiacol SOA (hydroperoxide)	C ₇ H ₁₀ O ₅	174	99.52	5.41×10^{-7}	0.1972	$9.89 \times 10^{+9}$
NAPH	Naphthalene	C ₁₀ H ₈	128	61.38	0.0398	3.64×10^{-6}	–
NAPHP	Radical	C ₁₀ H ₇ *	127	–	–	–	–
MNAPH	Methylnaphthalene	C ₁₁ H ₁₀	142	65.26	0.0150	8.73×10^{-6}	–
MNAPHP	Radical	C ₁₁ H ₉ *	141	–	–	–	–
BBPAHIN	Dihydroxyterephthalic acid	C ₈ H ₆ O ₆	198	131.62	1×10^{-12}	93817.62.59	$1.65 \times 10^{+19}$
BBPAHhN	Phthalic acid	C ₈ H ₆ O ₄	166	97.95	10^{-6}	97.95	$1.49 \times 10^{+9}$
USC>6phen	–	–	94	60.88	99.99×10^2	1.98×10^{-6}	–
USC>6CAT	Catechol	C ₆ H ₆ O ₂	110	76.91	6.5×10^{-4}	2.57×10^{-4}	–
USC>6ACIDMAL	Maleylacetic acid	C ₆ H ₆ O ₅	158	81.66	4.59×10^{-8}	2.56	8.68×10^{11}
USC>6naph	–	C ₁₀ H ₈	128	61.38	0.0398	3.64×10^{-6}	–
USC>6NAPHP	Radical	C ₁₀ H ₇ *	127	–	–	–	–
USC>6BBPAHIN	Dihydroxyterephthalic acid	C ₈ H ₆ O ₆	198	131.62	10^{-12}	93817.62.59	$1.65 \times 10^{+19}$
USC>6BBPAHhN	Phthalic acid	C ₈ H ₆ O ₄	166	97.95	10^{-6}	50	$1.49 \times 10^{+9}$

^a Molar weight (g mol⁻¹). ^b Enthalpy of vaporization (kJ mol⁻¹). ^c Saturation vapor pressure (torr). ^d Partitioning constant (m³ g⁻¹). ^e Henry's law constant (M atm⁻¹).

Table B2. Chemical structure of SOA compounds considered in this study.

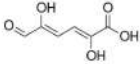
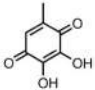
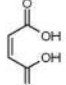
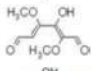
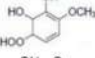
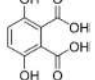
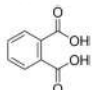
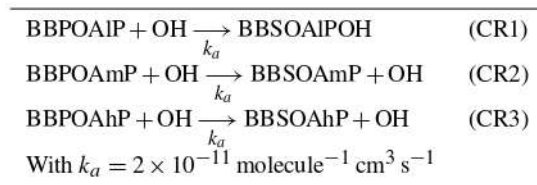
SOA species	Chemical structure
ACIDMAL	
DHMB	
Buten2COOH	
PSYR	
GHDPerox	
BBPAHIN	
BBPAHhN	

Table B3. Reactions leading to SOA formation added to CB05.

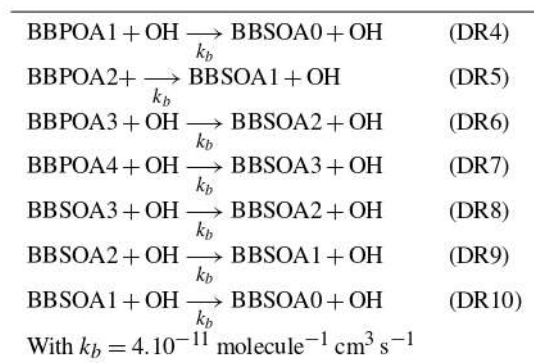
Reactions	Kinetic rate parameter (molecule ⁻¹ cm ³ s ⁻¹)
PHEN + OH → 0.75 CAT + OH	$4.7 \times 10^{-13} \exp(1220/T)$
CAT + OH → 0.28 ACIDMAL + OH	9.9×10^{-10}
BENZ + OH → 0.53 PHEN + OH	$2.3 \times 10^{-12} \exp(-190/T)$
CRESp + OH → 0.73 MCAT + OH	4.65×10^{-10}
MCAT + OH → 0.39 DHMB + OH	2×10^{-10}
FUR + OH → 0.87 ButDial + OH	4.19×10^{-11}
ButDial + OH → 0.83 RADButenalCOO + OH	5.20×10^{-11}
RADButenalCOO + HO ₂ → 0.15 ButenalCOOH + HO ₂	$5.20 \times 10^{-13} \exp(980/T)$
RADButenalCOO + NO → NO	$7.5 \times 10^{-12} \exp(290/T)$
RADButenalCOO + XO ₂ → 0.3 ButenalCOOH + XO ₂	1.0×10^{-11}
ButenalCOOH + OH → 0.3 RADButenCOOHCOO + OH	2.12×10^{-11}
RADButenCOOHCOO + HO ₂ → 0.15 Buten2COOH + HO ₂	$5.20 \times 10^{-13} \exp(980/T)$
RADButenCOOHCOO + NO → NO	$7.50 \times 10^{-12} \exp(980/T)$
RADButenCOOHCOO + XO ₂ → 0.3 Buten2COOH + XO ₂	1.0×10^{-11}
SYR + OH → RADSyr + OH	9.63×10^{-11}
RADSyr + HO ₂ → 0.57 PSyr + HO ₂	$2.91 \times 10^{-13} \exp(1300/T)$
RADSyr + NO → 0.36 PSyr + NO	$2.70 \times 10^{-13} \exp(360/T)$
RADSyr + NO ₃ → 0.36 PSyr + NO ₃	2.30×10^{-12}
GUAI + OH → RADGUAI + OH	7.53×10^{-11}
RADGUAI + HO ₂ → 0.37GHDPerox + HO ₂	$2.91 \times 10^{-13} \exp(1300/T)$
RADGUAI + NO → 0.32GHDPerox + NO	$2.70 \times 10^{-13} \exp(360/T)$
RADGUAI + NO ₃ → 0.32GHDPerox + NO ₃	2.30×10^{-12}
NAPHP + OH → NAPHP + OH	2.44×10^{-11}
NAPHP + HO ₂ → 0.44 BBPAHIN + HO ₂	$3.75 \times 10^{-13} \exp(980/T)$
NAPHP + MEO ₂ → 0.44 BBPAHIN + MEO ₂	$3.56 \times 10^{-14} \exp(708/T)$
NAPHP + C ₂ O ₃ → 0.44 BBPAHIN + C ₂ O ₃	$7.40 \times 10^{-13} \exp(765/T)$
NAPHP + NO → 0.26 BBPAHhN + NO	$2.70 \times 10^{-11} \exp(360/T)$
NAPHP + NO ₃ → 0.26 BBPAHhN + NO ₃	1.2×10^{-12}
MNAPHP + OH → 0.26 MNAPHP + OH	2.44×10^{-11}
MNAPHP + HO ₂ → 0.46 BBPAHIN + HO ₂	2.44×10^{-11}
MNAPHP + MEO ₂ → 0.46 BBPAHIN + MEO ₂	$3.56 \times 10^{-14} \exp(708/T)$
MNAPHP + C ₂ O ₃ → 0.46 BBPAHIN + C ₂ O ₃	$7.40 \times 10^{-13} \exp(765/T)$
MNAPHP + NO → 0.37 BBPAHhN + NO	$2.70 \times 10^{-11} \exp(360/T)$
MNAPHP + NO ₃ → 0.37 BBPAHhN + NO ₃	1.2×10^{-12}
USC>6 _{phen} + OH → 0.75 USC>6CAT + OH	$4.7 \times 10^{-13} \exp(1220/T)$
USC>6CAT + OH → 0.28 USC>6ACIDMAL + OH	9.9×10^{-10}
USC>6 _{NAPHP} + OH → USC>6NAPHP + OH	2.44×10^{-11}
USC>6NAPHP + HO ₂ → 0.44 USC>6BBPAHIN + HO ₂	$3.75 \times 10^{-13} \exp(980/T)$
USC>6NAPHP + MEO ₂ → 0.44 USC>6BBPAHIN + MEO ₂	$3.56 \times 10^{-14} \exp(708/T)$
USC>6NAPHP + C ₂ O ₃ → 0.44 USC>6BBPAHIN + C ₂ O ₃	$7.40 \times 10^{-13} \exp(765/T)$
USC>6NAPHP + NO → 0.26 USC>6BBPAHhN + NO	$2.70 \times 10^{-11} \exp(360/T)$
USC>6NAPHP + NO ₃ → 0.26 USC>6BBPAHhN + NO ₃	1.2×10^{-12}

Appendix C

Table C1. Ageing mechanism of I/S/L-VOCs using Couvidat approach (Couvidat et al., 2012).**Table C2.** Properties of primary and secondary I/S/L-VOCs.

Surrogates	Emission fraction	Molecular weight (g mol ⁻¹)	Log C*	Enthalpy of vaporization (kJ mol ⁻¹)
BBPOAlP	0.25	280	-0.04	106
BBPOAmP	0.32	280	1.94	91
BBPOAhP	0.43	280	3.51	79
BBSOAlP	-	392	-2.04	106
BBSOAmP	-	392	-0.06	91
BBSOAhP	-	392	1.51	79

Appendix D

Table D1. Ageing mechanism of I/S/L-VOCs using Ciarelli approach (Ciarelli et al., 2017).**Table D2.** Properties of the VBS species (primary and secondary I/S/L-VOCs).

Surrogates	Emission fraction	Molecular weight (g mol ⁻¹)	Log C*	Enthalpy of vaporization (kJ mol ⁻¹)
BBPOA0	0.2	216	-1	77.5
BBPOA1	0.1	216	0	70
BBPOA2	0.1	216	1	62.5
BBPOA3	0.2	216	2	55
BBPOA4	0.4	215	3	35
BBSOA0	-	194	-1	35
BBSOA1	-	189	0	35
BBSOA2	-	184	1	35
BBSOA3	-	179	2	35

Appendix E

Table E1. Summary of the parameters used to compute the dry-deposition velocities of the gaseous I/S/L-VOCs.

Species	Molecular weight ^a	C^{*b}	H_{eff}^c	Reactivity factor (f_0)	Diffusivity ^d	α^e	β^f
BBPOA1P	280	091	4.10^{+5}	0.1	0.0634	0	0.05
BBPOAmP	280	87.09	$1.6 \times 10^{+5}$	0.1	0.0634	0	0.05
BBPOAhP	280	3235	10^{+5}	0.1	0.0634	0	0.05
BBSOA1P	392	0.009	$1.3 \times 10^{+7}$	0.1	0.0388	0	0.5
BBSOAmP	392	0.87	$4. \times 10^{+5}$	0.1	0.0388	0	0.5
BBSOAhP	392	32.35	$1.45 \times 10^{+5}$	0.1	0.0388	0	0.5
BBPOA0	216	0.1	$3.2 \times 10^{+5}$	0.1	0.072	0	0.05
BBPOA1	216	1	$4 \times 10^{+5}$	0.1	0.072	0	0.05
BBPOA2	216	10	$1.3 \times 10^{+5}$	0.1	0.072	0	0.05
BBPOA3	216	100	$1.6 \times 10^{+5}$	0.1	0.072	0	0.05
BBPOA4	215	1000	10^{+5}	0.1	0.072	0	0.05
BBSOA0	194	0.1	$3.2 \times 10^{+5}$	0.1	0.0762	0	0.05
BBSOA1	189	1	$4.0 \times 10^{+5}$	0.1	0.0771	0	0.05
BBSOA2	184	10	$1.3 \times 10^{+5}$	0.1	0.0783	0	0.05
BBSOA3	179	100	$1.6 \times 10^{+5}$	0.1	0.0793	0	0.05

^a Molar weight (g mol^{-1}), ^b Saturation concentration ($\mu\text{g m}^{-3}$), ^c Effective Henry constant (Matm^{-1}), ^d Diffusivity ($\text{cm}^{-2} \text{s}^{-1}$), ^e Parameter for cuticle and soil resistance scaling to SO_2 , ^f Parameter for cuticle and soil resistance scaling to O_3 .

Author contributions. MM, KS, GL and FC developed the chemical mechanisms. ST and MM prepared VOC emissions from fires. MM performed the simulations, with help from MC and KS for the post-processing. MM, KS and GL prepared the paper with contributions from all co-authors.

Competing interests. The authors declare that they have no conflict of interest.

Acknowledgements. CEREIA is a member of the Institut Pierre-Simon Laplace (IPSL). A PhD grant from École des Ponts Paris-Tech partially funded this research.

Review statement. This paper was edited by Alma Hodzic and reviewed by two anonymous referees.

References

- Akagi, S. K., Yokelson, R. J., Wiedinmyer, C., Alvarado, M. J., Reid, J. S., Karl, T., Crounse, J. D., and Wennberg, P. O.: Emission factors for open and domestic biomass burning for use in atmospheric models, *Atmos. Chem. Phys.*, 11, 4039–4072, <https://doi.org/10.5194/acp-11-4039-2011>, 2011.
- Alvarado, M. and Prinn, R.: Formation of ozone and growth of aerosols in young smoke plumes from biomass burning: Three-dimensional Eulerian studies, *J. Geophys. Res.-Atmos.*, 114, D09306, <https://doi.org/10.1029/2008JD011144>, 2009.
- Alvarado, M. J., Lonsdale, C. R., Yokelson, R. J., Akagi, S. K., Coe, H., Craven, J. S., Fischer, E. V., McMeeking, G. R., Seinfeld, J. H., Soni, T., Taylor, J. W., Weise, D. R., and Wold, C. E.: Investigating the links between ozone and organic aerosol chemistry in a biomass burning plume from a prescribed fire in California chaparral, *Atmos. Chem. Phys.*, 15, 6667–6688, <https://doi.org/10.5194/acp-15-6667-2015>, 2015.
- Alves, C., Vicente, A., Nunes, T., Gonçalves, C., Fernandes, A., Mirante, F., Tarelho, L., Sanchez de la Campa, A., Querol, X., Caseiro, A., Monteiro, C., Evtugina, M., and Pio, C.: Summer 2009 wildfires in Portugal: emission of trace gases and aerosol composition, *Atmos. Environ.*, 45, 641–649, <https://doi.org/10.1016/j.atmosenv.2010.10.031>, 2011.
- Appel, K. W., Napelenok, S. L., Foley, K. M., Pye, H. O. T., Hogrefe, C., Luecken, D. J., Bash, J. O., Roselle, S. J., Pleim, J. E., Foroutan, H., Hutzell, W. T., Pouliot, G. A., Sarwar, G., Fahey, K. M., Gantt, B., Gilliam, R. C., Heath, N. K., Kang, D., Mathur, R., Schwede, D. B., Spero, T. L., Wong, D. C., and Young, J. O.: Description and evaluation of the Community Multiscale Air Quality (CMAQ) modeling system version 5.1, *Geosci. Model Dev.*, 10, 1703–1732, <https://doi.org/10.5194/gmd-10-1703-2017>, 2017.
- Atkinson, R. and Arey, J.: Atmospheric Degradation of Volatile Organic Compounds, *Chem. Rev.*, 103, 4605–4638, <https://doi.org/10.1021/cr0206420>, 2003.
- Aumont, B., Szopa, S., and Madronich, S.: Modelling the evolution of organic carbon during its gas-phase tropospheric oxidation: development of an explicit model based on a self-generating approach, *Atmos. Chem. Phys.*, 5, 2497–2517, <https://doi.org/10.5194/acp-5-2497-2005>, 2005.
- Bessagnet, B., Menut, L., Aymoz, G., Chepfer, H., and Vautard, R.: Modeling dust emissions and transport within Europe: the Ukraine March 2007 event, *J. Geophys. Res.*, 113, D15202, <https://doi.org/10.1029/2007JD009541>, 2008.
- Bian, Q., Jathar, S. H., Kodros, J. K., Barsanti, K. C., Hatch, L. E., May, A. A., Kreidenweis, S. M., and Pierce, J. R.: Secondary organic aerosol formation in biomass-burning plumes: theoretical analysis of lab studies and ambient plumes, *Atmos. Chem. Phys.*, 17, 5459–5475, <https://doi.org/10.5194/acp-17-5459-2017>, 2017.
- Bond, T. C., Doherty, S. J., Fahey, D. W., Forster, P. M., Berntsen, T., DeAngelo, B. J., Flanner, M. G., Ghan, S., Kärcher, B., Koch, D., Kinne, S., Kondo, Y., Quinn, P. K., Sarofim, M. C., Schultz, M. G., Schulz, M., Venkataraman, C., Zhang, H., Zhang, S., Bellouin, N., Guttikunda, S. K., Hopke, P. K., Jacobson, M. Z., Kaiser, J. W., Klimont, Z., Lohmann, U., Schwarz, J. P., Shindell, D., Storelvmo, T., Warren, S. G., and Zender, C. S.: Bounding the role of black carbon in the climate system: A scientific assessment, *J. Geophys. Res.-Atmos.*, 118, 5380–5552, <https://doi.org/10.1002/jgrd.50171>, 2013.
- Briant, R., Tuccella, P., Deroubaix, A., Khvorostyanov, D., Menut, L., Mailler, S., and Turquety, S.: Aerosol-radiation interaction modelling using online coupling between the WRF 3.7.1 meteorological model and the CHIMERE 2016 chemistry-transport model, through the OASIS3-MCT coupler, *Geosci. Model Dev.*, 10, 927–944, <https://doi.org/10.5194/gmd-10-927-2017>, 2017.
- Bruns, E., El Haddad, I., Slowik, J., Kilic, D., Klein, F., Baltensperger, U., and Prévôt, A.: Identification of significant precursor gases of secondary organic aerosols from residential wood combustion, *Sci. Rep.*, <https://doi.org/10.1038/srep27881>, 2016.
- Calvert, J., Atkinson, R., Becker, K., Kamens, R., Seinfeld, J., Wallington, T., and Yarwood, G.: *The Mechanisms of Atmospheric Oxidation of Aromatic Hydrocarbons*, Oxford University Press, 2002.
- Carlton, A., Pinder, R., Bhawe, P., and Pouliot, G.: What extent can biogenic SOA be controlled, *Environ. Sci. Technol.*, 9, 3376–3380, <https://doi.org/10.1021/es903506b>, 2010.
- Chan, A. W. H., Kautzman, K. E., Chhabra, P. S., Surratt, J. D., Chan, M. N., Crounse, J. D., Kürten, A., Wennberg, P. O., Flagan, R. C., and Seinfeld, J. H.: Secondary organic aerosol formation from photooxidation of naphthalene and alkylnaphthalenes: implications for oxidation of intermediate volatility organic compounds (IVOCs), *Atmos. Chem. Phys.*, 9, 3049–3060, <https://doi.org/10.5194/acp-9-3049-2009>, 2009.
- Chhabra, P. S., Ng, N. L., Canagaratna, M. R., Corrigan, A. L., Russell, L. M., Worsnop, D. R., Flagan, R. C., and Seinfeld, J. H.: Elemental composition and oxidation of chamber organic aerosol, *Atmos. Chem. Phys.*, 11, 8827–8845, <https://doi.org/10.5194/acp-11-8827-2011>, 2011.
- Chrit, M., Sartelet, K., Sciare, J., Pey, J., Marchand, N., Couvidat, F., Sellegri, K., and Beekmann, M.: Modelling organic aerosol concentrations and properties during ChArMEX summer campaigns of 2012 and 2013 in the western Mediterranean region, *Atmos. Chem. Phys.*, 17, 12509–12531, <https://doi.org/10.5194/acp-17-12509-2017>, 2017.
- Ciarelli, G., El Haddad, I., Bruns, E., Aksoyoglu, S., Möhler, O., Baltensperger, U., and Prévôt, A. S. H.: Constraining a hy-

- brid volatility basis-set model for aging of wood-burning emissions using smog chamber experiments: a box-model study based on the VBS scheme of the CAMx model (v5.40), *Geosci. Model Dev.*, 10, 2303–2320, <https://doi.org/10.5194/gmd-10-2303-2017>, 2017.
- Ciccioli, P., Centritto, M., and Loreto, F.: Biogenic volatile organic compound emissions from vegetation fires, *Plant Cell Environ.*, 37, 1810–1825, <https://doi.org/10.1111/pce.12336>, 2014.
- Coeur-Tourneur, C., Cassez, A., and Wenger, J. C.: Rate coefficients for the gas-phase reaction of hydroxyl radicals with 2-Methoxyphenol (guaiacol) and related compounds, *J. Phys. Chem. A.*, 114, 11645–11650, <https://doi.org/10.1021/jp1071023>, 2010a.
- Couvidat, F. and Sartelet, K.: The Secondary Organic Aerosol Processor (SOAP v1.0) model: a unified model with different ranges of complexity based on the molecular surrogate approach, *Geosci. Model Dev.*, 8, 1111–1138, <https://doi.org/10.5194/gmd-8-1111-2015>, 2015.
- Couvidat, F., Debry, E., Sartelet, K., and Seigneur, C.: A hydrophilic/hydrophobic organic (H²O) aerosol model: Development, evaluation and sensitivity analysis, *J. Geophys. Res.*, 117, D10304, <https://doi.org/10.1029/2011JD017214>, 2012.
- Couvidat, F., Kim, Y., Sartelet, K., Seigneur, C., Marchand, N., and Sciare, J.: Modeling secondary organic aerosol in an urban area: application to Paris, France, *Atmos. Chem. Phys.*, 13, 983–996, <https://doi.org/10.5194/acp-13-983-2013>, 2013.
- Dawson, M. L., Xu, J., Griffin, R. J., and Dabdub, D.: Development of aroC/MPPMO 1.0: a model to simulate secondary organic aerosol from aromatic precursors in regional models, *Geosci. Model Dev.*, 9, 2143–2151, <https://doi.org/10.5194/gmd-9-2143-2016>, 2016.
- Debry, E., Fahey, K., Sartelet, K., Sportisse, B., and Tombette, M.: Technical Note: A new Size Resolved Aerosol Model (SIREAM), *Atmos. Chem. Phys.*, 7, 1537–1547, <https://doi.org/10.5194/acp-7-1537-2007>, 2007.
- Donahue, N., Hartz, K., Chuong, B., Presto, A., Stanier, C., Rosenhorn, T., Robinson, A., and Pandis, S.: Critical factors determining the variation in SOA yields from terpene ozonolysis: a combined experimental and computational study, *Faraday Discuss.*, 130, 295–309, <https://doi.org/10.1039/B417369D>, 2005.
- Donahue, N. M., Robinson, A. L., Stanier, C. O., and Pandis, S. N.: Coupled partitioning, dilution and chemical aging of semivolatile organics, *Environ. Sci. Technol.*, 40, 2635–2643, <https://doi.org/10.1021/es052297c>, 2006.
- Donahue, N. M., Epstein, S. A., Pandis, S. N., and Robinson, A. L.: A two-dimensional volatility basis set: 1. organic-aerosol mixing thermodynamics, *Atmos. Chem. Phys.*, 11, 3303–3318, <https://doi.org/10.5194/acp-11-3303-2011>, 2011.
- Eldering, A. and Cass, G.: Source-oriented model for air pollutant effects on visibility, *J. Geophys. Res.-Atmos.*, 101, 19343–19369, <https://doi.org/10.1029/95JD02928>, 1996.
- Emmons, L. K., Walters, S., Hess, P. G., Lamarque, J.-F., Pfister, G. G., Fillmore, D., Granier, C., Guenther, A., Kinnison, D., Laepple, T., Orlando, J., Tie, X., Tyndall, G., Wiedinmyer, C., Baughcum, S. L., and Kloster, S.: Description and evaluation of the Model for Ozone and Related chemical Tracers, version 4 (MOZART-4), *Geosci. Model Dev.*, 3, 43–67, <https://doi.org/10.5194/gmd-3-43-2010>, 2010.
- Gómez, E., Borrás, E., Viidanoja, J., and Hjorth, J.: Unsaturated dicarbonyl products from OH-initiated photo-oxidation of furan, 2-methylfuran and 3-methylfuran, *Atmos. Environ.*, 43, 1603–1612, <https://doi.org/10.1016/j.atmosenv.2008.12.019>, 2008.
- Grieshop, A. P., Logue, J. M., Donahue, N. M., and Robinson, A. L.: Laboratory investigation of photochemical oxidation of organic aerosol from wood fires 1: measurement and simulation of organic aerosol evolution, *Atmos. Chem. Phys.*, 9, 1263–1277, <https://doi.org/10.5194/acp-9-1263-2009>, 2009.
- Grosjean, D.: Atmospheric Fate of Toxic Aromatic Compounds, *Sci. Total Environ.*, 100, 367–414, 1990.
- Guenther, A., Karl, T., Harley, P., Wiedinmyer, C., Palmer, P. I., and Geron, C.: Estimates of global terrestrial isoprene emissions using MEGAN (Model of Emissions of Gases and Aerosols from Nature), *Atmos. Chem. Phys.*, 6, 3181–3210, <https://doi.org/10.5194/acp-6-3181-2006>, 2006.
- Hand, K., Carlson, R., and Chyba, C.: Energy, Chemical Disequilibrium, and Geological Constraints on Europa, *Astrobiology*, 7, 1006–22, <https://doi.org/10.1089/ast.2007.0156>, 2007.
- Hildebrandt, L., Donahue, N. M., and Pandis, S. N.: High formation of secondary organic aerosol from the photo-oxidation of toluene, *Atmos. Chem. Phys.*, 9, 2973–2986, <https://doi.org/10.5194/acp-9-2973-2009>, 2009.
- Hodzic, A., Kasibhatla, P. S., Jo, D. S., Cappa, C. D., Jimenez, J. L., Madronich, S., and Park, R. J.: Rethinking the global secondary organic aerosol (SOA) budget: stronger production, faster removal, shorter lifetime, *Atmos. Chem. Phys.*, 16, 7917–7941, <https://doi.org/10.5194/acp-16-7917-2016>, 2016.
- Jathar, S. H., Gordon, T. D., Hennigan, C. J., Pye, H. O. T., Pouliot, G., Adams, J., Donahue, N. M., and Robinson, A. L.: Unspeciated organic emissions from combustion sources and their influence on the secondary organic aerosol budget in the United States, *P. Natl. Acad. Sci. USA*, 111, 10473–10478, <https://doi.org/10.1073/pnas.1323740111>, 2014.
- Jathar, S. H., Woody, M., Pye, H. O. T., Baker, K. R., and Robinson, A. L.: Chemical transport model simulations of organic aerosol in southern California: model evaluation and gasoline and diesel source contributions, *Atmos. Chem. Phys.*, 17, 4305–4318, <https://doi.org/10.5194/acp-17-4305-2017>, 2017.
- Jiang, X., Tsou, N. T., Jia, L., Liu, S., Zhang, H., Xu, Y., and Du, L.: Secondary organic aerosol formation from photooxidation of furan: effects of NO_x and humidity, *Atmos. Chem. Phys. Discuss.*, <https://doi.org/10.5194/acp-2019-89>, in review, 2019.
- Jimenez, J. L., Canagaratna, M. R., Donahue, N. M., Prevot, A. S. H., Zhang, Q., Kroll, J. H., DeCarlo, P. F., Allan, J. D., Coe, H., Ng, N. L., Aiken, A. C., Docherty, K. S., Ulbrich, I. M., Grieshop, A. P., Robinson, A. L., Duplissy, J., Smith, J. D., Wilson, K. R., Lanz, V. A., Hueglin, C., Sun, Y. L., Tian, J., Laaksonen, A., Raatikainen, T., Rautiainen, J., Vaattovaara, P. M., Ehn, M., Kulmala, J. M., Tomlinson, D. R., Collins, M. J., Cubison, E., Dunlea, J., Huffman, J. A., Onasch, T. B., Alfarra, M. R., Williams, P. I., Bower, K., Kondo, Y., Schneider, J., Drewnick, F., Borrmann, S., Weimer, S., Demerjian, K., Salcedo, D., Cottrell, L. R., Griffin, R., Takami, A., Miyoshi, T., Hatakeyama, S., Shimono, A., Sun, J. Y., Zhang, Y. M., Dzepina, K., Kimmel, J. R., Sueper, D., and Jayne, J. T., Herndon, S. C., Trimborn, A. M., Williams, L. R., Wood, E. C., Middlebrook, A. M., Kolb, C. E., Baltensperger, U., and Worsnop, D. R.: Evolution

- of organic aerosols in the atmosphere, *Science*, 326, 1525–1529, <https://doi.org/10.1126/science.1180353>, 2009.
- Johnston, F., Henderson, S., Chen, Y., Randerson, J., Marlier, M., and DeFries, R., Kinney, P., Bowman, D., and Brauer, M.: Estimated Global Mortality Attributable to Smoke from Landscape Fires, *Environ. Health Perspect.*, 120, 695–701, <https://doi.org/10.1289/ehp.1104422>, 2012.
- Karl, T., Harley, P., Emmons, L., Thornton, B., Guenther, A., Basu, C., Turnipseed, A., and Jardine, K.: Efficient atmospheric cleansing of oxidized organic trace gases by vegetation, *Science*, 330, 816–819, <https://doi.org/10.1126/science.1192534>, 2010.
- Kautzman, K. E., Surratt, J. D., Chan, M. N., Chan, A. W. H., Hersey, S. P., Chhabra, P. S., Dalleska, N. F., Wennberg, P. O., Flagan, R. C., and Seinfeld, J. H.: Chemical Composition of Gas- and Aerosol-Phase Products from the Photooxidation of Naphthalene, *J. Phys. Chem.*, 114, 913–934, <https://doi.org/10.1021/jp908530s>, 2010.
- Kim, Y., Couvidat, F., Sartelet, K., and Seigneur, C.: Comparison of Different Gas-Phase Mechanisms and Aerosol Modules for Simulating Particulate Matter Formation, *J. Air Waste Manage. Assoc.*, 61, 1218–1226, <https://doi.org/10.1080/10473289.2011.603999>, 2011.
- Kim, Y., Sartelet, K., Seigneur, C., Charron, A., Besombes, J. L., and Jaffrezo, J. L.: Effect of measurement protocol on organic aerosol measurements of exhaust emissions from gasoline and diesel vehicles., *Atmos. Environ.*, 140, 176–187, <https://doi.org/10.1016/j.atmosenv.2016.05.045>, 2016.
- Kim, Y., Sartelet, K., and Couvidat, F.: Modeling the effect of non-ideality, dynamic mass transfer and viscosity on SOA formation in a 3-D air quality model, *Atmos. Chem. Phys.*, 19, 1241–1261, <https://doi.org/10.5194/acp-19-1241-2019>, 2019.
- Kleinman, L. I.: Low and high NO_x tropospheric photochemistry, *J. Geophys. Res.*, 99, 16831–16837, <https://doi.org/10.1029/94JD01028>, 1994.
- Knote, C., Hodzic, A., and Jimenez, J. L.: The effect of dry and wet deposition of condensable vapors on secondary organic aerosols concentrations over the continental US, *Atmos. Chem. Phys.*, 15, 1–18, <https://doi.org/10.5194/acp-15-1-2015>, 2015.
- Kononov, I. B., Beekmann, M., Berezin, E. V., Petetin, H., Mielonen, T., Kuznetsova, I. N., and Andreae, M. O.: The role of semi-volatile organic compounds in the mesoscale evolution of biomass burning aerosol: a modeling case study of the 2010 mega-fire event in Russia, *Atmos. Chem. Phys.*, 15, 13269–13297, <https://doi.org/10.5194/acp-15-13269-2015>, 2015.
- Koo, B., Knipping, E., and Yarwood, G.: 1.5-Dimensional volatility basis set approach for modeling organic aerosol in CAMx and CMAQ, *Atmos. Environ.*, 95, 158–164, <https://doi.org/10.1016/j.atmosenv.2014.06.031>, 2014.
- Lauraguais, A., Coeur-Tourneur, C., Cassez, A., and Seydi, A.: Rate constant and secondary organic aerosol yields for the gas-phase reaction of hydroxyl radicals with syringol (2,6-dimethoxyphenol), *Atmos. Environ.*, 55, 48–48, <https://doi.org/10.1016/j.atmosenv.2012.02.027>, 2012.
- Lauraguais, A., Coeur-Tourneur, C., Cassez, A., Deboudt, K., Fourmentin, M., and Choel, M.: Atmospheric reactivity of hydroxyl radicals with guaiacol (2-methoxyphenol), a biomass burning emitted compound: Secondary organic aerosol formation and gas-phase oxidation products, *Atmos. Environ.*, 86, 155–163, <https://doi.org/10.1016/j.atmosenv.2013.11.074>, 2014.
- Lipsky, E. and Robinson, A.: Effects of dilution on fine particle mass and partitioning of semivolatile organics in diesel exhaust and wood smoke, *Environ. Sci. Technol.*, 40, 155–162, <https://doi.org/10.1021/Es050319P>, 2006.
- Majdi, M., Turquety, S., Sartelet, K., Legorgeu, C., Menut, L., and Kim, Y.: Impact of wildfires on particulate matter in the Euro-Mediterranean in 2007: sensitivity to some parameterizations of emissions in air quality models, *Atmos. Chem. Phys.*, 19, 785–812, <https://doi.org/10.5194/acp-19-785-2019>, 2019.
- Mallet, V., Qu'élo, D., Sportisse, B., Ahmed de Biasi, M., Debry, É., Korsakissok, I., Wu, L., Roustan, Y., Sartelet, K., Tombette, M., and Foudhil, H.: Technical Note: The air quality modeling system Polyphemus, *Atmos. Chem. Phys.*, 7, 5479–5487, <https://doi.org/10.5194/acp-7-5479-2007>, 2007.
- Marson, S., Trentmann, J., Winterrath, T., Yokelson, R., Christian, T., Carlson, L., Warner, W., Wolfe, L., and Andreae, M.: Intercomparison of Two Box Models of the Chemical Evolution in Biomass-Burning Smoke Plumes, *Environ. Sci. Technol.*, 55, 273–297, <https://doi.org/10.1007/s10874-006-9039-5>, 2006.
- May, A. A., Levin, E., Hennigan, C. J., Riipinen, I., Lee, T., Collett Jr, J., Jimenez, J. L., Kreidenweis, S. M., and Robinson, A. L.: Gas-particle partitioning of primary organic aerosol emissions: 3. Biomass burning, *J. Geophys. Res.-Atmos.*, 118, 327–338, <https://doi.org/10.1002/jgrd.50828>, 2013.
- Menut, L., Perez Garcia-Pando, C., Hausteijn, K., Bessagnet, B., Prigent, C., and Alfaro, S.: Relative impact of roughness and soil texture on mineral dust emission fluxes modeling, *J. Geophys. Res.-Atmos.*, 118, 6505–6520, <https://doi.org/10.1002/jgrd.50313>, 2013.
- Monahan, E. C.: In *The Role of Air-Sea Exchange in Geochemical Cycling*, Chap., The ocean as a source of atmospheric particles, 129–163, Kluwer Academic Publishers, 1986.
- Naeher, L., Brauer, M., Lipsett, M., Zelikoff, J., Simpson, D., Koenig, J., and Smith, R.: Woodsmoke Health Effects: A Review, *Inhalation Toxicol.*, 19, 67–106, <https://doi.org/10.1080/08958370600985875>, 2006.
- Nakao, S., Clark, C., Tang, P., Sato, K., and Cocker III, D.: Secondary organic aerosol formation from phenolic compounds in the absence of NO_x, *Atmos. Chem. Phys.*, 11, 10649–10660, <https://doi.org/10.5194/acp-11-10649-2011>, 2011.
- Nenes, A., Pandis, S., and Pilinis, C.: Continued development and testing of a new thermodynamic aerosol module for urban and regional air quality models, *Atmos. Environ.*, 33, 1553–1560, [https://doi.org/10.1016/S1352-2310\(98\)00352-5](https://doi.org/10.1016/S1352-2310(98)00352-5), 1999.
- Ng, N., Kroll, J., Chan, W., Chabara, P., Flagan, R., and Seinfeld, J.: Secondary organic aerosol formation from m-xylene, toluene, and benzene, *Atmos. Chem. Phys.*, 7, 3909–3922, <https://doi.org/10.5194/acp-7-3909-2007>, 2007.
- Odum, J., Hoffmann, T., Bowman, F., Collins, D., Flagan, R., and Seinfeld, J.: Gas/Particle Partitioning and Secondary Organic Aerosol Yield, *Environ. Sci. Technol.*, 30, 2580–2585, <https://doi.org/10.1021/es950943>, 1996.
- Olariu, R., Barnes, I., Bejan, I., Arsene, C., Vione, D., Klotz, B., and Becker, K.: FT-IR Product Study of the Reactions of NO₃ Radicals With ortho-, meta and para-Cresol, *Environ. Sci. Technol.*, 47, 7729–7738, <https://doi.org/10.1021/es401096w>, 2013.
- Pankow, J.: An absorption model of gas/particle partitioning involved in the formation of secondary organic aerosol, *At-*

- mos. Environ., 28A, 189–193, [https://doi.org/10.1016/1352-2310\(94\)90094-9](https://doi.org/10.1016/1352-2310(94)90094-9), 1994.
- Pankow, J. F. and Asher, W. E.: SIMPOL.1: a simple group contribution method for predicting vapor pressures and enthalpies of vaporization of multifunctional organic compounds, *Atmos. Chem. Phys.*, 8, 2773–2796, <https://doi.org/10.5194/acp-8-2773-2008>, 2008.
- Pilinis, C., Pandis, S., and Seinfeld, J.: Sensitivity of direct climate forcing by atmospheric aerosols to aerosol size and composition, *J. Geophys. Res.-Atmos.*, 1001, 18739–18754, <https://doi.org/10.1029/95JD02119>, 1995.
- Pope, C. A., Burnett, R. T., Thun, M. J., Calle, E. E., Krewski, D., and Thurston, K. I. G. D.: Lung cancer, cardiopulmonary mortality, and long-term exposure to fine particulate air pollution, *JAMA*, 287, 1132–1141, 2002.
- Pun, B. K., Seigneur, C., and Lohman, K.: Modeling secondary organic aerosol formation via multiphase partitioning with molecular data, *Environ. Sci. Technol.*, 40, 4722–4731, <https://doi.org/10.1021/es0522736>, 2006.
- Robinson, A. L., Donahue, N., Shrivastava, M., Weitkamp, E., Sage, A., Grieshop, A., Lane, T., Pierce, J., and Pandis, S.: Rethinking organic aerosols; Semivolatile emissions and photochemical ageing, *Science*, 315, 1259–1262, <https://doi.org/10.1126/science.1133061>, 2007.
- Sartelet, K., Couvidat, F., Seigneur, C., and Roustan, Y.: Impact of biogenic emissions on air quality over Europe and North America, *Atmos. Environ.*, 53, 131–141, <https://doi.org/10.1016/j.atmosenv.2011.10.046>, 2012.
- Sartelet, K., Zhu, S., Moukhtar, S., André, M., André, J., Gros, V., Favez, O., Brasseur, A., and Redaelli, M.: Emission of intermediate, semi and low volatile organic compounds from traffic and their impact on secondary organic aerosol concentrations over Greater Paris, *Atmos. Environ.*, 180, 126–137, <https://doi.org/10.1016/j.atmosenv.2018.02.031>, 2018.
- Saunders, S. M., Jenkin, M. E., Derwent, R. G., and Pilling, M. J.: World wide web site of a master chemical mechanism (MCM) for use in tropospheric chemistry models, *Atmos. Environ.*, 31, 1249–1249, [https://doi.org/10.1016/S1352-2310\(97\)85197-7](https://doi.org/10.1016/S1352-2310(97)85197-7), 1997.
- Schell, B., Ackermann, I. J., Hass, H., Binkowski, F. S., and Ebel, A.: Modeling the formation of secondary organic aerosol within a comprehensive air quality model system, *J. Geophys. Res.*, 106, 28275–28293, <https://doi.org/10.1029/2001JD000384>, 2001.
- Schwantes, R. H., Schilling, K. A., McVay, R. C., Lignell, H., Coggon, M. M., Zhang, X., Wennberg, P. O., and Seinfeld, J. H.: Formation of highly oxygenated low-volatility products from cresol oxidation, *Atmos. Chem. Phys.*, 17, 3453–3474, <https://doi.org/10.5194/acp-17-3453-2017>, 2017.
- Sheehan, P. and Bowman, F.: Estimated effects of temperature on secondary organic aerosol concentrations, *Environ. Sci. Technol.*, 35, 2129–2135, <https://doi.org/10.1021/es001547g>, 2001.
- Sillman, S., Logan, J. A., and Wofsy, S.: The sensitivity of ozone to nitrogen oxides and hydrocarbons in regional ozone episodes, *J. Geophys. Res.*, 95, 1837–1851, <https://doi.org/10.1016/j.agrformet.2004.12.007>, 1990.
- Stanier, C., Pathak, R., and Pandis, S.: Measurements of the volatility of aerosols from α -pinene ozonolysis, *Environ. Sci. Technol.*, 41, 2756–2763, <https://doi.org/10.1021/es0519280>, 2007.
- Stockwell, C. E., Veres, P., Williams, J., and Yokelson, R.: Characterization of biomass burning emissions from cooking fires, peat, crop residue, and other fuels with high-resolution proton-transfer-reaction time-of-flight mass spectrometry, *Atmos. Chem. Phys.*, 15, 845–865, <https://doi.org/10.5194/acp-15-845-2015>, 2015.
- Turquety, S., Menut, L., Bessagnet, B., Anav, A., Viovy, N., Maignan, F., and Wooster, M.: APIFLAME v1.0: high-resolution fire emission model and application to the Euro-Mediterranean region, *Geosci. Model Dev.*, 7, 587–612, <https://doi.org/10.5194/gmd-7-587-2014>, 2014.
- Wesely, M.: Parameterization of surface resistances to gaseous dry deposition in regional-scale numerical models, *Atmos. Environ.*, 23, 1293–1304, [https://doi.org/10.1016/0004-6981\(89\)90153-4](https://doi.org/10.1016/0004-6981(89)90153-4), 1989.
- Yarwood, G., Rao, S., Yocke, M., and Whitten, G.: Updates to the carbon bond chemical mechanism: CB05 Final report to the US EPA, 2005.
- Yee, L., Kautzman, K., Loza, C., Schilling, K., Coggon, M., Chhabra, P., Chan, M., Chan, A., Hersey, S., Crouse, J., Wennberg, P., Flagan, R., and Seinfeld, J.: Secondary organic aerosol formation from biomass burning intermediates: phenol and methoxyphenols, *Atmos. Chem. Phys.*, 13, 8019–8043, <https://doi.org/10.5194/acp-13-8019-2013>, 2013.
- Yokelson, R., Burling, I., Gilman, J., Warneke, C., Stockwell, C., De Gouw, J., Akagi, S., Urbanski, S., Veres, P., Roberts, J., Kuster, W. C., Reardon, J., Griffith, D. W. T., Johnson, T. J., Hosseini, S., Miller, J. W., Cocker, D., Jung, H., and Weise, D. R.: Coupling field and laboratory measurements to estimate the emission factors of identified and unidentified trace gases for prescribed fires, *Atmos. Chem. Phys.*, 13, 89–116, <https://doi.org/10.5194/acp-13-89-2013>, 2013.
- Zhu, S., Sartelet, K., Zhang, Y., and Nenes, A.: Three-dimensional modelling of the mixing state of particles over Greater Paris, *J. Geophys. Res.*, 121, 5930–5947, <https://doi.org/10.1002/2015JD024241>, 2016.

Annex C



Analysis and determination of secondary organic aerosol (SOA) tracers (markers) in particulate matter standard reference material (SRM 1649b, urban dust)

Alexandre Albinet¹ · Grazia Maria Lanzafame¹ · Deepchandra Srivastava¹ · Nicolas Bonnaire² · Frederica Nalin³ · Stephen A. Wise³

Received: 12 April 2019 / Revised: 13 June 2019 / Accepted: 2 July 2019 / Published online: 17 July 2019

© Springer-Verlag GmbH Germany, part of Springer Nature 2019

Abstract

Secondary organic aerosol (SOA) accounts for a significant fraction of particulate matter (PM) in the atmosphere. Source identification, including the SOA fraction, is critical for the effective management of air pollution. Molecular SOA markers (tracers) are key compounds allowing the source apportionment of SOA using different methodologies. Therefore, accurate SOA marker measurements in ambient air PM are important. This study determined the concentrations of 12 key SOA markers (biogenic and anthropogenic) in the urban dust standard reference material available from the National Institute of Standards and Technology (NIST) (SRM 1649b). Two extraction procedures, sonication and QuEChERS-like (quick easy cheap effective rugged and safe), have been compared. Three research laboratories/institutes using two analytical techniques (gas chromatography/mass spectrometry (GC/MS) and ultra-high-pressure liquid chromatography/tandem mass spectrometry (HPLC/MS-MS)) carried out the analyses. The results obtained were all in good agreement, except for 2-methylerythritol. The analysis of this compound still seems to be challenging by both GC/MS (large injection repeatability) and HPLC/MS-MS (separation issues of both 2-methyltetrols: 2-methylthreitol and 2-methylerythritol). Possible inhomogeneity in the SRM for this compound could also explain the large discrepancies observed. Sonication and QuEChERS-like procedures gave comparable results for the extraction of the SOA markers showing that QuEChERS-like extraction is suitable for the analysis of SOA markers in ambient air PM. As this study provides, for the first time, indicative values in a reference material for typical SOA markers, the analysis of SRM 1649b (urban dust) could be used for quality control/assurance purposes.

Keywords Aerosol · SOA · Tracers · QuEChERS · Analysis

Electronic supplementary material The online version of this article (<https://doi.org/10.1007/s00216-019-02015-6>) contains supplementary material, which is available to authorized users.

✉ Alexandre Albinet
alexandre.albinet@gmail.com; alexandre.albinet@ineris.fr

¹ Institut National de l'Environnement industriel et des RISques (INERIS), Parc technologique Alata BP2, 60550 Verneuil en Halatte, France

² Laboratoire des Sciences du Climat et de l'Environnement (LSCE), Unité Mixte CEA-CNRS-UVSQ, CEA/Orme des Merisiers, 91191 Gif-sur-Yvette, France

³ Chemical Sciences Division, National Institute of Standards and Technology (NIST), Gaithersburg, MD 20899, USA

Introduction and objectives

Organic matter (OM) accounts for a large fraction of the fine atmospheric particulate matter (PM, aerosol) (about 20 to 90%) [1]. Carbonaceous species that constitute the organic aerosol fraction (OA) are classified following their origins. Primary organic compounds directly emitted into the atmosphere belongs to the primary OA fraction (POA), while secondary organic particles, formed in the atmosphere by homogeneous or heterogeneous (photo)-chemical reactions of volatile or semi-volatile organic compounds (COVs) followed by gas-particle conversion processes such as nucleation and/or condensation, are defined as secondary OA (SOA) [2–5]. This latter fraction accounts for up to 80 to 90% of total OA under certain conditions [1, 6, 7] making its characterization and apportionment essential in terms of air quality or climate impacts.

Different methodologies have been developed and reported in the literature to apportion SOA (or secondary organic carbon, SOC) [7]. Several studies have identified key characteristic molecular compounds of the formation of SOA from specific precursors or sources and commonly defined as molecular SOA markers (or tracers if assuming that they are chemically stable) [7, 8] (Table 1). These compounds are used to apportion SOA in the so-called SOA tracer method [7, 9] or in source-receptor models, such as chemical mass balance (CMB) or positive matrix factorization (PMF) [7, 10–13]. The quantification of these SOA markers is critical because inaccurate values could lead to significant bias in the results obtained [7]. In most cases, no authentic standards are commercially available for these compounds and proxy compounds are generally used for their quantification. In addition, in terms of validation of analytical procedure, quality assurance, and control, the analysis of reference material is useful, but no SOA marker concentration values have been reported yet in any particulate matter reference material.

Thus, the objectives of this work were to evaluate the presence and to determine the concentration values of some typical molecular SOA markers in the commonly used National Institute of Standards and Technology's (NIST) urban dust standard reference material (NIST SRM 1649b). This material has been largely characterized in the past years [28–32], but to our knowledge, no concentration values for such compounds have been reported so far in the literature. Our objectives also included the comparison of the extraction efficiencies, for the analysis of molecular SOA markers in PM, of two different extraction procedures, namely, sonication and QuEChERS-like (Quick Easy Cheap Effective Rugged and Safe). Sonication is commonly used for the analysis of SOA marker compounds in aerosol samples [7–9, 16, 27, 33–40] while QuEChERS-like procedure has been developed and

successfully applied for the molecular chemical characterization of OA including polycyclic aromatic compounds (PAHs), nitro-PAHs, oxy-PAHs [31, 41–43], and also SOA markers [10, 11, 13, 44]. In addition, this latter technique should minimize the degradation of some fragile SOA marker and preserve the integrity of the sample as it is done at room temperature [31, 44]. Finally, three research laboratories/institutes (INERIS, NIST, and LSCE) using two extraction procedures and two analytical techniques (gas chromatography coupled to mass spectrometry (GC-MS) and high-pressure liquid chromatography/tandem mass spectrometry (HPLC/MS-MS)) performed the analysis of 12 key SOA markers in the SRM 1649b (Table 1, except 2-methylthreitol) and their results were compared.

Experimental

Chemical, gases, and solvents

Information about the chemicals, gases, and solvents used, their degrees of purity, and the supplier data are reported in the Electronic Supplementary Material (ESM). Pure and authentic SOA marker compounds (liquids or solids) were used in this study. They have been purchased or synthesized on purpose from/by different suppliers (ESM Table S1).

Standard reference material (SRM) 1649b (urban dust)

During the mid to late 1970s, NIST collected urban PM using a baghouse specially designed for the purpose from the Washington, DC, area. PM were collected over a period greater than 12 months and represents an atmospheric particulate matrix to validate analytical methods. SRM 1649b (urban

Table 1 Example of SOA markers identified in the literature and their precursors/sources

Organic markers	Predominant origin	Precursors/sources	References	
α -Methylglyceric acid	Biogenic	Isoprene	[14]	
2-Methylthreitol			[14, 15]	
2-Methylerythritol				
3-Methylbutane-1,2,3-tricarboxylic acid (MBTCA)	Anthropogenic	α -Pinene	[16, 17]	
3-Hydroxyglutaric acid			β -Pinene	[18]
Pinic acid			[17, 19–22]	
cis-Pinonic acid				
β -Caryophyllinic acid		β -Caryophyllene	[23]	
Succinic acid	Anthropogenic	Anthropogenic sources	[24]	
Phthalic acid			Naphthalene	[25]
2,3-Dihydroxy-4-oxopentanoic acid (DHOPA)			Toluene	[26]
4-Methyl-5-nitrocatechol			Phenolic compounds (biomass burning)	[27]
3-Methyl-5-nitrocatechol				

dust) has been prepared from the bulk material (SRM 1649) collected at this time but it has been sieved to a smaller particle size with a mean diameter of 105 μm [29].

For both extraction procedures tested, 5 to 13 (in total 5 for NIST, 10 for LSCE, and 23 for INERIS) samples of SRM 1649b of about 50 mg (balance precision = 0.01 mg) were analyzed. Triplicate analyses (3 injections of the sample extracts) were performed, except for 5 samples for each extraction procedure for INERIS, injected only once. Moisture content was determined using a Karl Fischer method (2.94% moisture, analyzer HR 73, Mettler Toledo). SOA marker concentrations were corrected and are reported here on dry-mass basis.

Extraction and derivatization procedures

SRM extraction was done by both sonication and QuEChERS-like procedures using methanol (MeOH) as solvent. SRM 1649b samples were placed in centrifuge glass tubes ($\varnothing = 16$ mm, $L = 100$ mm, screw cap with PTFE septum face; Duran), spiked with known amounts of 3 to 5 labeled surrogate standards (200 to 800 ng added, depending on the final volume of the extract after evaporation), and 7 mL of solvent was added for the extraction. Sonication was done for 15–20 min, while for QuEChERS-like extraction, the tubes were shaken by vortex mixing with a multiposition vortex mixer for 1.5 min (DVX-2500 Multi-Tube Vortexer; VWR). After extraction, samples were centrifuged at room temperature for 5 min at 4500 rpm or 30 min at 3800 rpm, for INERIS/LSCE and NIST, respectively (Sigma 3-16 PK and Beckman GS-6R centrifuge). For GC/MS analyses, supernatant extracts (4.5 or 5.5 ml) were collected and reduced to dryness under a gentle nitrogen stream to remove any trace of water or MeOH and avoid additional consumption of BSTFA or MSTFA. Extracts were dissolved into 50, 100, or 200 μL of acetonitrile and subjected to derivatization (silylation) for 30 min at 60 $^{\circ}\text{C}$ after addition of 50 or 100 μL of *N*-methyl-*N*-(trimethylsilyl)trifluoroacetamide (MSTFA) (INERIS) or 200 μL *N,O*-bis(trimethylsilyl)trifluoroacetamide (BSTFA) (NIST), both with 1% trimethylchlorosilane (TMCS) (ratio sample extract to derivatizing reagent of 1:1). For LC/MS-MS (LSCE) analyses, the supernatants were directly analyzed without any other sample preparation.

GC/MS analysis

The analysis of 11 to 12 SOA markers was achieved using GC/MS (Agilent 7890A GC coupled to 5975C MS at INERIS and Agilent 6890 GC coupled to 5973 MS at NIST) in electron ionization mode (EI, 70 eV). One or 2 μL of the extracts was injected in the splitless mode at 250 $^{\circ}\text{C}$ using, for INERIS, a programmed temperature vaporizer injector system (CIS-4 Gerstel, with a Restek Sky single baffle liner with wool, $3 \times$

2×71 mm, OD \times ID \times L), and for NIST, a splitless injector (with a Restek Sky low pressure drop precision inlet liner w/wool, $6.3 \times 4 \times 78.5$ mm). Compounds were separated using capillary columns with equivalent 5% phenylmethylpolysiloxane phase $60 \text{ m} \times 0.25 \text{ mm} \times 0.25 \mu\text{m}$ (Agilent J&W DB5-MS with 10 m guard column for INERIS or Restek Rtx-5MS for NIST), using the following temperature programs: INERIS—start at 70 $^{\circ}\text{C}$ for 1 min, then ramped to 260 $^{\circ}\text{C}$ at 5 $^{\circ}\text{C} \text{ min}^{-1}$, followed by a ramp to 290 $^{\circ}\text{C}$ at 20 $^{\circ}\text{C} \text{ min}^{-1}$, further followed by a ramp to 300 $^{\circ}\text{C}$ at 5 $^{\circ}\text{C} \text{ min}^{-1}$, then ramped at 10 $^{\circ}\text{C} \text{ min}^{-1}$ to 320 $^{\circ}\text{C}$ held for 10 min; NIST—start at 70 $^{\circ}\text{C}$ for 1 min, increased at a rate of 5 $^{\circ}\text{C} \text{ min}^{-1}$ to 300 $^{\circ}\text{C}$ held for 1 min. The carrier gas (He) flow was set to 1.2 (NIST) or 1.5 (INERIS) $\text{mL} \text{ min}^{-1}$ throughout the analysis and transfer line heated at 310 $^{\circ}\text{C}$. The ion source and quadrupole temperatures were 230 and 150 $^{\circ}\text{C}$, respectively.

Analyses were performed in selected ion monitoring mode (SIM). Autotune parameters were adopted for the electron multiplier conditions with a gain factor of 10. Monitored ions and dwell times are shown in Table 2. The quantification of the SOA markers was based on 8 to 10-points calibration curves (gravimetrically diluted stock standard solutions (prepared in acetonitrile (ACN) or MeOH) from 5 (or 20) to 5000 $\text{pg} \mu\text{L}^{-1}$ in MeOH; $0.99 > r^2 > 0.90$ for all compounds). All SOA marker compounds were quantified using authentic standards and labeled surrogate standards by internal calibration except for both methylnitrocatechols. Preliminary recovery tests performed on pre-cleaned SRM 1619a powder (twice, with DCM using pressurized liquid extraction and MeOH using sonication) spiked with known amount (500 ng) of SOA marker compounds showed significant differences in the results between internal and external calibration for the quantification of these compounds highlighting that the initial deuterated surrogate used (4-methylcatechol- d_3) to quantify them was not suitable for the GC/MS analyses (ESM Fig. S1). As no labeled methylnitrocatechol standards exist, both compounds were finally quantified by external calibration. In addition, the extraction recoveries obtained for DHOPA and 2-methylerythritol were quite low. The solvent of extraction used (MeOH) was probably not the best for the specific extraction of these compounds. However, it was the best compromise for the analysis of all the SOA markers targeted in this work. The labeled surrogates used (no labeled DHOPA and 2-methylerythritol are commercially available) to quantify these both compounds were not able to fully correct the sample preparation losses, but at least, they did not induce any analytical drift like in the case of methylnitrocatechols.

Using these conditions, the instrumental limits of quantification (LOQ), defined as the lowest concentration of the compound than can be determined with a signal to noise ratio of 10 (calculated using the chromatograms obtained from the calibration solution with the lowest concentration level), were within the range 0.6–14.3 pg injected.

Table 2 GC/MS conditions used for SOA marker analysis and typical instrumental limits of quantification (LOQ)

Compounds	Monitored ions (m/z)	Retention times ^d (min)	Dwell times (s)	LOQ (pg injected)
Succinic acid-2,3,3,3-d ₄	147, 251	19.54	<i>0.06/0.035</i>	–
Succinic acid ^a	129 , 247	19.61	0.035	1.0–1.3
α-Methylglyceric acid	219 , 306	19.74	<i>0.06/0.035</i>	1.0–2.3
2,3-Dihydroxy-4-oxopentanoic acid (DHOPA)	218 , 189, 350	24.71	<i>0.04/0.05</i>	3.7–11.0
cis-Pinonic acid	171 , 125	25.27	<i>0.04/0.05</i>	2.2–7.5
3-Hydroxyglutaric acid	185, 349	26.26	<i>0.08/0.05</i>	1.3–7.0
Pinic acid	129 , 171	28.50	<i>0.05/0.05</i>	6.3–7.6
Phthalic acid ^b	221, 295	29.04	<i>0.05/0.05</i>	0.9–8.4
Meso-erythritol-1,1,2,4,4-d ₆	208 , 220	24.50	<i>0.04/0.1</i>	–
2-Methylerythritol	116, 117, 219	25.74	<i>0.05/0.05</i>	1.1–4.2
1,9-Nonanedioic acid-d ₁₄	213, 331	31.10	<i>0.06/0.035</i>	–
3-Methylbutane-1,2,3-tricarboxylic acid (MBTCA)	204 , 245, 405	30.34	<i>0.08/0.05</i>	0.6–14.5
β-Caryophyllinic acid	117 , 200	36.08	<i>0.08/0.05</i>	8.9–14.3
4-Methyl-5-nitrocatechol ^f	296, 313	31.06	<i>0.06/0.035</i>	1.5–10.3
3-Methyl-5-nitrocatechol ^f	298 , 313	32.28	<i>0.10/0.10</i>	1.4–6.1

^a Not analyzed by NIST^b For NIST, quantified using 1,9-nonanedioic acid-d₁₄ as surrogate^c Quantified by external calibration^d For INERIS method

NIST parameters are italicized and quantification ions are in bold

The list of all SOA markers quantified, labeled surrogates used, retention times, monitored ions, and limits of quantification is given in Table 2 for both NIST and INERIS GC/MS analytical procedures.

HPLC/MS-MS analysis

The quantification of SOA markers was achieved by HPLC/MS-MS (HPLC Dionex U3000 coupled to a triple quadrupole MS AB Sciex 3200 QTRAP). Two different columns, Thermo porous graphic carbon (PGC) Hypercarb column (2.1 mm × 150 mm × 3 μm) and Waters Acquity C18 HSST3 column (2.1 mm × 100 mm × 1.8 μm), were employed for the chromatographic separation. For the HSST3 column, the mobile phases consisted of a 0.1% formic acid in Milli-Q water (A) and ACN (B). The following program was applied during the LC analysis: start with eluent B at 5% with a gradient to 60% in 10 min followed by a second one to 100% in 2 min kept at 100% for 4 min, decreased back to 5% in 1 min, and conditioned at 5% for 10 min for the following analysis. For the Hypercarb column, the mobile phases consisted of a 0.1% NH₃ in Milli-Q water (A) and ACN (B). The elution program used was the following: start with eluent B at 4% kept for 2.5 min followed by a with a gradient to 100% in 9.5 min kept at 100% for 4 min, decreased back to 4% in

1 min kept for 5 min for conditioning the following analysis. Samples were injected with an injection volume of 10 μL and the analysis was carried out using a flow rate of 0.2 (Hypercarb) and 0.3 (HSST3) mL min⁻¹, respectively.

The targeted compounds were ionized using electrospray ionization in the negative mode. The mass spectrometer, with unit mass resolution, was operated under the following conditions: source voltage at -4.5 kV, desolvation temperature at 650 °C, desolvation gas pressure (air) of 60 psi, nebulizer gas pressure (air) of 40 psi, collisional-activated dissociation (CAD) set on medium with nitrogen used as collision gas, compound-selective scheduled multiple reaction monitoring (MRM) mode with 40 or 140 s detection windows (HSST3 and Hypercarb, respectively), target scan time of 0.5 s, and MR pause of 5 ms.

The quantification of the compounds was based on 6-points calibration curves from 1 to 32 pg μl⁻¹ in MeOH (0.99 > r² > 0.90 for all compounds). Again, all SOA marker compounds were quantified by internal calibration, using authentic standards and labeled surrogate standards, except for 2-methylerythritol which was quantified by external calibration cause, using this method, the labeled meso-erythritol-1,1,2,4,4-d₆ surrogate standard was not well detected. Using these parameters, the instrumental LOQ were within the range 20–40 pg injected.

The compounds quantified, labeled surrogates used, retention times, parameters for each MRM transition, and limits of quantification are given in Table 3 for the HPLC/MS-MS analytical procedure.

Results and discussion

QuEChERS-like extraction vs sonication and GC/MS vs HPLC/MS-MS

The comparison of the results obtained according to the different extraction procedures and analytical techniques used is shown in Fig. 1 (see ESM Table S2 for details). Results are also presented by laboratories/institutes.

Overall, whatever the analytical protocol used, all the results were in quite good agreement, except for 2-methylerythritol, and to a lesser extent MBTCA and 3-hydroxyglutaric acid, which showed large discrepancies. First, this study highlighted that the SRM 1649b contains quantifiable and quite homogeneous amounts of SOA markers. Note that β -caryophyllinic acid has been reported by NIST as below LOQ (ESM Table S2). This SOA marker is usually observed at low concentration levels in

urban atmosphere [7, 10, 11, 36, 45]. Second, these results also showed that the extraction efficiencies of sonication and QuEChERS-like were similar demonstrating the validity of the QuEChERS-like extraction procedure for the analysis of SOA markers in PM. Except 2-methylerythritol, the results obtained showed also a good agreement between both analytical techniques used, GC/MS and HPLC/MS-MS. The differences observed were mainly due the discrepancies obtained between INERIS and NIST, both using GC/MS. In that case, it would be difficult to conclude on any influence of the derivatizing agent used (BSTFA and MSTFA). Finally, further tests showed that both 2-methyltetrol isomers, namely 2-methylthreitol and 2-methylerythritol, were not separated with the column and elution program used here for the analyses performed by HPLC/MS-MS (the exact same transitions were also observed). Thus, the concentration values reported in Fig. 1 for HPLC/MS-MS are the sum of both compounds. Based on the literature data about these compounds, 2-methylerythritol accounts generally for about 2/3 of the sum of 2-methyltetrols [9, 35–37, 39, 45–49]. However, this only explained in part the differences observed. In addition, the difference in the results reported by NIST and INERIS were still significant. The analysis of 2-methyltetrols seems still challenging and the results obtained here may also

Table 3 HPLC/MS-MS conditions used for SOA marker analysis and instrumental limits of quantification (LOQ)

Compounds	Transitions (m/z)	DP ^c	EP ^d	CEP ^e	CE ^f	CXP ^g	Retention time (min)	Column	LOQ (pg injected)
Succinic acid-2,3,3,3-d ₄	121 → 77	30	4	10	16	0	1.73	Hypercarb	–
3-Methylbutane-1,2,3-tricarboxylic acid (MBTCA)	203 → 185	30	5.5	12	16	4	1.61	Hypercarb	10
Succinic acid	117 → 73	25	8	10	14	0	1.82	Hypercarb	40
α -Methylglyceric acid	119 → 73	35	2	36	16	0	1.92	Hypercarb	40
2,3-Dihydroxy-4-oxopentanoic acid (DHOPA)	147 → 73	15	5	10	18	0	2.16	Hypercarb	10
3-Hydroxyglutaric acid ^a	–	–	–	–	–	–	–	–	–
Phthalic-3,4,5,6-d ₄ acid	169 → 125	25	2.5	12	14	0	1.78	Hypercarb	–
Phthalic acid	165 → 121	30	5	12	12	0	2.27	Hypercarb	20
1,9-Nonanedioic acid-d ₁₄	201 → 138	35	9.5	30	18	2	2.29	HSS T3	–
Pinic acid	185 → 141	35	9	12	18	0	5.97	HSS T3	40
cis-Pinonic acid	183 → 141	30	11.5	12	16	0	7.45	HSS T3	40
β -Caryophyllinic acid	253 → 209	40	6	10	14	2	10.64	HSS T3	40
4-Methylcatechol-d ₃	126 → 108	60	3	10	22	0	6.65	HSS T3	–
4-Methyl-5-nitrocatechol ^c	168 → 138	35	9	12	14	2	7.83	HSS T3	10
3-Methyl-5-nitrocatechol ^c	168 → 138	45	5.5	12	22	2	8.66	HSS T3	10
2-Methylerythritol ^b	135 → 85	30	10.5	12	22	0	2.64	Hypercarb	40

^a Not analyzed by HPLC/MS-MS

^b Quantified by external calibration

^c Declustering potential (V)

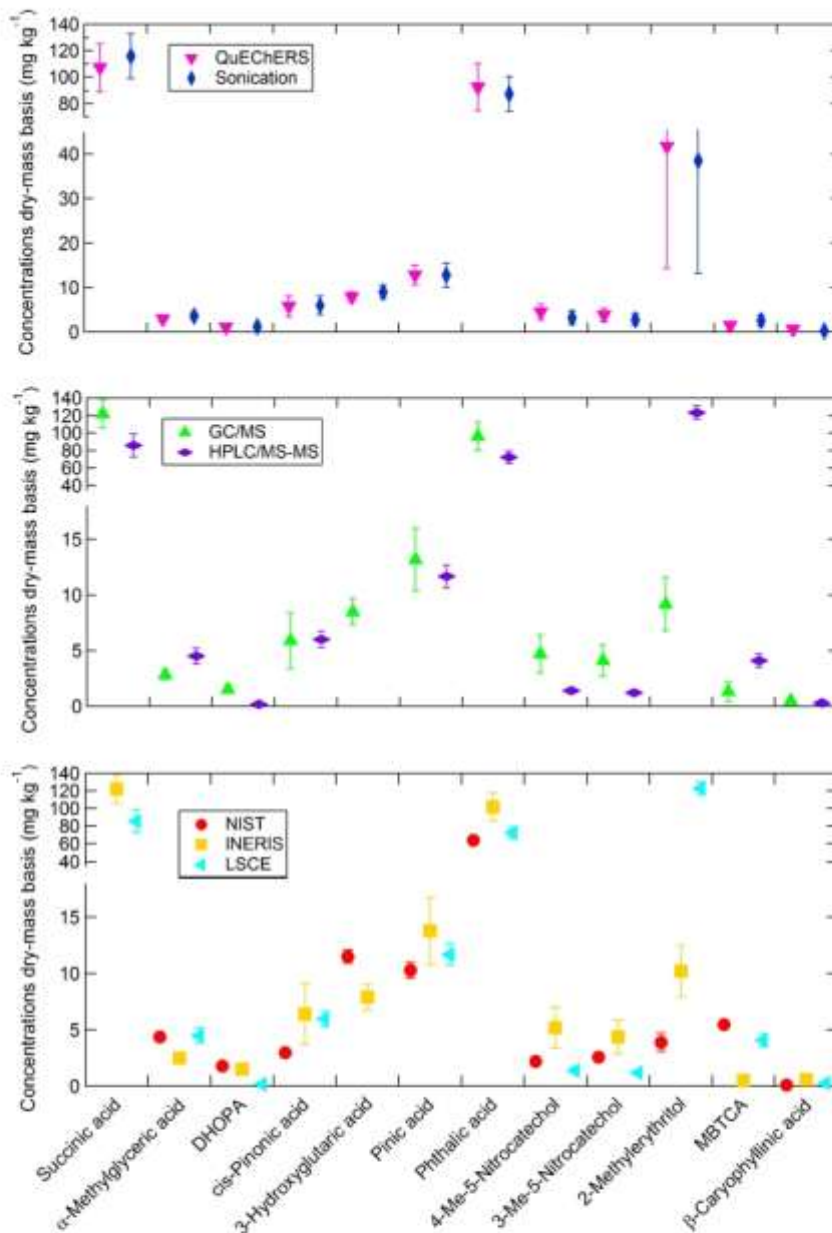
^d Entrance potential (V)

^e Collision cell entrance potential (V)

^f Collision energy (eV)

^g Collision cell exit potential (V)

Fig. 1 Comparison of the average SOA marker concentrations (mg kg^{-1}) (dry mass basis) in the SRM 1649b (urban dust) obtained according to the extraction procedure used (sonication or QuEChERS-like extraction), analytical method (GC/MS or HPLC/MS-MS), and by institution (INERIS, NIST, and LSCE). $n = 18$ to 20 for the extraction procedures, 10 to 28 for the analytical methods, and 5 to 23 for the laboratories/institutes. Sample extracts were 3 times injected and 50 mg of SRM was used. The error bars correspond to the standard deviation ($\pm 1 \sigma$) for the total number of analyses performed



indicate that the homogeneity in the SRM 1649b for this compound is not optimal. Further tests must be done to support our observations.

SOA marker concentrations in SRM 1649b (urban dust)

The final SOA marker concentration values determined in this study are presented on Table 4. A total of 28 to 38 full replicates (extraction + analysis, triplicate injections), depending on the compound considered, has been considered. Note that the concentrations of 2-methylethritol obtained by HPLC/MS-MS have been corrected by a factor 2/3 to consider that the sum of 2-methyltetrols was quantified in this case. The value reported here for this compound is given only for information.

Large standard deviations were obtained for some compounds such as DHOPA, pinonic acid, methylnitrocatechols, MBTCA, and 2-methylethritol with coefficients of variation (standard deviation/mean value, CV) larger than 70%. A detailed study of the different analytical steps showed that the injection repeatability (CV ranging from 2 to 15%) accounted for a low part in the variations observed (ESM Table S3). Only DHOPA for LSCE (37%) and 2-methylethritol (111%) for NIST showed large injection repeatability variations. This latter result highlighted again the challenge in the analysis of 2-methylethritol. Finally, the large standard deviations obtained for these SOA markers were due to the different analytical procedures used and the influence of the experimenter/laboratory/institute (variations in terms of reproducibility).

Table 4 SOA marker concentrations (mg kg^{-1}) (dry mass basis) in SRM 1649b (urban dust)

Compound	Mean ^a	Standard deviation ^a
Succinic acid	111.0	35.0
α -Methylglyceric acid	3.3	1.3
DHOPA	1.2	0.8
cis-Pinonic acid	5.9	4.4
3-Hydroxyglutaric acid	8.5	2.5
Pinic acid	12.8	4.9
Phthalic acid	89.7	30.7
4-Methyl-5-nitrocatechol	3.8	3.3
3-Methyl-5-nitrocatechol	3.3	2.7
2-Methylerythritol ^b	28.9	33.5
MBTCA	2.1	2.1
β -Caryophyllinic acid	0.4	0.3

^a $n = 28$ to 38 full replicates (extraction and analysis, triplicate injections). Mean values and standard deviations calculated considering all the results obtained

^b HPLC/MS-MS results were corrected by a factor 2/3 to consider that the sum of 2-methyltetrols was quantified in this case

Conclusions

The analysis of molecular SOA markers (tracers) is useful to apportion SOA mass in the atmosphere. The different SOA markers studied here were all present in the NIST SRM 1649b (urban dust). Sonication and QuEChERS-like procedures gave comparable results for the extraction of the SOA markers. As this study provides the first indicative values in a reference material for typical SOA markers, the analysis of SRM 1649b (urban dust) should be used for quality control/assurance purposes when such compounds are used to apportion the SOA fraction in ambient air.

Acknowledgements The authors wish to thank the French Ministry of Environment for their financial support. They also thank Siham Ayachi, Xavier Pollion (LSCÉ), and Jérôme Beaumont (INERIS), for their technical assistance and the chemical analyses performed.

Compliance with ethical standards

Conflict of interest S. Wise and F. Nalin worked at the NIST which also provides the standard reference materials (SRM). The other authors declare that they have no conflict of interest.

References

- Zhang Q, Jimenez JL, Canagaratna MR, Allan JD, Coe H, Ulbrich I, et al. Ubiquity and dominance of oxygenated species in organic aerosols in anthropogenically-influenced Northern Hemisphere midlatitudes. *Geophys Res Lett*. 2007;34(13):L13801.
- Ziemann PJ, Atkinson R. Kinetics, products, and mechanisms of secondary organic aerosol formation. *Chem Soc Rev*. 2013;41(19):6582–605.
- Carlton AG, Wiedinmyer C, Kroll JH. A review of Secondary Organic Aerosol (SOA) formation from isoprene. *Atmos Chem Phys*. 2009;9(14):4987–5005.
- Hallquist M, Wenger JC, Baltensperger U, Rudich Y, Simpson D, Claeys M, et al. The formation, properties and impact of secondary organic aerosol: current and emerging issues. *Atmos Chem Phys*. 2009;9(14):5155–236.
- Kroll JH, Seinfeld JH. Chemistry of secondary organic aerosol: formation and evolution of low-volatility organics in the atmosphere. *Atmos Environ*. 2008;42(16):3593–624.
- Zhang Q, Jimenez JL, Canagaratna MR, Ulbrich IM, Ng NL, Worsnop DR, et al. Understanding atmospheric organic aerosols via factor analysis of aerosol mass spectrometry: a review. *Anal Bioanal Chem*. 2011;401(10):3045–67.
- Srivastava D, Favez O, Perraudin E, Villenave E, Albinet A. Comparison of measurement-based methodologies to apportion secondary organic carbon (SOC) in PM_{2.5}: a review of recent studies. *Atmosphere*. 2018;9(11):452.
- Nozière B, Kalberer M, Claeys M, Allan J, D'Anna B, Decesari S, et al. The molecular identification of organic compounds in the atmosphere: state of the art and challenges. *Chem Rev*. 2015;115(10):3919–83.
- Kleindienst TE, Jaoui M, Lewandowski M, Offenberg JH, Lewis CW, Bhawe PV, et al. Estimates of the contributions of biogenic and anthropogenic hydrocarbons to secondary organic aerosol at a southeastern US location. *Atmos Environ*. 2007;41(37):8288–300.
- Srivastava D, Favez O, Bonnaire N, Lucarelli F, Haeffelin M, Perraudin E, et al. Speciation of organic fractions does matter for aerosol source apportionment. Part 2: intensive short-term campaign in the Paris area (France). *Sci Total Environ*. 2018;634:267–78.
- Srivastava D, Tomaz S, Favez O, Lanzafame GM, Golly B, Besombes J-L, et al. Speciation of organic fraction does matter for source apportionment. Part 1: a one-year campaign in Grenoble (France). *Sci Total Environ*. 2018;624:1598–611.
- Al-Naiema IM, Hettiyadura APS, Wallace HW, Sanchez NP, Madler CJ, Cevik BK, et al. Source apportionment of fine particulate matter in Houston, Texas: insights to secondary organic aerosols. *Atmos Chem Phys*. 2018;18(21):15601–22.
- Srivastava D, Favez O, Petit J-E, Zhang Y, Sofowote UM, Hopke PK, et al. Speciation of organic fractions does matter for aerosol source apportionment. Part 3: combining off-line and on-line measurements. *Sci Total Environ*. 2019. <https://doi.org/10.1016/j.scitotenv.2019.06.378>.
- Edney EO, Kleindienst TE, Jaoui M, Lewandowski M, Offenberg JH, Wang W, et al. Formation of 2-methyl tetrols and 2-methylglyceric acid in secondary organic aerosol from laboratory irradiated isoprene/NO_x/SO₂/air mixtures and their detection in ambient PM_{2.5} samples collected in the eastern United States. *Atmos Environ*. 2005;39(29):5281–9.
- Claeys M, Graham B, Vas G, Wang W, Vermeylen R, Pashynska V, et al. Formation of secondary organic aerosols through photooxidation of isoprene. *Science*. 2004;303(5661):1173.
- Szmigielski R, Surratt JD, Gómez-González Y, Van der Veken P, Kourchev I, Vermeylen R, et al. 3-methyl-1,2,3-butanetricarboxylic acid: an atmospheric tracer for terpene secondary organic aerosol. *Geophys Res Lett*. 2007;34(24):L24811.
- Mutzel A, Rodigast M, Iinuma Y, Böge O, Herrmann H. Monoterpene SOA – contribution of first-generation oxidation products to formation and chemical composition. *Atmos Environ*. 2016;130:136–44.
- Claeys M, Szmigielski R, Kourchev I, Van der Veken P, Vermeylen R, Maenhaut W, et al. Hydroxycarboxylic acids: markers for

- secondary organic aerosol from the photooxidation of α -pinene. *Environ Sci Technol*. 2007;41(5):1628–34.
19. Yu J, Cocker DR, Griffin RJ, Flagan RC, Seinfeld JH. Gas-phase ozone oxidation of monoterpenes: gaseous and particulate products. *J Atmos Chem*. 1999;34(2):207–58.
 20. Glasius M, Lahmiani M, Calogirou A, Di Bella D, Jensen NR, Hjorth J, et al. Carboxylic acids in secondary aerosols from oxidation of cyclic monoterpenes by ozone. *Environ Sci Technol*. 2000;34(6):1001–10.
 21. Jang M, Kamens RM. Newly characterized products and composition of secondary aerosols from the reaction of α -pinene with ozone. *Atmos Environ*. 1999;33(3):459–74.
 22. Christoffersen TS, Hjorth J, Horie O, Jensen NR, Kotzias D, Molander LL, et al. *cis*-Pinic acid, a possible precursor for organic aerosol formation from ozonolysis of α -pinene. *Atmos Environ*. 1998;32(10):1657–61.
 23. Jaoui M, Lewandowski M, Kleindienst TE, Offenberg JH, Edney EO. β -Caryophyllinic acid: an atmospheric tracer for β -caryophyllene secondary organic aerosol. *Geophys Res Lett*. 2007;34(5):L05816.
 24. Kawamura K, Bikkina S. A review of dicarboxylic acids and related compounds in atmospheric aerosols: molecular distributions, sources and transformation. *Atmos Res*. 2016;170:140–60.
 25. Kleindienst TE, Jaoui M, Lewandowski M, Offenberg JH, Docherty KS. The formation of SOA and chemical tracer compounds from the photooxidation of naphthalene and its methyl analogs in the presence and absence of nitrogen oxides. *Atmos Chem Phys*. 2012;12(18):8711–26.
 26. Kleindienst TE, Conner TS, Melver CD, Edney EO. Determination of secondary organic aerosol products from the photooxidation of toluene and their implications in ambient PM_{2.5}. *J Atmos Chem*. 2004;47(1):79–100.
 27. Inuma Y, Böge O, Gräfe R, Herrmann H. Methyl-nitrocatechols: atmospheric tracer compounds for biomass burning secondary organic aerosols. *Environ Sci Technol*. 2010;44(22):8453–9.
 28. Wise S, Poster D, Kucklick J, Keller J, VanderPol S, Sander L, et al. Standard reference materials (SRMs) for determination of organic contaminants in environmental samples. *Anal Bioanal Chem*. 2006;386(4):1153–90.
 29. NIST. Standard reference material 1649b, urban dust. Gaithersburg: National Institute of Standards and Technology; 2015.
 30. Albinet A, Leoz-Garziandia E, Budzinski H, Villenave E. Simultaneous analysis of oxygenated and nitrated polycyclic aromatic hydrocarbons on standard reference material 1649a (urban dust) and on natural ambient air samples by gas chromatography-mass spectrometry with negative ion chemical ionisation. *J Chromatogr A*. 2006;1121(1):106–13.
 31. Albinet A, Nalin F, Tomaz S, Beaumont J, Lestremieu F. A simple QuEChERS-like extraction approach for molecular chemical characterization of organic aerosols: application to nitrated and oxygenated PAH derivatives (NPAH and OPAH) quantified by GC-NICIMS. *Anal Bioanal Chem*. 2014;406(13):3131–48.
 32. Larsen RK, Schantz MM, Wise SA. Determination of Levoglucosan in particulate matter reference materials. *Aerosol Sci Technol*. 2006;40(10):781–7.
 33. Kitanovski Z, Grgić I, Vermeylen R, Claeys M, Maenhaut W. Liquid chromatography tandem mass spectrometry method for characterization of monoaromatic nitro-compounds in atmospheric particulate matter. *J Chromatogr A*. 2012;1268:35–43.
 34. Kitanovski Z, Grgić I, Yasmeen F, Claeys M, Čusak A. Development of a liquid chromatographic method based on ultraviolet-visible and electrospray ionization mass spectrometric detection for the identification of nitrocatechols and related tracers in biomass burning atmospheric organic aerosol. *Rapid Commun Mass Spectrom*. 2012;26(7):793–804.
 35. Clements AL, Seinfeld JH. Detection and quantification of 2-methyltetrols in ambient aerosol in the southeastern United States. *Atmos Environ*. 2007;41(9):1825–30.
 36. Fu P, Aggarwal SG, Chen J, Li J, Sun Y, Wang Z, et al. Molecular markers of secondary organic aerosol in Mumbai, India. *Environ Sci Technol*. 2016;50(9):4659–67.
 37. Hu D, Bian Q, Li TWY, Lau AKH, Yu JZ. Contributions of isoprene, monoterpenes, β -caryophyllene, and toluene to secondary organic aerosols in Hong Kong during the summer of 2006. *J Geophys Res Atmos*. 2008;113(D22):D22206.
 38. Rutter AP, Snyder DC, Stone EA, Shelton B, DeMinter J, Schauer JJ. Preliminary assessment of the anthropogenic and biogenic contributions to secondary organic aerosols at two industrial cities in the upper Midwest. *Atmos Environ*. 2014;84:307–13.
 39. Kourtchev I, Ruuskanen TM, Keronen P, Sogacheva L, Dal Maso M, Reissell A, et al. Determination of isoprene and α - β -pinene oxidation products in boreal forest aerosols from Hyytiälä, Finland: diel variations and possible link with particle formation events. *Plant Biol*. 2008;10(1):138–49.
 40. Gao S, Surratt JD, Knipping EM, Edgerton ES, Shahgholi M, Seinfeld JH. Characterization of polar organic components in fine aerosols in the southeastern United States: identity, origin, and evolution. *J Geophys Res Atmos*. 2006;111:D14.
 41. Albinet A, Tomaz S, Lestremieu F. A really quick easy cheap effective rugged and safe (QuEChERS) extraction procedure for the analysis of particle-bound PAHs in ambient air and emission samples. *Sci Total Environ*. 2013;450-451(0):31–8.
 42. Tomaz S, Jaffrezo J-L, Favez O, Perraudin E, Villenave E, Albinet A. Sources and atmospheric chemistry of oxy- and nitro-PAHs in the ambient air of Grenoble (France). *Atmos Environ*. 2017;161:144–54.
 43. Tomaz S, Shahpoury P, Jaffrezo J-L, Lammel G, Perraudin E, Villenave E, et al. One-year study of polycyclic aromatic compounds at an urban site in Grenoble (France): seasonal variations, gas/particle partitioning and cancer risk estimation. *Sci Total Environ*. 2016;565:1071–83.
 44. Mutzel A, Rodigast M, Inuma Y, Böge O, Herrmann H. An improved method for the quantification of SOA bound peroxides. *Atmos Environ*. 2013;67:365–9.
 45. Kleindienst TE, Lewandowski M, Offenberg JH, Edney EO, Jaoui M, Zheng M, et al. Contribution of primary and secondary sources to organic aerosol and PM_{2.5} at SEARCH network sites. *J Air Waste Manage Assoc*. 2010;60(11):1388–99.
 46. Kourtchev I, Ruuskanen T, Maenhaut W, Kulmala M, Claeys M. Observation of 2-methyltetrols and related photo-oxidation products of isoprene in boreal forest aerosols from Hyytiälä, Finland. *Atmos Chem Phys*. 2005;5(10):2761–70.
 47. Alier M, van Drooge BL, Dall'Osto M, Querol X, Grimalt JO, Tauler R. Source apportionment of submicron organic aerosol at an urban background and a road site in Barcelona (Spain) during SAPUSS. *Atmos Chem Phys*. 2013;13(20):10353–71.
 48. Yuan Q, Lai S, Song J, Ding X, Zheng L, Wang X, et al. Seasonal cycles of secondary organic aerosol tracers in rural Guangzhou, Southern China: the importance of atmospheric oxidants. *Environ Pollut*. 2018;240:884–93.
 49. Ion AC, Vermeylen R, Kourtchev I, Cafmeyer J, Chi X, Gelencsér A, et al. Polar organic compounds in rural PM_{2.5} aerosols from Kpuszta, Hungary, during a 2003 summer field campaign: sources and diel variations. *Atmos Chem Phys*. 2005;5(7):1805–14.

Publisher's note Springer Nature remains neutral with regard to jurisdictional claims in published maps and institutional affiliations.



Alexandre Albinet is a scientist in air quality at the French National Institute for Industrial Environment and Risks (INERIS) and the National Reference Laboratory of Air Quality Monitoring (LCSQA). He has been working for several years on the atmospheric chemistry field of research. His current work is focused on the study and the understanding of aerosol sources, (photo-)chemical processes, and fate together with their physicochemical characterization, toxicity, and impacts on health and climate.



Nicolas Bonnaire is an engineer in analytical chemistry applied to atmospheric chemistry (aerosol and gas) at the French National Centre for Scientific Research (CNRS), Laboratory for Sciences of Climate and Environment (LSCE). He is also a part-time lecturer in analytical chemistry at the Institute of Technology of University Paris-Sud 11.



Grazia Maria Lanzafame is a PhD candidate at the French National Institute for Industrial Environment and Risks (INERIS) and at Pierre and Marie Curie University (UPMC) in Paris (France). Her current work is about the measurement and modeling of organic aerosols, with a focus on secondary molecular markers.



Frederica Nalin is an analytical chemist with a clinical and environmental background. She worked at the French National Institute for Industrial Environment and Risks (INERIS) and at the National Institute of Standards and Technology (NIST, USA) where she developed and validated new analytical protocols for the determination of atmospheric organic compounds and she assisted in important measurements of clinically relevant analytes in human bio-fluid matrices, particularly vitamin D

metabolites in human serum.



Deepchandra Srivastava is working as a postdoctoral scholar in the Department of Environmental Toxicology at University of California, Davis (USA). Her current research work involves the chemical and physical characterization of biomass burning particles using soot particle aerosol mass spectrometry. She has been working on ambient aerosol for several years, and notably at the French National Institute for Industrial Environment and Risks (INERIS) to understand aerosol

fate and involved physicochemical processes, and source origins, which includes the use of different source apportionment methodologies.



Stephen Wise is Scientist Emeritus at the National Institute of Standards and Technology (NIST, USA) where he worked in the development of Standard Reference Materials (SRMs) for trace organic constituents in environmental, clinical, food, and dietary supplements. He is currently a scientific consultant in the Office of Dietary Supplements at the National Institutes of Health (NIH-ODS, USA) where he provides support for the Analytical Methods and Reference Materials Program.

Annex D

- Study upon γ cyclodextrine conjugates as carriers for anticancer drugs: synthesis and separation by column chromatography, NMR Analysis.
- Synthesis and functionalization of gold nanoparticles.

Education and Qualifications

2017	NCAS Climate Modelling Summer School, Cambridge (UK)
2016	Chimere Training Course, LMD, Paris
2015	Master's Degree in Environmental Chemistry - University of Turin (Italy)
2013	Bachelor's Degree in Chemistry - University of Catania (Italy)
2008	Graduated in Scientific Studies - High School "Principe Umberto Di Savoia" of Catania (Italy)

Publications

Lanzafame, G.M., Sarakha, M., Fabbri, D. and Vione, D.: Degradation of Methyl 2-Aminobenzoate (Methyl Anthranilate) by H₂O₂/UV: Effect of Inorganic Anions and Derived Radicals, *Molecules*, 22(4), 619, doi:10.3390/molecules22040619, 2017.

Srivastava, D., Tomaz, S., Favez, O., Lanzafame, G. M., Golly, B., Besombes, J.-L., Alleman, L. Y., Jaffrezo, J.-L., Jacob, V., Perraudin, E., Villenave, E. and Albinet, A.: Speciation of organic fraction does matter for source apportionment. Part 1: A one-year campaign in Grenoble (France), *Sci. Total Environ.*, 624, 1598–1611, doi:10.1016/j.scitotenv.2017.12.135, 2018.

Majdi, M., Sartelet, K., Lanzafame, G. M., Couvidat, F., Kim, Y., Chrit, M. and Turquety, S.: Precursors and formation of secondary organic aerosols from wildfires in the Euro-Mediterranean region, *Atmospheric Chem. Phys.*, 19(8), 5543–5569, doi:<https://doi.org/10.5194/acp-19-5543-2019>, 2019.

Lanzafame, G. M., Srivastava, D., Favez, O., Bonnaire, N., Gros, V., Alleman, L. Y., Couvidat, F., Bessagnet, B. and Albinet, A.: One-year measurements of secondary organic aerosol (SOA) markers in the Paris region: concentrations, seasonality, gas/particle partitioning and use in OA source apportionment, *Sci. Total Environ.*, In prep.

Lanzafame, G. M., Couvidat, F., Favez, O., Albinet, A. and Bessagnet, B.: Modelling organic aerosol markers in 3D air quality model. Part 1: Anthropogenic organic markers., *Atmospheric Chem. Phys.*, In prep.

Lanzafame, G. M., Couvidat, F., Favez, O., Albinet, A. and Bessagnet, B.: Modelling organic aerosol markers in 3D air quality model. Part 2: Biogenic secondary organic markers., *Atmospheric Chem. Phys.*, In prep.

Communications

Lanzafame G.M., Srivastava D., Couvidat F., Favez O., Bessagnet B. and Albinet A. "Benefits of cross modelling and field measurement approaches on the evaluation of SOA distribution: a case study in Grenoble, France" at the European Aerosol Conference (EAC) 2016, Tours, France (poster).

Lanzafame G.M., Srivastava D., Bonnaire N., Couvidat F., Favez O., Bessagnet B. and Albinet A. "Modelling of SOA markers: simulation through detailed mechanisms and validation by comparison with measurements. A new approach to understand SOA formation" at EAC 2017, Zurich, Swizerland (oral).

Lanzafame G.M., Srivastava D., Bonnaire N., Couvidat F., Favez O., Bessagnet B. and Albinet A. "Modelling of SOA markers: simulation through detailed mechanisms and validation by comparison with measurements. A new approach to understand SOA formation" at AAAR 2017, Raleigh, USA (oral).

Lanzafame G.M., Srivastava D., Bonnaire N., Couvidat F., Favez O., Bessagnet B. and Albinet A. "One-year comparison of SOA markers modelling and measurements: seasonality and gas/particle partitioning evaluation" at IAC 2018, Saint Louis, USA (oral).

Abstract

Organic aerosols (OA) account for a large fraction of ambient air particulate matter and have strong impacts on air quality and climate. As their sources and atmospheric formation processes, notably for secondary OA (SOA), are still not fully understood, their concentrations are often underestimated by air quality models. This work aimed at improving OA modelling by implementing specific organic molecular marker emissions and formation processes into the chemistry-transport model CHIMERE. It was based on the comparison of model outputs with measurements from field studies performed in the Paris region (suburban site of SIRTA, 25 km SW of Paris) over 2015 and 10 French urban locations in winter 2014-2015. 25 biogenic and anthropogenic SOA markers have been quantified in both, particulate and gas phases and the formation pathways of 10 have been developed and simulated using CHIMERE. The evolution of levoglucosan concentrations (biomass burning marker) has been also modeled. The results obtained showed that sources and precursor emissions (missing or underestimated), radical concentrations (NO, HO₂ and RO₂) and the lack of formation pathways, are key parameters for the simulation of SOA markers. Gas/particle partitioning seemed poorly linked to the T°C while the inclusion of hydrophilic non-ideal partitioning, usually neglected, seemed essential. Levoglucosan was well simulated, even if some underestimations existed in some regions. A significant theoretical gaseous fraction was also highlighted. The model/measurements comparison of molecular markers is a powerful tool to evaluate precursor emissions, physicochemical processes and in the end, to estimate OA sources.

Keywords: [Air quality; Particulate matter; Organic aerosol; Markers; Modelling; Chemical processes]

Résumé

L'aérosol organique (AO) constitue une large fraction des particules de l'air ambiant qui ont des impacts majeurs sur la qualité de l'air et le climat. Ses sources et processus de formation, surtout pour l'AO secondaire (AOS), sont encore méconnus induisant sa sous-estimation par les modèles de qualité de l'air. Ce travail a pour objectif d'améliorer la modélisation de l'AO en implémentant des émissions et processus de formation de marqueurs moléculaires organiques dans le modèle de chimie-transport CHIMERE. Il est basé sur la comparaison entre des sorties de modèle et de mesures réalisées en région parisienne (site périurbain du SIRTA, 25 km SO de Paris) en 2015 et sur 10 sites urbains en hiver 2014-2015. 25 marqueurs d'AOS biogénique et anthropique ont été quantifiés en phase particulaire et gazeuse et la formation de 10 a été simulée. L'évolution des concentrations en lévoglucosan (marqueur de la combustion de biomasse) a aussi été modélisée. Les résultats ont montré que les émissions de sources ou précurseurs (manquantes ou sous-estimées), les concentrations en radicaux (NO, HO₂ et RO₂) et le défaut de voies de formation, sont des paramètres clés pour la simulation des marqueurs d'AOS. Une faible dépendance à la T°C du partage gaz-particule a été observée alors que le partage hydrophile non idéal, souvent négligé, semble essentiel. Le lévoglucosan est bien modélisé, même si des sous-estimations existent dans certaines régions et une importante fraction gazeuse théorique a été mise en évidence. La comparaison mesures/modèle de marqueurs moléculaires est un outil puissant pour évaluer les émissions, les processus physico-chimiques et à terme, estimer les sources d'AO.

Mots clés: [Qualité de l'air; Particules en suspension; Aérosol organique; Marqueurs; Modélisation; Processus chimiques]